Agronomy Research

Established in 2003 by the Faculty of Agronomy, Estonian Agricultural University

Aims and Scope:

Agronomy Research is a peer-reviewed international Journal intended for publication of broad-spectrum original articles, reviews and short communications on actual problems of modern biosystems engineering incl. crop and animal science, genetics, economics, farm- and production engineering, environmental aspects, agro-ecology, renewable energy and bioenergy etc. in the temperate regions of the world.

Agronomy Research online:

Agronomy Research is available online at: https://agronomy.emu.ee/

Acknowledgement to Referees:

The Editors of *Agronomy Research* would like to thank the many scientists who gave so generously of their time and expertise to referee papers submitted to the Journal.

Abstracted and indexed:

SCOPUS, EBSCO, DOAJ, CABI Full Paper and Clarivate Analytics database: (Zoological Records, Biological Abstracts and Biosis Previews, AGRIS, ISPI, CAB Abstracts, AGRICOLA (NAL; USA), VINITI, INIST-PASCAL.)

Subscription information:

Institute of Technology, EMU
Fr.R. Kreutzwaldi 56,
51006 Tartu,
ESTONIA
E-mail: timo.kikas@emu.ee

ISSN 1406-894X

CONTENTS

Agronomy Research **18**(3), 1911–1925, 2020
https://doi.org/10.15159/AR.20.212

Municipal organic solid waste composting: development of a tele-monitoring and automation control system

T. Ahmadi[1,*], C.A. Casas[1], N. Escobar[2] and Y.E. García[1]

[1]University of Cundinamarca, Faculty of Engineering, 18th Diagonal 20-29, Fusagasugá, Colombia
[2]University of Cundinamarca, Faculty of Agricultural Sciences, 18th Diagonal 20-29, Fusagasugá, Colombia
[*]Correspondence: tahmadi@ucundinamarca.edu.co

Abstract. The Organic Solid Waste (OSW) generation have experienced high growth in the last decades. Moreover, the treatment and management of them have become a priority in the environmental policy of many cities, due to the sanitary and environmental problems related to the OSW elimination. Between 2 and 3 metric tons per day of organic residues are generated in the local market square of Fusagasugá-Colombia, without having any transformation program or technological alternatives for their decomposition. This paper presents the design and implementation of an experimental reactor for composting that includes a measurement stage, signal conditioning, data acquisition (DAQ), and data storage, together with a control and telemetric supervision system through a Human-Machine Interface (HMI), which allows manipulation of some key variables of the composting process remotely via the Internet.

Key words: compost, aerobic, municipal wastes, humane machine interface, telemetry, environment, process control.

INTRODUCTION

A compost is a material with plenty of plant nutrients, is very useful as organic fertilizer for soil crops, and is produced by the decomposition of organic matter from plant and animal residues, done by microorganisms in an adequate humidity, pH and oxygen environment.

In recent years, considerable studies have been done on organic solid waste composting. In (Xiao et al., 2017; Wu et al., 2019) a review of recent development in solid waste composting is provided. In (Petiot & de Guardi, 2004) a method of composting is presented to manage heat balance and oxygen and moisture supply to microorganisms. A similar method is introduced in (Kadir et al., 2016; Taeporamaysamai & Ratanatamskul, 2016). However, technological processes can improve production times or production quality (Rodríguez & Córdova, 2006; Gómez, 2017; Galeano, 2018). In (Peña, 2011), it is provided that to obtain a mixture with high energy content, it is needed an adequate proportion of materials with a rich content of Carbon and Nitrogen; then those materials are chopped to improve the speed of

microorganism biodegradation (Ameziane et al., 2020). As can be seen, to improve the composting time and quality it is need to control the process.

In (Luo et al., 2014; Jiang et al., 2015; Avidov et al., 2017; Soto-Paz et al., 2019b) review of turning techniques are done, that is to say, the process that homogeneously mixes the organic matter, the substrate soil and the atmosphere inside the reactor, improving the chemical properties like pH and oxygen concentration and homogenizing the temperature in its thermophile phase. In (Xiao et al., 2017), a review of recent development in biochar utilization as an additive in organic solid waste composting has been presented. Furthermore, it is founded that biochar addition in composting can improve compost mixture properties and microbial activities, reduce greenhouse gas emissions and upgrade compost quality.

Although the compost of organic matter is a natural process, ideally the compost production should be a fast, low energy process with a hygiene standard in production (Alvarado, 2018). This is achieved by controlling important variables like aeration, Carbon-to-Nitrogen ratio (C/N) and temperature and humidity (Mayorga, 2016). In (Hemidat et al., 2018) it is monitored the bio-waste composting process in Jordan to evaluate the final product quality. This control process is monitoring the temperature, moisture and oxygen content of the reactor. The effects of using remote control on the biowaste compost quality can be found in (Lozada, 2020). It is shown that this method has improved the composting time as well as its quality. In (Soto-Paz et al., 2019a) an approach to optimize the biowaste composting using machine learning methods is presented. However, in the literature it can found a gap between control process and Human-Machine Interface methods to measure stages, signal conditioning, data acquisition (DAQ), and data storage, together with a control and telemetric supervision.

For this reason, in this study to improve the composting efficiency with a control and telemetric supervision system, a new HMI system applied to the Organic Solid Waste (OSW) reactor. Furthermore, this paper shows a process of characterization for the Organic Solid Waste (OSW) produced in the local market of Fusagasugá, with both plant and animal type of residues. Similar to (Yimy Garcia et al., 2014) in this paper the prototype construction and startup are done in three phases: The first phase is a preliminary research about quantification and characterization of OSW, and a basic prototype design. In the second phase, the basic prototype is built and first laboratory experiments are done. In the third phase, a final prototype reactor is built and the basic operation manual is written.

The results of experiment approved that the compost produced adequate physical characteristics and compost quality. Due to the precise control over the composting environment inside the reactor, the process time was reduced.

PHYSICAL DESIGN OF THE EXPERIMENTAL REACTOR

A preliminary reactor structure design is designed and implemented using CAD software. Then an instrumentation system is added to the physical reactor, together with a temperature and humidity control system and a HMI for remote adjustment and supervision of the system.

The physical design is based on a drum-type closed system (Peña, 2011), because this design allows process speedup compared with an open system exposed to the atmosphere and also allows a fine control of the environment inside the reactor chamber.

This design also has a blade system for mixture homogenization inside the reactor. This physical model is presented in the Fig. 1.

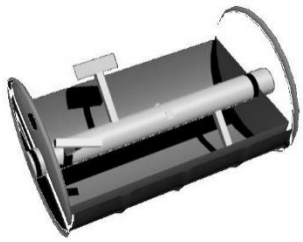

Figure 1. 3D model of the prototype reactor.

As presented in (Soto-Paz et al., 2019b), to improve the thermophilic phase peak, a reactor with a special rotation system can be used. In this rotation system a set of rotating opposite blades are connected to a rotating shaft in the center of the reactor. The 3D model of this system can be seen in the Fig. 2.

Figure 2. 3D model of the turning system.

Figure 3. Prototype reactor.

After confirming the results of simulations, the prototype reactor is built. In order to build this system, a 42 US gallons barrel with an isolated anti-corrosive coating is used as the reactor base. In this system, the rotating blades are made of 12-sheet metal and the rotating shaft is made of 2-caliber steel pipe (Fig. 3). Both the blades and the shaft have an isolated anti-corrosive coating.

ORGANIC MATTER TRANSFORMATION PROCESS

OSW characterization phase

To implement the composting process of the OSW produced in the local market of Fusagasugá, several methods for residue management are studied to get approximate characteristics and conditions of the generated OSW destined for a composting process. For the quantization and characteristics of the OSW a grouping based on the residue type (organic or inorganic) is done by using awnings, plastic bags, gloves, a scale, a residue crusher, the prototype reactor, a thermometer, a PH meter and a humidity sensor. The results are shown in the Table 1.

Table 1 shows that in municipal residues, the amount of organic waste is greater than the inorganic residues. The organic part includes shells, husks, fruits, vegetables, leafs, seeds and aromatic herbs. These residues are crushed to a size of 1 to 6 cm (Herodes et al., 2018). This allows a better decomposition of microorganisms, as well as homogeneous materials are also obtained at the end of the process.

Table 1. Results for separation and characterization of OSW

No. Garbage cans 3		Total weight: 140.35 kg
ORGANIC WASTE		INORGANIC WASTE
No. Weighing	Weight, kg	Type
1	14.3	Polystyrene, Plastic, Bottles
2	14.85	Metals, porcelains, cable
3	11.32	Paperboard and paper
4	15.79	wood
5	12.02	Others (soap)
6	12.54	
7	26.59	Total Inorganic Waste 9.43 kg
Leafs	22.43	
Animal waste	1	
Total organic waste	130.84	

In the Fig. 4, it is shown the separation and weighting process for OSW, for this step, it was necessary to use plastic bags, gloves and a scale.

Figure 4. Separation and weighing of organic residues.

At a municipal level, specifically for the OSW generation in Fusagasugá, according to studies of garbage collection routes done by the Fusagasugá public utility Emserfusa in 2011, each habitant generates 0.6 kg per day averagely. Comparing the characterization described before in Table 1 with the characterization at municipal level done by the integral solid waste management government program (in Spanish Programa gubernamental de Gestión Integral de los residuos Sólidos - PGIRS) in Table 2, both are similar although it is found that a bigger proportion of OSW is found in the local market.

Table 2. Municipal solid waste separation (Galeano Barrios, 2018)

Material	%
Recyclables material	
Plastics	6.03
Paperboard	1.98
Recyclable paper	11.35
Textile	0.11
Glass	11.35
Bone	0.18
Burnable material	0.0
Wood	0.84
Organic matter	64.67

Regarding the final garbage disposal, up until a few years ago, the town used a 7-hectare open-air landfill to store solid garbage generated by the residents. However, the Autonomous Regional Cundinamarca Corporation (CAR) canceled the authorization for garbage disposal in this site, attending to Resolution 1045 of 2003, which establish the shutdown of all open-air landfills. Later then, collected garbage is done in the Nuevo Mondoñedo landfill, with higher transportation costs for 72 metric tons a day of solid residues (Galeano, 2018).

According to the PGIRS (Galeano, 2018), the Fusagasugá city hall is wasting the opportunity to get additional income due to OSW recycling. It is shown that more than 55% of OSW can be recycled to produce useful materials for different productive

sectors; some of them can be processed by different options like composting or biogas production.

Particularly, in the space study that is the local market called 'La Galería', the local waste disposal service company (Emserfusa) informs that about 2 to 3 tons of OSW are produced daily, and unfortunately, this company does not have a proper waste management and recycling program.

Crush and triturate phase of organic material

Particle size is a key factor at the beginning of microbiologic activity for composting process, and for the result of the processed compost. In a compost with homogeneous particle size and shape, the microorganisms have better capacity for organic degradation; bigger particles have little contact surface for the degrading action of microorganisms and extending the processing time. Ideal particle size is between 3 cm to 6 cm (Alcantara & Roxana, 2018).

Due to the size of the organic materials previously characterized in the previous step, in order to improve the microorganism decomposition, process the organic material must have a bigger contact surface (Malat'ák et al., 2016). For this purpose, the OSW must be crushed and shredded through some mechanical treatments shown in Fig. 5. Type and intensity of the mechanical treatment depends on the structure, shape and size of the residues.

Figure 5. Organic material crusher (left) and plant material disposed in the reactor (right).

Carbon Nitrogen ratio (C/N)

The two essential elements involved in the composting process are Carbon and Nitrogen; its correct balance allows getting a high-energy mix. In order to get this desired high-energy mix, an adequate proportion of materials rich in Carbon and Nitrogen. Eq. (1) allows calculating the weight proportion between Carbon-rich material and Nitrogen-rich material. Eq. (2).

$$^{C}/_{N} > 30 \quad (1)$$

$$^{C}/_{N} < 30 \quad (2)$$

$$x = \frac{(30 \cdot N_N) - C_N}{C_c - (30 \cdot Nc)} \quad (3)$$

where x = weight amount of Carbon-rich material; N_N = % of Nitrogen, in the Nitrogen-rich material; C_N = % of Carbon, in the Nitrogen-rich material; N_C = % of Nitrogen, in the Carbon-rich material; C_C = % of Carbon, in the Carbon-rich material.

The optimal Carbon-to-Nitrogen ratio (C/N) for composting process is 30 to 1. For experimentation, trials with rice husks was used with a C/N of 30.02.

$$x = \frac{(30 \cdot 2.12) - 44.07}{30.42 - (30 \cdot 0.78)} = 2{,}782 \quad (4)$$

From the results shown in Eq. (4), a mix with a ratio of 2.8 weight parts of rice husks by 1 weight part of OSW must be used. However, the husk volume was not adequate and it gives a medium carbon contribution to the mix.

For the last two trials, a mix with sawdust gave excellent results because of their C/N ratio; sawdust has 51.90% of Carbon contribution.

$$x = \frac{(30 \cdot 2.12) - 44.07}{51.90 - (30 \cdot 0.06)} = 0.398 \quad (5)$$

According to Eq. 5), a mix of 0.4 weight parts of sawdust by 1 weight part of OSW must be used. Using this mix, the sawdust gives an adequate volume for the compost and a high Carbon contribution to the mix, an essential element for microorganism energy source. Using sawdust, an initial C/N ratio between 25 and 30 can be obtained for the beginning of the composting process, enough to get a mature compost with a final C/N ratio between 12 and 15. It is said that a compost with a final C/N ratio below 12 is ideally used for agricultural use (Bazrafshan et al., 2016; Romero-Cuero et al., 2016).

Humidity - temperature behavior

Using two physicochemical variables, temperature and humidity, the composting process can be evaluated and controlled (Robledo, 2018).

As shown in Fig. 6, the comparison between a reference pile covered by plastic and the compost processed by the proposed reactor with the sufficient physical conditions for composting process are performed.

The results of the experiments show that the compost in the prototype reactor reaches a temperature of 60 °C, while this temperature reaches 55 °C by the reference pile. This temperature cannot be maintained for a long time, because when the temperature reaches 50 °C, the rotation process takes place in order to supply oxygen to the microorganisms of the compost (Benjawan et al., 2015). As can be seen in Fig. 6, the temperature stabilizes after 12 days.

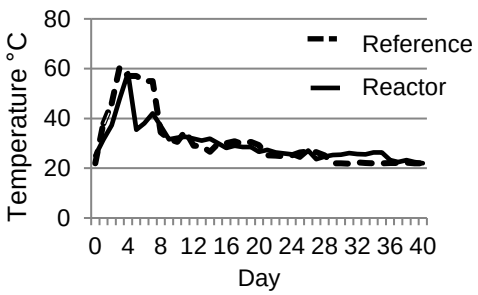

Figure 6. Composting Temperature vs Time.

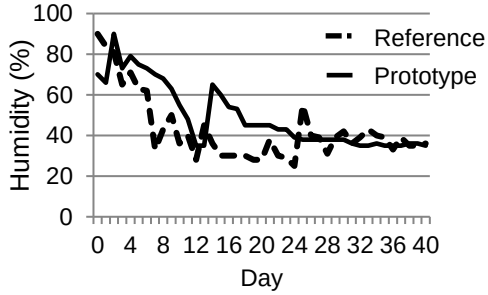

Figure 7. Composting Humidity vs Time.

As shown in Fig. 7, the humidity content of the materials used in the trials is high. However, from day 24 humidity in the prototype reactor is stabilized, as opposite to the reference pile that is stabilized up to day 38.

Physical Variables- Microorganisms Correlation

It is essential to correlate the Temperature (°C) and the amount of CFU g^{-1} of sample throughout the composting process. Due to this, a descriptive graph of the three

phases of composting was made together with the Temperature reached in each of these as observed in Fig. 8.

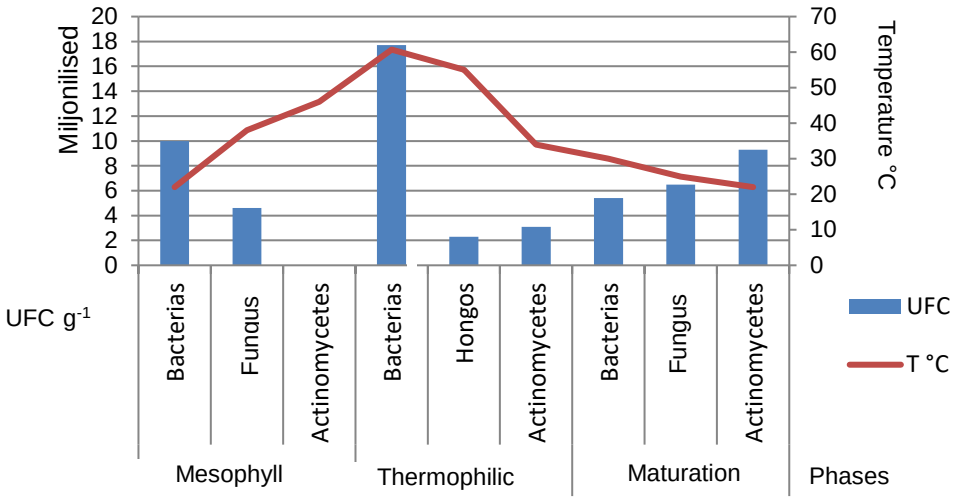

Figure 8. Compost temperature vs. Amount of CFU in each Phase.

In Fig. 8, the temperature line is starting with an ambient temperature where mesophilic bacteria and fungi initiate the degradation of organic matter until achieving homogeneity and accelerating the process during the first days. There the matter is acidified and the temperature later in the thermophilic stage reaches up to about 61 °C. When the temperature decreases, Actinomycetes continue to reproduce, unlike the bacteria that disappear due to the demand for food and energy that they suffered at the end of the thermophilic stage. The variation of temperature in the piles is one of the most important factors. In this study, the Correlation Coefficient (r) is 0.953. This value that is between 0.9 and 1.0 indicates that the variables Temperature and CFU g^{-1} are highly correlated.

TEMPERATURE AND HUMIDITY SENSORS

Instrumentation is a process based on the signal conditioning from the sensors used in a controlled environment. It is necessary to set the sensors optimal range of operation, with the maximum and minimum values. Once the sensors are selected for this application, sensor operation is analyzed and conditioning circuits for them are designed.

Humidity sensor

A common sensor is used to obtain humidity as shown in Fig. 9. Using this sensor, two parameters can be obtained namely the analog voltage corresponding to the humidity, and the digital output as an adjustable threshold.

Due to the high humidity content of the organic matter used in the prototype reactor, it is not necessary to use an additional system to supply water to the mix. However, a drying process controlled by HMI is required to reduce the humidity content of the mixture. The controller is such that an alarm is triggered when the humidity exceeds below the desired level (about 55%).

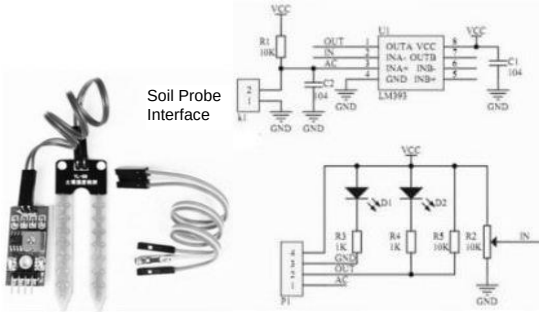

Figure 9. Humidity sensor used in the prototype.

Temperature sensor

A PT100 sensor is used due to its simple structure and lineal behavior. However a Wheatstone bridge is used, in order to increase its sensitivity (García, 2014). The 1NA106 is also used to amplify voltage of Wheatstone bridge. This amplifier has the ability to increase the voltage 10 times and is suitable for connecting this signal to a microcontroller or development board like Arduino.

Because the desired temperature of the organic matter is regulated by microbial action and artificial heating, a controlled water supply system using a 12-volt electric pump, along with a valve, a water tank and a nebulizer system are used to water the organic matter as homogeneous as possible. The control system of the water circuit is shown in the Fig. 10.

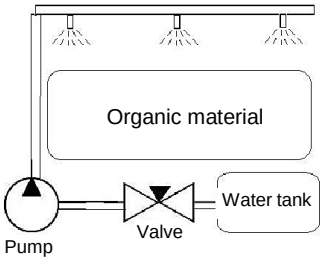

Figure 10. Irrigation system.

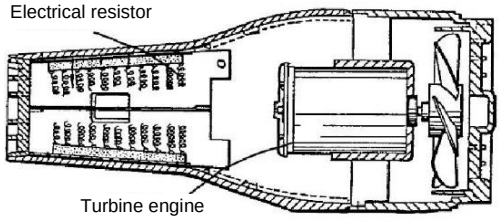

Figure 11. Temperature actuator.

A hot air circulatory system to perform the aerobic process. This system is responsible for controlling the oxygen level and temperature of the organic matter in the reactor. As can be seen from the Fig. 11, the heating system adjusts the system temperature using electrical resistors. These resistors can provide a maximum of 1,440 W of heat power and are controlled by a AC-AC PWM converter. In addition, using a turbine, airflow is created in the direction of the reactor.

The existence of this process with constant airflow and variable temperature over time is essential to accelerate the degradation of OSW.

Design and implementation of the temperature control

In the natural composting process, the temperature is not uniform. The higher temperatures are produced in the middle of the pile and lower temperatures at the ends. In addition, there is a maximum temperature difference in the thermophile stage. Asmentioned, the activity of microorganisms decreases at low temperatures. For this purpose, a temperature control system has been designed to maintain a constant temperature in all parts of the pile. In order to design the controller, the system under review becomes linear by using the IDENT tool in MATLAB (Fig. 12). As a result, the transfer function achieved and an appropriate PID controller with a delay time of 40 seconds designed to control the system (Fig. 13).

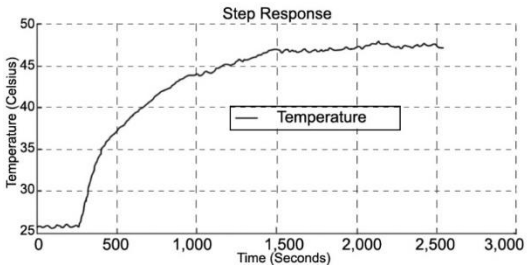

Figure 12. Step response for temperature.

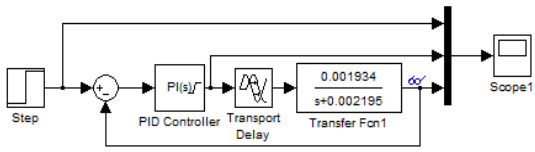

Figure 13. Simulink model controller.

HUMAN MACHINE INTERFACE (HMI)

The HMI for the reactor prototype is defined for monitoring and controlling the system parameters (airflow, watering and heating) via the Internet. The HMI diagram can be seen from the Fig. 14 and Fig. 15. In this study similar to (García, 2014), it is used Labview software to create HMI.

At the geographic location of the workshop, it is possible to use an Ethernet-based local area network (LAN) to connect the workshop and the Arduino module. For this purpose, a UDP-based communication is used because of its simple structure and fast response.

The sample time of the control system is 2 minutes, Due to the slow dynamics of the prototype reactor system. In addition, for the remote communication the 'Web Publishing Tool' tool of the LabVIEW is used. This tool runs a web server in the computer running the HMI that serves an HTML page with the same content visualized in the HMI. Therefore, users

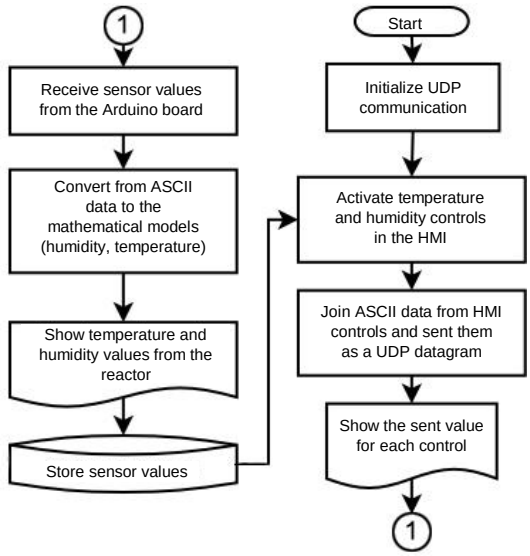

Figure 14. HMI Flowchart.

can view all stages of development in real time. The panel control viewed can be seen from the Fig. 16.

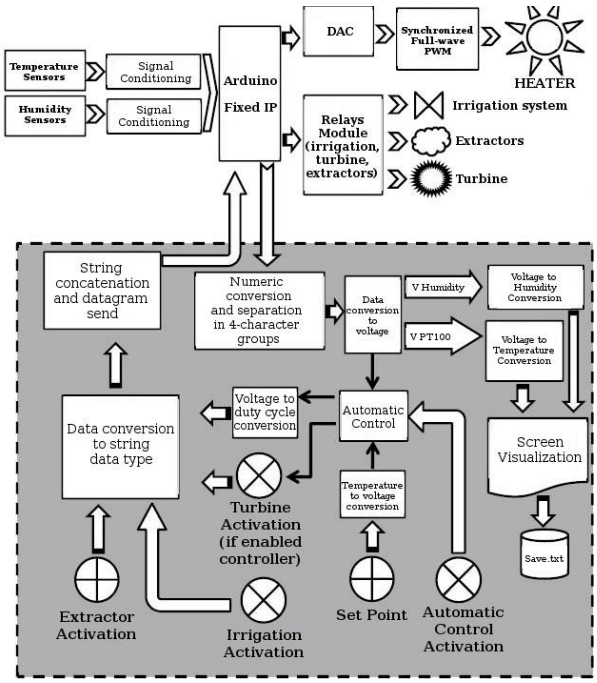

Figure 15. HMI Block Diagram.

Figure 16. View of HMI control panel from a web navigator.

DISCUSSION

Microbiological analysis of the mesophilic phase for composting in the prototype reactor

Nowadays, composting process is a complex activity that farmers do to obtain an organic fertilizer. However, for agricultural use this fertilizer need a certain quality level that depends of, among many things, microbiological activity on the composting process. For that reason, in the non-industrial scale it is essential to know each composting phase

and characterize the microorganism responsible of OSW decomposition process (Ahmadi et al., 2020).

In Table 3, it is shown the laboratory analysis results from the first phase of composting; these results are shown in terms of colony-forming units (CFU) for bacteria, fungus, pseudomonas and yeast. This analysis of the first composting phase, mesophilic phase, was done in the laboratory 'Dr. Calderón' in Bogotá D.C., Colombia on March 2014.

Table 3. Laboratory Analysis results mesophilic phase

Results No.	Scientif name	Population
1	Fungus	< 10 CFU g^{-1}
2	Yeast	11×10 E 7 CFU g^{-1}
3	Mesophilic Bacteria	24×10 E 7 CFU g^{-1}
4	Pseudomonas	17×10 E 5 CFU g^{-1}

In the Table 3 it is shown in detail that the result 3 from the mesophilic bacteria is the highest, meaning that these bacteria has the largest population measured in CFU in this phase. A brief explanation for this largest population is that these bacteria are responsible of the decomposition of lignin and other nitrogen-rich compounds to transform in Carbon. The thermophile bacteria use this Carbon in the next phase (thermophilic phase), those bacteria require high amounts of Carbon to raise the temperature in this phase. It must be noted that these bacteria are essential for initialize and activate all the process needed for composting, without mesophilic bacteria, it is impossible to degrade the organic matter.

The second highest microorganism population in terms of CFU for the first composting phase are the Pseudomonas. These microorganisms are important in the mesophilic phase for the decomposition of plant material like fruits, stems and leafs. It should be noted that pseudomonas also causes some plant diseases and those are initially found in past infected crops. Then in the thermophilic phase, its higher temperature (over 60 °C) kills the pseudomonas. Compost quality highly depends on this thermophilic phase because any pseudomonas that keep alive after this phase could cause plant diseases transmitted from the compost fertilizer.

Last in the result table, it is shown that both items 1 and 2 (fungus and yeast) had lower CFU because these microorganisms are not involved in organic matter decomposition and remain dormant until the decomposition of nitrogen-rich matter (Escobar et al., 2020). In the next two phases, it is observed an exponential growth of these two microorganism groups.

Quality and elaboration time of the compost

In order to check the quality and elaboration time of the compost, a comparison was done between a monitored conventional composting pile and the proposed prototype reactor with all the instrumentation, data acquisition and the manual turning mechanism. In many composting techniques it is unknown which microorganisms are responsible of organic material decomposition, and therefore the physicochemical factors involved in this process (Porras, 2016). Based on this, it can be said that the success in a composting process depends on the correct management of the physicochemical conditions inside the designed prototype reactor. A quality control analysis from a compost test produced was done; the results are show in Table 4.

The first quality parameter was the apparent density; according to (Storino et al., 2014) and its work on organic residue management, it can be considered that an ideal compost with adequate particle distribution and organic content had an apparent density between 0.2 and 0.5 g cm^{-3}. Compost produced in the tests done in the prototype reactor were around 0.2 g cm^{-3}, therefore it is in the ideal range.

The next quality parameter is the pH; measured values in the tests done were of 7.5, this value can be seen as near neutral or that it tends to neutrality. Moreover, in (Arregui Arellano et al., 2018) work about substrates composition in agriculture, they proposed that the electrical conductivity, as an indicator of salts concentration in a substrate for soil adjustment, should not exceed 100 dS m^{-1}. Measured electrical conductivity was around 23.8 dS m^{-1}, therefore it can be said that the compost met ideal characteristics by having low salt concentration, essential for a substrate used in agriculture.

Another quality parameter is relative humidity; its measurement was found below 30% that means the substrate has an adequate stability conditions). Furthermore, mention the ash content that is related to mineral content, with an 18% being a good mineral content. Substrates obtained in the tests measured around 25.87% of ash content, which means a very good mineral content.

Table 4. Compost Quality Control Analysis

Parameter	Value	Unit
Dry-Bulk Density	0.200	g cm^{-3}
Ph Satured paste	7.54	%
E.C Saturation Extract	23.80	dS m^{-1}
Moisture	31.89	%
Ashes	25.87	%
Acid Insoluble Residue	16.71	%
Cation-exchange capacity or CEC	31.19	meg/100
Total Nitrogen	1.47	%
Total Potassium	2.13	%
Total P2O5	0.68	%
Total MgO	0.44	%
Total K2O	2.56	%
Total CaO	1.98	%
Total Calcium	1.41	%
Total Magnesium	0.27	%
Total phosphorus	0.30	%
Sulfur	0.06	%
Boron	0.005	%
Cupper	0.001	%
Manganese	0.03	%
Iron	0.39	%
Zinc	0.007	%
Sodium	0.18	%
Total Oxidizable Organic Carbon	16.31	%
Carbon-to Nitrogen Ratio C/N	11.09	
Moisture Retention	147.58	%
volatilization losses	42.24	%

Regarding the Total Oxidizable Organic Carbon, the laboratory 'Agrilab' in Bogotá states that the minimum value for an organic fertilizer should be around 15%, elaborated compost in the tests is slightly higher showing adequate contents of humic and fulvic acids. In addition, about C/N ratio proposes a value between 25 and 30 as the ideal proportion. However, the elaborated compost in the tests had lower proportions and it was necessary to add carbon-rich materials like rice husks, sawdust or other materials with high carbon content. Quality measurement of this C/N ratio for the elaborated compost returned a value of 11.09. In (Ballardo et al., 2017), a compost reactor with enhanced biopesticide properties through solid-state fermentation of biowaste is presented. The process time of this reactor is about 50 days to reach to its ideal results. In (Zhang & Sun, 2016) the bacteria and fungi peak values can approximately reach to

19 (log_{10} CFU g^{-1}) and 10 (log_{10} CFU g^{-1}). The time needs to reach the final result in (Jalili et al., 2019) is about 60 days. in the mentioned study, the PH value after composting process the PH value finds a value of approximately 7.75. Furthermore, the C/N ratio has a value of 13. By comparing the results obtained in this investigation with the mentioned studies, it can be find that by applying the proposed control method in compost production, not only the time required for compost production is reduced but also the quality of the obtained results is improved. These benefits will also reduce energy consumption and improve the overall efficiency of the system.

CONCLUSIONS

This paper showed that the implementation of a closed system for compost elaboration minimized the climatic induced variations compared to the traditional composting piles. The installed controller could reduce the temperature variations inside the experimental reactor due to the composting process. Continuous measurement and data storage of the temperature and humidity by the HMI showed that environmental conditions affect organic material inside the reactor, particularly in the compost surface regions.

The experiment approved that the compost produced in this project maintained adequate physical characteristics like smell, color, C/N ratio and particle size; and it could be stated that this compost had a high quality standard. Because of the precise control over the composting environment inside the reactor, the process time was reduced up to 30%; from 65 days on the reference pile to 45 days in the experimental reactor. Furthermore, microbiological analysis performed from samples of experiments made in the prototype reactor showed the presence of bacteria, fungus and particularly actinobacteria; essential microorganisms for the decomposition process involved in quality composting production. This was evidenced by the laboratory analysis done in the certified laboratories 'Dr.Calderón' in accordance with the national standard NTC5167.

This project demonstrated to the local merchants of the local market 'La Galería' that it is possible to reduce the environmental impact due to the organic residues produced there. Future work will be focused in the automation of the turning process, the design and implementation of a large-scale reactor and the implementation of an OSW management program for the Fusagasugá local market 'La Galería'.

REFERENCES

Ahmadi, T., Casas, C.A., García Y.E. & Escobar, N. 2020. Prototype reactor to compost agricultural wastes of Fusagasuga Municipality. Colombia. *Agronomy Research* **18**(2), 314–323.

Alcantara, I. & Roxana, J. 2018. Efficiency of the treatment of organic livestock residues in composters by means of efficient micro. *Revista Chilena.* **34**(2), 59–98 (in Spanish).

Alvarado, R.L. 2018. Managment of poultry by composting. *Rev. PuertoNol* **2**(5), 131–134 (in Spanish).

Ameziane, H., Zouahri, A., Khamar, M. & Nounah, A. 2020. Composting olive pomace: evolution of organic matter and compost quality. *Agronomy Research* **18**(1), 5–17.

Arregui, M.J., Alcívar, M. & Indelira, M. 2018. E Evaluation of bio-fertilizers obtained from animal waste from the Camal Municipal de Guaranda, Escuela Superior Politécnica de Chimborazo. *Revista UMNG* **3**, 81–94 (in Spanish).

Avidov, R., Saadi, I., Krassnovsky, A., Hanan, A., Medina, S., Raviv, M., Chen, Y. & Laor, Y. 2017. Composting municipal biosolids in polyethylene sleeves with forced aeration: Process control, air emissions, sanitary and agronomic aspects. *Waste Management* **67**, 32–42.

Ballardo, C., Barrena, R., Artola, A. & Sánchez, A. 2017. A novel strategy for producing compost with enhanced biopesticide properties through solid-state fermentation of biowaste and inoculation with Bacillus thuringiensis. *Waste Management* **70**, 53–58.

Bazrafshan, E., Zarei, A., Mostafapour, F.K., Poormollae, N., Mahmoodi, S. & Zazouli, M.A. 2016. Maturity and stability evaluation of composted municipal solid wastes. *Health Scope* **5**. doi: 10.17795/jhealthscope-33202

Benjawan, L., Sihawong, S., Chayaprasert, W. & Liamlaem, W. 2015. Composting of biodegradable organic waste from Thai household in a semi-continuous composter. *Compost science & utilization* **23**, 11–17.

Escobar, N., Arenas, N.E. & Marques, S.M. 2020. Characterization of microbial populations associated with different organic fertilizers. *International Journal of Recycling of Organic Waste in Agriculture* **9**(2), 173–184.

García, M.Á.P. 2014. Electronic instrumentation. Ediciones Paraninfo, pp. 8–11 (in Spanish).

Gómez, L.J. 2017. Use of recyclable solid waste in the municipality of Pereira. *Revista Luna Azul* **8**, 101–113.

Garcia, Y., Restrepo, C.C. & Cedeño, K. 2014. Design of a telemetric monitoring system for temperature and humidity in an experimental prototype compost manufacturing plant. *INTERCON* 14, pp. 18–21 (in Spanish).

Hemidat, S., Jaar, M., Nassour, A. & Nelles, M. 2018. Monitoring of composting process parameters: A case study in Jordan. *Waste and Biomass Valorization* **9**, 2257–2274.

Herodes, K., Haiba, E., Nei, L., Lillenberg, M. & Ivask, M. 2018. On the degradation of metformin and carbamazepine residues in sewage sludge compost. *Agronomy Research* **16**(3), 696–707.

Jalili, M., Mokhtari, M., Eslami, H., Abbasi, F., Ghanbari, R. & Ebrahimi, A.A. 2019. Toxicity evaluation and management of co-composting pistachio wastes combined with cattle manure and municipal sewage sludge. *Ecotoxicology and Environmental Safety* **171**, 798–804.

Jiang, T., Li, G., Tang, Q., Ma, X., Wang, G. & Schuchardt, F. 2015. Effects of aeration method and aeration rate on greenhouse gas emissions during composting of pig feces in pilot scale. *Journal of Environmental Sciences* **31**, 124–132.

Kadir, A.A., Ismail, S.N.M. & Jamaludin, S.N. 2016. Food Waste Composting Study from Makanan Ringan Mas. *IOP Conference Series: Materials Science and Engineering* **136**, 012057.

Lozada, P.T., Rebellón, L.F.M., Giraldo, C.A., Zapata, K.F. & Paz, J.S. 2020. Effect of the incorporation of star grass on the improvement of the process and the quality of the bio-waste composting product. *Revista EIA* **17**, 321–325 (in Spanish).

Luo, W.H., Yuan, J., Luo, Y.M., Li, G.X., Nghiem, L.D. & Price, W.E. 2014. Effects of mixing and covering with mature compost on gaseous emissions during composting. *Chemosphere* **117**, 14–19.

Malat'ák, J., Bradna, J. & Velebil, J. 2016. Combustion of briquettes from oversize fraction of compost from wood waste and other biomass residues. *Agronomy Research* **14**, 525–532.

Mayorga, E.M. 2016. Acceleration and decomposition of organic substrates in compost making through the use of different substances (sugar, molasses, sugar cane). UTEQ **31**(1), 23–41 (in Spanish).

Peña, J.-R.A. 2011. How to make compost, Editorial Paraninfo, 106–111 (in Spanish).
Petiot, C. & Guardia, A. 2004. Composting in a Laboratory Reactor: A Review. *Compost Science & Utilization* **12**, 69–79.
Porras, Á.C. 2016. Use of organic agricultural and forestry waste in Ibero-America. *Revista Academia y Virtualidad* **9**, 6 (in Spanish).
Robledo, T. 2018. E iological indicators on waste water. *Journal of Alive Sciences* **14**,198–201.
Rodríguez, M. & Córdova, A. 2006. Municipal composting manual: urban solid waste treatment *Compostaje municipal* **9**, 131–133 (in Spanish).
Rodríguez, M. & Córdova, A. 2006. Manual de compostaje municipal: tratamiento de residuos sólidos urbanos. *Manual de compostaje municipal* **9**, 131–133 (in Spanish).
Romero-Cuero, J.M., Calderón-Maya, J.R. & Marmolejo-Uribe, A.M. 2016. Base Guidelines for Developing a Comprehensive Urban Solid Waste Management Plan in Ixtlahuaca, State of Mexico. *Quivera Revista de Estudios Territoriales* **18**, 89–115 (in Spanish).
Soto-Paz, J., Alfonso-Morales, W., Caicedo-Bravo, E., Oviedo-Ocaña, E.R., Torres-Lozada, P., Manyoma, P.C., Sanchez, A. & Komilis, D. 2019a. A New Approach for the Optimization of Biowaste Composting Using Artificial Neural Networks and Particle Swarm Optimization. *Waste and Biomass Valorization* **8**, 1–15.
Soto-Paz, J., Oviedo-Ocaña, E.R., Manyoma, P.C., Marmolejo-Rebellón, L.F., Torres-Lozada, P., Barrena, R., Sánchez, A. & Komilis, D. 2019b. Influence of mixing ratio and turning frequency on the co-composting of biowaste with sugarcane filter cake: a mixture experimental design. *Waste and Biomass Valorization* **6**, 1–15.
Storino, F., Arizmendiarrieta, J., Ganuza, E., Muro, J., Aparicio-Tejo, P. M. & Irigoyen, I. 2014. Comparison of small and large scale composting: Study of the process and of the compost obtained. *Spanish Composting Network* **10**, 40–44 (in Spanish).
Taeporamaysamai, O. & Ratanatamskul, C. 2016. Co-composting of various organic substrates from municipal solid waste using an on-site prototype vermicomposting reactor. *International Biodeterioration & Biodegradation* **113**, 357–366.
Wu, P., Ata-Ul-Karim, S.T., Singh, B.P., Wang, H., Wu, T., Liu, C., Fang, G., Zhou, D., Wang, Y. & Chen, W. 2019. A scientometric review of biochar research in the past 20 years (1998–2018). *Biochar* **1**, 23–43.
Xiao, R., Awasthi, M.K., Li, R., Park, J., Pensky, S.M., Wang, Q., Wang, J.J. & Zhang, Z. 2017. Recent developments in biochar utilization as an additive in organic solid waste composting: A review. *Bioresource Technology* **246**, 203–213.
Zhang, L. & Sun, X. 2016. Improving green waste composting by addition of sugarcane bagasse and exhausted grape marc. *Bioresource Technology* **218**, 335–343.

Agronomy Research **18**(3), 1926–1932, 2020
https://doi.org/10.15159/AR.20.195

Lighting source as cause of changes in cucumbers' physiology and morphology

I. Alsiņa[1,*], L. Dubova[1], M. Dūma[2], I. Erdberga[1], I. Augšpole[1], D. Sergejeva[1] and A. Avotiņš[3]

[1]Latvia University of Life Sciences and Technologies, Faculty of Agriculture, Institute of Plant and Soil Science, Liela street 2, LV-3001 Jelgava, Latvia
[2]Latvia University of Life Sciences and Technologies, Faculty of Food Technology, Department of Chemistry, Liela street 2, LV-3001 Jelgava, Latvia
[3]Riga Technical University, Faculty of Power and Electrical Engineering, Kaļķu street 1, LV-1658 Riga, Latvia
[*]Correspondence: Ina.Alsina@llu.lv

Abstract. The demand of fresh fruits and vegetables is growing. Therefore cultivation of them is essential all year round. The growth in the dark period of a year is not imaginable without artificial lighting sources. Therefore the experiments were carried out to investigate the effects of three different lighting sources on the growth of cucumbers at the early stages of development. Plants were grown in the polycarbonate greenhouse under three different lighting sources: Led cob Helle top LED 280, induction lamp and high pressure sodium lamp Helle magna. Cucumbers were grown in 16h photoperiod with PAR at the tips of plants 200 ± 20 µmol m^{-2} s^{-1}. Plant growth parameters, specific leaf area, pigments, phenols and flavonoids content in leaves, leaf light reflection parameters were determined. Results showed that cucumber plants grown under Led cob Helle top LED 280 in average were smaller, with less chlorophyll, carotenoids and phenols, but leaves have higher chlorophyll a and b ratio and specific leaf area in comparison with traditionally used in greenhouses High Presure Sodium Lamps (HPSL). Cucumber plants grown under Induction lamp in average were shorter, but with larger leaf area, with higher chlorophyll and carotenoids content, but decreased phenols content in comparison with HPSL. Lichtenthaler index 1 (LIC1) and NDVI are useful for assessing the physiological state of cucumber plants. Despite the fact that the plants grow well and develop normally under all lamps, the results show that sodium lamps are the most suitable for cucumbers. Further research is needed to adjust LED lighting for cucumber cultivation.

Key words: *Cucumis sativus*, LED, plant pigments, biochemical parameters, NDVI.

INTRODUCTION

The demand of fresh fruits and vegetables is growing. Therefore cultivation of them is essential all year round. Global change and development of technology provides new opportunities for influencing plant growth. The growth in the dark period of the year is not imaginable without artificial lighting sources. Development of high intensity light emitting diodes (LEDs) gives new opportunities for optimisation of light in horticulture (Dueck et al., 2016). LEDs have many benefits: they are easily integrated into digital

control system, they are safer to operate, and they are cooler in comparison with High Pressure Sodium Lamps (HPSL). As light output increases while devise costs decrease, LEDs continue to become economically feasible for horticultural lighting applications (Olle & Alsina, 2019). Light production efficiency is better in LEDs than HPSL and it is increasing (Särkkä et al., 2017). However, before use of LEDs as the sole source of light can be advanced, plant responses to light quality have to be investigated for the important horticultural plants (Hernández & Kubota, 2016).

Artificial lighting has been widely used to increase product quality and yield. Many research have been done to investigate changes of bioactive compounds under additional lightning. Kataoke et al., 2003 reported about changes of anthocyanin biosynthesis in grape and lettuce, but Zhou & Singh, 2002 reported, that additional light increased phenolic and anthocyanin content in cranberry fruits. There are also evidence, that supplemental far red (FR) LED decreased carotenoid and anthocyanin accumulation in lettuce (Li & Kubota, 2009).

Cucumbers are one of the most popular greenhouse grown vegetable and are known to be more sensitive to light quality changes then other vegetables (Hernandez & Kubota, 2016). Light and temperature are important growth factors for cucumbers known to respond well to light intensity. However, cucumber forms a tall canopy where self-shading affects vertical spectral light distribution. The vertical distribution of temperature and light may affect cucumber structure and photosynthesis efficiency with consequences for yield formation (Särkkä et al., 2017).

Nevertheless, LED technology in cucumber greenhouses is being introduced very slowly. This is due to the great variability of the LED lamp combinations, controversial data obtained in different experiments and insufficient amount of research.

The aim of this investigation is to compare three commercially available lighting sources which are produced for plant cultivation.

MATERIALS AND METHODS

The experiments were carried out in a polycarbonate greenhouse of Latvia University of Life Sciences and technologies during spring (1st set of experiments) and autumn (2nd set of experiments) seasons 2019. The temperature in the greenhouse was automatically regulated so that the temperature in the greenhouse did not exceed 30 ºC during the day, but did not fall below 15 ºC during the night.Two varieties of cucumbers 'Julian' and 'Victoria' were chosen for the experiments. Plants were grown in plastic pots (volume of pots was adapted to the plant size), filled with peat substratum KKS-S from Laflora (pH_{KCl} 5.8–6.6, EC 0.25 mS cm^{-1}, PG Mix (15–10–20) 1 kg m^{-3}, Ca 1.78%, Mg 0.21%). Total number of experimental plants for each variety at the beginning of experiment was 72. After appearance of the 1st true leaf plants were fertilized once a weak with 1% solution of Kristalon Green (18–18–18) with Mg, S and microelements in proportion $v:v_{pot}$ = 1:50.

Cucumbers were grown in 16 h photoperiod with PAR at the tips of plants 200 ± 20 µmol m^{-2} s^{-1}. Three different lighting sources: Led cob Helle top LED 280 (LED), induction lamp (IND) and high pressure sodium lamp Helle Magna (HPSL) were used. Lamp radiation distribution measured with portative spectrometer *Gigahertz*-Optic *MSC15* is shown at Fig. 1.

Six plants were analysed three times during the vegetative growth of cucumbers: at the stage of 1–2 true leaf; 3–5 leaves and inflorescence emergence stage). During cucumbers growth plant growth parameters (plant length, stem diameter under cotyledons, number of leaves), specific leaf area, pigments (spectrophotometrically determined in ethanol solution (Lichtenthaler & Buschmann, 2001) and with portative chlorophyll meter atLEAF^{+}, phenols and flavonoids content in leaves spectrophotometrically (Sergejeva et al., 2016), leaf light reflection parameters (with spectro-radiometer RS-3500) were determined. Indices used for evaluation of cucumbers vitality and biochemical composition as well as equations for their calculations (W- certain wavelength used for calculations) are shown in Table 1.

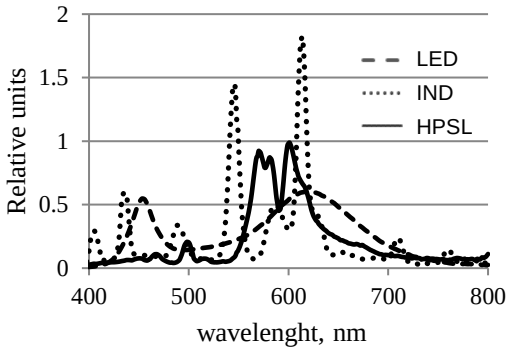

Figure 1. Lamp radiation distribution.

Table 1. Vegetation indices calculated from leaf reflectance at different wavelenghts

Vegetation index	Abbreviation	Equation	Reference
Carotenoids	CRI1	$\frac{1}{W510} - \frac{1}{W550}$	Gitelson et al., 2001
Carter 1(Stress index)	CTR1	$\frac{W695}{W420}$	Carter, 1994
Greenness Index	GI	$\frac{W554}{W677}$	Zarco-Tejada et al., 2001
Lichtenthaler index 1	LIC1	$\frac{W800 - W680}{W800 + W680}$	Lichtenthaler, 1996
Lichtenthaler index2	LIC2	$\frac{W440}{W690}$	Lichtenthaler, 1996
Normalized Difference Vegetation Index	NDVI	$\frac{W760 - W670}{W760 + W680}$	Padilla et al., 2017b
Plant Senescence Reflectance Index	PSRI	$\frac{W678 - W500}{W750}$	Merzlyak et al., 1999
Structure Intensive Pigment Index	SIPI	$\frac{W800 - W445}{W800 - W680}$	Peñuelas & Filella 1998, Zarco-Tejada et al., 2001
Simple Ratio Pigment Index	SRPI	$\frac{W430}{W680}$	Peñuelas et al., 1994
Vegetation fluorescence	DPI	$\frac{W688 + W710}{W697^2}$	Zarco-Tejada et al., 2003
Water use efficiency	WBI3	$\frac{W950}{W900}$	Peñuelas et al., 1993
Water Index	WI	$\frac{W900}{W970}$	Peñuelas et al., 1997

Biochemical analyses were performed in three replicates, Non-destructive leaf analyses in 10 replicates. Two way analyses of variance (Anova) and correlation analyse were calculated by software included in Microsoft Office Excel 2010. For mathematical

data processing the value of $P < 0.05$ was regarded as statistically significant. In cases of statistically significant differences, homogeneous groups were determined by Tukey's multiple comparison test at the level of confidence $\alpha = 0.05$.

RESULTS AND DISCUSSION

The obtained results showed that cucumber's growth significantly depends on used lighting source, growing season, plant development stage.

In average cucumber plant weight under LED lamp significantly decreased in comparison with Induction (IND) and High Pressure Sodium Lamps. (Fig. 2, A). Cucumber hypocotyl and whole plant length significantly decreased under LED and IND lamps in comparison with HPSL. It corresponds to research done by other researchers report about decrease of growth with increase blue light proportion in total light. (Hernández & Kubota, 2016, Sergejeva et al., 2018, Olle & Alsina, 2019).

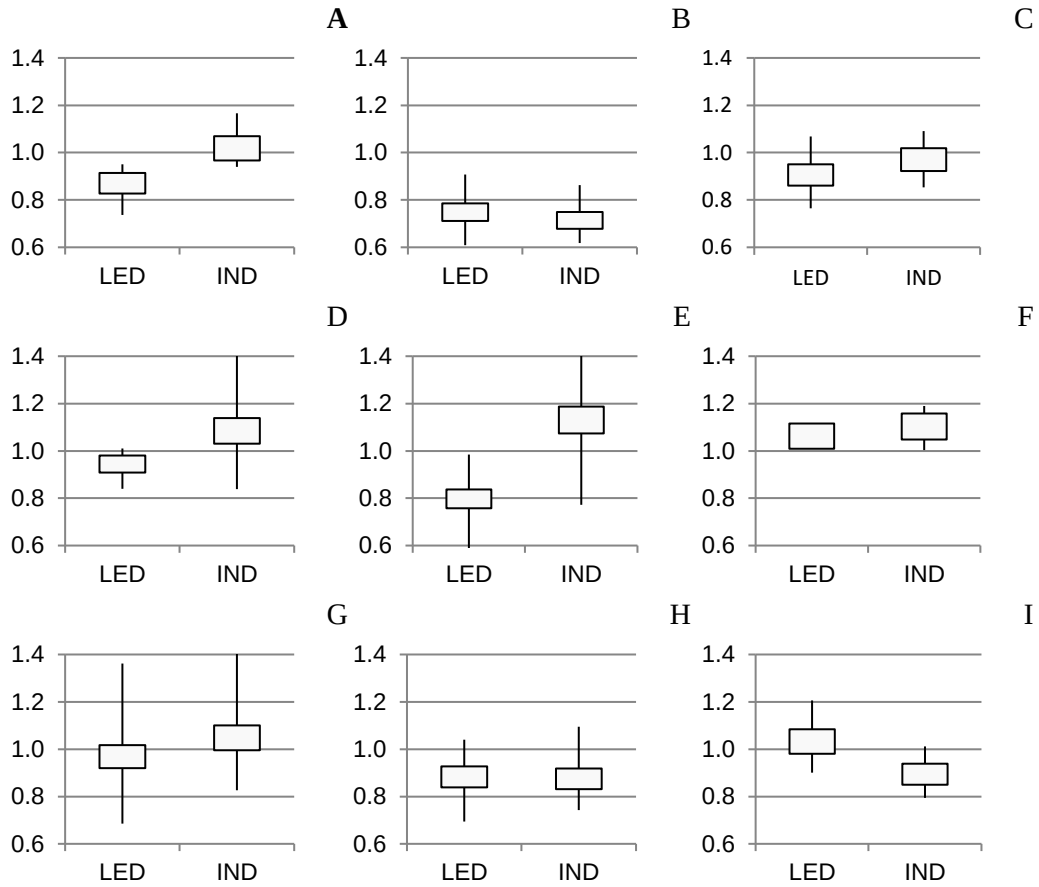

Figure 2. Ratio between plant parameters for growth under LED and IND lamps relative to the parameters obtained for growth under HPSL lamps. A – plant weight; B – plant length; C number of leaves; D – chlorophyll content; E – carotenoides content; F – ratio chlorophyll a and chlorophyll b; G – flavonoids conent; H – phenols content; I – specific leaf area.

Lighting source had significant effect of leaf properties. Cucumber leaves that had grown under the LED lamp had a smaller area, but thicker in comparison with IND and HPSL. These leaves characterized also with significantly larger specific leaf area (Fig. 2, I) in comparison with IND and HPSL. That corresponds to research done by Hernández & Kubota, (2016).

In average significant decrease of chlorophyll content in the cucumber leaves as result of LED ilumination was observed, in oposite to increase under IND ilumination in comparison with HPSL (Fig. 2, D), this difference in carotenoid content is even more noticeable ((Fig. 2, E). It is opposite to results by Sergejeva et al., 2018, Olle & Alsina, 2019. According to Padilla the average sufficiency value for all cucumber phenological phases for both maximum growth and maximum yield was 45.2 ± 0.7 SPAD units (Padilla et al., 2017a). Unfortunately leaves of our cucumbers contained chlorophyll in average 30–35 SPAD units and it leads to conclusion about unsufficiant nitrogen content in the cucumber leaves.

The most stable of the parameters studied was the ratio of chlorophyll a and b. In all vegetation seasons, for both varieties, under different lighting sources it varied between 2.0–2.76. In all sets of experiments the lowest value was observed under HPSL (Fig. 2, F).

No significant effect of used lighting source was observed on flavonoids content, but total phenols significantly decreased under LED and IND lamps. It is conversely our previous studies with leafy vegetables (Sergejeva et al., 2018).

Twelve vegetation indices were calculated from obtained cucumber leaves reflectance data (Table 2). Indices were chosen from different groups of published in the scientific literature, were previously by us and those which showed correlation with the studied morphological and biochemical parameters in our experiments.

Table 2. Vegetation indices calculated from leaf reflectance spectrums

Vegetation index	LED	IND	HPSL
CRI1	**0.086 a**	**0.126 b**	**0.122 b**
CRT1	1.332	1.228	1.347
GI	3.444	3.206	3.553
LIC1	**0.778 a**	**0.806 b**	**0.819 c**
LIC2	0.837	0.796	0.808
NDVI	**0.813 a**	**0.846 b**	**0.859 b**
PSRI	0.005	0.016	0.016
SIPI	**0.775 a**	**0.811 b**	**0.823 b**
SRPI	1.180	1.098	1.126
DPI	**0.225 a**	**0.329 b**	**0.279 a**
WBI3	**0.972 a**	**0.975 a**	**0.982 b**
WI	1.051	1.045	1.035

Significant differences in the reflected light from cucumber leaves were detected with Lichtenthaler indices 1 (LIC1). According to the literature, this index indicates the state of stress in the plant. By calculation, this index is similar to NDVI, which is the most commonly used index. The condition of plants is considered to be good if this index is larger than 0.8 (Berdugo et al., 2014). The results show that under all lamps the plants feel well. Vegetation indices connected with chlorophyll content (GI, SRPI) didn't show significant differences between lighting sources. Our previous experiments showed high correlation between SRPI and chlorophyll content in the plant leaves (Alsiņa et al., 2016).

Significant differences were found in Structure Intensive Pigment Index (SIPI) between LED and other two lamps used in experiments.

One of used water regime characterising index showed significantly higher value (WBI3 under HPSL), but in average seems that no water stress detected in cucumber leaves.

The results show that vegetative growth of cucumbers under the used LED and induction lamps is slightly inhibited compared to HPSL. Further research is required to optimize cucumber growing conditions

CONCLUSIONS

1. Cucumber plants grown under Led cob Helle top LED 280 in average were smaller, with less chlorophyll, carotenoids and phenols, but leaves have higher chlorophyll a and b ratio and specific leaf area in comparison with traditionally used in greenhouses High Pressure Sodium Lamps (HPSL).
2. Cucumber plants grown under Induction lamp in average were shorter, but with larger leaf area, with higher chlorophyll and carotenoids content, but decreased phenols content.
3. Lichtenthaler indices 1 (LIC1) and NDVI are useful for assessing the physiological state of cucumber plants.
4. Despite the fact that the plants grow well and develop normally under all lamps, the results show that sodium lamps are the most suitable for cucumbers. Further research is needed to adjust LED lighting for cucumber cultivation.

ACKNOWLEDGEMENTS. Research was supported by European Regional Development Fund project ‘New control methods for energy and ecological efficiency increase of greenhouse plant lighting systems (uMOL)’, Grant Agreement Nr. 1.1.1.1/16/A/261

REFERENCES

Alsiņa, I., Dūma, M., Dubova, L., Šenberga, A. & Daģis, S. 2016. Comparison of different chlorophylls determination methods for leafy vegetables. *Agronomy Research* **14**(2), 309–316.

Berdugo, C.A., Zito, R., Paulus, S. & Mahlein, A.K. 2014. Fusion of sensor data for detection and diffentation of plant diseases in cucumber. *Plant Pathology* **63**, 1344–1356.

Carter, G.A. 1994. Ratios of leaf reflectances in narrow wavebands as indicators of plant stress. *International Journal of Remote Sensing* **15**, 697–703.

Dueck, T., Wim Van Ieperen, W.V. & Kari Taulavuori. 2016. Light perception, signalling and plant responses to spectral quality and photoperiod in natural and horticultural environments. *Environmental and Experimental Botany* **121**, 1–3.

Gitelson, A.A., Merzlyak, M.N., Zur, Y., Stark, R. & Gritz, U. 2001. Non-destructive and remote sensing techniques for estimation of vegetation status. In: *Third European Conference on Precision Agriculture* France **1**, 301–306.

Hernández, R. & Kubota, C. 2016. Physiological responses of cucumber seedlings under different blue and red photon flux ratios using LEDs. *Environmental and Experimental Botany* **121**, 66–74.

Kataoke, I., Sugiyama, A. & Beppu, K. 2003. Role of Ultraviolet Radiation in Accumulation of Anthocyanin in Berries of 'Gros Colman' Grapes (Vitis vinifera L.). *Engei Gakkai zasshi*, **72**(1), 1–6.

Li, Q. & Kubota, C. 2009. Effects of supplemental light quality on growth and phytochemicals of baby leaf lettuce. *Environ. Exp. Bot*. **67**(1), 59–64.

Lichtenthaler, H.K. 1996. Vegetation Stress: an Introduction to the Stress Concept in Plants. *Journal of Plant Physiology* **148**, 4–14.

Lichtenthaler, H.K. & Buschmann, C. 2001. Chlorophylls and Carotenoids: Measurement and Characterization by UV-VIS Spectroscopy. *Current Protocols in Food Analytical Chemistry*. **1**(1), F4.3.1–F4.3.8.

Merzlyak, M.N., Gitelson, A.A., Chivkunova, O.B. & Rakitin, V.Y. 1999. Non-destructive optical detection of pigment changes during leaf senescence and fruit ripening. *Physiologia Plantarum* **106**, 135–141.

Olle, M. & Alsina, I. 2019. Influence of wavelength of light on growth, yield and nutritional quality of greenhouse vegetable, *Proc. of the Latvian Academy of Sciences*, Section B, Natural, Exact and Applied Sciences **73**(1), 1–9.

Padilla, F.M., Peña-Fleitas, M.T., Gallardo, M. Gimenez, C. & Thompson, R.B. 2017a. Derivation of sufficiency values of a chlorophyll meter to estimate cucumber nitrogen status and yield. *Computers and Electronics in Agriculture* **141**, 54–64.

Padilla, F.M., Peña-Fleitas, M.T., Gallardo, M. & Thompson, R.B. 2017. Determination of sufficiency values of canopy reflectance vegetation indices for maximum growth and yield of cucumber. *European Journal of Agronomy* **84**, 1–15.

Peñuelas, J. & Filella, I. 1998. Visible and near-infrared reflectance techniques for diagnosing plant physiological status. *Trends in Plant Science* **3**, 151–156.

Peñuelas, J., Gamon, J.A., Fredeen, A.L., Merino, J. & Field, C.B. 1994. Reflectance indices associated with physiological changes in nitrogen- and water-limited sunflower leaves. *Remote Sensing of Environment* **48**, 135–146.

Peñuelas, J., Gamon, J.A., Griffin, K.L. & Field, C.B. 1993. Assessing community type, plant biomass, pigment composition, and photosynthetic efficiency of aquatic vegetation from spectral reflectance. *Remote Sensing of Environment* **46**(2), 110–118.

Peñuelas, J., Pinol, J., Ogaya, R. & Filella, I. 1997. Estimation of Plant Water Concentration by the Reflectance Water Index WI (R900/R970). *International Journal of Remote Sensing* **18**(13), 2869–2875.

Särkkä, L.E., Jokinen, K., Ottosen, C.-O. & Kaukoranta, T. 2017. Effects of HPS and LED lighting on cucumber leaf photosynthesis, light quality penetration and temperature in the canopy, plant morphology and yield. *Agricultural and Food Science* **26**(2), 102–110. https://doi.org/10.23986/afsci.60293

Sergejeva, D., Alsina, I., Duma, M., Dubova, L., Augspole, I., Erdberga, I. & Berzina, K. 2018. Evaluation of different lighting sources on the growth and chemical composition of lettuce, *Agronomy Research* **16**(3), 892–899.

Zarco-Tejada, P.J., Miller, J.R., Noland, T.L., Mohammed, G.H. & Sampson, P.H. 2001. Scaling-up and model inversion methods with narrow-band optical indices for chlorophyll content estimation in closed forest canopies with hyperspectral data. *IEEE Transactions on Geoscience and Remote Sensing* **39**, 1491–1507.

Zarco-Tejada, P.J., Pushnik, J.C., Dobrowski, S. & Ustin, S.L. 2003. Steady-state chlorophyll a fluorescence detection from canopy derivative. *Remote Sensing of Environment* **84**(2), 283–294.

Zhou, Yu & Singh, B.R. 2002. Red light stimulates flowering and anthocyanin biosynthesis in American cranberry. *Plant Grown Reg*. **38**, 165–171.

Agronomy Research **18**(3), 1933–1943, 2020
https://doi.org/10.15159/AR.20.198

Olive pomace compost use for fenugreek germination

H. Ameziane*, A. Nounah & M. Khamar

Mohammed V University, High School of Technology, Civil Engineering and Environment Laboratory (LGCE), Materials Water and Environment team, MA11060 Sale, Morocco
*Correspondence: amezianehalima@gmail.com

Abstract. Morocco is among the major olive-growing countries around the Mediterranean, its productivity increases from one year to the next, especially after the introduction of the Green Morocco plan, which aims for an increase in the olive-growing area by the year 2020. The increase in productivity especially in olive oil is strictly accompanied by an increase in waste generated after crushing. The objective of this study is to value the olive pomace compost from traditional system as a soil amendment, and study its effect on the cultivation of herbaceous plants. The germination test is carried out in small pots, placed in a sunny place in a laboratory. 25 Fenugreek seeds were germinated in each pot which contains soil and a well-defined percentage of compost (5%, 10%, 15%, 20% and 25%). The seeds were irrigated regularly twice a week. All the tested seeds in different percentages of compost germinated at a rate of more than 90%. The final germination rate for the different concentrations was significantly important from the control (the pot that contains only soil). However, the 5% compost concentration allows an optimal germination rate. As well as the vigour of the seedlings that approves the positive effect of using olive pomace compost with a significantly high vigour index for all compost percentages (5%, 10%, 15%, 20% and 25%). The olive pomace compost use also improved the dry matter weight of the fenugreek seedlings for all percentages.

Key words: fenugreek germination, fertilizing power, olive pomace compost.

INTRODUCTION

In the Mediterranean countries, the environmental impact of olive oil production is significant. Indeed, the extraction of olive oil requires a large amount of water and generates huge amounts of waste during a limited period of 3 to 4 months per year (Ouzounidou et al., 2010; Mechri et al., 2011; Ntougias et al., 2013). According to the Food and Agriculture Organisation of the United Nations, 2.7 million tons of olive oil are annually produced worldwide, 76% of which are produced in Europe. Other olive oil producers are Africa (12.5%), Asia (10.5%) and America (0.9%) (Morillo et al., 2009).

In Morocco, the olive tree is the main planted fruit species. It is present throughout the national territory because of its capacity to adapt to all bioclimatic levels (El Mouhtadi et al., 2014). Indeed, the olive tree constitutes more than half of the arboricultural species, with more than 60 million trees on an area exceeding 560,000 ha (El Mouhtadi et al., 2014). In terms of production, the 2018–2019 campaign was marked

by a new production record of about 2 million tons of olives, an increase of 42% compared to the average olive production of the last five years (Harbouze, 2019).

The waste generated following olive crushing, used to be discharged directly into the surrounding environment, which causes strong phytotoxic and antimicrobial effects. In fact, olive waste increases soil hydrophobicity, decreases water retention and infiltration rate, and affects acidity, salinity, nitrogen immobilization, microbial activity, nutrient leaching, lipid concentration, organic acids and naturally occurring phenols (Sierra et al., 2007; Regni et al., 2016). However nowadays and with the emergence of the principle of sustainable development, which insists on the harmonious balance between the protection of the environment, including water resources, which are particularly fragile in Morocco (World bank group, 2017) on one hand, and industrial production on the other hand, force us to think differently.

The valuation of olive pomace constitutes a potential source of additional income that can contribute to improving the profitability of olive-growing farms. The olive pomace can be used as fuel, livestock feed, fertilizers and as thermal insulation in some construction materials (Ajmia Chouchene, 2010).

The pomace use as an organic amendment has been a widespread practice in olive groves for a long time. Indeed, in addition to being economical and easily achievable, it has positive effects on soil characteristics and crops (Amirante, 2003; Niaounakis & Halvadakis, 2006 and Lozano-Garcia et al., 2011). Similarly, the olive pomace use has improved the soil biological activity (Innangi et al., 2017). The amendment by olive pomace has gone beyond olive groves to be used in herbaceous crops. In fact Brunetti et al. (2005) found an increase in the production of Triticum turgidum L. related to grain weight, number of grains per square meter, and soil organic matter content after amendment by olive pomace. Another study carried out in central Italy by Regni et al., 2017, showed that the application of olive pomace and its compost for 8 consecutive years on the soil of olive groves, significantly increased olive trees vegetative activity and fruit yield, as well as the oil phenols concentration.

However the abusive use of raw pomace as an amendment has shown some problems related to the needed time for germination and root development due to their high organic load, the mineral salts it contains, its low pH and the presence of phytotoxic compounds (Del Buono et al., 2011; Gigliotti et al., 2012; Proietti et al., 2015). Therefore, composting is necessary to stabilize the high organic content and benefit from a soil amendment rich in humic compounds, cation exchange capacity and water retention capacity (Malik et al., 2009).

The objective of this work is to study the effectiveness of a compost composed of olive pomace and cattle manure, used as a soil amendment, when germinating fenugreek seeds. Different concentrations of compost (5%, 10%, 15%, 20% and 25%) are tested during the germination trial in order to determine the optimal dose. A set of parameters were determined during and at the end of the vegetative period, namely seedling vigour, germination rate, dry matter weight and root development.

MATERIALS AND METHODS

Experimental design

The experiment consists of germinating 25 fenugreek seeds in moderate percentages of olive pomace compost (Table 1) and soil, in order to identify the fertilizing power of this compost and to determine the optimal useful dose for plants.

Table 1. Percentages of compost and soil used in the experiment

Compost percentage	0%	5%	10%	15%	20%	25%
Soil percentage	100%	95%	90%	85%	80%	75%

The percentages are on weight.

The table below illustrates the percentages in used compost and soil:

The soil used in this study comes from 'Salé' city (Salé, Morocco, latitude 34°03'11" North, longitude 6°47'54" West, altitude above sea level: 34 m). It was sampled from the topsoil (0–20 cm deep) of a callistemon. It is a sandy type of soil with the following main properties (Table 2):

The compost used in this work is already prepared in a previous study (Ameziane et al., 2020b). It consists of 43% olive pomace and 57% cattle manure, which is mixed in a 30-litre barrel. The barrel is perforated to provide an aerated environment and placed in a sunny location. The composting process took 130 days to obtain mature compost, of which physico-chemical characteristics are presented in Table 3:

Before starting the germination test, the fenugreek seeds are disinfected with bleach, washed thoroughly with water and then rinsed with distilled water. Next, these seeds are put to germinate in small pots (φ (Top): 15 cm, Height: 14 cm, φ (Base): 10 cm). For each percentage of compost corresponds three pots, in each one of them 25

Table 2. Soil physico-chemical parameters (Ameziane et al., 2020a)

Physico-chemical parameters	Soil characteristics
Clay in %	9 ± 0.044
Sand in %	68 ± 0.088
Silt in %	23 ± 0.044
pH	7.61 ± 0.044
Electrical conductivity in μS cm^{-1}	85.5 ± 0.149
Moisture in %	4.51 ± 0.044
Organic matter in %	6.88 ± 0.125
Total organic carbon %	4.88 ± 0.333
Total nitrogen in %	0.134 ± 0.02
Total Phosphorus %	0.0103 ± 0.003
Calcium %	0.48
Potassium %	0.0445
Magnesium %	0.0243
Sodium %	0.0092

The obtained values represent the average of three repetitions.

Table 3. Physico-chemical properties and germination index of mature compost (Aameziane et al., 2020b)

Measured parameters	Mature compost
pH	8.61 ± 0.03
Humidity in %	30.4 ± 0.14
EC in mS cm^{-1}	2.06 ± 0.22
OM %	38.4 ± 0.76
K_2O %	2.8 ± 0.36
NTK %	1.3 ± 1.89
P_2O_5 %	0.42 ± 0.86
COT %	22.32 ± 0.89
C/N %	17.16
The germination index in %	73 ± 0.65

The obtained values represent the average of three repetitions.

Fenugreek seeds have been sown at a depth of approximately 0.5 cm with a space of 1.5 to 2 cm between seeds. The pots are then placed in a laboratory.

Each pot has been regularly irrigated twice a week with Salé High School of Technology well water, and of which physico-chemical characteristics are in accordance with the Moroccan standard for irrigation water (Ministry of Energy, Mines, Water and Environment, 2007) (Table 4). The germination test lasted for 12 days.

Table 4. Irrigation water physico-chemical parameters (Ameziane et al., 2020a)

Physico-chemical parameters	Irrigation water characteristics
pH	7.49 ± 0.047
Electrical conductivity in mS cm^{-1}	1.024 ± 0.016
Temperature in °C	18.13 ± 0.058
Suspended matter e mg L^{-1}	0.232 ± 0.033
Salinity in ppb	0.3 ± 0.1
Nitrates in mg L^{-1}	7.04 ± 0.007
Chlorides in mg L^{-1}	192.5 ± 0.044
Boron in mg L^{-1}	0
Sulphates in mg L^{-1}	21.33 ± 0.005
Ortophosphates in mg L^{-1}	0.0134 ± 0.0001
The SAR	0.53 ± 0.5

The obtained values represent the average of three repetitions.

Plant material

Fenugreek is a Fabaceae family member. This specie has several varieties. It adapts to various types of soils. The best soils are between permeable clay and sandy. It is generally cultivated in bour without additional irrigation in areas with rainfall between 300 and 450 mm (Bernard, 1999).

Measured parameters

Several parameters were regularly monitored during this germination test:

The germination rate is calculated by the formula of Belcher & Miller (1974):

$$G\,\% = 100 \times \frac{\sum n}{N} \quad (1)$$

where n is the number of sprouted seeds and N is the number of tested seeds.

The vigour is determined by the formula of Abdul-Baki & Anderson (1973):

$$VI = \%\,G \times SL \quad (2)$$

where SL is the length of the seedling in cm and % G is the germination rate.

Germination kinetics: this involves daily calculation of the germination rate under the different compost concentrations (Hajlaoui et al., 2007). It is expressed by the number of seeds germinated each day after the beginning of the experiment. This parameter allows a better understanding of the ecological significance of the germination behaviour of the studied seeds as well as the set of events that begin with the water absorption stage by the seed and end with the elongation of the embryonic axis and the emergence of the radicle.

Dry matter: Just after harvest, the seedlings dry matter weight of each pot, (stems + leaves + roots) was measured after drying in an oven at 105 °C to constant weight (Jacquemin, 2012).

Statistical analysis

The obtained results correspond to the average of 3 repetitions (three pots for each treatment). The experimental data were subjected to unidirectional variance analysis (ANOVA) and the average separations were made by the smallest difference (LSD) at

the significance level of $P < 0.05$, using the Statgraphics centurion XVI program for Windows.

RESULTS AND DISCUSSION

Olive pomace compost addition effect on germination kinetics and final germination rate

At the first observation of Fig. 1 it can be seen that seeds germination rate is important for all compost concentrations compared to the control. (Fig. 1). We note a slow-down in the germination process as the compost dose increases. But despite this decrease, the germination rate of the different percentages (5%, 10%, 15%, 20% and 25%) remains high compared to the control.

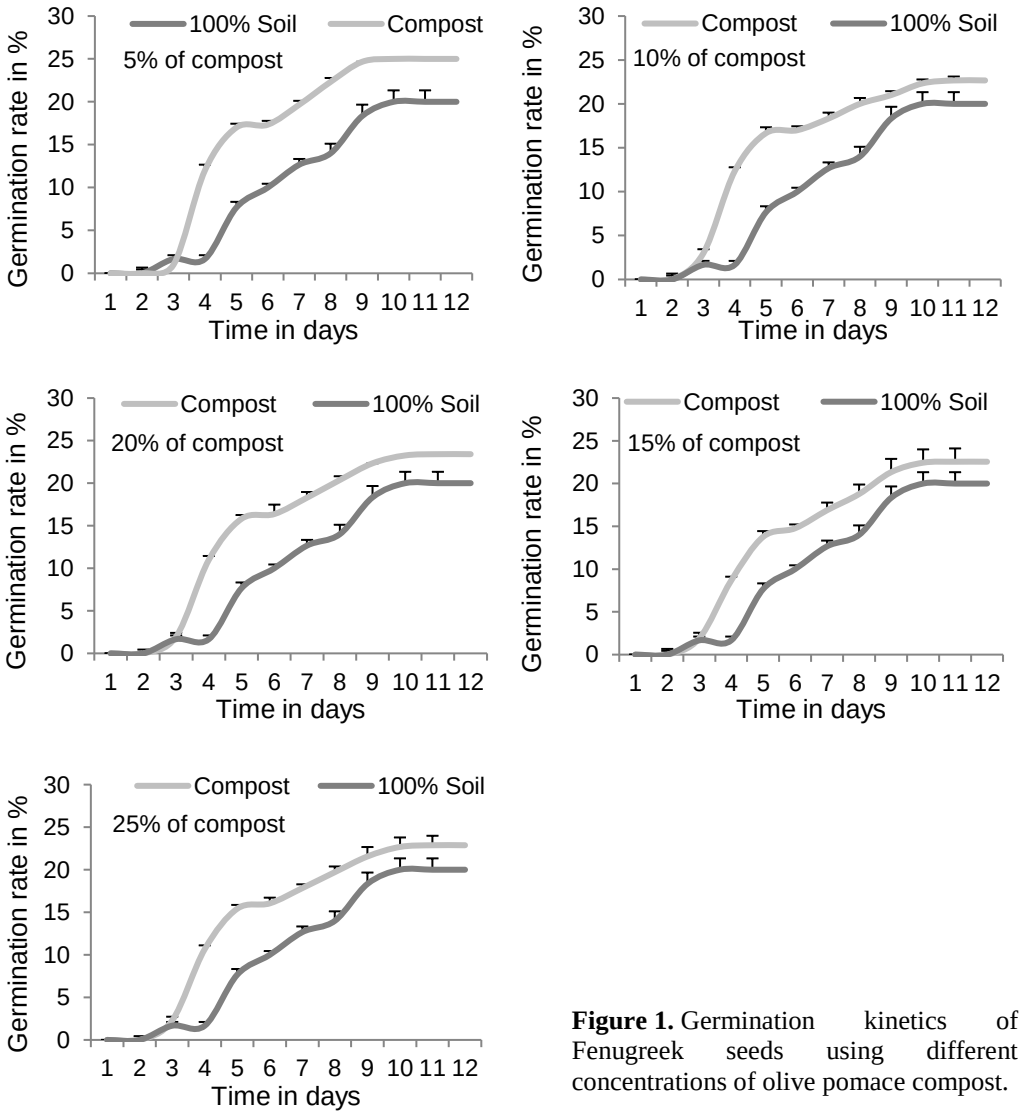

Figure 1. Germination kinetics of Fenugreek seeds using different concentrations of olive pomace compost.

The germination kinetics allows us to distinguish three important phases (Fig. 1):

– A latency phase, essential for the appearance of the first germs, and during which the germination rate remains low. The duration of this phase is short for the different concentrations (2 days), while it is longer for the control (4 days).

– A latency phase, essential for the appearance of the first germs, and during which the germination rate remains low. The duration of this phase is short for the different concentrations (2 days), while it is longer for the control (4 days).

– A more or less linear phase, corresponds to a rapid increase in the germination

– rate, which evolves proportionally to time (from the 2nd to the 10th day), during this phase an accelerated germination of the seedlings is noticeable for all compost concentrations compared to the control.

– A phase that corresponds to the final germination percentage, which is a stage that reflects the germination capacity of the fenugreek seeds for each concentration. This capacity seems important for all compost percentages compared to the control.

In general, all tested seeds germinated at a rate of more than 90% for all compost doses. Indeed, the final germination rate for the different concentrations is significantly different from the control. However, the 5% compost concentration allows an optimal germination rate (100%) (Fig. 2).

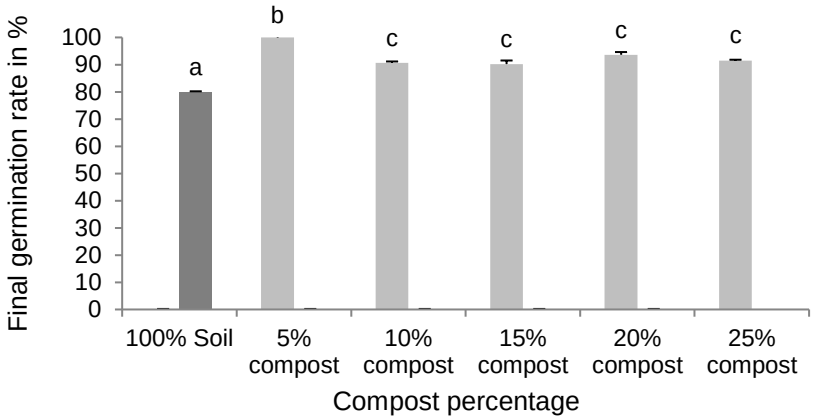

Figure 2. Final Fenugreek seedlings germination rate using different concentrations of olive pomace compost. (Values with different letters are significantly different: $p < 0.05$).

Plant germination is strongly linked to the availability of the nutrients elements, mainly nitrogen, which is responsible for the development of foliage and the plants aerial parts (Jean-François Morot-Gaudry, 1997). This explains the precocious germination of plants fertilized by the compost compared to control plants. In fact, the studied compost has a high nitrogen concentration (1.3%) (Table 3) compared to the control (0.134%) (Table 2).

Olive pomace compost addition effect on dry matter weight

The compost addition at different percentages improves the fenugreek seedlings dry matter weight (stems, leaves and roots), compared to the control (Fig. 3). The improvement is notable ($p < 0.05$) for 5%, 10% and 15% compost concentrations, while it is not significantly different from the control ($p > 0.05$) for 20% compost

concentration. The increase in the seedlings dry matter weight can be explained by the richness of the compost in nitrogen and macro-elements, namely sodium, calcium, magnesium and potassium, which participate in the formation of plant tissues and represent 99% of their mass (Union of Fertilizer Industries, 1998). It is noticeable that the added compost concentration is inversely proportional to the weight in dry matter, which could be attributed according to Del Buono et al. (2011) to a high phenols concentration contained in the compost. A similar result was observed when using olive pomace compost for germinating Festuca and Italian ryegrass (Del Buono et al., 2011).

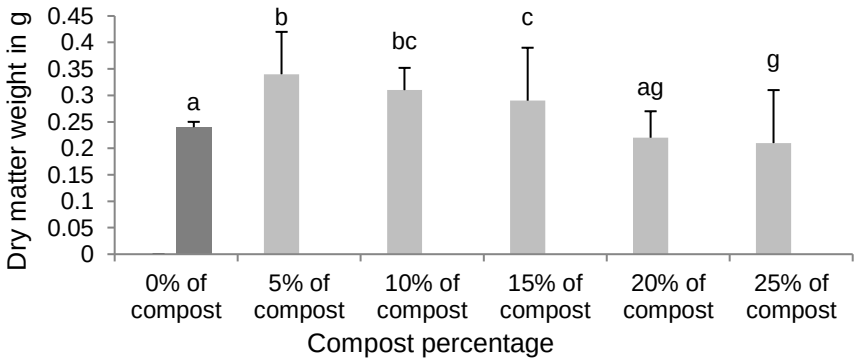

Figure 3. Effects of different percentages of compost on the weight of residual dry matter (Values with different letters are significantly different: $p < 0.05$).

Pomace compost addition effect on seedling vigour

The seedling vigour results (Fig. 4) show a positive effect of the use of olive pomace compost, which is reflected in a high vigour index compared to the control for the different percentages. In fact, the seedlings sown in the 5% compost percentage show an optimal vigour index (214.83) that is significantly different from the other percentages and from the control. Like the 10%, 15%, 20% and 25% percentages, the vigour index is high and significantly different from the control.

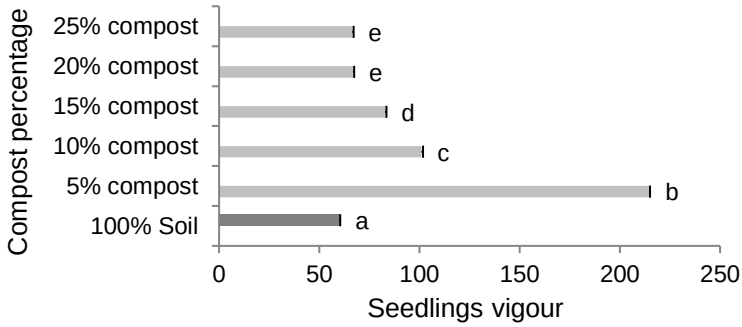

Figure 4. Fenugreek seedlings vigour using different olive-pomace compost concentrations. (Values with different letters are significantly different: $p < 0.05$).

In general, the fenugreek seedlings vigour index is significantly improved with the compost addition for all the used percentages compared to the control. Seedling vigour is linked to the presence of many nutrients, most important are nitrogen, which promotes

growth, phosphorus, which stimulates root development, and potassium, necessary for plant nutrients assimilation (Mickaël Delaire, 2005). All these elements are abundant in the compost (NKT: 1.3%; P_2O_5: 0.42%; K_2O: 2.8%) (Table 3) compared to the control soil (NKT: 0.13%; Total phosphorus: 0.01%; Total potassium: 0.04%) (Table 2). This explains the important vigour of plants fertilized by different compost doses compared to control plants. But as for the weight in dry matter, this vigour decreases when the concentration of compost increases, which approves the existence of a phytotoxic compound that affects the seedlings vigour.

Pomace compost addition effect on root development of seedlings

Concerning the pomace effect on fenugreek seedlings root structure; we note a positive effect on root formation (Fig. 5). This effect is apparent for all compost concentrations. Root length was significantly different from the control for 5%, 10%, 15% and 20% concentrations. Similarly, root thickness is important for all concentrations, except for 25% compost concentration which is similar to the control (Fig. 6). Root development and vigour are strictly related to the phosphorus abundance in the soil (Plassard et al., 2015). Therefore, the important phosphorus concentration in the compost (0.42%) (Table 3) compared to that of the control (0.01%) (Table 2) can explain the significant roots development of plants fertilized by the compost. Same results have been also observed during germination of Festuca and Italian ryegrass (Del Buono et al., 2011).

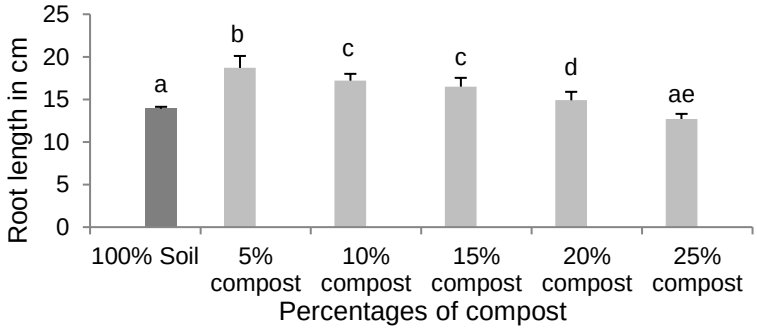

Figure 5. Root length for different concentrations of olive pomace compost. (Values with different letters are significantly different: $p < 0.05$).

Summarizing the obtained results we can say that the olive pomace compost presents an important nutritive contribution to the Fenugreek germination. Indeed, the pomace addition at different doses (5%, 10%, 15%, 20% and 25%) allowed an optimal germination compared to the control. The compost addition also increased the Fenugreek plants dry matter weight compared to the control for 5%, 10% and 15% compost concentrations. Similar results were observed by Del Buono et al. (2011) during the germination of Festuca and Italian ryegrass, as by Alburquerque et al. (2007), who reported a significant increase in Ryegrass plants dry matter weight, after been amended with olive pomace compost for 87 days. The present study also showed that the olive pomace compost addition allowed a significant improvement in the seedlings vigour and the root development of the plants, especially for 5%, 10%, 15% and 20% doses. This improvement could be attributed to the pomace compost richness in fertilizer elements (NTK, P_2O_5 and K_2O) required for the growth and development of most plants (Table 3)

(Regni et al., 2016). Likewise, Del Buono et al. (2011) found significant root development of Festuca and ryegrass following their amendment with olives pomace compost.

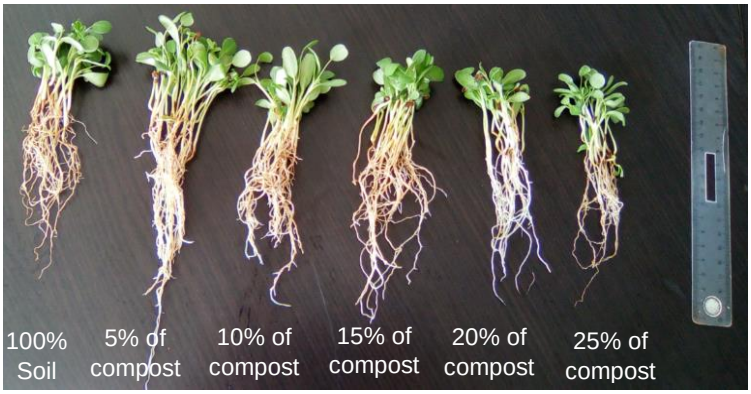

Figure 6. Fenugreek seedlings root development for different compost percentages.

Our results are consistent with studies carried out in other countries and on other plants. Indeed in Italy, the olive pomace compost amendment of olive trees for 8 years significantly increased the vegetative activity and fruit yield of olive trees (Regni et al., 2017). In an Italian study conducted by Proietti et al. (2015), an increase in vegetative activity and productivity of olive trees was observed after being amended with olive pomace compost for three consecutive years (Proietti et al., 2015). This increase in yield is due to the increase in organic matter, total nitrogen, assimilable phosphorus and exchangeable potassium content (Lopez-Pineiro et al., 2008). In fact, several studies show that soil amendment with pomace compost over time allowed an increase in soil organic matter and nutrient content (total nitrogen, phosphorus and exchangeable potassium) without modifying the soil pH and salinity (Ferarra et al., 2012; Chartzoulakis et al., 2010; Uygur & Karabatak, 2009; Montemurro et al., 2004). No negative effects on the quality of olive oil were observed in the studies mentioned above. This supports the view that pomace compost does not affect fruit quality.

CONCLUSIONS

In conclusion, in the present experiment, the used soil low fertility, and the olive-pomace compost important content in fertilizing elements, necessary for plant development (NTK, P_2O_5, K_2O), has allowed a significant Fenugreeks plants growth. The olive-pomace compost addition in different percentages (5%, 10%, 15%, 20% and 25%) to the Fenugreeks plants has improved their growth parameters (germination rate, seedling vigour and root development). Indeed the plants germination rate was important compared to the control for all compost percentages, the plant dry matter weight, the plants vigour and root development were significantly important compared to the control especially for 5%, 10% and 15% compost doses. Our study agrees with the results obtained by other authors and confirms that soil amendment with olive pomace compost can be a sustainable alternative to expensive and polluting chemical fertilizers. In perspective, further field trials on other crops are planned to confirm the obtained results.

REFERENCES

Abdul-Baki, A.A. & Anderson J.D. 1973. Vigor determination in soybean seed by multiple criteria. *Crop Science*, n° **13**, pp. 630–633.

Ajmia chouchene. 2010. *Experimental and theoretical study of processes for the valorisation of olive oil by-products by thermal and physicochemical means.* Doctoral thesis in Energy Engineering-Process Engineering, under the supervision of F. Zagrouba, Monastir, National Engineering School of Monastir, and G. Trouve, University of Haute-Alsace, Mulhouse, 220 pp. (in French).

Alburquerque, J.A., Gonzalvez, J., Garcia, D. & Cegarra, J. 2007. Effects of a compost made from the solid byproduct (alperujo) of the two-phase centrifugation system for olive oil L.). *Bioresour. Technol*. **98**(4), 940–945.

Ameziane, H., Nounah, A., Kabbour, M.R. & Khamar, M. 2020a. Agronomic valuation of olive pomace obtained by different extraction systems. *Eco. Env. & Cons*. **26**(1), 414–422.

Ameziane, H., Nounah, A., Khamar, M. & Zouahri, A. 2020b. Composting olive pomace: evolution of organic matter and compost quality. *Agronomy Research* **18**(1), 5–17.

Amirante, P. 2003. I sottoprodotti della filiera olivicola-olearia. In: Fiorino, P. (Ed.), Olea, Trattato di Olivicoltura. Edagricole, Bologna, pp. 291–303 (in Italian).

Belcher, E.W. & Miller, L. 1974. Influence of substrate moisture level on the germination of sweetgun and pine seed. *Proceeding of the Association of Official Seed Analysis* **65**, pp. 88–89.

Bernard, Le Clech. 1999. *Field crop production*. References 2nd edition. 412 pp. (in French).

Brunetti, G., Plaza, C. & Senesi, N. 2005. Olive pomace amendment in Mediterranean conditions: effect on soil and humic acid properties and wheat (*Triticum turgidum* L.). J. *Agric. Food Chem*. **53**, 6730–6737.

Chartzoulakis, K., Psarras, G., Moutsopoulou, M. & Stefanoudaki, E. 2010. Application of olive mill wastewaterto a Cretan olive orchard: effects on soil properties, plant performance and the environment. *Agric. Ecosyst. Environ*. **138**(3–4), 293–298.

Del Buono, D., Said-Pullicino, D., Proietti, P., Nasini, L. & Gigliotti, G. 2011. Utilization of olive husks as plant growing substrates: phytotoxicity and plant biochemical responses. *Compost Sci. Util*. **19**, 52–60.

El Mouhtadi, I., Agouzzal, M. & Guy, F.2014. The olive tree in Morocco. *OCL*, **21**(2) D203. (in French).

Ferarra, G., Fracchiolla, M., Al Chami, Z., Camposeo, S., Lasorella, C., Pacifico, A., Aly, A. & Montemurro, P. 2012. Effects of mulching materials on soil performance of cv. nero di troia grapevines in the Puglia region, southeastern Italy. *Am. J. Enol. Vitic*. **63**(2), 269–276.

Gigliotti, G., Proietti, P., Said-Pullicino, D., Nasini, L., Pezzolla, D., Rosati, L. & Porceddu, P.R. 2012. Co-composting of olive husks with high moisture contents: organic matter dynamics and compost quality. *Int.Biodeterior. Biodegradation* **67**, 8–14.

Hajlaoui, H., Denden, M. & Bouslama, M. 2007. Study of the intraspecies variability of saline stress tolerance of chickpeas (Cicer arietinum L.) at the germination stage. *Tropicultura*, **25**, 168–173 (in French).

Harbouze, R., Pellissier, J.-P., Rolland, J.-P. & Khechimi, W. 2019. *Synthesis report on agriculture in Morocco*. CIHEAM-IAMM, pp.104 (in French).

Innangi, M., Niro, E., D'Ascoli, R., Danise, T., Proietti, P., Nasini, L., Regni, L., Castaldi, S. & Fioretto, A. 2017. Effects of olive pomace amendment on soil enzyme activities. *Applied Soil Ecology* **119**, 242–249.

Jacquemin, L. 2012. *Production of hemicelluloses from straw and wheat bran on a pilot scale. Study of the technical performance and environmental assessment of an agro-process*. Doctoral thesis. National Polytechnic Institute of Toulouse, 345 pp. (in French).

Jean-François Morot-Gaudry. 1997. *Nitrogen assimilation in plants biochemical and molecular physiological aspects*, Paris, INRA-Quae, Mieux comprendre, 422 pp. (in French).

Lozano-Garcia, B., Parras-Alcantara, L. & del Toro Carrillo de Albornoz, M. 2011. Effects of oil mill wastes on surface soil properties, runoff and soil losses in traditional olive groves in southern Spain. *CATENA* **85**(3), 187–193.

Lopez-Pineiro, A., Albarran, A., Rato Nunes, J.M. & Barreto, C. 2008. Short and medium term effects of twophase olive mill waste application on olive grove production and soil properties under semiarid Mediterranean conditions. *Bioresour. Technol*. **99**, 7982–7987.

Malik, S.Y. Haddadin, Jamal Haddadin, & Omar, I. 2009. Arabiyat, Butros Hattar, Biological conversion of olive pomace into compost by using Trichoderma harzianum and Phanerochaete chrysosporium. *Bioresource Technology* **100**(20), 4773–4782.

Mechri, B., Cheheb, H., Boussadia, O., Attia, F., Ben Mariem, F., Braham, M. & Hammami, M. 2011. Effects of agronomic application of olive mill wastewater in a field of olive trees on carbohydrate profiles, chlorophyll a fluorescence and mineral nutrient content. *Environ. Exp. Bot.* **71**(2), 184–191.

Mickaël Delaire. 2005. *Variations in the mineral absorption capacity of the roots of young Acer pseu-doplatanus, L. (Aceraceae) as a result of the recent and ancient nutritional history of the plant. Application to off-ground cultivation of woody plants.* Plant biology. University of Angers, 180 pp. (in French).

Ministry of Energy, Mines, Water and Environment, in charge of Water and Environment. 2007. Quality Standards: Water intended for irrigation. (in French).

Montemurro, F., Convertini, G. & Ferri, D. 2004. Mill wastewater and olive pomace compost as amendments for rye-grass. *Agronomie* **24**, 481–486.

Morillo, J.A., Antizar-Ladislao, B., Monteoliva-Sánchez, M., Ramos-Cormenzana, A. & Russell, N.J. 2009. Bioremediation and biovalorisation of olive-mill wastes. *Applied Microbiology and Biotechnology* **82**, 25–39.

Niaounakis, M. & Halvadakis, C.P. 2006. *Olive Processing Waste: Management Literature Review and Patent Survey*, second ed. Elsevier Ltd., Kidlington, Oxford, UK. 514 pp.

Ntougias, S., Gaitis, F., Katsaris, P., Skoulika, S., Iliopoulos, N. & Zervakis, G.I. 2013. The effects of olives harvest period and production year on olive mill wastewater properties–evaluation of Pleurotus strains as bioindicators of the effluent's toxicity. *Chemosphere* **92**(4), 399–405.

Ouzounidou, G., Zervakis, G.I. & Gaitis, F. 2010. Raw and microbiologically detoxified olive mill waste and theirimpact on plant growth. *Terr. Aquat. Environ. Toxicol*. **4**, 21–38.

Plassard, C., Robin, A., Le Cadre, E., Marsden, C., Trap, J., Herrmann, L.,Waithaisong, K., Lesueur, D., Blanchard, E. & Chapuis-Lardy, L. 2015. Improving the bioavailability of phosphorus: how to make the most of plant skills and soil biological mechanisms?. *Innov. Agron*. **43**, 115–138 (in French).

Proietti, P., Federici, E., Fidati, L., Scargetta, S., Massaccesi, L., Nasini, L., Regni, L., Ricci, A., Cenci, G. & Gigliotti, G. 2015. Effects of amendment with oil mill waste and its derived-compost on soil chemical and microbiological characteristics and olive (Olea europaea L.) productivity. *Agric. Ecosyst. Environ*. **207**, 51–60.

Regni, L., Gigliotti, G., Nasini, L. & Proietti, P. 2016. Reuse of olive mill waste as soil amendment. In: Olive Mill Waste: Recent Advances for Sustainable Management, C.M. Galanakis Ed.; Elsevier-Academic Press: Oxford, UK, pp. 97–117.

Regni, L., Nasini, L., Ilarioni, L., Brunori, A., Massaccesi, L., Agnelli, A. & Proietti, P. 2017. Long term amendment with fresh and composted solid olive mill waste on olive groveaffects carbon sequestration by prunings, fruits and soil. *Front. Plant Sci*. **7**, 20–42.

Sierra, J., Marti, E., Garau, M.A. & Cruanas, R., 2007. Effects of the agronomic use of olive oil mill wastewater field experiment. *Sci. Total Environ* **378**, 90–94.

Union of Fertilizer Industries. *Fertilization*. 7th edition. 1998. 78 pp. (in French).

Uygur, V. & Karabatak, I. 2009. The effect of organic amendments on mineral phosphate fractions in calcareous soils. *J. Plant Nutr. Soil Sci*. **172**, 336–345.

World bank group. 2017. *Management of Urban Water Scarcity in Morocco*, 38 pp. (in French).

Agronomy Research **18**(3), 1944–1961, 2020
https://doi.org/10.15159/AR.20.232

Theoretical study on forced transverse oscillations of root in soil with provision for soil's elastic and damping properties

V. Bulgakov[1], I. Holovach[1], Z. Ruzhylo[1], V. Melnik[2], Ye. Ihnatiev[3] and J. Olt[4,*]

[1]National University of Life and Environmental Sciences of Ukraine, 15 Heroyiv Oborony Str., UA 03041 Kyiv, Ukraine
[2]Kharkiv Petro Vasylenko National Technical University of Agriculture, 44 Alchevskih Str., UA 61002 Kharkiv, Ukraine
[3]Dmytro Motornyi Tavria State Agrotechnological University, 18[B] Khmelnytsky Ave., UA 72310 Melitopol, Zaporozhye Region, Ukraine
[4]Estonian University of Life Sciences, Institute of Technology, 56 Kreutzwaldi Str., EE 51006Tartu, Estonia
[*]Correspondence: jyri.olt@emu.ee

Abstract. The topic of the paper is the theory of the forced transverse oscillations performed by the root fixed in the soil under the action of the harmonic perturbing force vectored at right angle to the root's centreline and along the line of the translational motion performed by the lifter. On the basis of applying the Ostrogradsky-Hamilton variational principle and using the equivalent schematic model developed by the authors, the expressions have been obtained that allow to determine the amplitude of the forced transverse root body oscillations as function of the perturbing force amplitude value as well as the soil's elastic deformation and damping coefficients. The ranges of the elastic soil deformation coefficient values, at which the resonant behaviour is observed, that is, at which the forced elastic root body oscillation amplitude value exceeds the tolerance limits, have been determined for the 10, 15 and 20 Hz frequencies of the perturbing force produced by the vibrational lifting tool. That said, the mentioned oscillation amplitude values can vary from 0.58 to 0.45 m, which is sufficient to result in the root breaking. Moreover, it has been proved that, with the increase of the perturbing force frequency, the resonant behaviour ranges shift towards the increased values of the elastic soil deformation coefficient. Therefore, such elastic soil deformation coefficient ranges should be avoided in case of the lifting tool design proposed in the paper. As regards the damping properties of the soil, it has been proved that they do not cause any resonance phenomena.

Key words: frequency, harvester, lifting tool, oscillation amplitude, soil, sugar beet root.

INTRODUCTION

Root-crop harvesters produced in the majority of countries worldwide are generally equipped with vibrational lifting tools, because such tools are capable of lifting roots from the soil without losing or damaging them (Gruber, 2005; Sarec et al., 2009; Gu et al., 2014). Also, the amount of energy required for digging roots from the soil with the use of vibrational lifting tools is significantly lower, than in case of using some other types of tools (Vasilenko et al., 1970; Bulgakov, 2005; Schulze Lammers, 2011).

At the initial stage of the development of vibrational lifting tools for beet harvesters, the forces were applied to the root sitting in the soil in the transverse horizontal plane at right angle to the vector of the lifter's translational motion (Dobrovsky, 1968). However, despite the considerable amount of sufficiently thorough theoretical research into the process of the vibrational sugar beet lifting (Vovk, 1936; Myata & Chumak, 1954), in which the perturbing forces were applied to the roots in the transverse horizontal plane, as well as the numerous engineering developments in that field followed by the industrial scale production of several prototypes and the implementation of comprehensive experimental investigations and official tests, such kind of vibrating digging tools did not gain popularity. The main reason for such an outcome was the fact established in practice that these vibrational lifting tools were unable to support sufficiently high rates of advance (which would, accordingly, provide for higher production rates), while maintaining the required harvesting quality parameters. That, in its turn, was due to the following negative events that took place regularly, when the perturbing forces were applied to the beet roots in the plane that was perpendicular to the line of the lifter's translational motion: the lifter's working throat got clogged with root bodies and soil, the tail parts of roots were broken off, the ability to clear itself was completely lost. The power consumption rate of the process was also unreasonably high (Pogorely & Tatyanko, 2004; Schulze Lammers & Schmittmann, 2013).

Following the above-mentioned unsuccessful attempt, it was found that there was a way to completely avoid those negative events. That could be achieved by changing the lines of action of the perturbing forces, that is, taking them away from the transverse horizontal plane and the perpendicular alignment with respect to the lifter's translational motion and placing them into the longitudinal vertical plane. Such a change resulted in very good indicators, when harvesting sugar beet roots at higher rates of advance. Hence, virtually all worldwide known manufacturers of beet root lifting machinery switched to the production of root-crop harvesters with the vibrational lifting tools that work on the principle of applying perturbing forces to the roots in the longitudinal vertical plane (Gruber, 2007).

In case of the root body performing transverse free and forced oscillations, i.e. when the line of action of the perturbing force coincides with the line of translational motion of the vibrational lifting tool, substantial changes are observed in the process of vibrational root lifting. For example, with such alignment of the perturbing forces, the bonds between the roots and the soil are disrupted more effectively (as a result of the so-called loosening effect) and also the accumulation of roots and soil in the working throat of the vibrational lifting tool becomes significantly reduced. Moreover, the designs of the vibrational lifting tools that work on the above principle are less energy intensive, metal intensive etc. (Boson et al., 2019).

The authors have developed a new vibrational lifting tool (Fig. 1), which during its operation imparts to roots sitting in the soil both longitudinal and transverse oscillations. The structural layout of the proposed digging tool is presented in Fig. 2. The vibrational lifting tool comprises the lifting shares 1 mounted at the ends of the posts 2, which are connected through the suspension brackets 3 with the drive mechanism 4 that sets the above-mentioned shares 1 into oscillatory motion. The mechanism 4 includes the system that allows to set (adjust) the frequency and amplitude of the shares' oscillatory motion within wide ranges (the frequency can be adjusted within 8.0 to 30.0 Hz, the amplitude – within 8 to 24 mm).

A distinctive feature of the proposed vibrational lifting tool is that the bracket 3 used for the suspension of the posts 2 is equipped with an additional hinge, which allows the coupled posts 2 to perform free movement within a small range in the longitudinal transverse plane. Such an arrangement provides for the self-adjustment of the shares 1 during their translational motion in the soil.

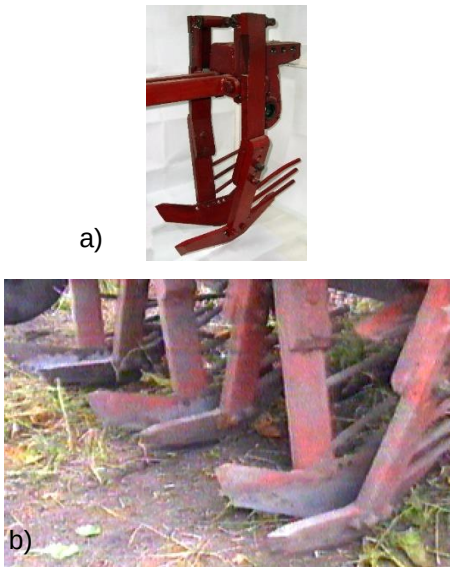

Figure 1. Vibrational lifting tool: a – general appearance; b – tools installed on experimental multiple-row root harvester.

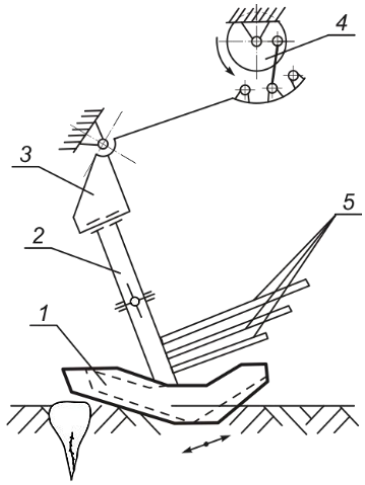

Figure 2. Design and process schematic model of vibrational lifting tool: 1 – lifting shares; 2 – posts; 3 – share spacing adjustment system; 4 – vibration drive with share oscillation amplitude and frequency adjustment system; 5 – guide pins.

However, despite its known considerable advantages, the vibrational method of root lifting features also certain shortcomings. The principal drawbacks are the insufficient reliability (which is true first of all for the vibration drive) that is more pronounced, when operating on heavy and strong soils, the increased metal and energy intensity of the process in general. The inclusion of vibration-type lifting tools, which have a significant weight and oscillate at a frequency of 20 Hz, in the design of the root-crop harvester contributes to the degradation in the reliability of the machine's operation overall.

All the said shortcomings generate the strong need for further development of new principles in the theory of vibrational root lifting, which are to be efficiently utilised for validating the design parameters assumed for further improved lifting tools in root-crop harvesters.

The first fundamental analytical study on the oscillations of the root body fixed in the soil was implemented and presented in the paper Vasilenko et al. (1970). In the study, the sugar beet root was modelled as a conical-shape body with its single lower point fixed, which had elastic properties. With that in view, the paper provided the detailed analysis of the transverse oscillations performed by the root body that were described by a fourth order partial differential equation. The solving of the generated equation provided the authors with the possibility of determining the natural frequencies of the

free transverse oscillations performed by the root body fixed in the soil. However, the paper did not provide analytical research into the process of specifically lifting sugar beet roots from the soil, but only stated that the conditions of their lifting had been obtained with the use of additionally generated kinetostatic equations.

In the paper Pogorely et al. (1983), the main principles and assumptions that had effectively been stated already in the paper Vasilenko et al. (1970) were defined and justified. Again, the paper Pogorely et al. (1983) did not present any mathematical model for the vibrational lifting of sugar beet roots from the soil.

The further development of the theory of vibrational root lifting with the perturbing forces applied to the roots specifically in the longitudinal vertical plane can be found in the papers (Vermeulen & Koolen, 2002; Pogorely & Tatyanko, 2004; Bulgakov et al., 2005; Bulgakov & Ivanovs, 2010). However, the case of a root body performing transverse free and forced oscillations, when the perturbing forces are vectored parallel to the translational motion of the vibrational lifting tool, had still not been researched. In the papers Bulgakov et al. (2014, 2015a, 2015b), the development of fundamentals for the theory of free transverse root body oscillations in the case, where the perturbing forces were vectored at right angle to the root's centreline, but parallel to the translational motion of the vibrational lifting tool, was presented.

The aim of this study is to substantiate the parameters of the oscillation process that takes place, when lifting beet roots from the soil, on the basis of developing the theory of the transverse oscillations performed by the root as an elastic body sitting in the soil as an elastic and damping medium for the case, where the perturbing forces have the same direction as the translational motion of the vibrational lifting tool.

MATERIALS AND METHODS

In the completed theoretical research, the fundamental principles of the theory of agricultural machines and the methods of the theoretical mechanics, in particular, the methods of the theory of oscillations, the variational calculus, generation and solution of differential equation systems have been used. In the PC-assisted numerical calculations, the methods of programming and presenting the obtained graphic relations between the main parameters have been applied.

Theory and modelling

In order to investigate the forced transverse oscillations performed by the root sitting in the soil during its vibrational lifting, it is necessary, first of all, to generate the equivalent schematic model of the root as an elastic cone-shaped body sitting in the soil as a medium with elastic and damping properties as well as the external forces applied to the root. Such a schematic model is presented in Fig. 3.

The root as a body has a conical shape (apex angle of the cone is equal to 2γ, its upper part is above the soil surface level) and is modelled as a variable cross-section bar with a fixed lower end (point *O*). The weight force $\overline{G}$ of the root is applied at the centre of mass represented by the point *C*. The overall length of the root is designated as *h*.

The vibrational lifting tool moving at a pre-set depth in the soil (along the vector $\overline{V}$) is conventionally presented as two planes at an angle with each other, which hold the root on its two sides and make contact with it at the points K_1 and K_2. Accordingly, at the above-mentioned points, the vibrational lifting tool imparts to the root the perturbing

forces $\bar{Q}_{df.1}$ and $\bar{Q}_{df.2}$, the vectors of which are directed forward and in parallel with each other and which are just the forces that generate the transverse oscillations of the root. These forces are applied at a distance of z_1 from the horizontal line passing through the point *O*.

The soil around the cone-shaped root body is represented by the two elastic and damping models with equal elasticity coefficients of c and damping coefficients of *b*.

The equivalent schematic model is referenced with the Cartesian coordinate system *xOz*, the origin of which is at the point *O* and the vertical axis *Oz* coincides with the axis of symmetry of the cone-shaped root body. The directions of oscillations of both the vibrational lifting tool planes are shown by arrows in the schematic model.

The next step is to analyse the oscillatory process of the transverse oscillations performed by the root body sitting in the soil and generated during the interaction between the root and the vibrating tool.

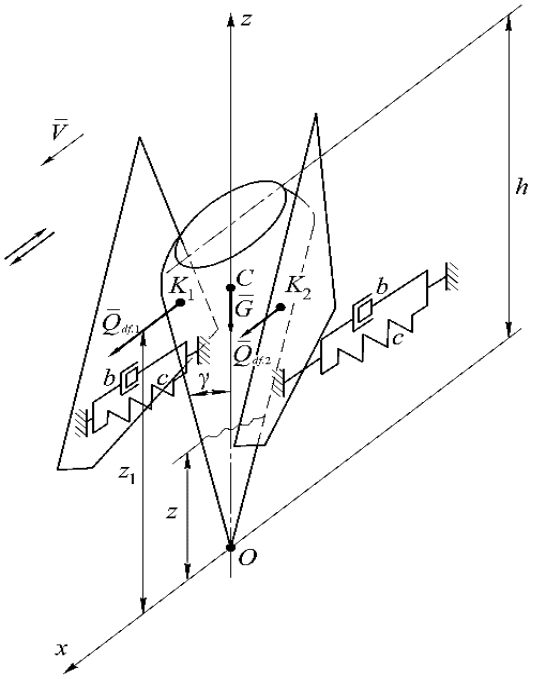

Figure 3. Equivalent schematic model of transverse oscillations performed by root sitting in soil during its vibrational lifting.

The Ostrogradsky-Hamilton principle can be used in the analysis of the forced transverse root oscillations that take place under the action of the horizontal perturbing force that varies in accordance with the following harmonic function (Dreizler & Lüdde, 2010):

$$Q_{df.} = H \cdot \sin(\omega t), \tag{1}$$

where *H* – amplitude of the perturbing force [N]; ω – frequency of the perturbing force [s^{-1}]; *t* – time interval [s].

However, as is obvious from the equivalent schematic model (Fig. 3), the above-mentioned perturbing force $\bar{Q}_{df}$ is applied to the root simultaneously on two sides of it by the two digging shares. Therefore, it is represented in the schematic model by the two components $\bar{Q}_{df.1}$ and $\bar{Q}_{df.2}$ and they are exactly what causes the transverse oscillations of the root that disrupt the bonds between the root and the soil and create the conditions needed for lifting the root from the soil.

On the basis of the conditions shown in the prepared equivalent schematic model, the Ostrogradsky-Hamilton functional can be generated, which will provide for

analytically describing this kind of root oscillations. Under the above assumptions, the displacements of the root centreline points during the transverse root oscillations are univalently determined by the following function of two variables:

$$y = y(z,t)\,, \tag{2}$$

where z – distance from the point on the axis Oz, through which the root cross-section passes, to the conventional point O of fixing the root in the soil [m]; t – current time [s].

Further, the following designations are introduced.

Thus, $\mu(z)$ – running mass (mass per unit of length) of the root [kg m^{-1}]; E – Young's modulus of the root material [N m^{-2}]; $J(z)$ – moment of inertia of the root cross-section with respect to the cross-section's neutral axis that is perpendicular to the oscillation plane [m^4]; $Q(z,t)$ – intensity of the external transverse load vectored at right angle to the root's centreline (axis Oz) along the axis Ox [N m^{-1}].

In accordance with Babakov (1968), the Ostrogradsky-Hamilton functional for a variable cross-section bar, which performs transverse oscillations under the action of an external transverse load, appears as follows:

$$S = \frac{1}{2}\int_{t_1}^{t_2}\int_{0}^{h}\left[\mu(z)\cdot\left(\frac{\partial y}{\partial t}\right)^2 - E\cdot J(z)\cdot\left(\frac{\partial^2 y}{\partial z^2}\right)^2 + Q(z,t)\cdot y\right]dz\,dt\,. \tag{3}$$

In view of the fact that the root is modelled as a cone-shaped body, the values present in the functional (3) can be expressed in terms of the main parameters of its conical surface.

It is obvious that the running mass of the root can be determined with the use of the following expression:

$$\mu(z) = \rho\cdot\pi\cdot z^2\cdot\tan^2\gamma\,, \tag{4}$$

where ρ – specific gravity of the root material [kg m^{-3}]; 2γ – taper angle of the cone used as the root body model [deg] (Fig. 3).

The root's moment of inertia $J(z)$ is determined as follows:

$$J(z) = \frac{\pi\cdot z^4\cdot\tan^4\gamma}{4}\,. \tag{5}$$

Since the value Q(z,t) that is a component of the functional (3) is the intensity of a distributed load measured in the N m^{-1} units, the perturbing force $\bar{Q}_{df.}$ that is a concentrated load measured in newtons must also have N m^{-1} as the unit of its measurement. For that purpose, the first-order impulse function $\sigma_1(z)$ is introduced (Babakov, 1968).

Hence, if $Q_{df.}(t)$ is a concentrated perturbing force applied at the point z_1 and measured in newtons [N], the function

$$Q_{df.}(z,t) = Q_{df.}(t)\cdot\sigma_1(z - z_1) \tag{6}$$

has N m^{-1} as the unit of its measurement and represents the intensity of the concentrated load at the point z_1. The function $\sigma_1(z - z_1)$ is equal to zero for all values of z, except $z = z_1$, where it goes to infinity.

Subsequently, taking into account the expression (1), the following can be written down:

$$Q_{df.}(z,t) = H\cdot\sin(\omega t)\cdot\sigma_1(z - z_1)\,. \tag{7}$$

At the start of the oscillatory process, the root is firmly bonded with the soil, the latter being an elastic and damping medium. Therefore, when the perturbing force, the value of which is determined by (1), acts on the root, the force of soil resistance to the transverse root oscillations emerges. Obviously, the soil resistance force (acting on the whole root body) is a load distributed over the area of contact between the root and the soil. Moreover, it is an external force with regard to the root body and it acts as a perturbing force generated by the soil acting on the root.

Further, the parameter c is introduced, which is the elastic deformation coefficient of the soil related to the area of contact between the root and the soil, measured in N m^{-3}. It is assumed that the root during its transverse oscillations is supported by the soil on half of its side surface along the whole depth of its sitting in the unbroken soil. The soil contacting with the said half of the side surface generates a distributed load vectored opposite to the perturbing force. Thus, when the root as well as the tool itself perform transverse oscillations, a distributed load, which is applied to the root by the surrounding soil and is opposite in direction to the perturbing force, arises in turn on one side of the root, then on the other side of it, and so on.

Hence, taking into account the above-said and subject to the condition that the root is conically shaped, it is possible to state to some approximation that the intensity $P(z, t)$ [N m^{-1}] of the distributed load generated by the elastic resistance of the soil is equal to:

$$P(z,t) = \pi \cdot c \cdot z \cdot \tan\gamma \cdot y(z,t) \tag{8}$$

In view of the fact that the perturbing forces generated by the vibrational lifting tool and the soil resistance have opposite directions, the resulting intensity of the external transverse load acting on the root has the following value:

$$Q(z,t) = Q_{df.}(z,t) - P(z,t), \quad [\text{N m}^{-1}], \tag{9}$$

or, taking into account the expressions (7) and (8), the following expression for the soil damping force is arrived at:

$$Q(z,t) = H \cdot \sin(\omega t) \cdot \sigma_1(z - z_1) - \pi \cdot c \cdot z \cdot \tan\gamma \cdot y(z,t), \tag{10}$$

Also, the damping properties of the soil have to be taken into account. They are, first of all: b – damping coefficient of the soil measured in (N s^2) m^{-3}.

The following considerations have to be taken into account with regard to the root sitting in the soil at the moment of its lifting. In view of the fact that the root grows and develops its shape in the soil during a considerable length of time, there are good reasons to believe that the area of contact between the whole conical root body and the soil is like a continuous body (it can be said that the root has rather strongly grown into the soil). Therefore, it is also reasonable to assume that great root body deformation rates result in also great deformation rates of the soil around the root. That is due to the certainly great value of the bonding force between the root and the soil enveloping it on all sides, especially in the case, when the root sits in (has grown in) dry and hard soil. Hence, the deformation rate of the soil surrounding the root is virtually equal to the deformation rate of the root body. It is common knowledge that, in case of high rates, the resistance forces follow not linear, but quadratic laws (Schmitz & Smith, 2012). Therefore, it can be assumed to some approximation that the soil damping force is in the quadratic relation with the root body deformation rate.

Therefore, taking into account the conical shape of the root, the soil damping force can be determined with the use of the following expression:

$$R(z,t)=\pi\cdot b\cdot z\cdot\tan\gamma\cdot\left[\frac{\partial y(z,t)}{\partial t}\right]^2,\ \text{[N]}. \tag{11}$$

Thus, taking into account the expressions (4), (5), (10) and (11), the functional (3) assumes the following form:

$$S=\frac{1}{2}\int_{t_1}^{t_2}\int_{o}^{h}\left[\rho\cdot\pi\cdot z^2\cdot\tan^2\gamma\left(\frac{\partial y}{\partial t}\right)^2-E\cdot\frac{\pi\cdot z^4\cdot\tan^4\gamma}{4}\left(\frac{\partial^2 y}{\partial z^2}\right)^2+\right.$$
$$\left.+H\cdot\sin(\omega t)\cdot\sigma_1(z-z_1)\cdot y(z,t)-\pi\cdot c\cdot z\cdot\tan\gamma\cdot y^2(z,t)-\pi\cdot b\cdot z\cdot\tan\gamma\cdot\left(\frac{\partial y}{\partial t}\right)^2\right]dz\,dt. \tag{12}$$

In order to analyse the forced transverse oscillations of the root body fixed in the soil, the Rietz method can be applied (Babakov, 1968).

In view of the fact that the perturbing force acts on the root at a frequency of ω, its solely forced oscillations occur in accordance with the following function (Babakov, 1968):

$$y(z,t)=\varphi(z)\sin(\omega t), \tag{13}$$

where $\varphi(z)$ – waveform of the forced oscillations.

The necessary partial derivatives have to be derived from the expression (13). They appear as follows:

$$\frac{\partial y}{\partial t}=\omega\cdot\varphi(z)\cdot\cos(\omega t),$$
$$\frac{\partial^2 y}{\partial z^2}=\varphi''(z)\cdot\sin(\omega t). \tag{14}$$

By substituting the expressions (13) and (14) into the functional (12), the latter's following representation is arrived at:

$$S=\frac{1}{2}\int_{t_1}^{t_2}\int_{o}^{h}\left\{\rho\cdot\pi\cdot z^2\cdot\tan^2\gamma\cdot\omega^2\cdot\varphi^2(z)\cdot\cos^2(\omega t)-\frac{E\cdot\pi\cdot z^4\cdot\tan^4\gamma}{4}\left[\varphi''(z)\right]^2\cdot\sin^2(\omega t)+\right.$$
$$+H\cdot\sigma_1(z-z_1)\cdot\varphi(z)\cdot\sin^2(\omega t)-\pi\cdot c\cdot z\cdot\tan\gamma\cdot\varphi^2(x)\cdot\sin^2(\omega t)- \tag{15}$$
$$\left.-\pi\cdot b\cdot z\cdot\tan\gamma\cdot\omega^2\cdot\varphi^2(z)\cdot\cos^2(\omega t)\right\}dz\,dt.$$

After integrating the expression (15) over z within the limits of one period, that is, within $T=\frac{2\pi}{\omega}$, the result is:

$$S=\frac{\pi}{2\omega}\int_{o}^{h}\left\{\rho\cdot\pi\cdot z^2\cdot\tan^2\gamma\cdot\varphi^2(z)\cdot\omega^2-\frac{E\cdot\pi\cdot z^4\cdot\tan^4\gamma}{4}\cdot\left[\varphi''(z)\right]^2+\right.$$
$$\left.+H\cdot\sigma_1(z-z_1)\cdot\varphi(z)-\pi\cdot c\cdot z\cdot\tan\gamma\cdot\varphi^2(z)-\pi\cdot b\cdot z\cdot\tan\gamma\cdot\omega^2\cdot\varphi^2(z)\right\}dz. \tag{16}$$

In accordance with the Rietz method, the values of the functional (16) have to be analysed on the class of linear combinations defined as follows:

$$\varphi(z)=\alpha\cdot\psi(z), \tag{17}$$

where α – parameter, the variation of which produces a class of admissible functions; $\Psi(z)$ – basis function.

After the expression (17) is substituted into the functional (16), the following is arrived at:

$$S=\frac{\pi}{2\omega}\int_o^h\left\{\rho\cdot\pi\cdot z^2\cdot\tan^2\gamma\cdot\alpha^2\cdot\psi^2(z)\cdot\omega^2-\frac{E\cdot\pi\cdot z^4\cdot\tan^4\gamma}{4}\alpha^2\left[\psi''(z)\right]^2+\right.$$
$$\left.+H\cdot\sigma_1(z-z_1)\cdot\alpha\cdot\psi(z)-\pi\cdot c\cdot z\cdot\tan\gamma\cdot\alpha^2\cdot\psi^2(z)-\pi\cdot b\cdot z\cdot\tan\gamma\cdot\alpha^2\cdot\psi^2(z)\cdot\omega^2\right\}dz. \tag{18}$$

Next, the following designations have to be introduced:

$$\int_o^h\rho\cdot\pi\cdot z^2\cdot\tan^2\gamma\cdot\psi^2(z)dz=M, \tag{19}$$

$$\int_0^h\frac{E\cdot\pi\cdot z^4\cdot\tan^4\gamma}{4}\left[\psi''(z)\right]^2dz=N, \tag{20}$$

$$\int_o^h\pi\cdot c\cdot z\cdot\tan\gamma\cdot\psi^2(z)dz=R, \tag{21}$$

$$\int_o^h\pi\cdot b\cdot z\cdot\tan\gamma\cdot\psi^2(z)dz=F, \tag{22}$$

$$\int_o^h H\cdot\sigma_1(z-z_1)\cdot\psi(z)dz=L. \tag{23}$$

After substituting the expressions (19) – (23) into (18), the result is:

$$S=\frac{\pi}{2\omega}\left[\omega^2\cdot(M-F)\cdot\alpha^2-(N+R)\cdot\alpha^2+L\cdot\alpha\right]. \tag{24}$$

Thus, on the class of functions (17), the functional (18) becomes a function of the free variable α. The necessary extremum condition of the function (24) is that its first-order derivative with respect to α is equal to zero. Accordingly, after differentiating the expression (24) with respect to α and equating the obtained derivative to zero, the following equation is arrived at:

$$2\omega^2\cdot(M-F)\cdot\alpha-2(N+R)\cdot\alpha-L=0, \tag{25}$$

from which the parameter α can be determined, that is:

$$\alpha=\frac{L}{2\left[N+R-\omega^2\cdot(M-F)\right]}. \tag{26}$$

Further, the waveform of the forced transverse oscillations performed by a homogeneous bar with a constant elastic stiffness of *EJ*, one end of which is rigidly fixed, under the action of a transverse harmonic unit force with a frequency of ω applied at the point $z=z_1$ is assumed to be the basis function $\Psi(z)$. In accordance with (Babakov, 1968), this waveform appears as follows:

$$\psi(z)=C\cdot U(kz)+D\cdot V(kz),\quad 0\le z<z_1, \tag{27}$$

$$\psi(z) = C \cdot U(kz) + D \cdot V(kz) + \frac{1}{k^3 \cdot EJ} \cdot V\left[k(z - z_1)\right], \quad z_1 \le z \le h, \tag{28}$$

where $U(kz)$, $V(kz)$ – Krylov functions (Babakov, 1968), $k = \sqrt[4]{\frac{\mu \cdot \omega^2}{EJ}}$ – coefficient representing the mass, kinematic and strength properties of the bar's material, μ – running mass of the bar; C, D – arbitrary constants. At the same time, the boundary conditions for the oscillations performed by the above-mentioned bar are as follows:

$$\begin{aligned} y(0) &= y'(0) = 0, \\ y''(h) &= y'''(h) = 0. \end{aligned} \tag{29}$$

Taking into account the said boundary conditions (29) for the free end of the bar ($z = h$), the following system of equations with respect to the unknown quantities $\Psi(z)$, C, D is obtained:

$$\left.\begin{aligned} -\psi(z) + C \cdot U(kz) + D \cdot V(kz) &= \begin{cases} 0, & 0 \le z < z_1, \\ -\frac{1}{k^3 \cdot EJ} \cdot V\left[k(z - z_1)\right], & z_1 \le z \le h, \end{cases} \\ C \cdot S(kh) + D \cdot T(kh) &= -\frac{1}{k^3 \cdot EJ} T\left[k(h - z_1)\right], \\ C \cdot V(kh) + D \cdot S(kh) &= -\frac{1}{k^3 \cdot EJ} S\left[k(h - z_1)\right]. \end{aligned}\right\} \tag{30}$$

For the problem under consideration, it is necessary to determine only such a basis function $\Psi(z)$ that meets the above-mentioned boundary conditions. Using the Cramer's rule, the target value of $\Psi(z)$ is obtained from the system of Eqs (30). It is equal to:

$$\begin{aligned} \psi(z) = {} & \frac{U(kz)}{\Delta \cdot k^3 \cdot EJ} \left\{ T\left[k(h - z_1)\right] S(kh) - T(kh) S\left[k(h - z_1)\right] \right\} - \\ & - \frac{V(kz)}{\Delta \cdot k^3 \cdot EJ} \left\{ T\left[k(h - z_1)\right] \cdot V(kh) - S\left[k(h - z_1)\right] S(kh) \right\}, \quad 0 \le z < z_1, \end{aligned} \tag{31}$$

or

$$\begin{aligned} \psi(z) = {} & -\frac{V\left[k(z - z_1)\right]}{\Delta \cdot k^3 \cdot EJ} \left\{ S^2(kh) - T(kh) \cdot V \cdot (kh) \right\} + \\ & + \frac{U(kz)}{\Delta \cdot k^3 \cdot EJ} \left\{ T\left[k(h - z_1)\right] \cdot S(kh) - T(kh) \cdot S\left[k(h - z_1)\right] \right\} - \\ & - \frac{V(kz)}{\Delta \cdot k^3 \cdot EJ} \left\{ T\left[k(h - z_1)\right] \cdot V(kh) - S\left[k(h - z_1)\right] \cdot S(kh) \right\}, \quad z_1 \le z \le h, \end{aligned} \tag{32}$$

where Δ – principal determinant of the system of Eqs (30) equal to:

$$\Delta = T(kh) \cdot V(kh) - S^2(kh). \tag{33}$$

Further, the following designations have to be introduced:

$$\frac{T\left[k\left(h-z_1\right)\right]\cdot S\left(kh\right)-T\left(kh\right)\cdot S\left[k\left(h-z_1\right)\right]}{\Delta\cdot k^3\cdot EJ}=B\,, \tag{34}$$

also:

$$\frac{T\left[k\left(h-z_1\right)\right]\cdot V\left(kh\right)-S\left[k\left(h-z_1\right)\right]\cdot S\left(kh\right)}{\Delta\cdot k^3\cdot EJ}=G\,, \tag{35}$$

finally:

$$\frac{S^2\left(kh\right)-T\left(kh\right)\cdot V\left(kh\right)}{\Delta\cdot k^3\cdot EJ}=K\,. \tag{36}$$

By substituting the expressions (34), (35), (36) into the expressions (31), (32), the following is obtained:

$$\psi\left(z\right)=B\cdot U\left(kz\right)-G\cdot V\left(kz\right),\qquad 0\le z<z_1\,, \tag{37}$$

$$\psi\left(z\right)=-K\cdot V\left[k\left(z-z_1\right)\right]+B\cdot U\left(kz\right)-G\cdot V\left(kz\right),\qquad z_1\le z\le h\,. \tag{38}$$

The next step is to determine the coefficients *M, N, R, F, L* that are present in the expressions (26).

For that purpose, the expressions (37), (38) are substituted into the expressions (19) and the value of the coefficient M is found. It is equal to:

$$\begin{aligned} M=&\rho\cdot\pi\cdot\tan^2\gamma\cdot\int_0^{z_1}z^2\cdot\left[B\cdot U\left(kz\right)-G\cdot V\left(kz\right)\right]^2dz+\\ &+\rho\cdot\pi\cdot\tan^2\gamma\cdot\int_{z_1}^{h}z^2\cdot\left\{-K\cdot V\left[k\left(z-z_1\right)\right]+B\cdot U\left(kz\right)-G\cdot V\left(kz\right)\right\}^2dz\,. \end{aligned} \tag{39}$$

In order to determine the coefficient *N*, the second derivatives of the expressions (37), (38) are obtained as follows:

$$\psi''\left(z\right)=B\cdot k^2\cdot S\left(kz\right)-G\cdot k^2\cdot T\left(kz\right),\qquad 0\le z<z_1, \tag{40}$$

$$\psi''\left(z\right)=-K\cdot k^2\cdot T\left[k\left(z-z_1\right)\right]+B\cdot k^2\cdot S\left(kz\right)-G\cdot k^2\cdot T\left(kz\right),\qquad z_1\le z\le h\,. \tag{41}$$

After the expressions (37), (38) are substituted into the expression (20), the value of the coefficient N is found as follows:

$$\begin{aligned} N=&\frac{E\cdot\pi\cdot\tan^4\gamma}{4}\cdot\int_0^{z_1}k^4\cdot z^4\cdot\left[B\cdot S\left(kz\right)-G\cdot T\left(kz\right)\right]^2dz+\\ &+\frac{E\cdot\pi\cdot\tan^4\gamma}{4}\cdot\int_{z_1}^{h}k^4\cdot z^4\cdot\left\{-K\cdot T\left[k\left(z-z_1\right)\right]+B\cdot S\left(kz\right)-G\cdot T\left(kz\right)\right\}^2dz\,. \end{aligned} \tag{42}$$

By substituting the expressions (40), (41) into the expression (21), the value of the coefficient *R* is obtained as follows:

$$\begin{aligned} R=&c\cdot\pi\cdot\tan\gamma\cdot\int_0^{z_1}z\cdot\left[B\cdot U\left(kz\right)-G\cdot V\left(kz\right)\right]^2dz+\\ &+c\cdot\pi\cdot\tan\gamma\cdot\int_{z_1}^{h}z\cdot\left\{-K\cdot V\left[k\left(z-z_1\right)\right]+B\cdot U\left(kz\right)-G\cdot V\left(kz\right)\right\}^2dz\,. \end{aligned} \tag{43}$$

By substituting the same expressions into the expression (22), the value of the coefficient F is found as follows:

$$F = b \cdot \pi \cdot \tan\gamma \cdot \int_0^{z_1} z \cdot \left[B \cdot U(kz) - G \cdot V(kz) \right]^2 dz + \\ + b \cdot \pi \cdot \tan\gamma \cdot \int_{z_1}^{h} z \cdot \left\{ -K \cdot V\left[k(z - z_1) \right] + B \cdot U(kz) - G \cdot V(kz) \right\}^2 dz. \tag{44}$$

The coefficient L is obtained by substituting the expressions (37), (38) into the expression (23). Its value is equal to:

$$L = \int_0^{z_1} H \cdot \sigma_1(z - z_1) \cdot \left[B \cdot U(kz) - G \cdot V(kz) \right] dz + \\ + \int_{z_1}^{h} H \cdot \sigma_1(z - z_1) \cdot \left\{ -K \cdot V\left[k(z - z_1) \right] + B \cdot U(kz) - G \cdot V(kz) \right\} dz. \tag{45}$$

The numerical values of the coefficients M, N, R and F can be calculated with the use of the PC either by directly taking integrals of the Krylov functions or after the transition to elementary functions in accordance with (Babakov, 1968).

In view of the fact that the expression (45) intended for finding the coefficient L contains the impulse function $\sigma_1(z - z_1)$ that does not fall into the category of classical functions, the integrals present in the said expression have to be calculated analytically with the use of the generalised function integration technique.

As a result of integrating the expression (45), the following is obtained:

$$L = H \left[B \cdot U(kz_1) - G \cdot V(kz_1) \right]. \tag{46}$$

Then, after substituting the expressions (39), (42), (43), (44) and (46) into the expression (26), the required value of the parameter α, at which the functional (16) has a stationary value, is obtained. Respectively, taking into account the expressions (17), (37) and (38), the expressions that represent the waveform of the forced transverse oscillations of the root body fixed in the soil are obtained.

These expressions appear as follows:

$$\varphi(z) = \alpha \cdot \left[B \cdot U(kz) - G \cdot V(kz) \right], \quad 0 \le z < z_1, \tag{47}$$

$$\varphi(z) = \alpha \cdot \left\{ -K \cdot V\left[k(z - z_1) \right] + B \cdot U(kz) - G \cdot V(kz) \right\}, \quad z_1 \le z \le h \tag{48}$$

where α is determined by the expression (26).

The substitution of the expressions (47) and (48) into the expression (13) results in obtaining the final representation of the function governing the forced transverse oscillations of the root body fixed in the soil:

$$y(z,t) = \alpha \cdot \left[B \cdot U(kz) - G \cdot V(kz) \right] \cdot \sin(\omega t), \quad 0 \le z < z_1, \tag{49}$$

$$y(z,t) = \alpha \cdot \left\{ -K \cdot V\left[k(z - z_1) \right] + B \cdot U(kz) - G \cdot V(kz) \right\} \cdot \sin(\omega t), \quad z_1 \le z \le h. \tag{50}$$

RESULTS

Following the results of the theoretical research into the forced transverse root body oscillations described above, the authors developed the algorithm for calculating the said oscillations.

The following initial data has been used in the calculations. In accordance with (Vasilenko et al., 1970), the ranges of the soil's elastic stiffness and damping coefficients were assumed to be as follows: b = 0–10 N s^2 m^{-3}, c = 0–20 105 N m^{-3}.

In accordance with (Pogorely et al., 1983), the average statistic values of the root's physical and mechanical properties were assumed to be as follows: h = 0.25 m; $\gamma = 14^\circ$; E = 18.4 10^6 N m^{-2}; ρ = 750 kg m^{-3}.

Calculations were carried out with the use of the compiled programme. Their results were used to plot the diagrams that represented the relations between the amplitude of the forced transverse oscillations performed by the root body as an elastic body, which sits (in practice, is fixed) in the soil as an elastic and damping medium, and the amplitude H of the perturbing force as well as the mechanical properties of the soil surrounding it. The obtained diagrams are presented in Figs 4–7.

Fig. 4 features the diagrams of the relations between the amplitude of the forced transverse elastic root body oscillations and the coefficient c of the elastic soil deformation at various perturbing force frequencies: 10 Hz, 15 Hz, 20 Hz. The calculations have been carried out for a perturbing force amplitude of H = 500 N and a soil damping coefficient of b = 6.5 N s^2 m^{-3}.

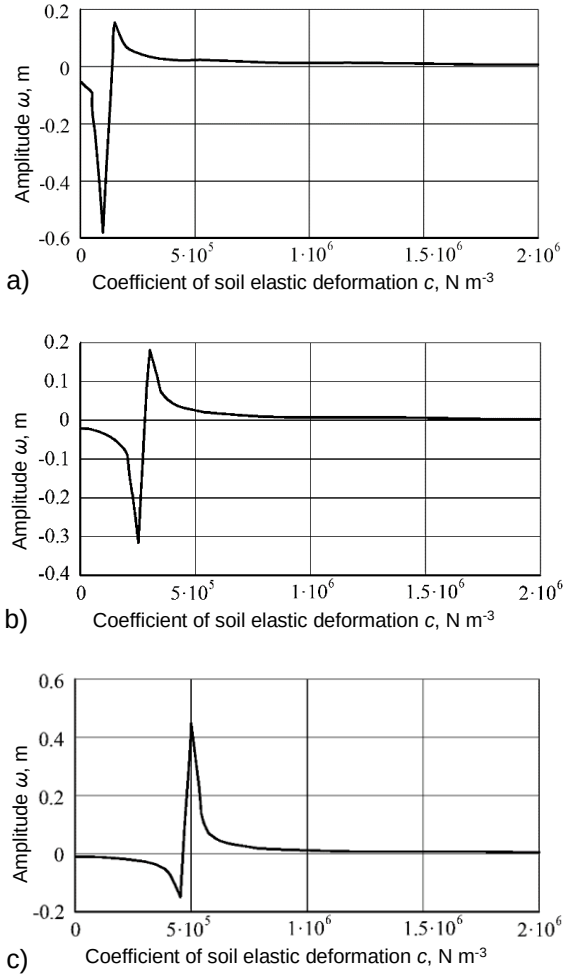

Figure 4. Relation between amplitude of forced transverse root body oscillations on one hand and coefficient of elastic soil deformation c and perturbing force frequency v on the other hand for root's cross-section at point of its gripping ($z = z_1 = 0.15$ m): a) ν = 10 Hz; b) ν = 15 Hz; c) ν = 20 Hz (perturbing force amplitude H = 500 N, b = 6.5 N s^2 m^{-3}, c = 0–20 N m^{-3}).

As is seen in the presented diagrams, the resonance state takes place at the following values of the parameters: ν = 10 Hz, c = 1.0–1.3·10^5 N m^{-3}; ν = 15 Hz, c = 2.5–2.7·10^5 N m^{-3}; ν = 20 Hz, c = 4.5–5.0·10^5 N m^{-3}.

Moreover, at ν = 10 Hz the amplitude of the root body oscillations in the resonance state varies within the range of – 0.58 to 0.17 m, at ν = 15 Hz within the range of – 0.31 to 0.18 m, at ν = 20 Hz within the range of – 0.17 to 0.45 m.

That said, it ought to be noted that the resonance state range shifts to the right with the increase of the perturbing force frequency, that is, the resonance takes place at higher values of the elastic soil deformation coefficient c.

Hence, within the above-mentioned resonance state ranges of the root body oscillation parameters, the chipping off of the root, especially in its tail part, can take place.

In Fig. 5, the diagrams are shown for the relations between the amplitude of the forced transverse root body oscillations on the one hand and the elastic soil deformation coefficient c and the distance z from the root's cross-section to the conventional point of its fixing in the soil O on the other hand at a perturbing force amplitude of H = 500 N and a damping coefficient of b = 6.5 N s^2 m^{-3}.

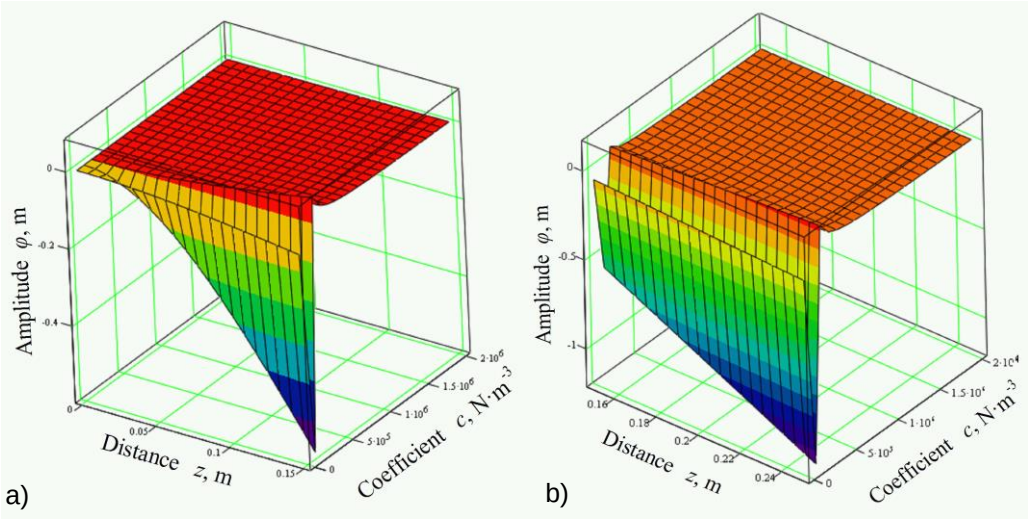

Figure 5. Relation between amplitude of forced transverse root body oscillations on one hand and coefficient of elastic soil deformation c and distance from root's cross-section to conventional point of its fixing z on the other hand: a) z = 0–0.15 m; b) z = 0.15–0.25 m; (perturbing force amplitude H = 500 N, b = 6.5 N s^2 m^{-3}, perturbing force frequency ν = 10 Hz).

As is obvious from the above diagrams, the amplitude of the forced transverse oscillations sharply rises at $c = 1.0 \cdot 10^5 \ldots 1.3 \cdot 10^5$, N m^3 and $z = 0.15\ m$, $z = 0.5\ m$, that is, at the point, where the tool grips the root and at the end of the root.

Also, in these cases the frequency of forced oscillations is virtually equal to the frequency of free oscillations of the root body. Within this range of parameters of the elastic soil deformation, the amplitude can reach up to 0.58 m. At all other values of the elastic soil deformation coefficients, the amplitude is close to zero and stays within the range of several millimetres.

Fig. 6 features the graphic relations between the amplitude of the forced transverse root body oscillations and the soil damping coefficient b at perturbing force frequencies v equal to 10 Hz, 15 Hz, 20 Hz, a perturbing force amplitude of $H = 500$ N and an elastic soil deformation coefficient of $c = 2.0 \cdot 10^5$, N m^{-3}.

As is seen in the diagrams, at $v = 10$ Hz and when the elastic deformation coefficient b varies within the range of 0 to 10 N s^2 m^{-3}, the amplitude of the forced transverse oscillations decreases from 0.088 to 0.056 m; at $v = 15$ Hz, it increases from 0.050 to 0.175 m; at $v = 20$ Hz, it increases from 0.015 to 0.025 m.

However, at $b = 6.5$ N s^2 m^{-3}, which is the most common value of the soil damping coefficient, the amplitudes in the above cases are equal to:

at $v = 10$ Hz – 0.063 m;

at $v = 15$ Hz – 0.085 m;

at $v = 20$ Hz – 0.020 m,

which is within the range of the permissible root body deformations.

As is seen in the diagrams presented in Fig. 6, the resonance phenomena in these cases do not take place.

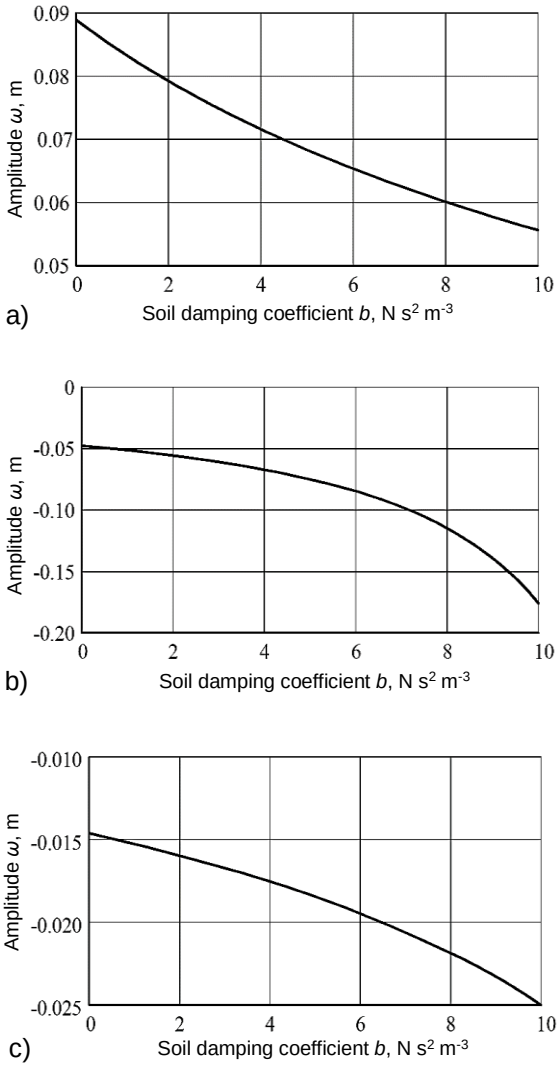

Figure 6. Relation between amplitude of forced transverse root body oscillations on one hand and soil damping coefficient b and perturbing force frequency v on the other hand for root's cross-section at point of its gripping by tool ($z = z_1 = 0.15$ m): a) $v = 10$ Hz; b) $v = 15$ Hz; c) $v = 20$ Hz (perturbing force amplitude $H = 500$ N, $b = 0$–10 N s^2 m^{-3}, $c = 2\ 10^5$ N m^3).

According to the diagrams shown in Fig. 7, the maximum amplitude of the transverse oscillations is reached at the point, where the tool grips the root (z = 0.15 m), and at the end of the root (z = 0.24 m), but again, resonance phenomena are not observed in these cases.

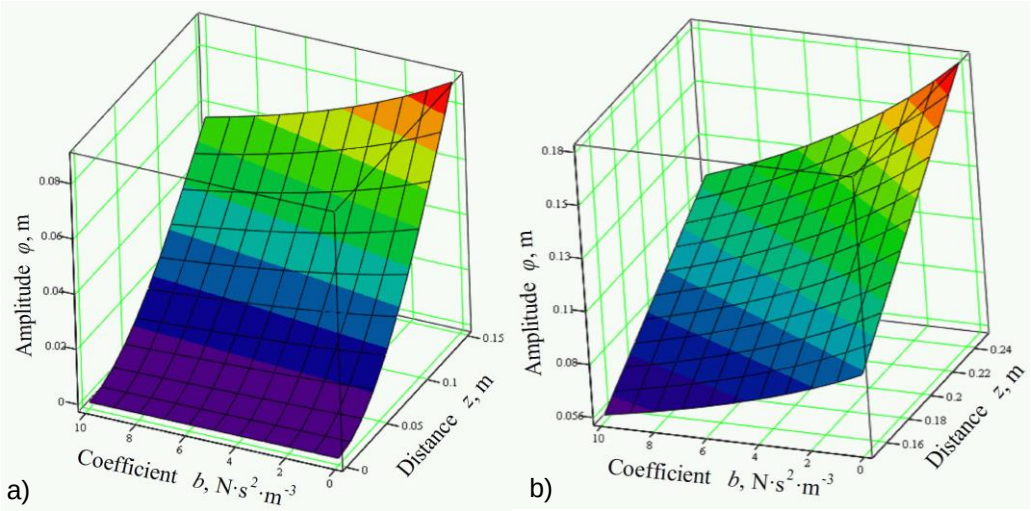

Figure 7. Relation between amplitude of forced transverse root body oscillations on one hand and soil damping coefficient b and distance from root's cross-section to conventional point of its fixing z on the other hand: a) z = 0–0.15 m; b) z = 0.15–0.25 m; (perturbing force amplitude H = 500 N, perturbing force frequency v = 10 Hz).

Thereby, by using the results of the PC-assisted calculations, the ranges of values have been obtained for the elastic soil deformation coefficient, within which the resonance state takes place. That is, the value of the amplitude of the forced transverse oscillations performed by the elastic root body exceeds the acceptable limit values.

CONCLUSIONS

1. The fundamental principles have been developed for the theory of the transverse oscillations performed by the root as an elastic body sitting in the soil as an elastic and damping medium during its vibrational lifting in the case, where the perturbing forces are vectored the same as the translational motion of the digging tool.

2. By using the generated equivalent schematic model and applying the Ostrogradsky-Hamilton variational principle, the analytical expressions have been obtained for calculating the amplitude of the forced transverse root body oscillations at any cross-section of the root.

3. The specially developed computer programme has been used to carry out the PC-assisted numerical calculations, which have provided for plotting the diagrams showing how the amplitude of the forced transverse oscillations of the root as an elastic body sitting in the soil as an elastic and damping medium varies in relation to the amplitude of the perturbing force and the coefficients of elastic soil deformation and soil damping.

4. The results of the calculations have been used to find the ranges of the elastic soil deformation coefficient values, within which the resonance state takes place. That is, the value of the amplitude of the forced transverse elastic root body oscillations exceeds the permissible limits, for the cases, when the frequency of the perturbing force generated by the vibrational lifting tool is equal to v = 10, 15 and 20 Hz. Under such conditions, the above-mentioned amplitudes of oscillations can vary within the range of 0.45 to 0.58 m, especially at the points of gripping the root and at the end of the root. That can result in chipping off the root's end, therefore, such ranges of the soil's elastic stiffness should be avoided.

5. When the soil damping coefficient b varies within the sufficiently wide range of 0–10 N s^2 m^{-3}, resonance phenomena are absent, the amplitudes of transverse oscillations stay within permissible limits. Therefore, the damping properties of the soil are acceptable within the whole range under consideration.

6. When engineering the lifting tools with the discussed direction of oscillations, it is necessary to take into account the elastic properties of the soil, with which such tools can operate efficiently.

7. The results of the completed analytical research have been used in the development of a new design of vibrational lifting tools.

REFERENCES

Babakov, I.M. 1968. *Theory of Oscillations*. Nauka, Moscow, 560 pp. (in Russian).

Boson, E.S., Verniaev, O.V., Smirnov, I.I. & Sultan-Shach, E.G. 2019. *Theory, Construction and Calculation of Agricultural Machines*. 2nd Ed., Scientific Publisher, 81 pp. ISBN: 9789388399838

Bulgakov, V.M. 2005. *Theory of beet harvesting machines*. Kiev, Publishing Centre of the National Agrarian University, 352 pp. (in Russian).

Bulgakov, V., Adamchuk, V., Kaletnik, G., Arak, M. & Olt, J. 2014. Mathematical model of vibration digging up of root crops from soil. *Agronomy Research* **12**(1), 41–58.

Bulgakov, V.; Adamchuk, V.; Arak, M. & Olt, J. 2015a. Theory of vibration-assisted sugar beet root lifting. *Agronomy Research* **13**(5), 1165−1192.

Bulgakov, V.; Adamchuk, V.; Olt, J. & Orszaghova, D. 2015b. Use of Euler equations in research into three-dimensional oscillations of sugar beet root during its vibration-assisted lifting. *Agronomy Research* **13**(1), 33−45.

Bulgakov, V., Golovats, I., Špokas, L. & Voitjuk, D. 2005. Theoretical investigation of a root crop cross oscillations at vibratinal digging up. *Research papers of IAg Eng LUA & LU of Ag*, **37**(1), 19–35 (in Russian).

Bulgakov, V. & Ivanovs, S. 2010. Mathematical simulation of beet vibration extraction. In: *Engineering for Rural Development*, pp. 25–31.

Dobrovsky, A.A. 1968. *Agricultural Machinery Vibration*. Mechanical Engineering, Moskow, 204 pp. (in Russian).

Dreizler, R.M. & Lüdde, C.S. 2010. *Theoretical Mechanics*. Springer, 402 pp.

Gruber, W. 2005. Trends in sugar beet harvesting. *Landtechnik* **60**(6), 320–322.

Gruber, W. 2007. Trends in sugar beet harvesting technology. *Landtechnik* **62**(6), 390–391.

Gu, F., Hu, Z., Wu, H., Peng, B., Gao, X. & Wang, S. 2014. Development and experiment of 4LT-A staggered-dig sugar beet combine. *Nongye Gongcheng Xuebao/Transactions of the Chinese Society of Agricultural Engineering* **30**(23), 1–9.

Myata, A.S. & Chumak, A.V. 1954. Research into tools of agricultural machines. *Collection of research papers of VISKhOM*. Moscow, Mechanical Engineering State Publishers, 148 pp.
Pogorely, L.V., Tatyanko, N.V. & & Bray, V.V. 1983. *Beet-harvesting machines (designing and calculation)*. Under general editorship of Pogorely, L. V. Tehnika, Kyiv, 232 pp.
Pogorely, L.V. & Tatyanko, N.V. 2004. *Beet-harvesting machines: History, Construction, Theory, Prognosis*, Feniks, Kyiv, 232 pp. (in Ukrainian).
Sarec, P., Sarec, O., Przybyl, J. & Srb, K. 2009. Comparison of sugar beet harvesters. *Listy cukrovarnicke a reparske* **125**(7–8), 212–216 (in Czech).
Schmitz, T.L. & Smith, K.S. 2012. *Mechanical vibrations: Modeling and measurement*. Springer, 378 pp. doi: 10.1007/978-1-4614-0460-6
Schulze Lammers, P. 2011. Harvest and loading machines for sugar beet – new trends. *International Sugar Journal* **113(**1348), 253–256.
Schulze Lammers, P.S. & Schmittmann, O. 2013. Testing of sugar beet harvesters in Germany 2012. *International Sugar Journal* **115**(1370), 100–106.
Vasilenko, P.M., Pogorely, L.V. & Brey, V.V. 1970. Vibrational Method of Harvesting Root Plants. *Mechanisation and Electrification of the Socialist Agriculture* **2**, 9–13 (in Russian).
Vermeulen, G.D. & Koolen, A.J. 2002. Soil dynamics oft he origination of soil tare during sugar beet lifting. *Soil & Tillage Research* **65**, 169–184.
Vovk, P.F. 1936. Agrophysical properties of sugar beet roots as regards mechanisation of their harvesting. Theory, design and production of agricultural machines. *Collection of scientific papers*. Leningrad, Agriculture State Publishers, **2**, pp. 269–284.

Agronomy Research **18**(3), 1962–1972, 2020
https://doi.org/10.15159/AR.20.200

Experimental research into the effect of harrowing unit's operating speed on uniformity of cultivation depth during tillage in fallow field

V. Bulgakov[1], V. Nadykto[2], V. Kaminskiy[3], Z. Ruzhylo[1], V. Volskyi[4] and J. Olt[5,*]

[1]National University of Life and Environmental Sciences of Ukraine, 15 Heroyiv Oborony street, UA03041 Kyiv, Ukraine
[2]Dmytro Motornyi Tavria State Agrotechnological University, 18[B] Khmelnytsky Avenue, UA72310 Melitopol, Zaporozhye Region, Ukraine
[3]National Scientific Centre, Institute of Agriculture of NAAS of Ukraine, 2b, Mashinobudivnikiv street, Chabany vil., Kyiv-Svyatoshin Dist., UA08162 Kyiv Region, Ukraine
[4]National Scientific Centre, Institute of Mechanization and Electrification of Agriculture, 11 Vokzalna street, Glevakha stl, Vasylkivsky Dist., UA08631 Kyiv Region, Ukraine
[5]Estonian University of Life Sciences, Institute of Technology, 56 Kreutzwaldi street, EE 51006 Tartu, Estonia
[*]Correspondence: jyri.olt@emu.ee

Abstract. Retention of soil moisture is an urgent topic of the day in the cultivation of agricultural crops. Using fallow fields is one of the ways to solve the named problem, but the tilling of such fields requires observing some special conditions, in particular, the capillary effects in their upper soil layers must be cut down. For that purpose, the authors have proposed a special harrow equipped with the tools capable of fulfilling the above-mentioned task. The authors have carried out extensive field experiment research into the tillage of fallow soils with the use of the said implement. In order to apply the implement, a new harrow unit has been developed. The results obtained during the experiment research have been processed with the use of statistical methods and it has been established that the depth of harrowing in the tilled field decreases, when the operating speed of the combined unit under consideration increases to 3.3 m s^{-1}. At the same time, the variances of oscillations of the parameter under research in accordance with the Cochran's C test remain uniform. Also, the frequency of the harrowing depth oscillations changes insignificantly. That is supported by the correlation lengths of the normalized correlation functions of the process under consideration, which, at the above-mentioned operating speed, stay within the sufficiently narrow range of values: 0.16–0.20 m. According to the results of the experimental investigations, the maximum value of the normalized cross-correlation function for the relation between the oscillations of the field harrowing depth and the oscillations of the field's longitudinal profile does not exceed 0.12. This testifies to the absence of any substantial interrelation between the said two stochastic processes, which is quite reasonable in view of the small values of the variance and period of the oscillations of the field's longitudinal profile. The probability of the new combined tractor and harrow unit maintaining the tolerance of the fallow field cultivation depth oscillations within the range of ± 1 cm is equal to 82%. Within each 1.85 m

of the distance travelled by the combined soil cultivation unit under consideration, only one instance of the field cultivation depth deviating from the ± 1 cm tolerance can be expected.

Key words: fallow, field profile, harrow, operating speed, tillage depth.

INTRODUCTION

As a result of the numerous field investigations, it has been established that, even at a sufficient amount of plant nutrients, the scarcity of soil moisture results in the reduced yield of the agricultural crops (Donaldson et al., 2001). In the absence of water in the soil, the sowing is either put off to some later date or completely postponed until spring (Schillinger & Papendick, 1997).

One of the ways to retain and even, to some extent, accumulate moisture in the soil is to apply the fallow land practice (Chang et al., 1990). The ripping of the upper soil layer up to the mulch condition virtually destroys its capillarity, which results in the development of the medium that separates the damp and relatively cold layer of soil from the dry and warm ground air. Under such conditions, the dissipation of water content from the uncultivated layer of soil gets substantially lower (Massee et al., 1978; Al-Mulla et al., 2009).

There are different kinds of agricultural machines for producing such soil mulch. Most commonly, they are equipped with V-blade tools, each one with a working span of 46 cm and more (Smith et al., 1996; Schillinger et al., 2006). Sometimes, rod weeders are applied as well as disc harrows and chisel cultivators (Lindwall & Anderson, 1981; Carman, 1997; Kornienko et al., 2016; Lovarelli & Bacenetti, 2017; Tagar et al., 2020).

The primary drawback of these implements is that they operate steadily only at a soil cultivation depth of greater than 10 cm. But it was as long ago as in 1909 that Russian scientist I. Ovsinskiy (1909) convincingly proved that the depth of the soil mulch might not exceed two inches, i.e. it had to be between 5 to 6 cm. From the previous field experiments, it has been established that this soil mulch layer is exactly the place, where the intensive water evaporation from the tilled soil takes place (Nadykto et al., 2012).

Moreover, it has to be taken into account that, when the field is tilled to a depth of 6 to 7 cm, the stirring of the soil and especially the carryover of its water content to the daylight surface of the field have to be kept to a minimum. Meanwhile, the numerous field experiments have shown that, even when single-row disc tools (Smith et al., 1996; Moreno et al., 2011) or bar harrows (Schillinger & Papendick, 1997) are used which in principle capable of tilling soil to the required depth of 6 to 7 cm, the discussed problem is still not solved completely. It results mostly from the fact that they rather intensively stir the cultivated soil layer (which is especially true for disc harrows).

MATERIALS AND METHODS

Taking into account the above-mentioned circumstances, the authors have developed an implement for cultivating fallow land, comprising different harrowing sections (Fig. 1), with each section containing 20 tools (5 rows with 4 tools in each of them) attached to the frame following a zigzag harrow pattern.

The tool in the section is a flat bar (spike tooth) with a thickness of 8 mm, to which a flat blade with a working width of 80 mm is welded. The front row of tools in the section can be equipped with vertically set blades. Such alignment of the front blades of the section facilitates cutting (shredding) those plant residues, which can be present in the upper (to a depth of up to 6 to 7 cm) soil layer. That action provides for the more stable motion of the harrowing section in the longitudinal and vertical plane.

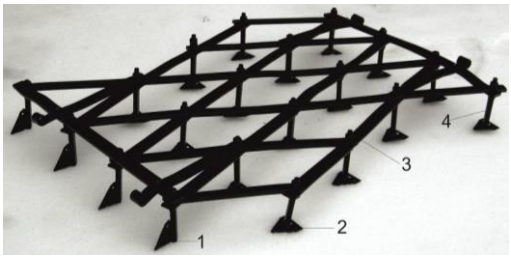

Figure 1. Isometric view of the proposed harrowing implement: 1 – vertically set blade; 2 – horizontally set blade; 3 – harrow frame; 4 – tool.

Each section is attached with the use of two drag bars to the common beam, the latter, in its turn, is connected with the carrying tractor. One of the problem points in the operation of such a harrowing section is the stability of its position in the longitudinal and vertical plane, when performing the harrowing operation.

In view of that, the aim of this study was to investigate theoretically and experimentally the effect of the operating speed of the developed harrowing unit on the uniformity of the soil ripping depth during fallow field tillage.

The experimental investigations were carried out during the spring harrowing of fallow fields. The fallow land was preceded by sunflower fields, the last soil tillage operation was mouldboard ploughing to a depth of 25 cm. In order to carry out the field investigations, a cultivated field with an area of 70 ha was selected, in which, prior to the experiments, multiple measurements of the moisture content and density of the soil in its upper 0–10 cm layer were made and also the longitudinal profile of the cultivated land was measured.

Figure 2. Combined tractor and harrow unit during fallow field tillage.

In the field experiment investigations, the harrowing unit for fallow land tillage was used, which comprised a wheeled tractor (MTZ-82, 60 kW) and the developed harrow, which included 9 harrowing sections (Fig. 2). In the process of the field investigations, the harrowing unit travelled using three different gears, which enabled its movement at three different speeds.

Specification of the harrowing unit:

Number of harrowing sections	9
Working width of section	0.91 m
Formation of sections in unit	line
Spacing between sections	0.06 m
Working width of harrowing unit	8.70 m

The following values were measured with three replications at each operating speed of the harrowing unit: the time t_a, in which the harrowing unit passed the recorded distance with a length of 250 m and the soil cultivation depth.

The time t_a was measured with the help of an FS-8200 electronic stopwatch with a measurement accuracy of ± 0.1 s. Then the operating speed of the combined tractor-implement unit V_a was calculated by the formula:

$$V_a = \frac{s}{t_a}. \quad (1)$$

The soil moisture content in the layer of 0–10 cm was measured with the use of the SHS-1 instrument, which was connected to the personal computer via the Arduino Uno interface unit (Fig. 3). The error in the measurement of the absolute value of the soil moisture content with the use of the SHS-1 instrument did not exceed ± 1%.

The data received from the Arduino Uno were transformed with the use of the CoolTerm software into the format suitable for the processing in the Microsoft Excel environment. After 100 soil moisture content measurements, taken at each 3 m, when moving along the diagonal of the field, had been completed, the mean value of the moisture content was calculated.

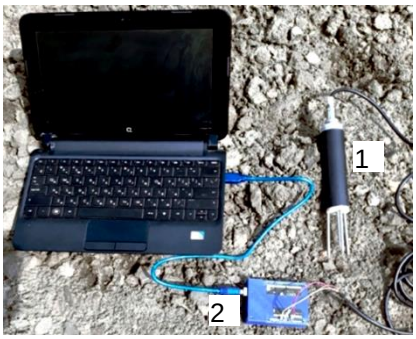

Figure 3. Soil moisture content measuring kit: 1 – SHS-1; 2 – Arduino Uno.

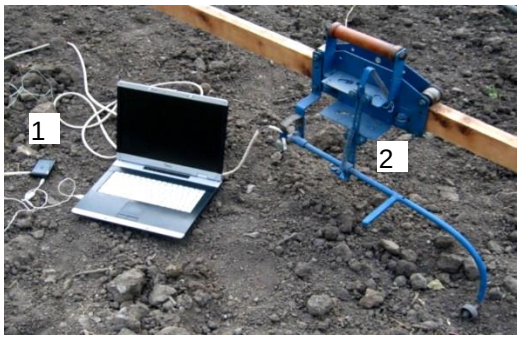

Figure 4. Device for measuring field profile oscillations: 1 − Arduino Uno; 2 – profilometer.

The longitudinal profile of the tilled field was measured with the help of a developed profilometer (Fig. 4). It was mounted on a rail positioned in parallel to the field surface. The lever of the instrument touched with its one end the surface of the field (i.e. sensed the profile), while the other end was pivoted to the axle connected to an SP-3A variable resistor. The resistor had a straight-line characteristic and a nominal value of 470 Ω.

As the instrument moved along the rail, the lever performed oscillatory motion in the longitudinal and vertical plane, which resulted in the variation of the resistance value in the SP-3A. The electric signal that was output in this process was sent to the analogue input of the Arduino Uno, then transmitted to the PC, where it was transformed to make it suitable for the processing in the Microsoft Excel environment.

The oscillations of the longitudinal profile of the field were recorded with 5 replications at a measurement interval of 0.1 m. With a rail length of 4 m, it provided for obtaining at least 350 points. The error in the measurement of the field profile oscillations with the use of the described instrument did not exceed ± 0.5 cm.

The density of the soil in the 0–10 cm layer was measured in accordance with the technique that is detailed in the paper.

For each operating speed of the combined tractor and harrow unit under consideration, three series of soil cultivation depth measurements were carried out. Each series comprised 200 measurements at an interval of 0.2 m. The accuracy of the instrument applied for this purpose (Fig. 5) was equal to ± 0.5 cm. The process of operating the instrument is as follows. For the purpose of taking a measurement, the cross bar 1 (Fig. 5) of the instrument is placed on the soil surface. Using the lever 3, the rod 4 is manually lowered until it is stopped by the untilled soil. After that, the value of the soil tillage depth is read on the measuring scale 2.

Figure 5. Instrument for measuring tillage depth: 1 – cross bar; 2 – measuring scale; 3 – lever; 4 − rod.

Apart from the standard statistical characteristics, normalized correlation functions were calculated for the tillage depth. These functions provide for estimating the frequency spectrum of the harrowing depth oscillation process. The impact of the field profile oscillations on the depth of its cultivation was estimated with the use of the normalized cross-correlation function.

RESULTS

The experimental investigations were carried out on dark chestnut soil in the conditions that were close to arid. The soil texture was heavy clay loam, since the alphitite content in the soil was at a level of 46–48%. The humus content was at a level of 2.8–3.6%, the reaction of soil solution was close to neutral.

At the time, when the experimental investigations were carried out, the mean value of the soil water content in the 0–10 cm layer was 18.3%, while the mean value of the soil bulk density in the same layer was 1.24 g cm^{-3}. The variance of the field surface profile oscillations was equal to 0.54 cm^2. The mean value of the period of the oscillations was equal to 0.17 m. When the combined harrow unit under consideration operated on such moving at different speeds of translation, the harrowing depth had the parameters presented in Table 1.

The analysis of the data from the table provides evidence of the following facts. When the operating speed was changes from 2.1 to 2.5 m s^{-1}, the mean value of the harrowing depth decreased by 0.2 cm. At a statistical significance level of 0.05 (that is, at a confidence coefficient of 95%), such a difference is non-random and significant, because in this case LSD_{05} is lower and equal to 0.1 cm.

As regards the mean value of the harrowing depth in the case, when the combined tractor and harrow unit travels at an operating speed of 3.3 m s^{-1} (Table 1), the null hypothesis of its equality to the two other statistical characteristics (5.0 and 4.8 cm) is

rejected even at a statistical significance level of 0.01. That can be explained by the wider confidence interval for the mean value of the soil cultivation depth at the unit's travel rate of 3.3 m s^{-1} (Table 1).

Table 1. Statistical characteristics of harrowing depth

Operating speed, m s^{-1} (km h^{-1})	Confidence interval, cm	Variance, cm^2	Standard deviation, ± cm	Coefficient of variation, %	Error of mean, cm
2.1 (7.6)	5.0 ± 0.1	0.49	0.70	14.0	0.06
2.5 (9.0)	4.8 ± 0.2	0.52	0.72	15.0	0.07
3.3 (11.9)	4.0 ± 0.3	0.58	0.76	19.0	0.06

The above-said leads to a conclusion that increasing the rate of travel of the combined tractor and harrow unit under investigation results in the decrease of the harrowing depth in the field under cultivation (Fig. 6). At the same time, the confidence interval for the said parameter demonstrates the uptrend.

In the discussed case, the described result can a priori be explained only by the suggestion that the towed members of the process part of the combined tractor and harrow unit under consideration (that is, the harrowing sections) tend to shallow up from the soil, when its rate of travel increases. It must be emphasized that such a phenomenon is quite common in the operation of towed implements.

The variance and correlation analysis of the results obtained during the field experiment investigations carried out by the authors provides evidence of the following facts:

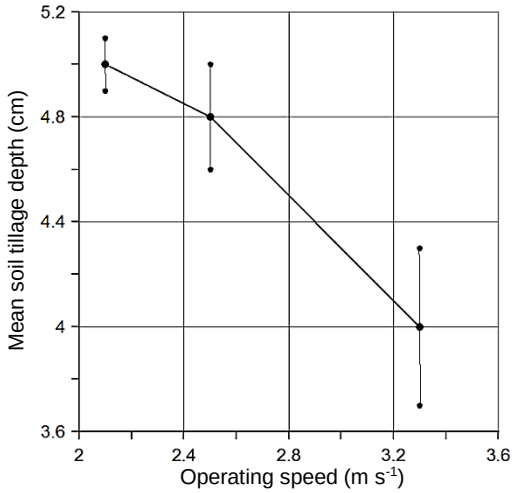

Figure 6. Relation between mean soil tillage depth and combined tractor and harrow unit's operating speed.

1. At a confidence level of 95% and greater, it can be stated that the null hypothesis of the equality of the compared variances of harrowing depth oscillations in the cases, when the soil cultivation unit travels at rates of 2.1 and 2.5 m s^{-1}, is not rejected. And that is true, because the actual value of the Fisher's ratio test F_r = 0.52 cm^2/0.49 cm^2 = 1.06 is smaller than the table value F_{tabl} = 1.39.

2. The three compared variances of harrowing depth oscillations do not significantly differ from each other. The statistical analysis shows that according to the Cochran's C test even the greatest of the discussed statistical characteristics (0.58 cm^2, Table 1) is uniform with the other two. As shown by the calculations, the actual value of the above-mentioned criterion for this case G_r = 0.58/(0.49 + 0.52 + 0.58) = 0.36 is smaller than the table value, which is equal to 0.58 at a statistical significance level of 0.05.

3. The harrowing depth oscillations during the operation of the unit under research take place within approximately the same frequency range. The basis for such a univalent conclusion is provided by the behaviour of the respective normalized correlation functions (Fig. 7).

The principal characteristic property of each of the functions is the correlation length, that is, the distance from zero to the first point of intersection between the function and the axis of abscissa.

It becomes evident from the analysis of the obtained correlation functions that the correlation length for all the three modes of motion of the discussed combined tractor and harrow unit is roughly the same. Despite the difference between the operating speeds of the harrowing unit (2.1, 2.5, and 3.3 m s^{-1}), these characteristics in terms of their values (correlation lengths) are situated in a sufficiently narrow range: 0.16–0.20 m (curves 1, 2, and 3, Fig. 7).

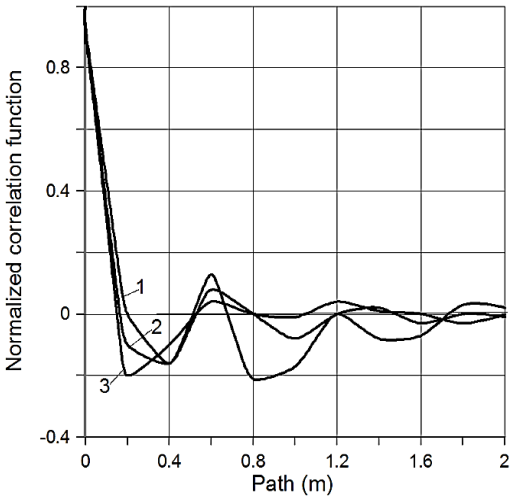

Figure 7. Normalized correlation functions of tillage depth oscillations at different operating speeds of combined tractor and harrow unit: 1) 2.1 m s^{-1}; 2) 2.5 m s^{-1}; 3) 3.3 m s^{-1}.

Nevertheless, taking a formal approach to the analysis of the obtained correlation functions it has to be noted that, as the rate of move of the soil cultivation unit under research increases, the spectrum of the harrowing depth oscillations spreads out to some extent. For example, while at the unit's operating speed of 2.1 m s^{-1} the correlation length of the process under consideration is equal to approximately 0.20 m (curve 1, Fig. 7), the increase of the unit's travel rate to 3.3 m s^{-1} results in this length decreasing to about 0.16 m (curve 3, Fig. 7). Essentially, that means that the spectrum of the harrowing depth oscillations in the latter case is to some extent wider. But the noted difference is small, therefore, it can be stated that the change of the harrowing unit's operating speed from 2.1 to 3.3 m s^{-1} has virtually no effect on the frequency of the soil cultivation depth oscillations during the operation of the unit under research.

One more statistical measure used for stationary ergodic processes is the cross-correlation function. As is known, in case of two stochastic processes $X_1(t)$ and $Y_1(t)$, this function describes the degree of correlation between the section of the process $X_1(t)$ at $t = t_1$ and the section of the process $Y_1(t)$ at $t = t_2$.

In the described research, the authors investigated the statistical interrelation between such stochastic processes as the oscillations of the tilled field profile in the longitudinal and vertical plane and the oscillations of the harrowing depth. Hypothetically, it could be expected that the two processes had a close correlation.

In effect, it was established that, in the case under consideration, virtually no closeness is observed in the above-mentioned correlation (Fig. 8).

For example, the level of the coefficients of the correlation between the field profile oscillations and the oscillations of the harrowing depth only slightly exceeds the 0.1 point. And that observation is true both for the positive (first and second quadrants, Fig. 8) and negative (third and fourth quadrants, Fig. 8) levels of the analysed correlation. Again, the presence of roughly identical, in terms of their values, maximum and minimum of the cross-correlation function excludes the possibility to determine, which of the processes is the input process and which is the output one.

This point needs to be analysed in greater detail. As is seen in Fig. 8, the cross-correlation function reaches its maximum negative value at a level of – 0.12, when its phase displacement is equal to approximately – 0.2 m (pt. A, Fig. 8). If the maximum of the positive correlation was at the same time below 0.12, it would be possible to state that the harrowing depth is the input factor, while the field surface profile is the output one. Moreover, in case of the negative correlation the situation is as follows: the greater the oscillations of the field surface irregularities, the smaller harrowing depth oscillations. Obviously, it would be very difficult to give a logical explanation for such a result.

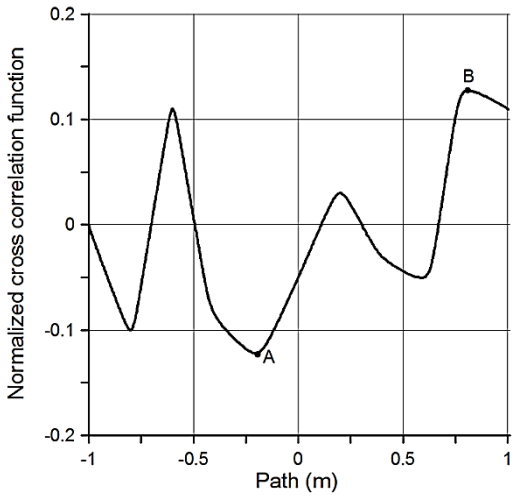

Figure 8. Normalized cross-correlation function for oscillations of longitudinal field profile and tilling depth.

On the other hand, the cross-correlation function reaches its maximum positive value at a level of 0.12 at a phase displacement of about 0.85 m (pt. B, Fig. 8). If the maximum of the negative correlation (its absolute value) was at the same time smaller and not equal to that of the positive correlation, the following conclusion could be arrived at: in case of a positive correlation, the profile irregularity oscillations are the input action, while the harrowing depth is the output action. The phase displacement in this case is equal to 0.85 m. In practical terms, that means that at a operating speed of, for example, 2.5 m s^{-1}, the time lag in the reaction of each harrowing section of the soil cultivation unit to the oscillations of the field profile irregularities in the longitudinal and vertical plane is equal to 0.85 m /2.5 m s^{-1} = 0.34 s.

When the maximum values of the negative and positive correlations in the cross-correlation function under consideration are equal, those statements are not true. Moreover, taking into account the very low maximum level of the normalized cross-correlation function, which does not exceed the 0.12 mark (Fig. 8), it is possible to state that, in the process of the research completed by the authors, no significant correlation was found between the oscillations of the profile irregularities of the cultivation field in the longitudinal and vertical plane and the oscillations of the depth of its harrowing.

The above result can be explained as follows. As earlier noted, the mean value of the period of the field profile irregularity oscillations during the research was equal to 0.17 m, while their variance was equal to 0.54 cm^2. The length of one harrowing section, which was equal to 1.2 m, contained 7 such periods. In view of that and taking into account the rather small variance of the track profile oscillations, it was quite logical to expect that the statistical characteristics of those oscillations could not have a significant effect on the oscillations of the soil cultivation depth.

When the soil is cultivated to a depth of 5–6 cm, the working tolerance for the oscillations of this parameter has to be low. The authors have set it at a level of $\Delta = \pm 1$ cm. In that case, it would be useful to know the probability P (%) of the harrowing unit maintaining such a tolerance and the frequency of deviating from it (ω, m^{-1}).

The first of the above-mentioned indicators can be calculated by the following formula (Lurye, 1970):

$$P = 2 \cdot F\left(\frac{\Delta}{\sigma}\right), \tag{2}$$

where F − Laplace's integral function; Δ – working tolerance for the oscillations of soil tillage depth (± cm); σ – standard deviation of the fallow field tillage depth (± cm).

In order to calculate the second indicator (that is, ω) the following relation is used (Lurye, 1970):

$$\omega = \frac{1}{2 \cdot T_p} \cdot exp\left(-\frac{\Delta^2}{2 \cdot \sigma^2}\right), \tag{3}$$

where T_p − half period of the soil tillage depth oscillation. If the correlation function of the process is known, the value of T_p can be found as follows:

$$T_p = \frac{1}{n} \cdot \sum_{i=0}^{n} (\tau_{i+1} - \tau_i), \tag{4}$$

where n – number of points of intersection between the normalized correlation function curve and the axis of abscissae; τ_i – successive values of the coordinates, at which the correlation function curve crosses the X-axis. For the normalized correlation functions shown in Fig. 7 the mean value of this parameter is T_p = 0.36 m.

As the mean value of the parameter σ in the case under consideration is equal to 0.73 (Table 1), the following value of the ratio is arrived at:

$$\frac{\Delta}{\sigma} = \frac{1}{0.73} = 1.37.$$

Then, in accordance with the well-known table, the value of Laplace's function is equal to 0.41. In view of the above-said, the expression (2) gives the following result: P = 0.82. In practical terms, that means that the probability of the combined unit under consideration maintaining the working tolerance of the soil cultivation depth at a level of ± 1 cm is equal to 82%.

Pursuant to the expression (4), at T_p = 0.36 m, $\Delta = \pm 1$ cm and $\sigma = \pm 0.73$ cm the value of ω is equal to 0.54 m^{-1}. The obtained result has to be interpreted as follows: in each 1/0.54 = 1.85 m of the travelling track of the soil cultivation unit under consideration, one instance of the harrowing depth deviating from a tolerance of ± 1 cm is possible.

CONCLUSIONS

When selecting the conditions of the harrow unit, it should be taken into account that increasing the operating speed results in the decrease of the harrowing depth in the cultivated field, while the variances of oscillations of the above-mentioned parameter in accordance with the Cochran's C test remain uniform. The frequency of the harrowing depth oscillations changes little. That is confirmed by the values of the correlation lengths in the normalized correlation functions of the process under consideration, which, in case of the above-mentioned mode of travel of the combined tractor and harrow unit, stay within the sufficiently narrow range: 0.16–0.20 m.

Following the results of the experimental investigations, the maximum value of the normalized cross-correlation function representing the relation between the oscillations of the field harrowing depth and the oscillations of the field's longitudinal profile does not exceed the 0.12 mark. That gives evidence of the absence of a significant interrelation between the two stochastic processes, which is quite reasonable in view of the small values of the variance and period of the longitudinal field profile oscillations.

The probability of the new combined tractor and harrow unit maintaining the tolerance of the fallow field cultivation depth oscillations within the range of ±1 cm is equal to 82%. Within each 1.85 m of the distance travelled by the combined soil cultivation unit under consideration, only one instance of the field tillage depth deviating from the ± 1 cm tolerance can be expected.

The above results of research can be used as practical guidelines, when selecting the unit's mode of travel in terms of its speed for ripping the soil to a depth of up to 6–7 cm. In case these guidelines are followed, the operation of the unit at speeds within the investigated range (2.1–3.3 m s^{-1}) will result in the high quality of soil tillage.

REFERENCES

Al-Mulla, Y.A., Wu, J.Q., Singh, P., Flury, M., Schillinger, W.F., Huggins, D.R. & Stöckel, C.O. 2009. Soil water and temperature in chemical versus reduced-tillage fallow in a mediterranean climate. *Applied Engineerin in Agriculture* **25**(1), 45–54.

Carman, K. 1997. Effect of different tillage systems on soil properties and wheat yield in Middle Anatolia. *Soil and Tillage Research* **40**(3–4), 201–207. doi: 10.1016/S0167-1987(96)01059-8

Chang, C., Sommerfeldt, T.G., Entz, T. & Stalker, D.R. 1990. Long-term soil moisture status in Southern Alberta. *Canadian Journal of Soil Science* **70**, 125–136.

Donaldson, E., Schilinger, W.F. & Dofing, S.M. 2001. Straw Production and Grain Yield Relationships in Winter Wheat. *Crop Science* **41**(1), 100–106.

Kornienko, S, Pashenko, V., Melnik, V., Kharchenko, S., Khramov, N. 2016. Developing the method of constructing mathematical models of soil condition under the action of a wedge. *Eastern-European Journal of Enterprise Technologies* **5**(7–8), 34–43. doi: 10.15587/1729-4061.2016.79912

Lindwall, C.W. & Anderson, D.T. 1981. Agronomic evaluation of minimum tillage systems for summer fallow in southern alberta. *Canadiab Journal of Plant Science* **61**(2), 247–253. https://doi.org/10.4141/cips81-037

Lovarelli, D. & Bacenetti, J. 2017. Seedabed preparation for acable crops: Environmental impact of alternative mechanical solution. *Soil and Tillage Research* **174**, 156–168. doi: 10.1016/j.still.2017.06.006

Lurye, A.B. 1970. *Statistical dynamics of agricultural sets*. Leningrad, Kolos, 128 pp. (in Russian).

Massee, T.W., Cary, J.W., Plains, G. & Desert, A. 1978. Potential for reducing evaporation during summer fallow. *J. Soil Water Conserv*. **33**, 126–129.

Moreno, M.M., Lacasta, C., Meco, R. & Moreno, C. 2011. Rainfed crop energy balance of different farming systems and crop rotations in a semi-arid environment: Results of a long-term trial. *Soil Tillage Res*. **114**, 18–27. https://doi.org/10.1016/j.still.2011.03.006

Nadykto, V.T., Kyurchev, V.M., Semenuk, V.L. & Nazin, A.E. 2012. *Separate harvesting of grain crops*. Zaporizhya, Inter-M. 132 pp. (in Ukrainian).

Ovsinskiy, I. 1909. *New Farming System*. Moscow, 123 pp. (in Russian).

Schillinger, W.F. & Papendick, R.I. 1997. Tillage Mulch Depth Effects during Fallow on Wheat Production and Wind Erosion Control Factors. *Soil Sci. Soc. Am. J*. **61**, 871–876.

Schillinger, W.F., Papendick, R.I., Guy, S.O., Rasmussen, P.E. & Van Kessel, C. 2006. Dryland Cropping in the Western United States. In: *Dryland Agriculture*. 2end Ed., Agronomy Monograph, 23. ASA, CSSA, and SSSA, Madison, WI, pp. 365–393.

Smith, E.G., Peters, T.L., Blackshaw, R.E., Lindwall, C.W. & Larney, F.J. 1996. Economics of reduced tillage fallow-crop systems in the dark brown soil zone of Alberta. *Canadian Journal of Soil Science* **76**, 411–416. https://doi.org/10.4141/cjss96-049

Tagar, A.A., Adamowski, J., Memon, M.S., Do, M.C., Mashori, A.S., Soomro, A.S. & Bhayo, W.A. 2020. Soil fragmentation and aggregate stability as affected by conventional tillage implements and relations fractal dimensions. *Soil and Tillage Research* **197**, Article number 104494. doi: 10.1016/j.still.2019.104494

Agronomy Research **18**(3), 1973–1991, 2020
https://doi.org/10.15159/AR.20.186

Investigation of the long-term toxic effect of nanoparticles of different physical-chemical characteristics

D.G. Churilov[1], S.D. Polischuk[2,*], G.I. Churilov[3], V.V. Churilova[2] and D.N. Byshova[4]

[1]Ryazan State Agrotechnological University, Road Transport Faculty, Department of Metal Technology and Machine Repair, Kostychev street 1, 390044 Ryazan, Russia
[2]Ryazan State Agrotechnological University, Technological Faculty, Department of Breeding and Seed Production, Agricultural Chemistry, Forestry and Ecology, Kostychev street 1, 390044, Ryazan, Russia
[3]Ryazan State Medical University, Faculty of Medicine, Department of General Chemistry, Vysokovoltnaya street 9, 390026 Ryazan, Russia
[4]Ryazan State Agrotechnological University, Faculty of Vet Medicine and Biotechnology, Kostychev street 1, 390044 Ryazan, Russia
[*]Correspondence: svpolishuk@mail.ru

Abstract. The purpose of this work is to study the effect of metal and oxide nanoparticles on some ecological and functional groups in the soil-plant-animal system to form the stability limits of organisms. Nanoparticles of cobalt, iron, zinc, copper, copper oxide, zinc oxide and titanium dioxide sized 20–80 nm were studied. The concentration range was 0.01–1,000 g of nanoparticles per ton of seeds or soil. Objects suitable for biotesting and environmental monitoring were selected: earthworms (*Lumbricina*), rats (white outbred) and Wistar rats. It was previously found that nanoparticles of the studied metals up to a concentration of 100 g t^{-1} of seeds, unlike oxides, practically do not affect bacterial populations. The use of indicators of biochemical and cytomorphologic reactions of invertebrates seems promising because worms are able to bind pollutants and reduce their penetration into plants. They are also an indicator of soil biotesting for metal contamination. Reactivity and toxic effects of nanoparticles (NPs) in natural conditions depend both on the type of soil and on the size and concentration of nanoparticles. With sizes (NPs) of up to 20 nm (depending on the type of soil and physicochemical characteristics), NPs are much more reactive and reduce the survival of microorganisms. Small nanoparticles (less than 20 nm) are characterized by a large interface. Such nano-objects exhibit high physical-chemical activity and are safe only at very low concentrations. The specifics of the environmental impact of oxide NPs compared to metal NPs was revealed. It was associated with accumulation of oxides in living systems and the peculiarities of changes in the morph physiological, histological and reproductive parameters of organisms and morphological and biochemical parameters of animals. Oxide nanoparticles accumulate in a living organism, exhibit toxic properties, lower the activity of enzymes and hormones and are transferred along trophic chains, which is not typical for metal nanoparticles.

Key words: toxicity, microorganisms, invertebrates, plants, laboratory animals, morphology, cytotoxicity, biochemistry, histology.

INTRODUCTION

In connection with the intensive development of nanotechnology, the flow of artificial nanoparticles entering the environment inevitably increases. This gives rise to the need to study and understand the routes of entry, distribution, accumulation and their effects on living organisms, including the degree of toxicity of nanoparticles, as well as the possibility of their inclusion in biogenic cycles. The environmental effects of nanoparticles of technogenic origin have not been fully studied yet due to the difficulty of isolating them in pure form from natural products for research (Edgington et al., 2010) and conflicting data in scientific studies when assessing their safety. There has been an increase in the number of publications demonstrating the toxic effects of nanoparticles (NPs) with a characteristic size of less than 100 nm (Oberdörster et al., 2005; Alekseeva, 2007; Elsaesser & Howard, 2012). But the properties of nanoparticles depend on many factors: the method of preparation, size, surface area, chemical composition. All these factors, including the effect of small doses, were studied in our earlier works (Churilov et al., 2019) and it was shown that nanoparticles of iron, copper and cobalt with a size of 20–80 nm have biological activity and can be used as growth stimulators of living systems. An analysis of the available scientific data, on the one hand, indicates a high degree of novelty and relevance of the proposed area - the study of the interaction of fine particles of technogenic origin with plant cells to develop technology for their use to stimulate the growth of agricultural plants. And on the other hand it shows the difficulties associated with the probability of bioaccumulation of heavy metals in the form of highly active particles and compounds, which requires special attention to environmental issues and safety of the developed approaches. The ecotoxicological assessment of nanoparticles remains the problem of creating algorithms for their comprehensive investigation, identifying key test objects and test functions, laying the foundations for the development of environmental safety standards. Studies are important to establish tolerance limits and assess the resistance of organisms to this factor of natural and technogenic origin.

The biological activity of metal and oxides nanoparticles indicates that the cause of this phenomenon is the processes associated with the action of a regulatory signal in biological systems (Burlakova et al., 1996; Voronkov et al., 2005; Rajput et al., 2018; Churilov et al., 2019). The biological effect produced by chemical and physicochemical factors is associated with the transfer of information that is universal for any biological objects that operate with a high degree of certainty in the system: an agent (a preparation) - a cell and its structures.

The system of supramolecular structures of the cellular microenvironment satisfies these requirements (Zaytsev et al., 1999). The authors of (Bogatyrenko et al., 1989; Churilov, 2009; Samoylova et al., 2017; Polischuk et al., 2018) showed that the energy of nanoparticles (NPs) of biogenic metals (iron, cobalt and copper) of a certain size (25–60 nm) stimulates the processes of self-organization of biological systems and their adaptation to external conditions. It is assumed that nanocrystalline metals have great potential in mineral nutrition and energy exposure and, thanks to uncompensated bonds, easily form complex compounds with organic substances. As a result, they activate the synthesis of various enzymes that affect carbohydrate and nitrogen metabolism, amino acid synthesis, photosynthesis and cellular respiration (Churilov, 2010; Antoņenko et al., 2016; Argentel-Martínez et al., 2019; Karpenko et al., 2019; Arutyunyan, et al., 2020).

In most cases, maximum activity is observed in a certain dose range, divided by the so-called 'dead zone' or a decrease in the index. For metal nanoparticles, an oscillatory character of the dose dependence is observed. In each case, the significance of the most important biological processes, including participation in gene expression, was identified and proved (Folmanis & Kovalenko, 1999; Churilov et al., 2015; Churilov et al., 2018a). The possibility of penetration and bioaccumulation of nanoparticles (NPs) of copper, zinc and titanium oxides with a size of 20–80 nm in various plant organs was established in (Churilov et al., 2018b; Stepanova et al., 2019). It was shown that bio-accumulation in plants led to transmission of NPs along food chains to animals. When introducing vetch grown after seed treatment with copper, zinc and titanium oxides at a concentration of 100 g t^{-1} into the rabbits' diet, a significant decrease in live weight of animals was observed throughout the experiment in experimental groups by an average of 15–9%.

There is no bioaccumulation for metal nanoparticles (copper, cobalt, zinc), 20–100 nm in size. Additional evidence of the lack of accumulation of metal NPs with a size of 20–100 nm is the effect of the introduction of crops pre-treated with NPs into the diet of animals on the state of animals. Vetch pre-treated with NPs of copper, iron and cobalt affects the growth of live weight of rabbits, increasing it by 12–16% relative to the control, while the main blood indicators were within the physiological norm. Therefore, NPs can be used in feed made of plants pre-treated with NPs of metals at concentrations up to 100 g t^{-1}. Moreover, the increased content of useful nutrients in such plants (Ampleeva, 2006) stimulates the growth and development of rabbits.

The effect of nanoparticles on the biological activity of soils and microorganisms that are sensitive to environmental changes has been studied. Metal nanoparticles have almost no effect on bacterial populations. The response to NPs of copper and zinc oxides is highly dependent on their concentration in the soil. Low oxide concentrations can stimulate bacteria that are thought to use resistance mechanisms to allow them to grow, but at high concentrations, population survival is significantly reduced. NPs in the range of up to 20 nm are much more reactive and dangerous. Oxide nanoparticles are more soluble and interact, which is especially characteristic of ZnO with membrane lipids and thiol groups of the enzyme and proteins, which are important for bacterial respiration, as well as transmembrane and intracellular transport. The generation of ROS (reactive oxygen species) plays a key role in this process, since damage to membranes, DNA and cellular proteins is the result of ROS.

The previous studies have considered the influence of nanoparticles on the biological activity of soils and microorganisms *Pseudomonas fluorescens*, Trichoderma koningii, *Bacillus cereus* and *E. coli M-17* (test system 'Ekolyum'), which are sensitive to environmental changes. There is some evidence of the effect of metal and metal complex nanoparticles and carbon nanotubes on bacterial populations (Bannikova 2017; Godymchuk, 2012). However, metal nanoparticles with certain physical-chemical characteristics studied in this work practically do not affect bacterial populations. The response of copper oxides and zinc to NPs is highly dependent on their concentration in the soil. Low concentrations of oxides can stimulate bacteria that are thought to use resistance mechanisms to allow them to grow, but at high concentrations, population survival is significantly reduced. When NPs reactivity is in the range of up to ~ 20 they are much more reactive and dangerous. Oxide nanoparticles are more soluble and interact, which is especially characteristic of ZnO with membrane lipids and thiol groups

of the enzyme and proteins, which are important for bacterial respiration, as well as transmembrane and intracellular transport. The generation of ROS plays a key role in this process, since damage to membranes, DNA and cellular proteins is the result of ROS.

Thus, in order to develop a unified approach to assessing the potential dangers of artificial nanoparticles, it is necessary to create an integrated system of phyto-toxicological studies.

The following tasks were set: 1. To reveal the patterns of morph physiological reactions of organisms of such ecological and functional groups as earthworms (*Lumbricina*), white outbred rats and Wistar rats on the effect of colloidal aqueous solutions of nanoparticles. 2. Given the possibility of penetration and bioaccumulation of NPs in tissues of higher plants, to evaluate the resulting biochemical and morph physiological effects. 3. To determine the environmental safety parameters of nanoparticles of different physical-chemical characteristics. The choice of these test objects was determined by the following criteria: a significant role in the functioning of terrestrial ecosystems, the prevalence of ecotoxicological studies in practice and the ease of growing in laboratory conditions.

MATERIALS AND METHODS

Physical-chemical properties of nanoparticles

Nanoparticles were obtained at RTU 'MISiS' by chemical precipitation of metal hydroxides from salt solutions, followed by their low-temperature reduction in a hydrogen stream with subsequent passivation (Dzidziguri et al., 2000; Novakova et al., 2001). Using a scanning electron microscope, the dispersion and morphology of the obtained metal nanoparticles were investigated. Physical-chemical properties of nanoparticles were determined by the following indicators: specific surface area (m^2 g^{-1}), size distribution of nanoparticles and form factor (Table 1). The specific surface area of the nanoparticles under study was measured by low-temperature nitrogen adsorption by BET using the Quantachrome NOVA 1,200e analyzer.

Table 1. Physical-chemical properties of nanoparticles

Parameter	Cu	Co	Zn	CuO	ZnO
Particle Size, nm	34–63	28–46	30–76	28–68	30–80
Specific Surface Area, m^2 g	6.5	52.1	5.7	90.5	37.9
Form Factor (ratio of the maximum size to the minimum one)	< 10	< 10	< 10	< 10	< 10
Solubility in Water wt. %	insoluble	insoluble	insoluble	insoluble	sparingly soluble
Solubility in Biological Fluids	< 1	< 1	insoluble	< 1	> 1
Charge	+	+	+	+	+
Aggregation Resistance	low	low	low	low	low
Hydrophobic Nature	+	+	+	+	+
Ability to Generate Free Radicals	low	low	low	revealed	revealed
Accumulation in Organs and Tissues	not found	not found	not found	revealed	revealed
Acute Toxicity	not hazard (class 4)	low-hazard (class 3)	low-hazard (class 3)	low-hazard (class 3)	low-hazard (class 3)

Toxic properties of nanoparticles

These studies were carried out in accordance with the Methodological Recommendations of the Pharmacological State Committee ('Guidelines for the experimental (preclinical) study of new pharmacological substances', Moscow, 2005, edited by R.U. Khabriev). Advanced development models of nanoparticles of copper, cobalt, iron, zinc, zinc oxide, copper oxide, sized 20–80 nm were used in the studies.

To establish the general toxic properties of the solution, white outbred rats were used. The animals were received from nursery 'Andreevka Branch of the State Center for Scientific Research of Biomedical Technologies of the Russian Academy of Medical Science'. They were grown on purpose and had not previously participated in experiments. The supplier of laboratory animals provides documents proving the last control of their health. The animals, newly arrived at the institute's vivarium, were kept in the quarantine and adaptation room for 14 days. During the quarantine period, their clinical indicators of health status were monitored. Animals were kept in polycarbonate cages, 5 animals each. Sawdust was use as litter. Animals were kept in the vivarium according to sanitary rules and on a standard diet in accordance with the Order of the Ministry of Health of the USSR No. 1045-73 dated April 6, 1973, The rules of laboratory practice and the Order of the Ministry of Health of the USSR No. 1179 dated October 10, 1983. Feeding was carried out in accordance with the Order of the Ministry of Health of the USSR No. 163 dated March 10, 1966 on the ration of laboratory animals, since January 1, 1979 the 'Temporary daily allowance of granular compound feeds for laboratory animals' adopted and approved by the Ministry of Health of the USSR on December 4, 1978 and following the guidelines 'Standardization of the ecological environment of laboratory animals by nutrition factor' (1980), Academy of Medical Science. Compound animal feedstuff extruded for laboratory animals (rats, mice, guinea pigs) GOST R 51849-2011 R.5 was delivered by LLC Labkorm, Moscow. The animals were watered from standard drinking bowls with tap water corresponding to GOST 'Drinking water'

The animals were kept in rooms with natural artificial lighting and controlled microclimate. Daily readings were taken from psychrometric hygrometer VIT-2 (all indications are documented). The temperature and humidity conditions were within normal limits: air temperature 20–22 °C and relative humidity 60–70%.

Preparation for the experiment was carried out in accordance with the instructions 'Toxicity test' GF XI. Before the experiment, food and water were taken from animals. Two hours later, they were weighed and divided into groups. The selection in groups was carried out arbitrarily by the method of 'random numbers', using body weight as a criterion. Individual body mass values did not deviate from the group average by more than 10%. Animals were weighed on a BP-05MS-3 0.5/BR scale (Russia). To conduct experiments on the acute toxicity of nanoparticles, white outbred rats weighing 190–220 g were used. 6 series of experiments were carried out, 48 groups of animals were formed, each of which consisted of 10 outbred rats. Their weight is indicated at the time of the preparation administration.

Nanoparticle bio-testing on representatives of the earthworm family

Objects of study were worms - representatives of the family of earthworms (*Lumbricina*), species: dung worm (*Eisenia fetida*) and White-bellied earthworm (*Octolasion lacteum*). Soil was taken from wheat cultivation sites. The test is considered

reliable according to GOST 33637-2015 when the following criteria are met for controls and experimental samples:

– at the end of the test, the total death during the absorption and elimination phases should not exceed 10% (for earthworms) or 20% (for enchitreides) of the total number of worms introduced into the test;

– the average weight loss for *Eisenia fetida* and *Eisenia andrei*, measured at the end of the absorption and elimination phases, should not exceed 20% compared to the initial wet weight (raw tissue mass).

A series of indicator cytochemical, cytomorphological, reproductive and restoration indicators of worms in contact with soils containing various concentrations of nanoparticles of various compositions and sizes was provided. The effect on the soil (substrate) was analyzed on the following soil options: 1 – a control sample of natural soil from areas where field tests were carried out; 2 – soil containing optimally permissible concentrations of 10 g t^{-1} of soil, 100 g t^{-1} and a maximum of 1,000 g t^{-1} of copper and cobalt NPs up to 20 nm; 3 – soil with copper or cobalt nanoparticles sized 30–80 nm; 4 – soil containing nanoparticles of copper and zinc oxides with a size of 20–80 nm, a concentration of 10 g t^{-1} and 100 g t^{-1}. All components were crushed, moistened and mixed until a homogeneous mass. At the end of the experiment, the worms were selected, washed with distilled water and then weighed. Then the bio-substrates were brought to a constant weight in an oven. Dried samples of soil and worm tissues were used to determine metals.

Determination of antioxidant enzyme activity

After cleansing the digestive tract, the tissues of the worms Eisenia fetida were homogenized with the help of a tissue homogenizer (QIAGEN, Germany). The homogenate was centrifuged for 18 minutes at 9,000 rpm, diluting to 10% solution. The resulting supernatant was diluted with a buffer mixture to 10% homogenate.

The content of lipid peroxidation products, malondialdehyde (MDA), as well as the activity of the key units of the antioxidant defence system (catalase and superoxide dismutase) was determined using a CS-T240 biochemical analyzer (Dirui Industrial Co., Ltd, China) in a homogenate of worm tissues using commercial Randox biochemical kits (USA). For this, hoods were prepared by homogenization in a buffer (Tris 50 mmol L^{-1}, DTT 1.0 mmol L^{-1}, EDTA 1.0 mmol L^{-1}, sucrose 250 mmol L^{-1}, pH 7.5), which was added in a ratio of 1:9. The activity of malonic aldehyde, catalase and superoxide dismutase was determined on a CS-T240 biochemical analyzer using commercial kits from Randox (USA). The activity of antioxidant enzymes was studied in *Eisenia fetida* worms under the action of Zn and zinc oxide nanoparticles sized 20–80 nm at various concentrations on natural soil. To evaluate potential acute and long-term effects, their effects were studied at a concentration of 1, 10, 100 and 1,000 g t^{-1} (g of nanoparticles per ton of soil). The effect of nanoparticles on growth, bioavailability and enzyme activity was determined. The worms were grown in horse manure without any medicine at 22 ± 2 °C. For each repetition, mature worms weighing 400–450 mg were selected, of which 9 groups were formed (n = 10). Group I included worms grown when adding zinc NPs at a concentration of 1 g t^{-1} of soil. Group II was connected with a concentration of 10 g t^{-1} of soil. Group III presupposed a concentration of 100 mg kg^{-1} of soil. Group IV was connected with a concentration of 1,000 g t^{-1} of soil. Group V included worms grown with the addition of zinc oxide nanoparticles at a concentration of 1 g t^{-1} of soil.

Group VI had a concentration of 10 g t^{-1} of soil. Group VII presupposed a concentration of 100 g t^{-1} of soil. Group VIII had 1,000 g t^{-1} of soil and group IX was the control without introducing NPs into the substrate.

Histological studies

Characteristics of the animals used and their conditions

Mature laboratory Wistar rats of both genders and weighing 200 ± 1 g were used in the studies. 96 females were involved in the experiment. All manipulations with laboratory animals were carried out in accordance with the legislation of the Russian Federation and met international principles of good laboratory practice (GOST R 33044-2014), taking into account recommendations for the management and use of laboratory animals (Guide for keeping ... 2001). During the experiment, the animals were kept in cages for rodents with a capacity of up to 13 individuals at a 12-hour light period, temperature of +22 °C and relative humidity of 40–60%. Autoclaved sawdust of deciduous tree species was used as litter. Standard granular feed Compound feed PK-120' specially developed for laboratory rats, mice and hamsters was used.

Five groups of animals, 8 animals each, were formed that received cobalt nanoparticles with a size of 20 nm, cobalt and copper nanoparticles with a size of 30–60 nm and copper and zinc oxides of 20–80 nm in size.

The animals' status observation was carried out within two weeks after the introduction of material with control of lethal action and such parameters of the general state of health as the intensity and nature of motor activity, the state of skin and hair, water and feed. The lethal effect of the introduced NPs was recorded by a number of deaths within the experimental groups of animals throughout the entire controlled period.

Before exposure, animals were kept in quarantine for 10 days. The studied materials were administered once intragastrically at a dose of 0.02, 0.2, 2.0 mg kg^{-1}. The control group was injected with distilled water. At the end of the control period, all animals were euthanized by dislocation of the cervical vertebrae (Mank, 1990). Then, the relative mass of visceral organs was calculated and histological studies were performed.

The liver, kidneys, adrenal glands, brain tissues, reproductive organs (tubes, uterus) were fixed in 10% formalin buffer solution, after which they were processed in a histological processor Tissue-Tek Xpress from SAKURA (Japan) and filled with homogenized paraffin medium for histological filling of tissues 'Meltex' company 'JLS Chemical' (Russia).

Slices with a thickness of 5–7 μm were obtained on a luge microtome 'MS-2' (Russia). For general purposes, connective and muscle tissues were stained with hematoxylin and eosin according to Van Gieson.

RESULTS AND DISCUSSION

Toxicological properties of nanoparticle additives

Nanoparticles were previously mixed with distilled water, kept in a plastic container in an ultrasonic bath for 20 minutes to achieve a uniform suspended state of particles in solution. Immediately after preparation, the suspension was administered to experimental animals once in the stomach using a probe in the form of a provided solution in an amount of 1 ml containing various dosages: 20, 40, 70, 100, 130, 160,

180 mg per animal. This was 1,000, 2,000, 3,500, 5,000, 6,500, 8,000, 9,000 mg kg^{-1} of the body weight and the control without additives.

To calculate the indicators of median lethal dose LD_{16}, LD_{50}, LD_{84}, the Miller-Teitner probit analysis method was used and GOST 12.0.007-76 was used to determine the hazard class.

As a result of studying the toxicological properties of nanoparticle additives, the following results were obtained:

• parameters of acute toxic effects with a single oral administration to white rats;

• parameters of toxic effects with repeated use of additives to white rats (chronic toxicity).

An experiment to determine chronic toxicity and cumulative properties was carried out in 3 series for 60 days using two methods (Lim, 1961; Yu.S. Kagan and V.V. Stankevich, 1968). In the first 5 days, each rat was injected 1/10; 1/20 or 1/50 of the previously established single doses of LD_{50}. Then, every subsequent 5 days, the dose increased 1.5 times from the previous daily administered dose. In the course of the experiment, the phenomena of toxicosis and death of animals were recorded and an autopsy of dead animals was performed.

For nanoparticles with a size of 20–80 nm, toxic characteristics were determined. Parameters of acute toxic effects after a single oral administration to white rats were as follows: LD_{50} (Zn NP) – 379.7 mg kg^{-1}, LD_{50} (ZnO NP) – 292.9 mg kg^{-1}, LD_{50} (Co NP) – 1233.3 mg kg^{-1}, LD_{50} (CuO NP) – 259.2 mg kg^{-1}, respectively, so additives were classified as moderately hazardous substances of hazard class 3. LD_{50} (Cu NP) – 7,000.0 mg kg^{-1}, LD_{50} (Fe NP) – 9,000.0 mg kg^{-1}, respectively, indicated additives belonging to low-hazard substances of hazard class 4 according to GOST 12.1.007-76.

Established chronic lethal doses were as follows: LD_{50} (Zn NP) chron. – 1,284.0 mg kg^{-1} of live weight, LD_{50} (ZnO NP) chron. – 1,183.8 mg kg^{-1}, LD_{50} (Co NP) chron. – 4,180.8 mg kg^{-1}, LD_{50} (CuO NP) chron. – 580 mg kg^{-1}, LD_{50} (Cu NP) chron. – 40,650.9 mg kg^{-1}, LD_{50} (Fe NP) – 56,000 mg kg^{-1}. The results were consistent with previously established hazard classes in experiments on the study of acute oral toxicity.

Biological and environmental safety of nanoparticles by the example of representatives of the earthworm family (*Lumbricina*)

If one compares the chemical method for analysing soil pollution, it shows the concentration of only the substances being determined, and the biological method using worms indicates the presence or absence of toxicity. The main soil load is derived from such pollutants as Cu, Zn, Co, Pb.

Table 2. The metal content in the soil during the experiment

	The content before the experiment, mg kg^{-1}	Content after 8 weeks of experiment, mg kg^{-1}, NP concentration 1,000 g t^{-1}	MPC, mg kg^{-1}
Cu	2.80 ± 0.03	2.9 ± 0.02	3.00
Zn	21.6 ± 0.022	24.0 ± 0.05	23.0
Co	4.60 ± 0.07	4.65 ± 0.04	5.04
Pb	5.40 ± 0.04	5.4 ± 0.03	6.00

The control soil contained these elements below the MPC and the indicators remained in this range for 3 days, 1, 4, and 8 weeks and did not depend on the composition of nanoparticles at the concentration range of 1–100 g t^{-1}. When the concentration of nanoparticles was 1,000 g t^{-1}, the indicators changed remaining in the MPC, excluding the zinc content (Table 2).

After the contact of nanoparticles with the soil, an increase in the weight of the worms (*Octolasion lacteum*) was gradually observed in the first, fourth, and eighth weeks (Fig. 1). The weight of the worms in the control variant was 200 mg, 240 mg, 604 mg, and 805 mg, depending on the time of the experiment. In soils where the content of Cu, Zn, Co nanoparticles was 10 g t^{-1} of soil, an increase in the mass of worms was observed and after 8 weeks it was higher by 28, 29, and 31%, respectively, relative to the control. After the 4th and 8th week the soil, where the content of Cu, Zn, Co nanoparticles was 1,000 g t^{-1} of soil, the mass of worms decreased from 10 to 12% compared with the control. At the same time, after the second week an increase in the mass of worms in soils with the content of ZnO and CuO nanoparticles of 10 g t^{-1} was only by 3 and 5%, respectively. After the 8th week, the mass of worms in this soil decreased by 25% and 45%, and in soils with a content of nanoparticles of 1,000 g t^{-1} the decrease was 46% and 58%, respectively. A similar pattern was observed for *Eisenia fetida*. For copper and zinc nanoparticles with sizes up to 20 nm an increase in the weight of worms was observed by 15% and 35% compared with the control after the 2nd week. After the 6th week the weight of worms decreased in soils where the content of nanoparticles was 10 g t^{-1} by 60% and 65%. The decrease after the 8th week amounted to 75% and in soils with a content of nanoparticles of 1,000 g t^{-1} the worms' death was observed.

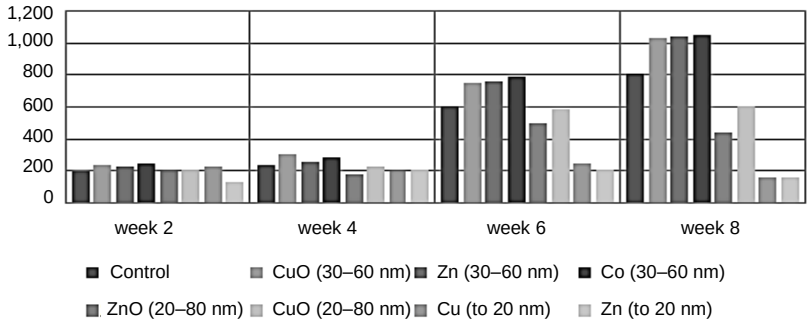

Figure 1. The change in the mass of worms during the experiment at a concentration of nanoparticles in the soil equal to 10 g t^{-1}.

After 5 weeks of the experiment the number of individuals and cocoons of all types of worms in the control soil did not change significantly. The survival rate of individuals was 97% and that of cocoons was 98%. When the content of Cu, Zn, Co, ZnO, CuO nanoparticles was 1–10 g ha^{-1}, the number of individuals, as well as their cocoons, did not change compared to the control. The number of individuals decreased by 15% and that of cocoons was 21% less at a concentration of Cu, Zn or Co nanoparticles of 1,000 g t^{-1} and by 24–29% for ZnO and CuO nanoparticles at a soil concentration of 100 g t^{-1}. The reproductive activity of worms, depending on environmental toxicity, is a reliable indicator of biotesting. It should be noted that the main parameters in the study of the propagation of worms are: the dynamics between the number of individuals and cocoons obtained from them and the number of hatched young individuals from these cocoons. When studying the relationship between the number of cocoons and the appearance of young worms, it was revealed in the third week, that the number of young worms increased on average by 30% compared with the control soil when contact with

metal nanoparticles (1–100 g t^{-1}) and by 5% when contacting oxides. At a higher concentration of oxides in the soil, the number of cocoons decreased with increasing the age of worms, and at the 6th week of ontogenesis they cease to postpone them.

When the concentration of nanoparticles was 100 g t^{-1} of soil the number of large granules in amebocytes increased by 0.6% and small granules decreased by 1.9%. A similar trend remained unchanged for the dung worm. For oxides at a concentration of 1–10 g t^{-1}, the cytochemical parameters in hemolymph cells were as follows: for large granules, an increase of 1.5% was observed and for small granules a decrease of 2–3% was noticed. At a concentration of more than 100 g t^{-1} in the amebocytes of the worms, compared with the norm, the number of large granules increased sharply and small granules practically disappeared. When evaluating the number of large and small glycogen granules in amoebocytes of worms exposed to anthropogenic effects of oxide nanoparticles, it was noted that their change had some negative effect, which was apparently associated with a higher solubility of copper oxides and especially zinc, as well as with an increase in the amount of these metals in the soil.

Determination of the activity of antioxidant enzymes in *Eisenia fetida* worms

To confirm the different toxicities of zinc and zinc oxide, the activity of the antioxidant enzymes of *Eisenia fetida* worms was studied. The tissues of the worms (after cleaning the digestive tract) were mixed with a homogenizer (QIAGEN, Germany).

The homogenate was centrifuged for 15 minutes at 10,000 rpm, diluting to 10% solution.

The activity of malonic aldehyde catalase and superoxide dismutase was determined on a CS-T240 biochemical analyzer using commercial kits from Randox (USA). The activity of antioxidant enzymes in *Eisenia fetida* worms was studied under the action of Zn nanoparticles and zinc oxide with a size of 20–80 nm, in natural soil. To evaluate the potential acute and long-term consequences of their impact, the effect of nanoparticles on growth, bioavailability and enzyme activity was determined at a nanoparticle concentration of 1, 10, 100 and 1,000 g t^{-1} of soil.

On the 30th day of exposure to zinc oxide nanoparticles, the development of oxidative stress was manifested in a sharp increase in the level of enzymes.

When a dose of Zn NP of 100 mg kg^{-1} the maximum level of malondialdehyde (MDA), the main indicator of lipid peroxidation, was higher than the control by 18%. At low and medium concentrations (1–10 g t^{-1}), the activity of MDA was in the range of 8–12% relative to the control values. The activity of superoxide dismutase (SOD) and catalase enzymes for zinc oxide nanoparticles increased, but deviations from the control were less than 30% and reached 70–120%. Evaluation of the antioxidant status of antioxidant enzymes, superoxide dismutase and catalase showed that under the influence of zinc NPs there was a slight increase in SOD at concentrations of 10 and 100 g t^{-1}, followed by a decrease of 32% at a dose of 1,000 g t^{-1}, respectively. An increase in load leads to inhibition of enzymatic reactions. There is a decrease in catalase activity by 10% relative to the control. Against the background of an increase in the level of antioxidant protection, the worm's body is able to withstand the amount of zinc NPs much higher than 100 g t^{-1} and, consequently, for metal NPs of 35–60 nm in size the stability limit of adaptation mechanisms is a concentration significantly exceeding 100 g t^{-1} and for oxides it exceeds 10 g t^{-1}.

The bio-accumulation of nanoparticles in the structure of worms depends on the level of nanoparticles in the soil substrate and on the ability of metal ions to return to the soil substrate. The level of zinc bio-accumulation in the presence of zinc and zinc oxide is 1.3 and 18.02, respectively, at a dose of 100 g t^{-1}, whereas it is 2.3 at 10 g t^{-1}. The degree of absorption and the rate of accumulation of metals in the body of the worms increased depending on the level of NP dose in the soil substrate. In particular, the degree of absorption in the control corresponded to a value of 0.48 mg % at 100 g t. With an increase in the concentration of zinc and zinc oxide, respectively, to 1,000 g t^{-1}, the rate of accumulation and degree of absorption of zinc was 2.3% and 29.8%, respectively, more than the control. The highest bio-accumulation value was found at a dose of oxide nanoparticles of 1,000 g t^{-1}, where the absorption and accumulation rates increased linearly with increasing the load on the soil substrate. It can be argued that the nanoparticles of oxides accumulate in structures of living systems, complicating their development and reducing survival.

Cytotoxicity of nanoparticles of copper, cobalt and oxides of copper and zinc for rats

With the introduction of suspensions of NPs of copper, cobalt and their oxides in a dose of 0.02 mg kg^{-1} of live weight to rats, blood hematological and biochemical parameters were studied for a month.

The analysis results showed that cobalt (Co NP) and copper (Cu NP) nanoparticles with particle sizes of up to 20 nm and 35–65 nm, respectively, did not significantly affect the blood hematological parameters of experimental animals compared with the control group. A slight change in the myelogram was observed: for example, leukocytes increased by 38% in the case of Cu NPs and by 39.3% in the case of Co NPs compared to the control, remaining within the normal range, which can be explained by stress during blood sampling. The percentage of components has not changed.

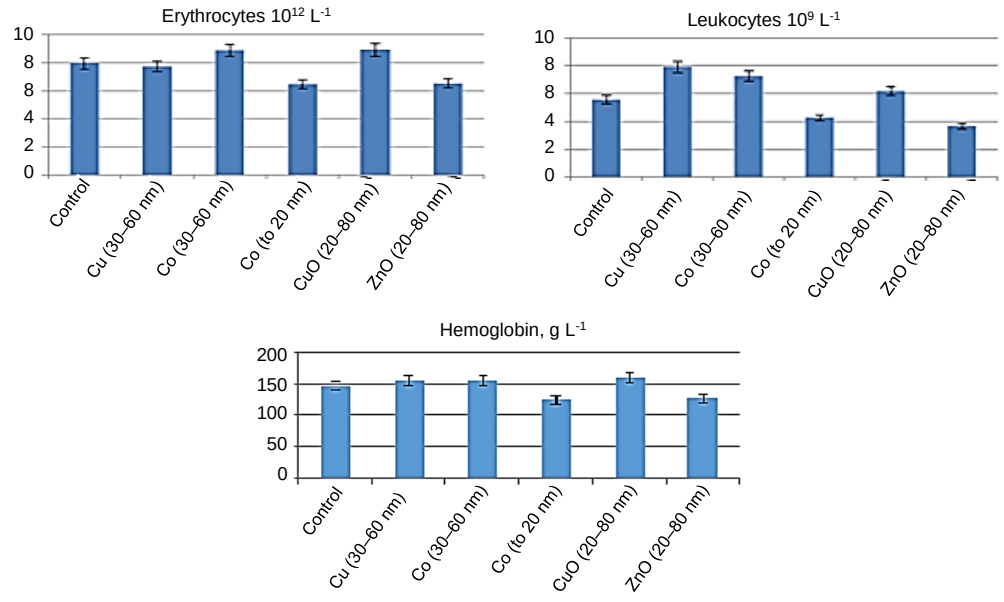

Figure 2. Hematological blood parameters of experimental animals.

When ZnO NPs (particle size 20–80 nm) were introduced into the diet of rats, the number of erythrocytes, leukocytes and hemoglobin decreased by 17.7% and 18.5%, 34.1% and 20.5%, 13.6% and 15%, respectively, compared with the control (Fig. 2). The total volume of erythrocytes, their distribution in blood and lymphocytes increased by 13.9%, 59.7% and 18.5%, respectively. ESR increased relative to the control by 5.5–8 times, which indicated the toxicity of ZnO and Co NPs (to 20 nm).

The introduction of CuO NPs (particle size 20–80 nm) contributed to an increase in all parameters (Fig. 2). So, erythrocyte distribution in blood increased by 17.7%, hemoglobin by 4.8% and segmented neutrophils by 18.75%. All NPs, except cobalt sized 20 nm and zinc oxide (20–80 nm) did not have any negative effect on morphological parameters of blood.

Nanoparticles of copper and cobalt with a size of 35–60 nm changed the biochemical parameters of blood approximately to the same extent within the physiological norm (Figs 3–8). NPs of copper and cobalt caused an increase in creatinine by 18.5% and 18.05% and glucose by 25.2% and 26.0%, respectively. The decrease in urea was 11.0% and 11.8%, the total bilirubin was 23.0% and 22%, respectively. The increase was insignificant and indicated the absence of toxic effects of NPs on hepatocytes.

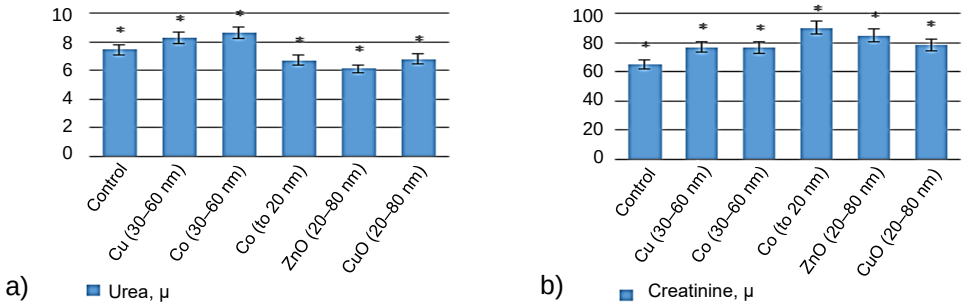

Figure 3. The effect of nanoparticles on the content of urea (a) and creatinine (b) in rats' blood (hereinafter, in section *, options are indicated in which a significant difference with control values is noted at $p < 0.05$).

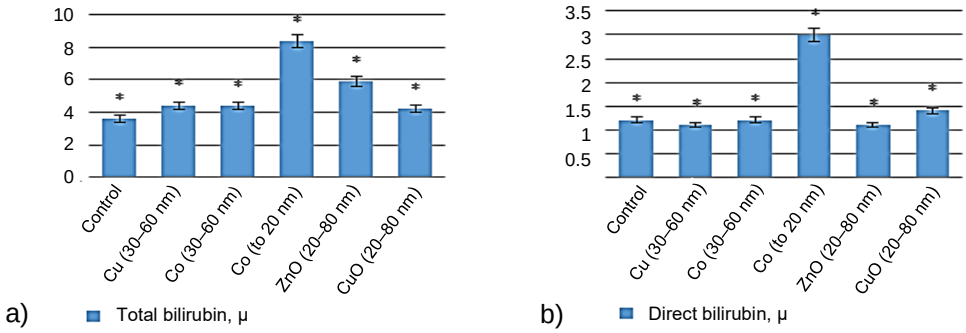

Figure 4. The effect of nanoparticles on the content of total bilirubin (a) and direct bilirubin (b) in rats' blood.

To determine the effect of nanoparticle sizes, rats were injected with Co NP, 18–20 nm in size (Figs 3–8). For this group there was an increase in comparison with the control values: creatinine by 38.46%, total bilirubin by 133.3%, direct bilirubin by 60.0%, glucose by 17.5%, albumin by 39.3% and cholesterol by 31.3%. AST increased by 15%. ALT decreased by 47.5% and de Ritis coefficient decreased by 2.3 times. At the same time, total protein and urea decreased by 5.8% and 9.8%, respectively. All these data indicate the toxic effect of Co NPs (to 20 nm) on internal organs (liver, kidneys). Such nanoparticles are extremely reactive and dangerous for living systems.

For CuO NPs the values of the parameters were as follows: urea decreased by 8.7%, AST increased by 14% and ALT became 55% lower, de Ritis coefficient decreased by 20%, relative to the control. Total bilirubin increased by 16.7%, alkaline phosphatase by 38.7%, total protein by 7.42% and globulins by 6% (Figs 3–8).

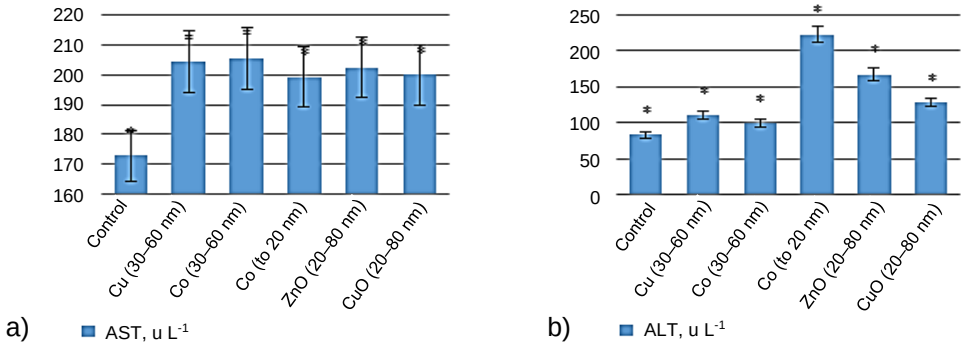

Figure 5. The effect of nanoparticles on the content of AST (aspartate aminotransferase) (a) and ALT (alanine aminotransferase) (b) in rats' blood.

When rats got ZnO NPs, urea decreased by 18%, total protein by 12.8% and the globulin fraction by 18.4%. The content of alkaline phosphatase increased by 4 times, AST by 17%, ALT by 2 times and de Ritis coefficient decreased by 1.7 times, which indicated the toxic effect of NPs on bone tissue, liver and kidney (Figs 3–8).

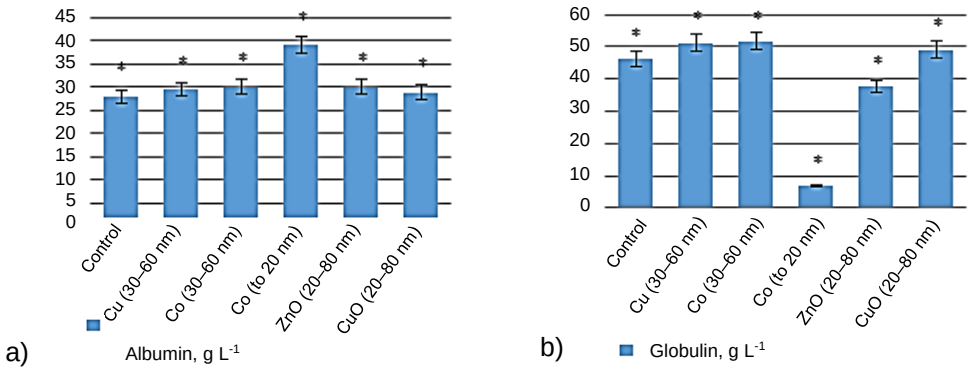

Figure 6. The effect of nanoparticles on the content of albumin (a) and globulin (b) protein fractions in rats' blood.

When comparing the effect of NPs of cobalt and copper, sized 35–60 nm, on morphological and biochemical parameters of blood, one can say they have a positive effect on the animal's organism, stimulating metabolic processes. Cobalt NPs, having a particle size of up to 20 nm, have a toxic effect, so they are dangerous for living systems. The effect of copper oxide NPs is not toxic, but it inhibits the metabolic processes of both plants and animals. Zinc oxide has a toxic effect and this is possibly due to higher solubility of zinc oxide in biological fluids.

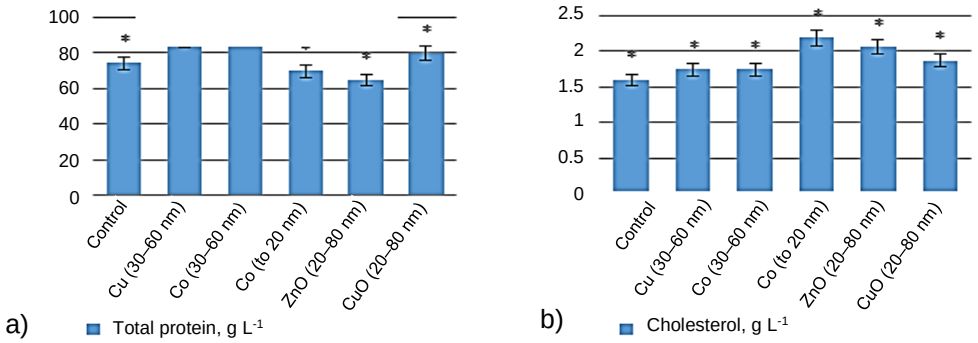

Figure 7. The effect of nanoparticles on total protein (a) and cholesterol (b) in rats' blood.

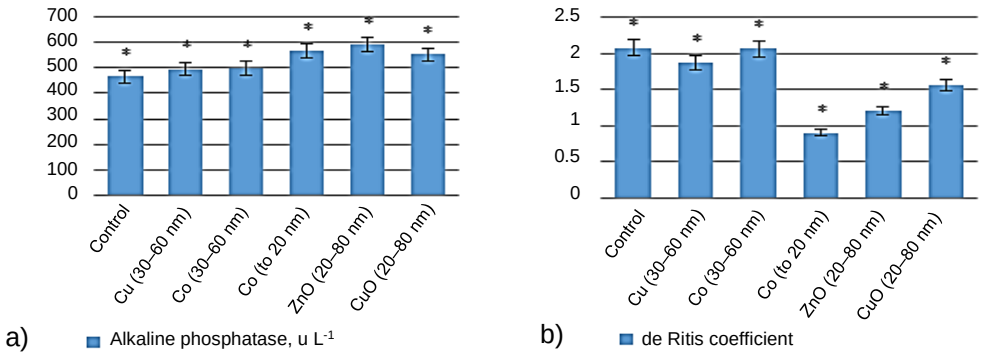

Figure 8. The effect of nanoparticles on the activity of alkaline phosphatase (a) in rats' blood and on the value of de Ritis coefficient (b).

Determination of the level of malondialdehyde and the activity of superoxide dismutase showed a different ratio for all studied groups. The MDA content in the group getting metal NP corresponds to the control group and is less than in the groups treated with oxides NP and especially cobalt, up to 20 nm in size. A decrease in the content of MDA indicates a decrease in the level of lipid peroxidation processes.

A change in the level of malondialdehyde, one of the final products of the lipid peroxidation process, allows to judge the intensity of processes that inevitably increase in pathogenic conditions. A decrease in the MDA level for 35–60 nm nanoparticles of copper and cobalt indicates a decrease in free-radical oxidative processes, i.e. a decrease in the level of oxidative stress, relative to the effect of cobalt oxide NPs and cobalt NPs, 20 nm in size.

Table 3. The content of malondialdehyde and the activity of superoxide dismutase in plasma and hemolysates of rat erythrocytes with the introduction of NP in a dose of 0.02 mg kg^{-1}

Indicator	Malondialdehyde, mol ml Hb		Superoxide dismutase, c.u. g Hb	
	Hemolysates	Plasma	Hemolysates	Plasma
With natural pathomorphism	17.8 ± 1.5	2.10 ± 0.32	1.45 ± 0.2	13.04 ± 0.73
NP of copper, size 35–60 nm	17.0 ± 2.6	2.04 ± 0.01	1.42 ± 0.3	12.32 ± 0.54
NP of cobalt, size 35–60 nm	17.1 ± 1.8*	2.0 ± 0.021	1.40 ± 0.41	12.42 ± 0.65
NP of copper oxide, size 20–80 nm	18.0 ± 2.6	2.09 ± 0.01	1.42 ± 0.3*	13.09 ± 0.65
NP of zinc oxide, size 20–80 nm	19.1 ± 2.6	2.36 ± 0.01	1.35 ± 0.3	13.45 ± 0.65
NP of cobalt, size 20 nm	19.5 ± 2.2	2.8 ± 0.5	1.33 ± 01	14.06 ± 1.01

*-$P \leq 0.05$.

The decrease in SOD activity against the background of an increase in the MDA level (Table 3) may indicate a decrease in the protective mechanisms of the cell, which is typical for the action of zinc oxide nanoparticles, 20–80 nm in size and cobalt NPs, sized 20 nm, at a concentration of 0.2–2.0 mg kg^{-1}. In this experiment, under the influence of copper and cobalt nanoparticles with a size of 35–60 nm, SOD decreases proportionally with a decrease in MDA, which suggests a decrease in the number of superoxide anions on the cell surface, i.e. a decrease in the intensity of peroxide oxidation processes.

Histological studies

For histological studies, 8 animals were selected. Samples were taken from 1.5 to 2.0 cm in size. A 10.0–12.0% formalin solution was used to fix the material. Samples were filled in paraffin blocks (7–8 days). Sections with a thickness of 5–7 μm were obtained on a luge microtome 'MS-2' (Russia) and stained with hematoxylin and eosin.

Some moderate expansion of the vessels of the venous channel with their pronounced plethora was noted in the liver of female rats treated with Cu NPs sized 35–60 nm at a dosage of 2.0 mg kg^{-1}. Some blood vessels of rats treated with 2.0 mg kg^{-1} CuO NPs were empty. Dystrophic processes developed in hepatocytes with the appearance of grains and vacuoles in the cytoplasm of cells. A moderate polymorphism of hepatocyte nuclei was observed, both in size and in the degree of chromatin staining.

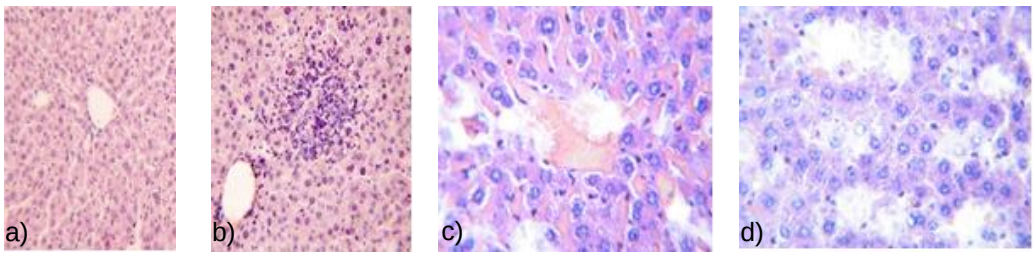

Figure 9. Histological studies of rats' liver: a – control, mp ×100; b – pathological changes in the experimental group, ZnO, mp ×400; c – expansion of the central veins and centrolobular sinusoids; d – focal necrosis of hepatocytes, ZnO, mp ×640.

Pathological changes were found in kidney tissues of animals in groups receiving Co NPs sized 20 nm and CuO and ZnO NPs sized 20–80 nm (Fig. 9). These included

congestive plethora of central veins (b) and expansion of the central veins and centrolobular sinusoids (c). One can see multiple focal necrosis of hepatocytes (d). However, in the case of cobalt with a size of 35–60 nm, the liver was characterized by plethora of central and portal veins, moderately expressed focal necrosis of hepatocytes.

In all experimental rats treated with nanoparticles of zinc, copper and cobalt oxides sized 20 nm the brain layer and a glomerular zone of the adrenal glands were with protein dystrophy, which was possibly associated with a decrease in the content of mineral corticoids in them. After NPs of copper and cobalt, sized 35–60 nm, the rats had moderate protein glomerular dystrophy. The reproductive function (tubes, uterus) in all groups, including the control, did not have gross violations.

Noticeable changes were detected in kidney tissues of animals in groups receiving cobalt NPs sized 20 nm and copper and zinc oxides of 2.0 mg kg^{-1} (Fig. 10). For the kidneys of the experimental groups (Fig. 10: 2, 3, 4), plethora of the capillary network and veins of the cortical substance was observed. In all series of experiments, the histo-structural organization of the proximal tubules is disrupted. This include multiple foci with turbid swelling of the nephocyte cytoplasm with fine granularity, a flattened form of nephrocytes, pycnosis of the nuclei and a large, filled lumen. In addition, in all series of experiments, one of the types of disturbance is observed. This is granular degeneration of cellular protein metabolism due to the decay of lipoprotein complexes, which form the basis of the membrane structures of the cell, primarily the mitochondria and the endoplasmic reticulum. The pronounced plethora of capillaries of the renal corpuscles and capillaries of the peritubular network found in all series can be the cause of granular dystrophy (Chen et al., 2007; Serrano et al., 2015).

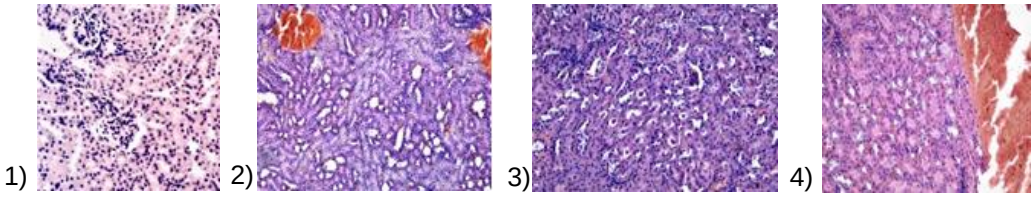

Figure 10. Histological studies of rats' kidneys in the control (1) mp ×400 and experimental groups at a nanoparticle concentration of 20 mg kg^{-1}: copper oxide (2); zinc oxide (3); cobalt (4). Stained with hematoxylin and eosin mp 10×16×160.

The observed effects were dose dependent 0.02, 0.2, 2.0 mg kg^{-1}. At the maximum dosage of cobalt NPs, 20 nm in size, pathological changes were manifested on the macroscopic level. The rats treated with NPs of metals and copper oxide in the same dosage did not have such violations.

The effect of nanoparticles on living systems depends on many factors. Important factors of their biological activity are the chemical interaction of nanoparticles with a liquid medium and a change in the pH of the medium due to the high reduction ability (Aleksanyan et al., 2005). These factors increase the permeability of membranes for nanoparticles, contributing in certain conditions to their bio-accumulation, which depends on the information (those properties) that particles of different sizes, composition and physicochemical properties possess (Auffan et al., 2009; Nel et al., 2009). When studying the dependence of the effect of nanoparticles on the oxidative

modification of proteins it was established that there was a decrease in the possibility of renewal of thymic tissue proteins due to low activity of cellular protease systems in groups of rats receiving nanoparticles of copper and zinc oxides at doses of 0.001 and 0.1 mg kg^{-1} (Abalenikhina, 2012), which directly depended on the activity of the biosynthetic mechanism of the cell. Histological studies in rats receiving 2.0 mg kg^{-1} of copper oxide and cobalt NPs sized 20 nm and zinc oxide NPs sized 20–80 nm showed that there was a change in nuclear cytoplasmic ratios in hepatocytes. There was moderate polymorphism of the hepatocyte nuclei, 'perforated nuclei' and dystrophy. In the cells of the kidneys and brain, protein dystrophy and pycnosis of the nuclei were noted, which mainly indicated some violation of the permeability of the nuclear membrane and indicated the decay of nucleoproteins and the release of nucleic acids. In addition, there was one type of violation in all the experiments, i.e. granular degeneration of cellular protein metabolism. All this indicated the influence of nanoparticles to varying degrees on the metabolism of protein synthesis and, in particular, on DNA.

CONCLUSIONS

To create environmentally friendly norms of nanoparticles in contact with biological objects, it is first necessary to determine the effects of nanoparticles on microorganisms, invertebrates (worms), plants and animals, studying their effect in the soil - plant - animal system. In this case, it is necessary to take into account the chemical composition and physical parameters of low frequencies, biocompatibility and bioaccumulation in the presence of the effect of 'low doses'. Nanoparticles are exposed to all components of a living organism, including bio-macromolecules, hormones, enzymes, especially cell membranes. Influence on the membrane structure leads to a change in the functional state of the cell, which changes the mechanism of action of nanoparticles depending on their concentration, structure and size.

Nanoparticles of copper, zinc and cobalt oxides belong to the III moderate toxicity class, but they accumulate in living systems, prolonging the time of interaction with them, which affects the survival of microorganisms, a decrease in the enzymatic activity of invertebrates, plants and animals (mice, rats, rabbits) biological, biochemical parameters of blood, the destruction of the protein structure and a decrease in the ability to update tissue proteins, which is confirmed by histological studies of internal organs.

Oxide nanoparticles accumulate in a living organism, exhibit toxic properties, lower the activity of enzymes and hormones and are transferred along trophic chains, which is not typical for metal nanoparticles.

Small nanoparticles (less than 20 nm) are characterized by a large interface. Such nano-objects exhibit high physical-chemical activity and are safe only at very low concentrations. Representatives of the family of earthworms, mice, rats are exposed to their negative effect, caused not by the toxicity of the particles themselves, but by a destructive effect on all metabolic processes and this leads to the accumulation of radicals (oxidation products) and the destruction of cell membrane proteins. Therefore, talking about favorable concentrations is impossible, they are dangerous.

ACKNOWLEDGEMENTS. This work was financially supported by the Russian Foundation for Basic Research in the framework of research project No. 18-33-00510.

REFERENCES

Abalenikhina, Yu.V., Fomina, M.A., Churilov, G.I. & Ivanycheva, Yu.N. 2012. Oxidative modification of rat thymus proteins under the influence of copper in ultrafine form. *Fundamental research* **11–6**, 1315–1319.

Aleksanyan, A.Yu., Podobaev, A.N., Reformatskaya, I.I. & Kiselev, V.D. 2005. Regularities of the initial stages of iron ionization in neutral environments. *Condensed matter and interphase boundaries* **7**(3), 329–334 (in Russian).

Alekseeva, O. 2007. A New Discipline - Nanotoxicology. *Promising Technologies* **14**(19) 2–4.

Ampleeva, L.E. 2006. *Physiological state of rabbits when introduced vetch grown using ultrafine powders of iron and cobalt into the diet.* Abstract of the dissertation for the degree of Candidate of Biological Science, Ryazan, Ryazan State Agricultural Academy, 23 pp. (in Russian).

Antoņenko, K., Duma, M., Kreicbergs, V. & Kunkulberga, D. 2016. The influence of microelements selenium and copper on the rye malt amylase activity and flour technological properties. *Agronomy Research* **14(**S2), 1261–1270.

Argentel-Martínez, L., Garatuza-Payán, J., Arredondo, T. & Yépez, E.A. 2019. Effects of experimental warming on peroxidase, nitrate reductase and glutamine synthetase activities in wheat. *Agronomy Research* **17**(1), 22–32.

Arutyunyan, A.V., Dubinina, E.E. & Zybina, N.N. 2000. *Methods for assessing free radical oxidation and the antioxidant system of an organism*. SPb., IKF Foliant, pp. 93–94.

Auffan, M., Rose, J., Bottero, J-Y., Lowry, G.V., Jolivet, J-P. & Wiesner, M.R. 2009. Towards a definition of inorganic nanoparticles from an environmental, health and safety perspective. *Nanotechnology* **4**, 634–641. https://doi.org/10.1038/nnano.2009.242

Bannikova, D.A., Kononenko, A.B. & Lobanov, A.V. 2017. The effect of metal and metal complex nanoparticles on bacterial populations. *Chemical Safety* **1**(2), 88–96.

Bogatyrenko, T.N., Redkozubova, G.P., Konradov, A.A. 1989. Influence of organic peroxides on the growth of cell cultures of higher plants *Biophysics* **34**(26), 327–329.

Burlakova, E.B., Boykov, P.Ya., Panina, R.I. & Karcev, V.G. 1996. The bimodal effect of picolinic acid derivatives on the germination rate of wheat and peas. *Izv. RAS. Ser. Biol*. **1**, 9–45.

Chen, Zh., Meng, H., Yuan, H., Xing, G., Chen, Ch., Zhao, F., Wang, Y., Zhang, Ch. & Zhao, Yu. 2007. Identification of target organs of copper nanoparticles with ICP-MS technique. *J. Radio and Nucl. Chem*. **272**(3), 599–603. doi: 10.1007/s10967-007-0631-1

Churilov, G.I. 2009. Herald of SamSU. *Nat. Sc. Series* **6**(72), 206–212.

Churilov, G.I. 2010. Ecological and biological effects of nanocrystalline metals. Dis. Dr. of Biol. Sc., Balashikha, 331 pp.

Churilov, G.I., Polischuk, S.D., Kutskir, M.V., Churilov, D.G. & Borychev, S.N. 2015. Activators of Biochemical and Physiological Processes in Plants Based on Fine Humic Acids. *IOP Conf. Ser.: Mater. Sci. Eng.* **98**.

Churilov, G.I., Polischuk, S.D., Kuznetsov, D., Borychev, S.N., Byshov, N.V. & Churilov, D.G. 2018a. Agro ecological grounding for the application of metal nanopowders in agriculture. *Int. J. Nanotechnol* **15(**4), 258–279.

Churilov, G.I., Churilov, D.G., Borychev, S.N., Byshov, N.V., Churilova, V.V. & Polischuk, S.D. 2018b. Plants Nutrition and Growth Stimulation with the Help of Nanotechnologies. *Int. J. Nanotechnol*. **7**(4.36), 231–236.

Churilov, D., Churilova, V., Stepanova, I., Polischuk, S., Gusev, A., Zakharova, O., Arapov, I. & Churilov, G. 2019. Size-dependent biological effects of copper nanopowders on mustard seedlings. *IOP Conf. Series: Earth and Environmental Science.* 012008, IOP Publishing, 392 pp. doi:10.1088/1755-1315/392/1/012008

Dzidziguri, E.L., Kuznetsov, D.V., Lyovina, V.V. & Sidorova, E.N. 2000 Perspective materials 6 Forestry 2019 *IOP Conf. Series: Earth and Environmental Science*, 7–92.

Edgington, A.J., Roberts, A.P., Taylor, L.M., Alloy, M.M., Reppert, J., Rao, A.M., Mao, J. & Klaine, S.J. 2010. The influence of natural organic matter on the toxicity of multiwalled carbon nanotubes. *Environ. Toxicol. Chem* **29**(11), 2511–8. doi: 10.1002/etc

Elsaesser, A. & Howard, C.V. 2012. Toxicology of nanoparticles. Adv Drug Deliv Rev. **64**(2), 129–37. doi: 10.1016/j.addr.2011.09.001

Folmanis, G.E. & Kovalenko, L.V. 1999. Ultradispersed metals in agricultural production. Moscow, IMET RAS, 80 pp.

Godymchuk, A.Yu., Savelyev, G.G. & Zykova, A.P. 2012. *Ecology of Nanomaterials*. Ed. by L.N. Patrikeeva and A.A. Revina. Moscow, BIN. Laboratory of Knowledge, 272 pp.

GOST 33637-2015 Test methods for chemical products that are hazardous to the environment. Bioaccumulation in earth worms. 2015.

GOST 33044-2014. Principles of good laboratory practice.

GOST 12.1.007-76 System of labor safety standards (SSBT). Harmful substance. Classification and General safety requirements.

Karpenko, V., Pavlyshyn, S., Prytuliak, R. & Naherniuk, D. 2019. Content of malondialdehyde and activity of enzyme glutathione-S-transferase in the leaves of emmer wheat under the action of herbicide and plant growth regulator. *Agronomy Research* **17**(1), 144–154.

Mank, M. 1990. Developed Mammal Biology: Methods. Moscow, Mir, 406 pp.

Nel, A.E, Mädler, L., Velegol, D., Xia, T., Hoek, E.M.V., Somasundaran, P., Klaessig, F., Castranova, V. & Thompson, M. 2009. Understanding biophysico-chemical interactions on nanobiodevice. *Nature Materials* **8**, 543–557. https://doi.org/10.1038/nmat2442

Novakova, A.A., Kiseleva, T.Y., Lyovina, V.V., Kuznetsov, D.V. & Dzidziguri, E.L. 2001. Low temperature formation of nanocrystalline Fe-Mo and Fe-W compounds. *J. of Alloys and Compounds* **317**, 423–427.

Oberdörster, G., Oberdorster, E. & Oberdorster, J. 2005. Nanotoxicology: An Emerging Discipline Evolving from Studies of Ultrafine Particles. *Environmental Health Perspectives* **7**(113) 823–839.

Polischuk, S., Fadkin, G., Churilov, D., Churilova, V. & Churilov, G. 2018. The stimulating effect of nanoparticle suspensions on seeds and seedlings of scotch pine (pinus sylvéstris). Forestry, *IOP Conf. Series: Earth and Environmental Science* **226**, 012020 doi:10.1088/1755-1315/226/1/012020

Rajput, V., Minkina, T, Suskova S., Mandzhieva, S., Tsitsuashvili, V., Chapligin, V. & Fedorenko, A.2018. Effects of Copper Nanoparticles (CuO NPs) on Crop Plants: a Mini Review *BioNanoSci*. **8**, 36. https://doi.org/10.1007/s12668-017-0466-3

Samoylova, M.V., Churilov, D.G., Nazarova, A.A., Polischuk, S.D. & Byshov, N.V. 2017. Biologically Active Nanomaterials in Potato Growing. *Nano Hybrids and Composites* **13**, 91–95. doi: 10.4028 /www.scientific.net /NHC.13.91

Serrano, D.R., Lalatsa, A., Auxiliadora Dea-Ayuela, M., Bilbao-Ramos, P.E., Garrett, N.L., Moger, J., Guarro, J., Capilla, J., Paloma Ballesteros, M., Schätzlein, A.G., Bolás, F., Torrado, J.J. & Uchegbu, I.F. 2015. Oral Particle Uptake and Organ Targeting Drives the Activity of Amphotericin B Nanoparticles. *Molecular Pharmaceutics* **12**(2), 420–431 doi: 10.1021/mp500527x

Stepanova, I.A., Polischuk, S.D., Churilov, D.G., Churilova, V.V., Obidina, I.V. & Churilov, G.I. 2019. The biological activity of cobalt and zinc oxide nanoparticles and their bioaccumulation by the example of vetch. *Herald of Ryazan State Agrotechnological University Named after P.A. Kostychev* **1**(41), 62–68 (in Russian).

Voronkov, M.G., Dolmaa, G., Tserenpil, C.X., Ugtakhbayar, O & Chimidtsogzol, A. 2005. Stimulating the germination of barley seeds in micromolar aqueous solutions of silatran and cresacin. *Report RAS* 404 562–564.

Zaytsev, S.V., Efanov, A.M. & Sazonov, L.A. 1999. General laws and possible mechanisms of action of biologically active substances in ultra-low doses. *Chem. J*., **5**, 28–33.

Agronomy Research **18**(3), 1992–2003, 2020
https://doi.org/10.15159/AR.20.179

Different proportion of root cutting and shoot pruning influence the growth of citronella plants

T.M. Daflon[1], C.M. Hüther[1,*], D. Cecchin[1], C.M.P.P. Santos[1], J. Borella[2], L.F. Carvalho[1], N.P.C. Correa[1], J.R. Oliveira[1], D.M. Correia[1], C.R. Pereira[1] and T.B. Machado[1]

[1]Federal Fluminense University. Postgraduate Program in Biosystems Engineering - Department of Agricultural Engineering and Environment. Street Passo da Pátria, n.156, São Domingos, Zip Code: 24210-240, Niterói- RJ, Brazil
[2]Federal University of Rio Grande. Institute of Biological Sciences, Zip Code: 96203-900, Rio Grande, RS, Brazil
[*]Correspondence: cristinahuther@yahoo.com.br

Abstract. Environment concern, sustainable products demand, and natural components conscious are currently global movement factors. Related to the global movement factors, citronella grass (*Cymbopogon nardus* L.) is being widely used in folk medicine, and has insect repellent activity, fungal and bactericidal action. Its essential oil has high content of citronellal, citronellol, geraniol. The essential oil is mostly extracted from leaves which turns this plant with high commercial demand. However, to obtain the best therapeutic quality and productivity of medicinal plants, which culminates in greater quantity and quality of the active compounds, the proper management of the crop is fundamental, as several factors can interfere during its growth and development. Thus, we analyzed the growth of citronella plants submitted to different levels of shoot and root cuts. Five different proportions of root pruning (0, 25, 50, 75, 100%), after 145 days of seedling planting and four cuttings in the shoots: blunt; a cut at 145 DAP (days after planting) along with the root cut; a cut at 228 DAP; and cuts at 145 and 228 DAP (two cuts). Four harvesting for dry matter accumulation and photoassimilate partition data were performed. The treatment with 100% root cut, but without leaf cut, increased the total dry mass accumulation of the plant in relation to the other treatments, for the last analysis period, demonstrating a recovery. Thus, the application of two leaf cuts or no leaf cutting within the 100% root cut treatment for leaf dry mass accumulation is more effective when compared to the blunt root treatment.

Key words: pruning, citronella growth, *Cymbopogon nardus* L., medicinal plant, photoassimilates, stress root.

INTRODUCTION

Concern for the environment and the quest to consume sustainable products with the conscious use of natural components is a growing movement worldwide (Chen et al., 2019; Xiong et al., 2019; Hatanaka, 2020; Yang et al., 2020). The research extends to several areas such as: medicines, cosmetics and food (De Hooge et al., 2018; Kozlowska et al., 2019). In Brazil, the juice and tea market grow 15% a year. Brazil has also stood

out in the market for products for hygiene, cosmetics and perfumes and has grown over 20% in exports over the last years (Corrêa Junior & Scheffer, 2013).

Thus, the species known as citronella grass (*Cymbopogon nardus* L.), is a plant of great interest as a raw material for natural products production (Kačániová et al., 2017; Silva & Ricci-Júnior, 2020). Citronella is a perennial species that fully develops in warm environments with fertile and well-drained soils, in addition to a large amount of biomass production, similarly to plants with C_4 metabolism (Sivashanmugam et al., 2009; Faria et al., 2018; Zhang et al., 2019).

The essential oil (EO) produced on leaves of citronella grass has several properties, such as repellent effect, especially for mosquitoes, and on negatively growth of fungi and bacteria (Solomon et al., 2012; Capoci et al., 2015; Hernandez-Lambraño et al., 2015), besides presenting aromatic characteristics (Gupta et al., 2018). Citronella leaves can also be used as a sedative and soothing in Brazilian folk medicine and in Indonesia as a soothing and digestive tea (Castro et al., 2007; Castro et al., 2010).

The leaves are the most economically valuable part of citronella grass, where EO is extracted. The EO is rich in citronellal aldehyde and contains high content of geraniol, citronellol and esters (Barbosa et al., 2008; Oliveira et al., 2010). The potential of EO has been reported to control pathogenic bacteria and fungi (Silva et al., 2010; Demuner et al., 2011; Nascimento et al., 2011).

The value of medicinal, aromatic or flavoring plants is determined by the production of chemical compounds, which are called active ingredients. In general, the active ingredients are mainly produced in leaves, flowers, roots or barks, depending on the plant species (Corrêa Junior & Scheffer, 2013). Moreover, the biosynthesis of chemical compounds vary according to several factors, ranging from changes in crop management to environmental factors such as light, temperature, soil state and photoperiod which can directly influence in growth and development, as well as yield (Peixoto et al., 2011; Pavarini et al., 2012; Nobre et al., 2013). The productivity is even reported as being widely affected according to weather conditions in the trial years (Plūduma-Pauniņa et al., 2019).

Thus, it is necessary to consider the optimal environmental conditions for each species, aiming high quantity and quality of chemical compounds, especially plants with high production of EO and can be highly impacted due to environmental changes that interfere on active compounds production (Souza et al., 2011).

Besides that, cutting processes mainly to obtain material for compound extractions can also be a stressful factor. Therefore, it is important to understand how the pruning of the shoot along with cuts in the root system during the citronella cultivation can influence biomass production, which is the main important raw material for EO extractions. In addition to the stress caused by pruning and cutting to the plants, it also can provide a better crop yield such as for example a better root and shoot development with high quantity and quality of EO (Kaczorowska–Dolowy et al., 2019).

Several studies have reported that pruning levels can influence plant metabolism: (i). pruning intensity influences growth, flower, and fruit development (Toit et al., 2020); (ii). early or late pruning influences EO yield; (Thakur et al., 2019); (iii). the number of pruned branches has a positive correlation with the growth attributes (Kathiresan et al., 2019); (iv). Partial root pruning lead to high plasticity of plants when the biomass of source organs is changed (Fanello et al., 2020); (v). the metabolite profile of shoots changes significantly after pruning (Arkorful et al., 2020).

Thus, to test how plants change the shoot growth when the roots are reduced (cut roots) by influencing the source-sink relationship during the critical period when leaves are removed from plants. Besides that, the requirement to comply with well-defined quality standards in medicinal and aromatic plants requires the elaboration of specific production strategies (Máthé & Franz, 1999). Therefore, the aim of this study was to analyze the biomass partitioning of citronella plants submitted different proportion of root cutting and shoot pruning.

MATERIALS AND METHODS

The experiment was carried out between March 2015 and May 2016 (22º54'00" S, 43º08'00" W and 8 m altitude). The annual average temperature was 23 ºC, with Aw climate, according to the Köppen classification. Citronella grass (*Cymbopogon nardus* (L.) Rendle) seedlings were planted in 8 L-polyethylene pots containing sandy soil, using a spacing of 40 cm between rows and between plants. Plants were watered to keep at field capacity. The plants were cultivated for five months until the beginning of the treatments, where they have adequate leaf area for the first pruning. For this, the experiment was conducted in a fully randomized design, with five different proportions of root cutting (0, 25, 50, 75 and 100%) and distinct shoot pruning after 145 days of seedling planting. The first pruning of all leaves was performed on the same day as the root cutting. The leaf pruning was composed of four treatments: blunt; pruning at 145 DAP (days after planting) along with the root cutting; pruning at 228 DAP; and pruning at 145 and 228 DAP (two pruning).

The roots were cut into a container with water and kept immersed in water for 24 h (at room temperature) to avoid cavitation in the vascular system. Root cutting treatments were through transverse cuts in the root system. After 24 h, the plants were replanted in 8 L-pots containing the same soil as above described. Throughout the experiment, the plants were fertilized (six and twelve months after seedling planting) using 300 g of Bokashi® compost plus 13 g of NPK (nitrogen: 0.4%; phosphorus: 14% and potassium: 0.8%) per pot.

To obtain the data of dry matter accumulation and photoassimilate partitioning, successive harvesting were performed, starting on the day of seedling planting, totaling four harvesting and in each harvesting the dry mass of the plant organs (leaf, stem and roots) was determined. The dry mas was getting by drying the fresh mass samples in an oven dried with forced air circulation at 65 °C until reach constant mass (± 72 h). The dry matter mass was calculated by the difference in fresh and dry mass for each analysis period.

The data was compared by its respective standard deviation with split plots. Treatment a: five different proportions of root cuts and treatment b: four different types of leaf cuts, with five samples per treatment.

RESULTS AND DISCUSSION

The growth analyzes show that when the roots are cut, but without pruning the leaves, there is an increase of the root dry mass in relation to other treatments. Leaf cutting alone showed the highest dry mass production for the leaves, and the treatments that remained at levels of non-leaf pruning were 50 and 75% root cutting.

Thus, the results of the evolution of citronella dry matter in internal comparisons (leaf pruning with different root cuts) (Fig. 1), with the first and second analysis being identical in all results, as the plants with no cutting and pruning. After 228 DAP, there was alterations, by being more relevant in the last analysis, since plants contained the treatments in the third and fourth analysis. After 145th day, changes were observed, with emphasis on the last analysis, since all plants had undergone some treatment.

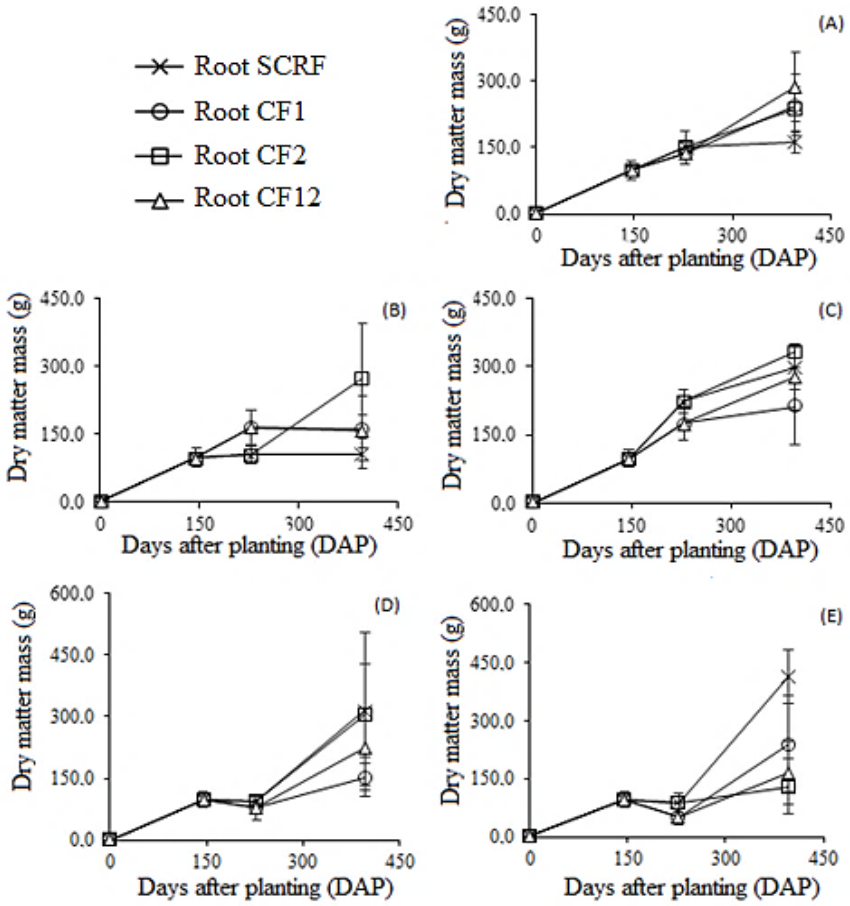

Figure 1. Evolution of citronella plant root dry matter accumulation in leaf cut treatments: (A) blunt root; (B) 25% root cut; (C) 50% root cut; (D) 75% root cut; (E) 100% root cut. (SCRF: no leaf pruning; CF1: leaf pruning at 145 DAP; CF2: leaf pruning at 228 DAP; CF12: leaf pruning at 145 and 228 DAP). Bar indicates Standard Deviation.

The treatment with no cutting on root (Fig. 1, A), which involved two leaf pruning at 145 and 228 DAP showed the highest root dry matter accumulation in the last analysis period. According to this treatment, it was observed that in the final analysis period the treatments with cutting at 145 and 228 DAP presented very similar values in their respective dry matter accumulation curves.

The treatment with 100% root cutting (Fig. 1, E) and no leaves pruning increased the root dry mass in relation to the other treatments, showing a 74.11% increase

compared to the 25% root cutting treatment (Fig. 1, B) for the same treatment of leaves in the last analysis period. This suggests that even under stress, the 100% root cutting plants had a higher root dry mass accumulation, as compared to the control (Fig. 1, A).

When the total dry mass accumulation of citronella was analyzed in the different root cutting treatments in relation to the four leaf pruning treatments, the treatment with 100% root cutting only and without leaf pruning showed a total of 838.67 g, as previously published data from this experiment (Daflon et al., 2019). This was the treatment that showed the largest increase in total mass in relation to the control, especially in the last analysis, where the root mass had a major contribution in the total mass of these plants, with an increase of 270 g, and soon after treatment with 50% of the root cut.

The redirection of photoassimilates to biomass production at the affected site (roots) is probably due to the fact that this energy is essential for the formation of new roots at this site, and most experiments involving root cutting demonstrate the reorientation of the roots assimilated toward the cut roots (Fanello et al., 2020). The same authors state that in cuttings performed on soybean roots in different proportions also promoted a greater accumulation of root biomass in pruned plants, causing a large increase in root respiration (increased alternative oxidase activity) and nitrate absorption, as well as also of water consumption towards the end of growth, as the pruned plants age.

Studies indicate that biomass accumulation by the plant and its productivity can be strongly affected by environmental conditions, among other factors (Lucas et al., 2013; Poorter et al., 2016; Xiao et al., 2016; Plūduma-Pauniņa et al., 2019; Yin et al., 2019), even if crop and weed mismanagement occurs, this can affect yield, which reflects the quality of the final product (Glatkova & Pacanoski, 2019).

In the treatments that suffered root cuts and a leaf pruning: i: 25% (Fig. 1, B), ii: 50% (Fig. 1, C) iii: 75% (Fig. 1, D) demonstrated higher dry mass accumulation compared to other treatments, including control (Fig. 1, A). However, the 75% treatment (Fig. 1, D) achieved a 36.19% reduction compared to the 100% treatment (Fig. 1, E) which showed higher root dry mass in relation to this leaf pruning.

Several factors can affect the growth and development of the crops, as well as the production of secondary metabolites, not only the injury caused by the application of pruning, but the characteristics of the soil, the temperature, among other environmental factors (Pavarini et al., 2012). However, such oscillations may be due to the fact that in some situations plants may show growth stimulus, including the production of secondary metabolites, in response to stress, in order to help organisms to establish adaptive responses, presenting the phenomena hormesia, which can contribute to improving the performance of plants when they are less aggressive to the plant (Tavares et al., 2015; Vargas-Hernandez et al., 2017; Hussain et al., 2019).

Regarding the data related to stem dry matter accumulation, under the action of treatments with pruned leaves in relation to the root cuts are presented in Fig. 2. The treatment that presented higher accumulation of stem dry mass in relation to the pruning of the leaves. The leaves did not contain root cuts, but with two leaf cuts (145 and 228 DAP) (Fig. 2, A), for the last period analyzed. Fanello et al. (2020) found the opposite in soybean plants subjected to longitudinal cutting in the roots of 15, 25 and 50%, where the plants whose roots were pruned showed large increases in dry matter in all vegetative organs compared with the plants intact.

When comparing the two leaf pruning with the different root cuts, the treatment with the lowest accumulation was the treatment of 75% of the root cut (Fig. 2, D) and

this reduction compared to the control was 38.25%. Thus, it can be analyzed that if there is no damage to the root system, the greatest accumulation of dry mass is in the stems, but when it contains two pruning in the leaves, because it can present energetic reserves for the plant, when in the absence of the photosynthetically active part (leaves), as several studies indicate that different parts of plants, such as stem and root, have an average accumulation of different nutrients, being able to present considerable individual development, despite these differences in allocated photoassimilates (Poorter et al., 2012; Rocha et al., 2014; Souza et al., 2018; Xu et al., 2018).

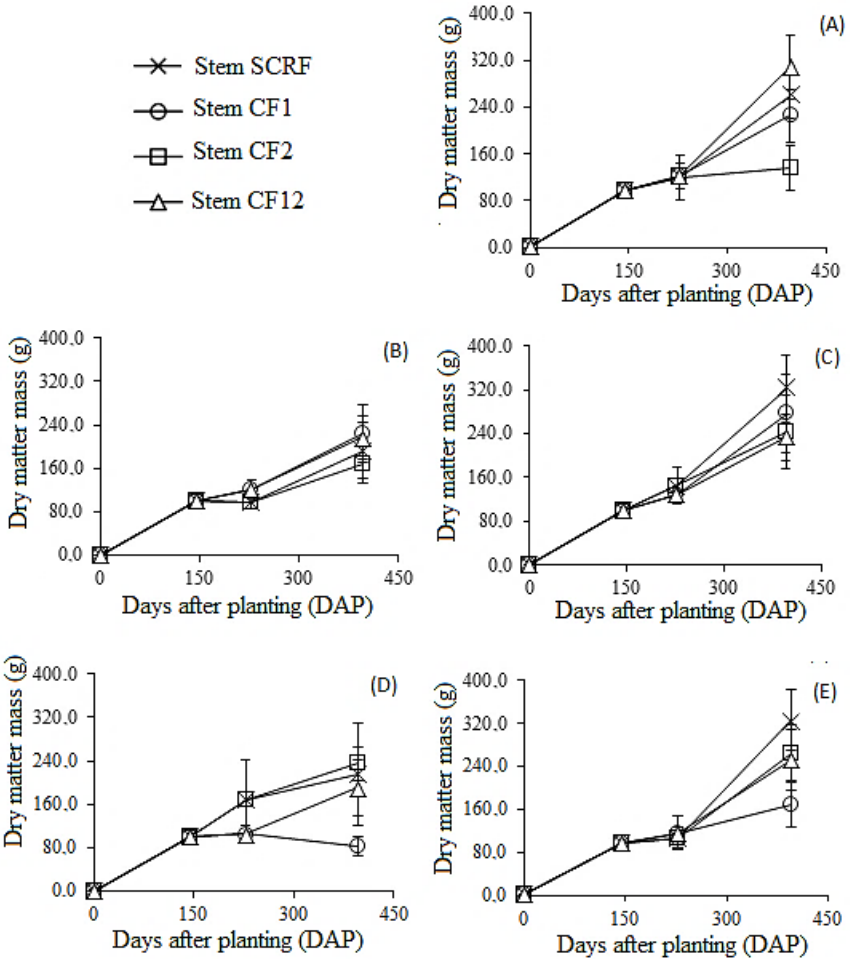

Figure 2. Evolution of citronella plant stem dry matter accumulation in leaf pruning treatments: (A) blunt root; (B) 25% root cut; (C) 50% root cut; (D) 75% root cut; (E) 100% root cut. (SCRF: no leaf pruning; CF1: leaf pruning at 145 DAP; CF2: leaf pruning at 228 DAP; CF12: leaf pruning at 145 and 228 DAP). Bar indicates Standard Deviation.

Depending on the species, up to 50% of the photoassimilates are consumed by the roots and the photoassimilate fraction used for root respiration increases with plant age as they are spent on maintenance respiration when root growth decreases (Lambers et al., 2002; Fanello et al., 2020). This energy expenditure in the primary metabolism

directly influences the production of the compounds of the secondary metabolism, such as essential oils, can provide an imbalance in the metabolism (Li et al., 2020).

When leaf pruning was analyzed only at 145 DAP in relation to the different root cuts, the treatment with the highest stem dry mass accumulation was 50% of the root cut (Fig. 2, C), followed by the blunt root treatment (Fig. 2, A), 25% (Fig. 2, B), 100% (Fig. 2, E), and to a lesser extent the treatment of 75% (Fig. 2, D), as it presented the greatest alterations between the values of stem dry matter accumulation, among their different types of leaf stress. Treatment involving leaf cutting at 145 DAP along with 75% root cutting (Fig. 2, D) decreased from the third analysis and continued this way until the last analysis period.

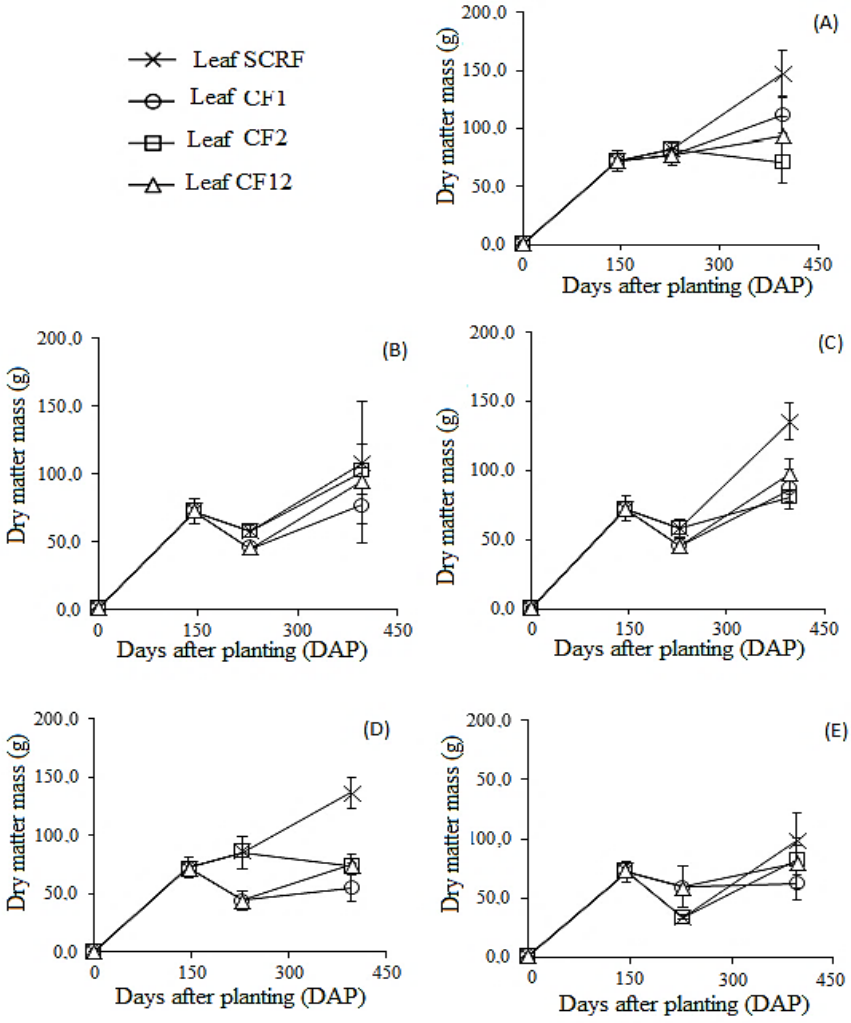

Figure 3. Evolution of leaf dry matter accumulation of citronella plant in leaf pruning treatments: (A) without root cutting; (B) 25% root cut; (C) 50% root cut; (D) 75% root cut; (E) 100% root cut. (SCRF: no leaf pruning; CF1: leaf pruning at 145 DAP; CF2: leaf pruning at 228 DAP; CF12: leaf pruning at 145 and 228 DAP). Bar indicates Standard Deviation.

Regarding the results of the evolution of leaf dry matter accumulation, for treatments of leaf pruning in relation to root cuts (Fig. 3), it was observed that the treatments in which the values were at control levels (Fig. 3, A) were 50% (Fig. 3, C) and 75% (Fig. 3, D), data from the analysis of 228 days after planting in relation to the treatment without pruning in the leaves, thus evidencing that the maintenance of both organs (root and leaves) influences the overall biomass of the plant.

When analysing the dry mass of the leaves and making two pruning in the leaves (145 and 228 DAP), these plants show a reduction, mainly among the analyzes, as can be seen mainly from the treatments with 100% root cut (Fig. 3, E) and 25% (Fig. 3, B). It was observed that the treatment that accumulated more dry matter in the leaf region was the one that did not have thinning neither in the root nor in the leaves, because it presented the maintenance of the two organs responsible for water and nutrient uptake and energy generation in the plant, respectively, which allowed its full growth and development, maintaining the photosynthetic activity for the production of organic molecules, being later distributed through the plant and transformed into biomass (Poorter et al., 2012; Sims et al., 2012; Reich et al., 2014; Li et al., 2019).

However, it is noteworthy that the plants that were not stressed with pruning in the shoots, these also have leaves that were senescent or entering senescence, all being accounted for dry mass, because they are retained in the plants, however, in other treatments presented leaves in senescence, due to the fact that the pruning was performed and these removed together with the other leaves at the time of pruning.

After pruning, many plants present an accelerated metabolic activity of the cells adjacent to the lesion, as in the case of citronella, which showed a rapid growth and increase of biomass after cutting, both in the root and shoots. was evidenced by the agility and ability to acclimate to these new situations imposed by the treatments, the same found by Fanello et al. (2020), where the soybean plants that suffered root cutting were able to fill the pods while regenerated their root system, well in the critical period of grain filling, without loss of yield, thus demonstrating the root plasticity in pruning situations.

Many agricultural crops use pruning, which may even be periodic to increase yield, among others (Albarracín et al., 2019; Gutierrez-Coarite et al., 2018; Fanello et al., 2020), experimental conditions, even the citronella undergoing drastic pruning, such as the complete removal of the root system, they survived and still showed greater biomass gain at the end, thus highlighting a positive reaction to its high metabolic adjustment capacity, including its relationship drain source.

Thus, the applicability of this form of cutting in the roots, can be carried out both in smaller crops, in pots, as well as in crops grown in beds, which facilitates the management of this crop and contributes, depending on the intensity of pruning, to a greater biomass production. However, there is a need for future work to also seek to relate this type of pruning in different environmental and cultivation conditions, in addition to relating to the production and yield of essential oil.

CONCLUSIONS

Citronella plants containing root cutting show compensatory growth in relation to root thinning, and the increase of root biomass gradually depends on the increase of thinning level, the same not being verified for stem and leaf biomass, which varied according to the levels of shoot pruning.

The treatment with 100% cut in the root, but without pruning in the leaves, increased the accumulation of total dry mass of the plant in relation to the other treatments, for the last period of analysis, showing a recovery.

The application of two pruning in the leaves or no pruning the leaves, within the treatment with 100% of the cut in the root for the accumulation of dry mass of the leaf is more effective when compared to the treatment without cutting in the roots.

ACKNOWLEDGEMENTS. The present work was carried out with the support of the Coordination of Improvement of Higher Education Personnel - Brazil (CAPES - Coordenação de Aperfeiçoamento de Pessoal de Nível Superior) - Financing Code 001, National Council for Scientific and Technological Development (CNPq - Conselho Nacional de Desenvolvimento Científico e Tecnológico); and Rio de Janeiro State Research Support Foundation (FAPERJ Fundação de Amparo à Pesquisa do Estado do Rio de Janeiro).

REFERENCES

Albarracín, V., Hall, A.J., Searles, P.S. & Rousseaux, M.C. 2019. Responses of shoot growth, return flowering, and fruit yield to post-pruning practices and growth regulator application in olive trees. *Scientia Horticulturae* **254**, 163–171.

Arkorful, E., Yu, Y., Chen, C., Lu, L., Hu, S., Yu, H., Ma, Q., Thangaraj, K., Periakaruppan, R., Jeyaraj, A., Chen, X. & Li, X. 2020. Untargeted metabolomic analysis using UPLC-MS/MS identifies metabolites involved in shoot growth and development in pruned tea plants (*Camellia sinensis* (L.) O. Kuntz). *Scientia Horticulturae* **264**, 109164. https://doi.org/10.1016/j.scienta.2019.109164

Barbosa, L.C.A., Pereira, U.A., Martinazzo, A.P., Maltha, C.R.A., Teixeira, R.R. & Melo, E.C. 2008. Evaluation of the chemical composition of Brazilian commercial *Cymbopogon citratus* (D.C.) Stapf samples. *Molecules,* Basel, **13**, pp. 1864–1874.

Capoci, I., Cunha, M.M., Bonfim-Mendonça, P., Ghiraldi-Lopes, L., Baeza, L., Kioshima, E. & Svidzinski, T. 2015. Antifungal activity of *Cymbopogon nardus* (l.) Rendle (citronella) against microsporum canis from animals and home environment. *Revista do Instituto de Medicina Tropical de São Paulo*, São Paulo, **57**(6), pp. 509–511.

Castro, H.G., Barbosa, L.C.A., Leal, T.C.A.B., Souza, C.M. & Nazareno, A.C. 2007. Growth, content and composition of the essential oil of *Cymbopogon nardus* L. *Revista Brasileira de Plantas Medicinais*, Botucatu, **9**, pp. 55–61 (in Portuguese).

Castro, H.G., Perini, V.B.M., Santos, G.R. Dos & Leal, T.C.A. B. 2010. Evaluation of the content and composition of *Cymbopogon nardus* (L.) essential oil at different harvesting times. *Revista Ciência Agronômica,* Fortaleza, **41**, pp. 308–314 (in Portuguese).

Chen, Z., Zhu, Q., Qi, J., Lu, Y. & Wu, W. 2019. Sustained and controlled release of herbal medicines: the concept of synchronized release. *International Journal of Pharmaceutics*, Amsterdam, **560**, pp. 116–125.

Corrêa Junior, C. & Scheffer, M.C. 2013. Good agricultural practice (BPA) of medicinal, aromatic and spice plants. Curitiba: EMATER, 55 pp. (in Portuguese).

Daflon, T., Hüther, C., Santos, C., Carvalho, L., Correa, N., Correia, D., Pereira, C. & Machado, T. 2019. Increases in citronella total biomass production due to severe stress in the root system. *Revista Brasileira De Ciências Ambientais* (Online), (**51**), 95–111 (in Portuguese).

De Hooge, I.E., Van Dulm, E. & Van Trijp, H.C.M. 2018. Cosmetic specifications in the food waste issue: supply chain considerations and practices concerning suboptimal food products. *Journal of Cleaner Production* **183**, 698–709.

Demuner, A.J., Barbosa, L.C.A., Magalhães, C.G., Silva, C.J., Maltha, C.R.A., Pinheiro, A.L. 2011. Seasonal variation in the chemical composition and antimicrobial activity of volatile oils of three species of Leptospermum (Myrtaceae) grown Brazil. *Molecules*, Basel, **16**, pp. 1181–1191.

Fanello, D.D., Santiago, J.K., Carlos Guillermo Bartoli, María Gabriela Cano, Santiago Martínez Alonso, Juan José Guiamet. 2020. Plasticity of root growth and respiratory activity: Root responses to above-ground senescence, fruit removal or partial root pruning in soybean, *Plant Science* **290**, 110296.

Faria, A.P. de, Marabesi, M.A., Gaspar, M. & França, M.G.C. 2018. The increase of current atmospheric CO_2 and temperature can benefit leaf gas exchanges, carbohydrate content and growth in C_4 grass invaders of the Cerrado biome. *Plant Physiology and Biochemistry* **127**, 608–616.

Glatkova, G. & Pacanoski, Z. 2019. Evaluating the effects of application modes and soil types on the herbicide efficacy and crop yield of pendimethalin and clomazone on transplanted pepper (Capsicum annuum L.). *Agronomy Research* **17**(2), 430–437.

Gupta, P., Mishra, A., Yadav, A. & Dawhan, S.S. 2018. Inter and intra-specific molecular and chemical diversity of elite accessions of aromatic grasses *Cymbopogon*s. *Journal of Applied Research on Medicinal and Aromatic Plants*, Stuttgart, **11**, pp. 54–60.

Gutierrez-Coarite, R., Mollinedo, J., Cho, A. & Wright, M.G. 2018. Canopy management of macadamia trees and understory plant diversification to reduce macadamia felted coccid (*Eriococcus ironsidei*) populations. *Crop Protection* **113**, 75–83.

Hatanaka, M. 2020. Beyond consuming ethically? Food citizens, governance, and sustainability. *Journal of Rural Studies* **77**, 55–62. https://doi.org/10.1016/j.jrurstud.2020.04.006

Hernandez-Lambraño, R., Pajaro-Castro, N., Caballero-Gallardo, K., Stashenko, E. & Olivero-Verbel, J. 2015. Essential oils from plants of the genus *Cymbopogon* as natural insecticides to control stored product pests. *Journal of Stored Products Research*, Oxford, **62**, pp. 81–83.

Hussain, S., Iqbal, N., Brestic, M., Raza, M.A., Pang, T., Langham, D.R., Safdar, M.E., Ahmed, S., Wen, B., Gao, Y., Liu, W. & Yang, W. 2019. Changes in morphology, chlorophyll fluorescence performance and Rubisco activity of soybean in response to foliar application of ionic titanium under normal light and shade environment. *The Science of the total environment* **658**, 626–637.

Kačániová, M., Terentjeva, M., Vukovic, N., Puchalski, C., Roychoudhury, S., Kunová, S., Klūga, A., Tokár, M., Kluz, M. & Ivanišová, E. 2017. The antioxidant and antimicrobial activity of essential oils against Pseudomonas spp. isolated from fish. *Saudi Pharmaceutical Journal* **25**, 1108–1116. https://doi.org/10.1016/j.jsps.2017.07.005

Kaczorowska–Dolowy, M., Godwin, R.J., Dickin, E., White, D.R. & Misiewicz, P.A. 2019. Controlled traffic farming delivers better crop yield of winter bean as a result of improved root development. *Agronomy Research* **17**(3),725–740.

Kathiresan, K., Narendran, R., Kalidasan, K. & Dinesh, P. 2019. Pruning of shoot branches: An efficient technique for stimulating the mangrove growth (*Rhizophora mucronata*). *Biocatalysis and Agricultural Biotechnology* **17**, 309–312. https://doi.org/10.1016/j.bcab.2018.12.006.

Kozlowska, J., Prus, W. & Stachowiak, N. 2019. Microparticles based on natural and synthetic polymers for cosmetic applications. *International Journal of Biological Macromolecules*, Greeley, **129**, pp. 952–956.

Lambers, H., Atkin, O. & Millenaar, F.F. 2002. Respiratory patterns in roots in relation to their functioning Y. Waisel, A. Eshel, U. Kafkafi (Eds.), Plant Roots, Hidden Half, Third, Marcel Dekker, Inc., New York, pp. 782–838.

Li, H., Si, B., Ma, X. & Wu, P. 2019. Deep soil water extraction by apple sequesters organic carbon via root biomass rather than altering soil organic carbon content. *Science of the Total Environment*, Amsterdam, **670**, pp. 662–671.

Li, L., Li, T., Jiang, Y., Yang, Y., Zhang, L., Jiang, Z., Wei, C., Wan, X. & Yang, H. 2020. Alteration of local and systemic amino acids metabolism for the inducible defense in tea plant (*Camellia sinensis*) in response to leaf herbivory by Ectropis oblique. *Archives of Biochemistry and Biophysics* **683**, 108301. https://doi.org/10.1016/j.abb.2020.108301

Lucas, J.A., García-Villaraco, A., Ramos, B., García-Cristobal, J., Algar, E. & Gutierrez-Mañero, J. 2013. Structural and functional study in the rhizosphere of Oryza sativa L. plants growing under biotic and abiotic stress. *Journal of Applied Microbiology*, Malden, **115**(1), pp. 218–235.

Máthé, A. & Franz, C. 1999. Good Agricultural Practices and the Quality of Phytomedicines. *Diário de Ervas, Especiarias e Plantas Medicinais* **6**(3), 101–113. doi: 10.1300/J044v06n03_10 (in Portuguese).

Nascimento, J.C., Barbosa, L.C.A., Paula, V.F., David, J.M., Fontana, R., Silva, L.A.M. & França, R.S. 2011. Chemical composition and antimicrobial activity of essential oils of Ocimum canum Sims. and Ocimum selloi Benth. *Anais da Academia Brasileira de Ciências*, Rio de Janeiro, **83**, pp. 787–799.

Nobre, R.G., Lima, G., Gheyi, H. R., Lourenço, G. Da S., Soares, L.A. & Dos, A. 2013. Emergence, growth and yield of papaya under saline stress and nitrogen fertilization. *Revista Ciência Agronômica,* Fortaleza, **44**(1), pp. 76–85 (in Portuguese).

Oliveira, M.M.M., Brugnera, D.F., Cardoso, M. Das, G., Alves, E. & Piccoli, R.H. 2010. Disinfectant action of *Cymbopogon sp.* essential oils in different phases of biofilm formation by Listeria monocytogenes on stainless steel surfasse. *Food Control*, Reading, **21**(4), pp. 549–553.

Pavarini, D.P., Pavarini, S.P., Niehues, M. & Lopes, N.P. 2012. Exogenous influences on plant secondary metabolite levels. *Animal Feed Science and Technology*, Amsterdam, **176**(1–4), pp. 5–16.

Peixoto, C.P., Cruz, T. & Peixoto, M. de F. da S.P. 2011. Quantitative analysis of plant growth: concepts and practice. *Enciclopédia Biosfera*, Goiânia, v. **7**(13), pp. 51–76 (in Portuguese).

Plūduma-Pauniņa, I., Gaile, Z., Bankina, B. & Balodis, R. 2019. Variety, seeding rate and disease control affect faba bean yield components. *Agronomy Research* **17**(2), 621–634.

Poorter, H., Fiorani, F., Pieruschka, R., Wojciechowski, T., Van Der Putten, W.H., Kleyer, M., Schurr, U. & Postma, J. 2016. Pampered inside, pestered outside? Differences and similarities between plants growing in controlled conditions and in the field. *New Phytologist*, New York, **212**(4), pp. 838–855.

Poorter, H., Niklas, K.J., Reich, P.B., Oleksyn, J., Poot, P. & Mommer, L. 2012. Biomass allocation to leaves, stems and roots: meta-analyses of interspecific variation and environmental control. *New Phytologist*, New York, **193**(1), pp. 30–50.

Reich, P.B., Luo, Y., Bradford, J.B., Poorter, H., Perry, C.H. & Oleksyn, J. 2014. Temperature drives global patterns in forest biomass distribution in leaves, stems, and roots. *Proceedings of the National Academy of Sciences of the United States of America*, Washington, **111**(38), pp. 13721–13726.

Rocha, J.G., Ferreira, L.M., Tavares, O.C.H., Santos, A.M. & Souza, S.R. 2014. Nitrogen absorption kinetics and accumulation of soluble nitrogenous fractions and sugars in sunflower. *Pesquisa Agropecuária Tropical,* Goiânia, **44**(4), pp. 381–390.

Silva, C. J., Barbosa, L. C. A., Demuner, A. J., Pinheiro, A. L., Dias, I., Andrade, N. J. 2010. Chemical composition and antibacterial activities from the essential oils of Myrtaceae species planted in Brazil. *Química Nova*, São Paulo, **33**, pp. 104–108.

Silva, M.R.M. da & Ricci-Júnior, E. 2020. An approach to natural insect repellent formulations: from basic research to technological development. *Acta Tropica*, In Press, Journal Pre-proof, 105419. https://doi.org/10.1016/j.actatropica.2020.105419

Sims, L., Pastor, J., Lee, T. & Dewey, B. 2012. Nitrogen, phosphorus and light effects on growth and allocation of biomass and nutrients in wild rice. *Oecologia*, Heidelberg, **170**(1), pp. 65–76.

Sivashanmugam, M., Paulsamy, S. & Senthilkumar, P. 2009. Energy dynamics in the C4 species dominated montane subtropical grassland at Nilgiri Biosphere Reserve, the Western Ghats, *India Acta Ecologica Sinica* **29**(4), 254–259.

Solomon, B., Gebre-Mariam, T. & Asres, K. 2012. Mosquito repellent actions of the essential oils of *Cymbopogon citratus*, *Cymbopogon nardus* and *Eucalyptus citriodora*: evaluation and formulation studies, journal of essential oil bearing plants. *Journal of Essential Oil Bearing Plants*, Pune, **15**, pp. 766–773.

Souza, G., Pinto, J., Resende, M., Bertolucci, S., Soares, A. & Castro, E. 2011. Growth, essential oil content and coumarin content of young guaco (Mikania glomerata Sprengel) plants grown under colored meshes. *Biotemas*, Florianópolis, **24**(3), pp. 1–11 (in Portuguese).

Souza, J., Rufini, J.C., Ferreira, E., Guedes, M., Ramos, M.C. & Campos, M. 2018. Nutrient absorption and accumulation in 'Paulista' and 'Sabara' jabuticaba cultivars. *Revista Brasileira de Fruticultura*, Jaboticabal, **40**(5), pp. 1–12.

Tavares, L.A.F., Sousa, S.F.G., Correia, T.P. da S., Silva, P.R.A. & Velini, E.D. 2015. Hormesis method for increasing oat straw with a view to viability of direct-seeding systems1. *Revista Ciência Agronômica* **46**(1), 48–53. https://doi.org/10.1590/S1806-66902015000100006

Toit, I.S du., Sithole J. & Vorster, J. 2020. Pruning intensity influences growth, flower and fruit development of Moringa oleifera Lam. under sub-optimal growing conditions in Gauteng, South Africa. *South African Journal of Botany* **129**, 448–456. https://doi.org/10.1016/j.sajb.2019.11.033

Thakur, M., Sharma, S., Sharma, U. & Kumar, R. 2019. Study on effect of pruning time on growth, yield and quality of scented rose (Rosa damascena Mill.) varieties under acidic conditions of western Himalayas. *Journal of Applied Research on Medicinal and Aromatic Plants* **13**, 100202, https://doi.org/10.1016/j.jarmap.2019.100202

Vargas Hernandez, M., Macias-Bobadilla, I., Guevara-Gonzalez, R.G., Romero-Gomez, S.J., Rico-Garcia, E., Ocampo-Velazquez, R.V., Alvarez-Arquieta, L.L. & Torres-Pacheco, I. 2017. Plant Hormesis Management with Biostimulants of Biotic Origin in Agriculture. *Frontiers in plant science* **8**, 1762. https://doi.org/10.3389/fpls.2017.01762

Xiao, L., Liu, G. & Xue, S. 2016. Elevated CO_2 Concentration and drought stress exert opposite effects on plant biomass, nitrogen, and phosphorus allocation in Bothriochloa ischaemum. *Journal of Plant Growth Regulation*, Dordrecht, **35**(4), pp. 1088–1097.

Xiong, X., Yang, X., Li, X., Yue, G., Xing, Y. & Cho, W. C. 2019. Efficacy and safety of Chinese herbal medicine for patients with postmenopausal hypertension: a systematic review and meta-analysis. *Pharmacological Research*, Milan, **141**, 481–500.

Xu, Z., Lai, T., Li, S., Si, D., Zhang, C., Cui, Z. & Chen, X. 2018. Promoting potassium allocation to stalk enhances stalk bending resistance of maize (Zea mays L.). *Fields Crops Research*, Davis, **215**, pp. 200–206.

Yang, Q., Shen, Y., Foster, T. & Hort, J. 2020. Measuring consumer emotional response and acceptance to sustainable food products. *Food Research International* **131**, 108992. doi: https://doi.org/10.1016/ j.foodres.2020.108992

Yin, Q., Tian, T., Han, X., Xu, J., Chai, Y., Mo, J., Lei, M., Wang, L. & Yue, M. 2019. The relationships between biomass allocation and plant functional trait. *Ecological Indicators*, Amsterdam, **102**, pp. 302–308.

Zhang, X., Pu, P., Tang, Y., Zhang, L. & Lv, J. 2019. C_4 photosynthetic enzymes play a key role in wheat spike bracts primary carbon metabolism response under water deficit. *Plant Physiology and Biochemistry* **142**, 163–172.

Agronomy Research **18**(3), 2004–2021, 2020
https://doi.org/10.15159/AR.20.180

A linear assignment based conceptual lifecycle assessment method for selecting optimal agri-industrial materials production pathway: A case study on Nigerian yam value chain

I. S. Dunmade

Mount Royal University, Faculty of Science & Technology, Department of Earth & Environmental Sciences, 4825 Mount Royal Gate SW, Calgary AB T3E 6K6, Canada
*Correspondence: idunmade@mtroyal.ca; israel_dunmade@yahoo.ca

Abstract. Lifecycle assessment is a robust tool for comprehensive environmental impact assessment of products and processes. It provides users opportunities to identify the hotspots along the lifecycle of a system and thereby enable them to implement improvement opportunities as deemed appropriate. Production of agri-based industrial raw materials could be energy and water intensive. Such endeavour could take a heavy toll on the environment in terms of resource consumption and environmental pollution. The goal of this study was to develop an easy to use and less data intensive conceptual LCA methodology for selecting optimal pathway along a value-chain under two decision scenarios: the optimal techno-environmentally friendly pathway, and optimal sustainability pathway. This proposed Linear Assignment Method integrated LCA is a less data intensive conceptual LCA method that facilitates the selection of an optimal production and processing pathway for agri-industrial materials, minimizes resource consumption and reduction of potential climate change impact of agri-industrial materials value chain. The LCA ISO 14040s aligned conceptual LCA method will be found useful in identifying potential hotspots in a agri-industrial production process lifecycle, in selecting activity options that would result in minimum ecological footprint, and help in removing obstacles in implementing a scoping lifecycle analysis where cost, time and data availability are the impediments.

Key words: Africa, agri-industrial materials, ecological footprint, LAM (linear assignment method), yam.

INTRODUCTION

Agri-industrial materials refer to agricultural produce used as feedstocks in the textile, dairy, fashion, food, beverage and paper industry. It includes crops like cocoa, coffee, tea, orange, sorghum, millet, cassava, yam, cocoyam, kenaf, sisal, and jute. Their industrial applications include in the production of starch, biofuels, pharmaceuticals, and other industrial chemicals. Decisions in this sector of the economy are often based on profitability and regulatory compliance. The emerging trend in this sector is the incorporation of corporate social responsibility and concept of sustainability.

Production of agri-based industrial raw materials could be energy and water intensive. Such endeavour could take a heavy toll on the environment in terms of resource consumption and environmental pollution. There is, therefore, a need to address

environmental issues along with other social and economic factors. Lifecycle assessment (LCA) is a robust tool for evaluating environmental-, social-, and social sustainability of a product, a process or a system. Originally, LCA is utilized for comprehensive environmental impact assessment of products and processes. It provides users with opportunities to identify the hotspots along the lifecycle of a system and thereby enable them to implement improvement opportunities as deemed appropriate. Lifecycle tool has been used for evaluating environmental impacts of products and processes from various sectors of our economy. Its use in agriculture includes using it to determine the ecological footprint of various types of crops cultivation (Avadí et al., 2020; Romero-Gámez & Suárez-Rey, 2020); livestock production systems (Ottosen, 2020), and products from agro-based companies (Mfitumukiza et al., 2019; Farahani et al., 2019). Although LCA is a comprehensive tool has been widely used in the agricultural sector but its use is mostly in the developed countries. Its complexity and associated cost has limited its utilization by agricultural stakeholders in the developing countries. The goal of this study was to develop an easy to use and less data intensive conceptual LCA methodology for selecting optimal pathway along a value-chain. This study proposed the use of Linear Assignment Method based, less data intensive conceptual LCA method that facilitates the selection of an optimal production and processing pathway for agri-industrial materials, minimizes resource consumption and reduction of potential climate change impact of agri-industrial materials value chain. The LCA ISO 14040s aligned conceptual LCA method will be found useful in identifying potential hotspots in an agri-industrial production process lifecycle, in selecting activity options that would result in minimum ecological footprint, and help in removing obstacles in implementing a scoping lifecycle analysis where cost, time and data availability are the impediments.

One of the contributions of this research is that this is the first time that Linear Assignment Method (LAM) is integrated with the Lifecycle Assessment (LCA) methodology to simplify the LCA process by eliminating the need for intensive data as is the case with the traditional LCA (Fava and Cooper, 2004). There is no known literature on the use of LAM integrated LCA approach. The use of the LAM integrated LCA approach enables the stakeholders in the agri-industrial materials production value chain to select the 'best' (i.e. optimal) pathway along the value chain under two decision scenarios: environmental friendly pathway or sustainability pathway.

Environmentally friendly pathway is the decision scenario that evaluates the value chain to select the combination of technically sound processes with the lowest ecological footprint. This pathway favors processes with the lowest resource consumption and minimum emissions. The sustainability pathway goes beyond the environmental sustainability to include the consideration of economic and sociocultural factors in the process of designing/selecting the best pathway along the value chain.

This conceptual LCA methodology is particularly beneficial to agri-industrial materials producers, processors and marketers in developing countries that may want to carry out an LCA but cannot afford to purchase commercial LCA software necessary to carry out the traditional LCA. It is also suitable for those that may not be able to handle the complexity, data requirement and time commitment necessary for the conventional LCA (Udo de Haes, 2004; Rebitzer & Hunkeler, 2006).

MATERIALS AND METHODS

This proposed conceptual LCA method involved hybridization of linear assignment decision method (LAM) with the ISO 14040s based LCA process in an easily understandable and utilizable manner. The integration of LAM with the LCA process was done at the lifecycle inventory stage of LCA. This proposed method is easy to employ and it produces actionable results that would be found useful in decision-making processes along agri-industrial materials value-chain.

Linear assignment method and reasons for its choice as a method to integrate with LCA

Linear assignment method (LAM) is one of the multiple attribute decision making (MADM) methods that utilize quantitative and qualitative data in facilitating the decision maker's selection of the best choice out of a small number of possible options. In LAM, the choices are ranked based on their points of each criterion and are rank ordered on the basis of their overall performance across the criteria. The evaluation of the available choices often involve considering multiple conflicting attributes (Abdolazimi et al., 2015; Azar, 2000). At each stage of agri-industrial material production, a farmer/processor is often confronted with the need to choose among a small number of options. Their choices at each stage often have to be based on a set of weighted or unweighted criteria that may eventually have far reaching effect on profitability, environmental impacts and socio-cultural consequences. So, their decisions are of multiple attributes in nature.

Although there are many MADM methods, LAM was selected because it is simpler/easier to understand and to use. In addition, it is technically sound and has been used in many real-life situations requiring making choices from a small number of options on the basis of a set of criteria. Examples of areas of applications of LAM were in logistics (Liu & Wang, 2009); material selection (Jahan et al., 2010); optimum maintenance strategy selection (Bashiri et al., 2011), and spare parts inventory classification (Baykasoglu et al., 2016). Further literature on the theory and applications of MADM and LAM specifically can be found in the works of Herrera & Herrera-Viedma, 2000; Liu & Wang, 2007 and Chen, 2013.

The ISO 14040s based LCA process

Life-cycle assessment (LCA) is a robust tool for evaluating potential environmental impacts of products, processes and systems. LCA enables the users to determine the potential environmental impacts of their products or process even before they are developed, thereby facilitating taking preventive measures rather than curative steps that may be necessary after the facts. LCA also allows for consistent comparisons of alternative system designs with respect to their environmental performance. LCA consists of four major steps, namely: goal and scope definition, inventory analysis, impact analysis, and LCA interpretation (Fig. 1) (ISO, 2006a and 2006b; Dunmade, 2013a and 2013b; Kazulis et al., 2018; Dunmade, 2019a).

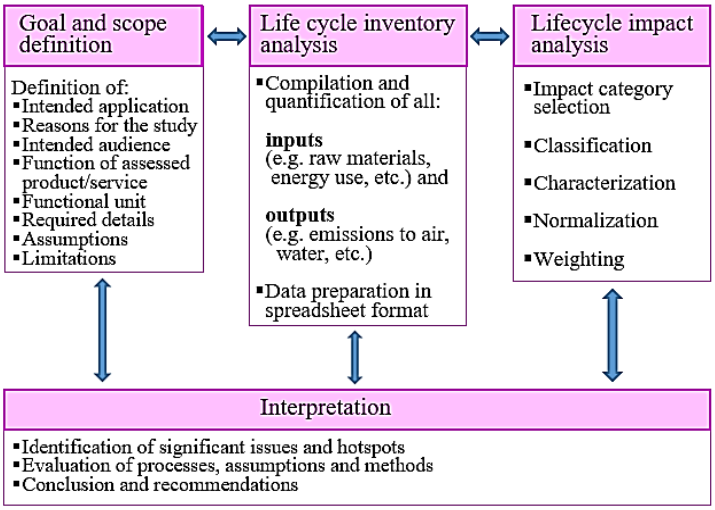

Figure 1. The four steps life cycle assessment process.

Conceptual LCA

The conceptual level of LCA, which is also referred to as scoping LCA or lifecycle thinking, generally involves the use of generic secondary data and scoring of possible alternative course of actions over a set of criteria. It is often used for selecting a more promising option from among two or more available options. It is commonly used in selecting conceptual product designs pending a more detailed analysis of the selected option. It is useful when there are cost, time or data availability issues affecting carrying out a more rigorous LCA. This level of LCA facilitates getting a rough idea/ identification of potential hotspots in a process, products, or system without the use of a more rigorous level of LCA.

Goal and scope definition

ISO 14040s require that the goal of an LCA should articulate the intended applications, reasons for implementing the LCA and the audience that will use the information from the results. The scope definition set the boundary for the LCA study. It specifies the function of the system, the functional unit, the data cut-off criteria.

Lifecycle inventory (LCI)

This second stage of the LCA involves quantification and compilation of data, usually in spreadsheet format. This is the most time consuming step in the LCA process. This is because the needed data are either not kept or it is not available in a usable form. Intended users of LCA are usually discouraged/ frustrated for those reasons. Consequently, an effort to address this problem would greatly enhance utilization

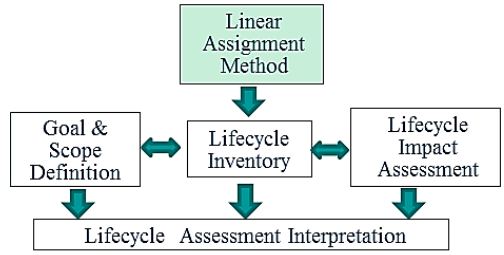

Figure 2. An illustration of LAM integrated LCA process.

of LCA for various purposes. This is where the use of LAM comes in handy because of its simplicity and less data demanding. Fig. 2 is an illustration of LAM incorporated LCA. It shows that LAM is integrated at the lifecycle inventory analysis stage of the LCA.

The incorporation of LAM to the LCA process

The integration of LAM into the life cycle inventory stage involves a professional or manager evaluating each of the available options A_j, $_{j=1, 2,..., n}$ for a production unit process against a set of criteria S_1 .... S_m that are essential for the successful implementation of that unit process. The professional comparatively rate the options in terms of how good they are on each of the criteria and compile the numerical score of each option across all the criteria. He/she then rank order the options based on their total scores. The option with the least total score across the criteria is the best option while the option with the highest total score is the worst option for the unit process/opperation of the value chaim. The professional or manager repeats the rank ordering and totaling the score for each of the unit processes in the value chain. The rank ordering of the options on the basis of their total score at the unit process/operational level enables the decision maker to easily see the best and the worst options. Assemblage of all the (operation level) best options is the optimal production pathway along the value chain (Dunmade, 2013b; Dunmade & Anjola, 2019b).

Metrics of measurement

The aforemention rank ordering process starts with articulating the criteria by which the various unit process options would be assessed and the metric for measuring the performance of each process. The framework allows the use of mixed qualitative and quantitative metric or purely qualitative metric wherever necessary/relevant. The qualitative evaluation is done on the basis of a six ordinal linguistic scale that ranks available choices in order of their goodness and assign numerical values according to the ranking. Generally, in ordinal scales, it is the order of the choices/values that is important and significant because the magnitude of the differences between the choices may not really be known. Ordinal scales therefore provide good information about the order of choices (Triola, 2007; MRK, 2020). Table 1 shows the six ordinal linguistic scale levels and the numerical conversion of the linguistic ratings.

Table 1. The six linguistic scale levels

Linguistic rating	Assigned numerical value
The best	1
Second best	2
Third best	3
Fourth best	4
Fifth best	5
Sixth best (i.e. worst case)	6

Decision analysis

Having determined the available options and articulating the basis for their evaluation, it is necessary to determine the characteristics of the decision maker. This methodology is premised on a single decision maker that is assumed to be rational and wants to choose a unit process option that maximize his utility. Furthermore, it is also assumed that in choosing the best out of the available options, he/she may set some minimum limits/value on the performance of the options below which he will not be ready to accept to choose any of the options.

For a specific decision scenario, let $A_{j,\ j=1,\ 2,\ldots,\ n}$ be the identified unit process options from which he/she wants to choose while $S_{i,\ i=1,\ 2,\ \ldots,\ m}$ are criteria/attributes on which the options are to be evaluated. As a rational decision maker who intends to maximize his utility, he/she will select the option with the lowest total score (Dunmade, 2004):

$$A_j = min \sum_{i=1}^{m} w_i S_{ij} \quad (1)$$

But if he/she has set some minimum performance limit for any acceptable option on the sustainability factors, this limit can be written as

$$\sum_{i=1}^{m} w_i S_i^o \quad (2)$$

where S_i^o is the required minimum performance for any acceptable option A_j on criterion S_i.

Thus, he/she will choose process A^* that both satisfy his/her minimum performance requirements and maximize his/her utility. This can be written as

$$A^* = min \sum_{i=1}^{m} w_i S_{ij} < \sum_{i=1}^{m} w_i S_i^o \quad (3)$$

Lifecycle impact analysis (LCIA)

This third step in LCA is the point at which the data collected and processed regarding resource use and environmental releases at lifecycle inventory stage are mapped/ modelled into environmental effects. This stage conventionally consists of three mandatory steps of impact category selection, classification and characterization. The other non-mandatory steps at this stage in the LCA process are normalization, grouping and valuation. For this LAM integrated conceptual LCA method, the LCIA step involves trying, compiling and diagrammatic illustration of possible combinations of operational options and determining the outcomes. The set of best choice (A^*) from individual operations of the value chain (Fig. 3) constitute the optimal pathway for the scenario under consdideration.

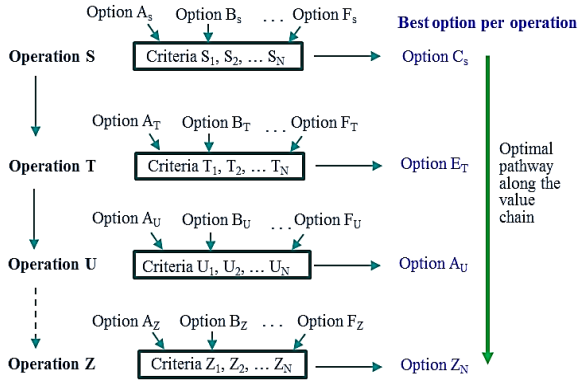

Figure 3. An illustration of the optimal pathway selection in LAM integrated LCA process.

Lifecycle interpretation

This last step in the LCA process involves evaluating the LCI and LCIA data, and determining environmentally significant issues from those data. Significant issues can be identified by doing contribution analysis or anomaly assessment of the data. This stage of LCA also involves evaluating the soundness of the decisions taken and validity of assumptions made at each stage of the LCA process. Such evaluation ensures correct interpretation of the results, and adequacy of conclusions and recommendations. It also

improves confidence in the outcomes of the LCA study. Conclusion on the outcomes of the study and recommendations for necessary actions are made after the evaluation. The results of the LCA study may also be subjected to either internal or external peer/critical review before the report is submitted to the client or published.

An illustration on the use of LAM integrated conceptual LCA method for the selection of an optimal agri-industrial material production value chain/pathway

Agri-industrial material production system: yam as an example.

The process of producing and transforming a typical agricultural produce to a final industrial material or products involve so many activities. Using yam as an example, the production process involves land clearing, mound/ridge making, seed yams planting, weeding, fertilizer and chemicals application, staking and harvesting (Hori & Oshima, 1986; Diop, 1998; IITA, 2013; Ike & Inoni, 2006; Maroya et al., 2014; Bassey, 2017; Eze, 2018; FMAWRRD, 2020). And according to ANOL (2018), the postharvest processing of yam into instant pounded yam flour, involves yam selection and weighing, washing, peeling and slicing, parboiling, drying, milling, and packaging. Fig. 4 illustrates the various processes involved in yam value chain resulting in multiple industrial products obtainable from yam processing (Suzan & Gameiro, 2007; Sadh et al., 2018; USOTA, 2020).

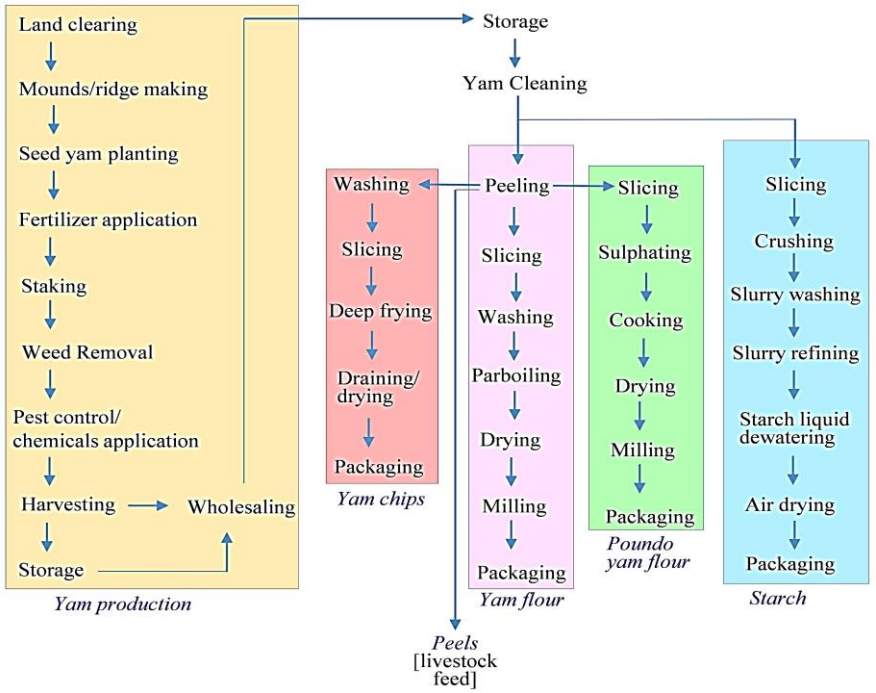

Figure 4. A network of main operational activities involved in yam production value chain system boundary and its products.

Yam production process

Land clearing is the process of removing vegetation cover from a piece of land for crop planting planting. It often involves removing trees, stumps, brush, stones and other

obstacles from an area as required to increase the size of the crop producing land base of an existing farm or to provide land for a new farm operation. Methods used to clear land will vary depending on the type and density of native cover, prevailing regulations, available technology, and affordability of modern methods. The choice of land clearing method would in turn affect soil properties and agricultural produce yields. Umeghalu & Ngini (2013) in their article on the effect of poor land clearing on soil and agricultural produce highlighted five methods of land clearing operation. However the four commonly used methods in Nigeria are:

1. Manual method involving the use of hand tools such as matchet, hoes, axes and diggers for land clearing. It is a tedious method that leads to drudgery. Land cleared by this method may be difficult to later work with machines as some stumps and roots may be left in the soil.

2. Burning method involves setting the vegetation on fire. It is commonly used in the savanna vegetation region of Nigeria. It is fast and not labor intensive. It however can lead to decrease in the soil organic matter, nitrogen content, earthworm and microbial population, as well as general fertility of the soil.

3. Chemical method utilizes arboricides to kill stumps and forest regrowth thereby avoiding the utilization of the commonly used mechanical means of land clearing. However some arboricides are highly poisonous and could have unexpected consequences on humans and other organisms.

4. Mechanical method employs heavy machinery such as bulldozer and tractors to clear vegetation. This method is adopted by large scale farmers. It is more costly than the other three methods.

The rank ordering and scoring of the land clearing operational options is as shown in Table 2 below.

Table 2. Land clearing options and their scores

Option	Resource consumption	Environmental pollution	Efficiency of operation	Total	Path ID
Manual	1	1	4	6	A1
Burning	2	2	2	6	A2
Chemical	3	4	3	10	A3
Mechanical	4	3	1	8	A4

Mound/ridge making

This refers to the piling up of earthen materials either in rounded forms (mounds) or continuous earthen elevation in a row or rows (ridges) above the plane. It is done in preparation for seed yam planting to facilitate easy penetration of seed yam roots thereby fostering its growth and eventual yield. There are three commonly used methods in Nigeria, namely:

1. Manual method involving the use of hoes designed for the purpose. The use of manual methods for mound /ridge making is generally plagued with drudgery and is only suited for small scale farming.

2. Animal draught methods involve the use of animals such as donkey and bull to which farm implements such as disk or mouldboard plough are attached, which draw those implement to make ridges. This method is commonly utilized in Northern Nigeria.

3. Mechanical method. This is similar to animal draught method except that tractors are used instead of donkey or bull. This method is often used for large scale farming.

The rank ordering and scoring of the mound/ridge making operational options is as shown in Table 3 below.

The same rank ordering and scoring process was used for the rest unit processes in the yam production value chain.

Table 3. Mound/ridge making options and their scores

Option	Resource consumption	Environmental pollution	Efficiency of operation	Total	Path ID
Manual	1	1	3	5	B1
Animal	2	1	2	5	B2
Mechanical	3	2	1	6	B3

Seed planting

Yam seed planting and fertilizer application operations are often carried out manually by small scale farmers while large scale farmers use mechanical methods involving the use of planters and fertilizer applicators.

Staking involves the insertion/erection of long sticks in the soil near each sprouting yam seed is used to train the yam vine to hang onto those stakes in order to facilitate healthy growth. The staking operation involves cutting sticks of about 40–70 mm thick and about 180–200 cm height, transporting them to the site, inserting each stick for one or two growing yam vines, and training the vines to wind around the stakes. The staking design could be in various patterns, namely: standalone, 4-across two rows, or stakes in each row linked by horizontally lying top ones that are tied to the top of the standing ones. To date it is only done manually. Transportation of the stakes may be manual, animal drawn carriage or by a machine.

Weed control is often necessary at the early growth stage of the yam seedling before the vines form a canopy. There are four commonly used weed control methods.

1. Manual method. This often involves the use of hoe and cutlass. This method is often plagued with drudgery and suited for only small sized farms, just like other manual farming operations.
2. Chemical method. This method involves the use of herbicides. It requires careful handling as it may kill other things that were not the target of the application. It could be done manually or mechanized.
3. Animal draught weeding method. This involves the attachment of weeding implement to a set of farm animals such as donkey and bulls, and directing their movement.
4. Mechanical weeding method. This involves the use of weeding tool mounted farm machinery that may be self-propelled or manually driven. The weeding tool may be cutters that farm machinery like mower or trimmers can be used. It may also involve a tool that turns the soil on the weed.

Pest control/chemical application

1. Chemical method. This common method involves the use of pesticides/insecticides. It also requires careful handling as it may kill other things that were not the target of the chemical application. It could be done manually or mechanized.

2. Biological method. This involves raising and releasing insects, birds or animals that kill/feed on the pests.

3. Mechanical method. This usually involves the use of noise making devices that scare away the pest. The most common one consists of string suspended metal gongs that periodically hit each other as wind blows. The level of effectiveness of this method is yet to be established.

Harvesting

There are two usable methods for yam harvesting.

1. Manual method. Majority of yam harvesting is done by using hoes or cutlass to dig out the tuber from the soil. It usually involves cutting off the vine from the tuber, removing the soil around the tuber, shaking the tuber and lifting it up from the soil.

2. Mechanical method. Tuber harvesting implement can also be attached to a tractor that digs out the yams from the soil. This is suitable for mechanized large farms.

Storage

Losses in farm produce in many developing countries are largely due to lack of appropriate storage facilities for storing harvested produce. This is often because small holders can not afford the cost of modern storage facilities and these losses poses threat to food security and constitute serious economic losses in many developing countries. Yam is one of the farm produce that suffer from such losses (Amponsah et al., 2015). There are two common methods of yam storage in Nigeria:

1. Traditional method. There are various versions of this method. One common version involves tying yams unto erected stakes. The stakes are fenced to prevent human theft and easy access by animals such as rodents that may want to feed on the yams. This version allows cross circulation of air that elongates the lifespan of the tubers by preventing decay and mold growth on the tubers.

2. Improved yam storage facility. In recent years, there are concerted efforts being devoted to the design and development of modern yam storage facilities in Nigeria and in Ghana (FAO, 1990; Amponsah et al., 2015 and Knoth, 2020). Improved storage methods generally consist of ventilated buildings of various sizes with shelves on which yams are stored. The storage facility may be naturally or artificially ventilated.

Yam post-harvest processing

Cleaning

The processing of yam to any industrial material or product requires the removal of remaining soil that may still be clinging to it after harvesting it. A number of marketers do put identification marks on their yams. The markings may be with paints, chalk or charcoal. All these would need to be removed by washing before further processing. There are two main methods of tuber washing which are also applicable to yam washing:

1. Traditional method involves hand washing each yam tuber in water usually with a sponge. Like other operations involving the usual manual method, this method is tedious and generally applicable to small scale processing.

2. Mechanized methods could be either continuous or batch type. The most common ones involve a motorized sieve-like cylinder rotating in a pool of water that is fed with yams. The continuous version is often fitted with an auger or worm like device that moves yams from feeding point to the output end.

Other yam processing operations to various industrial materials/products such as slicing, crushing, frying, parboiling/cooking, drying, milling and packaging are amenable to both traditional manual method and mechanized method depending on the scale of operations as well as availability and affordability of the technology. Options available for each operation are comparatively assessed in terms of their energy, material and water consumption. Their environmental impacts are also comparatively evaluated with regards to the extent to which they affect land degradation, water contamination, air pollution and loss of biodiversity.

This example to illustrate this conceptual LCA method involves the use of the method by a corporate organization that produce 'pando yam' flour, chips, and starch from yam. The company has two farms under cultivation for the production of yams and other crops. It also has a facility that process the yam into pando yam flour.

Limitations to the utilization of the method

The use of this method requires in-depth knowledge of operations required to produce a product. The method is also based on the user's sufficient knowledge of all methods that could be used to accomplish a task/operation and his/her ability to correctly evaluate and rank order them in terms of the various attributes developed to assess the usable methods.

RESULTS AND DISCUSSION

Lifecycle inventory

Two decision scenarios were evaluated. The first scenario is that of that individual that wants to choose the best environmentally friendly pathway along the value-chain. The second scenario went beyond the consideration of just the technical and environmental factors to include the economic and social factors (Zamagni et al., 2013).

1. Techno-environmental Scenario:

The LAM integrated LCA process starts with setting the goal and scope of the LCA study using the ISO 14044 standard. Then comes the role of a decision maker that is knowledgeable in: the operations constituting the value chain, available choices within each operation, and the various characteristics of each choice in relation to the environmental factors such as resource requirements and environmental releases. He/she considers these factors and rank order the choices from the best to the worst. If there are three available choices for an operation, the best choice in term of environmental performance is assigned 1 while the worst choice is assigned 3. If there are six possible choices, rank ordering them means the best choice is assigned 1 while the worst choice is assigned 6. The decision maker goes through the rank ordering of available choices for each operation till the last operation in the value chain. The set of choices that is ranked 1 for each of the operations in the value chain constitute the optimal environmentally friendly pathway along the value chain. Table 4 is an extract of environmental focus analysis results where the goal of the conceptual LCA analysis is

only to select a technically sound and environmental friendly optimal pathway for yam production value chain.

Table 4. A sample results of technical effectiveness and environmental friendliness based analysis

Land clearing operation					
Option	Res. cons.	Env. pol.	Tech. eff.	Total	Path ID
Manual	1	1	4	6	A1
Burning	2	2	2	6	A2
Chemical	3	4	3	10	A3
Mechanical	4	3	1	8	A4
Mound/ridge making operation					
Option	Res. cons.	Env. pol.	Tech. eff.	Total	Path ID
Manual	1	1	3	5	B1
Animal	2	1	2	5	B2
Mechanical	3	2	1	6	B3
Seed planting					
Option	Res. cons.	Env. pol.	Tech. eff.	Total	Path ID
Manual	1	1	3	5	C1
Mechanical	3	2	1	6	C3
Fertilizer application					
Option	Res. cons.	Env. pol.	Tech. eff.	Total	Path ID
Manual	1	1	2	4	D1
Mechanical	2	2	1	5	D2
Staking					
Option	Res. cons.	Env. pol.	Tech. eff.	Total	Path ID
Manual	1	1	3	5	E1
Manual-animal	2	2	2	6	E2
Manual-mechanical	3	3	1	7	E3
Weed control					
Option	Res. cons.	Env. pol.	Tech. eff.	Total	Path ID
Manual	1	1	2	4	F1
Chemical	2	3	1	6	F2
Animal	2	2	3	7	F3
Mechanical	4	3	4	11	F4
Pest control					
Option	Res. cons.	Env. pol.	Tech. eff.	Total	Path ID
Chemical	2	3	1	6	G1
Biological	1	1	2	4	G2
Mechanical	3	2	3	8	G3
Harvesting					
Option	Res. cons.	Env. pol.	Tech. eff.	Total	Path ID
Manual	1	1	2	4	H1
Mechanical	2	2	1	5	H3
Storage					
Option	Res. cons.	Env. pol.	Tech. eff.	Total	Path ID
Traditional	1	1	2	4	I1
Improved	2	2	1	5	I2

Res. cons. – resource consumption; Env. pol. – environmental pollution; Tech. eff. – technical effectiveness; Econ. – economic sustainability.

2. Sustainability Scenario:

There are three main dimensions of sustainability: namely, environmental, social, amd economic sustainability. Consequently, this scenario considers the three dimensions in the selection of the optimal pathway. This is particularly important in view of the ongoing trend in agri-industrial system analysis that necessitates going some steps further to include potential economic and sociocultural/sociopolitical impacts of our choices. Social factors consider various aspects of human well-being. The methods are evaluated in terms of elimination/reduction of drudgery, minimization of exposure to health risk, emotional trauma, and other possible hazards that could affect human well-being (Jørgensen et al., 2008). Looking at the options available for each operation, the use of mechanical methods facilitate the attainment of the aforementioned goals. This scenario follows the same process as in the case of techno-environmental scenario. However, in addition to evaluating the available choices for each operation on the basis of environmental factors, it also consider social and economic factors (Roos, 2016). The choice that has the lowest total of the combination of the environmental, social and economic factors is ranked first. The choices are thus ordered from the lowest total to the highest total for each operation. The set of choices that are ranked first over the value chain operations constitutes the optimal pathway. Table 5 shows a sample results of sustainability based analysis that included economic and social considerations along with the technical effectiveness and environmental friendliness.

Table 5. A sample results of sustainability based analysis

Land clearing operation							
Option	Res. cons.	Env. pol.	Tech. eff.	Econ.	Social	Total	Path ID
Manual	1	1	4	4	4	14	A1
Burning	2	2	2	1	2	9	A2
Chemical	3	4	3	2	2	14	A3
Mech	4	3	1	3	1	12	A4
Mound/ridge making operation							
Option	Res. cons.	Env. pol.	Tech. eff.	Econ.	Social	Total	Path ID
Manual	1	1	3	3	3	11	B1
Animal	2	1	2	1	2	8	B2
Mech	3	2	1	2	1	9	B3
Seed planting							
Option	Res. cons.	Env. pol.	Tech. eff.	Econ.	Social	Total	Path ID
Manual	1	1	3	2	2	9	C1
Mech	3	2	1	1	1	8	C2
Fertilizer application							
Option	Res. cons.	Env. pol.	Tech. eff.	Econ.	Social	Total	Path ID
Manual	1	1	2	2	2	8	D1
Mech	2	2	1	1	1	7	D2
Staking							
Option	Res. cons.	Env. pol.	Tech. eff.	Econ.	Social	Total	Path ID
Manual	1	1	3	3	3	11	E1
Manual-animal	2	2	2	1	2	9	E2
Manual-mech	3	3	1	2	1	10	E3

Table 5 (continued)

Weed control							
Option	Res. cons.	Env. pol.	Tech. eff.	Econ.	Social	Total	Path ID
Manual	1	1	2	4	4	12	F1
Chemical	2	3	1	2	3	11	F2
Animal	2	2	3	2	2	11	F3
Mech	4	3	4	1	1	13	F4
Pest control							
Option	Res. cons.	Env. pol.	Tech. eff.	Econ.	Social	Total	Path ID
Chem	2	3	1	3	3	12	G1
Biol	1	1	2	1	2	7	G2
Mech	3	2	3	2	1	11	G3
Harvesting							
Option	Res. cons.	Env. pol.	Tech. eff.	Econ.	Social	Total	Path ID
Manual	1	1	2	2	2	8	H1
Mech	2	2	1	1	1	7	H2
Storage							
Option	Res. cons.	Env. pol.	Tech. eff.	Econ.	Social	Total	Path ID
Tradi	1	1	2	2	2	8	I1
Improv	2	2	1	1	1	7	I2

Res. cons. – resource consumption; Env. pol. – environmental pollution; Tech. eff. – technical effectiveness; Econ. – economic sustainability.

Lifecycle impact analysis

An evaluation of the results shown in Tables 4 and 5 provides us some insights into the best pathway for each of the two yam production value chain decision scenarios. Fig. 5 shows the best yam production value chain pathway for the techno-environmentally focussed decisions while Fig. 6 shows the best yam production value chain pathway for an all encompassing sustainability based decision. It would be observed that the environmentally friendly optimal pathway largely consist of manual methods. The reason for this is because manual methods generally require less resource to operate and they generate no or smaller emissions than other approaches.

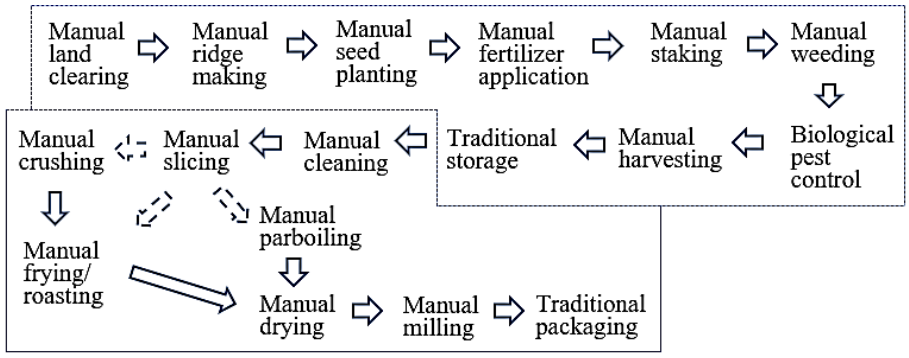

Figure 5. An illustration of the best pathway for techno-environmental focused yam production value chain.

The sustainability optimal pathway (Fig. 6) mainly consist of mechanical approaches. The main reason is because the use of mechanical methods generally protect workers from drudgery and facilitates higher productivity. Thus, it is preferred to the manual and other approaches. The combine effect of economic and social sustainability balances the environmental sustainability for the attainment of all round sustainability.

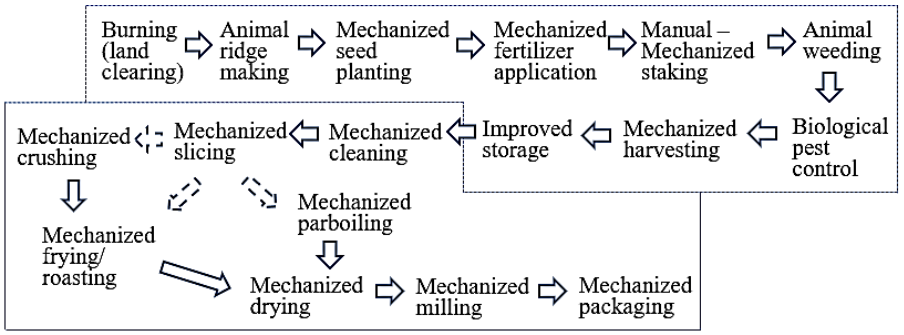

Figure 6. An illustration of the best pathway for sustainability focused yam production value chain.

Systems Lifecycle Interpretation

Techno-environmental focused analysis results in Table 4 and Fig. 5 revealed an emphasis on the use manual labour in majprity of the operaions along the yam production value chain. The reason is not far fetched. Manual labour based operations minimizes resource consumption and eliminates environmental releases that could lead to resource depletion, loss of biodiversity, air polltion, water contamination and a number of other environmental problems. However, business decisions would need to also consider economic implications of its choices. Consequently, there is a need to include economic and social factors in the analysis. A look at results of sustainability analysis results in Table 5 and Fig. 6 showed that major emphasis is on the use of mechanized systems. The reason being that mechanized systems facilitate mass production, reduced unit cost, increased profit margin and drudgery elimination. A comparison of the environmental results and sustainability results revealed only in pest control operation that both analysis recommed the same approach, that is biological pest control.

Comparing both decision scenarios, sustainability based optimal pathway is more comprehensive and it is a more balanced decision than environmentally optimal pathway as it also consider social and economic factors. The only challenge is that the sustainability decision scenario require someone with not only the indepth knowledge of environmental characteristics of the system to implement the LCA process, it also requires the decision maker to have the knowledge of the social and economic characteristics of various choices available along the value chain.

CONCLUSIONS

This paper presented a simplified less data intensive linear assignment based conceptual LCA method. The used of the LCA methodology was illustrated with a case study yam production value chain. Contributions of this study includes its provision of opportunity to choose the best pathway to produce agri-industrial materials in technically

efficient and environmentally friendly manner. It also facilitates the use of lifecycle concepts in selecting agri-industrial material production operations without going through the rigour of data collection and related analytical issues. The methodology would enable small to medium scale farmers and agri-processors in developing countries to conduct an LCA of their products because many of the LCA software and databases are beyond their affordability. In addition, this methodology is much easier to use than the conventional lifecycle assessment method. Moreover, this LCA approach is less costly and less time consuming than other known methods. The methodology can be used by a manager, a policy maker or any professional to identify the best operational pathway that is technically sound, environmental friendly, warrants economic profitability and incorporate human welfare consideration. This methodology would be found useful, not only for any agri-industrial material production value chain but also for other production or service systems decision scenarios that require an evaluation of environmental and socioeconomic consequeces of our choices.

REFERENCES

Avadí, A., Marcin, M., Biard, Y. Renou, A.; Gourlot, J-P & Basset-Mens, C. 2020. Life cycle assessment of organic and conventional non-Bt cotton products from Mali. *Int. J. Life Cycle*, 678–697. https://doi-org.libproxy.mtroyal.ca/10.1007/s11367-020-01731-x

Abdolazimi, A., Momeni, M & Montazeri, M. 2015. Comparing ELECTRE and Linear Assignment Methods in Zoning Shahroud-Bastam Watershed for Artificial Recharge of Groundwater with GIS Technique. *Modern Applied Science* **9**(1), 68–82.

Azar, F.S. 2000. Multiattribute Decision-Making: Use of Three Scoring Methods to Compare the Performance of Imaging Techniques for Breast Cancer Detection. Accessed online on 26 Jan 2020 at https://repository.upenn.edu/cgi/viewcontent.cgi?referer=https://www.google.com/&httpsredir=1&article=1121&context=cis_reports

Amponsah, S.K., Akowuah, J.O., Adu-Kwarteng, E. & Bessah, E. 2015. Design and Construction of Improved Yam Storage Structure Using Locally-Available Materials. *International Journal of Research in Agriculture and Forestry* **2**(10), 1–11.

ANOL (Agriculture Nigeria on Line). 2018. Yam flour production trend now. Accessed online on 12 December 2019 at https://agriculturenigeria.com/agro-processing/processing-of-crops/yam-processing

Bashiri, M., Badri, H. & Hejazi, T.H. 2011. Selecting optimum maintenance strategy by fuzzy interactive linear assignment method. *Appl. Math. Model*. **35**(1), 152–164.

Bassey, E.E. 2017. Constraints and prospects of yam production in Nigeria. *European journal of physical and Agricultural Sciences* **5**(1), 55–64. Accessed online on 12 December 2019 at https://www.idpublications.org/wp-content/uploads/2016/12/Full-Paper-constraints-and-prospects-of-yam-production-in-nigeria.pdf

Baykasoglu, A., Subulan, K. & Karaslan, F.S. 2016. A new fuzzy linear assignment method for multi-attribute decision making with an application to spare parts inventory classification. *Applied Soft Computing* **42**, 1–17.

Chen, T.-Y. 2013. A linear assignment method for multiple-criteria decision analysis with interval type-2 fuzzy sets. *Applied Soft Computing***13**, 2735–2748.

Diop, A. 1998. Storage and processing of roots and tubers in the tropic. FAO. Chapter 1.4.2 Yams. http://www.fao.org/docrep/X5415E/x5415e00.htm#Contents

Dunmade, I.S. 2004. *PLETS model: A sustainability concept based approach to product end-of-life management.* In the Proceedings of Environmental conscious manufacturing IV: (Philadelphia PA, 26–27 October 2004) **5583**, pp. 118–126. ISBN 0-8194-5536-9

Dunmade, I.S. 2013a. A Multi-criteria model for sustainability Assessment of an Agri-Industrial Technology meant for a Developing Economy. *International Journal of Engineering Research and Applications* **3**(1), 445–456.

Dunmade, I.S. 2013b. An investigation on Alpaca Fibre's Microstructure as a renewable material for engineering applications. *International journal of engineering science invention* **2**(31), 45–49.

Dunmade, I.S. 2019a. Lifecycle assessment education in Nigeria: An exploratory evaluation of the trend. *Procedia Manufacturing* **35**, 447–452.

Dunmade, I.S. & Anjola, A. 2019b. Social lifecycle impact assessment of cocoyam chips hawking in Lagos, Nigeria. *Procedia Manufacturing* **35**, 453–458.

Eze, C. 2018. How to plant yam in Nigeria. Accessed online on 12 December 2019 at https://infoguidenigeria.com/plant-yam/

FAO. 1990. Handling and storage methods for Fresh Roots and Tubers. Accessed online on 18 January 2020 at http://www.fao.org/docrep/X5415E/x5415e04.htm

Farahani, S.S., Soheilifard, F., Raini, M.G.N & Kokei, D. 2019. Comparison of different tomato puree production phases from an environmental point of view. *Int J Life Cycle Assess* **24**, 1817–1827. https://doi-org.libproxy.mtroyal.ca/10.1007/s11367-019-01613-x

Fava, J.A. & Cooper, J.S. 2004. LCA Capacity Building in North America: An Update on Capacity Building. *Journal of Industrial Ecology* **8**(3), 8–10.

FMAWRRD (Federal Ministry of Agriculture, Water Resources and Rural Development) (2020). Agricultural policy for Nigeria. Accessed online 4th Feb 2020 at http://extwprlegs1.fao.org/docs/pdf/nig149296.pdf

Herrera, F. & Herrera-Viedma, E. 2000. Linguistic decision analysis: steps for solving decision problems under linguistic information. *Fuzzy Sets Syst*. **115**, 67–82.

Hori, Y. & Oshima, Y. 1986. Life history and population dynamics of the Japanese Yam, *Dioscorea japonica*. Botanical Magazine Tokyo **99**(4), pp. 407–418. https://doi.org/10.1007/BF02488719

IITA (International Institute of Tropical Agriculture) (2013). Report, achievement, challenges and prospects of yam production in Nigeria, IITA, Ibadan, Nigeria. Accessed online on 15 May 2020 at https://www.iita.org/wp-content/uploads/2016/04/Annual-Report-2013.pdf

Ike, P.C. & Inoni, O.E. 2006. Determinants of yam production and economic efficiency among small holder farmers in South Eastern Nigeria. *Journal of Central European Agriculture* **7**(2), 337–342.

International Standard Organisation (ISO). 2006a. Environmental Management_Life Cycle Assessment: Principles and Framework. ISO14040, Geneva.

International Standard Organisation (ISO). 2006b. Environmental Management_Life Cycle Assessment: Requirements and Guidelines. ISO14044, Geneva.

Jahan, A., Ismail, M.Y.; Mustapha, F. & Sapuan, S.M. 2010. Material selection based on ordinal data. *Mater. Des.* **31**(7), 3180–3187.

Kazulis, V., Muizniece, I. & Blumberga, D. 2018. Conceptual cradle to gate analysis of GHG emissions from wood, agricultural plant and synthetic fibres. *Agronomy Research* **16**(1), 1069–1076. https://doi.org/10.15159/AR.18.099

Knoth, J. 2020. Traditional Storage of Yams and Cassava and its Improvement (GTZ). Accessed online at www.nzdl.org/gsdlmod?.

Jørgensen, A, Le Bocq, A., Nazarkina, L. & Hauschild, M. 2008. Methodologies for Social Life Cycle Assess-ment. *Int J LCA* **13**(2), 96–103. doi: http://dx.doi.org/10.1065/lca2007.11.36

Liu, H.W. & Wang, G.J. 2007. Multi-criteria decision-making methods based on intuitionistic fuzzy sets. Eur. *J. Oper. Res*. **179**, 220–233.

Liu, H.T. & Wang, W.K. 2009. An integrated fuzzy approach for provider evaluation and selection in third-party logistics. *Expert Syst. Appl*. **36**, 4387–4398.

Maroya, N.G., Asiedu, R., Kumar, P.L., Lopez-Montes, A. Orchard, J. &Ndiame, F. (2014). YIIFSWA Working Paper Series No. 1. Yam Improvement for Income and Food Security in West Africa. International Institute of Tropical Agriculture, Ibadan, Nigeria, 18 pp. Accessed online on 18 June 2020 at https://www.researchgate.net/publication/265291980_Yam_Improvement_for_Income_and_Food_Security_in_West_Africa_YIIFSWA

Mfitumukiza, D., Nambasa, H. & Walakira, P. 2019. Life cycle assessment of products from agro-based companies in Uganda. *Int J Life Cycle Assess* **24**, 1925–1936. https://doi-org.libproxy.mtroyal.ca/10.1007/s11367-019-01629-3

MRK (Market research guy)(2020). Types of Data & Measurement Scales: Nominal, Ordinal, Interval and Ratio. https://www.mymarketresearchmethods.com/types-of-data-nominal-ordinal-interval-ratio/

Ottosen, M., Mackenzie, S.G., Wallace, M. & Kyriazakis, I. 2020. A method to estimate the environmental impacts from genetic change in pig production systems. *Int. J. Life Cycle Assess* **25**, 523–537. https://doi-org.libproxy.mtroyal.ca/10.1007/s11367-019-01686-8

Rebitzer, G & Hunkeler, D. 2006. The Future of Life Cycle Assessment. *Int. J. LCA* **1010101010**(5), 305–308.

Romero-Gámez, M. & Suárez-Rey, E.M. 2020. Environmental footprint of cultivating strawberry in Spain. *Int. J. Life Cycle Assess* **25**, 719–732. https://doi-org.libproxy.mtroyal.ca/10.1007/s11367-020-01740-w

Roos, S., Zamanib, B., Sandin, G., Peters, G.M. & Svanstrom, M. 2016. A life cycle assessment (LCA)-based approach to guiding an industrysector towards sustainability: the case of the Swedish apparel sector. *Journal of Cleaner Production* **133**, 691–700.

Sadh, P.K., Duhan, S. & Duhan, J.S. 2018. Agro-industrial wastes and their utilization using solid state fermentation: a review. *Bioresour. Bioprocess* **5**(1). https://doi.org/10.1186/s40643-017-0187-z

Suzan, E. & Gameiro, A.H. 2007. The Agri-industrial system of Ostrich in Brazil. Accessed online on 15 January 2020 at http://paineira.usp.br/lae/wp-content/uploads/2017/02/2007_Suzan_Gameiro_pensa.pdf

Triola, M.F. 2007. Elementary Statistics using Excel, 3rd edition. Chapter **1**, pp. 5–9.

Udo de Haes, H.A. 2004. Life-Cycle Assessment and Developing Countries. *Journal of Industrial Ecology* **8**(1/2), 8–10.

Umeghalu, I.C.E. & Ngini, J.O. 2013. Effect of poor land clearing on soil and agricultural produce. *Inter. J. Appl. Sci. Engr*. **1**(2), 56–60. www.ijapscengr.com

USOTA (U.S. Congress, Office of Technology Assessment), Agricultural Commodities as Industrial Raw Materials, OTA-F-476 (Washington, DC: U.S. Government Printing Office, May 1991). Accessed online on 28 Jan 2020 at https://govinfo.library.unt.edu/ota/Ota_2/DATA/1991/9105.PDF

Zamagni, A., Pesonen, H.-L. & Swarr, T. 2013. From LCA to Life Cycle Sustainability Assessment: concept, practice and future directions. *Int. J. Life Cycle Assess* **18**,1637–1641. doi: 10.1007/s11367-013-0648-3

Agronomy Research **18**(3), 2022–2032, 2020
https://doi.org/10.15159/AR.20.197

Effects of lake sediment on soil chemical composition, dehydrogenase activity and grain yield and quality in organic oats and spring barley succession

L. Edesi[1,*], T. Kangor[2], V. Loide[1], R. Vettik[1], I. Tamm[2], H.J. Kennedy[3], M. Haljak[2], Ü. Tamm[2], T. Võsa[1], K. Tamm[1], T. Talve[1] and E. Karron[1]

[1]Estonian Crop Research Institute, Department of Agrotechnology, Aamisepa 1, EE48309 Jõgeva alevik, Estonia
[2]Estonian Crop Research Institute, Department of Plant breeding, Aamisepa 1, EE48309 Jõgeva alevik, Estonia
[3]Estonian Crop Research Institute, Department of Development, Aamisepa 1, EE48309 Jõgeva alevik, Estonia
[*]Correspondence: liina.edesi@etki.ee

Abstract. In organic farming, it is important to maintain soil fertility with organic fertilisers; often organic compost, manure, or slurry is used. However, the effects of lake sediment in maintaining and improving soil fertility are less studied. The direct and residual effects of a one-time application of 50 t ha^{-1} or 100 t ha^{-1} of lake sediment were compared to an unfertilised control for oats *(Avena sativa)* (2015) followed by spring barley *(Hordeum vulgare)* in 2016, under organic farming conditions. Soil chemical composition, microbial activity in the 0–20 cm soil layer, grain yield, and grain quality were tested. The application rate, 100 t ha^{-1}, increased ($P < 0.05$) the soil organic carbon (SOC), the amount of mobile calcium (Ca), total nitrogen (N_{tot}), and boron (B) content in soil. Both application rates increased ($P < 0.05$) the amount of magnesium (Mg), copper (Cu), and manganese (Mn) content in the soil. The application rate had no effect on soil pH. Soil dehydrogenase activity (DHA) was higher ($P < 0.05$) at 100 t ha^{-1} than the control and the lower application rate. Both rates of lake sediment application significantly ($P < 0.05$) increased the grain yield and test weight for oats in 2015. Positive residual effects on spring barely yield only occurred in the 100 t ha^{-1} treatments in 2016. No residual impact of lake sediment was found on spring barely quality.

Key words: *Avena sativa*, *Hordeum vulgare*, lake sediments, organic farming, soil chemical composition, soil dehydrogenase activity.

INTRODUCTION

There are 1,534 natural, 525 reservoir, and 489 artificial lakes in Estonia, as of 2020 (Estonian Environmental Register, 2020). The main stages of development of Estonian lakes are dystrophic, with high levels of humic substances, and eutrophic, with high levels of nutrients (Kõiv, 2012). The result is that lakes become overgrown and a bog begins to develop. To stop this phenomenon, remediation plans have been drawn up for several lakes (Kahala lake, Jõepere lake, Elistvere lake etc.). According to these plans,

the sediment would be partially removed from the lakes. It is not advisable to leave the removed sediment on the shore of the lake as most of the nutrients would drain back into the lake. In addition, depending on the lake, the amount of sediment may be too much for the shoreline to accommodate, for example, at lake Kahala about 12.07 million m^3 of sediments was removed. Therefore, the sediments recovered during the restoration process must be placed somewhere else (Metsur et al., 2015).

In organic farming, it is important to maintain soil fertility, but only via organic methods. In addition to other organic fertilisers, such as organic compost, manure, or slurry, the use of lake sediments could be also a possible method of maintaining and improving soil fertility.

Lake sediment (sapropel) rich in organic matter and minerals are formed from different organic compounds, such as the remains of aquatic plants and animals (Stankevica et al., 2016). Lake sediments are recommended for use on soils with lighter texture, where fertilisation effects occur more quickly (Kalmet et al., 1996).

Several studies on lake sediments have been published in nearby countries – other Baltic countries such as Latvia and Lithuania (Baksiene, 2009; Baksiene & Asakaviciute, 2013; Grantina-Ievina et al., 2014; Baksiene et al., 2015), Finland (Salonen et al., 2001), and Russia (Bogush et al., 2013). Positive effects on soil chemical, physical (Baksiene, 2009; Baksiene & Asakaviciute, 2013), and microbial properties (Grantina-Ievina et al., 2014; Hristeva & Bozhinova, 2017) have been found from sapropel application. Some studies show that fertilisation with lake sediments increases crop yields (Baksiene, 2004; Baksiene, 2009; Baksiene & Asakaviciute, 2013). However, Naumova and her colleagues (2017) found no effect of lake sediments application on yields.

At the same time, there may be some risks associated with using lake sediment as an organic amendment. Rapid industrialization and urbanization have led to a high accumulation of heavy metals in lake sediments, mainly originating from industrial discharge and waste from municipal activities (Li et al., 2012). Due to their toxicity, persistence, and bioaccumulation, heavy metals pose a potential threat to ecological system and human health (Li et al., 2012). However, heavy metal content analyses of freshwater sediment in Poland (Tylmann et al., 2011), Lithuania (Kruopiene, 2007), and Latvia (Stankevica et al., 2012) showed that the concentrations in sediment were generally low.

To our knowledge this is the first study in Estonia to examine the effects of lake sediment on soil chemical and microbial properties and on cereal yield and quality when used as an organic fertiliser in organic agriculture. The objective of this study was to assess the soil chemical composition, soil microbial activity, grain yield and quality of oats and spring barley when fertilised with various rates of lake sediment in organic farming conditions.

MATERIALS AND METHODS

Field experiment and treatments

The field experiment was conducted at the Estonian Crop Research Institute (ECRI) in Jõgeva (58°45'N, 26°24'E) during 2015–2016. The field trial was arranged as randomized plots of 10.5 m^2 with six replications. The trial area was already under organic farming cultivation. The soil of the experimental field is classified as *Calcaric*

Cambic Phaeozem (Loamic) clay loam soil (WRB, 2015). The initial soil chemical composition in spring 2015 was as follows: pH_{KCl} 7.4, P 47.4 mg kg^{-1}, K 101.0 mg kg^{-1}, Ca 4884.1 mg kg^{-1}, Mg 86.8 mg kg^{-1}, Mn 53.3 mg kg^{-1}, Cu 1.9 mg kg^{-1}, B 0.6 mg kg^{-1}, N_{tot} 0.2% and SOC 1.9.

Two fertiliser rates were tested: 50 t ha^{-1} and 100 t ha^{-1} of lake sediments (Table 1). The control had no fertiliser. No fertiliser was used in 2016 in order to measure the residual effects of the lake sediments fertiliser.

Table 1. Dry matter (DM), organic matter (OM), and amount of main nutrients in lake sediment applied in May 2015

Lake sediment, t ha^{-1}	DM, t ha^{-1}	OM, t ha^{-1}	N_{tot} (kg ha^{-1})	P_{tot}	P^M	K_{tot}	K^M	Ca	Mg	Mn	Cu	B	Fe^M
50	13.6	3.5	62	37.7	0.3	34.8	3.5	1,301	59	15	0.1	0.4	7.9
100	27.1	7.0	125	75.3	0.6	69.7	7.0	2,602	118	30	0.2	0.8	15.7

[M]Mehlich 3 method.

In the first year (2015), the lake sediment was applied and ploughed into the soil before sowing the oat seeds. The sowing rate of oat var. *Eugen* was 600 seeds per m^2. In the second year (2016), when the residual effect of lake sediments was studied, 500 seeds per m^2 of spring barley var. *Maali* were sown. Both crops were sown at the optimal sowing time for eastern Estonia (the first week of May) with a Pöttinger sowing machine. In both years at growth stages 13–14 on the Biologische Bundesan-stalt, Bundessortenamt and CHemical Industry (BBCH) scale, harrowing was used to control weeds (Meier, 2001). All plots were harvested in August with a Hege combine harvester.

Soil and lake sediment sampling and analyses

Soil samples (approximately 0.5 kg) for chemical and soil dehydrogenase activity (DHA) analyses were taken from each treatment in six replications from the 0–20 cm layer with a 16 mm auger. Soil samples were taken in the spring before lake sediment application in 2015 and in the fall at harvest in 2015 and 2016. Additionally, soil samples were taken one month after the lake sediment application to analyse soil DHA. The chemical composition of lake sediment was analysed before application.

For soil chemical properties the following analyses were carried out: pH_{KCl}–ISO 10390; P, K, Ca, Mg, Mn – Mehlich 3 (Mehlich, 1984); N_{tot} – ISO 13878; B – Berger & Truog method; SOC – ISO 10694. Lake sediments were characterized for different parameters: dry matter content (DM) –gravimetric method; organic matter content (OM) – GOST 27980-88; N_{tot} – Kjeldahl method; pH_{KCl} – GOST 27979-88; P_{tot}, K_{tot}, Ca, Mg – PMK–JJ–4C; Mn, Cu, B– PMK–JJ–1A; available P, K and Fe – Mehlich 3. The soil and lake sediment chemical analyses were determined in an accredited laboratory at the Estonian Agricultural Research Centre.

Soil samples for DHA analyses were sieved (2 mm) and stored at 4 °C until they were analysed in ECRI's laboratory. Measurement of soil DHA were based on methods from Tabatabai (1982). Soil samples (5 g) were incubated at 30 °C for 24 h in the presence of an alternative electron acceptor (triphenyltetrazoliumchloride). The red-tinted product, triphenylformazan (TPF), was extracted with acetone and measured in a spectrophotometer (BioPhotometer plus).

Crop yield and quality

The grain from each plot was dried, cleaned and weighed separately. Grain yield was calculated at 14% moisture content. Grain quality characteristics such as thousand-kernel weight (TKW) (g), test weight (g L^{-1}), and protein content (%) were measured in ECRI's laboratory. TKW were measured by the ISTA method, test weight by an automatic grain analyser (Infratec 1241Analysis), protein content by the near-infrared method (NIR) using an XDS Rapid Content Analyser (Foss, Cheshire, UK) and a Monochromator (NIR).

Phenological growth stages were determined according to BBCH identification keys for cereals. Number of ears per m^2 was determined at BBCH 77–79.

Meteorological data

Meteorological data were obtained from a field meteorological weather station (Metos Compact) located at Jõgeva, close to the trial site. The meteorological data of the month is divided into three parts (I, II, III). I – the first 10 days of a month, II – the middle 10 days of a month and III – the last 10 days of a month.

Data from each year were different (Figs 1, 2). The average air temperature and precipitation of the 2015 growing period was similar to the long-term average (1922–2015) of the same period, though there were some drier stretches. The period from May II to June III (tillering, stem elongation), there was less precipitation which caused drought conditions for the oat plants. The second drier period was prior to harvesting (grain filling) through harvest, from July III to the end of August. Oats were harvested August 27.

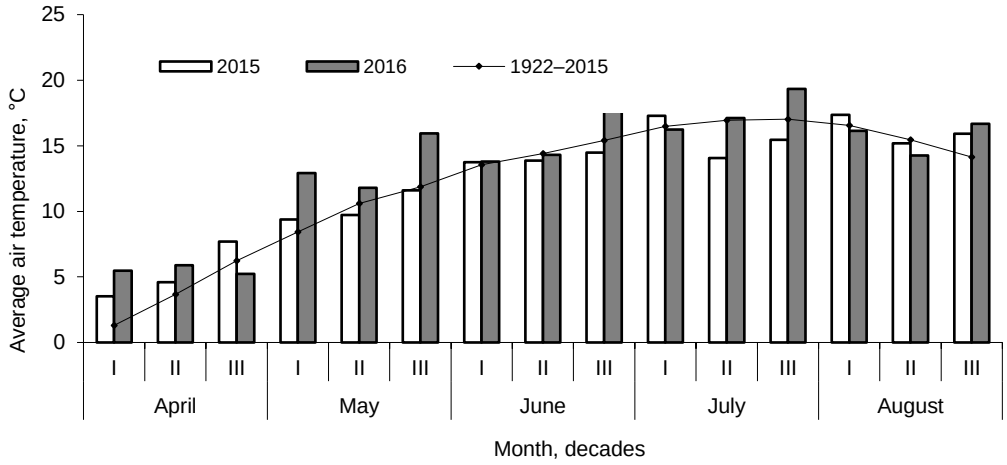

Figure 1. Average air temperature during growing periods of 2015–2016 and long-term average (1922–2015).

In 2016, the average air temperature during the growing period was somewhat higher than in 2015 and there were extreme precipitation fluctuations. May was very dry with only 4 mm of rain. During the same time, the average temperature was high and drought conditions occurred. The large amount of precipitation (120 mm) at the end of June saved the barley yield. Barley was harvested August 18.

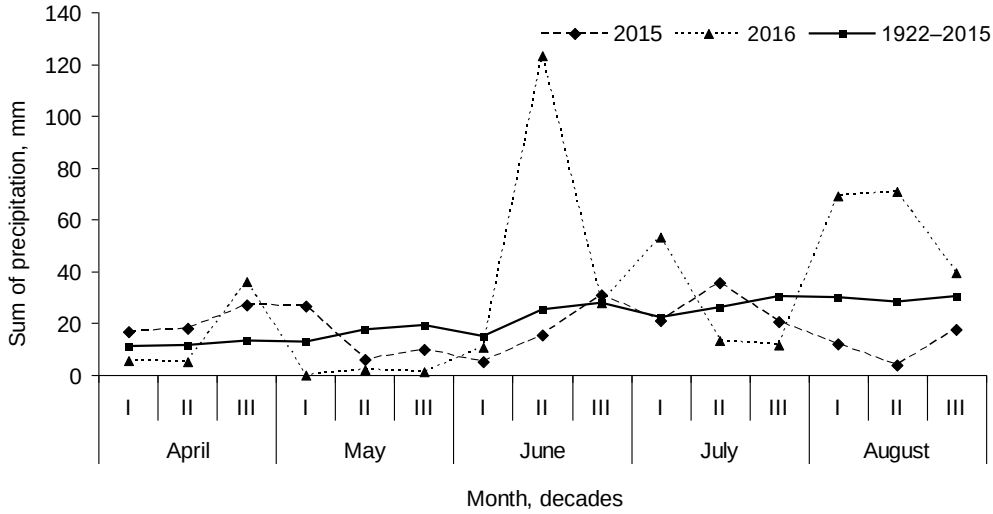

Figure 2. Sum of precipitation during growing periods of 2015–2016 and long-term average (1922–2015).

Statistical analyses

One-way ANOVA was used to test the effect of lake sediment on soil chemical properties, microbial activity, and grain yield and quality ($n = 6$) of oats and spring barley. In case of significant effects, differences between treatments were tested post-hoc using the *Tukey-Kramer (HSD) test*. The statistical analyses were performed using the *JMP 5.0.1.2* software.

RESULTS AND DISCUSSION

Soil chemical composition

The lake sediment application rate of 100 t ha^{-1} had significant direct and residual effects on some of the soil agrochemical parameters, while minor or no effect was found at the 50 t ha^{-1} rate (Table 2). In 2015, the use of lake sediment at 100 t ha^{-1} significantly ($P < 0.001$) increased the SOC content of the soil. Similar results were found by Baksiene and Asakaviciute (2013); they reported higher humus content in soil fertilised with a rate of 40 t DM ha^{-1} of lake sediment. Lake sediment (sapropel) is rich in organic matter and minerals are formed from different organic compounds, such as the remains of aquatic plants and animals (Stankevica et al., 2016). The proportion of organic matter in the lake sediment applied was 7.0 t ha^{-1} OM out of 100 t ha^{-1} lake sediment (Table 1). The second year showed that the residual effect of both sediment treatments on SOC was noticeable, but not significant.

The use of lake sediment at a rate of 100 t ha^{-1} significantly ($P = 0.002$) increased the amount of available Ca in the soil since a considerable amount (2,602 kg ha^{-1}) of Ca was applied in the lake sediment (Table 1). The soil pH was neutral before (7.4) and application of lake sediment did not change the soil acidity. Baksiene and Asakaviciute (2013) also found no effect of various rates of lake sediment application (10, 20 and 40 t DM ha^{-1}) on soil pH.

The content of Mg, Cu, and Mn in the soil was significantly influenced by the use of lake sediment (Table 2). Significantly ($P < 0.001$) higher N_{tot} and B content was found in the 100 t ha^{-1} treatment. In the case of Mn and B, the soil levels were quite low before the application of lake sediment and remained low afterwards.

Table 2. The average agrochemical properties of the 0–20 cm soil layer in fall 2015 and 2016

Treatment	Year	pH_{KCl}	SOC, %	N_{tot}, %	P	K	Ca	Mg	Cu	Mn	B
					mg kg^{-1}						
Control	2015	7.40^{a}	1.65^{b}	0.12^{c}	44.5^{ab}	114.8^{a}	4,037.3^{b}	75.3^{c}	1.70^{c}	49.5^{b}	0.72^{b}
50 t ha^{-1}		7.40^{a}	1.75^{b}	0.13^{b}	41.3^{b}	97.8^{b}	4,527.8^{b}	79.3^{b}	1.88^{b}	60.3^{a}	0.74^{b}
100 t ha^{-1}		7.40^{a}	1.98^{a}	0.16^{a}	49.5^{a}	118.3^{a}	5,713.8^{a}	90.8^{a}	2.25^{a}	63.8^{a}	0.89^{a}
P value		*ns*	*<0.001*	*<0.001*	*0.008*	*0.004*	*0.002*	*<0.001*	*<0.001*	*0.004*	*<0.001*
Control	2016	7.30^{a}	1.65^{a}	0.13^{a}	52.5^{a}	125.5^{a}	4,465.5^{b}	100.0^{a}	2.05^{b}	60.0^{a}	0.65^{b}
50 t ha^{-1}		7.40^{a}	1.80^{a}	0.13^{a}	46.5^{a}	113.0^{b}	5,306.5^{ab}	95.5^{a}	2.05^{b}	73.5^{a}	0.66^{ab}
100 t ha^{-1}		7.35^{a}	1.85^{a}	0.14^{a}	51.5^{a}	125.5^{a}	,6539.0^{a}	95.0^{a}	2.35^{a}	73.0^{a}	0.74^{a}
P value		*ns*	*ns*	*ns*	*ns*	*0.035*	*0.019*	*ns*	*0.037*	*ns*	*0.043*

Different letters indicate significant differences between treatment means ($n = 6$) (*Tukey-Kramer HSD test*, $P < 0.05$).

The sediment application had no effect on P and K content in soil. It could be because the total P and K content of the lake sediment at a rate 100 t ha^{-1} was 75.3 and 69.7 kg ha^{-1} of which only 0.6 and 7.0 kg ha^{-1}, respectively, was in plant available form, according to the Mehlich 3 test (Table 1). In iron-rich sediments, if the ratio of Fe to P is greater than 15, P will be unavailable to plants because oxidized iron ($FePO_4^{3-}$) is capable of binding all the dissolved P, under aerobic conditions (Jensen et al., 1992, Heinsalu et al., 2003). The soluble Fe to P ratio of the sediments used in the field trial was over 20.

Based on the second year soil data, a significant residual effect of lake sediments occurred only in case of Ca, Cu and B content at the 100 t ha^{-1} application rate with no significant residual effects at the 50 t ha^{-1} application rate.

Soil dehydrogenase activity

One month after lake sediment application, in June 2015, the soil DHA was significantly ($P < 0.001$) higher in the 100 t ha^{-1} treatment compared to the control and 50 t ha^{-1} treatment (Fig. 3). In fall 2015, the soil DHA remained significantly ($P = 0.003$) higher in the 100 t ha^{-1} treatment compared to the 50 t ha^{-1} treatment and the control. Compared to the control, the significantly ($P = 0.0204$) positive impact on soil DHA continued to be noticeable the following spring (2016). However, by fall 2016 the soil DHA of all treatments had returned to the pre-treatment level. The lake sediment application had no statistically significant effect on soil DHA in the 50 t ha^{-1} treatment throughout the experimental period.

The significant effect of the highest rate of lake sediment application on the soil DHA was probably caused by the higher SOC and nutrient content in this treatment (Table 2). It has been found that freshwater sapropel contains high levels of aerobic heterotrophic bacteria and yeasts (Grantina-Ievina et al., 2014). In addition, in 2015 there were extraordinarily dry periods in the two months prior to lake sediment application which consequently reduced soil moisture content (Fig. 2). At the same time, a large

portion of the 100 t ha^{-1} of lake sediment applied was water (about 72.9 t ha^{-1}, equivalent to 7.29 mm of precipitation). A negative effect of drought on the size and activity of the soil microbial biomass was found by Hueso et al. (2012), while Siebert et al. (2019) found that soil microbial activity and biomass in grasslands were not affected by drought.

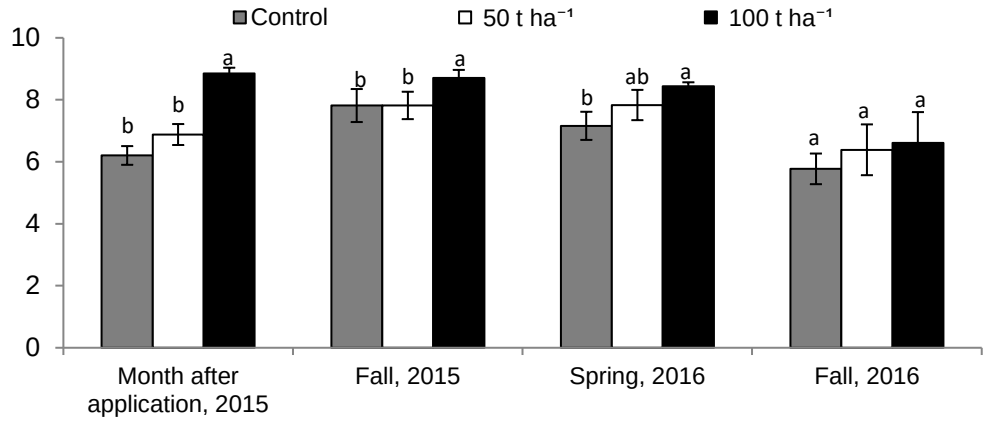

Figure 3. Soil dehydrogenase activity (DHA, TPF μg g^{-1} h^{-1}) in the 0–20 cm layer in 2015 and 2016. Different letters indicate significant differences between treatment means (n = 6) (*Tukey-Kramer HSD test*, month after application, $P < 0.001$; fall 2015, $P = 0.003$; spring 2016, $P = 0.0204$; fall 2016, $P > 0.05$).

Although the effect of lake sediment specifically on soil microbiological activity has been little studied, more generally there are many studies which have shown a strong positive relationship between soil microorganisms and organic fertilisers. Organic amendments such as manure provide a direct source of C for soil organisms (Bünemann et al., 2006; Fliessbach et al., 2007). Knapp et al. (2010) found that the compost amendments impact the soil microbiota and leave a distinct imprint on the soil.

Grain yield and quality

The first-year data showed that there was significant ($P = 0.005$) direct effects on oat yield from fertilisation with lake sediment. Compared to the control yield (4,353 kg ha^{-1}), both treatments increased oat yield; the additional yield was 417 kg ha^{-1} for the 50 t ha^{-1} treatment and 974 kg ha^{-1} for the 100 t ha^{-1} treatment (Table 3). The first year data showed that even the lowest rate of lake sediment application significantly increased the yield compared to the control. Similar results were found by Baksiene (2004), Baksiene & Asakaviciute (2013), and Kiani et al. (2018); however, the magnitude of extra yield depends on the

Table 3. Direct effect of lake sediment fertiliser on grain yield and quality characteristics of oats in 2015

Treatment	Yield, kg ha^{-1}	Plant height cm	Test weight, g L^{-1}	TKW, g	Protein content, %
Control	4,353^{b}	91^{b}	533^{b}	39.4^{b}	9.9^{a}
50 t ha^{-1}	4,770^{ab}	93^{ab}	537^{ab}	38.9^{b}	10.0^{a}
100 t ha^{-1}	5,327^{a}	97^{a}	538^{a}	41.7^{a}	9.2^{b}
P value	*0.005*	*0.007*	*0.013*	*0.001*	*0.008*

Different letters indicate significant differences between treatment means (n = 6) (*Tukey-Kramer HSD test*, $P < 0.05$).

crop species and its nutritional requirements. Plants require nutrients for their growth and development. In an organic farming system, the available amount of nutrients is usually limited. An adequate supply of nutrients for oats results in taller plants and more aboveground biomass (Daugviliene et al., 2014; Baksiene et al., 2015; Kiani et al., 2018). Oat plant height was significantly (P = 0.007) higher in the 100 t ha^{-1} treatment (97 cm) than in the 50 t ha^{-1} treatment (93 cm) and in control (91 cm). Despite this, no significant increase was found in the number of productive tillers when using lake sediment as fertiliser (data not shown). As known, the number of productive tillers, TKW and the number of kernels per ear or panicle determine cereal yield.

In the second year, when the residual effects of lake sediment were studied, barley yield was significantly (P = 0.023) higher in the plots where the highest rate of lake sediment (100 t ha^{-1}) was applied. The additional yield was 359 kg ha^{-1} (Table 4).

The barley plants grew significantly (P = 0.023) higher in the 100 t ha^{-1} plots as well (Table 4). However, the yield in the 50 t ha^{-1} plots was the same as in the control plots. As demonstrated, taller barley plants and significant additional yields were obtained, probably due to higher organic matter content and other nutrients in the soil where the highest rate of lake sediment was applied the previous year. Obviously, the additional yield of both crops (2015 and 2016) where the highest rate of lake sediment was applied was supported by higher soil microbial activity. This is because soil microbiota plays an important role in productivity of agricultural crops as it is responsible for the biochemical degradation of organic matter and other chemicals in soil (Munnoli et al., 2010).

Table 4. Residual effect of lake sediment fertiliser on grain yield and quality characteristics of spring barley in 2016

Treatment	Yield, kg ha^{-1}	Plant height, cm	Test weight, g L^{-1}	TKW, g	Protein content, %
Control	2,908^{b}	56^{b}	641^{a}	46.7^{a}	9.6^{a}
50 t ha^{-1}	2,873^{b}	57^{ab}	640^{a}	45.7^{a}	9.4^{a}
100 t ha^{-1}	3,266^{a}	60^{a}	645^{a}	46.2^{a}	9.4^{a}
P value	*0.011*	*0.023*	*ns*	*ns*	*ns*

Different letters indicate significant differences between treatment means (n = 6) (*Tukey-Kramer HSD test* $P < 0.05$).

Oat test weight increased significantly (P = 0.013) in both the 50 t ha^{-1} and 100 t ha^{-1} treatments. TKW only increased (P = 0.001) in the 100 t ha^{-1} treatment. Kernel weight is one of the most important components affecting yield. This research revealed that organic sediment does not always have positive effects on grain quality characteristics. There was no effect on oat protein content in the 100 t ha^{-1} treatment, but in the 50 t ha^{-1} treatment the protein content significantly (P = 0.008) decreased so the effect of fertilisation was negative compared to the control. Organic farming often has a lack of nutrients. This is a crucial aspect to achieve sufficient protein content of cereals (Bilsborrow et al., 2013; Tamm et al., 2016).

There were no residual effects of lake sediment on barley grain quality characteristics in the second year (2016).

CONCLUSIONS

The rate of lake sediment applied had significant effects on soil chemical composition, soil dehydrogenase activity, as well as on grain yield and quality, with responses being strongest in the 100 t ha^{-1} treatment. The 100 t ha^{-1} treatment increased

the amount of mobile Ca and B content in soil the first year. A residual effect was seen in the soil Ca, Cu and B content. Both application rates (50 and 100 t ha^{-1}) increased the N_{tot}, Mg, Cu, and Mn content in the soil the first year but had no effect on soil pH or P and K content. The higher application rate increased the SOC content, which could be a reason why soil DHA was higher in 100 t ha^{-1} treatment. Positive effects on soil DHA could be also due to the addition of a large amount of water along with the sediment.

The application of lake sediment increased grain yield, test weight, and thousand-kernel weight of oats in the first year. However, there were only small residual effects the following year. Barley yield was only positively impacted in the 100 t ha^{-1} treatment.

To use lake sediment as an organic fertiliser the ratio of Fe to P in the sediment should be considered in order to avoid a plant available P deficit in the soil. In order to recommend using lake sediment as an organic fertiliser to farmers, further research is needed to evaluate and avoid the risks of contaminating soils with heavy metals.

ACKNOWLEDGEMENTS. This research was supported by National Programme 'Agricultural Applied Research and Development Programme for 2015–2021'. We are also grateful to Laine Keppart for providing us the weather data.

REFERENCES

Baksiene, E. 2004. Effects of lake sediments on changes in sandy loam cambisol properties and on crop productivity. *Agronomy Research* **2**(2), 111–119.

Baksiene, E. 2009. The influence of lake sediments on the fertility of Cambisol. *Agronomy Research* **7** (Special Issue I), 175–182.

Baksiene, E. & Asakaviciute, R. 2013. The effects of organic lake sediments on the crop rotation yield and soil characteristics in Southeast Lithuania. *Applied Ecology and Environmental Research* **11**(4), 557–567.

Baksiene, E., Asakaviciute, R., Romanovskaja, D., Tripolskaja, L. & Razukas, A. 2015. The influence of lake sediments on sandy loam soil properties and crop yield. *Romanian Agricultural Research* **32**(1), 1–9.

Bilsborrow, P., Cooper, J., Tétard-Jones, C., Średnicka-Tober, D., Baranński, M., Eyre, M., Schmidt, C., Shotton, P., Volakakis, N., Cakmak, I., Ozturk, L., Leifert, C. & Wilcockson, S. 2013. The effect of organic and conventional management on the yield and quality of wheat grown in a long-term field trial. *European Journal of Agronomy* **51**, 71–80.

Bogush, A.A., Leonova, G.A., Krivonogov, S.K., Bobrov, V.A., Tikhova, V.D., Kondratyeva, L.M., Kuzmina, A.E. & Maltsev, A.E. 2013. Diagenetic transformation of sapropel from Lake Dukhovoe (East Baikal region, Russia). *Procedia Earth and Planetary Science* **7**, 81–84.

Bünemann, E.K., Schwenke, G.D. & Van Zwieten, L. 2006. Impact of agricultural inputs on soil organisms - a review. *Australian Journal of Soil Research* **44**, 379–406.

Daugviliene, D., Burba, A. & Baksiene, E. 2014. Changes of sandy loam Cambisol properties at application for calcareous sapropel and limestone. *Journal of Food, Agriculture and Environment* **12**(1), 1532–1536.

Estonian Environmental Register, 2020. Available at http://register.keskkonnainfo.ee/envreg/main#HTTP1iGilmPYdf6FWgbQfdhr2HWP6QJaPK accessed on 17.06.2020. (in Estonian).

Fliessbach, A., Oberholzer, H.-R., Gunst, L. & Mäder, P. 2007. Soil organic matter and biological soil quality indicators after 21 years of organic and conventional farming. *Agriculture, Ecosystems and Environment* **118**, 273–284.

Grantina-Ievina, L., Karlsons, A., Andersone-Ozola, U. & Ievinsh, G. 2014. Effect of freshwater sapropel on plants in respect to its growth affecting activity and cultivable microorganism content. *Zemdirbyste-Agriculture* **101**(4), 355−366.

Heinsalu, A., Vassiljev, J. & Veski, S. 2003. *Sediment properties of Lake Kääriku* /Kääriku järve lõunapoolse osa setete lasund ja omadused/. Institte of Geology at Tallinn University of Technology Report Series, 34 pp. (in Estonian).

Hristeva, T.H. & Radka P. Bozhinova, R.P. 2017. Microbiological characteristic of cinnamon pseudopodzolic soil (Planosol) at using of Black sea deep-water sediments (Sapropels). International *Journal of Current Microbiology and Applied Sciences* **6**(4), 125–133.

Hueso, S., García, C. & Hernández, T. 2012. Severe drought conditions modify the microbial community structure, size and activity in amended and unamended soils. *Soil Biology and Biochemistry* **50**, 167−173.

Jensen, H.S., Kristensen, P., Jeppesen, E. & Skytthe, A. 1992. Iron: phosphorus ratio in surface sediment as an indicator of phosphate release from aerobic sediments in shallow lakes. In *Sediment/Water Interactions*, Springer, Dordrecht, pp. 731–743.

Kalmet, R., Kanger, J., Kevvai, L., Kevvai, T., Kuldkepp, P., Kärblane, H., Raudväli, E. & Turbas, E. 1996. Mineral fertilisers. *Handbook of plant nutrition and fertilisation* /Mineraalväetised. Taimede toitumise ja väetamise käsiraamat/. H. Kärblane (Eds.), Estonian Ministry of Agriculture, Tallinn, 284 pp. (in Estonian).

Kiani, M., Simojoki, A., Tammeorg, O. & Tammeorg, P. 2018. Impacts of lake sediment reuse on plant growth and soil properties in the field. 21st World Congress of Soil Science in Rio de Janeiro, Brazil in August 12–17 (poster presentation). Available at https://researchportal.helsinki.fi/en/publications/impacts-of-lake-sediment-reuse-on-plant-growth-and-soil-propertie accessed 17.06.2020.

Knapp, B.A., Ros, M. & Insam, H. 2010. Do composts affect the soil microbial community? In: Insam H, Franke-Whittle I, Goberna M (Eds.), *Microbes at work*. Springer, Berlin, pp. 271–291.

Kruopiene, J. 2007. Distribution of Heavy Metals in Sediments of the Nemunas River (Lithuania). *Polish Journal of Environmental Studies* **16**(5), 715–722.

Kõiv, T. 2012. Development of the Estonian lakes /Eesti järvede arenguteed/. Available at http://lakeontogeny.weebly.com/eesti-jaumlrvede-arenguteed.html accessed on 11.06.2015. (in Estonian).

Li, H.B., Yu, S., Li, G.L., Liu, Y., Yu, G.B., Deng, H., Wu, S.C. & Wong, M.H. 2012. Urbanization increased metal levels in lake surface sediment and catchment topsoil of waterscape parks. *Science of the Total Environment* **432**, 202–209.

Meier, U. 2001. Growth stages on mono- and dicotyledonous plants. BBCH Monograph 2. Federal Biological Research Centre for Agriculture and Forestry. Available at https://www.politicheagricole.it/flex/AppData/WebLive/Agrometeo/MIEPFY800/BBCHengl2001.pdf accessed 19.02.2019.

Metsur, M. & Vreimann, T. 2015. A remedial action plan for the lake Kahala, the draft environmental impact assessment report /Kahala järve tervendamise insenertehnilise tegevuskava keskkonnamõju hindamise aruande eelnõu/. http://www.keskkonnaamet.ee/public/Kahala_KMH_aruande_eelnou.pdf accessed on 24.08.2015. (in Estonian).

Mehlich, A. 1984. Mehlich 3 soil test extractant a modification of Mehlich 2 extractant. *Communications in Soil Science and Plant Analysis* **15**, 1409–1416.

Munnoli, P.M., Teixeira da Silva, J.M. & Bhosle, S. 2010. Dynamics of the Soil Earthworm-Plant Relationship: A Review. *Dynamic Soil, Dynamic Plant* **4**(Special Issue), 1–21.

Naumova, N., Nechaeva, T., Smirnova, N., Fotev, Y. & Belousova, V. 2017. Effect of sapropel addition on selected soil properties and field tomato yield in south west Siberia. Asian *Journal of Soil Science and Plant Nutrition* **1**(3), 1–11.

Salonen, V-P., Varjo, E & Rantala, P. 2001. Gypsum treatment in managing the internal phosphorus load from sapropelic sediments; experiments on Lake Laikkalammi, Finland. *Boreal Enviroment Research* **6**, 119–129.

Siebert, J., Sünnemann, M., Auge, H., Berger, S., Cesarz, S., Ciobanu, M., Guerrero-Ramírez, N.R. & Eisenhauer, N. 2019. The effects of drought and nutrient addition on soil organisms vary across taxonomic groups, but are constant across seasons. *Scientific Reports* **9**. https://doi.org/10.1038/s41598-018-36777-3

Stankevica, K., Klavins, M. & Rutina, L. 2012. Accumulation of metals in sapropel. *Material Science and Applied Chemistry* **26**, 99–105.

Stankevica, K., Vincevica-Gaile, Z., Muter, O. & Klavins, M. 2016. Physiological response of bacteria consortium to the presence of intact and autoclaved freshwater sapropel (gyttja) derived in the eastern Latvia. In Mendez-Vilas, A. (ed.): *Microbes in the Spotlight: Recent Progress in the Understanding of Beneficial and Harmful Microorganisms*. Brown Walker Press, Boca Raton, 111–115. Available at: https://books.google.ee/books?id=s2C8DAAAQBAJ&pg=PA111&lpg=PA111&dq=sapropel+as+organic+fertiliser&source=bl&ots=dE0d84UMJs&sig=ACfU3U0WVu3BVSOIoN74BkasdJZIZeYxUw&hl=et&sa=X&ved=2ahUKEwjMyvC16MfgAhUyw8QBHV0xBWA4FBDoATAHegQIABAB#v=onepage&q=sapropel%20as%20organic%20fertiliser&f=false accessed on 19.02.2019.

Tabatabai, M.A., 1982. Soil enzymes. In: Page A.L., Miller R.H., Keeney D.R. (eds.). *Methods of Soil Analysis*. Part 2. American Society of Agronomy & Soil Science Society of America. Madison. Wisconsin, pp. 903–949.

Tamm, I., Tamm, Ü., Ingver, A., Koppel, R., Tupits, I., Bender, A., Tamm, S., Narits, L. & Koppel, M. 2016. Different leguminous pre-crops increased yield of succeeding cereals in two consecutive years. *Acta Agriculturae Scandinavica, Section B — Soil & Plant Science* **66**(7), 593–601.

Tylmann, W., Łysek, K., Kinder, M. & Pempkowiak, J. 2011. Regional Pattern of Heavy Metal Content in Lake Sediments in Northeastern Poland. *Water, Air, & Soil Pollution*. **216**, 217–228.

WRB, 2015. World reference base for soil resources 2014, update 2015. International soil classification system for naming soils and creating legends for soil maps. *World Soil Resources Reports* **106**, FAO, Rome, 203 pp.

Agronomy Research **18**(3), 2033–2048, 2020
https://doi.org/10.15159/AR.20.165

Combustion and emission studies of a common-rail direct injection diesel engine with various injector nozzles

M. Hissa*, S. Niemi and A. Niemi

University of Vaasa, School of Technology and Innovations, P.O. Box 700, FI-65101 Vaasa Finland
*Correspondence: Michaela.Hissa@univaasa.fi

Abstract. Fuel injection has a critical role in an internal combustion engine and a significant effect on the quality of the fuel spray. In turn, fuel spray directly affects an engine´s combustion, efficiency, power and emissions. This study evaluated three different injector nozzles in a high-speed, non-road diesel engine. It was run on diesel fuel oil (DFO) and testing was conducted at three different engine loads (100%, 75% and 50%) and at two engine speeds (2,200 rpm and 1,500 rpm). The nozzles had 6, 8 and 10 holes and a relatively high mass flow rate (HF). The study investigated and compared injection and combustion characteristics, together with gaseous emissions. The combustion parameters seemed to be very similar with all studied injector nozzles. The emission measurements indicated general reductions in hydrocarbons (HC), carbon monoxide (CO) and nitrogen oxides (NOx) at most load/speed points when using the 6- and 10-hole nozzles instead of the reference 8-hole nozzles. However, smoke number increased when the alternative nozzles were used.

Key words: diesel engine, fuel injection, injector nozzle, combustion performance, emissions.

INTRODUCTION

The European Parliament has set three key targets for more efficient energy use: improve energy efficiency by 35%; increase the share of renewables in energy consumption to at least 35%; and ensure that at least 12% of energy in transport comes from renewable sources (European Parliament, 2018). The deadline to achieve all three targets is 2030, so, coupled with changing fuel prices and fuel availability issues, significant shifts in the fuel market can be expect during the next decade. Diesel engines and their injection systems in the future must be capable of handling various alternative fuels as efficiently as possible.

When modifying a diesel engine to suit new fuels, one of the most critical elements is fuel injection. It has a key role in the optimisation of the trade-off between thermal efficiency and exhaust emissions (Jääskeläinen, 2017; Heywood, 2018; Salvador et al., 2018). The injection system has a significant impact on the duration of both fuel injection and combustion, as well as combustion noise (Salvador et al., 2018). Moreover, the injector nozzle´s design - the number of nozzle holes, the hole diameter and the spray angle - affects spray atomisation and fuel-air mixing (Sarvi et al., 2008; Jääskeläinen, 2017; Dong et al., 2018a). Fuel atomisation and fuel-air mixing must improve to meet

the EU's energy efficiency target and more stringent emission regulations, including those for nitrogen oxides (NOx) (Salvador et al., 2018).

The injector nozzle is responsible for delivering the fuel spray. The injected spray consists of fuel droplets smaller than the nozzle hole diameter (Sarvi et al., 2008). Reducing nozzle hole diameter has been shown to improve atomisation efficiency, leading to increased heat release rate (HRR) and less soot formation (Sarvi et al., 2008; Jääskeläinen, 2017; Dong et al., 2018a). However, those studies found that there are limits to the reduction of nozzle diameter. These are related to total injection time and combustion durations (especially at high loads) or the potential for nozzle coking. Additionally, the accelerated combustion leads to rising combustion temperature that increases NOx emissions (Satyanarayana & Muraleedharan, 2012). NOx formation in the combustion chamber is related to the flame area, which depends on the number and size of the fuel nozzle holes (Sarvi et al., 2008; Dong et al., 2018a). Decreasing the number of holes gives a smaller cone angle of fuel spray, changing the fuel/air mixing and reducing NOx production.

If nozzle hole diameter is reduced it is necessary to increase injection pressure or raise nozzle hole count to maintain the same fuel injection rate and nozzle flow area for maximum engine torque, power objectives and engine efficiency (Jääskeläinen, 2017). Jääskeläinen (2017) states that coupling hole size reduction to several other factors may improve combustion characteristics, like reducing the potential for overlapping of the burning zones of individual fuel sprays. These factors are: injection pressure increase, changes in combustion chamber design, improvements in nozzle flow performance and increase in the number of nozzle holes.

Increasing the number of nozzle holes, however, affects the fuel penetration length. Sayin et al. (2013), reported that raising the hole count could lead to poor combustion efficiency, mainly because the shorter penetration weakens the fuel/air mixing. Lee et al. (2010) noticed a decrease in penetration length when the hole count was raised. That led to a reduction in cylinder pressure and HRR, despite the improved evaporation and atomisation.

Overall, the optimal injector nozzle parameters depend on the engine type and have to be found by testing, since there is no theory that properly describes nozzle performance (Sarvi et al., 2008). Furthermore, the suitability for each fuel has to be studied individually (Niemi et al., 2011).

The present study compares three different injector nozzles in a high-speed, non-road diesel engine powered by DFO fuel. Tests were carried out at three different engine loads (100%, 75%, 50%) and at engine speeds of 2,200 rpm and 1,500 rpm. The nozzles had 6, 8 and 10 holes and a relatively high mass flow rate (HF). No other modifications were made to the engine components or control settings. Engine performance was kept constant. Detailed injection and combustion characteristics and gaseous emissions were measured. The injection map was optimized for the reference 8-hole nozzles and the map was kept constant with the other nozzles.

The study´s main aim was to evaluate how the selected fuel nozzles affect the combustion and emission characteristics of a modern high-speed, common-rail diesel engine using commercial low-sulphur DFO. The measurements generated new information relating to nozzle choice, supporting the aim to increase efficiency of high-speed non-road engines.

MATERIALS AND METHODS

Experimental setup

The experiments were conducted by the University of Vaasa (UV) at the Internal Combustion Engine (ICE) laboratory of the Technobothnia Research Centre in Vaasa, Finland. The laboratory is managed by Novia University of Applied Sciences.

Engine setup and nozzles

The experimental engine, an AGCO Power 44 CWA, was a turbocharged, high-speed four-cylinder diesel engine for non-road applications. It was intercooled (air-to-water) and had a Bosch common-rail fuel-injection system. The engine had no exhaust after treatment devices. It was loaded by means of a Horiba eddy-current dynamometer WT300. Table 1 lists the engine´s main specification.

Testing was conducted at three different engine loads (100%, 75%, 50%) and at two engine speeds of (2,200 rpm and 1,500 rpm). Three solenoid-driven injector nozzles were compared. The nozzles had 6, 8 and 10 holes and a high mass flow rate (1.2 L min^{-1} at 100 bar). The spray angle (umbrella angle) was 149° for all nozzles. Most diesel combustion systems include spray angles in the range of 145−158° (Salvador et al., 2018). The injection map was optimised for the 8-hole nozzles by the engine manufacturer. The map was kept constant with the other nozzles. Fig. 1 and Table 2 provide detailed information about the nozzles.

The fuel used was a commercial low-sulphur diesel fuel oil (DFO). It had a cetane number (CN) of 54, lower heating value of 43 MJ kg^{-1}, its was density 835 kg m^{-3} and kinematic viscosity 3 mm^2 s^{-2}.

Table 1. Main engine specifications

Engine	AGCO POWER 44 CWA
Cylinder number	4
Bore (mm)	108
Stroke (mm)	120
Swept volume (dm^{-3})	4.4
Rated speed (min^{-1})	2,200
Rated power (kW)	96
Intermediate speed (min^{-1})	1,500

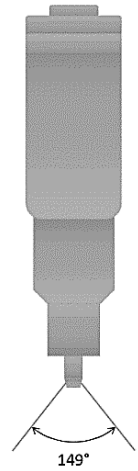

Figure 1. Spray angle schematics of the injector nozzles.

Table 2. Specifications of different injector nozzles

Number of nozzle holes	6	8	10
Orifice diameter (mm)	0.2	0.162	0.139
Total orifice areas (mm^2)	0.188	0.165	0.152
Included spray angle	149°	149°	149°
Nozzle flow rate (L min^{-1}) at 100 bar	1.2	1.2	1.2
Needle lift (mm)	0.4	0.4	0.4

Analytical instruments

LabVIEW system-design software was used to collect sensor data from the engine. The recorded variables were engine speed and torque, cylinder pressure and injection timing, duration and quantity. WinEEM3 diagnostic and service software provided by the engine manufacturer, AGCO Power, controlled fuel injection according to load-speed requests. The basic settings of WinEEM3 were the same for all nozzles and fuels. Fig. 2 depicts a schematic of the test bench setup.

Injected fuel mass flow rate was measured with a Kern digital fuel scale for 300 seconds at every load point once engine operation was stabilised. The average result was saved via LabVIEW software. The relative uncertainty for fuel mass flow measurement was 0.03%.

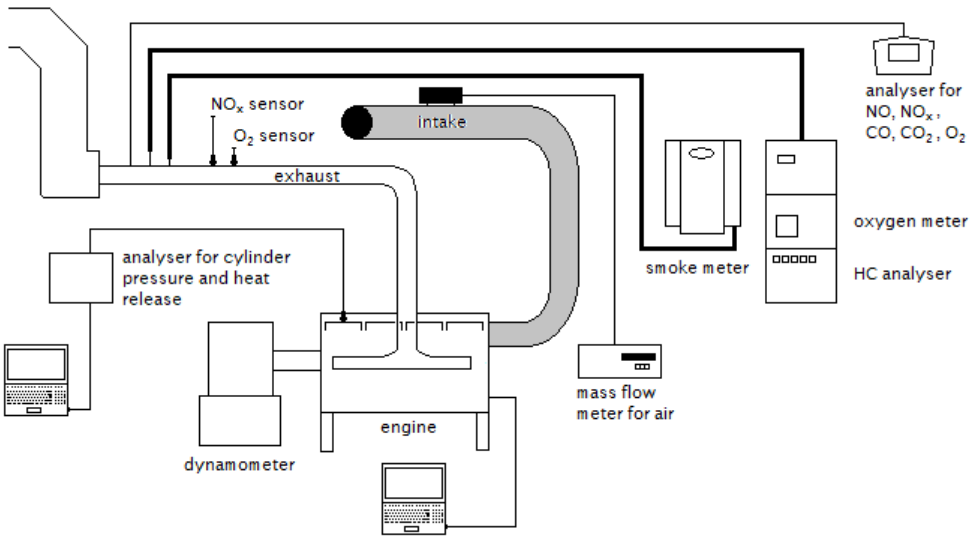

Figure 2. Engine measurement setup.

A piezoelectric Kistler 6125C pressure sensor was used to measure in-cylinder pressure. The sensor was mounted into the head of the fourth cylinder. A charge amplifier filtered and amplified the signal, which was then transmitted to a Kistler KIBOX combustion analyser. The crankshaft position was recorded by a crank-angle encoder (Kistler 2614B1), which can output a crank-angle signal with a resolution of 0.1° CA by means of an optical sensor. Cylinder pressure data were averaged over 100 consecutive cycles to smooth irregular combustion. The averaged data were used to calculate HRR. The raw data over 100 cycles were used to calculate the standard deviations for the maximum cylinder pressures.

HRR and MFB were calculated via AVL Concerto's data-processing platform, using the Thermodynamics2 macro. The macro used a calculation resolution of 0.2 °CA. The start of the calculation was set at -30 °CA. Data were filtered with the DigitalFilter macro and a frequency of 2,000 Hz. For HRR results, the average values of in-cylinder pressure were calculated first. Thereafter, the macro calculated HRR values. Finally, the HRR curve was filtered. In contrast, for MFB results, pressure values were first filtered

and then the macro was used. Average values of 100 cycles were not used for MFB results, thus establishing the standard deviations.

Exhaust temperatures were recorded by K type thermocouples (NiCu-NiAl). Air and exhaust pressures were determined by industrial transmitters. Engine air-flow was measured by an ABB Sensyflow FMT700-P air mass flow rate meter. Exhaust emissions were determined by means of the instruments listed in Table 3.

Table 3. Instruments for emission measurements

Parameter	Analyser	Technology	Accuracy*
CO	TSI CA-6203 CA-CALC	Electrochemical	0−100 ppm: ± 10% 100−5,000 ppm: ± 5%
O2	Siemens Oxymat 61	Paramagnetic	± 0.25%
NO, NOx	TSI CA-6203 CA-CALC	Electrochemical	0−100 ppm: ± 10% 100−4,000 ppm: ± 5%
HC	J.U.M. VE 7	HFID	0−100,000 ppm: ± 1%
Smoke	AVL 415 S	Optical filter	± 5%

* Accuracy provided by manufacturer.

Experimental matrix and measurement procedure

All measurements were performed under steady operation conditions without engine modifications. The comparison of injector nozzles used six load/speed points from the ISO 8178-4 standard: 100%, 75%, 50% loads at engine speeds of 2,200 rpm and 1,500 rpm. Brake mean effective pressure (BMEP) values ranged from 17.4 to 5.7 bar. The load/speed points are listed in Table 4.

Table 4. Engine operating conditions

Engine speed (rpm)	2,200			1,500		
BMEP (bar)	11.4	8.6	5.7	17.4	13.1	8.7
Load (%)	100	75	50	100	75	50

At the beginning of every measurement, the engine was warmed-up and the load was applied. The intake-air temperature was adjusted to 85 ± 1 °C downstream of the charge-air cooler to support auto-ignition of the fuels at each load. The temperature was controlled manually by regulating the flow of cooling water to the heat exchanger. The valve setting was kept constant. Therefore, the charge temperature changed with the load. All measurements were taken after the engine had stabilised, as determined by the stability of the temperatures of coolant water, intake air and exhaust upstream the turbine.

RESULTS AND DISCUSSION

Injector nozzles

The measurement results from the three injector nozzles were compared. The nozzles had 6, 8 and 10 holes but each had the same mass flow rate of 1.2 L min^{-1} at 100 bar. The rail pressure values of 8-hole nozzles were 83, 74, 66 MPa at measurement points of 11.4, 8.6 and 5.7 bar 2,200 rpm. Respectively, 61, 46 and 40 MPa at 17.4, 13.1 and 8.7 bar BMEP 1,500 rpm. The 6- and 10-hole nozzles had a minor increase in rail pressures. The maximum rail pressure increase was 4% with 6-hole nozzles at medium load (8.6 bar BMEP) at 2,200 rpm compared to rail pressure with 8-hole nozzles. The

following sections provide results and discussion from the measurements of injection timing, specific fuel consumption, heat release rate and cylinder pressure, brake thermal efficiency, mass fraction burned and combustion duration as well gaseous emissions and smoke.

Injection timing and brake specific fuel consumption

For all test conditions, pilot injections were set before top dead centre (BTDC) while main injections occurred after top dead centre (ATDC). The exact timings and durations are shown in Table 5. Fig. 3 depicts brake specific fuel consumption (BSFC).

Only main injections occurred at load points of 11.4 bar and 8.6 bar BMEP (engine speed 2,200 rpm). At this engine speed, pilot injections occurred only with the lowest BMEP of 5.7 bar (50% load). The timing and duration of these pilot injections were similar for all the nozzles. The main injection duration was slightly shorter (by just one crank angle degree) with the 8-hole nozzles. There was no post injection for any of the three loads at 2,200 rpm.

Pilot injection was used for all the nozzles at all loads (17.4, 13.1 and 8.7 bar) at the lower engine speed of 1,500 rpm. Minor variations of starting times and durations were noticed. At full load (17.4 bar) at this engine speed, post injection occurred only with the 8-hole nozzles. Post injection occurred with all the nozzles at the two smaller loads at 1,500 rpm.

Table 5. Injection timing

Nozzle	BMEP	Pilot Injection (BTDC)		Main injection (ATDC)		Post injection (ATDC)	
		Start	Duration	Start	Duration	Start	Duration
	bar	°CA	°CA	°CA	°CA	°CA	°CA
6	11.4	8.6	0	4	21	31	0
8		8.6	0	4	20	30	0
10		8.6	0	4	21	31	0
6	8.6	7.6	0	3	17	28	0
8		7.6	0	3	16	27	0
10		7.6	0	3	17	28	0
6	5.7	13	4	3.5	12	22	0
8		13	4	3.5	12	22	0
10		13	4	3.5	12	22	0
6	17.4	8.3	2.8	2.4	25	31	0
8		8	2.8	2	24	31	2.2
10		8.3	2.8	2.4	24	31	0
6	13.1	8.6	3.2	2.3	20	28	3.1
8		8.5	3.3	2.1	20	27	3.1
10		8.6	3.2	2.3	21	28	3.1
6	8.7	8.7	3.5	2.1	13	21	4.5
8		8.7	3.7	1.9	12	20	4.7
10		8.7	3.5	2.1	13	21	4.6

The amount of injected fuel was assumed to correlate to injection durations because fuel injection was controlled according to load/speed requests. Overall, the differences in main injection durations of all the nozzles did not exceed 1 °CA.

As expected, pilot injection duration increased when the engine load was reduced and main injection duration increased when the engine load was raised. At 1,500 rpm, post injection duration increased when the engine load was reduced. A longer pilot is used to shorten the ignition delay (ID) of a fuel by increasing in-cylinder temperatures for main injections. Post injections, in turn, are used to reduce particulate and soot emissions, primarily at lighter loads and lower engine speeds (Heywood, 2018).

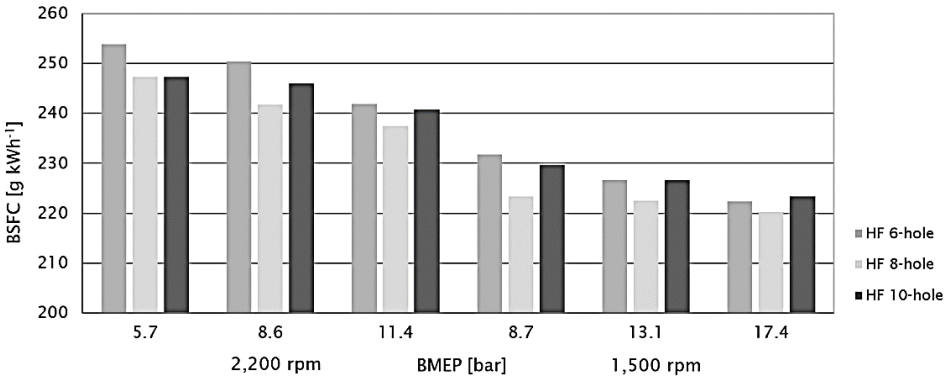

Figure 3. Brake specific fuel consumption at rated and intermediate speeds.

Brake specific fuel consumption (BSFC) is the fuel flow rate per hour (g h^{-1}) divided by engine brake power (kW). Generally, BSFC decreased when brake mean effective pressure (BMEP) or load of the engine increased. The 8-hole nozzles produced the lowest BSFC at five out of the six load/speed points. In other words, either raising the hole count to 10 or reducing it to 6 increased BSFC. The highest BSFC values were measured for the 6-hole nozzles at all load/speed points, except at full load at 1,500 rpm, where BMEP was at its maximum value of 17.4 bar. At this point, however, the difference between the 10-hole and 8-hole nozzles was minor (3.1 g kWh^{-1}, 1.4%). The maximum difference was 8.7 g kWh^{-1} or 3.6% at 8.6 bar BMEP, between the 6-hole and 8-hole nozzles.

Sayin et al. (2013) investigated 2-, 4-, 6- and 8-hole nozzles in a single-cylinder diesel engine using DFO. They also observed that increasing or decreasing the number of nozzle holes increased BSFC compared to the original nozzle. They assumed that a reduction in hole count led to enlarged fuel droplets and lengthened the ignition delay period, increasing BSFC. Conversely, raising the hole count shortened the ID period, reducing homogeneous mixture, and so once again BSFC increased. Mekonen et al. (2020) studied 3-, 4- and 5-hole nozzles in a single-cylinder diesel engine using preheated palm oil methyl ester. They observed decrease in BSFC when nozzle hole number increased from 3 to 4, due to increased fine droplets of injected fuel and improved fuel atomisation. However, BSFC increased when the nozzle hole count was raised further, from 4 to 5. They assumed that was caused by the higher number of fine droplets leading to a shorter ID and hence increasing the chance of non-homogeneous mixing.

Heat release rate (HRR)

The compression pressure was at its maximum at 2°CA before top dead centre at an engine speed of 1,000 rpm. This had no effect on measurement results, but must be considered when the results are examined.

Combustion starts with a rapid burning phase that lasts only a few CA degrees and produces the first spike in the heat release rate curve. It is followed by the main heat release period, which has a longer duration and more rounded profile. The HRR curve´s tail is the remainder of the fuel's chemical energy released when burnt gases mix with excess air that was not involved in the main combustion (Heywood, 2018). Fig. 4 shows HRR curves for the studied injector nozzles. The small dip near the beginning of each curve is the loss due to the heat transfer into the liquid fuel for vaporising and heating (Heywood, 2018).

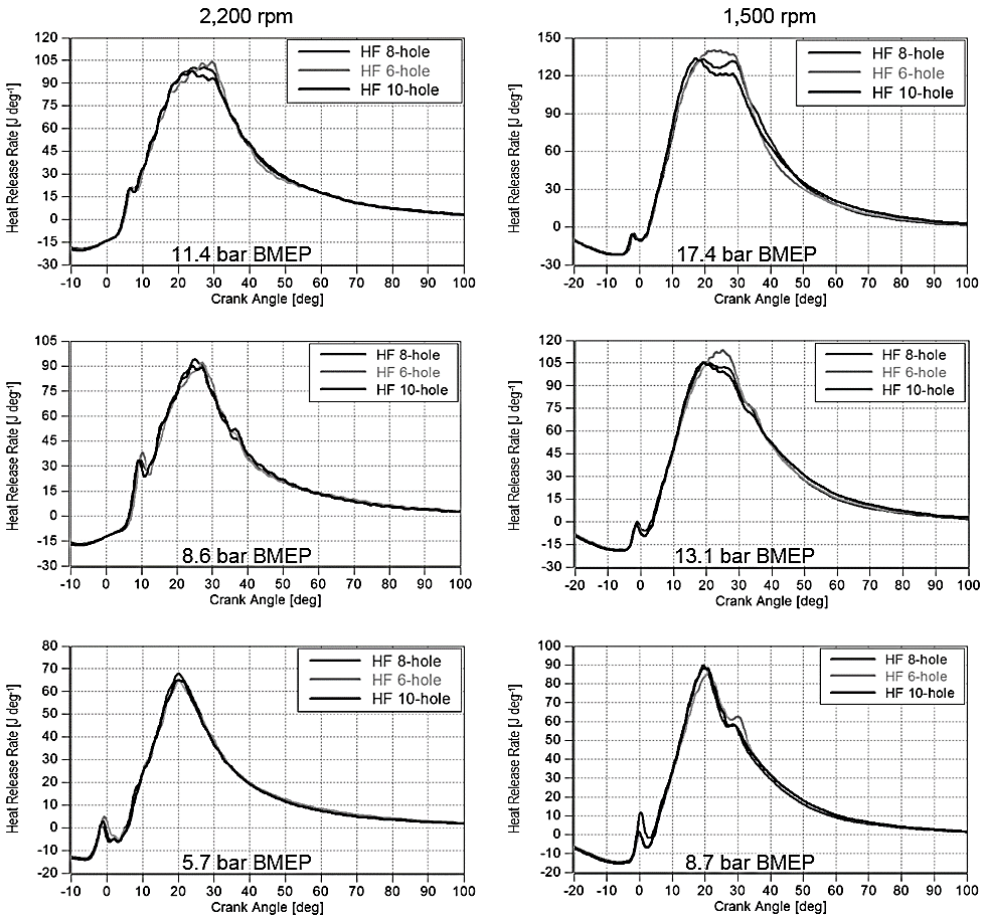

Figure 4. Heat release rates at rated and intermediate speeds.

At rated speed (2,200 rpm) and full load (11.4 bar BMEP), the maximum HRR for the 6-hole nozzles was 104 J °CA^{-1}, just before the start of post injection (27 °CA). The 10-hole nozzles´ maximum HRR peak (98 J °CA^{-1}) came earlier, at the end of main injection (24 °CA). This difference in the arrival of the HRR peak may be due to the

larger droplet sizes created by the 6-hole nozzles evaporating more slowly than the smaller droplet sizes from the 10-hole nozzles. The start of all injections, as well as injection durations, were similar for the 6- and 10-hole nozzles.

A slightly longer ignition delay observed for the 6-hole nozzles at medium (8.6 bar BMEP) and low (5.7 bar BMEP) loads is due to larger droplet size generated by larger nozzle hole diameter. Otherwise, the HRR curves are similar. The 8-hole nozzles achieved a higher HRR than the other two nozzles at medium and low loads (94 J $°CA^{-1}$ and 68 J $°CA^{-1}$ respectively).

At intermediate speed and full load (17.4 bar BMEP), only the 8-hole nozzles had a post injection, although this is not evident on the HRR curve. The curve of the 6-hole nozzles differs from those of the other two nozzles at peak HRR.

At high loads, the maximum HRR decreased as the nozzle-hole count rose. Maximum HRR occurred later at intermediate speed with the 6-hole nozzles due to the larger droplet size generated by the greater hole diameter. Additionally, this delayed HRR peak with the 6-hole nozzles also may be due to increased spray penetration length, decreased cone angle and the slower mixing that is the consequence of the larger fuel droplets´ longer evaporation time (Hoang, 2019), combined with slightly increased BSFC or fuel amount. Lee et al. (2010) studied 6-, 8- and 10-hole nozzles in a diesel engine and noticed that the strongest penetration of liquid spray from 6-hole nozzles impinged against the piston bowl, lowering in-cylinder temperature. Without the impingement, the HRR of the 6-hole nozzles should be the highest due to less uniform fuel/air distribution that enhanced combustion. They also observed the lowest HRR values for the 10-hole nozzles due to incomplete combustion caused by the poorly distributed fuel/air mixture and the highest concentration of unburned fuel during combustion process.

Cylinder pressure

Maximum cylinder pressures (MCP) were very similar with all injector nozzles at all studied load/speed points (Fig. 5 and Table 6). MCP at rated speed and full load with all nozzles were 106 to 108 bar. At 1,500 rpm, MCP at full load was 116 to 117 bar. Table 6 shows the standard deviations of MCP of 100 consecutive cycles.

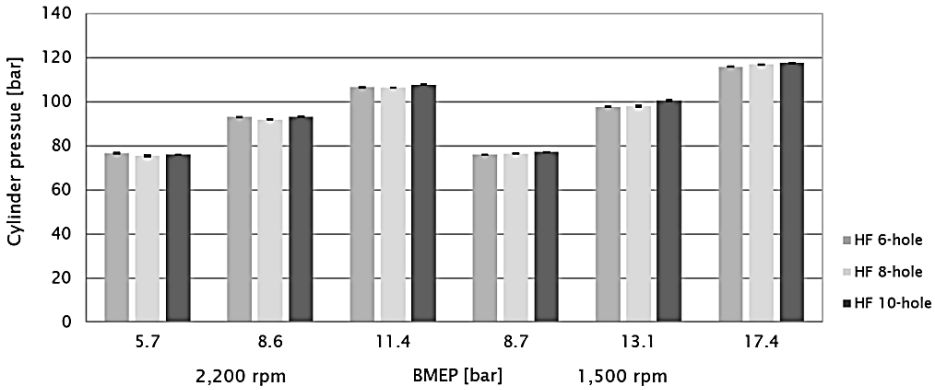

Figure 5. Maximum cylinder pressures at rated and intermediate speed with standard deviations.

Maximum cylinder pressure depends on the burned fuel fraction during the premixed combustion phase. A larger amount of fuel burned in premixed phase shows a higher MCP (Hissa et al., 2019). The fuel/air mixing rate mainly controls the combustion process of diesel engines. Slowing the rate results in retarded ignition and lower MCP. Dong et al. (2018b) noticed a lower pressure peak with a reduced number of nozzle holes, mainly due to the slower fuel/air mixing rate. In turn, Lee et al. (2010) noticed shorter penetration length when the number of nozzle holes was increased. This led to lower cylinder pressure and HRR, despite the improved evaporation and atomisation.

Table 6. Maximum cylinder pressure and standard deviations

Nozzle	BMEP	Max. cylinder pressure (avg)	StDev	Nozzle	BMEP	Max. cylinder pressure (avg)	StDev
	bar	°CA			bar	°CA	
6	11.4	107	0.135	6	17.4	116	0.165
8		106	0.150	8		117	0.147
10		108	0.173	10		117	0.189
6	8.6	93.0	0.114	6	13.1	97.7	0.179
8		91.9	0.140	8		97.9	0.209
10		93.1	0.133	10		100	0.264
6	5.7	76.6	0.251	6	8.7	75.9	0.154
8		75.4	0.192	8		76.4	0.237
10		76.0	0.187	10		77.2	0.158

Brake thermal efficiency (BTE)

BTE indicates how efficiently the energy in the fuel was converted into mechanical output. BTE increased with load for all nozzles due to relative reductions in heat and mechanical losses at higher load (e.g., Perumal et al., 2017). Fig. 6 shows BTE was very similar with different nozzles. At full load at 2,200 rpm, BTE was 34 to 35% and at half load 33 to 34%. At full load at 1,500 rpm, BTE was 37 to 38% and at half load 36 to 37%. Differences between nozzles were minimal and within the measurement accuracy.

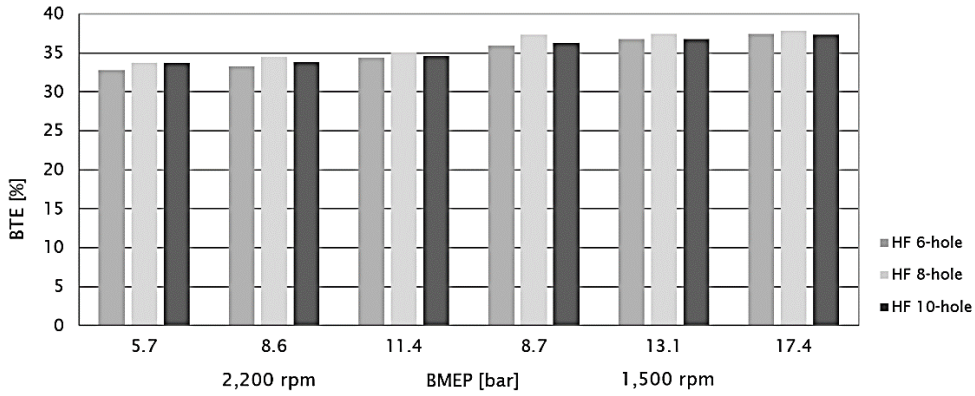

Figure 6. Brake thermal efficiency at rated and intermediate speeds.

Sayin et al. (2013) noticed an increase in BTE with higher number of nozzle holes and assumed it was because of finer atomisation of fuel. However, they also noticed an

increase in the nozzle-hole count could lead to poor combustion efficiency, mainly stemming from the shorter penetration weakening the fuel/air mixing. Mekonen et al. (2020) also measured an increased BTE when nozzle-hole number was increased from 3 to 4. This was attributed to a better fuel spray and turbulence. BTE fell when the number of nozzle holes was increased from 4 to 5. It is assumed that when the nozzle-hole count exceeds a certain range, combustion and emissions are adversely affected due to lack of the air entrainment required for the achievement of a stoichiometric mixture (Lee et al., 2010; Mekonen et al., 2020).

Mass fraction burned (MFB)

Table 7 presents MFB values with their standard deviations. It shows that the nozzles had the same MFB 5% values, except at full load at 2,200 rpm (11.4 bar BMEP) and 75% load at 1,500 rpm (13.1 bar BMEP). At these two load/speed points, the 6-hole nozzles achieved MFB 5% slightly later than the other nozzles. This may be due to increased droplet size leading to increased ID. At 50% load at 1,500 rpm (8.7 bar BMEP), the 8-hole nozzles had the earliest MFB 5%.

Table 7. Mass fraction burned and standard deviations

Nozzle	BMEP bar	MFB 5% °CA	StDev	MFB 50% °CA	StDev	MFB 90% °CA	StDev
6	11.4	19	0.14	32	0.21	65	1.0
8		18	0.15	32	0.22	63	1.1
10		18	0.13	32	0.26	64	1.3
6	8.6	20	0.14	32	0.22	67	1.1
8		19	0.15	32	0.24	65	1.2
10		20	0.11	32	0.28	64	1.1
6	5.7	17	0.17	30	0.30	67	1.6
8		17	0.16	29	0.32	65	1.6
10		17	0.16	29	0.27	64	1.3
6	17.4	14	0.13	28	0.22	55	1.2
8		14	0.11	29	0.21	53	1.0
10		14	0.14	29	0.31	58	1.5
6	13.1	16	0.15	29	0.23	58	1.3
8		15	0.13	29	0.23	56	0.94
10		15	0.15	30	0.33	61	1.1
6	8.7	16	0.17	29	0.26	58	1.2
8		15	0.13	28	0.26	56	1.1
10		16	0.12	29	0.26	58	0.97

MFB 50% values were similar with all nozzles at high loads. However, some difference between the nozzles was observed at lower cylinder pressures. At rated speed and 50% load (5.7 bar BMEP), MFB 50% of the 6-hole nozzles occurred one CA degree later than with the other nozzles. At 1,500 rpm and 75% and 50% loads (13.1 and 8.7 bar BMEP respectively), MFB 50% for the 8-hole nozzles was one CA degree ahead of the other nozzles. As a whole, differences in MFB 5% and 50% values were very small.

MFB 90% was achieved first with the 8-hole nozzles in the majority of cases. However, the 10-hole nozzles had the earliest MFB 90% values at rated speed with 75% and 50% loads (8.6 and 5.7 bar BMEP respectively). Conversely, the 10-hole nozzles

showed the latest values of MFB 90% at all loads with an engine speed of 1,500 rpm. At rated speed, the cylinder pressure and in-cylinder temperature were, perhaps, more favourable for formation, evaporation and burning of the smaller droplets from 10-hole nozzles (Chauhan et al., 2010; Hoang, 2019).

Combustion duration

Combustion duration (CD) can be defined either as the time interval between MFB 5% and MBF 50% or the time interval between MFB 5% and MFB 90%. Measurements using both definitions of CD are depicted in Fig. 7 and 8 respectively, using the data from Table 7. MFB 5% always occurred during the main injection, irrespective of nozzle or load. MFB 50% was achieved at 30 ± 2° CA. MFB 90% was observed after the end of any post injections.

CD values of MFB 5−50% were fairly similar for all the nozzles at all load/speed points, with two exceptions (Fig. 7). In the first of these, the 6-hole nozzles had a shorter CD at rated speed and full load (11.4 BMEP) because increased fuel supply at higher loads with the 6-hole nozzles enhance combustion. However, at lower loads mixing with the six-hole nozzles is poorer, ID may be delayed and combustion is more prolonged relative to the other nozzles. The second exception relates to the 10-hole nozzles; these showed longer CD values at 1,500 rpm with 75% and 100% loads (13.1 and 17.4 bar respectively). Effective fuel/air mixing with the 10-hole nozzles gave a shorter CD at low loads but at higher load CD increased, due to smaller orifice diameters that led to lengthened combustion duration. Studies of Sarvi et al. (2008), Jääskeläinen (2017) and Dong et al. (2018) stated that there is a limit to the reduction of nozzle diameter that related to e.g. total injection time and combustion durations especially at high loads.

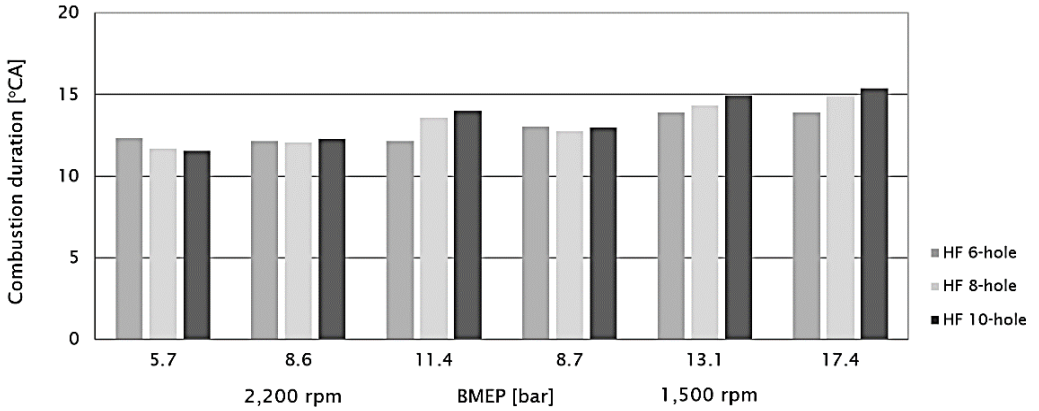

Figure 7. Combustion duration (°CA) at all engine loads, determined as crank angles between MFB 5% and MFB 50%.

Fig. 8 shows MFB 5−90% values at all load/speed points. At 2,200 rpm, the 6-hole nozzles always had the longest CD. Their larger hole diameters created larger droplets than the other nozzles; larger droplet sizes require more time to evaporate and burn (Heywood, 2018). At 1,500 rpm engine speed, the 10-hole nozzles had the longest CD and the difference compared to the other nozzles increased as engine load grew.

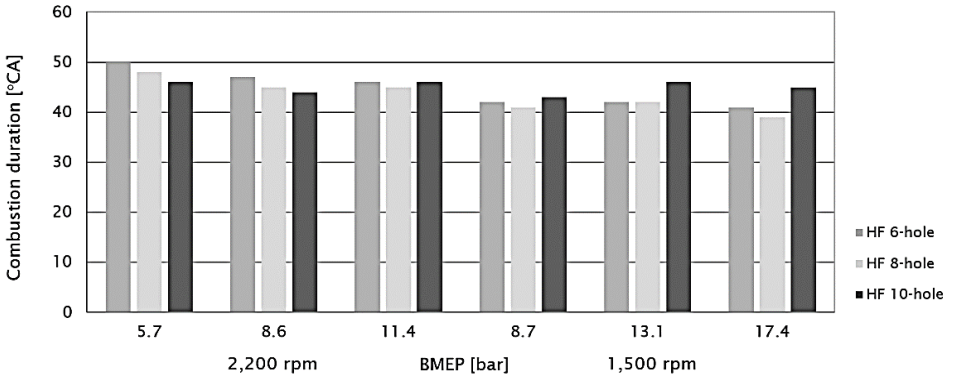

Figure 8. Combustion duration (°CA) at all engine loads, determined as crank angles between MFB 5% and MFB 90%.

Gaseous emissions and smoke

Fig. 9 illustrates the brake specific emissions of NOx, CO and HC. The smoke numbers are also depicted.

Using 6- and 10-hole nozzles instead of 8-hole nozzles generated less NOx. The 6-hole nozzles gave the lowest NOx at low loads at both speeds: 14% lower at rated speed and 18% lower at intermediate speed compared with the 8-hole nozzles. At full loads, the lowest NOx values were measured with the 10-hole nozzles. They cut NOx emissions by 11% at 2,200 rpm and by 13% at 1,500 rpm compared with 8-hole nozzles. Low smoke and high BTE indicate that combustion was efficient with 8-hole injectors, although that often is accompanied by the trade-off involving greater NOx formation. Mekonen et al. (2020) observed more NOx when they increased nozzle hole number from 3 to 4, attributing it to smaller particles that increased the combustion rate and in-cylinder gas temperature. They also measured a reduction in NOx when the nozzle number was raised from 4 to 5. The reason given was greater fuel supply to the cylinder, reducing in-cylinder gas temperature and NOx emissions. The results are consistent with the experimental observations of Lee et al. (2010) where the highest NOx emission was measured for the 8-hole nozzles. The lowest NOx values with the 10-hole nozzles were due to presence of fuel-rich zones developed from the poor mixture formation.

Carbon monoxide (CO) is mainly formed due to lack of oxygen in locally rich mixtures in the cylinder, although dissociation of CO_2 may also increase CO. The 6-hole nozzles improved CO performance at rated speed, cutting CO emissions by 20% at low load and by 39% at full load compared with the 8-hole nozzles. The 10-hole nozzles reduced CO by 15% at low load and by 19% at medium load, respectively. The 8-hole and the 10-hole nozzles produced the same amount of CO at full load. At intermediate speed, the 10-hole nozzles now produced the highest CO emissions at all load points. The increases compared with the 8-hole nozzles were considerable: 36% at low load, 26% at medium load and 83% at high load. Conversely, the 6-hole nozzles performed better than the 8-hole nozzles, reducing CO by 2%, 39% and 54% at low, medium and high loads respectively. At full load at 1,500 rpm, CO formation with 10-hole nozzles was four times higher than with the 6-hole nozzles, maybe due to the prolonged combustion. The effects of CO_2 dissociation on CO were assumed to be quite similar for all nozzles because the high temperatures prevailed in the cylinder for quite similar periods with them all.

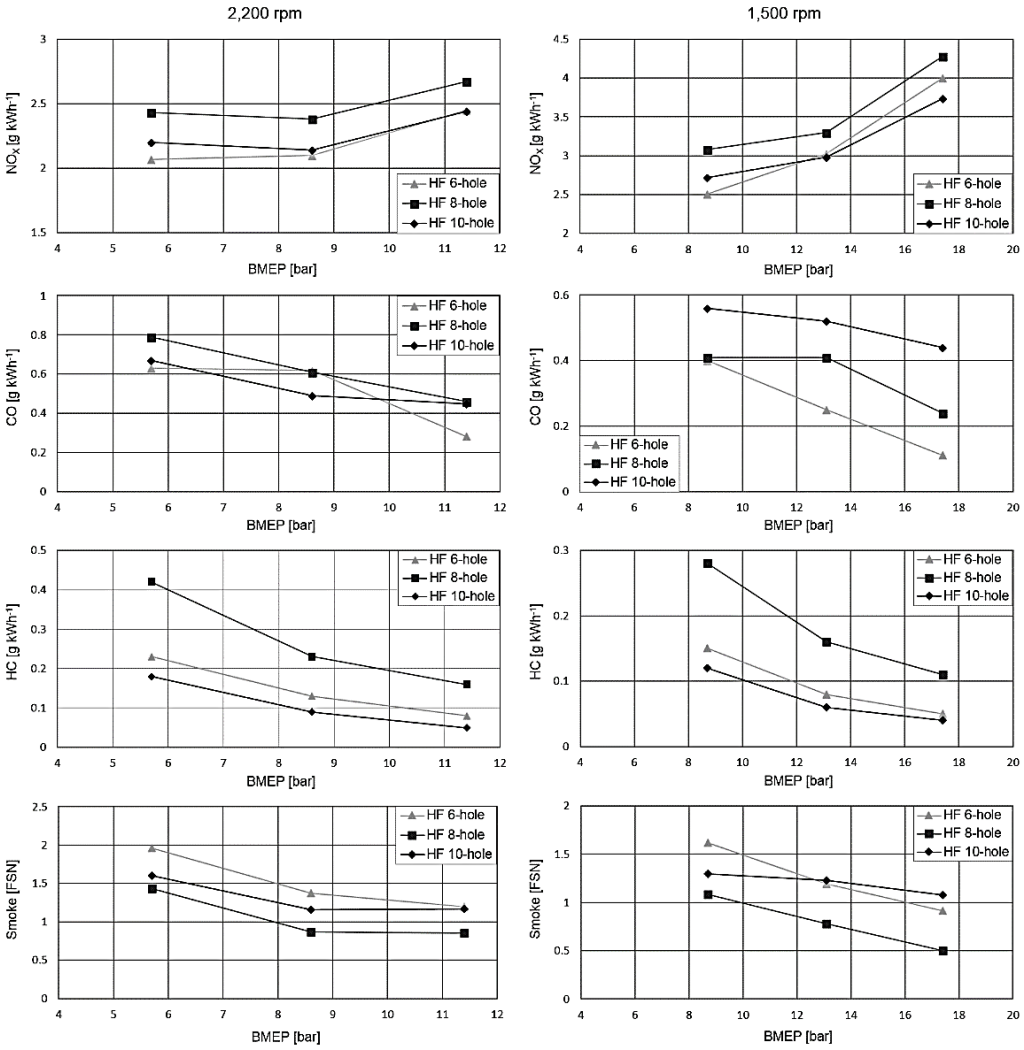

Figure 9. Brake specific emissions of NOx, CO and HC and smoke numbers versus engine load at two speeds.

Total hydrocarbon emissions (HC) are considered to reflect the presence of unburnt or partially burnt fuel in the exhaust gas (Hoang, 2019). Most exhaust HC originate from the fuel but some are formed by unknown chemical reactions within the cylinders (Satyanarayana & Muraleedharan, 2012). An increase in HC emissions is indicative of reduced thermal efficiency and a raised level of pollutants (Hoang, 2019). In our study, both the alternative nozzles gave better HC performance than the reference nozzles at all loads and speeds, with the 10-hole nozzles being slightly the most beneficial. At rated speed, the 10-hole nozzles reduced HC emissions by 57% at low load, 60% at medium load and 68% at high load compared with 8-hole nozzles. At intermediate speed, 10-hole nozzles achieved HC reductions of 57%, 62% and 63% respectively.

Exhaust smoke increased when engine load reduced. Smoke number at the engine´s rated speed was always highest with 6-hole nozzles. The smoke result was less clear-cut

at intermediate speed: the 6-hole nozzles generated the highest smoke at low load but the 10-hole nozzles produced the most smoke at the highest load. The 8-hole nozzles gave the lowest smoke at both speeds and all loads, ranging from 0.9 to 1.5 FSN at rated speed and from 0.5 to 1.1 at intermediate speed.

Sarvi et al. (2008) reported that NOx decreased when the number of nozzle holes was reduced for a given fuel consumption in a medium-speed diesel engine driven with light fuel oil (LFO). However, that was accompanied by the penalty of greater smoke (FSN), HC and CO concentrations. Dong et al. (2018a), say that combustion efficiency improves with smaller fuel droplets. Heat release is accelerated and combustion temperature rises, giving higher NOx. On the other hand, NOx formation in the combustion chamber is related to the flame area. A lower number of nozzle holes gives a smaller fuel jet area, resulting in different fuel/air mixing which reduces NOx production (Dong et al., 2018a; Sarvi et al., 2008).

Generally, NOx formation increased with engine load. Higher combustion temperature promoted NOx formation. Fig. 8 shows that higher engine load improved fuel/air mixing and fuel oxidation processes. The improved mixing rate led to reductions of CO, HC and smoke when engine load was increased.

CONCLUSIONS

The present study compared three different injector nozzles in a high-speed non-road diesel engine at different engine loads and speeds. The main aim was to find out how the selected nozzles affect combustion and emission characteristics of the common-rail experimental engine, fuelled by commercial low-sulphur DFO. The nozzles had 6, 8 and 10 holes. The injection map was kept constant and the engine control module set the injection for each nozzle automatically. The measurements generated new information of fuel injection nozzles supporting the development of more efficient high-speed non-road engines.

Based on the performed measurements and analyses, the following conclusions could be drawn:

- The BSFC for the 6- and 10-hole nozzles were higher than that of the 8-hole nozzles.
- The HRRs were fairly similar for all nozzles at all loads. However, the HRR remained slightly longer at a high level with 6-hole nozzles.
- Differences in maximum cylinder pressures and BTE were minimal between the nozzles.
- Combustion durations were almost similar for all the nozzles.
- The 6- and 10-hole nozzles improved CO and HC formation.
- The 8-hole tips generated the highest NOx but lowest smoke at all loads.

ACKNOWLEDGEMENTS. This project was one part of the national Future Combustion Engine Power Plant research program. The authors wish to thank Business Finland for the financial support of the program.

The authors offer their appreciation to Dr. Katriina Sirviö, Mr. Olav Nilsson, Mr. Markus Uuppo and Mr. Teemu Ovaska for the assistance in the measurements. The authors also express their gratitude to Mr. Henri Huusko and Mr. Marko Vallinmäki at AGCO Power Inc. for their kind assistance in providing test nozzles and their specifications for the study.

REFERENCES

Chauhan, B.S., Kumar, N., Du Jun, Y. & Lee, K.B. 2010. Performance and emission study of preheated Jatropha oil on medium capacity diesel engine. *Energy* **35**, 2484−2492.

Dong, S., Wang, Z., Yang, C., Ou, B., Lu, H., Xu, H. & Cheng, X. 2018a. Investigations on the effects of fuel startification on auto-ignition and combustion process of an ethanol/diesel dual-fuel engine. *Applied Energy* **230**, 19−30.

Dong, S., Yang, C., Ou, B., Lu, H. & Cheng, X. 2018b. Experimental investigation on the effects of nozzle-hole number on combustion and emission characteristics of ethanol/diesel dual-fuel engine. *Fuel* **217**, 1−10.

European Parliament. 2018. MEPs set ambitious targets for cleaner, more efficient energy use. https://www.europarl.europa.eu/news/en/press-room/20180112IPR91629/meps-set-ambitious-targets-for-cleaner-more-efficient-energy-use. Accessed 15.1.2020.

Heywood, J.B. 2018. *Internal Combustion Engine Fundamentals*, 2nd Edition, McGraw-Hill Education, USA, 1028 pp.

Hissa, M., Niemi, S., Sirviö, K., Niemi, A. & Ovaska, T. 2019b. Combustion Studies of a Non-Road Diesel Engine with Several Alternative Liquid Fuels. *Energies* **12**, 2447.

Hoang, A.T. 2019. Experimental study on spray and emission characteristics of a diesel engine fueled with preheated bio-oils and diesel fuel. *Energy* **171**, 795−808.

Jääskeläinen, H. 2017. *DieselNet Technology Guide − Diesel Fuel Injection Nozzles.* https://dieselnet.com/tg. Accessed 20.9.2019.

Lee, B.H., Song, J.H., Chang, Y.J. & Jeon, C.H. 2010. Effect of the number of fuel injector holes on characteristics of combustion and emissions in a diesel engine. *International Journal of Automotive Technology* **11**(6), 783−791.

Mekonen, M. W. & Sahoo, N. 2020. Combined effects of fuel injection pressure and nozzle holes on the performance of preheated palm oil methyl ester used in a diesel engine. *Biofuels* **11**(1), 19−35.

Niemi, S., Uuppo, M., Virtanen, S., Karhu, T., Ekman, K., Svahn, A., Vauhkonen, V., Agrawal, A. & Hiltunen, E. 2011. Animal Fat Based Raw Bio-Oils in a Non-Road Diesel Engine Equipped with a Diesel Particulate Filter. In Bartz, W.J. (ed) (2011): *8th International Colloquium Fuels; Conventional and Future Energy for Automobiles*. Ostfildern, Germany: Technische Akademie Esslingen. pp. 517–528.

Perumal, V. & Ilangkumaran, M. 2017. Experimental analysis of engine performance, combustion and emission using pongamia biodiesel as fuel in CI engine. *Energy* **129**, 228–236.

Salvador, F.J., Lopez, J.J., De la Morena, J. & Crialesi-Esposito, M. 2018. Experimental investigation of the effect of orifices inclination angle in multihole diesel injector nozzles. Part 1 – Hydraulic performance. *Fuel* **213**, 207−214.

Sarvi, A., Fogelholm, C-J. & Zevenhoven, R. 2008. Emissions from large-scale medium-speed diesel engines: 1. Influence of engine operation mode and turbocharger. *Fuel Processing Technology* **89**, 510−519.

Satyanarayana, M. & Muraleedharan, C. 2012. Experimental Studies on Performance and Emission Characteristics of Neat Preheated Vegetable Oils in a DI Diesel Engine. *Energy Sources, Part A: Recovery, Utilization, and Environmental Effects* **34**, 1710−1722.

Sayin, C., Gumus, M. & Canakci, M. 2013. Influence of injector hole number on the performance and emissions of a DI diesel engine fueled with biodiesel-diesel fuel blends. *Applied Thermal Engineering* **61**, 121–128.

Agronomy Research **18**(3), 2049–2059, 2020
https://doi.org/10.15159/AR.20.176

Winter wheat, winter rape and poppy crop growth evaluation with the help of remote and proximal sensing measurements

Z. Jelínek[1,*], K. Starý[1], J. Kumhálová[1], J. Lukáš[2] and J. Mašek[3]

[1]Czech University of Life Sciences Prague, Faculty of Engineering, Department of Machinery Utilization, Kamýcká 129, CZ165 00 Prague, Czech Republic
[2]Crop Research Institute, v.v.i., Drnovská 507, CZ161 00 Prague, Czech Republic
[3]Czech University of Life Sciences, Faculty of Engineering, Department of Agricultural Machines, Kamýcká 129, CZ165 00 Prague, Czech Republic
[*]Correspondence: jelinekzdenek@tf.czu.cz

Abstract. Monitoring of agricultural crops with the help of remote and proximal sensors during the growing season plays important role for site-specific management decisions. Winter wheat, winter rape and poppy are representatives of typical agricultural crops from the family Poacea, Brassicaceae and Papaveraceae, growing in relative dry area of Rakovník district in the Czech Republic. Ten Sentinel 2 satellite images acquired during vegetation season of the crops were downloaded and processed. Crops were monitored with the help of unmanned aerial vehicles (UAV) equipped with consumer grade Red Green Blue (RGB) camera and multispectral (MS) MicaSense RedEdge MX camera. In-field variability was assessed by computing RGB-based vegetation indices Triangular Greenness Index (TGI), Green Leaf Index (GLI) and Visible Atmospherically Resistant Index (VARI) and commonly used vegetation indices as Normalised Difference Vegetation Index (NDVI) and Green NDVI (GNDVI). The results derived from satellite and UAV images were supported with in-situ measurements of hand-held GreenSeeker and Chlorophyll Meter Content sensors. The study showed the usability of individual vegetation indices, especially the TGI index for chlorophyll content estimation, and VARI index for green vegetation fraction detection and leaf area index estimation, in comparison with selected hand-held devices. The results showed as well that leaf properties and canopy structure of typical characteristics of selected families can significantly influence the spectral response of the crops detected in different phenological stages.

Key words: satellite images, unmanned aerial vehicles, vegetation indices, winter wheat, winter rape, poppy.

INTRODUCTION

Monitoring the vitality of agricultural crops during the whole growing season is significant for increasing crop yields and reducing input resources and costs for the agricultural system (Brisco et al., 1998). Knowledges of vegetation indices are fundamental for understanding of agricultural ecosystems as well (Wang et al., 2010). Vegetation indices can describe health and condition of agricultural crops, but each of indices uses different part of electromagnetic spectrum and therefore each of indices has different informative value.

Triangular Greenness Index (TGI) index calculates the triangle area of the reflectance spectrum in red, green and blue wavelengths, allows estimation of chlorophyll concentration in leaves and the canopy (Hunt et al., 2013). Green Leaf Index (GLI) is one of the important indices commonly used for yield forecasting. This spectral index was originally designed for use with RGB camera in data range from 0 to 255 (Gobron et al., 2000; Hunt et al., 2013). Visible Atmospherically Resistant Index (VARI) estimates the fraction of crops in scene with low sensitivity to atmospheric effects (Gitelson et al., 2002). Normalised Difference Vegetation Index (NDVI) is measure of healthy, green vegetation. The combination of it is normalized difference formulation and use of the highest absorption and reflectance regions of chlorophyll make it robust over a wide range of conditions (Rouse et al., 1974). Green NDVI (GNDVI) has similar algorithm to NDVI, but green part of electromagnetic spectrum (in 540 to 570 nm) is measured instead of the red part. GNDVI is more sensitive to chlorophyll content (Gitelson et al., 2002).

Data from Copernicus program can be free downloaded and used for evaluation of crop plots with using commercial software or open access software. Optical satellite imaging have borders in usability for example in cloudy weather (Domínguez et al., 2017). Compared to satellite images, unmanned aerial vehicles represent a much more accurate source of images for crop growth monitoring, especially in terms of spatial and temporal resolution. We can say, that UAVs are the most important technologies in agriculture and their flexibility help scientific sectors development and farmers in praxis (De Rango et al., 2017). One of UAV's benefits is possibility to add various devices for example high resolution multispectral camera, digital camera, thermal camera, LiDAR etc. (Grenzdorffer et al., 2008).

The use of modern technologies in precision agriculture is the reply to new epoch of farming systems, private companies or scientists. Good informations in precision agriculture, especially satellite and UAV's scanning or results from precise measurements, may affect the production function of immediate yield monitoring. That is why the main aim of this study was to evaluate crop growth of winter wheat, winter rape and poppy with the use of proximal and remote sensing measurements. The other objective of this study was to compare the utilization of selected RGB indices with most common spectral indices and prove use for common agricultural practice.

MATERIALS AND METHODS

Study area

The study area was located near to Lišany village (N 50° 9'31.57", E 13°44'37.12"), the Czech Republic. Experimental field with winter wheat was in size of 16.48 ha with average elevation of 355.96 m a.s.l. and 3.32% slope. Winter rape field had 19.30 ha with 360.35 m a.s.l. average elevation and 4.14% slope. Poppy field had 18.77 ha with average elevation of 349.25 m a.s.l. and 2.90% slope. Weather condition, total monthly precipitation and temparatures data for the years 2018 and 2019 and then total monthly average of 1961–1990 were provided by the hydrometeorological station Heřmanov in district Rakovník (see Table 1). The experimental fields are owned by Agricultural Company Lupofyt s.r.o. Soil tillage minimalization technology with alternately conventional arable soil technology (ploughing) were used on experimental plots. Since 2015 the crop rotation for the field with winter wheat has been: winter wheat (2015),

lupine (2016), winter wheat (2017), winter rape (2018) and winter wheat (2019); for the field with winter rape: winter rape (2015), winter wheat (2016), winter rape (2017), winter wheat (2018) and winter rape (2019); and for the field with poppy: winter rape (2015), winter wheat (2016), winter rape (2017), winter wheat (2018) and poppy (2019).

Table 1. Weather conditions (monthly precipitations and temperatures) for the years 2018 and 2019 and total monthly average of 1961–1990 for hydrometeorological station Heřmanov

	Precipitation (mm)			Temperature (°C)		
Month/Year	2018	2019	Avg 1961–1990	2018	2019	Avg 1961–1990
I.	25.0	34.0	32.0	1.1	1.9	-2.0
II.	2.0	5.0	30.0	2.7	0.5	-0.4
III.	36.0	40.0	36.0	6.9	4.8	3.4
IV.	33.0	26.0	43.0	10.6	8.4	8.1
V.	121.0	41.0	70.0	12.6	13.2	13.0
VI.	27.0	60.0	75.0	16.7	16.5	16.3
VII.	94.0	28.0	72.0	20.1	20.8	17.8
VIII.	64.0	70.0	73.0	16.6	22.1	17.2
IX.	85.0	20.0	46.0	14.7	13.7	13.6
X.	51.0	54.0	36.0	10.6	8.4	8.6
XI.	18.0	64.0	40.0	6.4	6.6	3.3
XII.	31.0	17.0	35.0	2.5	4.9	-0.2
Sum	587.0	459.0	590.0	-	-	-
Mean	49.0	38.0	49.0	10.2	10.1	8.2

Data description

Measurements were performed during vegetation season 2019 on winter wheat, winter rape and poppy crops. Measurements consisted of spectral indices derived from Sentinel 2A/B MSI images, UAV images and handheld devices (GreenSeeker and Chlorophyllmeter). The details can be found in Table 2.

Yield and remote sensing data

Combine harvester New Holland CR9080 was used for yield measurement. This machine was equipped with yield monitor and DGPS receiver. EGNOS correction ensure the accuracy of this system (± 0.1–0.3 m in horizontal and ± 0.2–0.6 m in vertical direction). The yield data were saved every 1 second with coordinates to the external memory. The yield data were processed by basic statistical method in order to eliminate the errors of yield measurement system. The yield data sets were then interpolated to kriging maps (see Fig. 1) using experimental variograms and common procedures. The method is detailed described for example in Kumhálová et al., 2011. Because of problems with poppy yield measurement, the special correction of this yield data set was used. Geographically Weighted Regression (GWR; ArcGIS 10.4.1 SW, ESRI Redlands, CA, USA) with the use of last satellite images from poppy vegetation season (28 June) was used for this correction. GWR is one of several spatial regression techniques increasingly used in geography and other disciplines. GWR provides a local model of the variable or process by fitting a regression equation to every feature in the dataset. GWR constructs these separate equations by incorporating the dependent and explanatory variables of features falling within the bandwidth of each target feature (ESRI, 2019).

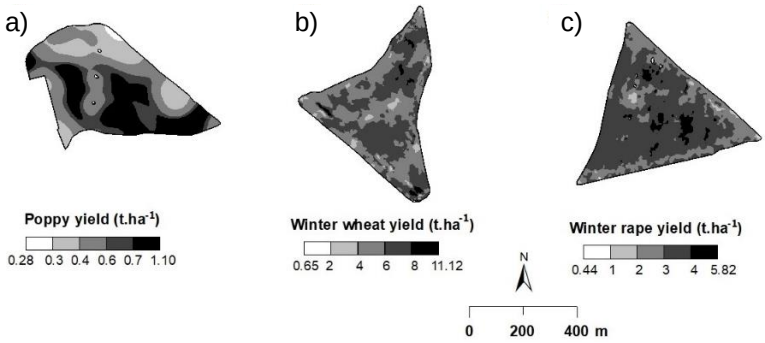

Figure 1. Yield maps (in t ha^{-1}) of poppy (a); winter wheat (b); and winter rape (c).

Table 2. Measurements (date, platform with sensors and spectral indices) used in this study for individual crops for the vegetation season 2019

Date	Platform and sensor	Winter wheat Indices	Winter rape Indices	Poppy Indices
4 April	S2A MSI	GNDVI, NDVI, TGI, VARI	GNDVI, NDVI, TGI, VARI	GLI*, GNDVI*, NDVI*, TGI*, VARI*
12 April	UAV with RGB camera	-	TGI	-
	GreenSeeker	NDVI	NDVI	-
	N-Sensor	NDGI	NDGI	-
	Chlorophyllmeter	CFR	CFR	-
19 April	S2B MSI	GNDVI, NDVI, TGI	GNDVI, NDVI, TGI	GLI*, GNDVI*, NDVI*, TGI*, VARI*
24 April	S2A MSI	GNDVI, NDVI, TGI	GNDVI, NDVI, TGI	GLI*, GNDVI*, NDVI*, TGI*, VARI*
1 May	GreenSeeker	NDVI	-	-
	N-Sensor	NDGI		
	Chlorophyllmeter	CFR		
19 May	S2B MSI	clouds – only parts of the fields usable, not used for the study		
24 May	S2A MSI	GNDVI, NDVI, TGI	Clouds, shadows	GNDVI, NDVI, TGI
3 June	S2A MSI	GNDVI, NDVI, TGI	GNDVI, NDVI, TGI	GNDVI, NDVI, TGI
8 June	S2B MSI	GNDVI, NDVI, TGI	clouds	GNDVI, NDVI, TGI
13 June	S2A MSI	GNDVI, NDVI, TGI	GNDVI, NDVI, TGI	GNDVI, NDVI, TGI
17 June	UAV with MicaSense camera	-	-	GLI, GNDVI, NDVI
18 June	S2B MSI	clouds	GNDVI, NDVI, TGI	clouds
28 June	S2B MSI	GNDVI, NDVI, TGI	GNDVI, NDVI, TGI	GNDVI, NDVI, TGI
30 June	GreenSeeker	-	-	NDVI

**= spectral indices calculated for the bare soil; CFR = Content of Chlorophyll, GLI = Green Leaf Index; GNDVI = Green Normalised Difference Vegetation Index; NDVI = Normalised Difference Vegetation Index; NDGI = Normalised Difference Green Index; TGI = Triangular Greenness Index; VARI = Visible Atmospherically Resistant Index; S2A/B MSI = Sentinel 2A/B Multispectral Instrument.*

The Sentinel 2A or B satellite images for vegetation season of 2019 were downloaded from Copernicus Open Access Hub (https://scihub.copernicus.eu/). The satellite images in level of BOA reflectance (Bottom of Atmosphere) L2A were resampled to 10 m spatial resolution with the help of SW ENVI 5.5 (Excelis, Inv. Mc Lean, USA) or SNAP 6.0.4 (ESA, http://step.esa.int/main/). Aerial survey were performed using common UAV with common RGB camera on 12 April for winter wheat and winter rape monitoring, and using Phantom UAV with MicaSense RedEdge-MX camera (MicaSense, Inc. Seattle, WA, USA) with five spectral bands (RED, GREEN, BLUE, Red Edge and NIR channels) and 1.2 Mpx per EO band sensor resolution on 17 June for poppy monitoring.

Spectral indices (see Table 3) were calculated from each of Sentinel 2 image (see Table 2). The images were acquired for the whole vegetation season with the aim to reach essential growth stages (see Fig. 2 and Table 4).

Table 3. Vegetation indices used in this study

RGB Spectral Index	Algorithm	References
Normalized Difference Vegetation Index	$NDVI = \frac{\mathrm{NIR} - \mathrm{R}}{\mathrm{NIR} + \mathrm{R}}$	(Rouse et al., 1974)
Green Normalized Difference Vegetation Index	$GNDVI = \frac{\mathrm{NIR} - \mathrm{G}}{\mathrm{NIR} + \mathrm{G}}$	(Gitelson et al., 1996)
Green Leaf Index	$GLI = \frac{(\mathrm{G} - \mathrm{R}) + (\mathrm{G} - \mathrm{B})}{2\mathrm{G} + \mathrm{R} + \mathrm{B}}$	(Gobron et al., 2000; Hunt et al., 2013)
Visible Atmospherically Resistant Index	$VARI = \frac{\mathrm{G} - \mathrm{R}}{\mathrm{G} + \mathrm{R} - \mathrm{B}}$	(Gitelson et al., 2002)
Triangular Greenness Index	TGI =G-0.39×R-0.61×B	(Hunt et al., 2013)

Where g = G/(R+G+B); b = B/(R+G+B); r = R/(R+G+B); and green (G), red (R), blue (B) and NIR are the reflectance values of each band.

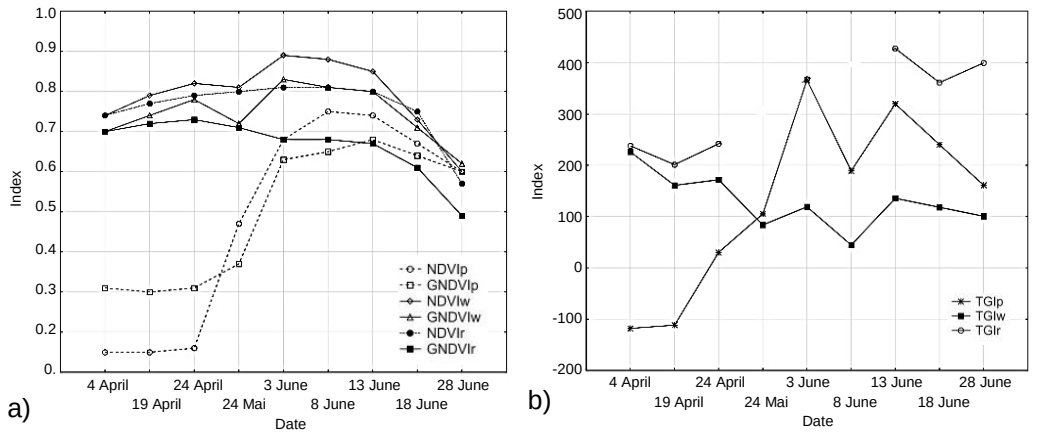

Figure 2. Graphs of Normalised Difference Vegetation Index (NDVI), Green NDVI (GNDVI) (a); and Triangular Greenness Index (TGI) (b) for winter wheat, winter rape and poppy calculated from Sentinel 2 images for vegetation season.

Table 4. Growth stages of monitored crops, expressed in BBCH scale

BBCH	Winter wheat	Winter rape	Poppy
0–19	21.9.2018–10.11.2018	6.8.2018–31.3.2019	25.3.2019–20.4.2019
20–29	11.11.2018–10.4.2019	-	21.4.2019–10.5.2019
30–59	11.4.–31.5.2019	1.4.–15.4.2019	11.5.2019–15.6.2019
60–89	1.6.2019–27.7.2019	16.4.–24.7.2019	16.6.2019–28.7.2019

Data were compared for each of the selected crop (winter wheat, winter rape and poppy). Correlation coefficients (R) were calculated between generally known and used NDVI and GNDVI spectral indices and TGI index for Sentinel 2 images, and then these indices derived from Sentinel 2 images were compared with other measurements (Chlorophyllmeter, GreenSeeker, N-Sensor, indices derived from UAV images and yield data).

RESULTS AND DISCUSSION

The coefficients of correlation for selected parameters are shown in Table 5, 6 and 7. The coefficients of correlation were calculated for a 5% significance level.

Table 5. Coefficients of correlation between Triangular Greenness Index (TGI) and Normalized Different Vegetation Index (NDVI) a Green NDVI (GNDVI) derived from Sentinel 2 images for the vegetation season of winter wheat, winter rape and poppy (at 5% significance level)

		Winter wheat		Winter rape		Poppy	
Date	Index	NDVI	GNDVI	NDVI	GNDVI	NDVI	GNDVI
4 April	TGI	-0.14	-0.28	0.59	0.47	-0.04	-0.64
	VARI	-0.31	-0.25	-0.48	-0.43	0.61	0.84
19 April	TGI	-0.34	-0.50	0.63	0.51	0.10	-0.43
24 April	TGI	-0.33	-0.49	0.55	0.37	0.11	-0.41
24 May	TGI	0.80	0.80	-	-	0.85	0.74
3 June	TGI	-0.19	-0.32	0.17	-0.10	0.82	0.52
8 June	TGI	-0.10	-0.39	-	-	0.85	0.73
13 June	TGI	0.12	-0.16	0.45	0.15	0.74	0.70
18 June	TGI	-	-	0.42	0.53	-	-
28 June	TGI	0.70	0.49	0.47	-0.12	0.78	0.60

Table 5 showed comparison between RGB indices (TGI and VARI) and NDVI and GNDVI spectral indices with near-infrared band, mostly used in literature (e.g. Domínguez et al., 2017) for crop vigor evaluation. The indices were calculated for Sentinel 2 images only. The results showed that TGI index developed for chlorophyll estimation calculated using RGB spectral bands had the strongest correlations with NDVI and GNDVI for poppy crops in comparison with the other (winter wheat and winter rape). Higher values of correlations in 24 May and 8 June were probably caused by light condition over the experimental field (clouds shadows on crop canopy). Nevertheless, results from 3 June, when the images was clear, showed that correlation between NDVI and TGI in case of poppy was relatively high as well. It means that the shadows affect the measured values to some extent, but the trend is generally maintained. Generally, correlations between TGI and NDVI were more significant for poppy (calculated from end of April – see BBCH scale in Table 4) and winter rape. On the

contrary, winter wheat crops showed more significant dependence between TGI and GNDVI during the growth season, when the plants were green. The last image captured on 28 June showed opposite results because of partly matured canopy. As the results on 4 April in case of winter wheat and winter rape showed, VARI index developed for vegetation faction and leaf area estimation could be used only for early growth stages evaluation, when canopy is uneven. The development of NDVI and GNDVI indices calculated from Sentinel 2 images are given in the Fig. 2, a. The graph showed relatively similar development of the values of these spectral indices. Early values of crop growth were evaluated only in case of winter wheat and winter rape canopy (see Table 4). On the contrary, TGI index in Fig. 2, b showed uneven development of this index and plant growth during the time which is probably caused by light condition over the experimental field (clouds shadows on crop canopy) how it is explained higher.

Table 6. Coefficients of correlation between handheld sensors (CFR = Chlorophyllmeter; N-Sensor a GreenSeeker = GSK) and UAV images (Triangular Greenness Index = TGI) used in this study and spectral indices (NDVI, GNDVI, TGI and VARI) derived from Sentinel 2 (S2) images for winter wheat and winter rape and crop yield (at 5% significance level)

Date	Sensor	Winter wheat				Winter rape			
		NDVI S2	GNDVI S2	TGI S2	VARI S2	NDVI S2	GNDVI S2	TGI S2	VARI S2
12 April		4 April – S2 images				4 April – S2 images			
	CFR	-0.21	-0.25	0.07	-0.01	-0.20	-0.21	-0.07	0.15
	NDGI N-Sensor	-0.19	-0.21	0.02	0.03	-	-	-	-
	NDVI GSK	0.47	0.50	-0.41	-0.08	0.52	0.53	0.18	-0.34
	TGI UAV	-	-	-	-	0.36	0.33	0.22	-0.18
12 April		19 April – S2 images				19 April – S2 images			
	CFR	-0.02	-0.03	0.00	-	-0.15	-0.16	-0.08	-
	NDGI N-Sensor	0.05	0.06	-0.07	-	-	-	-	-
	NDVI GSK	0.29	0.31	-0.36	-	0.47	0.46	0.23	-
	TGI UAV	-	-	-	-	0.34	0.29	0.19	-
1 May		24 April – S2 images							
	CFR	-0.09	-0.07	0.08	-	-	-	-	-
	NDGI N-Sensor	-0.02	0.00	-0.18	-	-	-	-	-
	NDVI GSK	0.19	0.17	0.00	-	-	-	-	-
		28 June – S2 images				28 June – S2 images			
	Yield	0.37	0.31	0.27	-	0.10	-0.15	0.41	-

Table 6 described the coefficients of correlation between selected handheld sensors and UAV images, and spectral indices (NDVI, GNDVI, TGI) calculated from Sentinel 2 images. The dependences between selected variables were relatively low. Nevertheless, more significant correlations (R = 0.47/0.50 – NDVI /GNDVI for winter wheat; 0.52/0.53 NDVI/GNDVI for winter rape on 12 April vs. 4 April) were found between NDVI measured with GreenSeeker and indices derived from Sentinel 2. Similarly higher correlations between NDVI measured by GreenSeeker on 30 June and Sentinel 2 spectral indices (28 June) derived for poppy are given in Table 7. Significantly higher correlations (around the R values of 0.6 for NDVI and GNDVI; and around 0.46 R value

for TGI) between spectral indices calculated from UAV images (from 17 June) and Sentinel 2 images (13 June) are given in Table 7 as well. Comparison between last satellite images (see Fig. 3) and crop yield are given in Table 6 for winter wheat and winter rape, and Table 7 for poppy.

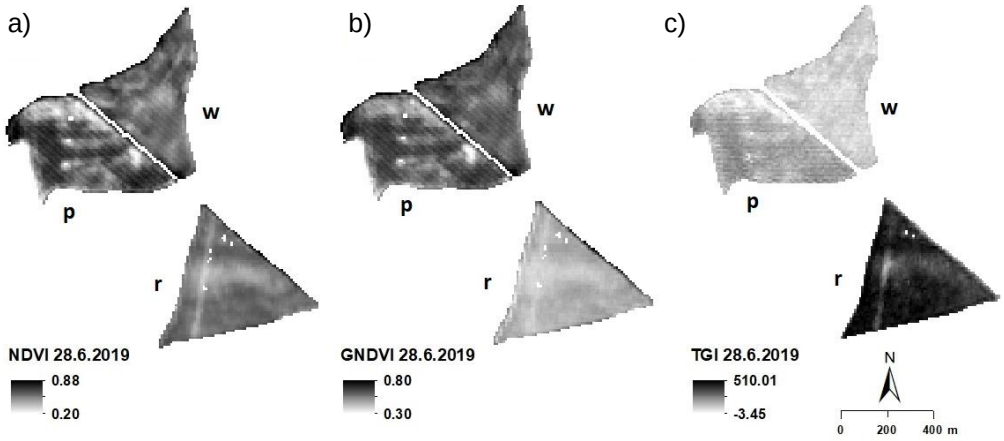

Figure 3. Normalised Difference Vegetation Index (NDVI) a); Green NDVI (GNDVI) (b); Triangular Greenness Index (TGI) (c) for winter wheat (w), winter rape (r) and poppy (p).

Table 7. Coefficients of correlation between handheld sensors and UAV images used in this study and spectral indices derived from Sentinel 2 (S2) images for poppy and crop yield (at 5% significance level)

Date	Sensor	Poppy			
		NDVI S2	GNDVI S2	TGI S2	
		13 June – S2 images			
17 June	GLI UAV	0.61	0.57	0.46	
	GNDVI UAV	0.64	0.61	0.46	
	NDVI UAV	0.63	0.59	0.47	
		28 June – S2 images			NDVI GSK 30 June
30 June	NDVI GSK	0.47	0.31	0.68	-
	Yield	0.62	0.54	0.58	0.48

These results showed that normalised indices calculated from UAV images could suitably complement the time series of satellite images, if any are missing, for example due to cloud cover. This statement is in accordance with study of Cucho-Padin et al. (2019). They tested usability of agricultural UAV based remote sensing methods to increasing productivity with high-quality multispectral camera and open-access software. Their study proved high usability and higher accuracy of UAV images than satellite images from Sentinel 2. The development of high-precision agricultural techniques has been observed for at least two decades (e.g. Moran et al., 1997). However, our results show that even low-cost cameras can be useful for crop scanning.

Hunt et al. (2005), Lelong et al. (2008), Sakamoto et al. (2011), Lebourgeois et al. (2012) wrote in their studies about UAV's with multispectral camera, that can be quickly deployed to acquire data. Because of agricultural purposes, data from UAV had to be processed quickly for providing recommendations. These findings are supported by our

research. Based on our measurements during season, we found UAV with multispectral camera as a good source of data to assess the health of the crop and crop predict yield as well. Compared to data collection from Sentinel 2, we are able to obtain data with higher spatial resolution without the risk of cloudy. On the other hand our results are similar as conclusion by Hunt & Stern (2019) that RGB spectral indices (TGI and VARI) derived from UAV camera are crucial dependent on lighting conditions. Barbosa et al. (2019) confirmed the dependence of scanned vegetation on light conditions as well.

Handheld devices like GreenSeeker, Chlorophyllmeter or N-sensor can be useful especially for quickly determining the current state of the crops at selected locations. Because of in-situ measurements, it is hard to select the representative leaf for measurements. Kumhálová & Matějková (2017) used in their study GreenSeeker to find out the usability of this handheld crop sensor for estimation of winter barley crop condition and yield. They presented that GreenSeeker handheld crop sensor is not suitable for large area of crops estimation due to point measurement. Our results are in accordance with theirs.

On the other hand our results confirm the usability of UAV with multispectral camera to evaluate and predict the yield. The results also show a more suitable use of the TGI index to cereals and poppy than winter rape. Domínguez et al. (2017) found, that NDVI are more accuracy to cereals than winter rape as well. It can be caused by different canopy and leaves structure of agricultural crops of different family (in our case Poacea, Brassicaceae and Papaveraceae). Jelínek et al. (2019) found it, that according to Sentinel 2 image to estimate crop structure from 96% for winter wheat. Hunt et al. (2013) researched topic of a visible spectrum band indices. They described TGI as a significant spectral index for crop evaluation. This theory has also been confirmed by our research, primarily for winter wheat and poppy than winter rape. Broge & Leblanc (2000) compared TGI index and canopy reflectance and their results indicated strong correlation, mainly for NDVI, SAVI indices. Although Masoni et al. (1996) found, that high TGI index may be a symptom of other problems. These conclusions are mostly in accordance with ours. Among other crops, our study focused on poppy monitoring as a crop that is relatively commonly cultivated in the Czech Republic, especially for the food or technical purposes, but at the same time it is not allowed worldwide for legislative reasons. Our study can be useful for agricultural practice. Nevertheless next year of poppy monitoring could be useful for making our results more significant.

ACKNOWLEDGEMENTS. The authors wish to deep thank the farmers in Agricultural Company Lupofyt for their time, inputs data and provided experimental fields.

CONCLUSIONS

Our research showed solution with the use of visible spectral indices (GLI, TGI and VARI) derived not only from Sentinel 2 images, but from UAVs with common used multispectral or low-cost RGB camera as well. Nevertheless the highest coefficient of correlation between TGI index and NDVI derived from Sentinel 2 images is for poppy in average 0.69, with the maximum of 0.85. This points to the use of the TGI index in case of poppy as an alternative to NDVI when only common RGB camera is available. Generally, the results showed potential in UAV data collection as provide high spatial resolution, lower weather independence and select the best term of imaging. The devices

used in this study need to be more used and proved in selected terms during the crop growth in the future.

REFERENCES

Barbosa, B.D.S., Ferraz, G.A.S., Goncalves, L.M., Marin, D.B., Macield, D.T., Ferraz, P.F.P. & Rossi, G. 2019. RGB vegetation indices applied to grass monitoring: a qualitative analysis. *Agronomy Research* **17**(2), 349–357.

Brisco, B., Brown, R.J., Hirose, T., McNairn, H. & Staenz, K. 1998. Precision agriculture and the role of remote sensing: A review. Can. *J. Remote Sens*. **24**, 315–327.

Broge, N.H. & Leblanc, E. 2000. Comparing predictive power and stability of broadband and hyperspectral vegetation indices for estimation of green leaf area index and canopy chlorophyll density. *Remote Sensing of Environment* **76**, 156–172.

Cucho-Padin, G., Loayza, H., Palacios, S., Balcazar, M., Carbajal, M. & Quiroz, R. 2019. Development of low-cost remote sensing tools and methods for supporting smallholder agriculture. *Applied Geomatics* **11**, 1–17.

De Rango, F., Palmieri, N., Santamaria, A.F. & Potrino, G. 2017. A simulator for UAVs management in agriculture domain. 2017 international symposium on performance evaluation of computer and telecommunication systems (SPECTS), 345.

Domínguez, J.A., Kumhálová, J. & Novák, P. 2017. Assessment of the relationship between spectral indices from satellite remote sensing and winter oilseed rape yield. *Agronomy Research* **15**(1), 055–068.

Gitelson, A., Kaufman, Y. & Merzlyak, M. 1996. Use of green channel in remote sensing of global vegetation from EOS-MODIS. *Remote Sensing of Environment* **58**, 289–298.

Gitelson, A.A., Kaufman, Y.J., Stark, R. & Rundquist, D. 2002. Novel Algorithms for Remote Estimation of Vegetation Fraction. *Remote Sensing of the Environment* **80**, 76–87.

Gobron, N., Pinty, B., Verstraete, M.M. & Widlowski, J.L. 2000. Advanced Vegetation Indices Optimized for up-Coming Sensors: Design, Performance, and Applications. *IEEE Transactions on Geoscience and Remote Sensing* **38**(6), 2489–2505.

Grenzdorffer, G.J., Engel, A. & Teichert, B. 2008. *The photogrammetric potential of low-cost UAVs in forestry and agriculture.* The international archives of the photogrammetry, Remote sensing and spatial information sciences. XXXVII. Part **B1**.

Hunt, E.R., Cavigelli, M., Daughtry, C.S.T., McMurtrey, J.E. & Walthall, C.L. 2005. Evaluation of digital photography from model aircraft for remote sensing of crop biomass and nitrogen status. *Precision Agriculture* **6**, 359–378.

Hunt, E.R., Doraiswamy, P.C., McMurtrey, J.E., Daughtry, C.S.T., Perry, E.M. & Akhmedov, B. 2013. A Visible Band Index for Remote Sensing Leaf Chlorophyll Content at the Canopy Scale. *International Journal of Applied Earth Observation and Geoinformation* **21**, 103–112.

Hunt, E.R. & Stern, A.J. 2019. Evaluation of incident light sensors on unmanned aircraft for calculation of spectral reflectance. *Remote Sensing* **11**(22), 2622.

Jelínek, Z., Starý, K. & Kumhálová, J. 2019. Assessment of production zones modelling accuracy based on satellite imaging and yield measurement of selected agriculture plot. *Agronomy Research* **17**(2), 447–455.

Kumhálová, J., Kumhála, F., Kroulík, M. & Matějková, Š. 2011. The impact of topography on soil properties and yield and the effects of weather conditions. *Precision Agriculture* **12**, 813–830.

Kumhálová, J. & Matějková, Š. 2017. Yield variability prediction by remote sensing sensors with different spatial resolution. *International Agrophysics* **31**, 195–202.

Lebourgeois, V., Bégué, A., Labbé, S., Houlès, M. & Martiné, J.F., 2012. A light-weight multi-spectral aerial imaging system for nitrogen crop monitoring. *Precision Agriculture* **13**, 525–541.

Lelong, C.C.D., Burger, P., Jubelin, G., Roux, B., Labbé, S. & Baret, F. 2008. Assessment of unmanned aerial vehicles imagery for quantitative monitoring of wheat crop in small plots. *Sensors* **8**, 3557–3585.

Masoni, A., Ercoli, L. & Mariotti, M. 1996. Spectral properties of leaves deficient in iron, sulfur, magnesium, and manganese. *Agronomy Journal* **88**, 937–943.

Moran, M.S., Inoue, Y. & Barnes, E.M. 1997. Opportunities and limitations for image based remote sensing in precision crop management. *Remote Sensing of Environment* **61**, 319–346.

Rouse, J.W., Haas, R.H., Schell, J.A. & Deering, D.W. 1974. Monitoring vegetation systems in the Great Plains with ERTS. In: Freden, S.C., Mercanti, E.P., Becker, M. (Eds.), Third Earth Resources Technology Satellite-1 Symposium, Vol. **1**: *Technical Presentations, NASA SP-351*. National Aeronautics and Space Administration, Washington, DC, pp. 309–317.

Sakamoto, T., Shibayama, M., Kimura, A. & Takada, E. 2011. Assessment of digital camera-derived vegetation indices in quantitative monitoring of season rice growth. *ISPRS Journal of Photogrammetry and Remote Sensing* **66**, 872–882.

Wang, K., Franklin, S.E., Guo, X. & Cattet, M. 2010. Remote sensing of ecology, biodiversity and conservation: Areview from the perspective of remote sensing specialists. *Sensor* **10**, 9647–9667.

Agronomy Research **18**(3), 2060–2068, 2020
https://doi.org/10.15159/AR.20.178

The effect of nitrogen fertilization on root characteristics of *Camelina sativa* L. in greenhouse pots

I. Kakabouki[1,*], A. Folina[1], S. Karydogianni[1], Ch. Zisi[1] and A. Efthimiadou[2]

[1]Agricultural University of Athens, Department of Crop Science, Laboratory of Agronomy, 75 Iera Odos Str., GR11855 Athens, Greece
[2]Institute of Soil and Water Resources, Department of Soil Science of Athens, Hellenic Agricultural Organization-DEMETER, Sofokli Venizelou 1, GR14123 Lycovrissi, Attica, Greece
[*]Correspondence: i.kakabouki@gmail.com

Abstract. Climate change has made mandatory the introduction of new crops in Greece, such as the cultivation of camelina [*Camelina sativa* (L.) Crantz]. Nitrogen (N) and the development of root system are two important factors affecting crop growth and yield. Camelina has been studied mainly for its composition and oil. In the present study, root development of camelina crop was thoroughly investigated; mainly in terms of Nitrogen fertilization. Therefore, a camelina greenhouse experiment was established in Western Greece, in the region of Agrinio, in March 2019 in completely randomized design with four treatments, (control 0 ppm N, 30 ppm N, 60, ppm N and 90 ppm N). The N rates had statistically significant affected root density and root surface from 40 to 120 days after treatment (DAT) with highest values at 100 DAT and 90 ppm N, 52.54 cm of root 100 cm^{-3} and 27.59 cm^2 of root 100 cm^{-3}, respectively. The root volume was significantly affected by N fertilizer from 40 to 100 DAT and highest value was 13.18 cm^3 of root 100 cm^{-3} soil in the 90 ppm at 120 DAT. The plant leaf area was significantly affected by the highest rate of N. Yield per plant had not statistically significant difference with the 60 and with the 90 and highest weight per plant 292.25 g $plant^{-1}$ in 90 ppm. In conclusion, N fertilization significantly affected growth or camelina's root system after 40 DAT. Plant growth was significantly affected by fertilization and the highest yield and 1,000 seed weight were recorded with the highest amount of N.

Key words: camelina, N rates fertilizer, root system, thousand-seed weight, yield.

Abbreviations: N Nitrogen; DAT Days After Transplanting.

INTRODUCTION

Camelina [*Camelina sativa (L.*) Crantz] belongs to the family Brassicaceae and has many benefits, environmental, industrial, as well as nutritional, since seed oil has a unique profile of fatty acid (Angelopoulou et al., 2019). A direct result of climate change is the change of temperatures that offer alternative cultivation zones and allow in Greece the introduction of new species (Bilalis et al., 2017). *Camelina sativa* is well-adapted to semi-arid region and grown for its seed and oil (Obour et al., 2015). Camelina oil is rich in fatty acid with high levels of alpha-linolenic acid and linoleic acid (Toncea et al.,

2013). Also, in many areas it is used as a raw material for biofuels due to the great potential for plant mass growth (Solis et al., 2013). It is an alternative plant for biofuel production with significant economic and environmental impact, mainly in areas where corn and soybeans are grown. In these areas, camelina is a great option to increase biodiversity, while at the same time, prevents weed expansion and limits pathogenic weed cycles (Johnson & Gesch, 2013). The environmental impact of camelina cultivation is also characterized by the fact that camellia oil used as jet fuel has low emissions (Shonnard et al., 2010). In the past, it was an important oil crop, while today has additional characteristics such as low weed management need and low soil tillage requirements (Bilalis et al., 2017).

Although camelina is a non- legume plant and has high need of N, while compared with other oil plants, camelina is a crop that does not need high inputs (Dobre & Jurcoane, 2011; Gao et al., 2018). According Francis & Warwick (2009) important factors that influence the yield of camelina are sowing density and available nutrients. The application of N fertilizer significantly increases the yield (Solis et al., 2013; WysockI et al., 2013) and plant growth (Dobre et al., 2014). The different fertilization in camelina result in different quality of feed (Henriksen et al., 2009). Additionally, the oil content decreased with the increase of the N rate (Solis et al., 2013). However, there is a great variability in the effect of N fertilization on yields and oil quality depending on climatic and soil conditions. (Malhi et al., 2014). The N rate should not be excessive because it can have negative effects. A negative effect of N fertilization is the reduction of crop productivity (Johnson & Gesch, 2013). Johnson & Gesch (2013) regarding its use as biodiesel. In this aspect fertilization should not exceed 800 kg ha^{-1}. In organic farming, the yield of camelina cultivation was higher with compost addition, followed by inorganic fertilization (Bilalis et al., 2017). In another oil crop such as linseed cultivation, there was a high correlation between oil content and seed yield (Bilalis et al., 2010).

The plant's ability to absorb nutrients is directly related to the development of the root system especially in dry thermal conditions (Sidiras et al., 2001; Anderson et al. 2012). In safflower crop the linoleic acid and fatty acids contents were reduced to dry conditions (Ashrafi & Razmjoo, 2010). Therefore, in order to ensure the quality of the oil, the root system plays a primary role, and with the appropriate agricultural practices it has the highest density and absorbs more nutrients. In corn cultivation the N fertilization increased the length of the root while the weight of the root decreased with the increase of N rate (Durieux et al., 1994). The applied N has positive significant affected the ratio shoot/ root of camelina, even in dry conditions camelina has the root mechanisms to use N (Gao et al., 2018).

While camellia is considered a low-input plant, the exact amount of fertilizer that gives the best yield has not been determined. Also, since the literature shows great variability in yields depending on the climatic conditions of each region, there is a knowledge gap for implementing its cultivation in Greece. The objective of this study was to identify the effect of different nitrogen amounts on the development of the root system, growth of the aboveground part of the plant and seed yield. Our hypothesis is that different levels of nitrogen fertilization, influence the growth of the root system of camelina plants.

MATERIALS AND METHODS

Experimental Design

A camelina greenhouse experiment (*Camelina sativa* L.) was set up in Western Greece, in the region of Agrinio, in March 2019. The cultivated variety was Calena, produced by Saatbau Linz in Austria

The experiment followed a completely randomized design (CRD), with four treatments, different amounts of added nitrogen (control 0 ppm N, 30 ppm N, 60 ppm N and 90 ppm N). The fertilizer applied was potassium nitrate, KNO_3, 13% N and 46% K In the control treatment 0 g KNO_3 (without fertilizer) were added, in the 30 ppm N treatment, 3.655 g KNO_3 were added, in 60 ppm N, 7.311 g KNO_3 and in 90 ppm N, 10.966 g KNO_3. The quantity of K that was changing was not taken into account why K fertilization does not have a direct effect on a small biological life plant cycle and the release of potassium ions often takes place over a long period of time as opposed to nitrates (Thorne, 1954).

A total of 320 pots, 20 pots per treatment and 80 pots per replicate were used. The capacity of the pots was 12 L. They were filled with 8 L of soil and 4 L of compost (natural product of aerobic degradation of See weed *Posidonia oceanica*). Nitrogen content of compost 2%. The soil was clay loam (CL) with pH 6.72, organic matter 2.17%, total nitrogen 0.1125%, N-NO_3 10 ppm and 12 ppm N-NH_4, 18% $CaCO_3$, and a good supply of available phosphorus (P-Olsen 48 ppm) and potassium (335 ppm) The greenhouse conditions remained the same for all pots (temperatures, sunshine and water). Irrigation rate was 8 times of 0.5 L during the camelina life cycle.

So that all plants have the same biological life cycle and the same time point of emergence seedligns were prepared. The growth of seedlings was done in a seedbed with the method of the floating system, where the germination of the seeds as well as the growth of the plants took place. Large water tanks were created, in which the discs were placed. The discs contained plant substrate. The plants remained there until they reached a height of 5 cm. The plants were then transplanted into pots., one plant per pot.

Measurements

The measurements were performed in different days after transplanting (DAT). Root characteristics (root density, root surface and root volume) and plants agronomic characteristics (height, seed yield, leaf area and 1,000 seed weight) were measured.

Regarding the root measurements, the samples were collected in 6 different DAT (20, 40, 60, 80, 100 and 120 DAT) 2 samples per treatment. There were washed over a 5 mm mesh sieve. Also there was used a formalin/acetic acid/alcohol (FAA) staining solution. Root density (cm of root 100 cm^{-3} soil), root surface (cm^2 of root 100 cm^{-3} soil), as well as root volume ($cm^3$of root 100 cm^{-3} soil) were determined in millimeters using a high resolution scanner, using DT-software (Delta-T Scan version 2.04; Delta Devices Ltd, Burwell, Cambridge, UK) (Bilalis et al., 2012).

In terms of plant characteristics, plant height (cm), was measured in 100 DAT. At the end of the experiment, 120 DAT, there were measured the plantseed yield (g), the leaf area (cm^2 $plant^{-1}$) and the 1,000 seed weight (g). The leaf area was determined in 100 DAT, by the use of an automatic leaf area meter (Delta-T Devices Ltd., Burrwell, Cambridge, UK).

Statistical Analysis

The experimental data analysis was conducted using the software Statistica (StatSoft, 1996), according to the completely randomized design. Differences among the means were compared using the Least Significant Difference (LSD) test, at the *5%* level of significance ($P \leq 0.05$). correlation The tests of correlation coefficients and linear regression by Statistica software were set at two levels with significance ($\alpha = 0.05$) and remarkable significance ($\alpha = 0.01$).

RESULTS

In Fig. 1, the changes in the root density are presented. The nitrogen treatments had statistically significant difference between them, from 40 to 120 DAT. At 20 DAT no treatment was statistically significant. The 0 ppm treatment had the lowest value of root density, in all measurements from the 20 DAT to 120 DAT and the 90 ppm had the highest value from the first measurement to the last (Fig. 1). At 80 DAT, at the 0 ppm treatment, the root density was 32.82 cm of root 100 cm^{-3}, in the 30 ppm was 39.77 cm of root 100 cm^{-3}, in the 60 ppm was 45.82 cm of root 100 cm^{-3} and in the 90 ppm was 51.58 cm of root 100 cm^{-3}. At 100 DAT the highest value was recorded, which was 52.54 cm of root 100 cm^{-3} soil in the 90 ppm and the lowest was 12.85 cm of root 100 cm^{-3} in the 0 ppm treatment at 40 DAT. Up to 100 DAT there was an increase in root density, but at 120 DAT there was a small decrease in all treatments (Fig. 1).

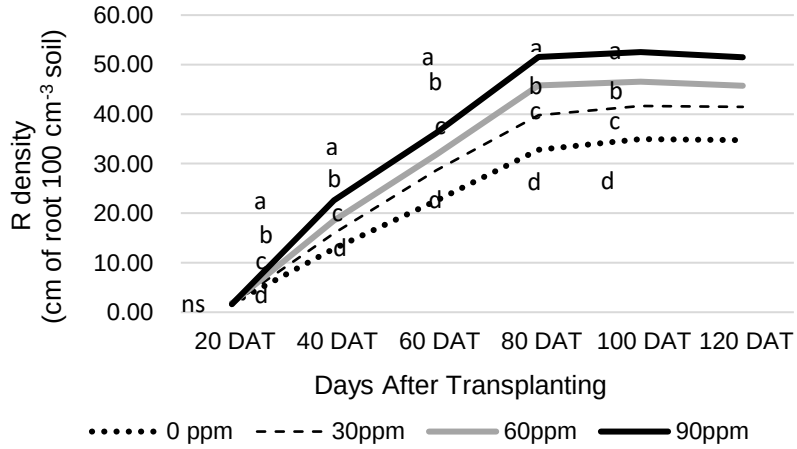

Figure 1. Changes in root density (affected by different nitrogen levels) in different Days After Transplanting (DAT) (‘*ns’: not statistically significant at P = 0.05).*

Moreover, in Fig. 2, at 20 DAT none treatment were statistically significant, concerning the root surface. From 40 DAT to 120 DAT, all treatment had statistically significant difference between them. At 120 DAT there was a declining trend at all levels of nitrogen. The 0 ppm had the lowest values in all Days After Transplanting. On the other hand, the 90 ppm had the highest values in all Days After Transplanting.

The values ranged from 6.85 to 27.59 cm^2 of root 100 cm^{-3} soil. The highest value was 27.59 cm^2 of root 100 cm^{-3} soil at 100 DAT, in the 90 ppm and the lowest was 6.85 cm^2 of root 100 cm^{-3} soil at 40 DAT, in the 0ppm (Fig. 2). Also, in the root surface and in the root density the same path is presented in the different DAT, increasing trend from 20 DAT to 100 DAT and in 120 DAT there is a decrease in all treatments.

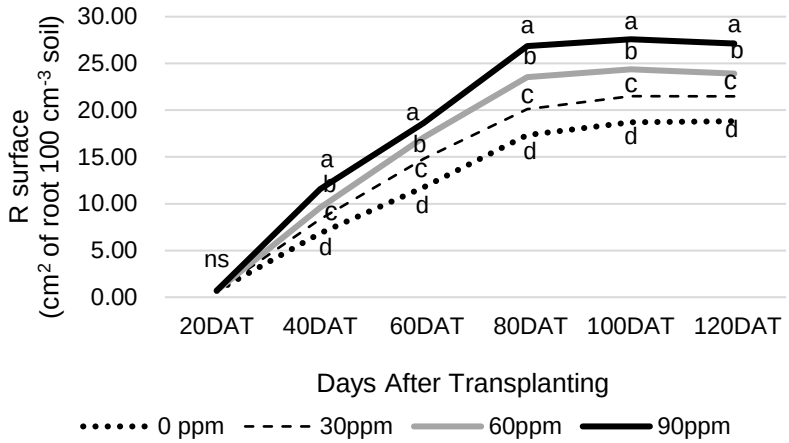

Figure 2. Changes in root surface (affected by different nitrogen levels) in different Days After Transplanting (DAT) (*'ns': not statistically significant at P = 0.05*).

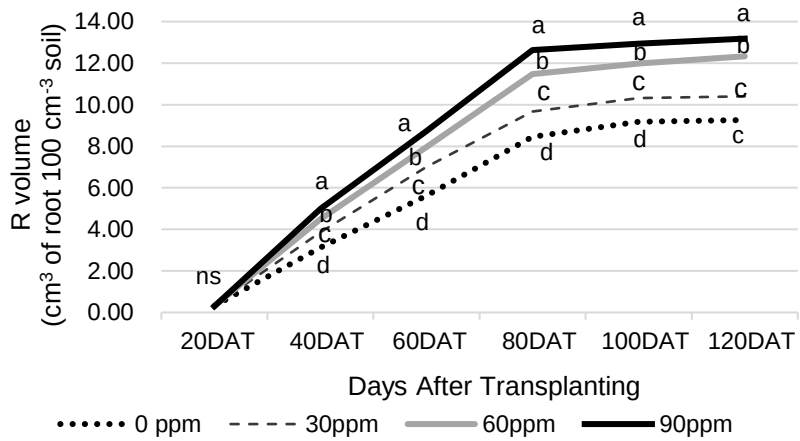

Figure 3. Changes in root volume (affected by different nitrogen levels) in different Days After Transplanting (DAT) (*'ns': not statistically significant at P = 0.05*).

Furthermore, in root volume changes, which are shown in the Fig. 3, at 20 DAT no treatment was statistically significant. From the 40 DAT to 100 DAT all nitrogen levels had statistically significant difference between them. At 120 DAT the 60 ppm had not statistically significant differences with the 90 ppm. The lowest value was 3.12 cm^3 of root 100 cm^{-3} soil in the 0 ppm and the highest was 13.18 cm^3 of root 100 cm^{-3} soil in the 90 ppm at 120 DAT. Compared to the other measurements of the root system, the

growth trend continues up to 120 DAT. The largest increase was observed from 40 DAT to 80 DAT (Fig. 3). At 40 DAT the values were, in 0 ppm 3.12 m^3 of root 100 cm^{-3} soil, in 30 ppm 3.86 m^3 of root 100 cm^{-3} soil, in 60 ppm 4.50 m^3 of root 100 cm^{-3} soil and in 90 ppm 4.99 m^3 of root 100 cm^{-3} soil. At 80 DAT the values were, in 0 ppm 8.45 m^3 of root 100 cm^{-3} soil, in 30 ppm 9.67 m^3 of root 100 cm^{-3} soil, in 60 ppm 11.47 m^3 of root 100 cm^{-3} soil and in the 90 ppm 12.63 m^3 of root 100 cm^{-3} soil (Fig. 3).

Also, in the plant height the values ranged from 57 to 72.75 cm. All treatments had statistically significant differences between them. The highest value was 72.75 cm in the 90 ppm and the lowest was 57 in the 0 ppm (Table 1). In the leaf area, the 30 ppm had not statistically significant differences with the 0 ppm and with the 60 ppm. The lowest value was 1.41 cm^2 $plant^{-1}$ in the 0 ppm and the highest was 2.26 cm^2 $plant^{-1}$ in the 90 ppm. Moreover, the yield per plant of the 30 ppm had not statistically significant differences to the 60 ppm and to the 90 ppm. The highest value was 292.25 g per plant in the 90 ppm and the lowest was 169.50 g per plant in the 0 ppm (Table 1). In the 1,000 seed weight measurement, all treatments had statistically significant differences between them. The values ranged from 1.29 to 1.66 g. The lowest value was 1.29 g in the 0 ppm and the highest was 1.66 g in the 90 ppm.

Table 1. The agronomic characteristics as affected by different nitrogen levels

	Plant height (cm)	Leaf area (cm^2 $plant^{-1}$)	Yield (g $plant^{-1}$)	1,000 seed weight (g)
0 ppm	57.00^{a}	1.41^{a}	169.50^{a}	1.29^{a}
30 ppm	63.00^{b}	1.92^{ab}	208.75^{b}	1.36^{b}
60 ppm	66.50^{c}	2.12^{b}	231.00^{bc}	1.48^{c}
90 ppm	72.75^{d}	2.26^{c}	292.25^{c}	1.66^{d}
F_{ppm}	74.16^{***}	25.25^{***}	66.57^{***}	141.75^{***}

*F-test ratios are from ANOVA. Different letters within a column indicate significant differences according to LSD (P = 0.05). Significance levels: * P < 0.05; ** P < 0.01; *** P < 0.001; ns, not significant (p > 0.05).*

DISCUSSION

It is known that the development of the root system is affected by the availability of nutrients (Drew, 1975). According to Pavlista et al. (2012), who studied camelina and two other crops, the fertilization as well as irrigation are critical factors for the first six weeks of root growth. This is also shown in the figures above, as there was an almost linear increase in all root characteristics during the first 40 DAT (Fig. 1, Fig. 2, and Fig. 3). In addition, there was positive correlation between the roots with the agronomic characteristics (Table 2). More specifically, the root density was positively correlated with the plant height, the yield, the leaf area and with the 1,000 seed weight ($r = 0.94$, $P < 0.001$; $r = 0.90$, $P < 0.001$; $r = 0.91$, $P < 0.001$ *and* $r = 0.92$, $P < 0.001$ respectively), (Table 2). In several studies was reported that higher plant growth and yield were related with root system characteristics (Vamerali et al., 2000; Den Herder et al., 2010).

Moreover, there was positive correlation between the root characteristic. Thus root density was positively correlated with root surface ($r = 0.98$, $P < 0.001$) and with root volume ($r = 0.94$, $P < 0.001$), while root volume was positively correlated with the root surface ($r = 0.94$, $P < 0.001$) (Table 2). The different amounts of N application significantly affected the development of roots, in accordance with several studies who

observed that the variation in nitrogen supply leads to differences in root development (Tausz et al., 2017).

Table 2. Correlation matrix between root and agronomic characteristics

	Root density 120 DAT	Root surface 120 DAT	Root volume 120 DAT	Plant Height	Yield	Leaf area per plant	1,000 seed weigh
Root density 120 DAT	1	0.98***	0.94***	0.95***	0.90***	0.91***	0.92***
Root density 120 DAT	0.98***	1	0.94***	0.93***	0.87***	0.94***	0.95***
Root density 120 DAT	0.94***	0.94***	1	0.89***	0.86***	0.85***	0.88***
Plant height	0.95***	0.93***	0.89***	1	0.89***	0.80***	0.90***
Yield	0.90***	0.87***	0.86***	0.89***	1	0.77***	0.85**
Leaf area per plant	0.91***	0.94***	0.85***	0.80***	0.77***	1	0.92***
1,000 seed weight	0.92***	0.95***	0.88***	0.90***	0.85***	0.92***	1

Significance levels: * $P < 0.05$; ** $P < 0.01$; *** $P < 0.001$; ns, not significant ($P > 0.05$).

Urbaniak et al. (2007), reported that the plant height of the camelina increased as the applied dose of nitrogen fertilizer increased. Similar results were obtained in our study where the highest plant height was recorded in the higher amounts of nitrogen. Furthermore, Johnson & Gesch (2013) presented in their study that different nitrogen levels had no effect on the photosynthetic capacity of the leaves. On the other hand, Field & Mooney (1986); Pan et al. (2011) emphasized that as nitrogen levels increased, resulted in greater leaf area, leaf N, as well as increased leaves photosynthetic capacity. Also, Karydogianni et al. (2020) reported that the effect of nitrogen on canopy photosynthesis was due to the effect of nitrogen on the production of the leaf area as well as on light interception. In our study, the leaf area increased as the applied dose of nitrogen increased.

In addition, the yield per plant increased with increased rate of nitrogen fertilizer. Czarnik et al. (2017), reported that increasing nitrogen fertilization significantly increases the number of silicles per plant, as well as the number of seeds per silicles. Henriksen et al. (2009), said that the camelina showed an increase in yield at 40 kg N ha^{-1} compared to the control. Czarnik et al. (2017), demonstrated that the 1,000 seeds weight increased significantly as the nitrogen applied to the fertilizer increased. Similar results were presented in our study, where at 90 ppm the largest weight of 1,000 seeds was recorded. The yield per plant had a positive correlation with the plant height ($r = 0.89$, $P < 0.001$) as well as with the weight of 1,000 seeds ($r = 0.85$, $P < 0.001$), (Table 2).

CONCLUSION

In conclusion, the different levels of nitrogen fertilization, influenced the growth of the root system, as well as the agronomic characteristics of the camelina plant. More specifically, at the level of 90 ppm nitrogen, the highest growth rates were recorded for

the characteristics of the root such as root density, as well as in the agronomic characteristics such as the yield per plant. Also in the measurements of the root system at 100 DAT the maximum growth was presented.

REFERENCES

Anderson, H.M., Barlow, P.W., Clarkson, D.T., Jackson, M.B. & Shewry, P.R. 2012. In *Plant Roots-From Cells to Systems: Proceedings of the 14th Long Ashton International Symposium Plant Roots, From Cells to Systems*, (Eds.) Springer Science & Business Media held in Bristol, UK, **73**, 13–15.

Angelopoulou, F., Tsiplakou, E. & Bilalis, D. 2019. Impact of Compost Application on Fall-seeded Camelina Yield and Seed Quality. *Bulletin of University of Agricultural Sciences and Veterinary Medicine Cluj-Napoca Horticulture* **76**(2), 151–153. doi:10.15835/buasvmcn-hort: 2019.0028

Ashrafi, E. & Razmjoo, K. 2010. Effect of irrigation regimes on oil content and composition of safflower (*Carthamustinctorius* L.) cultivars. *Journal of the American Oil Chemists' Society* **87**(5), 499–506.

Bilalis, D.J., Karkanis, A., Papastylianou, P., Patsiali, S., Athanasopoulou, M., Barla, G. & Kakabouki, I. 2010. Response of Organic Linseed ('Linumusitatissimum'L.) to the Combination of Tillage Systems, (Minimum, Conventional and No-Tillage) and Fertilization Practices: Seed and Oil Yield Production. *Australian Journal of Crop Science* **4**(9), 700.

Bilalis, D., Katsenios, N., Efthimiadou, A., Efthimiadis, P. & Karkanis, A. 2012. Pulsed electromagnetic fields effect in oregano rooting and vegetative propagation: A potential new organic method. *Acta Agriculturae Scandinavica, Section B - Soil & Plant Science* **62**(1), 94–99. doi:10.1080/09064710.2011.570374

Bilalis, D., Roussis, I., Fuentes, F., Kakabouki, I. & Travlos, I. 2017. Organic agriculture and innovative crops under Mediterranean conditions. *Notulae Botanicae Horti Agrobotanici Cluj-Napoca* **45**(2), 323–331.

Czarnik, M., Jarecki, W. & Bobrecka-Jamro, D. 2017. The effects of varied plant density and nitrogen fertilization on quantity and quality yield of *Camelina sativa* L. *Emirates Journal of Food and Agriculture* **29**(12), 988–993. doi:10.9755/ejfa.2017.v29.i12.1569

Den Herder, G.D., Van Isterdael, G., Beeckman, T. & De Smet, I. 2010. The roots of a new green revolution. *Trends Plant Science* **15**(11), 600–607.

Dobre, P. & Jurcoane, S. 2011. Camelina crop opportunities for a sustainable agriculture. *Scientific Papers-Series A, Agronomy* **54**, 420–424.

Dobre, P., Jurcoane, S., Cristea, S., Matei, F., Moraru, A.C. & Dincă, L. 2014. Influence of N, P chemical fertilizers, row distance and seeding rate on camelina crop. *AgroLife Scientific Journal* **3**(1), 49–53. ISSN 2285-5718

Drew, M.C. 1975. Comparison of the effects of a localised supply of phosphate, nitrate, ammonium and potassium on the growth of the seminal root system, and the shoot, in barley. *New Phytologist* **75**(3), 479–490. doi:10.1111/j.1469-8137.1975.tb01409.x

Durieux, R.P., Kamprath, E.J., Jackson, W.A. & Moll, R.H. 1994. Root distribution of corn: the effect of nitrogen fertilization. *Agronomy journal* **86**(6), 958–962.

Field, C. & Mooney, H.A. 1986. The photosynthesis-nitrogen relationship in wild plants. In: Givnish, T.J. (ed.): *On the Economy of Plant Form and Function*. Cambridge Univ. Press, Cambridge–London–New York–New Rochelle–Melbourne–Sydney, 25–55.

Francis, A. & Warwick, S.I. 2009. The biology of Canadian weeds. 142. *Camelina alyssum* (Mill.) Thell. *C.; microcarpa* Andrz. ex DC.; *C. sativa* (L.) Crantz. *Canadian Journal of Plant Science* **89**(4), 791–810.

Gao, L., Caldwell, C. D. & Jiang, Y. 2018. Photosynthesis and growth of camelina and canola in response to water deficit and applied nitrogen. *Crop Science* **58**(1), 393–401.

Henriksen, B.I.F., Lundon, R.A., Prestløkken, E, Abrahamsen, U. & Eltun, R. 2009. Nutrient supply for organic oilseed crops, and quality of potential organic protein feed for ruminants and poultry. *Agronomy Research* **7**(Special issue II), 592–598.

Johnson, F.M.J. & Gesch, W.R. 2013. Calendula and camelina response to nitrogen fertility. Ind. *Crops and Products* **43**, 684–691

Karydogianni, S., Darawsheh, M.K., Kakabouki, I., Zisi, Ch., Folina, A.E., Roussis, I., Tselia, Z. & Bilalis, D. 2020. Effect of nitrogen fertilizations, with and without inhibitors, on cotton growth and fiber quality. *Agronomy Research* **18**(2), 432–449. doi: 10.15159/AR.20.148

Malhi, S.S., Johnson, E.N., Hall, L.M., May, W.E., Phelps, S. & Nybo, B. 2014. Effect of nitrogen fertilizer application on seed yield, N uptake, and seed quality of *Camelina sativa*. *Canadian Journal of Plant Science* **94**(1), 35–47.

Obour, A.K., Sintim, H.Y., Obeng, E. & Zheljazkov, V.D.J. 2015. Oilseed camelina *Camelina sativa* L. Crantz production systems prospects and challenges in the USA great plains. *Advances in Plants & Agriculture Research* **2**(2).

Pan, X., Lada, R., Caldwell, D.C. & Falk, C.K. 2011. Photosynthetic and growth responses of *Camelina sativa* (L.) Crantz to varying nitrogen and soil water status. *Photosynthetica* **49**(2), 316–320. doi: 10.1007/s11099-011-0035-x

Pavlista, A.D., Baltensperger, D.D., Isbell, T.A. & Hergert, G.W. 2012. Comparative growth of spring-planted canola, brown mustard and camelina. *Industrial Crops and Products* **36**(1), 9–13. doi:10.1016/j.indcrop.2011.07.020

Shonnard, D.R., Williams, L. & Kalnes, T.N. 2010. Camelina-derived jet fuel and diesel: Sustainable advanced biofuels. *Environmental Progress & Sustainable Energy* **29**(3), 382–392.

Sidiras, N., Bilalis, D. & Vavoulidou, E. 2001. Effects of tillage and fertilization on some selected physical properties of soil (0–30 cm depth) and on the root growth dynamic of winter barley *(Hordeum vulgare* cv. Niki*). Journal of Agronomy and Crop Science* **187**(3), 167–176.

Solis, A., Vidal, I., Paulino, L., Johnson, B.L. & Berti, M.T. 2013. Camelina seed yield response to nitrogen, sulfur, and phosphorus fertilizer in South Central Chile. *Industrial Crops and Products* **44**, 132–138.

Tausz, M., Bilela, S., Bahrami, H., Armstrong, R., Fitzgerald, G., O'leary, G. & Rennenberg, H. 2017. Nitrogen nutrition and aspects of root growth and function of two wheat cultivars under elevated [CO_2]. *Environmental and Experimental Botany* **140**, 1–7. doi: 10.1016/j.envexpbot.2017.05.010

Thorne, G.N. 1954. Absorption of nitrogen, phosphorus, and potassium from nutrient sprays by leaves. *Journal of Experimental Botany* **5**(1), 37–48.

Toncea, I., Necseriu, D., Prisecaru, T., Balint, L.N., Ghilvacs, I. & Popa, M. 2013. The seed's and oil composition of Camelia-first romanian cultivar of camelina (*Camelina sativa*, L. Crantz). *Romanian Biotechnological Letters* **18**(5), 8594–8602.

Urbaniak, D.S., Caldwell, D.C., Zheljazkov, D.V., Lada, R. & Luan, L. 2007. The effect of cultivar and applied nitrogen on the performance of Camelina sativa L. in the Maritime Provinces of Canada. *Canadian Journal of Plant Science* **88**(1), 111–119. doi: 10.4141/CJPS07115

Vamerali, T., Bona, S., Mosca, G. & Sambo, P. 2000. Is the root system the key to higher nitrogen uptake in rapeseed? In *The Supporting Roots of Trees and Woody Plants: Form, Function and Physiology* Stokes, A. (Ed.). doi: 10.1007/978-94-017-3469-1

Wysocki, D.J., Chastain, T.G., Schillinger, W.F., Guy, S.O. & Karow, R.S. 2013. Camelina: seed yield response to applied nitrogen and sulfur. *Field Crops Research* **145**, 60–66.

Agronomy Research **18**(3), 2069–2075, 2020
https://doi.org/10.15159/AR.20.190

Electric infrared heating panels as an alternative source of heating for greenhouses

P. Kic

Czech University of Life Sciences Prague, Faculty of Engineering, Department of Technological Equipment of Buildings, Kamycka 129, CZ165 21 Praha 6, Czech Republic
Correspondence: kic@tf.czu.cz

Abstract. The aim of this article is to show the possibilities of supplementary heating of greenhouses. There was used for this research an electric infrared heating panel ITA 700. The average total power was 630.8 W in laboratory measurements, of which 504.3 W has been transferred by the front part of the panel, of which 267.2 W has been transmitted by radiation. The total radiation efficiency of the front part was 42.4%. Similar measurements have been carried out in an experimental greenhouse (length 24 m, width 3.5 m). Approximately 448 W of average total power 603.7 W has been transferred by the front part of the panel, of which 159 W has been transferred by radiation. The total radiation efficiency of the front part was 26.3%. Differences between measured surface temperatures confirmed the influence of panel radiation on the flower bed. The average temperature in the soil (9 °C) shows that the influence of heating is mainly on the surface of the flower bed, where it could protect cultivated plants during the lowest temperature period. The obtained results can be useful for choosing suitable panel parameters for the placement in small horticultural or hobby greenhouse.

Key words: convection, heat transfer, low temperature, measurement, radiation, soil.

INTRODUCTION

The aim of this article is to show the possibilities of supplementary heating of greenhouses. Construction, calculation and design of heating systems in large scale greenhouses are well described and studied in special publications e.g. Has, 2004; Pokluda & Kobza, 2011. The heating systems (hot water, electricity or gas) recommended for large scale greenhouses are usually very sophisticated, but very expensive and they are supposed to be used permanently during the long period e.g. in the Czech Republic (autumn, winter and spring). Considerable attention is paid to the construction of greenhouses in terms of the use of progressive techniques (Avotins et al., 2018; Hart & Hartova, 2018).

There are also used some simple constructions of greenhouses (mostly made from plastics) used in many parts of the world. Constructions of these greenhouses are well described in (Cermeno, 2002). There is no supposed heating. Small greenhouses, which are used for growing seedlings, vegetables, flowers and other plants in the cold season unsuitable for growing in free garden, are usually without heating. These greenhouses, unlike large commercial greenhouses, are not equipped with a conventional overhead or

underground heating system. A drop of outdoor air temperature and insufficient solar radiation e.g. in night, can cause plant destruction (spring frosts). That is the reason why some scientific publications are focused on this issue. E.g. (Anifantis et al., 2017) carried out an assessment of thermal energy with the use of small scale photovoltaic, hydrogen and geothermal stand-alone system for greenhouse heating.

The influence of heating systems on greenhouse microclimate for low-cost, plastic covered greenhouses is studied in (Tadj et al., 2014) as it greatly influences crop growth and development. It is focused on heating pipes and air heater. In conclusion, it is stated that precise evaluation of the behaviour of heating equipment in a greenhouse is necessary.

One of solutions for heating in the critical period is the use of electric infrared heating panels. Infrared emitters have considerable applications in many sectors (Bulgakov et al., 2014). Unlike conventional convection heating panels, which first heat the air and thus a lot of energy escapes (heat losses) through the surrounding walls, the electric infrared heating panels transfer part of energy from their surface in the form of radiation, i.e. directly on the plants and soil. This makes more efficient use of input power. The research work focused on the theory and construction of the electric heating panel is described in Greppi & Fabbri (2017). Unlike electric heating cables, which must be in the soil, these panels are easy to install.

This research is focused on the verification of the function of electrical infrared low-temperature panels in laboratory conditions and in an experimental greenhouse. The energy transfer and influence on the soil surface has been studied in real conditions.

MATERIALS AND METHODS

There was used for this research an electric infrared heating panel ITA 700 with rated power 680 to 730 W, which is recommended to install on the wall or ceiling. The front part of the panel which is the principal source of heat transmission has surface area $S_F = 0.75$ m^2 and the back part together with side parts ($S_O = 0.85$ m^2) are insulated and covered with the aim to reduce the heat transfer through these parts. The panel was set at an angle of 75° to the floor during the measurements.

This paper includes the results of two types of experiments. There were carried out laboratory experiments inside the Faculty of Engineering, which enabled to install heating panel and all instruments together for long distance measurement on the floor. The aim was to find out properties of heating panel in protected laboratory conditions with average indoor temperature about 22 °C and relative humidity approximately 26%.

Similar measurements have been carried out in an experimental greenhouse (length 24 m, width 3.5 m and height 2.22 m) at outside air temperature about -2 °C, relative humidity approximately 65% and a solar radiation 520 W m^{-2}. This greenhouse is not equipped with any heating system.

Instrumentation

Air temperatures and relative humidity were measured by data loggers ZTH65 with registration at 1- minute intervals. Parameters of ZTH65 are: temperature operative range –30 to +70 °C with accuracy ± 0.4 °C and operative range of relative humidity 5–95% with accuracy ± 2.5%.

The surface temperatures of tested infrared heating panel were measured by special surface infra sensor FIA 260-MV with temperature operative range -18 to 260 °C with accuracy ± 0.1 K. The surface temperatures in some specific places were measured by special surface sensor S 106 9R (NiCr-Ni, with adapter G017R) connected to the instrument THERM 2253-2 (Ahlborn GmbH, Germany) for contact temperature measurement. This instrument was used also with sensor for air temperature measurement AMR TK 127 10R. This instrument and sensors can be used in operative range from –100 to 1,370 °C, with display resolution 0.1 °C and with accuracy ± 1% from the measured value.

There were installed during the measurements surface thermocouples NiCr-Ni (type K) in operative range from –50 to +200 °C, with display resolution 0.1 °C and with accuracy ± 1% from the measured value.

Temperatures of the soil in the greenhouse were measured by the thermocouples NiCr-Ni (type K) in operative range from –25 to +400 °C, with display resolution 0.1 °C and with accuracy ± 1% from the measured value, completed by the compensation line NiCr-Ni in operative range from –10 to +105 °C in the length installed according to the needs of measurements.

The heat flux density on the rear part of the panel was measured by special heat flux sensor FQA018C (Ahlborn GmbH, Germany) which has dimensions 120×120×1.5 mm. It is made from epoxy resin with the resistance to 80 °C and calibration constant 9.69 W m^{-2} mV^{-1} and relative measurement uncertainty 5%.

Temperature and humidity of surrounding air has been measured by sensor FHA 646–21 including temperature sensor NTC type N with operative range from –30 to +100 °C with accuracy ±0.1 °C, and air humidity by capacitive sensor with operative range from 5 to 98% with accuracy ±2%. All measured data were stored at 1-minute intervals to measuring instruments ALMEMO 2590-9 and ALMEMO 2690.

The measurement results were processed by Excel software and some of results were verified by statistical software Statistica 12 (*ANOVA* and *TUKEY HSD Test*).

Theory and modelling

To evaluate the function and efficiency of the panel, it is necessary to assess its energy balance (Eq. 1), expressing the total power consumption of panel P:

$$P = P_C + P_R \tag{1}$$

where P – total power consumption (W); P_C – power (heat) transmitted by convection (W); P_R – power (heat) transmitted by radiation (W).

Radiation heat transfer follows Newton-Richman law, Eq. (2). Basic principles and equations are described in many publications focusing on heat transfer, e.g. Sazima et al., 1989; Szekyova et al., 2006, which creates a theoretical background described in the next part of this article.

$$P_C = \alpha \cdot S \cdot \Delta t \tag{2}$$

where α – heat transfer coefficient (W m^{-2} K^{-1}); S – convective heat-transmitting surface (m^2); Δt – temperature difference between the panel surface and ambient air (K).

The heat transfer coefficient α depends on the Nusselt criterion *Nu* according to Eq. (3):

$$\alpha = \frac{Nu \cdot \lambda}{L} \tag{3}$$

where *Nu* – Nusselt number; λ – coefficient of thermal conductivity of air (W m^{-1} K^{-1}); *L* – characteristic dimension (height) of the panel (m).

For the vertical or inclined planar surface of the panel, *Nu* is determined by Eq. (4) depending on the Rayleigh's criterion *Ry*.

$$Nu = C \cdot Ry^n \tag{4}$$

where *C* – constant which depends on *Ry*; *Ry* – Rayleigh's criterion; n – exponent which depends on *Ry*.

The Rayleigh's criterion *Ry* is determined according to Eq. (5):

$$Ry = \frac{g \cdot \beta \cdot \Delta t \cdot L^3}{\nu \cdot a} \tag{5}$$

where g – gravitational acceleration (m s^{-2}); β – expansion coefficient (K^{-1}); ν – kinematic viscosity of air (m^2 s^{-1}); a – coefficient of thermal diffusivity of the air (m^2 s^{-1}).

The expansion coefficient β is expressed by Eq. (6):

$$\beta = t_m^{-1} \tag{6}$$

where t_m – characteristic temperature (K).

$$t_m = \frac{1}{2}\,(t_P - t_a) \tag{7}$$

where t_P – surface temperature (°C); t_a – air temperature (°C).

The total power transmitted by the panel can be divided into power P_F transferred by the front part of the panel and power P_O transferred by the other parts (back and side).

$$P = P_F + P_O \tag{8}$$

where P_F – power transferred by the front part of the panel (W); P_O – power transferred by the other parts of the panel (W).

The power transfer efficiency η_F of the front part of the panel is calculated according to Eq. (9):

$$\eta_F = \frac{P_F}{P} \cdot 100 \tag{9}$$

where η_F – power transfer efficiency of the front part of the panel (%).

The efficiency of power transfer by radiation of the front part η_{FR} is calculated according to Eq. (10):

$$\eta_{FR} = \frac{P_{FR}}{P} \cdot 100 \tag{10}$$

where η_{FR} – power transfer efficiency by radiation of the front part of the panel (%); P_{FR} – power transferred by radiation of the front part of the panel (W).

RESULTS AND DISCUSSION

Main parameters measured in laboratory and greenhouse experiments are given in Tables 1,2 and 3. The data are the mean values ± SD (standard deviation). Total power consumption P was lower than was the nominal information. As results of the surface insulation of back and side parts of the heating panel ($S_O = 0.85$ m^2) the power transferred through these parts $P_O = 126.5$ W is not too big and the power transfer efficiency of the front part ($S_F = 0.75$ m^2) of the panel is rather high, in the laboratory $\eta_F = 80\%$, in the greenhouse $P_O = 155.7$ W and $\eta_F = 74.2\%$.

Table 1. Results of power (W) and power transfer efficiency (%) (average and standard deviation) measured and calculated in the laboratory and experimental greenhouse

Experiments in	$P \pm$ SD	$P_O \pm$ SD	$P_F \pm$ SD	$\eta_F \pm$ SD
Laboratory	630.8 ± 1	126.5 ± 42.6	504.3 ± 42	80.0 ± 6.7
Greenhouse	603.7 ± 6	155.7 ± 20.5	448.0 ± 23.7	74.2 ± 3.4

SD – standard deviation.

Table 2 presents main results calculated for the power convection of the front part of the radiant heating panel. Final results of power calculation of the front part of the radiant heating panel in the laboratory and greenhouse experiments are presented in Table 3.

Table 2. Results of Nusselt criterion Nu, Rayleigh criterion Ry and heat transfer coefficient α (average and standard deviation) of the front part of the radiant heating panel calculated in the laboratory and greenhouse experiments

Experiments in	$Ry \pm$ SD	$Nu \pm$ SD	$\alpha \pm$ SD
Laboratory	$7.83\times10^9 \pm 2.7\times10^9$	256.5 ± 45.1	5.57 ± 1
Greenhouse	$9.27\times10^9 \pm 1.1\times10^9$	278.1 ± 18.6	6.04 ± 0.4

SD – standard deviation.

The average total power consumption was 630.8 W in laboratory measurements, of which 20% has been transferred by the rear part of the panel and the remaining 504.3 W has been transferred by the front part of the panel. It has been transmitted 237.1 W by convection to the ambient air and 267.2 W by radiation mainly to the floor.

Similar measurements carried out in an experimental greenhouse show that approximately 25.8% of average total power 603.7 W has been transferred by rear and side panel parts, and remaining 448 W has been transferred by the front part of the panel. It has been transferred by convection 289 W to ambient air and 159 W by radiation mainly to the soil surface.

Table 3. Results of power and power transfer efficiency (average and standard deviation) of the front part of the radiant heating panel calculated in laboratory and greenhouse experiments

Experiments in	$P_{FC} \pm$ SD	$P_{FR} \pm$ SD	$\eta_{FR} \pm$ SD
Laboratory	237.1 ± 94.3	267.2 ± 135.9	42.4 ± 21.6
Greenhouse	289 ± 42.5	159 ± 59.7	26.3 ± 9.7

SD – standard deviation.

The efficiency of power transfer by radiation of the front panel part are rather different (in the laboratory η_F = 42.4% and η_F = 26.3% in the greenhouse). It can be explained by bigger heat transfer coefficient α and higher percentage of the heat transferred by the convection in greenhouse.

Table 4 presents measured surface temperatures in 2 m, 4 m and 6 m distance from the installed heating panel in the laboratory as well as in the greenhouse experiment. The statistically significant differences between these temperatures are caused by increased distance from the panel.

Table 4. Results measurements of soil temperature at 5 cm deep in flower bed of greenhouse and surface temperatures 2 m, 4 m and 6 m distance from heating panel (average and standard deviation) measured in the laboratory and greenhouse experiments. Different letters (*a, b, c*) in the superscript are the sign of high significant difference (*ANOVA; Tukey HSD Test; P≤ 0.05*) between the surface temperatures of floor (laboratory) or soil surface in the greenhouse

Experiments in	t_{soil} ± SD	t_{s2} ± SD	t_{s4} ± SD	t_{s6} ± SD
Laboratory	-	23.0 ± 0.3^a	22.5 ± 0.1^b	22.3 ± 0.1^c
Greenhouse	8.9 ± 0.6	30.3 ± 4.6^a	28.1 ± 5.3^b	26.3 ± 3.6^c

SD – standard deviation.

The surface temperature of the floor in the laboratory measured at a distance of 2 m from the panel was 23.0 °C, at 4 m about 22.5 °C and at 6 m about 22.3 °C. The surface temperature of the soil in the greenhouse measured at a distance of 2 m from the panel was 30.3 °C, at 4 m about 28.1 °C and at 6 m about 26.3 °C. Higher surface temperatures in greenhouses than in the laboratory are caused by the influence of solar radiation (520 W m^{-2}) and greenhouse effect. The average soil temperature at 5 cm deep was 9 ºC.

CONCLUSIONS

The measurement results show the possibility of using a radiant low-temperature electric panel as a possible source of greenhouse heating, but the total output power was lower than nominal.

The total radiation efficiency of the panel front part was approximately 42.4% during the laboratory experiments. In similar measurements carried out in an experimental greenhouse total radiation efficiency of the panel front part was about 26.3%.

The energy transferred through the rear and side panels and the energy transferred by convection of the front panel part are also brought to the greenhouse and used to heat the indoor air. So, it has also positive impact on the indoor greenhouse conditions.

Differences between surface temperatures confirm the influence of panel radiation on the flower bed. The average temperature in the soil shows that the influence of heating is mainly on the surface of the flower bed, there it could protect cultivated plants, leaves and flowers during the lowest temperature period.

The obtained results can be useful for choosing suitable panel dimensions and parameters for the placement in small horticultural or hobby greenhouse. The future research could be focused on the long-time experiments and application in special greenhouses.

ACKNOWLEDGEMENTS. The author wishes to express his thanks to the employees of the CULS Prague Garden Centre, who made it possible to perform measurements in an experimental greenhouse.

REFERENCES

Anifantis, A.S., Colantoni, A. & Pascuzzi, S. 2017. Thermal energy assessment of a small scale photovoltaic, hydrogen and geothermal stand-alone system for greenhouse heating. *Renewable Energy* **103**, 115–127.

Avotins, A., Potapovs, A., Apse-Apsitis, P. & Gruduls, J. 2018. Crop weight measurement sensor for IoT based industrial greenhouse systems. *Agronomy Research* **16**, 952–957.

Bulgakov, V., Bandura, V., Arak, M. & Olt, J. 2018. Intensification of rapeseed drying process through the use of infrared emitters. *Agronomy Research* **16**, 349–356.

Cermeno, Z.S. 2002. *Construction of greenhouses.* Ediciones Mundi-Prensa, Madrid, Barcelona, Mexico, 499 pp. (in Spanish).

Greppi, M. & Fabbri, G. 2017. Thermal characterization of radiative and convective heating devices. *Energy Procedia* **126**, 74–81.

Hart, J. & Hartova, V. 2018. Development of new elements to automatized greenhouses. *Agronomy Research* **16**, 717–722.

Has, S. 2004. *Greenhouses, characteristics and equipment*. UZPI, Praha, 56 pp. (in Czech).

Pokluda, R. & Kobza, F. 2011. *Greenhouses, plastic greenhouses, utilization and growing technologies.* Profi Press s.r.o., Praha, 253 pp. (in Czech).

Sazima, M., Kmonicek, V., Schneller, J., Ambroz, J., Bayer, Z., Cerny, V., Hlavacka, V., Pikman, M., Streda, I. & Sifner, O. 1989. *Heat.* SNTL, Praha, 588 pp. (in Czech).

Szekyova, M., Ferstl, K. & Novy, R. 2006. *Ventilation and air-conditioning.* JAGA, Bratislava, 359 pp. (in Czech).

Tadj, N., Bartzanas, T., Fidaros, D., Draoui, B. & Kittas, C. 2010. Influence of heating system on greenhouse microclimate distribution. *Transactions of the ASABE* **53**(1), 225–238.

Agronomy Research **18**(3), 2076–2086, 2020
https://doi.org/10.15159/AR.20.185

A comparative study of the properties of industrially produced humic substances

M. Klavins[1,*], K. Upska[1,2], A. Viksna[2], M. Bertins[2], L. Ansone-Bertina[1] and J. Krumins[1]

[1]University of Latvia, Department of Environmental Science, 19 Raina Blvd, LV-1586 Riga, Latvia
[2]University of Latvia, Department of Analytical Chemistry, 19 Raina Blvd, LV-1586 Riga, Latvia
[*]Correspondence: maris.klavins@lu.lv

Abstract. Humic substances (HSs) are produced industrially in large quantities from low rank coal, weathered coal, peat, also from soils, composts and other sources. Considering that the applications of industrially produced HSs also include food, pharmaceutical applications and environmental technologies, it is important to evaluate their composition and quality and to identify their sources. The aim of the present study is to compare the properties of industrially produced HS samples. HSs were characterised using spectroscopic and other methods. For the identification of origin of HSs, different methods can be used, such as elemental analysis and ratios of light stable isotopes. The results of the study indicate that many industrially produced HSs are of poor quality (low concentration of basic substance, admixture of undesirable substances, pollutants, no quality indications). In this situation, rigorous quality control should be implemented, providing detailed characteristics of the product. The composition of materials suggested for agricultural applications has not been analysed much. Most of the studied materials were designated as HAs, followed by fulvic acids (FAs) and HSs. However, an analysis of the humic matter types indicates that the majority of substances offered on the market are in fact mixtures of HAs and FAs; so, it would be more appropriate to designate them as HSs or their salts. This study identifies the main quality problems of industrially produced humic substances: 1) lack of strict quality indicators, 2) absence of indication of source materials/origins of HSs.

Key words: peat, humic substances, humic acids, characterisation, spectroscopy.

INTRODUCTION

Humic substances (HSs), being a refractory part of natural organic matter, are compounds with high molecular mass (from < 1,000 up to several millions Da) and acidic nature due to presence of carboxylic and phenolic hydroxyl groups (Tan, 2014). HSs are products of decay of living organic matter formed in its degradation reactions and can provisionally be classified as humic acids (HAs), fulvic acids (FAs) and humin, depending on their solubility (Stevenson, 1994). Both degradation and synthetic processes in decaying organic matter are described as humification. Humification is a process of the transformation of organic molecules of living organic matter into groups of substances with similar properties – humic substances. All these processes are

important for understanding the carbon cycle and transformation processes of originally living matter (Ciais et al., 2013). HSs can be extracted from the source materials using alkaline compounds, ion exchange and other techniques; however, their structure is changed during the isolation and purification process (Tan, 2014). As HSs form from any living organic matter, they can be found not only in any organic fossil but also in any recent organic decay product. Typically, HSs are extracted from low rank coal (lignite, leonardite and others), weathered coal, sediments of waterbodies, peat, also from soils, composts and other organic matter degradation products. Despite a long lasting history of research of humic matter, many questions about humification processes and about structure and properties of HSs are still open, including questions concerning the relation of properties of HSs to their biological precursor material, humification conditions and length (age of HSs).

Nowadays HSs are produced industrially in quantities of hundreds (maybe even thousands and more) of tonnes, first of all for agricultural applications. They are produced worldwide from all types of source materials. Since the major source of HSs is soil, they are an important material in various areas of agriculture, such as soil chemistry, fertility, plant physiology and others. At the same time, HSs can be considered as an important resource, because they can be extracted in industrial amounts from sources where they are abundant and then applied to achieve or increase their positive impacts. The role of HSs in soil environments and their possible use in agriculture have been examined in reviews (Nardi et al., 2002; Peña-Méndez et al., 2005; Calvo et al., 2014; Olk et al., 2018). Considering that the applications of industrially produced HSs also include food, pharmaceutics and environmental technologies, it is important to evaluate their composition and quality and to identify their sources. Until now, properties of HSs of different origins have been analysed; however, their comparative studies have not been done.

The aim of the present study is to compare the properties of samples of industrially produced HSs with ones isolated from known source materials and with reference humic samples as well as to examine approaches for identification of HS sources.

MATERIALS AND METHODS

The studied humic substances containing samples

In the study, HSs produced in China, USA, Russia, Germany, Belarus, Finland, Switzerland, Mexico, Latvia and Poland were used (to avoid conflicts of interest, the producers and trade names of the studied products were kept anonymous). Humic substances were analysed as obtained (in solid state).

The source materials of industrially produced HSs included low rank coal (such as leonardite and lignite), peat and, in some cases, waste products of cellulose production (lignosulphonates). For comparison, HAs and potassium humate were isolated from well characterised samples of raised bog peat, fen peat, soil and vermicompost. HAs were extracted and purified, using procedures recommended by the International Humic Substances Society (IHSS) (Tan, 2005). IHSS reference materials were also used (https://humic-substances.org/#products). In this study industrially produced HSs are classified by their source material and producer country: coal – Czech Republic (HA), Germany (HA), USA (HA), China (FA), Russian Federation (HS), Mexico (FA); peat – Belarus (HA), Latvia (HA), Finland (HA), USA (HA), USA (FA), Finland (FA);

water – USA (FA), Latvia (FA), Estonia (FA), Lithuania (FA), Russia (FA), Latvia (HS); lignite – Russia (HS); soil – USA (HA), Latvia (HS); unknown – Switzerland (HA).

Most of the studied materials were designated as HAs, followed by FAs and HSs. Altogether, 32 industrially produced HS samples of different types and origins and 18 reference samples were studied.

Characterisation of humic substances

Elemental analysis (C, H, N, S and O) was carried out using an Elemental Analyzer Model EA–1108 (Carlo Erba Instruments), and the found values were normalised with respect to ash content. Ash content was measured after heating 50 mg of each humic sample at 750 °C for 8 h.

Atomic ratios were calculated from elemental analysis using the Eqs (1) and (2),

$$O/C = \frac{(Mc \cdot O\%)}{(Mo \cdot C\%)} \quad (1)$$

$$H/C = \frac{(Mc \cdot H\%)}{(M_H \cdot C\%)} \quad (2)$$

where MX is the element molecular mass, and X% is the percentage of the element (C, O, H) in the sample.

UV–Vis Spectroscopy

UV–Vis spectra were recorded on a Thermospectronic Helios γ UV (Thermo Electron Co) spectrophotometer in a 1 cm quartz cuvette. The E4/E6 ratio (Chen et al., 1977), i.e. ratio of absorbances at 465 and 665 nm, was determined for 5 mg of a humic sample solution in 10 mL of 0.05 N $NaHCO_3$.

Fluorescence Spectroscopy

Fluorescence spectra were recorded using a Perkin Elmer LS 55 fluorescence spectrometer on the aqueous solutions of each sample at a concentration of 25 mg L^{-1}, adjusted to pH 7 with 0.5 M HCl. Emission spectra were recorded at a fixed excitation wavelength of 350 nm (scan speed 500 nm min^{-1}, with 10.0 nm slit over the wavelength range of 380 to 650 nm). The ratio of fluorescence intensity of 460 to 510 nm (I,460/I,510) was used as a humification indicator, as previously suggested by Milori et al. (2002).

Excitation-Emission Matrix (EEM) Fluorescence Spectroscopy

Excitation-emission matrices were recorded for humic substances (as obtained from producer, reference samples or isolated) aqueous solutions using an Aqualog total luminescence spectrometer. Matrices were recorded in the excitation range of 250–600 nm and emission range of 250–600 nm with 5 nm increments to reflect major fluorescent components in HAs. Data were processed with parallel factor analysis.

Determination of inorganic element content

1.00 g humic matter samples were weighed into Teflon tubes, adding 8 mL of 69% HNO_3 and 2 mL of H_2O_2. The tubes were closed to provide high pressure. The prepared samples were mineralised using a microwave sample preparation system (Milestone Advanced Microwave digestion system, Ethos Easy) at 200 °C for 20 min. The resulting

samples were filtered through filter paper and diluted to 50 mL with deionised water. The concentrations of inorganic elements in HSs were determined by inductively coupled plasma spectrometry with optical emission detection (ICP-OES), using a Thermo Scientific iCAP 700 series ICP spectrometer.

FT-IR absorption spectra of humic substances

A Fourier Transform Infrared Spectrophotometer Shimadzu IR-Tracer 100 was used with the following settings: wave number: 4,000–400 cm^{-1}, resolution: 2 cm^{-1}, the number of scans: 20. 3 mg of the sample of the studied humic substance and 200 mg of KBr powder were mixed, and 30 mg of the mixture was weighed and compressed into a tablet. Spectra were taken in the infrared spectrum of 400 cm^{-1} to 4,000 cm^{-1}.

Determination of stable isotope ratios of δ13C, δ15N and δ18O

For determination of the ratio of C and N stable isotopes, samples were weighed into tin capsules on an analytical balance with an accuracy of ± 0.01 mg and within a weight range of 0.80 to 1.20 mg. Glutamic acid standards were used for calibration (0.20, 0.50, 0.80, 1.00 and 1.50 mg). For determination of the ratio of O stable isotopes, silver capsules were used, and sucrose was used for calibration. The measuring system consisted of a EuroVector Euro EA3000 element analyser (a quartz reaction tube filled with chromium (III) oxide and silvered cobaltous oxide (1,030 °C), a quartz reduction tube filled with copper shards (650 °C) for determination of C and N, and an HT-PyrOH block with a ceramic outer tube and a glassy carbon inner tube filled with glassy carbon chips (1,450 °C) for O analysis. Measurements were taken using a Nu HORIZON mass spectrometer by Nu Instruments (acceleration voltage: 5 kV, mass range: 2–100 Da, mass dispersion: > 30 cm). The results were processed by the Nu Stable Control Software v1.69.

Statistical analysis of data

One-way analysis of variance (ANOVA) with post hoc Tukeys HSD test ($p < 0.05$) was performed using SAS JMP®, Version 15 (SAS Institute Inc., Cary, NC, USA).

RESULTS AND DISCUSSION

Most of the studied materials were designated as HAs, followed by FAs and HSs (data not shown). However, the analysis of the humic matter types (HAs or FAs, based on the solubility at pH 2) indicated that the majority of the substances offered on the market are in fact a mixture of HAs and FAs; so, it would be more appropriate to designate them as HSs or their salts.

The analysis of the amounts of organic matter in the compositions of humic materials indicated that only few of the industrially produced HSs indeed predominantly consist of organic matter, while the majority contain significant amounts of inorganic substances, as indicated by the ash content in the compositions: the ash content in some compounds reached even 35%; on average it was 6% (Fig. 1). So high concentrations of inorganic substances in industrial humic products is an indicator of poor quality of prepared products as in pure humic substances only traces of inorganic substances has been found. The highest ash content was characteristic of the HSs isolated from lignite, leonardite and weathered coal.

An important quality indicator of HSs for agricultural applications can be the presence of inorganic elements. The inorganic components of HSs mostly are major elements. For instance, Na (up to 44 mg g^{-1}) and K (up to 100 mg g^{-1}) in highest concentrations can be found in such preparations as potassium and sodium humates. Notably, these elements in high concentrations can even be found in products sold under such trade names as 'Humic Substance' and 'Humic Acid'. In humic products, Al, Ca and Fe can also be found in high concentrations (up to 33 mg g^{-1}, 20 mg g^{-1} and 5 mg g^{-1} respectively). Further, high concentrations (up to 70 mg g^{-1}) of S were found in products obtained from cellulose production waste materials (lignohumates). High concentrations of P (up to 5 mg g^{-1}) were found in several products, indicating amendments of phosphorus fertilizers. Next, toxic trace elements can be found in relatively high concentrations in some humic products: for example, 197 µg g^{-1} Sr in an industrially produced FA obtained from lignite, 50.8 µg g^{-1} Cr and 30.7 µg g^{-1} Cu in a HA from leonardite, 27 µg g^{-1} As and 51 µg g^{-1} Ba in a lignohumate preparation, as well as high concentrations in other products.

Comparatively, in the reference samples and in the samples isolated in laboratory, trace elements were found in trace concentrations (for elements such as Na, Ca, Mg, Fe < 0.1 mg g^{-1}, but for trace elements, such as Pb, As, Co, Ni < 0.2 µg g^{-1}).

To characterise elemental composition, atomic ratios (Van Krevelen graphs) were used. H/C versus O/C ratios (Fig. 3) illustrate the relative percentage of aromaticity in HS structures. By far the most important

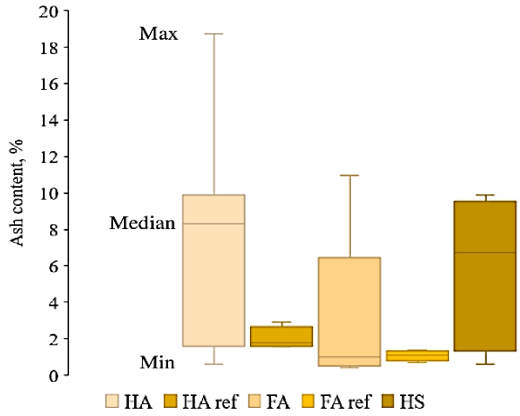

Figure 1. The box plot of ash content in the studied industrially produced (n = 32) and reference (n = 18) HAs, FAs and HSs (Max – the highest value; Min – the lowest value; Median – the mid-point of the data).

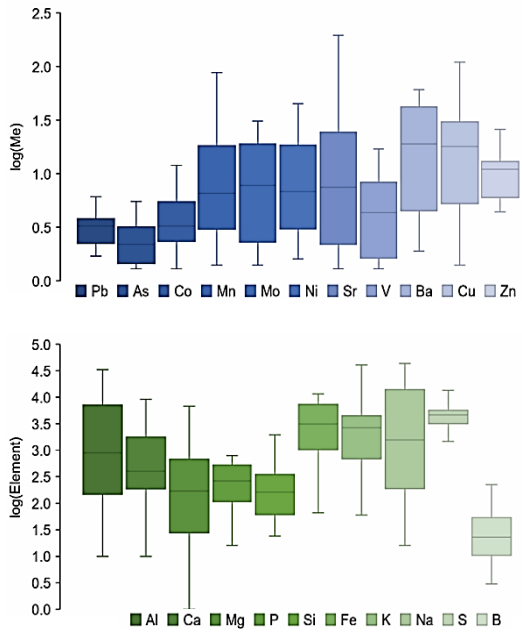

Figure 2. Box plot of major and trace element concentration (µg g^{-1}) in the studied industrially produced (n = 32) humic substances. Error bars represent the highest and lowest values. The median of data is presented. (log(Me) – the logarithm of metal concentration; log(Element) – the logarithm of element concentration) (results are represented in logarithmic values on account of large concentration of element presented in sample).

reactions influencing the HS structure are demethylation (split off of -CH_3 groups), dehydration and decarboxylation (split off of -COOH groups). Van Krevelen graph characterises the depth of the humification process (Klavins et al., 2019). The demethylation, dehydration and decarboxylation processes result in an increased aromaticity and an increased humification degree and is characteristic of HSs isolated from deeply humified materials, such as lignite and leonardite. Soil, peat and aquatic HSs demonstrate a lower humification degree and their application for agricultural purposes (as biostimulant, soil amendment, fertiliser) is more beneficial, than of material which has undergone deep transformation process (Nardi et al., 2002).

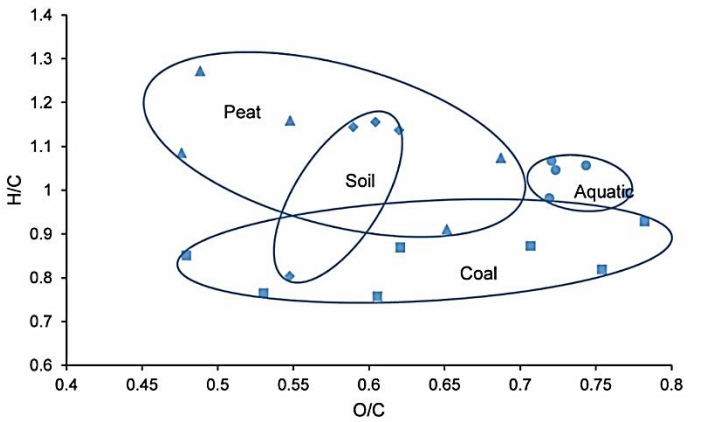

Figure 3. Van Krevelen graph of industrial and reference HS composition element H/C ratio *versus* O/C ratio (Peat (▲), Coal (■), Soil (♦), Water (●), Lignite (-)).

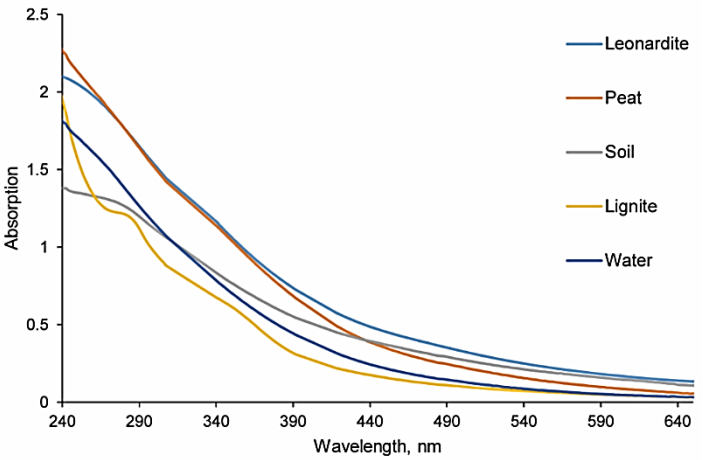

Figure 4. UV–Vis spectra of the studied HSs depending on their origin.

The UV–Vis spectra of the FAs and HAs obtained (Fig. 4) do not have well expressed sorption lines and decrease with increasing wavelength. However, the HSs isolated from highly transformed organic material demonstrate a shoulder at 280 nm characteristic of aromatic structures (not so expressed for HSs of other origins). The UV

spectra of both HAs and FAs are relatively similar. The UV sorption ratios at 465 and 665 nm are used as condensation of aromatic groups measure (aromaticity), but they also reflect the particle size and molecular weight of HS (Chen et al., 1977). The E4/E6 ratio for the studied HSs varied from 3.46 to 16.35, demonstrating high variability of the studied HSs. The highest E4/E6 ratios were found for the aquatic FA as well as for HSs from soil as described also in literature (Stankevica et al., 2019). The E4/E6 ratio for FAs is higher than for HAs (Zalba et al., 2016), thus indicating lower molecular weight, higher acidity and thus also better accessibility for plants.

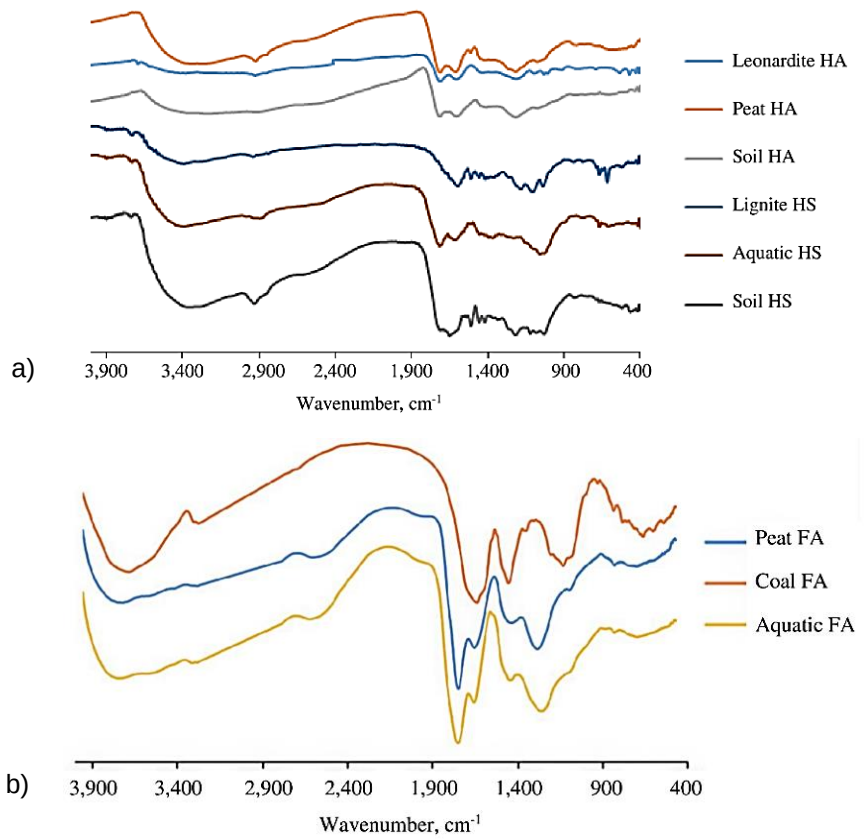

Figure 5. Fourier transform infrared (FTIR) spectra of the studied HAs, HSs (a) and FAs (b) depending on their origin.

The IR spectra of the FAs (Fig. 5, b) and HAs (Fig. 5, a) obtained have general similarity. The FTIR spectra of the analysed HSs can be split by regions, depending on the informativity and the presence of important functional groups. The Fourier transform infrared spectra (Fig. 5, a, b) can also be used to discriminate between FAs and HAs and to identify the origin and quality of HSs. However, the presence of mineral substances and, possibly, other mixtures delimit the possibilities to obtain good quality spectra. Absorption bands in the spectral region of 3,600–2,800 cm^{-1} are broad. Absorbance in this spectral region is determined by the presence of -OH groups. Sorption at the wavelengths of 2920 and 2,860–2,850 cm^{-1} characterise the presence of the CH_3-

and CH_2- groups. The FTIR spectra data of soil HSs show that methylene groups - $(CH_2)_n$- exist as short alkane chains (n < 4). Intensive sorption at 1,700 cm^{-1} (1,725–1,700 cm^{-1}), is common for carbonyl groups in aldehydes, ketones and carbonic acids.

Fig. 6 shows a separation between the four origin of HSs. ANOVA results represent that the values of δ18O and δ15N of the soil and water origin of HSs relate to the one group (C). According to statistical analyses the values of δ13C of peat origin of HSs relate to two groups – A (coal) and B (soil).

The isotope ratio measurements show a difference of up to 5‰ for each HS group (Fig. 6), which allows to distinguish them one from another. The C, N and O isotopic patterns of water and soil HSs are very similar. The reason for that most probably is their common source of origin, i.e. water. HSs leach into water bodies from soil. Also, the C and N isotopic patterns of coal and peat HSs are very similar, except for δ18O, which is dependent mostly on temperature changes and, in this case, is indicative of different environmental temperatures at the time of coal and peat HS formation time. For all sample groups, δ15C changes within the range from -25‰ to -30‰. Since C is accumulated in plants mostly from air by means of photosynthesis, as the δ13C values show, all humic substance groups are formed from the C3 type plants. The δ15N values depend on many factors, including the isotopic composition of soil in different geographical locations. If we assume that the isotope ratio is fixed at the time of formation of a humic substance, then, taking into account the N15 discrimination processes in plants, larger δ15N values, as in the soil and water HS, are indicative of the lower amounts of N available for plants at the time of formation of the humic substance.

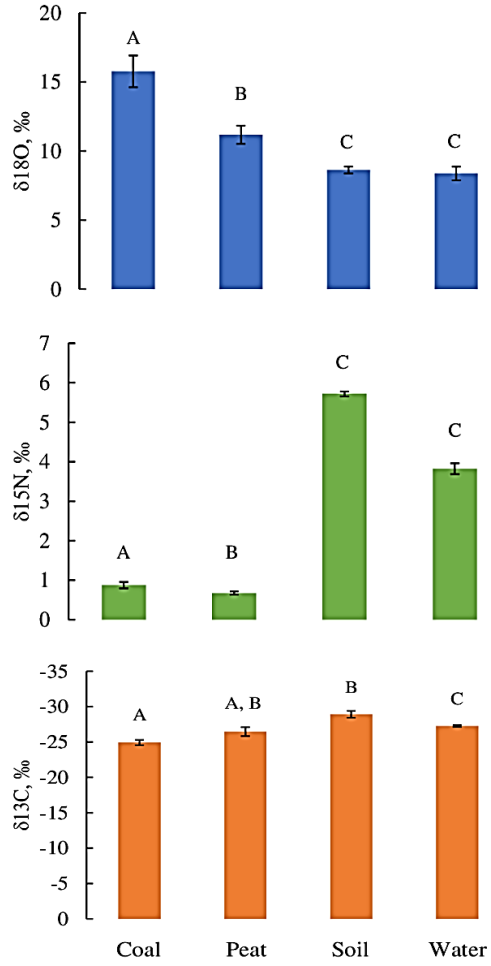

Figure 6. Isotope ratios of the studied HSs depending on their origin. Error bars represent standard deviation ($n = 5$). Letters above bars represent significant differences among different groups (Tukeys HSD $p < 0.05$).

The excitation-emission matrix fluorescence spectra illustrate the fluorescent components in HSs, HAs and FAs (Figs 7, 8, 9). In a mixture of HAs and FAs, the most intensive fluorescence signal comes from FAs (approximately 350 nm excitation and 450 nm emission), while the fluorescence intensity of HAs (present at approximately

470 nm excitation and 540 nm emission) is comparatively less expressed. FAs have a stronger fluorescence signal due to higher phenolic group content, while HAs have more condensed structures. EEM spectra can be used as a tool to identify the type of an HS: whether it is an HA, or an FA, or a mixture of both. Moreover, EEM spectra can be used for the identification of other groups of substances with fluorescent characteristics, for instance, if there is chlorophyll in vermicompost, and the like. In this study, the excitation-emission fluorescence spectra were recorded at the excitation and emission range between 250 and 650 nm, and the data show evident differences between the fluorescence characteristics in HAs, FAs and mixtures of both.

Lignite HA has a typically weak fluorescence peak at 470 nm excitation and 540 nm emission (Fig. 7). At the same time, the EEM spectra results also show the presence of low quantities of FA in this industrial HA. Additionally, there is a signal of some plant remnants, which shows that lignite is originally formed from peat/plants.

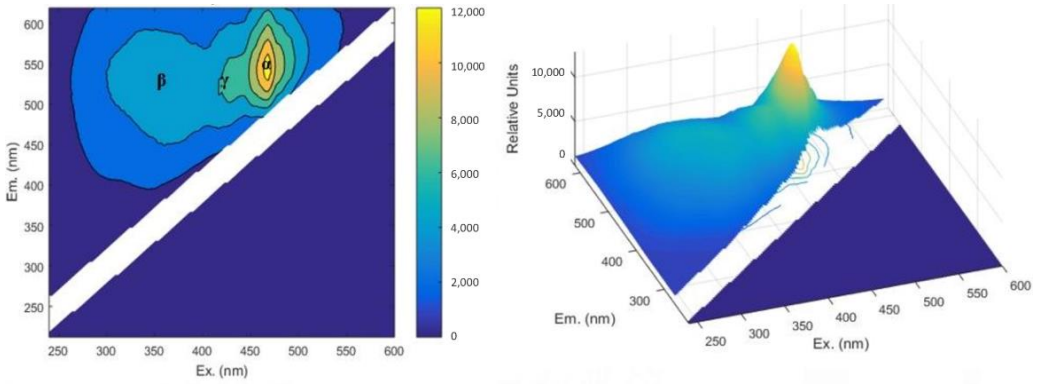

Figure 7. Lignite HA 2D (left) and 3D (right) EEM spectra.

Lignite FA (Fig. 8) has a typical, intensive and complex fluorescence signal at around 350 nm excitation and 450 nm emission. This is due to high phenolic concentration. However, the data also show a weak HA signal. HA could have got into the FA solution during the isolation procedure.

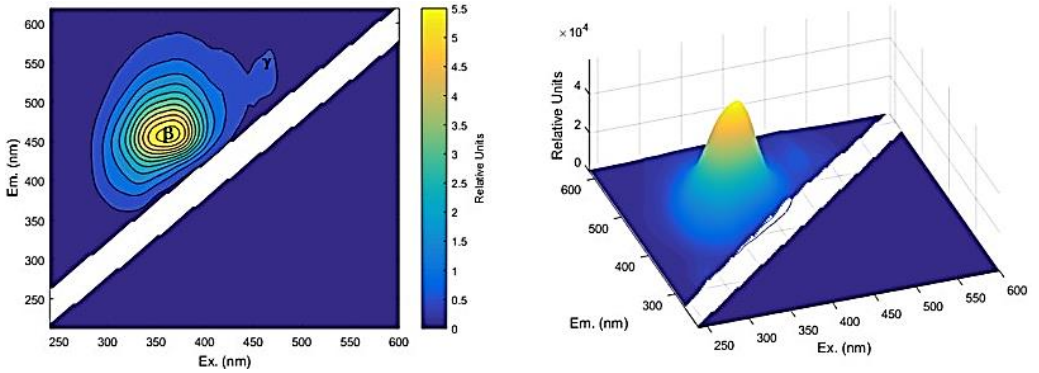

Figure 8. Lignite FA 2D (left) and 3D (right) EEM spectra.

The excitation-emission matrix of soil HSs shows a mixture of HA and FA fluorescence signals and indicates small amounts of FA in the soil (Fig. 9).

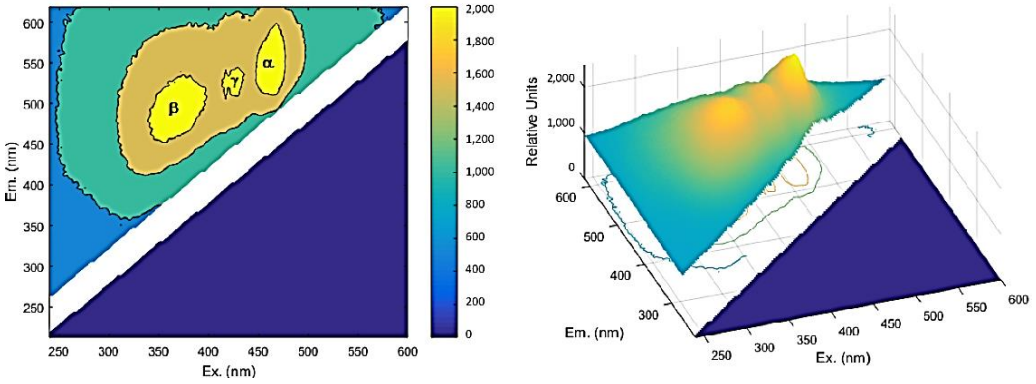

Figure 9. HS (isolated from soil) 2D (left) and 3D (right) EEM spectra.

CONCLUSIONS

As HSs increasingly become an industrially produced material for agricultural applications, their quality analysis and control is of utmost importance. The quality assessment of HSs is yet more important in view of the fact that there are no strict definitions of HSs and regulations of their quality control. The properties of HSs depend on their origin, and significant differences have been observed depending on the source materials. Major differences are common for freshly humified humic substances (isolated from soil, vermicompost, but also peat) on one hand, but on the other – for humic substances isolated from highly humified materials, such as lignite, leonardite and others. In addition, the comparison with the IHSS reference materials can be used for research purposes and not so much for describing the properties of industrially produced products. Most industrially produced HSs are very poorly characterised, sometimes chemical characteristics are absent, including, for example, the amount of the claimed product (HS), ash content and other parameters. This study reveals the main quality problems of industrially produced HSs: 1) lack of strict quality indicators; 2) absence of indication of a source material/origin of the HS.

ACKNOWLEDGEMENTS. This research was funded by the European Regional Development Fund grant No. 1.1.1.2/I/16/001 under the post-doctoral research project No. 1.1.1.2/VIAA/1/16/008 as well as Latvia Science Council project 'Properties and structure of peat humic substances and possibilities of their modification' lzp-2018/1-0009.

REFERENCES

Calvo, P., Nelson, L. & Kloepper, J.W. 2014. Agricultural uses of plant biostimulants. *Plant and Soil* **383**(1–2), 3–41.

Chen, Y., Senesi, N. & Schnitzer, M. 1977. Information provided on humic substances by E4/E6 ratios. *Soil Science Society of America Journal* **41**, 352.

Ciais, P., Sabine, C., Bala, G., Bopp, L., Brovkin, V., Canadell, J., Chhabra, A., DeFries, R., Galloway, J., Heimann, M., Jones, C., Le Quéré, C., Myneni, R.B., Piao, S. & Thornton, P. 2013. Carbon and Other Biogeochemical Cycles. In: *Climate Change 2013: The Physical Science Basis. Contribution of Working Group I to the Fifth Assessment Report of the Intergovernmental Panel on Climate Change* [Stocker, T.F., Qin, D., Plattner, G.-K., Tignor, M., Allen, S.K., Boschung, J., Nauels, A., Xia, Y., Bex, V. & Midgley, P.M. (eds.)]. Cambridge University Press, Cambridge, United Kingdom and New York, USA, 465–570.

Klavins, M., Purmalis, O., Grandovska, S. & Klavina, L. 2019. Properties of soil and peat humic substances from Latvia. *Agronomy Research* **17**(2), 499–508. https://doi.org/10.15159/AR.19.045

Milori, D.M.B.P., Martin-Neto, L., Bayer, C., Mielniczuk, J. & Bagnato, V.S. 2002. Humification degree of soil humic acids determined by fluorescence spectroscopy. *Soil Science* **167**, 739–749.

Nardi, S., Pizzeghello, D., Muscolo, A. & Vianello, A. 2002. Physiological effects of humic substances in higher plants. *Soil Biology and Biochem*istry **34**, 1527–1537.

Olk, D.C., Dinnes, D.L., Scoresby, J.R., Callaway, C.R. & Darlington, J.W. 2018. Humic products in agriculture: potential benefits and research challenges – a review. *Journal of Soils and Sediments* **18**(8), 2881–2891.

Peña-Méndez, E.M., Havel, J. & Patočka, J. 2005. Humic substances–compounds of still unknown structure: applications in agriculture, industry, environment, and biomedicine. *Journal of Applied Biomedicine* **3**(1), 13–24.

Stankevica, K., Vincevica-Gaile, Z. & Klavins, M. 2019. Role of humic substances in agriculture and variability of their content in freshwater lake sapropel. *Agronomy Research* **17**(3), 850–861. https://doi.org/10.15159/AR.19.094

Stevenson, F.J. 1994. *Humus Chemistry: Genesis, Composition, Reactions*. John Wiley & Sons, 538 pp.

Tan, K.H. 2005. Soil sampling, preparation, and analysis. Second Edition. Taylor & Francis, New York, 628 pp.

Tan, K.H. 2014. *Humic matter in soil and the environment: principles and controversies*. CRC Press, 465 pp.

Zalba, P., Amiotti, N.M., Galantini, JA. & Pistola, S. 2016. Soil humic and fulvic acids from different land-use systems evaluated by E4/E6 ratios. *Communications in Soil Science and Plant Analysis* **47**(13–14), 1675–1679. https://doi.org/10.1080/00103624.2016.1206558

Agronomy Research **18**(3), 2087–2102, 2020
https://doi.org/10.15159/AR.20.213

UAV photogrammetry for volume calculations

K. Kokamägi[1,*], K. Türk[2] and N. Liba[2]

[1]Estonian University of Life Sciences, Institute of Agricultural and Environmental Sciences, Chair of Environmental Protection and Landscape Management, Kreutzwaldi 5, EE51006 Tartu, Estonia
[2]Estonian University of Life Sciences, Institute of Forestry and Rural Engineering, Chair of Geomatics, Kreutzwaldi 5, EE51006 Tartu, Estonia
[*]Correspondence: kaupo.kokamagi@student.emu.ee

Abstract. This research assesses the suitability of UAV (Unmanned Aerial Vehicle) photogrammetry for calculating stockpile volumes and analyses the compliance of the accuracy of results to current laws. In addition two different UAV's and two different objects are compared and the necessity of using GCP's (Ground Control Points) is investigated. The time spent on each work stage is also evaluated. Data used in this study was collected in two sites, where the objects differed in shape, colour and texture. The investigated objects were a regularly shaped peat stockpile and an irregularly shaped gravel stockpile. Data was collected with a terrestrial laser scanner, a GNSS (Global Navigation Satellite System) device and two different UAVs. Volume of the models calculated from different data was compared to the volume of the models based on laser scanning data for accuracy assessment. Relative errors of all of the photogrammetric models compared to the laser scanning based model were under 4%. It was concluded that the advantages of UAV based photogrammetry become apparent as the complexity and size of the measured objects grow. Results of the study show that using UAV photogrammetry to determine stockpile volumes is sufficiently accurate with both of the tested UAVs. The results show that without using GCPs (Ground Control Points), sufficient accuracy was still achieved. Nevertheless accuracy was increased by using GCP's. It was concluded that using UAV's can significantly reduce the time spent on collecting data for volume calculations, especially when GCP's are not necessary.

Key words: stockpile, 3D modelling, GCP's.

INTRODUCTION

Thanks to the overall development of technology the use of UAV's is increasing. Using UAV photogrammetry for volume calculations and mapping large areas is in accordance with the principles of sustainable development. It is possible to measure large objects relatively quickly using an UAV. This saves time, human resources and also transportation costs, because it is possible to map a large object in one day using an UAV, whereas mapping the same object using traditional methods could take up to a week. Furthermore it is possible to map areas that are dangerous or difficult to access using an UAV, whereas it would be necessary to use some form of special equipment for mapping it otherwise. Using an UAV is also contactless, so it is possible to map

sensitive areas, without driving or walking on the endangered area. In endangered areas, where getting a flight permit is difficult, terrestrial photogrammetry or laser scanning could be used as an alternative (Dlouhy et al., 2016; Burdziakowski, 2017). Thanks to the development of software and hardware it is possible to use smaller, low-priced UAV's and cameras, which makes work more efficient and less resource heavy, which is one of the main aspects of sustainable development.

UAV's are used for various different purposes from military, postal services and assessing forest health to different forms of entertainment. UAV's can be used as an alternative way to create DEM (Digital Elevation Model) for agricultural purposes (Moravec et al., 2017) and also in precision agriculture, for example to estimate hops canopy area (Starý et al., 2020). As the technology has advanced it is also possible to autonomously navigate UAV's even without GNSS signal (as in extremely low altitudes or indoors) (Dlouhy et al., 2016; Burdziakowski, 2017). Even data from a commercial remotely piloted aircraft can be successfully used in agriculture, when georeferenced with GCP's (Santos et al., 2019). In Estonia, some years ago UAV's were mainly used for inspecting power line corridors, calculating mining volumes and state control of agricultural sector (Liba & Berg-Jürgens, 2015). Photos collected with an UAV can be used both in mapping and creating 3D models (Kokamägi, 2018b; Burdziakowski et al., 2020). Surveying with UAV's is mostly used for large or hardly accessible areas but as the technology evolves, some surveys that were formerly done via total stations or RTK are also beginning to be replaced by UAV's. It is a technology that is rapidly expanding all over the world (Eisenbeiß, 2009). Because of the popularity of UAV's, the smaller models are in mass production and therefore available for a wider scope of users.

The study assesses the accuracy of stockpile volume calculations based on UAV photos and analyses the compliance of this accuracy to current laws. Besides that the impact of using different GCP's and different characteristics of the objects is also investigated. Also, the amount of time spent on each working stage was measured. Many similar studies were analysed to choose a suitable methodology.

Rhodes (2017) investigated using a low-priced UAV for creating 3D models. Different data collecting and processing methods were compared and the results were compared with known volumes and reference measurements. The investigated objects were hay bales and large water tanks (Rhodes, 2017).

In 2014 there was a study carried out in Canada, which researched using UAV's and terrestrial laser scanning (TLS) for collecting data to create digital elevation models (DEM). For accuracy assessment the results were compared to GNSS survey results. It was found that UAV's have great potential for collecting the needed data for this kind of purpose (Ouédraogo et al., 2014).

A research done in 2015 compared using an UAV and a total station for collecting data for stockpile volume calculations. The results were compared with the actual volume that was given by the engineers working on site. The relative errors compared to reference data were -0.67% for the UAV and 2.88% for the total station. The time spent on collecting data was also compared and it was found that surveying with a total station took about six times more time than surveying with an UAV (Arango & Morales, 2015).

Raeva, et al. (2016) compared using a GNSS device and an UAV for volume surveys in their study in 2016. An open-pit quarry stockpile was measured via RTK GNSS and an UAV. The collected photos were processed in Pix4D software and volume calculations were done in Civil 3D software. It was pointed out that in many countries

the relative error of the calculated volume compared to the actual volume is not allowed to exceed 3%. The error between the two surveys was 1.1%, which fits in the given limit. It was also pointed out that collecting photogrammetric data took a lot less time than collecting GNSS data. It was found that using UAV in open-pit quarries is justified, especially because the technology is continually developing (Raeva et al., 2016).

In Estonia the main focus of research has been on dermining vertical or horizontal accuracy (Berg-Jürgens, 2015; Huul, 2016; Köök, 2018). Based on the study of Natalja Liba et al. (2016), it became clear that an orthophotomosaic with sufficient accuracy in the national geodetic system can be created only by using reference points, and by automating other processes, the geometric accuracy remain within 0.1 meters.

As the determination of volumes by this method had not been studied in Estonia before, the accuracy of the determination of volumes on the basis of photographs taken from unmanned aircraft had to be studied, among other things, for updating legislation and making investment decisions for surveying companies. During the work, two different unmanned aircraft and two different objects were compared. The models generated by photogrammetric method were compared with the model based on measurements with RTK GNSS device and based on terrestrial laser scanning. In order to find out the efficiency of different methods of determining volumes, the time spent on different work steps of different methods is compared.

A master's thesis (Kokamägi, 2018a) was prepared and defended at the Estonian University of Life Sciences in the spring of 2018 based on the data presented in the article, which is reviewed in the article 'Accuracy of stockpile volume calculations based on UAV photogrammetry' Kokamägi, 2018b).

This study aims to assess the accuracy of stockpile volume calculations based on UAV photos and analyse the compliance of this accuracy to current laws and to investigate the impact of using different types of GCP's and UAV's to the accuracy.

MATERIALS AND METHODS

Two objects were selected for the research. The first object was a regular-shaped dark-coloured peat stockpile in a peat extraction area in Western Estonia, and the second was a light-coloured irregular-shaped gravel stockpile in the Karude quarry in Central Estonia (Fig. 2). Measuring volumes of peat stockpiles is a daily work of surveyors, and since they have to be measured several times during the season, it is useful to study the possibilities to make the work more efficient, therefore the time spent on different work stages was taken into account during the research.

During the preparation of the object, ground control points were installed and their locations were measured with a Trimble R4-3 GNSS device. After that, the contours of the object were measured using a GNSS device and then laser scanning was performed.

The area of the peat stockpile was 463 m^2 and the area of the gravel stockpile 394 m^2. Both the Laiküla peat extraction area and the Karude quarry are currently in use and are typical objects where it is necessary to determine the volumes of material on a regular basis.

The Trimble R4-3 GNSS instrument was used to measure the contours and control points of both objects, and both dumps were scanned with a Trimble SX10 scanning total station.

The process of the methodology that was used to achieve the set goal is shown in Fig. 1.

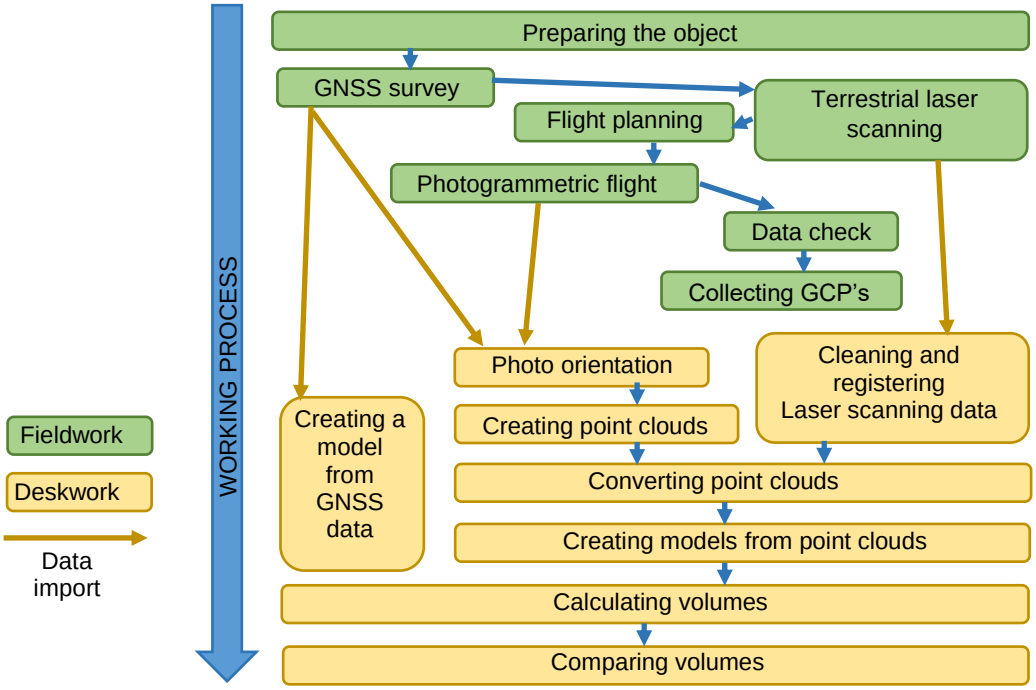

Figure 1. Working process (Kokamägi, 2018a).

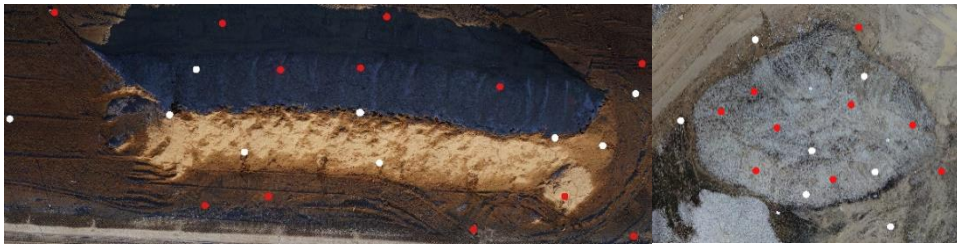

Figure 2. On the left an orthophotomosaic of the peat stockpile in Laiküla and on the right an orthophotomosaic of the selected object in Karude quarry. On the left special photogrammetric GCP's are marked with white and spray painted GCP's are marked with red dots. On the right the selected seven GCP's are marked with white and selected nine GCP's are marked with red dots.

The first object (Laiküla peat stockpile) was surveyed on October 24, 2017.

Measuring a peat stockpile is generally difficult and dangerous, as it is a soft material and it is generally necessary to use special instruments or heavy machinery to measure its ridge using conventional methods.

21 ground control points were installed on the first object: 12 points made with spray paint and 9 special photogrammetric markers. It took about 20 minutes to install them.

A total of 20 points were collected during the GNSS survey. Measurements yielded data from 13 to 19 satellites and PDOP (Position of Dilution of Precision) ranged from

1.3 to 2.0. According to the GNSS device report, the horizontal accuracy of the points was within three cm horizontally and 5 cm vertically. This step took about 40 minutes.

The stockpile was scanned from four points of view and it took about an hour to scan.

Two different UAVs were used for imaging (Table 1). Unmanned aircraft DJI Phantom 4 pro v2.0, (Fig. 3), a relatively inexpensive and widely used unmanned aerial vehicle, and the Aibotix Aibot X6, built specifically for photogrammetric use (Fig. 3). The first has a 20 MP (megapixel) integrated camera and the second had a 32.4 MP Sony ILCE-7RM2 camera on board.

Table 1. DJI Phantom 4 pro v2.0 and Aibotix Aibot X6 specifications (Phantom 4 Pro 2020, Aibot X6 2018, Sony ILCE-7RM2 Full 2020)

	DJI Phantom 4 Pro v2.0	Aibotix Aibot X6
Size	Diagonal 35 cm	105×105×45 cm
Weight	1,375 kg (including camera)	3.4 kg
Payload	-	2 kg
Max flight time	30 minutes	20 minutes
Max speed	20 km s^{-1}, positioning mode 13–89 m s^{-1}	11.11 m s^{-1}
Max ascent speed	6 m s^{-1}, positioning mode, 5m s^{-1}	8 m s^{-1}
Rotors	4	6
Camera	Integrated 1'' CMOS 20 MP	Sony ILCE-7RM2
Effective pixels	5,472×3,648 (20 MP)	7,952×5,304 (42.4 MP)
Focal length	8.8 mm	35 mm
Sensor size	Diagonal 1 inch	1.4×0.9 inches
Image format	JPEG, DNG (RAW)	JPEG, RAW

The flight planning of the DJI Phantom 4 pro v2.0 was done with DroneDeploy software and lasted about five minutes. 415 photos were collected during the flight. To create the model, 76 of them, which were photographed at the correct height and had the object or a control point visible, were used. The flight height was 33 meters (AGL – above ground level) and the GSD (ground sampling distance) was 8 millimeters. The flight lasted about five minutes.

Figure 3. Aibotix Aibot X6 on the left and DJI Phantom 4 Pro v2.0 on the right (Leica-Geosystems, 2020; DJI, 2020).

The Aibot X6 flight was planned using AiProFlight software. Flight planning and aircraft assembly took about 15 minutes, which is significantly more than with the DJI Phantom. The flight lasted about 5 minutes. 95 photos were collected, of which 48 were used. The flight height was 47 (AGL) meters and the GSD was 6 mm.

The second object (Karude Gravel Quarry) is more accessible and manually measurable, but gravel quarries are also one potential place to make work more efficient with an UAV. The survey took place on April 10, 2018.

18 special photogrammetric markers were installed on the second object, which took about 20 minutes.

A total of 100 points were measured using the RTK GNSS method. Because the dump was quite complex in shape and had many bumps, it was measured quite densely. Measurements yielded data from 14 to 17 satellites and PDOP ranged from 1.2 to 1.8. According to the GNSS device report, the horizontal accuracy of the points was within 8 mm horizontally and 12 mm vertically. This step took about 55 minutes.

Scanning was performed with a Trimble SX10 scanning total station, the stockpile was scanned from eight positions and the point cloud was assembled automatically during field work. It took about two hours to scan.

Only the DJI Phantom 4 Pro UAV was used for imaging. The flight was planned using DroneDeploy software. The flight lasted less than 5 minutes, during which 139 photographs were collected, of which 55 were used. The flight height was 28 meters (AGL) and the GSD was 6 mm.

Data processing

Then the data was processed, during which 3D models of objects were created from the data collected with different devices and their volumes were calculated. After that, the volumes of the different 3D models were compared and absolute and relative errors compared to the scanning model were found.

The photos were oriented and point clouds created using Agisoft Photoscan Professional 1.4.0 software. Trimble Business Center and Autodesk Recap 2019 software were used to process the point clouds. Autodesk Civil 2019 drawing software was used to create models from point clouds and calculate volumes. The results were analysed using Microsoft Excel.

The research used the coordinates of points collected with a GNSS receiver, point clouds obtained with a laser scanner, and JPEG images collected with an unmanned aircraft with data about the location of the images. Data was collected on two objects.

Based on the coordinates of the points representing the surface of the objects measured by the GNSS method, the contours were drawn, and then the bottom of the dump and its surface were created as separate surfaces. The heights of these surfaces were then compared and the volume between the two surfaces was calculated.

In the Civil 3D software, the lower contour of the stockpile measured by the GNSS device was fixed to the height according to one of the selected control points. The surface of the base was then formed from the contour. After that, the surface of the scanned point cloud was created. For this, only the points inside the base contour were used, the cloud was thinned to a point spacing of 5 cm and the kriging method was used to create the grid. The heights of these surfaces were then compared and the volume of the model was calculated.

Agisoft PhotoScan Professional was used to find volumes by the photogrammetric method, the images were oriented and then the surveyed control points were attached to the GCP's on the images. It was a time consuming process and lasted about one hour. After marking the GCP's, the images were reoriented using the Medium accuracy class.

Then a point cloud was created, Medium was also chosen as the quality. For Aibot X6 data, camera orientation data collected on-board using an IMU device was also used.

After creating the point clouds, they were processed in the same way as the laser scanning point cloud described above. The control points used to position the base contour were not used in the photo orientation process.

Using the photogrammetric method, 8 different models were created for the first object (peat stockpile) and 4 different models for the second object (gravel stockpile) (Table 2). The volumes derived from laser scanning and GNSS survey were 722.52 m^3 and 680.55 m^3 for the first object and 674.04 m^3 and 651.94 m^3 respectively.

Table 2. Different models created by the photogrammetric method (Kokamägi, 2018a)

Object	UAV	GCP's used	Volume (m^3)
First object: Laiküla peat extraction area	Aibotix Aibot X6	no GCP's	704.92
		spray paint GCP's	715.02
		photogrammetric GCP's	730.27
		all GCP's	717.49
	DJI Phantom 4 Pro	no GCP's	708.21
		spray paint GCP's	699.50
		photogrammetric GCP's	742.23
		all GCP's	730.48
Second object: Karude gravel quarry	DJI Phantom 4 Pro	no GCP's	698.97
		7 photogrammetric GCP's	652.30
		9 photogrammetric GCP's	653.60
		16 photogrammetric GCP's	658.41

Assessment of the accuracy of volumes

After finding all the volumes from laser scanning, GNSS and photogrammetric data by different methods (Table 2), they were compared. As laser scanning is considered to be more accurate than other methods used in creating the models, the volume of the model obtained by laser scanning was considered correct for the sake of research. Both the absolute and the relative volume error were found and it was monitored whether the relative error was within the permissible limits.

Similar to the research conducted by Richard Kramer Rhodes (Rhodes, 2017), in addition to the relative error. the root mean square errors (*RMSE*) of different models created by photogrammetric method were also found in both objects. The Gaussian *RMSE* formula was used to calculate the *RMSE* (Randjärv, 1997).

$$m = \pm\sqrt{\frac{[\Delta^2]}{n}} \quad (1)$$

where Δ^2 – the sum of the squares of the errors of the volume of the model obtained by the photogrammetric method compared to the model obtained from laser scanning data; n – the number of different models.

To evaluate the accuracy of the *RMSE* m. the *RMSE* of the result was calculated by the formula (Randjärv, 1997)

$$m_m = \pm\frac{m}{\sqrt{2n-1}} \quad (2)$$

where m – the *RMSE*; n – the number of different models.

In addition, the time spent on the different steps of the volume determination methods were analysed and compared.

RESULTS AND DISCUSSION

For the first object (Laiküla peat stockpile) a total of 10 models were created and their volumes and errors compared to the model created using the laser scanning data were calculated.

Table 3. Errors of the volumes of models created on the basis of surveys of Laiküla peat stockpile compared to the model created from laser scanning data with mean squared errors (Kokamägi, 2018a)

Instrument	GCP's	Volume (m^3)	Error (m^3)	Relative Error (%)	*RMSE* (m^3)		
Scanning total station Trimble SX10		722.52	0	0			
GNSS Device Trimble R4-3		680.55	-41.97	-5.81			
UAVAibot X6	no GCP's	704.92	-17.60	-2.44		10.62	14.31
	Spray paint GCP's	715.02	-7.50	-1.04	6.87		
	photogrammetric GCP's	730.27	7.75	1.07			
	all GCP's	717.49	-5.03	-0.70			
UAV DJI Phantom 4 Pro	no GCP's	708.21	-14.31	-1.98		17.23	
	spray paint GCP's	699.50	-23.02	-3.19	18.09		
	photogrammetric GCP's	742.23	19.71	2.73			
	all GCP's	730.48	7.96	1.10			

The errors in the volumes of the models created on the basis of the surveys made in Laiküla peat extraction area compared to the scanning model with the mean square errors are shown in Table 3. The relative differences of the volumes are shown in Fig. 4.

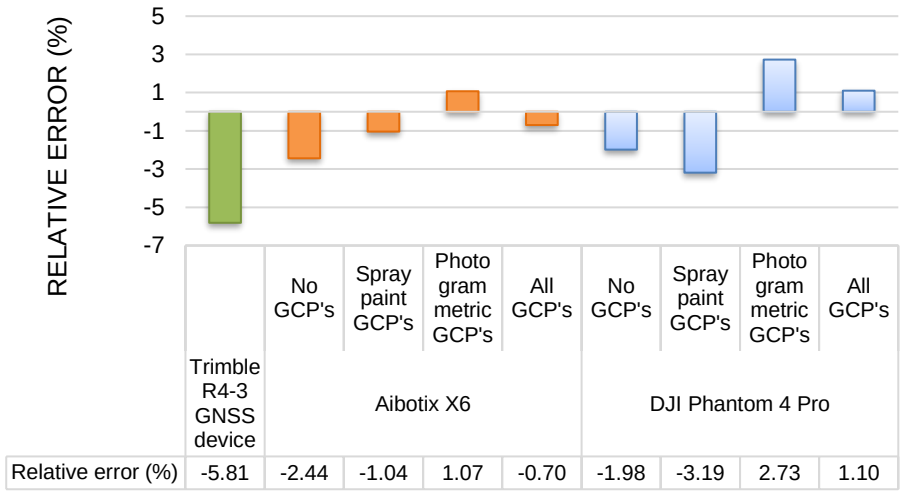

Figure 4. Relative errors of the volumes of the models of Laiküla peat stockpile (Kokamägi, 2018a).

The errors of the volumes of the models created by the photogrammetric method in different methods at the Laiküla peat stockpile show that the errors in the models created with the data collected by the special surveying UAV Aibot X6 with a better camera were more accurate than the models created using cheaper Phantom 4 Pro data. The mean square errors of the different models were 10.62 m^3 and 17.23 m^3, respectively. It is likely that the superiority of the more expensive instrument will come out even more when measuring objects in the global coordinate system, as the Aibot X6 positioning devices are more accurate. As the Phantom 4 Pro flew lower, the pixel sizes were about the same size for both aircrafts - 8 mm for the Phantom 4 Pro and 6 mm for the Aibot X6. For a larger object, of course, this means a longer flight for the Phantom 4 Pro, but since photogrammetric surveying is a lot faster than other surveys, it shouldn't be a big problem.

Also, no significant effect on the accuracy of the volumes was observed when using different types of GCP's. For the Phantom 4 Pro, the relative volume error was -3.19% using spray paint GCP's and 2.73% for special photogrammetric GCP's. For the Aibot X6, the relative errors were -1.04% and 1.07%, respectively. At the same time, the use of all GCP's at the Laiküla site improved the accuracy of the models created from the data collected by both aircraft. The relative error using all GCP's was only -0.7% for Aibot X6 and 1.1% for Phantom 4 Pro.

For the second object (Karude gravel stockpile) a total of 6 models were created and their volumes and errors of compared to the model created from the laser scanning data were calculated.

The errors in the volumes of the models created from the surveys done in the Karude gravel quarry compared to the model created from the laser scanning data with the mean square errors are shown in Table 4. The relative errors in the volumes of the models of Karude gravel stockpile are shown in Fig. 5.

Table 4. Error of the volume of models created on the basis of surveys of Karude gravel stockpile compared to the model created from laser scanning data with mean squared errors (Kokamägi, 2018a)

Instrument	GCP's	Volume (m^3)	Error (m^3)	Relative error (%)	*RMSE* (m^3)
Scanning total station Trimble SX10		674.04	0	0	
GNSS Device Trimble R4-3		651.94	-22.1	-3.28	
UAV DJI Phantom 4 Pro	no GCP's	698.97	24.93	3.70	20.95
	spray paint GCP's	652.3	-21.74	-3.23	19.45
	photogrammetric GCP's	653.6	-20.44	-3.03	
	all GCP's	658.41	-15.63	-2.32	

The error of the model created on the basis of GNSS measurements at the Karude gravel quarry remained in the same order of magnitude as the models obtained by photogrammetric method.

In Karude gravel quarry, where only Phantom 4 Pro data and special photogrammetric GCP's were used, the results obtained using different amounts of

GCP's were quite as expected - the more markers used, the more accurate the model. The relative errors were 3.70% without GCP's. -3.23% with 7 GCP's. -3.03% with 9 GCP's, and -2.32% using all 16 GCP's.

	Trimble R4-3 GNSS device	No GCP's	7 Photogrammetric GCP's	9 Photogrammetric GCP's	16 Photogrammetric GCP's
		DJI Phantom 4 Pro			
Relative error (%)	-3.28	3.70	-3.23	-3.03	-2.32

Figure 5. Relative errors of the volumes of the models of Karude gravel stockpile (Kokamägi, 2018a).

A comparison of the relative volume errors of models created from GNSS data and the DJI Phantom 4 Pro data generated for the two objects is shown in Fig. 6.

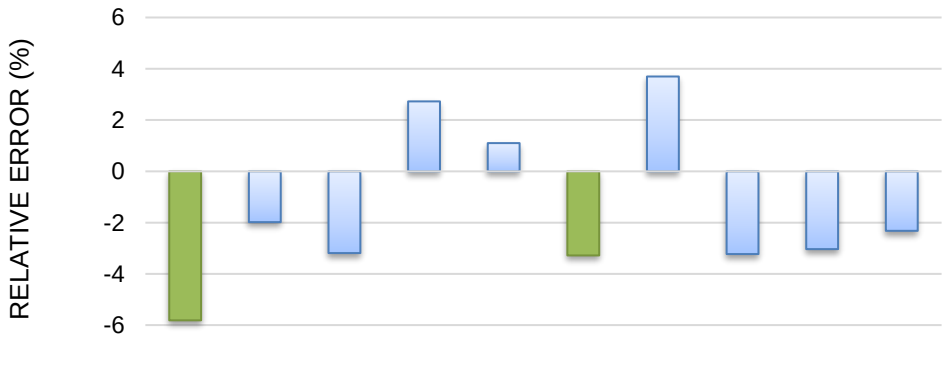

	Trimble R4-3 GNSS receiver	No GCP's	Spray paint GCP's	Photo-gram-metric GCP's	All GCP's	Trimble R4-3 GNSS receiver	No GCP's	Spray paint GCP's	Photo-gram-metric GCP's	All GCP's
	Laiküla	DJI Phantom 4 Pro Laiküla				Karude	Phantom 4 Pro Karude			
Relative error (%)	-5.81	-1.98	-3.19	2.73	1.10	-3.28	3.70	-3.23	-3.03	-2.32

Figure 6. Relative errors in the volumes of the models created from the GNSS and DJI Phantom 4 Pro data of Laiküla and Karude objects compared to the results obtained from the laser scanning data (Kokamägi, 2018a).

Looking at the relative errors of the two objects, we see that, when using all the GCP's in the Laiküla object (peat stockpile), the relative difference was 1.10% compared to the volume of the model formed from the laser scanning data and 2.32% in the case of the Karude object (gravel stockpile). GNSS survey of Laiküla peat stockpile had the largest error, this could have been caused by measuring too few points and oversimplifying the shape of the stockpile and also by the soft material.

Differences of photogrammetrical models could have been caused by the different distribution of GCP's in the area (Fig. 2). For the first object (Laiküla peat stockpile), shadows and the amount and distribution of GCP's in the shadow could also affect the result.

Time spent on different methods

In the course of the work, the time taken to determine the volumes in different ways was also assessed. Table 5 shows the stages of determining the volume of the Laiküla peat stockpile with different methods and the time spent on each. Fig. 7 compares the total time taken to determine the volume with different methods.

Table 5. Stages of determining the volume of Laiküla peat stockpile with different methods and the time spent on (Kokamägi, 2018a)

	GNSS device Trimble R4-3	Scanning total station Trimble SX10	UAV DJI Phantom 4 Pro using GCP's	UAV DJI Phantom 4 Pro no GCP's	UAV Aibotix Aibot X6 using GCP's	UAV Aibotix Aibot X6 no GCP's
Object preparation (min)			20		20	
RTK GNSS survey (min)	15		25		25	
Laserscanning (min)		60				
Flight planning (min)			5	5	15	15
Photogrammetric flight (min)			5	5	5	5
Collecting GCP's (min)			10		10	
Data processing (min)	15	30	90	30	90	30
Total (min)	30	90	155	40	165	50

The fastest way to determine the volume of the Laiküla peat stockpile was to use GNSS measurements, but this is misleading because it was only one small object with a regular shape. The larger the area and the more irregular the objects, the more the advantage of laser scanning and especially unmanned aircraft becomes apparent. In addition, it took more time than usual to prepare the object and measure the GCP's, as different types of GCP's were used. Using GCP's in this case took so long to process, as the locations of the tags were determined manually in the photographs and this is a time consuming process.

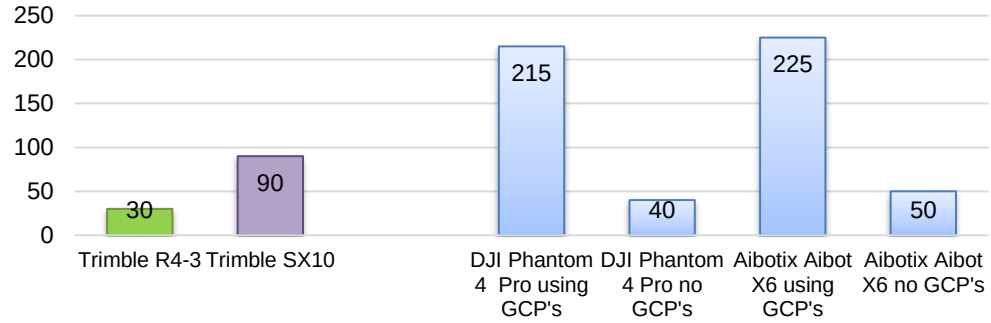

Figure 7. Total time spent to determine the volume of Laiküla peat stockpile using different methods (minutes). (Kokamägi, 2018a)

Table 6 shows the stages of determining the volume of the Karude gravel stockpile with different methods and the time spent on each. Fig. 8 compares the total time taken to determine the volume with different methods.

Table 6. Stages of determining the volume of Karude gravel stockpile with different methods and the time spent on each (Kokamägi, 2018a)

	GNSS device Trimble R4-3	Scanning total station Trimble SX10	UAV DJI Phantom 4 Pro using GCP's	UAV DJI Phantom 4 Pro no GCP's
Object preparation (min)			20	
RTK GNSS survey (min)	30		25	
Laserscanning (min)		120		
Flight planning (min)			5	5
Photogrammetric flight (min)			5	5
Collecting GCP's (min)			10	
Data processing (min)	20	30	90	30
Total (min)	50	150	155	40

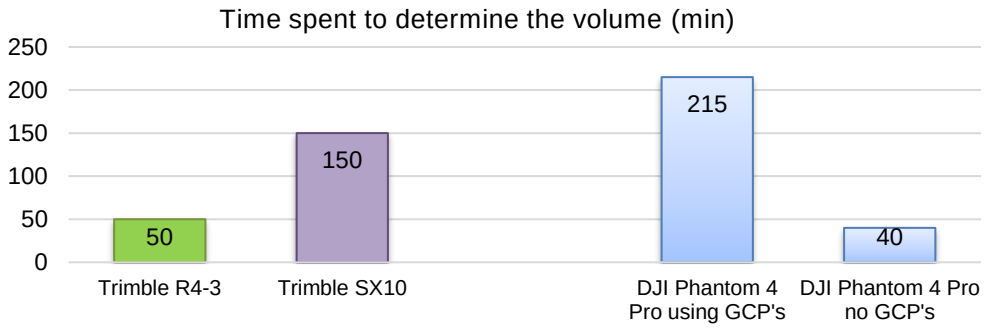

Figure 8. Total time spent to determine the volume of Karude gravel stockpile using different methods (Kokamägi, 2018a).

In the case of the Karude gravel quarry, the fastest determination of volume was made by photogrammetric method without markings. The time taken for GNSS measurements is again misleading for the reasons mentioned above. The Karude object

also took more time than usual to prepare the object and survey the GCP's, as more GCP's were used than usual. It was also more time-consuming to create a model using GCP's during data processing for the reasons mentioned earlier. During laser scanning, the Karude object was surveyed from eight points of view, but normally three or four points of view would be sufficient to measure such an object, so the time taken for scanning could be considerably shorter.

DISCUSSION

As expected, more accurate results were obtained from regularly shaped peat stockpile located in the Laiküla peat extraction area. The exception here is GNSS measurements, where the error compared to the volume of the laser scanning model was -5.81%. This may have been due to errors caused by the soft ground in the field measurements, as well as excessive simplifications and measuring too few points. Surprisingly. the photogrammetric models made without using GCP's gave errors in the same order of magnitude and in some cases even more accurate results than the models made using GCP's. However, the use of all GCP's in both objects helped to improve the accuracy of the results. However, if it is necessary to georeference the coordinates of objects, the GCP's should of course be used.

Comparing the two objects, it became clear that the differences in the volumes calculated on the basis of GNSS data were -5.81% for the Laiküla object and -3.28% for the Karude object. In the case of the regularly shaped Laiküla peat stockpile, the relative error of the model created from the DJI Phantom 4 Pro data created without GCP's was -1.98% and 1.10% using all symbols. In the case of the irregularly shaped Karude gravel stockpile, the relative error of the model created from the DJI Phantom 4 Pro data created without GCP's was 3.70% and -2.32% using all the GCP's.

For comparison, the research of Richard Kramer Rhodes using unmanned aerial vehicles resulted in volume errors of less than 5% from the reference data for 13 sites, more than 15% for four sites and between 5% and 15% for three sites. In this research the measured objects were more regularly shaped hay bales and water tanks. A commercial UAV and camera were used for the research (Rhodes, 2017).

In the study of Arango & Morales (2015), the error of the model created from the total station data compared to the reference data was 2.88% and for the model based on unmanned aircraft data -0.67%. In this research the surveyed object was a soil stockpile and a commercial UAV was used for photogrammetric purposes.

In the work carried out by Raeva et al. (2016), the relative error of the model created on the basis of unmanned aircraft data was also quite good at 1.1%. An eBee UAV was used in this study and the surveyed object was the stockpile of an open quarry.

The results of current research regarding volume errors are similar to the results of previous studies. However in addition to that, using different amounts and different types of GCP's and using two different UAV's was also investigated in this study. It was found that using different types of GCP's does not affect the accuracy of results significantly. It was also found that sufficient accuracy was achieved even without any GCP's with both UAV's. However using GCP's did increase the accuracy.

Comparing the times spent on different methods to determine volumes, it turned out that GNSS is useful for measuring objects as small as those selected for research in the present work, but the larger and more complex the object, the more useful the

photogrammetric method becomes. For a larger object, the photogrammetric data collection time would not be greatly extended, but GNSS measurements would take much longer.

CONCLUSIONS

The research revealed that the use of photographs collected from unmanned aircraft to determine volumes would significantly reduce the time spent on fieldwork. The volumes of all models created by the photogrammetric method in this work were within the limits of 12% of the permitted error established in Estonia with a fairly large margin (Markšeideritöö kord, 2012). It also turned out that simple spray paint GCP's could be used, which also increases the speed of field work. It turned out that sufficient accuracy of calculating volumes can also be achieved by using an inexpensive UAV and camera kit. It would be particularly useful to use unmanned aircraft to determine the volumes of larger and hard-to-reach objects.

Similar measurements could be investigated for larger objects in the future. The effect of using different photogrammetric software on the result of the volume calculation should also be tested. In addition, the effect of automatic GCP detection on the volume calculation results in photogrammetry software should be investigated, as in the present study, manual tagging of images was the most time-consuming part of data processing.

ACKNOWLEDGEMENTS. We would like to thank Kristo Must, who was a co-supervisor of the master's thesis (Kokamägi, 2018a), which this article is based on and also Raxoest OÜ, which is the surveying company, that allowed their equipment to be used for this study.

REFERENCES

Aibot X6, 2018. Aibotix. https://aibotix.com/products/aibot-x6 Accessed 03.05.2018.

Arango, C. & Morales, C.A. 2015. Comparison between multicopter UAV and total station for estimating stockpile volumes. *The International Archives of the Photogrammetry, Remote Sensing and Spatial Information Sciences* **XL-1/W4**, In: *International Conference on Unmanned Aerial Vehicles in Geomatics*. Toronto, Canada, 131–135. https://www.int-arch-photogramm-remote-sens-spatial-inf-sci.net/XL-1-W4/131/2015/isprsarchives-XL-1-W4-131-2015.pdf Accessed 06.07.2020.

Berg-Jürgens, J. 2015. *The quality of orthophoto generation methods using unmanned airplane MUST Q aerial Imagery*. Master's thesis. Estonian University of Life Sciences, Tartu, Estonia, 105 pp. https://dspace.emu.ee/xmlui/bitstream/handle/10492/2360/Jaano_Berg-Jürgens_2015MA_GEm_täistekst.pdf?sequence=1&isAllowed=y Accessed 06.07.2020. (in Estonian).

Burdziakowski, P. 2017. Towards Precise Visual Navigation and Direct Georeferencing for MAV Using ORB-SLAM2. In: *2017 Baltic Geodetic Congress (BGC Geomatics)*. Gdansk, Poland, 394–398. doi: 10.1109/BGC.Geomatics.2017.21. https://www.researchgate.net/publication/320517598_Towards_Precise_Visual_Navigation_and_Direct_Georeferencing_for_MAV_Using_ORB-SLAM2 Accessed 08.09.2020.

Burdziakowski, P. 2018. UAV IN TODAYS PHOTOGRAMMETRY – APPLICATION AREAS AND CHALLENGES. In: *18th International Multidisciplinary Scientific GeoConference SGEM2018.* Albena, Bulgaria, 241–248. https://www.researchgate.net/publication/328269878_UAV_IN_TODAYS_PHOTOGRAMMETRY_-_APPLICATION_AREAS_AND_CHALLENGES Accessed 08.09.2020.

Burdziakowski, P., Specht, C., Dabrowski, P.S., Specht, M., Lewicka, O. & Makar, A. 2020. Using UAV Photogrammetry to Analyse Changes in the Coastal Zone Based on the Sopot Tombolo (Salient) Measurement Project. *Sensors Special Issue - Sensors and Sensor's Fusion in Autonomous Vehicles* **20**(14), 4000. https://doi.org/10.3390/s20144000 Accessed 08.09.2020

DJI 2020. https://www.dji.com/ee/phantom-4-pro-v2 Accessed 05.05.2020

Dlouhy, M., Lev, J. & Kroulik, M. 2016. Technical and software solutions for autonomous unmanned aerial vehicle (UAV) navigation in case of unavailable GPS signal. *Agronomy Research* **14**(3), 733–744.

Eisenbeiß, H. 2009. *UAV Photogrammetry*. Doctoral thesis. Swiss Federal Institute of Technology. Zürich, Switzerland, 203 pp.

Huul, K. 2016. *Implementing drone photogrammetry to create ortophotos and digital elevation models in Raadi strip mine*. Bachelor's thesis. University of Tartu, Tartu, Estonia, 46 pp. http://dspace.ut.ee/bitstream/handle/10062/52945/Huul_Kaspar.pdf Acessed 06.07.2020

Kokamägi, K. 2018a. *Accuracy of stockpile volume calculations based on UAV photogrammetry.* Master's thesis, Estonian University of Life Sciences, Tartu, Estonia, 89 pp. (in Estonian).

Kokamägi, 2018b. Accuracy of stockpile volume calculations based on UAV photogrammetry. In: *CLGE Student Contest 2018* https://issuu.com/mairoltkakko/docs/geodesy_kaupo_kokamagi_stockpile_vo Accessed 06.07.2020.

Köök, R. 2018. *Accuracy of UAV Photogrammetry With Applications to Road Construction Works*. Master's thesis. Tallinn University of Technology, Department of Civil Engineering and Architecture. Tallinn, Estonia, 92 pp.

Leica Geosystems 2020. https://leica-geosystems.com/blog-content/2016/new-solutions-standard-sensors-and-workflows-for-your-uav-aibot-x6-v2 Accessed 05.05.2020.

Liba, N. & Berg-Jurgens, J. 2015. ACCURACY OF ORTHOMOSAIC GENERATED BY DIFFERENT METHODS IN EXAMPLE OF UAV PLATFORM MUST. *IOP Conference Series: Materials Science and Engineering* **96**, In: *Proceedings of the 2nd International Conference on Innovative Materials, Structures and Technologies: 2nd International Conference "Innovative Materials, Structures and Technologies"*, IOP Publishing Ltd, Riga, Latvia.

Liba, N., Berg-Jürgens, J. & Järve, I. 2016. IMPACT OF THE USE OF GROUND CONTROL POINTS ON THE ACCURACY OF ORTHOMOSAIC IN EXAMPLE OF UAV PLATFORM "MUST Q". In: *16th INTERNATIONAL MULTIDISCIPLINARY SCIENTIFIC GEOCONFERENCE SGEM 2016*. 901−909.

Markšeideritöö kord. 2012. Riigi Teataja. Estonian legislation. https://www.riigiteataja.ee/akt/125012012004 Accessed 06.07.2020. (in Estonian).

Moravec, D., Komárek, J., Kumhálová, J., Kroulík, M., Prošek, J. & Klápště, P. 2017. Digital elevation models as predictors of yield: Comparison of an UAV and other elevation data sources. *Agronomy Research* **15**(1), 249–255.

Ouédraogo, M.M., Degré, M., Debouche, C. & Lisein, J. 2014. The evaluation of unmanned aerial system-based photogrammetry and terrestrial laser scanning to generate DEMs of agricultural watersheds. *Geomorphology* **214**, 339–355.

Phantom 4 Pro Specs. 2020. DJI. https://www.dji.com/phantom-4-pro/info Accessed 09.09.2020.

Raeva, P.L., Filipova, S.L. & Filipov, D.G. 2016. Volume computation of a stockpile – a study case comparing GPS and UAV measurements in an open pit quarry. *The International Archives of the Photogrammetry, Remote Sensing and Spatial Information Sciences* **XLI-B1**. In: *2016 XXIII ISPRS Congress.* Prague, Czech Republic. 999–1004. https://www.int-arch-photogramm-remote-sens-spatial-inf-sci.net/XLI-B1/999/2016/isprs-archives-XLI-B1-999-2016.pdf Accessed 06.07.2020.

Randjärv, J. 1997. *Geodesy I*. Tartu, Estonia, 360 pp. (in Estonian).

Rhodes, R.K. 2017. *UAS as an Inventory Tool: A Photogrammetric Approach to Volume Estimation*. Master's thesis. University of Arkansas, Monticello, 104 pp. http://scholarworks.uark.edu/cgi/viewcontent.cgi?article=3963&context=etd Accessed 06.06.2020.

Santos, L.M.D., Ferraz, G.A.S., Andrade, M.T., Santana, L.S., Barbosa, B.D.S., Maciel, D.T. & Rossi, G. 2019. Analysis of flight parameters and georeferencing of images with different control points obtained by RPA. *Agronomy Research* **17**(5), 2054–2063.

Sony ILCE-7RM2 Full Specifications. 2020. Sony. https://www.sony.com/electronics/interchangeable-lens-cameras/ilce-7rm2/specifications Accessed 09.09.2020.

Starý, K., Jelínek, Z., Kumhálová, J., Chyba, J. & Balážová, K, 2020. Comparing RGB – based vegetation indices from UAV imageries to estimate hops canopy area. *Agronomy Research* Running Issue. Tartu, Estonia. https://agronomy.emu.ee/wp-content/uploads/2020/06/AR2020_201_Star%C3%BD_V_doi_169.pdf#abstract-7788 Accessed 10.08.2020.

Agronomy Research **18**(3), 2103–2116, 2020
https://doi.org/10.15159/AR.20.187

Effect of winter wheat variety, hydrothermal coefficient (HTC) and thousand kernel weight (TKW) on protein content, grain and protein yield

M. I. Kulyk[1], A. O. Rozhkov[2], O. V. Kalinichenko[1], A. O. Taranenko[1,*] and O. V. Onopriienko[1]

[1]Poltava State Agrarian Academy, Faculty of Agrotechnology and ecology, 1/3 Skovorody street UA36003 Poltava, Ukraine
[2]Kharkiv National Agrarian University. V. V. Dokuchaev, Agronomy Department, p/v Dokuchaevske – 2, UA62483 Kharkiv, Ukraine
[*]Correspondence: anna.taranenko@pdaa.edu.ua

Abstract. The aim of the research is to clarify the physiological and biochemical processes in the plant organism that occur in the optimal and stressful conditions, as well as to search for anthropogenic methods of their manifestation in connection with the protein content in grain of wheat varieties of different origin in the conditions of the Forest-Steppe Ukraine. The impact of temperature factor and the moistening mode of the period of winter wheat seed formation and ripening (*Triticum aestivum* L.) has been studied. The impact of varieties of Ukrainian and foreign plant breeding on the protein content in grain of the obtained offspring (reproduction yield) has been studied too. The ways to eliminate the influence of weather conditions on the protein content in grain and on the bases of sowing of different seed fractions have been searched. Research methods: field (studying the influence of growing conditions on grain quality), laboratory (determination of protein content), correlation-regression (establishing connection between factors), statistical method (to confirm the difference between variants). According to the results of the first stage of research, the dependence has been established: sowing with seed, grown in the arid conditions, allows obtaining offspring with high protein content, and vice versa. This is confirmed by the strong correlation both for winter wheat variety. At the second stage of research it has been determined that sowing with fine seed raises the yield protein content in grain, and protein yield without additional costs, but using seed, formed in the arid conditions.

Key words: winter wheat, varieties, protein content in grain, air temperature, precipitation, seed size.

INTRODUCTION

In terms of harvested area *Triticum aestivum L.* and *Triticum turgidum ssp*. Durum are the most cultivated cereal in the world. Today, wheat cultivation accounting 220.11 million of hectares and 749.46 million tonnes (Falcone et al., 2019). Today, countries with the advanced agricultural production, in particular Ukraine, strive to increase the yield and quality of grain crops not expanding the sown areas. Winter wheat is the main grain crop in Ukraine. However, the level of yield and quality of grain remains low in comparison with European countries (Asseng et al., 2015).

Marenych et al. (2019) showed that the problem of increasing of yield crops (including winter wheat), can be solved by humic growth stimulators with keeping of soil fertility. Using of foliar crops fertilization with growth stimulant leads to improve plant nutrition conditions and increases the efficiency of mineral fertilizers. This is confirmed by our previous studies, which found that increasing of winter wheat yield is achieved by fertilizing of winter wheat crops (complex and microfertilizers). Also the influence of the average daily air temperature and the amount of precipitation during the spring-summer vegetation period and period of accumulation of nutrients in the grain on the winter wheat yield was established (Barabolia et al., 2018).

Protein and gluten content in winter wheat grain is a major indicator of its commercial and technological value (Asseng et al., 2018). Therefore, the price of grain in the world market is directly proportional to the value of these indicators. In this regard, improving the quality of grain is a pressing issue, which depends on the quality of bakery products and the selling price of products in the domestic and foreign markets.

The problem of protein content of winter wheat always encourages scientists to find ways to increase the protein content in winter wheat grain without additional agronomic measures and significant material resources. At the same time weather conditions significantly affected the process of triticale organogenesis at the early stages and yield (Mazurenko et al., 2020) and protein content is significantly affected by weather conditions, which are difficult to regulate. It is requiring more costs for increase protein content of winter wheat grain. The biochemical processes that take place in winter wheat plants under the influence of stressful weather conditions (high temperatures et al.) require more detailed study (Argentel-Martínez et al., 2019).

Recently agrarian variety policy has been aimed, first of all, at increasing the grain yields. Thus, the yields of grain crops and legumes in Ukraine in 1990–2018 varied in the range of 1.8 to 4.7 t ha^{-1} (Central Statistical Bureau of Ukraine, 2020). It has been determined that the increase of air temperature and the number of hot days will adversely affect the crop production, which is very difficult for world food security (Tripathi et al., 2016; Ruiz-Ramos et al., 2017). It has been established that the quality of winter wheat grain raised mainly in the hot favorable conditions. They are almost opposite to the conditions in which the high yields are obtained (Mondal et al., 2013; Iqbal et al., 2017; Ruiz-Ramos et al., 2017; Pandey et al., 2019).

Another, no less important problem is that the grain protein indicator is poorly inherited in generations, since it relates to the modification variability, which, in turn, largely depends on the certain weather and climate conditions (Ferris et al., 1998). That is why, while creating new varieties of winter wheat, breeders establish only the potential capabilities of this variety, which are realized depending on the environmental conditions (Dupont et al., 2006). It has been proved (Allen & Ingram, 2002; Almeselmani et al., 2009; Narayanan, 2018), that the violation of physiological and biochemical parameters in a plant, caused by high temperature or moisture deficit, is the weaker, the greater their resistance to these conditions. Hence, it can be concluded that the more drought-resistant variety, the weaker the biochemical processes violation will be under the lower values of the hydrothermal coefficient (HTC). Accordingly, there will be less possibility of the structural connections destruction and the hydrolysis of functional compounds. But, growth of the protein content in grain more than biologically optimal level is impossible without destruction and hydrolysis (Almeselmani et al., 2012; D'Amico et al., 2013). This suggests that the drought resistanse of a variety is a factor that reduces the ability

of plant to respond to HTC decrease, and ultimately to increase the protein content in winter wheat grain.

Therefore, in our opinion, the deterioration of grain quality of modern winter wheat varieties is largely due to the selection of more drought-resistant and plastic varieties. The contrast of the optimal conditions for increasing yields, on the one hand, and grain quality improvement, on the other hand, result in the opposition of the processes that occur in a plant under the stressful weather and climatic conditions. In the optimal conditions of growth and development of winter wheat plants, prevailing mass of nodal roots is located in the upper soil layers. Due to soil drying (stressful conditions), they die off and their functions pass to the germinal roots, which, in search of moisture, develop a considerable mass, using carbon dioxide. As a result, the growth of aboveground mass is inhibited, grain yield decreases, and protein content increases.

Previous researches have established features regarding the physiological mechanism of protein content variability in winter wheat grain. It has been determined that due to the lack of moisture in the stress conditions the ratio of 'bound - free water' increases in a plant, whereas under the optimal conditions the opposite phenomenon is observed. In turn, the reduction of moisture in the soil almost to its dead reserve leads to the nodal roots dying off with a simultaneous intensive growth of the germinal ones. At the same time, with optimal moisture and nutrients supply, the intensity of their growth is almost absent. The genetic program of winter wheat is aimed at preserving itself as a species. Such preservation is based not only on the creation of offspring but also (and equally importantly) on the stable obtaining of viable seed, which can provide seedlings in any environmental conditions, within certain limits. Thus, in the optimal weather conditions, winter wheat grain which is more adapted to germination under the similar conditions is formed. The winter wheat grain, obtained under the stress conditions, better germinates in the dry conditions. This is the biochemical essence of protein content variability depending on the weather and climatic conditions (Sidorenko & Kulik, 2007).

Studying the issue of protein content in winter wheat grain, the authors (Zhemela et al., 2007) concluded that if the amplitude of fluctuations of protein content in grain under the influence of varieties, agrarian and technical measures varies from 9 to 14%, and under the influence of weather and climatic conditions varies from 9 to 24%. As grain protein is considerably dependent on the weather and climatic conditions (Chapman et al., 2012), maximum attention should be paid to this area of research. At the same time, we state that the inability to manage weather conditions necessitates their imitation. Changes in physiological and biochemical processes similar to the natural ones would take place in the plant under such imitation.

The problem of the impact of the temperature factor, precipitation and the combination of their influence of the winter wheat generative period on grain protein content remains to be fully clarified. The search for effective ways to decrease this effect on winter wheat plants and their ability to form high protein grain in the offspring without additional costs for its production is also of high priority.

The research results of foreign and Ukrainian authors indicate that improve the quality of wheat grain due to weather conditions is an actual problem today. Following issues (confirmed or disproved hypotheses) need to discovering:

1) will the ‘encoded information’ in seed (the amount of protein substances), formed in the arid, wet or optimal conditions, affect the formation of quality indicators of grain in the offspring?

2) is it possible to influence the offspring and to increase the protein content in it by selecting a certain fraction of the seed material?

Thus, the aim of the research is to clarify the physiological and biochemical processes in the plant organism that occur in the optimal and stressful conditions, as well as to search for anthropogenic methods of their manifestation in connection with the protein content in grain

MATERIALS AND METHODS

To study the response of winter wheat varieties of different origin to the weather conditions during the period of seed filling and formation on the variability of protein content in the obtained products (grain), we have conducted the relevant investigations.

The experiment was carried out in the fields of the training and experimental farm of the Poltava State Agrarian Academy, which by territorial distribution belongs to the central part of the Forest-Steppe of Ukraine. The arable soil layer has the following agrochemical characteristics (Table 1).

Table 1. Characteristics of the soil conditions of the experimental field

Soil type	Typical podzolic black soil
Humus content	3.07–3.23%
Moving phosphorus content	10 mg per 100 gram of soil
Exchangeable potassium content	13 mg per 100 gram of soil
Degree of soil saturation with substrates	84–87%
pH (salt)	6.8–7.1
Hydrolytic acidity	4.37–9.9 mg eqv^{-1}

The weather conditions were contrasting during the investigation. Deviations from a norm (average long-term indicators) of both air temperature and precipitation were fixed. These indicators were uneven at the stages of winter wheat organogenesis, especially during the period of formation and filling of winter wheat grain (Figs 1–2).

Agricultural techniques of winter wheat cultivation combined step-by-step implementation of agrarian measures: basic (disking, plowing, 3 autumn cultivations), fertilizing with 30 kg ha^{-1} N, 60 kg ha^{-1} P, 60 kg ha^{-1} K (autumn plowing) and sowing taking into account the sowing qualities of seed (at the rate of 4.5 million seeds per 1 ha and taking into account the experiment factors), fertilizing with KAC (urea-ammonia mixture) in period of restoration of spring vegetation, harvesting (full grain ripening).

The experiment is multifactorial and combines two stages. The variants in the experiment were laid out by a randomized method in a fourfold repetition. The accounting area of the plot is 50 m^2.

The scheme of multifactorial experiment included the following factors (Fig. 3):

– factor A – the conditions in which winter wheat seed was formed at the stage 71–77 according to BBCH codes: A.1 – optimal (HTC is about 1.0), A.2 – arid (HTC < 1.0), A.3 –wet (HTC > 1.0);

– factor B – winter wheat varieties: B.1 – ‘Chyhyrynka’ (Ukrainian plant breeding) and B.2 – ‘Kubus’ (foreign plant breeding);

– factor C – size of seed material: C.1 – initial seed sample (control), (TKW 40.8 ± 0.5 g), C.2 – large seed (TKW 50.4 ± 0.5 g), C.3 – average seed (TKW 41.5 ± 0.3 g), C.4 – fine seed (TKW 30.6 ± 0.7 g).

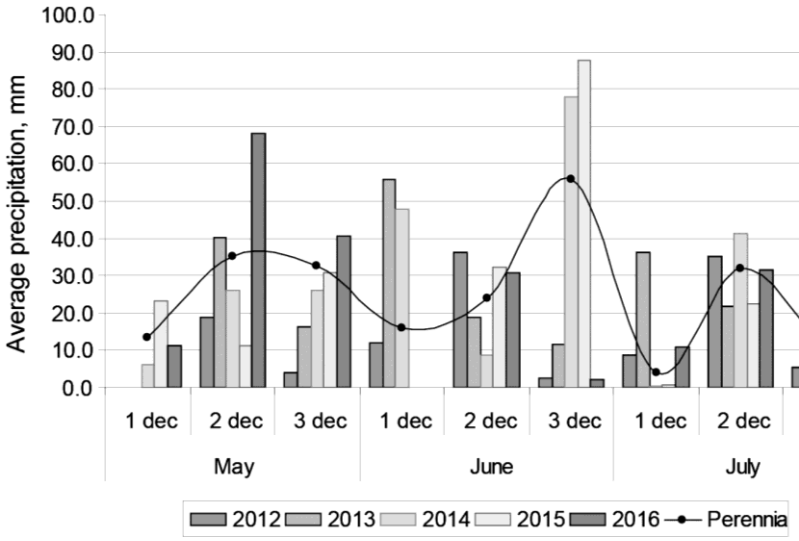

Figure 1. Weather conditions (precipitation) during spring-summer vegetation of winter wheat, 2012–2016.
Note: dec- ten day period; Perennial – average value of long-term data.

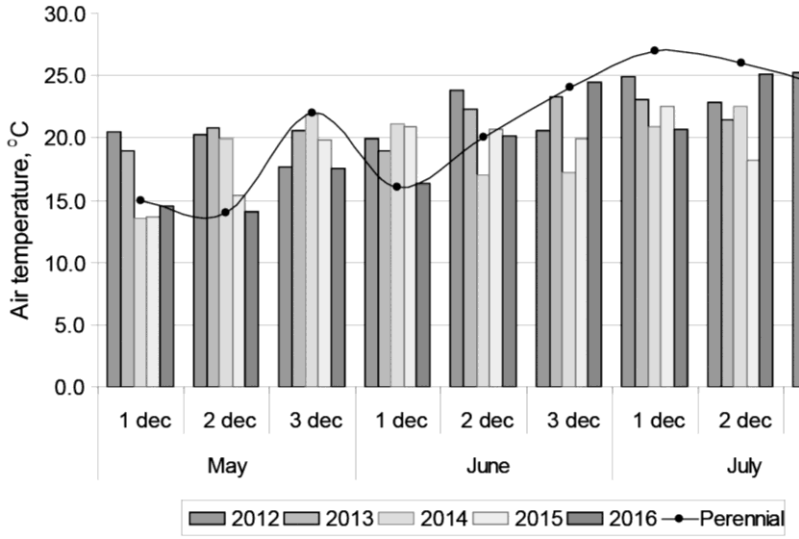

Figure 2. Weather conditions (air temperature) during spring-summer vegetation of winter wheat, 2012–2016.
Note: dec- ten day period; Perennial – average value of long-term data.

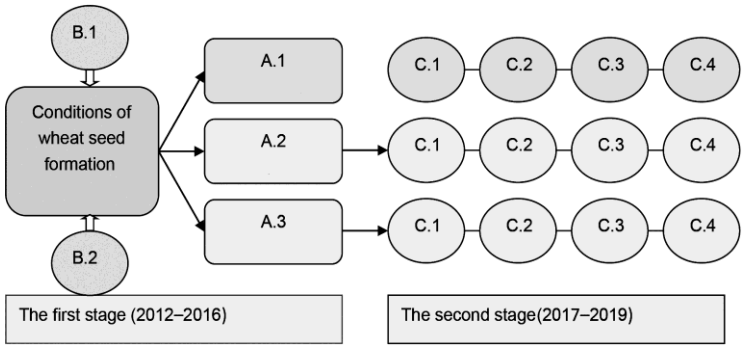

Figure 3. Stages of researches.
Note: B.1 – variety 'Chyhyrynka', B.2 – variety 'Kubus'; A.1, A.2, A.3 – conditions of seed cultivation; C.1 – initial seed sample (control), C.2 – large seed, C.3 – average seed, C.4 – fine seed.

Analyses and accountings during vegetation period were performed according to the generally-accepted methods (Tekrony, 2006; Tkachyk, 2014).

Hydrothermal coefficient (HTC) was determined by the formula that reflects both temperature factor and precipitation during the certain period (period of grain formation and filling). Hydrothermal coefficient (HTC), precipitation and the air temperature **(**above +10) were calculated by the following relation:

$$HTC = \Sigma R \times 10 / \Sigma t,$$

where R – is the sum of precipitation (mm) during the period; t – the sum of average daily temperatures °C during the same period; 10 – coefficient.

The given condition, if HTC < 0.4 – very strong drought, HTC from 0.4 to 0.5 – strong drought, HTC from 0.6 to 0.7 – medium drought, HTC from 0.8 to 0.9 – weak drought, HTC from 1.0 to 1.5 – sufficiently wet conditions, HTC > 1.5 – excessively wet conditions.

Yield was calculated on each plot of land, weighing grain from each variant by repetitions. Protein content in wheat grain was determined according to Kjeldahl method (by Kjeldahl digestion) (Kjeldahl, 1983).

The research results were calculated by the dispersion analysis (ANOVA and MANOVA) in order to define the significant differences between the variants. Fisher's LSD test ($p < 0.05$) was applied to determine the effect of weather conditions and significance assessment on the grain quality. Correlation-regression analysis using correlation coefficients (r) and trait determination (d) at significance levels ($p < 0.05$) was also applied.

RESULTS AND DISCUSSION

Effect of HTC and variety on protein content

The data on air temperature and precipitation was used in order to characterize the weather conditions of the period of grain formation and filling. HTC has been calculated for each year as well.

It has been determined that the weather conditions during the research years – in the period from jelly-like state to full grain ripening differed from each other (Table 2).

Table 2. Characteristics of the climatic factors in the period from jelly-like state to full ripening of winter wheat grain

Research year	Period duration, days	Sum of active air temperatures, °C		Sum of precipitation, mm		HTC
		average	deviance from a norm	average	deviance from a norm	
2012	24.0	68.4	-8.7	8.6	+ 14.6	1.3
2013	28.0	67.8	-9.3	36.4	+ 32.4	5.4
2014	22.0	60.6	-16.5	1.3	- 3.7	0.2
2015	23.0	60.5	-16.4	0.8	- 3.2	0.1
2016	25.0	70.3	-6.8	10.9	+ 6.9	1.6
Norm (average annual value)	-	77.0	-	4.0	-	-

It has been determined that the duration of the period of winter wheat seed formation and filling is longer, if HTC is lower, and vice versa.

The period of seed formation and filling in 2012 was at the average daily air temperature of 22.8 °C, which is 2.9 °C below the average annual temperature. The effective temperature sum was 68.4 °C. The period was characterized by precipitation at the level of 18.6 mm, while the average annual precipitation was 4.0 mm. The hydrothermal coefficient was 1.3, indicating the sufficiently wet conditions of this period. Excessively wet conditions were formed during the winter wheat seed formation in 2013: the temperature factor was below the norm by 3.1 °C, and the precipitation was excessive – more than the norm by 32.4 mm, the HTC was at a level of 5.4. During 2014 and 2015, the average daily air temperature raised from 17.0–20.7 (jelly-like state of grain) to 22.5–22.7 °C (waxy grain ripening) while precipitation decreased by 3.2–3.7 mm compared to the norm.

The average daily air temperature in 2016 during the period of grain filling and formation was almost at the level of norm, and precipitation is higher by 6.9 than HTC – at the level of 1.6.

Therefore, the results of observations described the periods of wheat grain formation and filling in the conditions of 2012 and 2016 as the sufficiently wet conditions, 2014 and 2015 as very arid, and 2013 as excessively moist.

Weather conditions significantly affected the protein content in winter wheat grain of the studied varieties (Table 3). That is why, the conditions of the period of grain formation and filling have been distinguished as follows: close to the optimal (2012 and 2016), arid (2014 and 2015), and wet (2013). This made it possible to fairly analyze their effect on the accumulation of protein content in winter wheat grain, grain and protein yield, which subsequently served as a seed material for the second stage of research.

High precipitation during the period of seed formation and ripening and low average daily air temperature in 2013 reduced the protein content in winter wheat grain of the studied varieties. The protein content was lower in grain, which was formed in the conditions close to optimal (2012 and 2016). The best quality of grain was provided by winter wheat varieties in 2014 and 2015 in arid and stressful conditions during the period of grain formation and filling.

Table 3. Winter wheat yield and Protein content in grain of 'Chyhyrynka' and 'Kubus' varieties, 2012–2016

Conditions of seed formation (Factor A)	Varieties (Factor B)	Protein content in grain, %	Grain yield, kg ha^{-1}	Protein yield, kg ha^{-1}
Optimal	Chyhyrynka	13.0* ^{a}	4,400.0* ^{a}	572.0* ^{a}
	Kubus	13.4* ^{b}	4,800.0* ^{b}	643.2* ^{b}
Dry	Chyhyrynka	13.9* ^{a}	3,900.0* ^{a}	542.1* ^{a}
	Kubus	14.0* ^{b}	4,100.0* ^{b}	569.9* ^{b}
Wet	Chyhyrynka	12.7* ^{a}	4,500.0* ^{a}	571.5* ^{a}
	Kubus	13.2* ^{b}	4,900.0* ^{b}	646.8* ^{b}

MANOVA: Factor A *; Factor B ^{ab}. Different letters indicate significant differences. Significant effects: $p < 0.05$ (*). Same letters indicate that no significant differences were found.

On the basis of correlation-regression analysis, a similar effect of weather conditions on the HTC index of the period of grain formation and filling on the protein content in winter wheat grain, irrespective of the origin of the varieties, has been determined (Fig. 4).

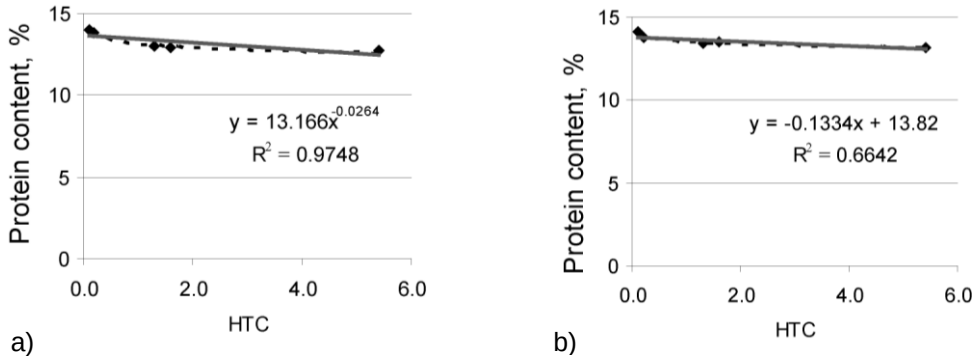

Figure 4. Dependence (according to the coefficient of approximation of traits) between protein content in grain of winter wheat variety 'Chyhyrynka' (a) and variety 'Kubus' (b) and HTC of the period of seed formation and ripening, 2012–2016.

The strong correlation was observed ($R^2 = 0.97$) during the interaction of HTC (period of grain formation and filling) and protein content in winter wheat grain of variety 'Chyhyrynka'. The variety 'Kubus' shows a similar dependence: in dry years of the period of grain formation and filling at HTC, the protein content increases in the dry season, these indicators have a correlation of mean force was observed $R^2 = 0.66$.

Our researches are consistent with the data obtained by the authors (Linana & Ruza, 2015). They found the following peculiarity: if during the period of grain ripening, warm weather with the lowest precipitation is observed, wheat accumulates more protein. The amount and quality of gluten was mostly affected by the weather conditions of the research year, but the variety also slightly affected the variability of the grain protein content (Linina & Ruza, 2015).

Other studies of these authors (Linina & Ruza, 2018) determined the impact of nitrogen application and growing technology on the yield and found a medium strong positive correlation between HTC in the period from the formation to the ripening of winter wheat grain.

Petrenko et al., 2017 found out that wheat grain, grown by the intensive farming system, had better quality than other variants of the experiment. In some experimental years, weather conditions played an important role in the formation of baking properties, as well as the efficiency of plant nutrition and protection was noted.

In the following experiment, the authors (Mäkinena et al., 2018) evaluated the sensitivity of European wheat yields to the extreme weather phenomena connected with the sowing phenology while testing varieties across Europe (latitude from 37.21 °C to 61.34 °C and longitude from 6.02 °C to 26.24 °C) in the period of 1991–2014. All observed agro-climatic extremes (≥ 31 ° C, ≥ 35 °C, or drought from ear formation to seed ripeness; excessive precipitation; heavy precipitation and low global radiation) resulted in significant yield losses of the studied European varieties. There were no European wheat varieties that responded positively to drought after sowing at + 10 °C or to low temperatures in winter (in the range of −15 °C and −20 °C). These data correspond to our investigations, carried out in the conditions of the central Forest-Steppe of Ukraine.

Effect of seed formation and fraction of seed material on protein content and yield

The second stage of the research involved the study of influence of the conditions of seed formation and its size on the protein content in grain of the new winter wheat yield (Table 4, 5).

Table 4. Winter wheat yield and Protein content in grain of variety 'Chyhyrynka' in relation to the period of seed formation and ripening and its size, 2017–2019

Conditions of seed formation (Factor A)	Seed fraction (Factor C)	Protein content in grain, %	Grain yield, kg ha^{-1}	Protein yield, kg ha^{-1}
Optimal	control	13.7	3,800.0	520.6
	large	13.4	4,200.0	562.8
	average	13.8	4,400.0	607.2
	fine	14.1	4,900.0	690.9
Dry	control	13.6	3,900.0	530.4
	large	13.8	4,400.0	607.2
	average	14.2	4,500.0	639.0
	fine	14.5	5,000.0	725.0
Wet	control	13.2	5,400.0	712.8
	large	13.0	5,700.0	741.0
	average	13.3	6,200.0	824.6
	fine	13.7	5,900.0	808.3
$LSD_{0.95}$(Factor A)		0.06	11.3	12.9
$LSD_{0.95}$(Factor C)		0.04	75.4	6.5
$LSD_{0.95}$(Factor A and C)		0.08	8.1	7.8

*Note – The obtained differences between the variants of winter wheat variety 'Chyhyrynka' are confirmed by the mathematical analysis MANOVA.

Table 5. Winter wheat yield and protein content in grain of variety 'Kubus' in relation to the period of seed formation and ripening and its size, 2017–2019

Conditions of seed formation (Factor A)	Seed fraction (Factor C)	Protein content in grain, %	Grain yield, kg ha^{-1}	Protein yield, kg ha^{-1}
Optimal	control	13.8	4,700.0	648.6
	large	13.6	5,000.0	680.0
	average	14.1	5,200.0	733.2
	fine	14.3	5,900.0	843.7
Dry	control	13.9	4,800.0	667.2
	large	14.2	5,300.0	752.6
	average	14.6	6,100.0	890.6
	fine	14.8	6,400.0	947.2
Wet	control	13.3	5,100.0	678.3
	large	13.5	5,300.0	715.5
	average	13.8	5,900.0	814.2
	fine	13.6	5,600.0	761.6
$LSD_{0.95}$(Factor A)		0.04	108.2	13.4
$LSD_{0.95}$(Factor C)		0.02	71.3	7.5
$LSD_{0.95}$(Factor A and C)		0.05	80.4	8.9

**Note* – The obtained differences between the variants of winter wheat variety 'Chyhyrynka' are confirmed by the mathematical analysis MANOVA.

It has been found that the protein content in winter wheat grain of variety 'Chyhyrynka' varied in the range of 13.0 to 14.5%, grain yield varied from 3,800 to 6,200 kg ha^{-1}, protein yield varied from 520.6 to 824.6 kg ha^{-1} depending on the studied factors. The lowest protein content in winter wheat grain was formed during sowing with large seed: in the range of 13.0 to 13.8%, protein yield –520.6; 530.4 and 712.8 kg ha^{-1}. Index of protein yield depending on grain yield also.

Variety 'Chyhyrynk' a provided the highest protein content in winter wheat of the new yield by sowing fine seed, obtained in the optimal conditions (14.1%) and arid conditions (14.5%). The shallow fraction of seed, obtained in the wet years, although increases the protein content in winter wheat grain, but this index was greatly lower (< 14.0%) compared to grain, formed during the optimal and dry years. In research years increase in protein yield was formed during sowing with small seeds fraction, except wet conditions where increase in protein yield was formed during sowing with average seeds fraction.

Protein content in winter wheat grain of variety 'Kubus' varied in the range of 13.1 to 14.8% depending on the studied factors. The lowest protein content in grain was formed during sowing with large seed: in the range of 13.5 to 13.9%. Protein yield from 843.7–947.2 kg ha^{-1} was formed during sowing with small seeds fraction, except wet conditions of seeds forming where protein yield (814.2 kg ha^{-1}) was formed during sowing with average seeds fraction (Table 5).

Winter wheat variety 'Kubus' provided the highest protein content in grain due to sowing with fine seed that was formed under the optimal conditions (14.3%) and the arid conditions (14.8%). Compared to the control and other variants, the shallow fraction of seed, obtained in wet years, did not increase the protein content in winter wheat grain and protein yield.

Graphs 3-D show and confirm the connection between the conditions of the period of seed formation and filling, its size and protein content (Fig. 5).

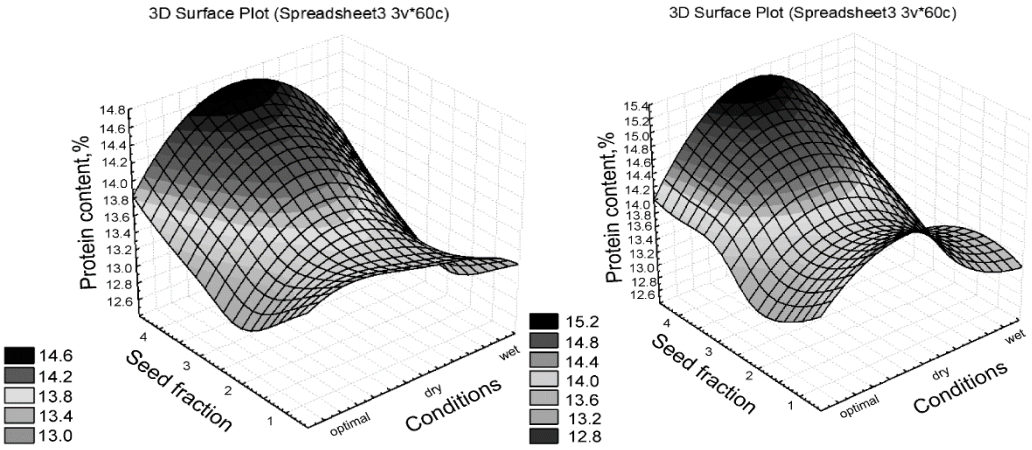

Note: C.1 is the initial sample of winter wheat seed (control), C.2 is the large winter wheat seed, C.3 is the average winter wheat seed, C.4 is the fine winter wheat seed.

Figure 5. Connection between the seed growing conditions, its size and protein content in grain of wheat varieties: a – variety 'Chyhyrynka', b – variety 'Kubus', 2017–2019.

While establishing a correlation between protein content and seed size, it has been determined that these indicators are interdependent at r = 0.59 for winter wheat variety 'Chyhyrynka' and r = 0.53 for variety 'Kubus'.

Our researches correspond with the findings of scientists (Savill et al., 2018) who have developed a new method of analysis for the quantitative assessment of both protein concentration gradients and protein body size distribution in wheat plants endosperm. The plants were grown at two different temperatures (20.0 °C or 28.0 °C) during the period of seed formation and filling. It has been determined that the protein content of wheat grain also varies depending on the fertilizing options: high or low nitrogen content. The authors of the publication found out that increased temperatures of the period of generative development of wheat at the background of high nitrogen supply increases the protein content of grain. This feature can also be used in the plant breeding process (Pereira & Coimbra, 2019).

The results of field experiments by other scientists (Popko at al., 2018) showed that the application of amino acid-based products had an effect on growth of the grain yield of winter wheat (5.4% and 11%, respectively, when using AminoPrim at a dose of 1.0 L ha^{-1} and AminoHort at a dose 1.25 L ha^{-1}) in comparison with the control group (without biostimulant). Laboratory trials have shown the improvement of such technological characteristics of winter wheat grain, as ash content, Zeleny sedimentation index and protein content. This is in line with the perspectives of our further investigations, which will aim at the determination of the effect of weather conditions and foliar nutrition with chelate preparations in the different phases of winter wheat growth and development on its yield and grain quality. The study of the complex effect

of weather conditions and agrarian measures of cultivation in connection with the size of winter wheat seed and protein content is also envisaged.

CONCLUSIONS

1. The nature of the physiological mechanism and the biochemical essence of the protein content in winter wheat grain under the influence of weather factors have been discovered on the basis of intellectual search and experimental studies. Dependencies have been established: stressful conditions of wheat cultivation at high air temperature and low-effective precipitation during the period of grain formation and filling increase the protein content in it, and vice versa.

2. The tendency of impact of temperature and precipitation of the period of seed formation and filling in winter wheat maternal plants on quality of the obtained grain has been determined. It has been found out that the highest protein content in grain of the studied winter wheat varieties was observed at the low hydrothermal coefficient (< 0.5). The correlation between protein content in grain and HTC of the period of seed formation and ripening of winter wheat variety $R^2 = 0.97$ for variety 'Chyhyrynka' and $R^2 = 0.66$ for variety 'Kubus'.

3. The variability of protein content in winter wheat grain was determined depending on the formation conditions and in relation to the size of seed fraction of the offspring. When sowing larger seed, the protein content in obtained grain of variety 'Chyhyrynka' will be lower by 0.6–0.7% and protein content of variety 'Kubus' will be lower by 0.6–0.8%, compared to the sowing of fine seed. The correlation between grain protein content and seed size has been confirmed at $r = 0.59$ for variety 'Chyhyrynka' and $r = 0.53$ for variety 'Kubus'. It is established that sowing with medium and small seeds fraction obtained in optimal and dry conditions allows to increase grain yield, protein content and yield at the same time. Small seeds obtained in humid conditions do not increase grain and protein yield. This regularity is established for both varieties.

REFERENCES

Allen, M.R. & Ingram, W.J. 2002. Constraints on future changes in climate and the hydrologic cycle. *Nature* **419**, 224–232. https://doi. org/10.1038/nature01092

Almeselmani, M, Deshmukh, P.S. & Chinnusamy, V. 2012. Effect of prolonged high temperature stress on respiration, photosynthesis and gene expression in wheat (*Triticum aestivum* L.) varieties differing in their thermotolerance. *Plant Stress* **6**, 25–32. http://www.globalsciencebooks.info/Online/GSBOnline/images/2012/PS_6(1)/PS_6(1)25-32o.pdf

Almeselmani, M., Deshmukh, P.S. & Sairam, R.K. 2009. High temperature stress tolerance in wheat genotypes: Role of antioxidant defence enzymes. *Acta Agronomica Hungarica* **57**, 1–14. doi: 10.1556/AAgr.57.2009.1.1

Argentel-Martínez, L., Garatuza-Payán, J., Arredondo, T. & Yépez, E.A. 2019. Effects of experimental warming on peroxidase, nitrate reductase and glutamine synthetase activities in wheat. *Agronomy Research* **17**(1), 22–32. https://doi.org/10.15159/AR.19.003

Asseng, S., Ewert, F., Martre, P., Rötter, R.P., Lobell, D.B., Cammarano, D. & Zhu, Y. 2015. Rising temperatures reduce global wheat production. *Nature Climate Change* **5**, 143–147. https://doi.org/10. 1038/nclimate2470

Asseng, S., Martre, P., Maiorano, A., O'Leary, G.J., Fitzgeraldat, G.J., Girousse, C., Motzo, R., Giunta, F., Babar, M. Ali, Reynolds, M.P., Kheir, A.M.S., Thorburn, P.J., Waha, K., Ruane, A.C., Aggarwal, P.K., Ahmed, M., Balkovič, J., Basso, B., Biernath, C., Bindi, M., Cammarano, D., Challinor, A. J., Sanctis, G., Dumont, B., Rezaei, E.E., Fereres, E., Ferrise, R., Garcia-Vila, M., Gayler, S., Gao, Y., Horan, H., Hoogenboom, G., Izaurralde, R.C., Jabloun, M., Jones, C.D., Kassie, B.T., Kersebaum, K., Klein, C., Koehler, A.-K., Minoli, L.S., Montesino, M., Martin, S., Müller, C., Naresh, S., Claas, K., Jørgen, N., Olesen, E., Palosuo, T., Porter, J.R., Priesack, E., Ripoche, D., Semenov, M.A,. Stöckle, C., Stratonovitch, P., Streck, T., Supit, I., Tao, F., Van der Velde, M., Wallach, D., Wang, E., Webber, H., Wolf, J., Xiao, L., Zhang, Z., Zhao, Z., Zhu, Y., Ewert, F. 2018. Climate change impact and adaptation for wheat protein. *Global Change Biology* **25(**1), 155–173. doi: 10.1111/gcb.14481

Barabolia, O.V., Barat, Yu.M., Kyluk, M.I. & Onoprienko, O.V. 2018. Crop capacity of winter wheat depending on system and weather condition of a vegetation period. *Bulletin of Uman National University of Horticulture* **2**, 3–9. doi: 10.31395/2310-0478-2018-21-3-9

Central Statistical Bureau of Ukraine. 2020. Plant growing. Available at: http://www.ukrstat.gov.ua/operativ/operativ2006/sg/sg_rik/sg_u/rosl_u.html

Chapman, S.C., Chakraborty, S., Dreccer, M.F. & Howden, S.C. 2012. Plant adaptation to climate changeopportunities and priorities in breeding. *Crop and Pasture Science* **63(**3), 251–268. https://doi.org/10.1071/CP11303

D'Amico, S., Müller, U. & Berghofer, E. 2013. Effect of hydrolysis and denaturation of wheat gluten on adhesive bond strength of wood joints. *Journal of Applied Polymer Science* **129**(5), 2429–2434. doi: 10.1002/app.38686

Dupont, F.M., Hurkman, W.J., Vensel, W.H., Tanaka, C., Kothari, K.M., Chung, O.K. & Altenbach, S.B. 2006. Protein accumulation and composition in wheat grains: Effects of mineral nutrients and high temperature. *European Journal of Agronomy* **25(**2), 96–107. doi: 10.1016/j.eja.2006.04.003

Falcone, G., Stillitano, T., Montemurro, F., De Luca, A.I., Gulisano, G. & Strano, A. 2019. Environmental and economic assessment of sustainability in Mediterranean wheat production. *Agronomy Research* **17**(1), 60–76. https://doi.org/10.15159/AR.19.011

Ferris, R, Ellis, R.H., Wheeler, T.R. & Hadley, P. 1998. Effect of high temperature stress at anthesis on grain yield and biomass of field-grown crops of wheat. *Annals of Botany* **82**, 631–639. https://doi.org/10.1006/anbo.1998.0740

Iqbal, M., Raja, N.I., Yasmeen, F., Hussain, M., Ejaz, M. & Shah, M.A. 2017. Impacts of heat stress on wheat: a critical review. *Advances in Crop Science and Technology* **5**, 251–259. doi:10.4172/2329-8863.1000251

Kjeldahl, J. 1983. Neue Methode zur Bestimmung des Stickstoffs in organischen Körpern (New method for the determination of nitrogen in organic substances). *Zeitschrift für analytische Chemie* **22**(1), 366–383.

Linina, A. & Ruza, A. 2015. Weather conditions effect on fresh and stored winter wheat grain gluten quantity and quality. 25th Congress. Nordic view to sustainable rural development June 16–18,52015,5148–153. https://llufb.llu.lv/conference/NJF/NJF_2015_Proceedings_Latvia-148-153.pdf

Linina, A. & Ruza, A. 2018 The influence of cultivar, weather conditions and nitrogen fertilizer on winter wheat grain yield. *Agronomy Research* **16(**1), 147–156. https://doi.org/10.15159/AR.18.034

Mäkinena, H., Kasevab, J., Trnka, M., Balekcd, J., Kersebaumat, K.C., Nendele, C., Gobin, A., Olesen, J.E., Bindi, M., Ferrise, Moriondo, R.M., Rodríguez, A., Ruiz-Ramos, M., Takáč, J., Bezák, P., Ventrella, D., Ruget, F., Capellades, G. & Kahiluoto, H. 2018. Sensitivity of European wheat to extreme weather. *Field Crops Research* **222**(1), 209–217 https://doi.org/10.1016/j.fcr.2017.11.008

Marenych, M.M., Hanhur, V.V., Len, O.I., Hangur, Yu.M., Zhornyk, I.I. & Kalinichenko, A.V. 2019. The efficiency of humic growth stimulators in pre-sowing seed treatment and foliar additional fertilizing of sown areas of grain and industrial crops. *Agronomy Research* **17**(1), 194–205. https://doi.org/10.15159/AR.19.023

Mazurenko, B., Kalenska, S., Honchar, L. & Novytska, N. 2020. Grain yield response of facultative and winter triticale for late autumn sowing in different weather conditions. *Agronomy Research* **18**(1), 183–193. https://doi.org/10.15159/AR.20.008

Mondal, S., Singh, R.P., Crossa, J., Huerta-Espino, J., Sharma, I., Chatrath, R., Singh, G.P., Sohu, V.S., Mavi, G.S., Sukaru, V.S.P., Kalappanavarg, I.K., Mishra, V.K., Hussain, M., Gautam, N.R., Uddin, J., Barma, N.C.D., Hakim, A. & Joshi, A.K. 2013. Earliness in wheat: a key to adaptation under terminal and continual high temperature stress in south Asia. *Field Crops Research* **15**, 19–26. doi: 10.1016/j.fcr.2013.06.015

Narayanan, S. 2018. Effects of high temperature stress and traits associated with tolerance in wheat. *Open Access J Sci*. **2**(3), 177–186. doi: 10.15406/oajs.2018.02.00067

Pandey, G.C, Mehta, G., Sharma, P. & Sharma, V. 2019. Terminal heat tolerance in wheat: An overview. *Journal of Cereal Research* **11**(1), 1–16. doi. org/10.25174/2249-4065/2019/79252

Pereira, A.M. & Coimbra, S. 2019. Advances in plant reproduction: from gametes to seeds. J*ournal of Experimental Botany* **70**(11), 2933–2936. https://doi.org/10.1093/jxb/erz227

Petrenko, V., Liubich, V. & Bondar, V. 2017. Baking quality of wheat grain as influenced by agriculture systems, weather and storing conditions. *Romanian agricultural research* **34**, 69–76. https://www.incda-fundulea.ro/rar/nr34/rar34.9.pdf

Popko, M., Michalak, I., Wilk, R., Gramza, M., Chojnacka, K. & Górecki, H. 2018. Effect of the new plant growth biostimulants based on amino acids on yield and grain quality of winter wheat. *Molecules* **23**(2), 470 https://doi.org/10.3390/molecules23020470

Ruiz-Ramos, M., Ferrise, R., Rodríguez, A., Lorite, I.J., Bindi, M., Carter, T.C. & Rotter, R.P. 2017. Adaptation response surfaces for managing wheat under perturbed climate and CO2 in a Mediterranean environment. *Agricultural Systems* **159**, 260–274. doi:10.1016/j.agsy.2017.01.009

Savill, G.P., Michalski, A., Powers, S.J., Wan, Y., Tosi, P., Buchner, P. & Hawkesford, M.J. 2018. Temperature and nitrogen supply interact to determine protein distribution gradients in the wheat grain endosperm. J*ournal of Experimental Botany* **69**(12), 3117–3126. doi:10.1093/jxb/ery127

Sidorenko, A.V. & Kulik, M.I. 2007. The process of increasing the technologically qualitative indicators of the reproductive organs of agricultural crops // Patent of Ukraine No. 25516, class AO1 G7 /, publ.10.08.07. Bul. No. 12.

Tekrony, D.M. 2006. Seeds: the delivery system for crop science. *Crop Science* **3**, 467–472. https://doi.org/10.2135/cropsci2005.12.0445

Tkachyk, S.O. 2014. *Method for grain, cereal and leguminous varieties VCU expert examination in Ukraine. (Metodyka provedennia ekspertyzy sortiv roslyn hrupy zernovykh, krupianykh ta zernobobovykh na prydatnist do poshyrennia v Ukraine (PSP))*. Kyiv: Nilan-LTD. (in Ukrainian)

Tripathi, A., Tripathi, D.K., Chauhan, D.K., Kumar, N. & Singh, G.S. 2016. Paradigms of climate change impacts on some major food sources of the world: a review on current knowledge and future prospect. *Agriculture, Ecosystems and Environment* **216**, 356–373. doi: 10.1016/j.agee.2015.09.034

Zhemela, G., Sydorenko, A. & Kulyk, M. 2007. The part of weather factors in the process of crop capacity formation and improvement of quality of winter wheat grain. *Poltava State Agrarian Academy Journal* **2**, 10–16. (in Ukrainian).

Agronomy Research **18**(3), 2117–2126, 2020
https://doi.org/10.15159/AR.20.191

Feasibility study of the grinding process of grain materials

A. Lebedev, R. Iskenderov*, Y. Zhevora, P. Lebedev, N. Marin, R. Pavlyuk and A. Zaharin

Federal State Budgetary Educational Institution of Higher Education 'Stavropol State Agrarian University', Faculty of Agricultural Mechanization, Department of Technical Service, Standardization and Metrology, 12 Zootechnicheskiy Ln, RU355017 Stavropol, Russia
*Correspondence: iskenderov_ramil@inbox.ru

Abstract. For a comparative assessment of the effectiveness of various types of grinders of grain materials, various approaches are used. As the main criterion, the correspondence of the crushed material according to the particle size distribution can be taken as an indicator of the reliability of the grinding process. A comparative assessment of rotary crushers is carried out using the technical and economic indicator E_g, which is the ratio of total costs to the implementation of a given amount of work. Under the reliability of the grinding process, we have accepted the condition that the particle size distribution will comply with the requirements for agricultural feeding animals, which is possible while maintaining a rational gap between the stator and rotor riffles. The contradiction manufacturing techniques for the experiment are divided into: option No. 1 – steel 3 (HRC 10–12), option No. 2 – steel 45 (HRC 15–17), option No. 3 – hardened steel 45 (HRC 45–50), option No. 4 – steel 45 hardened and having a thin-film coating of FPH (finish plasma hardening), microhardness of 13 GPa. If reliability of the grinding process equal to 80%, wear on the fourth option, the cost was 1,171 rubles per ton, which is 16% lower than the cost of the first version of the production of a rotor crusher equal to 1,405 rubles per ton, respectively, this all speaks of the possible use of the proposed options for various forms of ownership of agricultural enterprises.

Key words: grain crushing, rotary crusher, working clearance, finished product quality, reliability of the grinding process, cutting element, wear resistance, feasibility.

INTRODUCTION

One of the main operations of preparing feed for feeding is the grinding of grain materials. Its implementation accounts for up to 75% of energy and 45% of labor costs. High quality and aligned size distribution of the crushed grain material are providing increase animal productivity and are the criteria it evaluating the performance of grinding devices (Lebedev et al., 2016).

Currently, hammer and impact centrifugal crushers are widely used in feed preparation lines, but during their operation, the content of the dust fraction increases to 30% with fine grinding, and under-crushed to 20% with coarse (Lebedev et al., 2012; Iskenderov et al., 2018).

The practice of operating hammer crushers has shown that there is a problem of excessive wear of the working bodies and low quality grinding of grain material, which decreases significantly with increasing humidity. The hammers of feed crusher have a minimum resource (their service life is from 72 to 300 hours). Resource of other working bodies is up to 2 times higher. However, this trend leads to the need for about 50 maintenance services per year. The data of the experiment we conducted in the agricultural production cooperative 'Kazminsky' in the Stavropol Territory, Russian Federation on the DM-10 hammer crusher are shown in Fig. 1. New sieve and hammers were installed on the it. Tests were carried out during the 35 days (every week 5 kg of crushed seed were selected). The weekly threshing was about 300 tons (Lebedev et al., 2012).

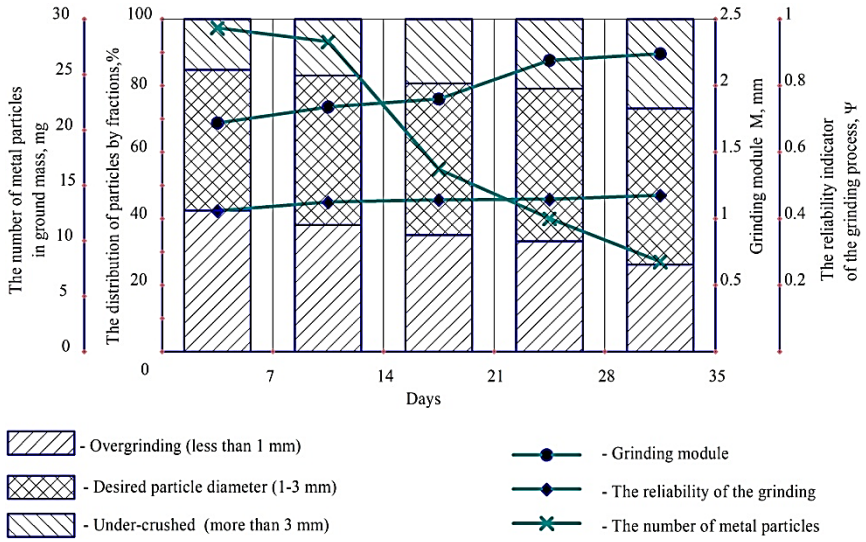

Figure 1. Experimentally determined indicators of grinding crushers DM-10.

As can be seen in the graph of Fig. 1, the average particle size in the first period of operation was 1.72 mm for a given grinding module M = 1.8–2.6 mm, i.e. the finished product contained more fine particles. Subsequently, an increase in the average particle size was observed. At the beginning of operation of the crusher the fraction of overgrinding was 42.4%, under-crushed 15.2%, at the end 26.2%, and 26.8%, respectively. This is due to the wear of sieve and hammers, which lost an average of 4.5 kg from the initial mass of 24.7 kg. For the entire experiment, the amount of ground mass corresponding to a given grinding module did not exceed 47%. And although the average particle size was in the specified range, in fact, only half of the feed mixture met the zootechnical requirements (Lebedev et al., 2012).

Thus, with the wear of the working bodies of the crusher, the degree of grinding of the starting material will also change. But the studies of grinders are mainly aimed at improving the structural and technological schemes of grinding, determining the optimal design or modes of its operation. Moreover, the analysis shows that the development of issues of increasing the durability of the working bodies of shredders is currently gaining particular importance.

In addition to everything, the question more often arises of the appropriateness of using and manufacturing hammer crushers, and way of replacing them with more modern designs that provide the best indicators with high-quality grinding (Sabirov et al., 2018; Thomas et al., 2018), for example, horizontal rotor crushers (Patent EA 026179, 2017).

The development of new and modernization of existing designs of crushers to provide animals with high-quality feeds is becoming an increasingly popular and urgent task against the backdrop of an annual increase in food prices. At the same time, there is a need to create new, more informative methods for evaluating grinding, both from the qualitative and the technical and economic aspects of this important technological process (Lebedev et al., 2011; Tumuluru et al., 2014; Sabirov et al., 2019).

MATERIALS AND METHODS

Experiments on grain refinement winter wheat were carried out on a horizontal rotary crusher produced in the training workshop of FSBEI HE 'Stavropol State Agrarian University'. The design of the crusher without changing initials parameters correspond, description in the (Lebedev et al., 2018; Iskenderov et al., 2019) and shown in Fig. 2.

Clarification of rational technical and economic indicators was carried out by performing a cutting element 5 of various structural materials. To carry out the experiment were made 3 cutting element with a length of 0.06 m. Each of them (Fig. 3, a) consisted of 4 independent segments of the same size, they are put on the rod base. These segments different depending on the type of steel grade and its processing technologyare divided into: Option No. 1 – St3 (HRC 10–12), Option No. 2 – Steel 45 (HRC 15–17), Option No. 3 – Steel 45 hardened (HRC 45–50), Option No. 4 – Steel 45 hardened and having a thin-film coating of FPH (finish plasma hardening), microhardness of 13 GPa. The segments, as shown in Fig. 3, b, were marked on the back (number of the experimental group from 1 to 3) and side (number of the type of manufacturing technology from 1 to 4).

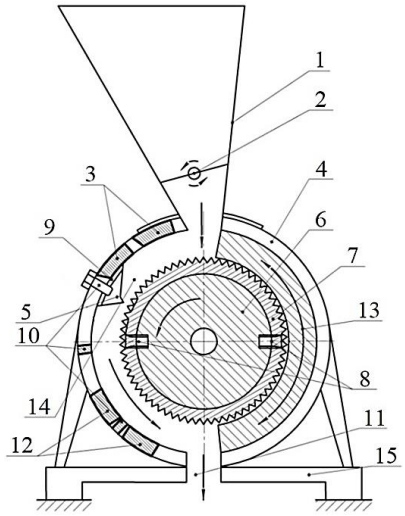

Figure 2. Scheme of a prototype rotary crusher: 1 – receiving hopper; 2 – damper; 3 – plugs in add. places of a loading window; 4 – a stator; 5 – cutting element; 6 – a rotor; 7 – a removable surface of a rotor; 8 – fastenings of a surface of a rotor; 9 – a lining for variation of a backlash; 10 – fastening and caps in add. locations of the counter-blade; 11 – discharge hopper; 12 – plugs in add. places of unloading; 13 – limiting lip; 14 – crushing chamber; 15 – frame.

The replaceable rotor surfaces of the prototype crusher were made of hardened Steel 45, with a hardness of HRC 45–50, their diameter was D = 0.1 m, and their length l = 0.06 m. The geometric parameters of the rotor riffles for grinding wheat were as

follows: the number of riffles on the rotor is 38, with a pitch of t = 8 mm and the height of the riffle h = 1.2 mm, the angle of the riffle tip is 60°, and the wall angle 15° (Fig. 3, c) (Iskenderov et al., 2018; Iskenderov et al., 2019). During operation of the rotor crusher to maximum wear, an increase in the gap occurs between the rotor and cutting element, which, with the corresponding operating time, also causes a process disruption in the form of crushed grain material that does not meet the specified quality.

a)  b)  c) 

Figure 3. General view of: the cutting element (a), markings its segments (b) and the grinding zone in a horizontal rotary crusher (c).

To determine the probability of failure-free operation of the rotary crusher, we establish the relationship between its reliable and unreliable applications. Therefore, for the subsequent evaluation of the grinding process, an indicator of the actual grinding result was used. The grinding process is reliable provided that the particle size distribution meets the specified requirements for feeding livestock and poultry. Then, as an unreliability of the process, the appearance in the finished product of non-crushed and over-crushed grain fractions was considered.

Under normal operating conditions, the rotor crusher in question does not produce more than 5% of substandard products. In this case, the detection of undestructed wheat grains occurs with a gap between the stator and the rotor having more than 0.8 mm. This is due to the wear of their working surfaces, primarily the cutting element, which perceives several times more impacts per revolution of the rotor.

One indicator of equipment reliability is the probability of uptime. Considering the grinding process, based on the theory of reliability, we take that the under-crushed grain material is a failure of the system:

$$P(g) = 1 - F(g), \quad (1)$$

where $P(g)$ – the probability of uptime; $F(g)$ – the probability of failure or the occurrence of a under-crushed grain.

Fig. 4 shows the dependence that characterizes the changes in the main characteristics of the process of grinding grain in a rotary crusher.

As can be seen in the Fig. 4, grind with the observance of the required quality (for a specific grinding module) is characterized by almost 100% process reliability, that is, up to the section with the value of W_0. With further operation of the grinder, the probability of failure increases, which is characterized by the formation on the graph of the zone with a violation of the quality of grinding. At the same time, the probability of failure-free work begins to decline.

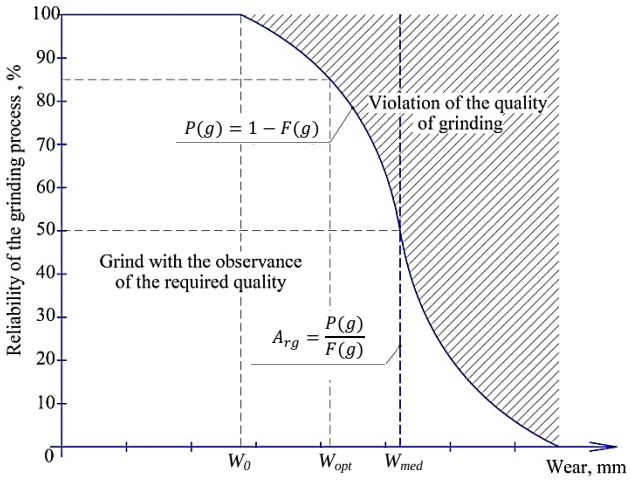

Figure 4. Theoretical probability of failure-free operation of the rotor crusher depending on the wear of the rotor and stator.

Any crusher has a state of equilibrium – the optimum reliability of the grinding process. After reaching and overcoming this boundary, operability drops and it is advisable to carry out preventive or scheduled maintenance to restore it.

Depending on the operating conditions, different requirements can be applied to the quality of grinding of the grain material, that is, a different value of the process reliability. For example, with an average level of wear of W_{med} work surfaces, which corresponds to the reliability of the grinding process of 50%, the crushed grain will contain both large fractions and very fine particles of the finished product. If their separation is carried out, the first (large) fraction can be used as feed for poultry, and small for pigs. However, often modern producers tend to use fast and productive methods of animal husbandry without intermediate feed preparation operations, as this entails additional energy and time costs.

So, the higher the reliability of the process, the more products of a given quality will be generated by the crusher, and the more preventive work will be required to maintain a given level of wear resistance of work surfaces. We take the optimal gap size for the W_{opt} rotary crusher, which meets the specified requirements for the quality of the crushed product and 85 ± 5% process reliability. For a more accurate and informative monitoring of the process reliability, we use the indicator of the actual result of the A_{rg} process (Lebedev, 2011). Using this indicator, we get:

$$A_{rg} = \frac{P(g)}{F(g)} \tag{2}$$

where A_{rg} – indicator of actual result of grinding process.

When calculating the reliability indicators of the rotor crusher, variation coefficients are used, which make it possible to choose the distribution law (normal or Weibula). The calculations were performed automatically in the MSExcel environment, based on the quality indicators obtained during operational tests of the rotary crusher.

For a comparative assessment of the effectiveness of various types of grinders of grain materials in practice, various approaches are used. A feature of our approach is the condition for an objective assessment of various types and types of grinders according to the quality of the grinding process, which is the *purpose* of these machines. Such an indicator, in our opinion, is *the reliability of the process being implemented*. The main criterion in assessing the reliability index of the grinding process is the *goal function*, that is, *the whole crushed mass must correspond in terms of particle size distribution to the given module and degree of grinding.*

A comparative assessment of rotary crusher is carried out using the technical and economic indicator E_g, which is the ratio of the total costs C_t of a predetermined space of work S_w and is determined by the formula:

$$E_g = \frac{C_t}{S_w} \tag{3}$$

The total cost of performing a given amount of work S_w can be determined by the formula:

$$C_t = C_m + C_l + C_e + C_{pw} \cdot k \tag{4}$$

where C_m – manufacturing cost; C_l – the cost of labor when grinding the mass of grain; C_e – the cost of energy consumed by grinding grain mass; C_{pw} – costs of preventive work; k – number of preventive work.

In view of the above, additional prophylaxis must be carried out upon reaching the rejection wear of the cutting element of rotor crusher W_{opt} corresponding to the reliability of the technological process 80–90%. It should take into account the additional costs, related to the elimination of the C_Δ revealed deviations in the grinding and used for additional crushing volume of products $S_{w\Delta}$ not corresponding task parameters.

Feasibility study criterion E_g cereal material grinding process at maximum wear working surfaces of the rotor and a cutting element must consider violation process and compensation additional costs for bringing the entire predetermined amount of work to the required quality. In this case, its value can be determined from the expression:

$$E_{\mathrm{g}} = \frac{\mathrm{C_t}}{S_w - S_{w\Delta}} + \frac{C_\Delta}{S_{w\Delta}} \tag{5}$$

Reducing the scope of work $S_{w\Delta}$ does not match the standards of the grinding is possible during timely preventive maintenance or by reducing wear of the cutting surface during the operation of the crusher. To calculate the basic indicators of costs, generally accepted methods of economic calculation are used to evaluate agricultural technical means. The total cost values may differ taking into account depreciation and costs different for each country and other indicators associated with the characteristics of certain industries, so we did not specifically take them into account. First of all, the feasibility study presented is aimed at identifying the possibility and profitability of increasing the reliability of the grinding process through the use of highly wear-resistant structural materials, taking into account the costs of their use.

RESULTS AND DISCUSSION

The analysis of the experimental results in Fig. 5 showed that the wear of the cutting element during running to its limit value (resource), on average, amounted to W = 1.26–1.48 mm. These data correspond to the values of wear, which are determined

in real operating conditions. When evaluating the efficiency of the grinding process according to the proposed method, the reliability indicator is $P(g)$ = 10–25%, and the actual result indicator is extremely low – A_{rg} = 0.1–0.3.

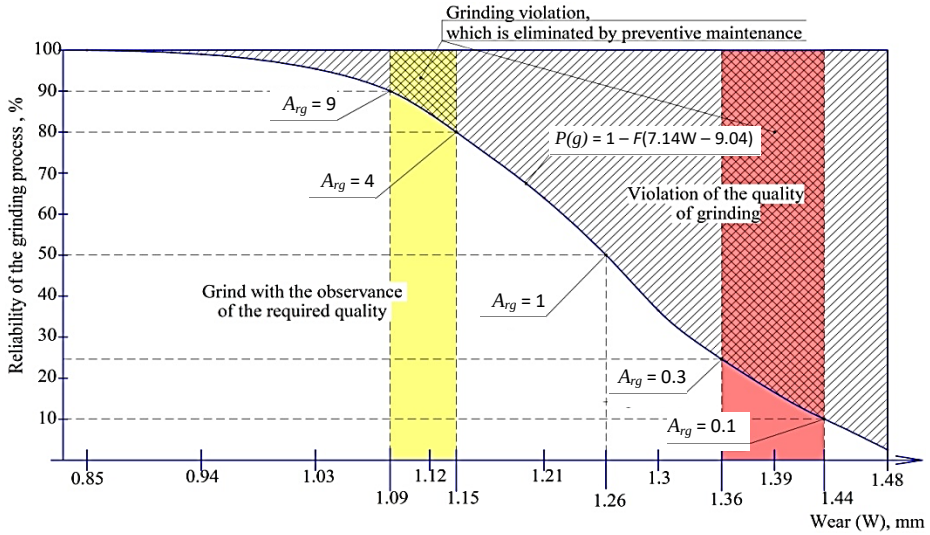

Figure 5. Dependence of reliability grinding process of grain materials wear riffles cutting element.

The obtained dependences are used to determine the amount of wear of the cutting edge (riffle) of the cutting element, which corresponds to the specified quality of grinding, according to the level of reliability of this process. So, for reliability $P(g)$ = 80–90%, the maximum allowable clearance should not exceed the range of 1.09–1.15 mm under these operating conditions.

The data obtained make it possible to build the dependences of ensuring the guaranteed grinding process on the tolerance for wear of the riffle of the cutting element, forming a gap between the working surfaces of the rotor and it. After an increase in the clearance value of more than 0.9 mm, periodically occurring failures in the loss of operation of the rotor crusher occur, consisting in a deviation of the norm of grinding of agricultural crops and the passage of full size grains. When changing the reliability of the grinding process by 10%, which corresponds to a change in the gap by 0.19 mm, out of 10 threshed tons of agricultural products, 1 ton does not meet the specified grinding requirements.

Therefore, to perform grain grinding with a process reliability of 90%, excluding disturbances in the operation of the rotary crusher, it is recommended to timely control the gap between the cutting element and the rotor at the level of 1.09 mm.

Techno-economic assessment of increasing resource rotor crusher with reference to four embodiments considered producing cutting element, for which made experiments with the grain of wheat s varieties ‘Yuka’, having microtrauma of seeds 27% and the content of mineral impurities 0.4%. Experiments were carried out at other equal conditions (the drive power of the electric motor of 1.5 kW, the length of the working part l = 0.06 m,

the diameter of the rotor 0.1 m, circumferential speed of the rotor v = 5 m s^{-1}) and design parameters, which provided to productivity 0.3 ton h^{-1} (Table 1).

Table 1. The results of the evaluation of the technical and economic efficiency of the proposed options for rotary crushers

Indicators	Units	Options			
		1	2	3	4
S_w	ton	40.4	46.8	77.2	171.2
$S_{w80\%}$	ton	29.6	34	56.8	140
$S_{w\Delta 80\%}$	ton	10.8	12.8	20.4	31.2
$S_{w50\%}$	ton	34	39.2	65	152.8
$S_{w\Delta 50\%}$	ton	6.4	7.6	12.2	18.4
Time of work	hour	134	156	257	570
C_m	rubles	6,500	6,800	9,000	15,000
C_e	rubles	480	559	921	2,042
C_l	rubles	16,750	19,500	32,125	71,250
C_{pw}	rubles	300	1,000	1,400	1,950
C_t	rubles	24,030	2,7859	43,446	90,242
E_g	rubles ton^{-1}	594	595	562	527
$C_{\Delta 80\%}$	rubles	6,423	7619	11,480	16,445
$E_{g80\%}$	rubles ton^{-1}	1,405	1,414	1,326	1,171
$C_{\Delta 50\%}$	rubles	3,801	4,522	6,856	9,696
$E_{g50\%}$	rubles ton^{-1}	1,299	1,305	1,229	1,116

The calculation results in accordance with formulas (4) and (5) show that, without taking into account the quality (full wear) for the coated cutting element (option No. 4), the productivity and the criterion of technical and economic efficiency E_g respectively reach 171.2 tons and 527 rubles ton^{-1}, which indicates a greater wear resistance by 4.2 times compared with steel St3 (option No. 1) and an 11% decrease in technical and economic criteria.

When taking into account the quality of grinding, the volume corresponding to a given level of reliability will become less, but the additional volume $S_{w\Delta}$ will increase, requiring repeated processing, at least once. In this case, additional costs C_Δ are also required, which takes into account the technical and economic criterion E_g.

When the process reliability is 50% and 80%, the productivity is reduced, respectively, by 18.1–12.2% and 36.5–22.3% for all options, and the technical and economic criterion rises on average by 2.16 and 2.28 times.

These data allow us to confirm the hypothesis of the legitimacy of using all the proposed options for various forms of ownership of agricultural enterprises. For example, the crusher's maximum resource in the first and second manufacturing options, from the point of view of reducing their economic costs, can be recommended for private farms and peasant farms, in which the volume of processing and consumption of animal feed is from 30 to 35 tons per year. With an average cost of work equal to 1,410 rubles per ton of grinding. Also in favor of less durable structural materials is the simplicity of their machining, which makes it possible to carry out operations to restore working capacity in place without the use of spare parts.

The calculations are given in the currency of the Russian Federation (rubles), taking into account the cost of structural materials and technological operations to improve their characteristics according to data for December 2019.

CONCLUSIONS

– With the wear of the working bodies of the crusher, the degree of grinding of the source material, and hence the quality of the finished product, will also change. Grinding in compliance with the required quality is characterized by 100% process reliability, but during operation of the grinder, the probability of failure increases. According to an additional analysis should be carried out prevention when the culling wear of cutting element suitable the process reliability 80–90%.

– Analysis of the experimental results allows us to formulate several recommendations for grinding wheat on a horizontal rotary crusher:

1) for reliability $P(g)$ = 80–90%, the maximum allowable clearance should not exceed the range of 1.09–1.15 mm under these operating conditions;

2) an increase in the gap value of more than 0.9 mm leads to periodically occurring failures and loss of operability of the rotor crusher;

3) given the reliability of the grinding process at 90% and to avoid disruption in the operation of the rotary crusher, it is recommended to replace or adjust the cutting element with a gap of 1.09 mm.

– Comparative evaluation of shredders recommend performed using technical-economic indicator E_g. This is due to the appearance of additional costs C_Δ in the form of carrying out an additional amount of work $S_{w\Delta}$ related to bringing the substandard product to a given particle size distribution. Based on this, two types of the process can be distinguished:

1) at the maximum wear (the reliability 10–25%) of the cutting element according to option No. 4, the productivity amounted to 171.2 tons of crushed grain, and the efficiency criterion was 527 rubles/ton, which is 4.2 times higher compared to according option No. 1 on productivity, and by 11% lower by technical and economic criteria;

2) taking into account the reliability of the process, 50% and 80%, the operating time is reduced, respectively, by 18.1–12.2% and by 36.5–22.3% for all options, and the technical and economic criterion rises on average by 2.16 and 2.28 times.

– The cost of manufacturing more expensive, but wear-resistant cutting surfaces will not always be the best option, for example, inexpensive and less durable options No. 1 and No. 2 can be recommended for small forms of ownership, the productivity of which is up to 35 tons per year.

ACKNOWLEDGEMENTS. The authors would like to acknowledge rector of FSBEI HE ‘Stavropol State Agrarian University’ V ruhachev and the chairman of agricultural production cooperative ‘Kazminsky’ in the Stavropol Territory of Russian Federation S. Shumsky for comprehensive support in conducting research work.

REFERENCES

Iskenderov, R., Lebedev, A., Zacharin, A. & Lebedev, P. 2018. Evaluating effectiveness of grinding process grain materials. In: *Engineering for Rural Development, 17th international scientific conference*, pp. 102–108.

Iskenderov, R., Lebedev, A., Zacharin, A., Lebedev, P. & Marjin, N. 2019. Constructive and regime parameters of horizontal impact crusher of grain materials. In: *IOP Conf. Series: Earth and Environmental Science, INTERAGROMASH 2019*, vol. **403**. *https://iopscience.iop.org/article/10.1088/1755-1315/403/1/012057/pdf*. Accessed 28.01.2020.

Lebedev, A.T., Pavlyuk, R.V., Zaharin, A.V. & Lebedev, P.A. 2016. Providing for quality grinding grain for the implementation of the biological potential of productive animals. In: *Research Journal of Pharmaceutical, Biological and Chemical Sciences* **7(**2), 1525–1528.

Lebedev, A.T. 2011. Influence of reliability of technical means on their efficiency. *Technique in agriculture.* No. **6**, pp. 22–23 (in Russian).

Lebedev, A.T., Tskhovrebov, V.S., Simonovsky, A.Ya., Makarenko, D.I., Kaa, A.V. & Shumsky, A.S. 2012. Wear resistance of the working bodies of hammer crushers for feeding animals In: *Bulletin of the agro-industrial complex of Stavropol.* No. **3**, pp. 50–53 (in Russian).

Lebedev, A.T., Iskenderov, R.R. & Shumsky, A.S. 2018. Substantiation of construction parameters of the horizontal rotor unit for crushing forked grain. *Agricultural machinery and technology* **12**(5), 9–13 (in Russian).

Patent EA 026179. *https://www.eapo.org/ru/patents/reestr/patent.php?id=26179* (in Russian). Accessed 28.01.2020.

Sabirov, A.A., Barakova, N.V., Nsengumuremyi, D. & Samodelkin, E.A. 2019. Enrichment of the grains from rye wort after shock-activator-disintegrating processing. *Agronomy Research* **17**, 1424–1434.

Sabirov, A.A., Barakova, N.V. & Samodelkin, E.A. 2018. Effect of impact-activating-disintegration treatment on grain protein fraction of autumn rye. *Agronomy Research* **16**, 1466–1474.

Thomas, M., Hendriks, W.H. & van der Poel, A.F.B. 2018. Size distribution analysis of wheat, maize and soybeans and energy efficiency using different methods for coarse grinding. In: *Animal Feed Science and Technology* **240**, 11–21.

Tumuluru, J.S., Tabil, L.G., Song, Y., Iroba, K.L. & Meda, V. 2014. Grinding energy and physical properties of chopped and hammer-milled barley, wheat, oat, and canola straws. In: *Biomass and Bioenergy* **60**, 58–67.

Agronomy Research **18**(3), 2127–2137, 2020
https://doi.org/10.15159/AR.20.229

Relation between first lactation milk yield and functional traits in dairy cows

Iv. Marinov[1], V. Valchev[1], D. Dimov[2] and T. Penev[2,*]

[1]Trakia university, Faculty of agriculture, Department of Animal Husbandry – Ruminants and Dairy Farming, BG6000 Stara Zagora, Bulgaria
[2]Trakia University, Faculty of Agriculture, Department of Applied Ecology and Animal Hygiene, BG6000 Stara Zagora, Bulgaria
[*]Correspondence: tonchopenev@abv.bg

Abstract. The aim of the study was to analyze the relationship between first lactation milk yield (FLMY) and age at first calving (AFC), longevity and productive life in dairy cows. The study covered 944 Holstein cows housed in 5 dairy cattle farms in Bulgaria. All cows from the five farms culled in the period 2012–2018 with FLMY data were included. The average AFC for all culled cows included in the study was relatively high for the Holstein-Friesian breed - 29.75 months. The average FLMY of the herds included in the study was 7,660.94 kg with significant herd variation from 5,899.09 kg to 8,646.0 kg. Significant effect of the herd ($P < 0.001$), AFC and the associated effect of the herd and AFC ($P < 0.05$) on the average FLMY were found. The highest FLMY was reported in primiparous with AFC of 28–30 months -7,860.8 kg, and the lowest in those with AFC ≤ 24 months - 7322.8 kg. In the herd with the lowest average FLMY - 5,899.09 kg 27.5% of the heifers had calved at age over 34 months. A statistically significant effect of AFC ($P < 0.001$) was found on longevity, whereas the productive life was significantly influenced by FLMY ($P < 0.05$). A tendency for higher longevity for cows with higher AFC of 34–37 months and over 37 months – 5.9 and 5.8 years, respectively was observed. The lowest were the longevity values for cows calved at age up to 24 months - 4.9 years. The cows with the lowest average FLMY (up to 4,000 kg) had the shortest productive. Both very low and high AFC were associated with lower first lactation cow productivity and shorter productive life. The losses for farmers were greater when keeping a high AFC in heifers, which increases the cost for housing them, and the lower productivity and longer productive life reduce the probability.

Key words: milk performance, primiparous, age at first calving, longevity, productive life.

INTRODUCTION

Basic functional traits such as age at first calving (AFC), longevity and productive life affect genetic progress and economic indicators in dairy cows (Teke & Murat, 2013; Penev et al., 2014; Caetano et al., 2017). The AFC is particularly important since it affects fertility, milk performance and duration of productive life and hence the economic return in the dairy sector (Cooke et al., 2013; Zavadilová & Štipková, 2013; Sawa et al., 2018; Fodor et al., 2019). Heifer rearing equals 15 to 20% of total milk production costs, thus representing the second largest share of costs after feed costs at

farms (Tozer & Heinrichs, 2001). The goal of dairy farm owners is to minimize costs and maximize future income from heifers, but contemporary goals also include considerations for ecological impacts and animal welfare (Heinrichs et al., 2017).

There are many reasons for dairy farmers to want animals that are used longer. Although the most important consideration is economic benefits, achieving a long life in the herd is still a great challenge. Although the natural life of a cow may exceed 15–20 years, cows in modern farms are culled on average age of 4.5–6.6 years (Cielava et al., 2017). In Belgium, it was found that less than one third of the cows reach the fourth lactation (Gengler et al., 2005). Other authors in other countries report relatively short productive life of dairy cows. The average productive life of a cow in Sweden is 2 to 2.5 lactations (Carlén & Eriksson, 2013), which means that a cow that has its first calf at the age of 30 months may not be able to pay back it's rearing cost before culling. There are several studies on the relationship between cow use duration and survival and the milk yield (Pool et al., 2003; Ajili et al., 2007; M'hamdi et al., 2010; Grayaa et al., 2019). An important indicator of selection and culling in primiparous is their first lactation milk yield (FLMY). It is largely influenced by the AFC, which in turn is a factor related to the duration of rearing. Clarifying these dependencies, which are specific for the various herds, is important for the overall strategy of dairy farms. The aim of the study was to analyze the relationship between FLMY and AFC, longevity and productive life in dairy cows.

MATERIAL AND METHODS

The study was conducted in 944 Holstein cows housed in 5 cattle farms in the Sliven region Bulgaria. All cows from the five farms culled in the period 2012–2018 with milk yield data for the first lactation (for standard lactation - from 240 to 305 days in milk) were included in the study. The farms surveyed were in a region with identical climatic and forage conditions - Southeast Bulgaria. The feeding of the cows and replacement heifers was based on corn silage, hay and green forage (seasonal) and compound feed. Animals from all farms were not grazed. Cows in farms 2 and 5 were housed in free stall barns and in the other three - under the conditions of bedded pack housing system. All cows were milked in a milking parlor 'Herringbone' type, with number of places corresponding to farm capacity. All farms produced their own replacement heifers. The rearing of female calves and heifers was the same in all farms. During the preweaning period calves were housed in individual hutches outdoors and during the rest of the periods – they were group housed on deep straw bedding, subject to the requirements for technological sizing of group stalls, depending on the age of the animals. The AFC was calculated from the date of birth to the date of the first calving, in months. The longevity was calculated as the difference between date of birth and date of culling of the cow, and the productive life, respectively - as the difference between the date of culling and the date of first calving. Both traits are presented in years.

For better approximation in data processing, the AFC is represented in classes, respectively: 1 – up to 24 months, 2 – from 25 to 27 months, 3 – from 28 to 30 months, 4 – from 31 to 33 months, 5 – from 34 to 36 and 6 – over 37 months. To study the relationship between FLMY and duration of productive life, it is presented in classes respectively: 1 – up to 1 year, 2–1 to 2 years, 3–3 to 4, 4–5 to 6 and 5–7 and more years.

The classes of FLMY are respectively: 1 – up to 4,000 kg, 2 – from 4,001 to 6,000 kg, 3 – from 6,001 to 8,000 kg, 4 – from 8001 to 10,000 kg and 5 – over 10,001 kg.

For the basic statistical processing, the corresponding modules of software packages of MS EXEL and STATISTICA of Stat Soft were used.

The following models were used to determine the degree of influence of the different factors and to derive reliable models:

$$Y_{ijkl} = \mu + H_i + AFC_j + H \cdot AFC_k + e_{ijkl} \quad (1)$$

where Y_{ijkl} – is the depended variable(first lactation milk yield); μ – is the population mean; H_i – is the i^{-ht} effect of the herd; AFC_j – is the j^{-th} effect of the age at first calving; $H \cdot AFC_k$ – is the k^{-th} related effect of the herd and age at first calving; e_{ijkl} – is the effect of the not included random effects, except μ.

$$Y_{ijk} = \mu + AFC_j + ML_j + e_{ijk} \quad (2)$$

where Y_{ijk} – is the depended variable(longevity and productive life); μ – is the population mean; AFC_i – is the i^{-th} effect of the age at first calving; ML_j – is the j^{-th} effect of the FLMY; e_{ijk} – is the effect of the not included random effects, except μ.

By analysis of variances (ANOVA) for each model by classes of fixed factors are evaluated the least squares of means (LSM), representing the sums of squares calculated as deviation from the mean value of the trait derived from the model.

RESULTS AND DISCUSSION

Table 1 presents the main statistics for the traits studied - FLMY, AFC, longevity and productive life by herds. The average AFC for all culled cows included in the study was 29.75 months. The variation of AFC across herds was not large (the difference was about 2 months), although the differences were statistically significant between herds with higher and lower AFC. The lowest was the average AFC for cows from herd 1–28.32 months and the highest for herd 3–30.84 months.

Table 1. Average values for FLMY and functional traits by herds

Herds	n	AFC, months	FLMY, kg	Longevity, years	Productive life, years
		x ± SE	x ± SE	x ± SE	x ± SE
1	226	28.32 ± 0.29^{abc}	$6,748.91 \pm 98.29^{abcd}$	5.14 ± 0.10^{ab}	2.74 ± 0.09^{abc}
2	83	30.75 ± 0.43^{ad}	$6,057.43 \pm 122.85^{ae}$	5.92 ± 0.15^{ac}	3.31 ± 0.16^{a}
3	33	30.84 ± 0.81^{be}	$5,899.09 \pm 315.20^{bfg}$	5.31 ± 0.32^{d}	2.78 ± 0.31^{d}
4	78	28.71 ± 0.31^{def}	$6,137.54 \pm 129.78^{cfh}$	6.06 ± 0.19^{bdf}	3.70 ± 0.19^{bde}
5	524	30.30 ± 0.17^{cf}	$8,646.00 \pm 48.42^{degh}$	5.32 ± 0.06^{cf}	2.83 ± 0.06^{ce}
Average	944	29.75 ± 0.13	7,660.94 ± 54.41	5.39 ± 0.05	2.92 ± 0.05

^{a,b,c,d} – differences between herds with identical letters are statistically significant at $P < 0.05$.

A 24-month AFC is considered as optimal for maximizing FLMY (Nilforooshan and Edriss, 2004), and achieving higher production profitability (Ghavi Hossein-Zadeh, 2011; Wathes et al., 2014). In fact, this target is rarely achieved in the various countries and the average AFC ranges from 24.5 to 31 months. Cooke et al. (2013) indicate that within the UK, the industry-recognized target for AFC is 24 months. Nevertheless, Eastham et al. (2018) indicate that the average AFC for Holstein heifers calved in the period 2006–2008 in the UK was 29.1 months. Cole & Null (2010) indicate for Holstein

breed in US AFC of 26 months, Haworth et al. (2008) for Australia - 28.8 months, Wu et al. (2012) in China - 29.3 months.

In our country over the years, several studies have been conducted on AFC in Black-and-white Holstein cattle. Gergovska & Yordanova (2011) found an average AFC of 29.7 months in 1460 Black-and-white cows calved in the period 1995–2006. Lower average AFC in Bulgaria was reported by Penev et al. (2014) in 818 Black-and-white cows from 7 farms - 26.6 months, with variations from 25 to 28 months by farms.

Fig. 1 shows the percentage of cows depending on the AFC. The highest percentage of cows calved for the first time at 25–27 and 28–30 months of age, respectively 26.2 and 26.6%. Quite a high percentage of cows have calved for the first time at a high age - 31 months or more, respectively 35.7%. Only 11.5% of the cows in the studied herds have calved at 24 months of age or less. The high percentage of heifers calved at over 34 months of age was due, on the one hand, to the failures in the management of the herds and, on the other, to the subjective decisions of the owners. Some owners deliberately postpone the first insemination of the heifers to a later age because of fear of negative consequences associated with calving and productivity due to the early conception. Such concerns were also indicated by Pirlo et al. (2000) among Italian farmers. Other reason is the neglected feeding and housing of replacement female calves and heifers, leading to delay of reaching the desired live weight and development for conception. Moreover, traits related to the development of young animals such as live weight and conformation traits were not controlled on our farms. Popova (2003) indicate that the practice of relatively late conception of heifers in Bulgaria (on age 16–18 months) was mainly consequence of inadequate feeding.

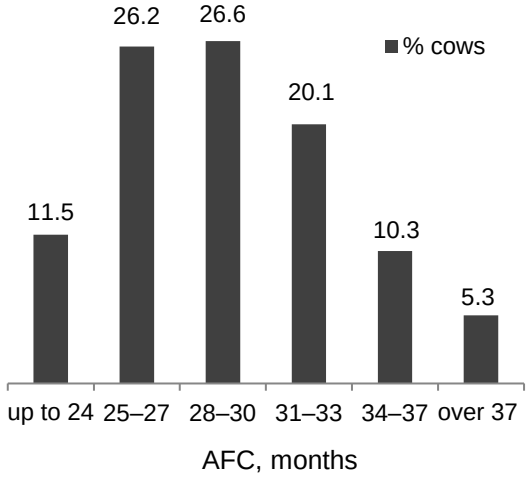

Figure 1. Percentage of cows depending on AFC.

Eastham et al. (2018), in a study covering 6,985 farms in UK report an average AFC for all heifers of 29.1 months, with only 12.3% calved for the first time at 24 months of age or younger and 40.9% calved for the first time at age of 30 months or older. Similar results reported and Sherwin et al. (2016), from other smaller scale British research where the average AFC was 29.6 months, with 35.9% of heifers calved for the first time at age over 30 months.

Sawa et al. (2018) in a study covering 10% of cows in Poland found that the percentage of cows calved before reaching the age of 22 months was the lowest (2.1%). he proportion of the cows calved for the first time at 24.1–26.0 and 26.1–28.0 months was considerable, 30.7% and 22.4%, respectively, and 9.1% of cows calved for the first time at the age of 30 months.

Fig. 2 presents the percentage of cows from the two extreme AFC groups - the youngest - 24 and less months and the oldest - over 34 months by herds. The data shows

a large difference in the percentage of cows from the two age groups in the individual herds. With the highest percentage of heifers with AFC of 24 months or less was herd 1–26.1%, and with the lowest in herd 4 - only 2.6%. In the other three herds, the proportion of heifers with AFC up to 2 years of age was similar and was up to 10%. This definitely shows the reluctance and lack of interest of the owners for the early conception of replacement heifers. On the other hand, in herd 3 there were a very high percentage of heifers with AFC over 34 months - 27.5%. This was the farm with the lowest average milk yield per a primiparous - 5,899.09 kg. With the lowest proportion of such animals were herds 5 and 4, respectively 1.5 and 3.3%. These large differences by herds were definitely related to the subjective decisions of the owners.

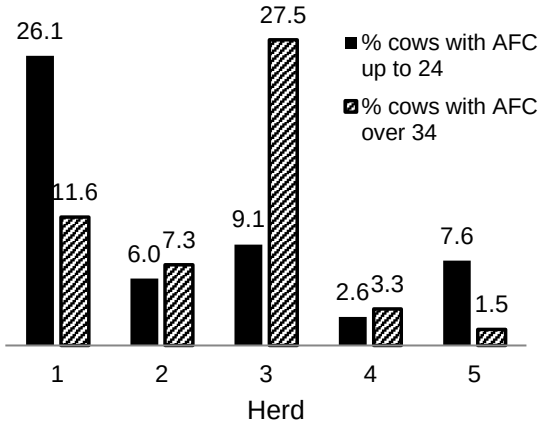

Figure 2. Percentage of cows with AFC up to 24 and over 34 months by herds.

The average FLMY of the herds included in the study was 7,660.94 kg, with significant herd variation, Table 1. The highest milk yield was in primiparous of herd 5 - 8,646.0 kg. This was the largest farm with the highest milk yield per a cow. The milk yield was the lowest in primiparous from herd 3 - 5,899.09 kg, which was also with the smallest capacity. For the other 3 herds, the average milk yield was with values from 6,057.43 to 6,748.91 kg.

Table 2 shows the result of the analysis of variance for the effect of the two studied factors - herd and AFC on FLMY. The herd had effect with a high significance ($P < 0.001$), while the AFC effect and the associated herd*AFC effect were with less degree of significance ($P < 0.05$). The reported significance of the associated herd*AFC factor was related to the presented difference in the variation of the age classes by herds, Fig. 2.

Table 2. Analysis of variance for the influence of the herd and AFC on FLMY

Source of variation	Degrees of freedom (n-1)	FLMY, kg		
		MS	F	P
Total for the model	29	10,546	28.51***	
Herd	4	1,996	131.80***	
AFC	5	4,408	2.91*	
Herd*AFC	20	2,619	1.73*	
Error	914	1,514		

* – significance at $P < 0.05$; ** – significance at $P < 0.01$; *** – significance at $P < 0.001$; – no significant effect.

Fig. 3 shows the LS-means for FLMY depending on the AFC of the primiparous. The highest FLMY was reported in the primiparous with AFC 28–30 months - 7,860.8 kg, followed by those with AFC 31–33 months - 7,773.1 kg. The mean FLMY gradually decreased with the increase of AFC over 33 months, with 297.6 kg lower FLMY in primiparous with AFC over 37 months compare to the highest average milk yield for primiparous with AFC 28–30 months. The lowest FLMY was reported in primiparous with AFC of ≤ 24 months - 7,322.8 kg. The mean milk yield of the primiparous with AFC ≥ 37 months was also relatively low, almost equal to the mean milk yield of the primiparous with AFC ≥ 37 months - 7,526.7 kg. The mean FLMY of

the cows from the two youngest age classes was lower by 538 and 334.1 kg, respectively, compared to the highest FLMY in the class with AFC 28–30 months. These results clearly indicate an underestimation of management, especially with regard to the feeding of young replacement calves and heifers, whereby younger heifers do not reach the desired optimal levels of live weight and body condition at the first calving.

Several authors have found that cows' age at first calving influences milk yield for standard lactation (Ettema & Santos, 2004; Mohd Nor et al., 2013). An increase in milk yield at a greater AFC is associated with an increase in the body size of the primiparous and the development of the mammary glands (Mohd Nor et al., 2013). The authors found that milk yield has increased significantly in primiparous that have calved at age of 23 and 25 months. In primiparous that have calved at a later age, the increase in milk yield was less pronounced.

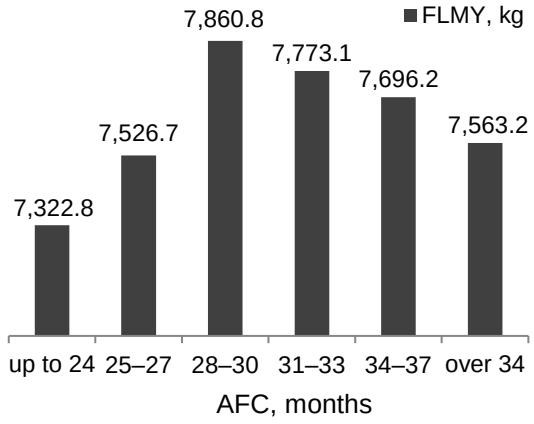

Figure 3. LS-mean values for FLMY (kg) depending on AFC (months).

Eastham et al. (2018) found that the lowest predicted average milk yield for lactation (6,617 kg) was reported for cows with an AFC of 21 months, considerably lower than any other age class. Heifers with AFC of 36 months had the highest predicted average milk yield (7,774 kg), but it was not significantly higher than that in heifers with AFC of 34–42 months.

According to Meyer et al. (2004) data on the effect of lower AFC on milk yield for first lactation in Holstein cows in the USA were contradictory. Some authors found no effect, while others reported a negative effect. Most studies suggested that a decrease in AFC from 24.7 to 21.9 months results in an approximately 4.8% reduction in first lactation milk yield. The authors indicated that the biology associated with the interaction between low AFC and FLMY was difficult to identify and quantify. This is because a decrease in AFC is often associated with higher pre-pubertal daily growth/gain, reduced live weight at calving, or both, which appear to affect future milk yield. According to Dobos et al. (2001) with increasing AFC by one month during the first three lactations cows are 56.7 L milk, 1.78 kg milk fat, 1.45 kg milk protein and 3.23 kg fat + protein over the first 3 lactations.

Fig. 4 shows the inverse dependence, the mean AFC is determined depending on the FLMY (in classes). The average AFC of the cows with low FLMY - up to 4,000 kg was highest - 33 months. The lowest was the average AFC of cows with a FLMY from 4,001 to 6,000 kg. Primiparous with a milk yield of more than 8,000 kg had an average AFC of about 30 months. These results mainly show that the very high AFC does not favor the higher milk performance on first lactation.

The studies of other authors on the relationship between AFC and FLMY also are contradictory, the reasons for this being the differences in the management applied in the studied populations. Curran et al. (2013) concluded that the AFC between 23 and 30

months did not cause differences in milk yield of the primiparous and that calvings between 20 and 22 months were associated with lower milk yield, whereas Cooke et al. (2013) found no significant effect of AFC on the milk yield of the primiparous.

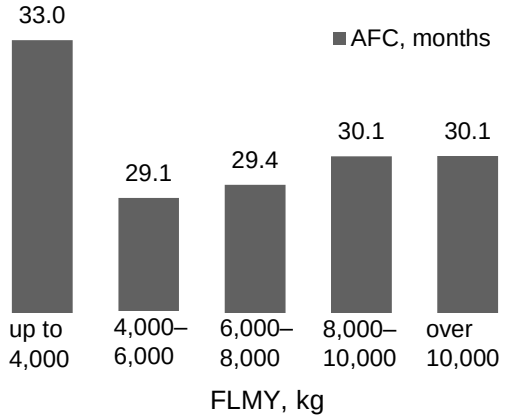

Figure 4. Average AFC (months) depending on FLMY (kg).

The average longevity for the cows included in the study was 5.39 years, and although significant differences were reported between the average values for the herds, the differences were small, Table 1. With the highest longevity were the cows from herd 4–6.06 years and with the lowest in herd 1–5.14 years, with difference being less than 1 productive life of all cows was 2.92 years. Again, the variation in this trait was within 1 year, year. Similar results were reported for the trait productive life. The average duration of although significant differences by herds were reported. With the longest productive life were the cows in herd 4–3.70 years and with the shortest in herd 1–2.74 years.

Table 3. Analysis of variance for the influence of AFC and FLMY on the functional traits

Source of variation	Degrees of freedom (n-1)	Longevity			Productive life		
		MS	F	P	MS	F	P
Total for the model	9	9.103	4.38	***	2.839	1.318	*
AFC	5	16.058	7.743	***	3.228	1.576	-
FLMY	4	1.17	0.565	-	2.425	0.041	*
Error	934	2.074			2.047		

* – significance at $P < 0.05$; ** – significance at $P < 0.01$; *** – significance at $P < 0.001$; - no significant effect.

As shown on Table 3 a statistically significant effect of AFC ($P < 0.001$) was found only on longevity, whereas the productive life was significantly influenced by FLMY ($P < 0.05$).

Fig. 5 shows the LS-means for the two traits - longevity and productive life depending on the cows' AFC. Although the AFC does not have a significant effect on productive life, the presentation of the mean values of the two traits gives a clearer picture of the relationship between them. From the presented LS - means a tendency

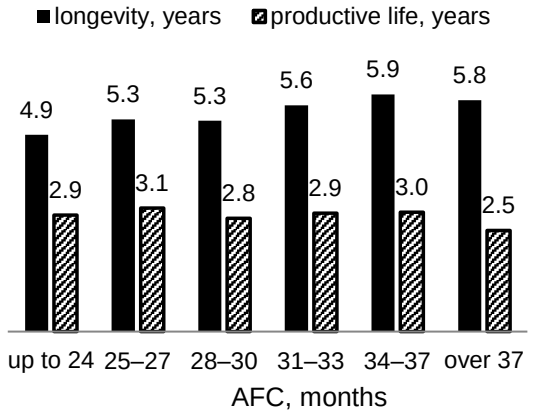

Figure 5. LS-mean values for longevity and productive life (years) depending on AFC (months).

for longer longevity was observed for cows with AFC 34–37 months and over 37 months - 5.9 and 5.8 years, respectively. The lowest were the mean values for longevity in cows calved at the lowest AFC up to 24 months - 4.9 years. No such clear trend was observed in the trait productive life. The shortest productive life was reported for cows with an AFC of over 37 months - 2.5 years. In other age classes a certain pattern was not observed, length of productive life ranged from 2.8 to 3.1 years. From the results presented, it can be concluded that the longer longevity for cows with AFC over 34 months mainly due to the unproductive part of their lives - until first calving.

Sawa et al. (2018) found a very low correlation between AFC and longevity (r = 0.062**), also noting that the longer life is a result of a longer unproductive life (until first calving), and not of a longer productive life. Similar low (0.039–0.061) but significant correlation coefficients have been reported previously by Sawa & Bogucki (2010) and Do et al. (2013) (r = 0.0131).

The possibility of increasing the productive life of cows is of particular interest to livestock farmers. In their study, Sawa et al. (2018) found that the longest productive life (3.54 years) was typical for cows that calved for first time at age of 22.1–24.0 months, and for the other groups the productive life decreases to 3.49 years in cows with early AFC and up to 2.94 years with higher AFC. Similar trends for reduced productive life have been reported by Sawa & Bogucki (2010) and Jankowska et al. (2014).

Zavadilova & Stipkova (2013) and Olechnowicz et al. (2016) also report shorter productive life in cows with higher AFC. According to Cielava et al. (2017), the AFC has a significant effect on the life of cows, finding that the difference between the longevity of cows calved for the first time at < 24 and > 30 months is 1.4 years (5.9 vs. 7.3 years). In turn, Adamczyk et al. (2017) reported that the productive life of cows that calved before 24 months of age decreased compared to those that calved for the first time at age > 31 months, from 5.9 to 5.4 years.

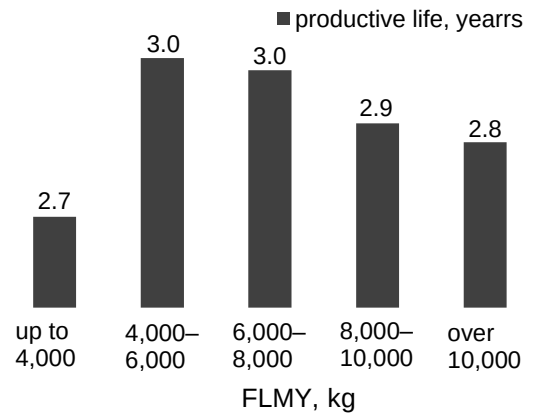

Figure 6. LS-mean values for productive life (years) depending on FLMY (kg).

Fig. 6 shows the LS - means for the productive life of cows, depending on their FKMY. With the highest mean productive life - 3 years were cows with a FLMY of 4,001–6,000 and 6,001–8,000 kg. Cows with FLMY up to 4,000 kg had the shortest productive life - 2.7 years. A trend of shorter productive life was also observed in cows with over 10,000 kg FLMY (2.8 years). The results obtained suggest that cows with low FLMY were culled for various reasons, including various diseases that led to the reported low milk yield. The reported tendency for shorter productive life in cows with very high FLMY more than 10,000 kg is a prerequisite for exhaustion in young animals with high first lactation productivity.

Fig. 7 shows the inverse relationship - the average FLMY in cows with different duration of productive life. Cows with the shortest productive life - up to 1 year had the lowest average FLMY – 6,437.1 kg. The cows with the highest FLMY 7,915.5 and 7,891.1 kg had a productive life of 3 and 2 years, respectively. Cows with a long productive life of more than 6 years had an optimal average FLMY - 7,364.3 kg.

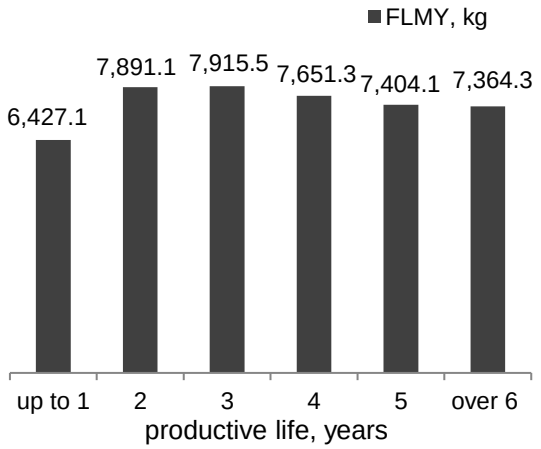

Figure 7. Average FLMY (kg) depending on productive life (years).

These results support the view that low milk yield primiparous are often culled within the first lactation, i.e. up to 1 year after calving. Primiparous with very high first lactation productivity had a relatively short productive life (2–3 years), and the longest productive life, over 6 years, was reported in cows with medium-high FLMY.

Usually, 1 to 1.5 lactations are needed to cover the cost of rearing the replacement heifers, therefore FLMY and longevity affect the payback period of the rearing costs (Boulton et al., 2017). Moreover, cows that are culled or die shortly after the first calving will not cover their costs of rearing, leading to large losses (Fodor et al. 2019).

Both very low and high AFC are associated with lower first lactation cow productivity and shorter productive life. From an economic point of view, losses are greater when keeping a high AFC in heifers, which increases the cost for housing them, and the lower productivity and longer productive life reduce the probability of covering them.

CONCLUSIONs

The average AFC for the herds studied is relatively high - 29.75 months with a slight variation by the herds (about 2 months). The highest percentage of cows (52.8%) - are calved for the first time at 25–30 months. The highest FLMY was reported in cows with AFC 28 to 30 months – 7,860.8 kg, and the lowest in cows with AFC 24 and less months. Cows with both very low and high AFC had lower FLMY. The longer longevity for cows with higher AFC (over 34 months) was due to the greater unproductive share of their life (until first calving). The cows with the lowest average FLMY (up to 4,000 kg) had the shortest productive life. There was a tendency for shorter productive lives also for cows with very high FLMY (over 10,000 kg).

REFERENCES

Adamczyk, K., Makulska, J., Jagusiak, W. & Węglarz, A. 2017. Associations between strain, herd size, age at first calving, culling reason and lifetime performance characteristics in Holstein-Friesian cows. *Animal* **11**, 327–334.

Ajili, N., Rekik, B., Ben Gara, A. & Bouraoui, R. 2007. Relationships among milk production, reproductive traits, and herd life for Tunisian Holstein-Friesian cows, *Afr. J. Agr. Res*. **2**, 57–61.

Boulton, A.C., Rushton, J. & Wathes,D.C. 2015. Analysis of the management and costs associated with rearing pregnant dairy heifers in the UK from conceptio to calving. *Open J. Anim. Sci*. **5**, 474–485.

Caetano, S.L, Rosa, G.J., Savegnago, R.P., Ramos, S.B., Bernardes, P.A., Bezzera, L.A., Lôbo, R.B., de Paz C.C. & Munari, D.P. 2017. Estimation of genetic parameters for longevity considering the cow's age at last calving. *J. Appl. Genetics* **58**, 103–109.

Carlén, E. & Eriksson, J.Å. 2013. The lifespan of the cows - how is the farm's results affected? *Animal Health and Feeding Conference (D&U)* 2013 (in Swedish).

Cielava, L., Jonkus, D. & Paura, L. 2017. The effect of cow reproductive traits on lifetime productivity and longevity. World Academy of Science, Engineering and Technology, International Science Index 123, *International Journal of Biological, Biomolecular, Agricultural, Food and Biotechnological Engineering* **11**, 220–223.

Cole, J.B. & Null, D.J. 2009. Genetic evaluation of lactation persistency for five breeds of dairy cattle, *J. Dairy Sci.* **92**, 2248–2258.

Cooke, J.S., Cheng, Z., Bourne, N.E. & Wathes, D.C. 2013. Association between growth rates, age at first calving and subsequent fertility, milk production and survival in Holstein-Friesian heifers, *Open J. Anim. Sci.*, **3**, 1–12.

Curran, R.D., Weigel, K.A., Hoffman, P.C., Marshall, J.A., Kuzdas, C.K. & Coblentz, W.K. 2013. Relationships between age at first calving; herd management criteria; and lifetime milk, fat, and protein production in Holstein cattle. *The Professional Animal Scientist* **29**, 1–9.

Do, C., Wasana, N., Cho, K., Choi, Y., Choi, T., Park, B. & Lee, D. 2013. The effect of age at first calving and calving interval on productive life and lifetime profit in Korean Holstein. *Asian-Australasian J. Anim. Sci.* **26**, 1511–1517.

Dobos, R.C., Nandra, K.S., Riley, K., Fulkerson, W.J., Lean, I.J. & Kellaway, R.C. 2001. Effects of age and liveweight at first calving on first lactation milk, protein and fat yield of Friesian heifers. *Australian Journal of Experimental Agriculture* **43**, 13–19.

Eastham, N.T., Coates, A., Cripps, P., Richardson, H., Smith, R. & Oikonomou, G. 2018. Associations between age at first calving and subsequent lactation performance in UK Holstein and Holstein-Friesian dairy cows. *PLoS ONE* **13**(6), 1–13.

Ettema, J.F. & Santos, J.E.P. 2004. Impact of age at calving on lactation, reproduction, health, and income in first-parity Holsteins on commercial farms. *J. Dairy Sci.* **87**, 2730–2742.

Fodor, I., Lang, Z. & Ózsvári, L. 2019. Relationship of dairy heifer reproduction with survival to first calving, milk yield and culling risk in the first lactation. *Asian-Australas J Anim Sci.* in press (doi: 10.5713/ajas.19.0474.)

Gengler, N., Vanderick, S., Mayeres, P., Gillon, A. & Croquet, C. 2005. Genetic evaluation of cow survival using a lactation random regression model, *Interbull Bulletin* no. **33**, Interbull, Sweden, 176–180.

Gergovska, Zh. & Yordanova, L. 2011. Effect of the age at first calving on the evaluation of breeding potential of dairy cattle and its correlation to test day productivity. *Agricultural Science and Technology* **3,** 1, 3–7.

Ghavi Hossein-Zadeh, N. 2011. Estimation of genetic and phenotypic relationships between age at first calving and productive performance in Iranian Holsteins. Tropical *Animal Health and Production* **43**, 967–973.

Grayaa, M., Vanderick, S., Rekik, B., Ben Gara, A., Hanzen, C., Grayaa, S., Reis Mota, R., Hammami, H. & Gengler, N. 2019. Linking first lactation survival to milk yield and components and lactation persistency in Tunisian Holstein cows. *Arch. Anim. Breed*. **62**, 153–160.

Haworth, G.M., Tranter, W.P., Chuck, J.N., Cheng, Z. & Wathes, D.C. 2008. Relationships between age at first calving and first lactation milk yield, and lifetime productivity and longevity in dairy cows. *Vet. Rec.* **162**, 643–647.

Heinrichs, A.J., Zanton, G.I., Lascano, G.J. & Jones, C.M. 2017. A 100-Year Review: A century of dairy heifer research. *J. Dairy Sci*. **100**, 10173–10188.

Jankowska, M., Sawa, A. & Kujawska, J. 2014. Effect of certain factors on the longevity and culling of cows, *Acta Sci. Pol., Zootech.* **13**, 19–30.

M'hamdi, N., Aloulou, R., Bouallegue, M., Brar, S.K. & Ben Hamouda, M. 2010. Study on functional longevity of Tunisian Holstein dairy cattle using a Weibull proportional hazard model, *Livest. Prod. Sci.*, **132**, 173–176.

Meyer, M.J., Everett, R.W. & Van. Amburgh, M.E. 2004. Reduced age at first calving: effects on lifetime production, longevity, and profitability. *Kansas Agricultural Experiment Station Research Reports*: **0**, 2, 42–52.

Mohd Nor, N., Steeneveld, W., van Werven, T., Mourits, M.C.M. & Hogeveen, H. 2013. First-calving age and first-lactation milk production on Dutch dairy farms. *J. Dairy Sci.* **96**, 981–992.

Nilforooshan, M.A. & Edriss, M.A. 2004. Effect of Age at First Calving on Some Productive and Longevity Traits in Iranian Holsteins of the Isfahan Province. *Journal of Dairy Science*, **87**, 2130–2135.

Olechnowicz, J., Kneblewski, P., Jaśkowski, J.M. & Włodarek, K. 2016. Effect of selected factors on longevity in cattle: a review. *J. Anim. Plant Sci.* **26**, 1533–1541.

Penev, T., Vasilev, N., Stankov, K., Mitev, J. & Kirov, V. 2014. Impact heifers, age at first Breeding and first calving on some parameters of economic effectiveness at dairy cattle farms. *International Journal of Current Microbiology and Applied Sciences*, **3**, 772–778.

Pirlo, G., Miglior, F. & Speroni, M. 2000. Effect of Age at First Calving on Production Traits and on Difference Between Milk Yield Returns and Rearing Costs in Italian Holsteins. *J. Dairy Sci.* **83**, 603–608.

Pool, M.H., Olori, V.E., Calus, M.P.L. & Veerkamp, R.F. 2003. Aspects of milk yield adjustment in the parameter estimation for genetic evaluation of survival, in: proceedings of the Interbull technical workshop, 2–3 March 2003, USA, *Interbull Bulletin no. 30*.

Popova, Y. 2003. Economic effectiveness of rearing own female calves and heifers at dairy cattle farms. *Bulgarian Journal of Animal Husbandry* **40**, 5–7 (in Bulgarian).

Sawa, A. & Bogucki, M. 2010. Effect of some factors on cow longevity. *Arch. Tierzucht* **53**, 403–414.

Sawa, A., Siatka, K. & Krężel-Czopek, S. 2018. Effect of age at first calving on first lactation milk yield, lifetime milk production and longevity of cows, *Annals of Animal Science*. doi: 10.2478/aoas-2018-0044

Sherwin, V.E., Hudson, C.D., Henderson, A. & Green, M.J. 2016. The association between age at first calving and survival of first lactation heifers within dairy herds. *Animal*. **10**, 1877–1882.

Teke, B. & Murat, H. 2013. Effect of age at first calving on first lactation milk yield, lifetime milk yield and lifetime in Turkish Holsteins of the Mediterranean Region in Turkey. *Bulgarian Journal of Agricultural Science* **19**(5), 1126–1129.

Tozer, P.R. & Heinrichs, A.J. 2001. What affects the costs of raising replacement dairy heifers: A multiple-component analysis. *J. Dairy Sci.* **84**, 1836–1844.

Wathes, D.C., Pollott, G.E., Johnson, K.F., Richardson, H. & Cooke, J.S. 2014. Heifer fertility and carry over consequences for life time production in dairy and beef cattle. *Animal* **8**(Suppl 1), 91–104.

Wu, J.J., Wathes, D.C., Brickellm, J.S., Yang, L.G., Cheng, Z., Zhao, H.Q., Xu, Y.J. & Zhang, S.J. 2012. Reproductive performance and survival of Chinese Holstein dairy cows in central China. *Animal Production Science* **52**(1) 11–19.

Zavadilova, L. & Stipkova, M. 2013. Effect of age at first calving on longevity and fertility traits for Holstein cattle. *Czech J. Anim. Sci.* **58**(2), 47–57.

Agronomy Research **18**(3), 2138–2147, 2020
https://doi.org/10.15159/AR.20.184

Properties of *Populus* genus veneers thermally modified by two modification methods: wood treatment technology and vacuum-thermal treatment

A. Meija[1,*], I. Irbe[2], A. Morozovs[1] and U. Spulle[1]

[1]Latvia University of Life Sciences and Technologies, Forest Faculty, Department of Wood Processing, Liela street 2, LV3001 Jelgava, Latvia
[2]Latvia State Institute of Wood Chemistry, Laboratory of Wood Biodegradation and Protection, Dzerbenes street 27, LV1006 Riga, Latvia
[*]Correspondence: meija.anete@gmail.com

Abstract. Due to environmental concerns the use of wood materials is becoming more extensive and is causing wood supply shortage, therefore the use of *Populu*s genus wood species with a short rotation period is vital. *Populus* genus species wood has several shortcomings - it is not durable, has low density and is hygroscopic. Thermal modification is a technology that can be used to improve the situation. In this study aspen (*Populus tremula* L.) was thermally treated using the Wood Treatment Technology (WTT) device for 50 min at 160 °C (50-160 WTT) and poplar (*Populus x canadensis* Moench) was vacuum-treated (VT) 120 min at 204 °C (120-204 VT), 120 min/ 214 °C (120-214 VT), 180 min 217 °C (180-217 VT) and 30 min 218 °C (30-218 VT). Mass loss (ML), colour change, density, tensile strength along the fibres, moisture exclusion efficiency and weight loss (WL) after brown rot fungus *Coniophora puteana* were determined and also light microscopy images were taken. Aspen veneers showed a ML of 5.3% between 120-214 VT (6.2%) and 30-218 VT (4.6%) treatment that coincided with the same mass loss in aspen boards cited in the literature. The highest ML was 8.7% calculated from 180-217 VT, while the lowest ML was 2.9% computed from 120-204 VT. The total colour change ΔE was 44, where lightness parameter L provided the greatest impact that was reduced twice after modification. Tensile strength reduced by 47% in the WTT process and had ~29% reduction in the VT process. The WL after fungus *C. puteana* was 33% at 50-160 WTT. After VT treatment, WL was 0–2.4%. 120-214 VT and 180-217 VT poplar veneers were the most suitable for plywood production.

Key words: aspen, poplar, thermal modification, decay resistance.

INTRODUCTION

Due to the constantly growing eco-awareness around the world, wood products are increasingly being utilized in indoor and outdoor applications (Li et al., 2017). One way of reducing the emission of carbon dioxide is to use a larger portion of wood products and to increase the lifetime of these products so that carbon is stored over a longer period (Sandberg et al., 2013). Climate change should be considered, since it has strong negative effects on boreal timber supply (Brecka et al., 2018).

Plywood is an engineered wood material, which is widely used. Its production reached 107.4 million cubic meters in 2017 (Raute, 2017) and has a growing tendency to be used for different purposes. Traditionally plywood in Latvia is made from birch wood (Meija-Feldmane et al., 2020), but, due to climate changes, population growth and urbanization and infrastructure development, the potential area for forests might decrease that causes risk of a potential birch wood supply shortage. Therefore, it is crucial to investigate other species suitable for plywood production. Poplar tree species, including all their wide varieties, are largely cultivated in the world as a fast-growing energy crop (Todaro et al., 2017) and it may open the opportunities for the forest industry to widen Populus spp wood usage (Brecka et al., 2018). Aspen (*Populus tremula* L.) is usually the raw material of choice for the production of matches and interior materials (Biziks et al., 2015) in Latvia and it covers 3% from the species growing in Latvia's forests (Mezataksacija, 2016). It is timber with the highest potential from the point of view of the national economy in Latvia (Iejavs et al., 2018). Poplar (*Populus* × *euramericana*) is a fast-growing species with a short rotation period of 10 to 20 years and it is commonly used in veneer and plywood production, as a cellulose material, for lumber production, as biofuel, and in the production of packaging material (Lovrić et al., 2014) and therefore it has been extensively investigated (Aydin et al., 2006; Bulcke et al., 2012; Denes & Lang, 2013).

The material that is used for plywood production, as well as the adhesives used and manufacturing technology strongly affect the end-product quality (Tymyk et al., 2013). Poplar plywood tends to warp greatly with the absorption of moisture. This is one of the problems presented by such plywood that may be caused by its high hygroscopicity (Murata et al., 2013). Generally, shrinkage and swelling create the biggest problems in manufacturing of wood construction and carpentry elements (Spulle et al., 2018).

One of the environmentally friendly methods to improve the dimensional stability and biodurability of wood is its thermal modification (Zanuttini et al., 2019). Heat treatment process changes the composition of wood (Hyttinen et al., 2010). Chemical composition alterations are result of dehydration, hydrolysis, oxidation, decarboxylation and transglycosylation, and the wood becomes less hygroscopic (Kocaefe et al., 2008). In 2007, Jones predicted that in 5 years there would be thermally modified veneer supply in the market. Thermal wood treatment is the most commercialized and the most investigated method for modifying wood composition (Willems et al., 2013). Thermally modified veneers can also be used for decorative purposes indoors as a laminated layer for board materials (Wang et al., 2018).

Although poplar veneers had been previously investigated, there was no direct comparison between Wood Thermal Technology (WTT) and vacuum-thermo (VT) processes. According to Hill (2006) WTT is a closed and wet process, while VT is an open and dry process. WTT process operate at 140–160 °C, 7 bar pressure, while VT modifies wood at reduced pressure and higher temperatures (0. 25 bar, 204–218 °C).

In this paper, the properties of two *Populus* genus veneers treated with two treatment technologies, the VT modification and the WTT were compared to choose the most suitable for plywood production.

MATERIALS AND METHODS

Samples

The experiments were conducted with rotary-cut veneers from aspen (*Populus tremula* L.) and poplar (*Populus x canadensis* Moench) with moisture content of 7.5–8.1%. The samples were obtained directly from the production unit - peeling and wet veneer sorting line after drying and dry veneer sorting process, without visual wood defects with regular annual rings not wider than 2 mm.

Thermal modification

Thermal modification of 290×290×1.5 mm aspen veneers was conducted using Wood Treatment Technology under the previously determined optimal regime of 50 min/160 °C (50-160 WTT) 5–9 bar pressure in water vapour environments in packs of 10 sheets per each. The process applied was described in detail previously by Grīniņš (Grinins et al., 2016).

Rotary-cut 600×600×1.5 mm poplar veneers were treated at four experimental regimes: 120 min/204 °C (120-204 VT), 120 min/214 °C (120-214 VT), 180 min/217 °C (180-217 VT), 30 min/218 °C (30-218 VT) in VT process under 250 mbar pressure in dry environment, which was described in more detail by (Sandak et al., 2015) although this process was modified – veneers were treated under convective heat regime, between aluminium plates in packs of 3 to 12 pieces per pack, which was similar to the processes used in manufacturing.

Laboratory Characterisation

Mass loss (ML)

ML was determined by weighing each sample before and after the treatment and it was calculated according to Hill (2006).

Colour

A MicroFlash 200D portable spectrophotometer (DataColor Int, Lawrenceville,

USA), suitable for direct determination of the CIE L*a*b* colour coordinates according to ISO 11664–4 (2008) was used for the measurement over an 18 mm diameter spot with a standard light source D65 and an observer angle of 10°. Colour was also measured with minolta CM-2500d spectrometer with D65 light source and d/8 measuring geometry and 10° standard observer. Each sample was measured 3 times at the same spot before and after the modification (30 samples per regime in total). The total colour change ΔEab was the difference between the colour before and after the modification, it was calculated according to the suggestions of Technical report of the Calorimetry (International Commission on Illumination, 2004).

Tensile strength

Tensile strength was determined according to the standard GOST 20800-75 (GOST, 1976). After the thermal treatment, 20 random samples were cut both from treated and untreated veneers. The size of these samples was 20×200×1.5 mm. To avoid sample slipping out of the clamps, plywood pieces with the dimensions of

20×50×4.5 mm were glued on both sides of the veneers and both ends of samples, using a one component polyurethane glue. Afterwards, the samples were conditioned at 20 ± 3 °C and at a relative humidity of 65 ± 5%. A tensile strength test was performed with the INSTRON 5500 device with a constant speed (~1mm min^{-1}) to obtain a rupture of the samples in 60 ± 30 s.

Density

Density was measured by weighing the 30 samples of each treatment and measuring their dimensions. Calculation of density was done according to the standard ISO 13061-2 (ISO, 2014). To analyse the results standard deviation and coefficient of variation were calculated.

Moisture exclusion efficiency (MEE)

Twenty samples were weighed after each environment condition and afterwards an oven-dry mass was calculated according to the standard ISO 13061-1 (ISO, 2014).

Then samples were equilibrated in chambers at 20 °C with RH 30%, 65% and 85% and mass changes were measured. The MEE of samples equilibrated at each condition was estimated according to Hill (2006). The equilibrium moisture content was the MC that was constant at the corresponding relative humidity and temperature of the surrounding environment.

The MEE of samples equilibrated at each condition was estimated by Eq. 1:

$$MEE = \frac{EMC_{NT} - EMC_{HT}}{EMC_{NT}} \quad (1)$$

where EMC_{NT} (%) is the EMC of untreated reference samples and EMC_{HT} (%) is the EMC of treated samples.

Decay resistance

Decay resistance was determined according to modified European Prestandard ENV 12038 (2002) using brown rot fungus *Coniophora puteana* BAM Ebw 15. The fungus was cultivated on a medium which contained 5% malt extract concentrate and 2% Fluka agar. Six samples with the dimensions of 50×25×1.5 mm were aseptically placed on 3 mm steel supports in Petri dishes on fungal mycelium and incubated at 22 ± 2 °C and 70 ± 5% RH for 6 weeks. After cultivation, the samples were removed from the culture vessels, brushed free of mycelium and oven-dried at 103 ± 2 °C. The weight loss (WL) of the samples expressed as a percentage was the measure for the extent of fungal degradation.

Statistics

To find out whether a statistically significant difference exists between two groups of data, an unpaired two-tailed t-test with a confidence level of 0.05 was used.

The correlation was the measure of how two or more variables were related to one another. To estimate that, the CORREL function in MS EXCEL was used, where the correlation coefficient r was used to determine the relationship between the two properties.

RESULTS AND DISCUSSION

Mass loss (ML)

ML is a property that allows one to compare different processes that had different temperatures, different treatment times and treatment environments. Heat treatment of wood in the WTT and VT processes differs in water vapours content in the reaction environment, and with hydrolysis reactions prevalence in the first one. Fig. 1 shows that aspen veneers treated in the 50-160 WTT had a ML 5.3% between 120-214 VT and 30-218 VT treatment that coincided with 5% mass loss for aspen boards 60 min 160 °C WTT process (Biziks et al., 2015). The highest ML 8.7% was observed in 180-217 VT with the longest treatment time that was close to ML 9%, obtained in VT process 120–210 °C treated poplar plywood (Zanuttini et al., 2019).

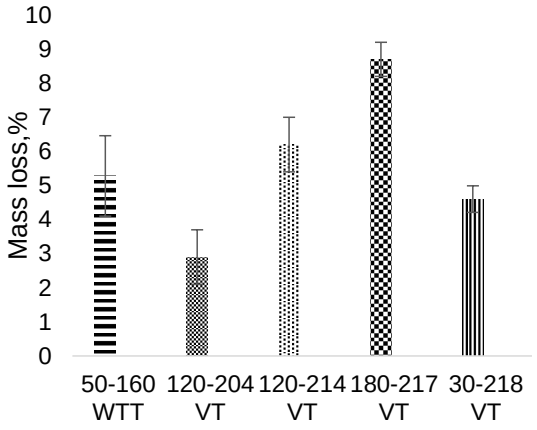

Figure 1. The ML after different thermal treatments of veneer samples.

Colour

The colour of the material is a result of selective light absorbance by the conjugated double bond chemical systems with chromophore groups, which are present in lignin and also in certain sort of extractives in natural wood (Nemeth et al., 2016). Structural change of lignin during thermal modification is mainly responsible for colour change (Kim et al., 2014). Lightness parameter L* was the one that changed the most during thermal modification as showed in Table 1.

Table 1. Colour of untreated and thermally modified veneers.

	L	a	b	ΔE
Untreated aspen	87.6 ± 1.6	1.4 ± 0.4	19.2 ± 1.0	x
Untreated poplar	89.5 ± 2.5	0.8 ± 1.4	18.4 ± 1.2	x
50-160 WTT	46.6 ± 2.2	13.7 ± 0.6	27.4 ± 1.8	43.5 ± 12.9
120-204 VT	52.9 ± 1.2	11.4 ± 0.2	26.8 ± 0.7	39.0 ± 11.1
120-214 VT	43.2 ± 1.5	11.0 ± 0.2	21.8 ± 0.9	47.5 ± 8.5
180-217 VT	40.4 ± 1.2	10.1 ± 0.2	25.8 ± 1.0	50.0 ± 9.2
30-218 VT	44.4 ± 1.7	11.3 ± 0.3	22.9 ± 1.1	46.6 ± 8.4

Zanuttini et al. (2019) states that lightness parameter L is 85 ± 2 for untreated poplar and 41 ± 1.4 for thermally treated aspen samples, which coincides with the findings in this research. Lightness parameter L has close correlation with mass loss (r = 0.90).

Total colour change ΔE values showed that thermally modified veneer colours are considered as different colours (Allegretti et al., 2009), which could be an advantage for customers who prefer a tropical-like appearance of wood.

Density

Density changes during the thermal modification of *Populus deltoides* were reported by (Mirzaei et al., 2017), implying density increase with an increase in temperature. The results of the present study show that density after thermal modification was not affected in both species (Table 2) which agreed with Chaouch et al.(2010a) that species of lower density presented better stability to thermo-degradation than species with higher density.

Table 2. Density of untreated and thermally treated veneers

	Density	stdev
Untreated aspen	442	58
50-160 WTT	420	54
Untreated poplar	300	29
120-204 VT	295	25
120-214 VT	289	35
180-217 VT	312	35
30-218 VT	309	18

Density of untreated aspen was 442 ± 58 kg m^{-3} which was slightly lower than 524 kg m^{-3} (Biziks et al., 2015), but it coincided with Li et al. (2017) 400 kg m^{-3} *Populus* spp. Density of untreated poplar was 300 ± 29 kg m^{-3}, which was less than *Populus nigra* (Chaouch et al., 2010b) 437 kg m^{-3} and poplar (Willems et al., 2013) 437 kg m^{-3}. Minor differences were expected, hence density depends not only on the species but also on growth conditions.

Tensile strength

The tensile strength (Fig. 2) along the fibres for unmodified aspen of 65 MPa was slightly higher than 60 MPa, reported in the literature (Volinsky, 2009). Aspen veneers, treated in the WTT process reduced tensile strength from 65 to 35 MPa, which was statistically significant ($p = 2.81 \cdot 10^{-7}$). After modification in the VT process, the tensile strength of poplar veneers reduced from 45 to ~34 MPa. The difference between tensile strength of untreated and VT treated poplar veneers was statistically significant $p = 2.24 \cdot 10^{-5}$ (120-204 VT), $p = 2.19 \cdot 10^{-5}$ (120-214 VT), $p = 0.003$ (180-317 VT), $p = 0.006$ (30-218 VT) and it was insignificantly affected by a treatment regime, except with 30-218 VT regime, which had significant ($p = 0.01$–0.02) difference compared to the other VT regimes. Although the remaining tensile strength was comparable in MPa, the strength decrease was considerably higher (47%) in WTT process than (29%) the decrease in VT process due to low molecular acids that were formed during thermal treatment and catalysed wood decomposition reactions if not removed in the closed WTT process.

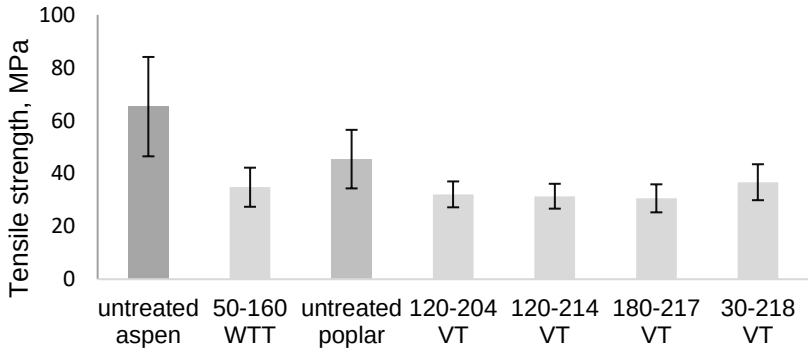

Figure 2. The tensile strength of veneer samples.

Comparing the density and tensile strength changes after modification, the major difference in 50-160 WTT process could be observed. Both properties showed an average correlation (r = 0.64).

Moisture exclusion efficiency (MEE)

Moisture is a critical parameter for nearly all properties of wood, and one of the ways to provide better dimensional stability and decay resistance is wood thermal treatment (Thybring et al., 2018). MEE results are shown in Table 3, which very well correlate with ML (r = 0.95) at RH 30% and RH 65%, at RH 80% it is slightly lower (r = 0.71). Hemicelluloses are the major contributors to the hygroscopicity of the plant fibres. Removal of hemicelluloses decreases hygroscopicity (Kocaefe et al., 2008), although Willems et al. (2013) stated that hemicelluloses were not removed, but dehydrated to furans leading to the subsequent formation of carbonaceous condensation products within the wood structure. The more intense the treatment regime, the less hygroscopic the obtained material. Li et al. (2017) and Mirzaei et al. (2017) stated that the hygroscopicity of poplar wood decreased with increasing temperature in the heat treatment process. Thybring et al. (2018) implied that MEE above 40% was a threshold for decay resistance, 50-160 WTT regime was an exception, although MEE RH80% was 40.4%, WL after fungus *Coniophora puteana* was 33% (Fig. 3).

Table 3. Moisture exclusion efficiency after thermal modification in different relative humidity (RH) environments

	MEE RH 30%	MEE RH 65%	MEE RH 80%
50-160 WTT	-38.9%	-39.4%	-40.4%
120-204 VT	-37.5%	-32.9%	-23.0%
120-214 VT	-43.2%	-42.1%	-31.4%
180-217 VT	-46.6%	-44.1%	-38.4%
30-218 VT	-39.9%	-38.2%	-31.1%

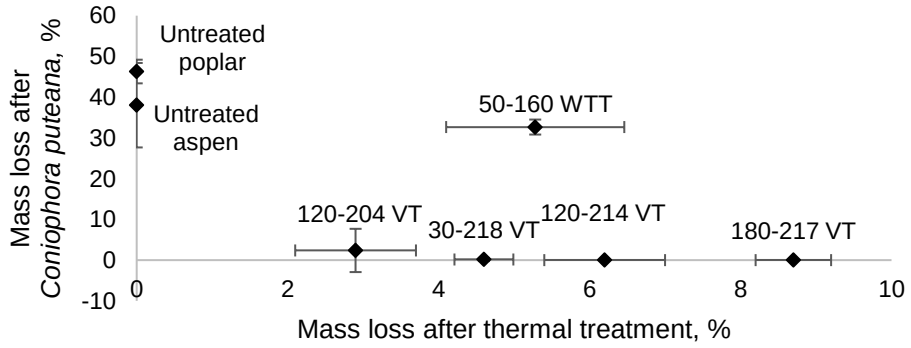

Figure 3. The WL after fungus *C. puteana* and its correlation with the ML after thermal treatment.

Decay resistance

86% of wood construction damage in Latvia is caused by brown rot (Irbe, 2008). Decay resistance and ML correlation can be seen in Fig. 3. WL caused by brown rot fungus *Coniophora puteana* for untreated aspen samples was 46 ± 3%, 50-160 WTT treatment decreased WL till 33 ± 2%. According to Janberga et al. (2013) 60 min 160 WTT aspen boards showed WL 7 ± 4% while WL for untreated aspen was 50 ± 3%. Veneer samples had a higher surface to volume ratio that could affect the WL by brown rot fungus.

The WL for untreated poplar was 38 ± 10%, which was close to 24% of *Populus nigra* (Chaouch et al., 2013). After the VT treatment, mass loss was 0–2.4%, which was an insignificant decrease. Poplar veneers showed significantly better decay resistance compared to commonly used silver birch veneers treated under the same regime (Meija-Feldmane et al., 2020.).

The only regime that differs is 50-160 WTT where the relatively high ML of 5.3% after modification resulted in 33% WL after brown rot fungi. Poplar (*Populus* spp) plywood glued with urea-melamine-formaldehyde adhesive treated for 120 min at 210 °C WL after *Coniophora puteana* is 0.1% (Zanuttini et al., 2019) which was comparable with 0.0% 120-214 VT regime.

CONCLUSIONS

VT treated poplar veneers show better properties, compared to the WTT process treated aspen due to the less severe conditions during the treatment.

All the veneers can be used for decorative purposes (as outer lamination layers) as they become significantly darker during the thermal modification.

Aspen treated in 50-160 WTT is not suitable for plywood production as it has no relevant improvement regarding decay resistance against *Coniophora puteana*, but it has tensile strength reduction by 47%.

120-214 VT and 180-217 VT poplar veneers were the most suitable for plywood production due to the achieved WL 0% after degradation by brown rot fungus *Coniophora puteana* and 32% tensile strength loss along the fibre.

To have a better comparison between both treatment technologies, the same species of veneers should be used.

ACKNOWLEDGEMENTS. The research was carried out within the project P5 ‘Plywood with improved durability’ co-financed by Implementation of Research Programme at Latvia University of Life Sciences and Technologies.

Special gratitude to Ottaviano Allegreti and Ignazia Cuccui from Bioeconomy Institute CNR-IBE for vacuum-thermo modification of poplar veneers and EMC measurements.

REFERENCES

Allegretti, O., Travan, L. & Cividini, R. 2009. Drying Techniques to obtain White Beech. Bled. Proceedings of the COST E53 Meeting: *Quality control for wood and wood products. EDG Drying Seminar: improvement of wood drying quality by conventional and advanced drying techniques 2009*, Bled, Slovenia, pp.7–512.

Aydin, I., Colakoglu, G., Colak, S. & Demirkir, C. 2006. Effects of moisture content on formaldehyde emission and mechanical properties of plywood. *Building and environment* **41**, 1311–1316.

Biziks, V., Andersons, B., Sansonetti, E., Andersone, I., Militz, H. & Grinins, J. 2015. One-stage thermo-hydro treatment (THT) of hardwoods: an analysis of form stability after five soaking-drying cycles. *Holzforschung* **69**(5), 563–571.

Brecka, A.F.J., Shahi, C. & Chen, H.Y.H. 2018. Climate change impacts on boreal forest timber supply. *Forest Policy and Econimics* **92**, 11–21.

Bulcke, J., Windt, I.D., Defoirdt, N. & Acker, J.V. 2012. Plywood under the scanner: linking moisture dynamics and 3D structure. In *The 43rd international research group on wood protection:* Kuala Lumpur, Malaysia, pp. 1–12.

Chaouch, M., Dumarçay, S., Pétrissans, A., Pétrissans, M. & Gérardin, P. 2013. Effect of heat treatment intensity on some conferred properties of different European softwood and hardwood species. *Wood Science and Technology* **47**(4), 663–673.

Chaouch, M., Petrissans, M., Petrissans, A. & Gerardin, P. 2010a. Prediction of Decay Resistance of Different Softwood and Hardwood Species after Heat Treatment Based on Analysis of Wood Elemental Composition. In *The fifth European conference on wood modification : ECWM5,* Riga, Latvia, pp. 135–141.

Chaouch, M., Pétrissans, M., Pétrissans, A. & Gérardin, P. 2010b. Use of wood elemental composition to predict heat treatment intensity and decay resistance of different softwood and hardwood species. *Polymer Degradation and Stability* **95**(12), 2255–2259.

Denes, L. & Lang, E. M. 2013. Journal of Photochemistry and Photobiology B : Biology Photodegradation of heat treated hardwood veneers. *Journal of Photochemistry & Photobiology, B: Biology* **118**, 9–15.

ENV 12038. Durability of wood and wood-based products –Wood-based panels –Method of test for determining the resistance against wood-destroying basidiomycetes. 2000.

GOST 20800-75. 1976. Rotary cut veneer. Test methods, (in Russian).

Grinins, J., Andersons, B., Irbe, I., Andersone, I., Meija-Feldmane, A., Janberga, A., Pavlovics, G. & Sansonetti, E. 2016. Thermo-hydro treated (THT) birch veneers for producing plywood with improved properties. *Holzforschung* **70**(8), 739–746.

Hill, C. 2006. *Wood modification: chemical, thermal and other processes.* John Wiley & Sons, Ltd, 249 pp.

Hyttinen, M., Masalin-Weijo, M., Kalliokokski, P. & Pasanen, P. 2010. Comparison of VOC emissions between air-dried and heat-treated Norway spruce (*Picea abies*), Scots pine (*Pinus sylvestris*) and European aspen (*Populus tremula*) wood. *Atmospheric environment* 44(38), 5028–5033.

Iejavs, J., Spulle, U., Jakovlevs, V., Buksans, E. & Zelmenis, A. 2018. Effect of environmental temperature on bending strenght of the finger jointed aspen lumber. *Agronomy Research* **16**(4), 1677–1685.

International Commission on Illumination. 2004. Technical report Calorimetry, International Comission in Illumination, 72 pp.

ISO 13061-1:2014. 2014. International Organization for Standardiazation. Physical and mechanical properties of wood 4 Test methods for small clear wood specimens – Part 1: Determination of moisture content for physical and mechanical tests.

ISO 13061-2:2014. 204. International Organization for Standardization. Physical and mechanical properties of wood 4 Test methods for small clear wood specimens – Part 2: Determination of density for physical and mechanical tests.

Irbe, I. 2008. *Wood Brown-Rot: Basidiomycetes and their Destructive Action on Lignocellulose*. Doctoral thesis. University of Latvia, 119 pp. (in Latvian).

Janberga, A., Irbe, I., Biziks, V., Kurnosova, Ņ., Asatiani, M. D., Andersons, B. & Andersone, I. 2013. Biodegradation of treated softwood and hardwood species by brown rot fungi. *Environmental and Experimental Biology* **11**, 17–22.

Jones, D. 2007. Wood modification in the composites industry - its present and medium-term viability. In *Proceedings of the International Panel Products Symposium* Cardiff, Wales, UK, pp. 3–10.

Kim, J.Y., Hwang, H., Oh, S., Kim, Y.S., Kim, U.J. & Choi, J.W. 2014. Investigation of structural modification and thermal characteristics of lignin after heat treatment. *International Journal of Biological Macromolecules* **66**, 57–65.

Kocaefe, D., Poncsak, S. & Boluk, Y. 2008. Effect of thermal treatment on the chemical composition and mechanical properties of birch and aspen. *BioResources* **3**(2), 517–537.

Li, T., Cheng, D., Avramidis, S., Walinder, M.E. & Zhou, D. 2017. Response of hygroscopicity to heat treatment and its relation to durability of thermally modified wood. *Construction and Building Materials* **144**, 671–676.

Lovrić, A., Zdravković, V. & Furtula, M. 2014. Influence of thermal modification on colour of poplar (*populus* × *euramericana*) rotary cut veneer. *Wood Research* **59**(2), 661–670.

Mezataksacija. 2016. *http://www.mezataksacija.lv/koki/apse/*. Accessed 28.11.2019 (In Latvian)

Meija-Feldmane, A., Cuccui, I., Irbe, I., Morozovs, A. & Spulle, U. 2020. Properties of Wood Treatment Technology and Thermo-Vacuum process treated birch (Betula pendula Roth.) veneers. *BioResources* **15**(2), 4150–4164.

Mirzaei, G., Mohebby, B. & Ebrahimi, G. 2017. Glulam beam made from hydrothermally treated poplar wood with reduced moisture induced stresses. *Construction and Building Materials* **135**, 386–393.

Murata, K., Watanabe, Y. & Nakano, T. 2013. Effect of Thermal Treatment of Veneer on Formaldehyde Emission of Poplar Plywood. *Materials* **6**, 410–420.

Nemeth, R., Tolvaj, L., Bak, M. & Alpar, T. 2016. Colour stability of oil-heat treated black locust and poplar wood during short-term UV radiation. *Journal of Photochemistry and Photobiology* **329**, 287–292.

Raute. 2017. Plywood production and consumption. *https://www.raute.com/documents/10157/880369/Plywood+production+and+consumption_20171031+update.pdf.* Accessed 20.11.2019.

Sandak, A., Sandak, J., Cuccui, I., Allegretti, O., Zanuttini, R., Negro, F., Cremonini, C., Rosso, L. & Castro, G. 2015. Thermal modification of poplar veneers in vacuum conditions. *In 8th European Conference of Wood Modification*, Helsinki, Finland, pp. 1–7.

Sandberg, D., Navi, P. & Haller, P. 2013. Thermo-hydro and thermo-hydro-mechanical wood processing: An opportunity for future environmentally friendly wood products. *Wood Material Science and Engineering* **8**(1), 64–88.

Spulle, U., Buksans, E., Iejavs, J. & Rozins, R. 2018. Swelling pressure and form stability of cellular wood material. *Agronomy Research* **16**(1), 263–275.

Thybring, E.E., Kymäläinen, M. & Rautkari, L. 2018. Moisture in modified wood and its relevance for fungal decay. *iForest* **11**(3), 418.

Todaro, L., Russo, D., Cetera, P. & Milella, L. 2017. Effects of thermo-vacuum treatment on secondary metabolite content and antioxidant activity of poplar (*Populus nigra* L.) wood extracts. *Industrial Crops and Products* **109**, 384–390.

Tymyk, D., Bekhta, P. & Sedliacik, J.A.N. 2013. The effect of chemical modification of wood veneer surfaces on their bondability. **273**(81), 269–273.

Volinsky, V.N. 2009. *Tehnologia kleyennih materialov*. Profvi, Sankt-Peterburg, 392 pp. (in Russian).

Wang, J., Wang, X., Zhan, T., Zhang, Y., Lv, C. & He, Q. 2018. Preparation of hydro-thermal surface-densified plywood inspired by the stiffness difference in 'sandwich structure' of wood. *Construction and Building Materials* **177**, 83–90.

Willems, W., Gérardin, P. & Militz, H. 2013. The average carbon oxidation state of thermally modified wood as a marker for its decay resistance against Basidiomycetes. *Polymer Degradation and Stability* **98**(11), 2140–2145.

Zanuttini, R., Castro, G., Cremonini, C., Negro, F. & Palanti, S. 2019. Thermo-vacuum treatment of poplar (*Populus* spp.) plywood. *Holzforschung* **72**, 1–8.

Agronomy Research **18**(3), 2148–2155, 2020
https://doi.org/10.15159/AR.20.216

The combined impact of energy efficiency and embodied energy of external wall over 30 years of life cycle

M. Miljan, M.-J. Miljan*, K. Keskküla (Leiten) and † J. Miljan

Estonian University of Life Sciences, Institute of Forestry and Rural Engineering, Chair of Rural Building and Water Management, Fr. R. Kreutzwaldi 5, EE51006 Tartu, Estonia
*Correspondence: martti-jaan.miljan@emu.ee

Abstract. Decreasing the energy consumption in production and building activity is the main aim nowadays as well as in the future. Taking into account that almost 50% of European Union's final energy consumption is used for heating and cooling, of which 80% is used in buildings it is essential to minimize this amount beforehand. Looking at the energy losses we see that the main heat losses are caused due to the transmission through the envelope and ventilation system.
EU energy efficiency target for buildings to 2030 is at least 32.5%. According to this, national energy efficiency action plans were done, which mean that existing building stock need renovation and new buildings will be constructed according to the energy efficiency requirements. One important factor to improve energy efficiency is to modify thermal transmittance of the envelope. In 2017 minimum energy efficiency requirements were validated in Estonia and determined that the thermal conductance of outer wall must be less than 0.22 W m^{-2} K^{-1} (recommended range of U = 0.12–0.22 W m^{-2} K^{-1}). According to this the energy loss through the envelope was calculated over the year taking degree-days as bases. In our area this number is 4,933 degree days per year, what gives us the calculated heat loss through the envelope 10.22 kWh m^{-2} if the thermal conductance of the wall is 0.092 W m^{-2} K^{-1}. This required value of thermal conductance we can achieve using good insulation materials. Still there are possibilities to choose between insulations.
Done tests and calculations allow to conclude that energy consumption during building life cycle together with embodied energy of building materials gives us more realistic overview of the energy efficiency of the building. Our results confirm that the use of local natural insulation materials is 1.67 times more sustainable and energy saving than using industrial materials.

Key words: embodied energy, thermal conductance, energy efficiency.

INTRODUCTION

'Energy use in buildings and for building construction represents more than one-third of global final energy consumption and contributes to nearly one-quarter of greenhouse gases emissions worldwide' (GBS, 2016). Minimising energy consumption is one of the important goals in nowadays production and construction activities. Referring to Eurostat: buildings account for 40% of energy consumed (EC, 2019).

As we see from the Fig. 1 the energy consumption in building hasn't decreased since 2014 comparing to 2019. Big amount of energy losses (heating and cooling energy mainly) is caused by ventilation and through envelopes, what are not sufficiently

insulated (ECS, 2016). Speaking about energy savings it is recommended to use more energy efficient products. On the whole this mean energy efficient technologies and new generation insulation materials (EC, 2019; Wang et al., 2020). Increasing concern of climate and environmental change distress people and transform the way they live to limit the impacts of everyday life on environment (Probst et al., 2014). More and more customers are seeking alternative solutions that could improve their quality of life being environmentally-friendly. One approach to sustainable building includes the use of alternative building materials (Schroeder, 2019; Cornaro et al., 2020).

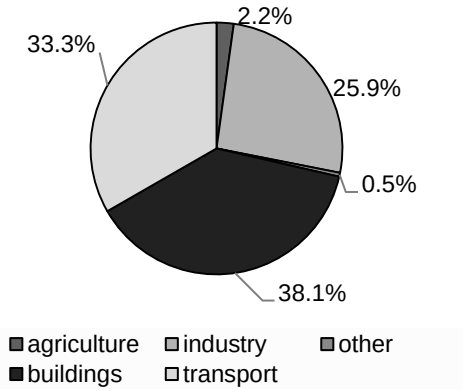

Figure 1. Energy consumption by sectors in EU in 2014 (ECS, 2016).

The possibility to obtain the energy efficiency aims planned by EU until 2030 is to build new constructions according to the demands and to renovate existing building stock as well and as quickly as possible (EPB-EU, 2016; SGF, 2014). By Estonian national energy and climate plan European Union funds are planned to use for renovating business and public sector buildings and living stock as well. The plan is to renovate totally about 290,000 m^2 of flooring (NECP 2030, 2019).

Although calculations of buildings energy efficiency don't pay attention to consumed embodied energy in building materials. B. Berge has divided the energy use during building life cycle as presented on the Fig. 2.

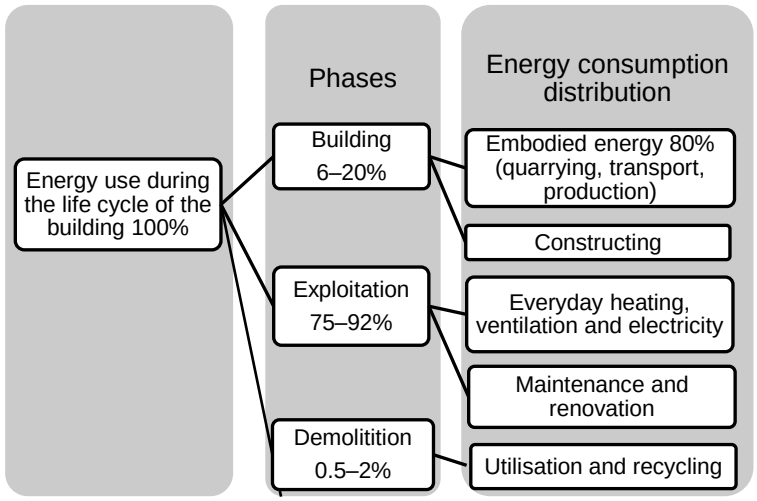

Figure 2. The energy use in different stages of the building life cycle (Berge, 2009).

From the Fig. 2 we see that in the exploitation phase the energy use is the greatest, until 92% of the total energy use. So the amount of embodied energy in the materials is

in the range of 8–25%. The exploitation phase of residential buildings is considered to be 30 years. In our research and by B. Berge embodied energy of materials consists of energy used for extracting, transporting and producing materials, in other words it means energy used from 'the cradle to the gate' (Miljan, J. & Miljan, R., 2012). This method to calculate embodied energy has been used by many researchers (May et al., 2012; Fernandes et al., 2019). Embodied energy amount in building materials has been researched by Bath's University for years and done database will give the wide overview of embodied energy consumed in different building materials (ICE, 2008). One possibility to minimise energy consumption of construction materials is to use local renewable sustainable and natural materials. These materials are also considered to be healthy and improving the indoor climate quality. Renewable materials have been investigated by many researchers (Brencis et al., 2017) and results have been promising.

So one possibility to ensure good and healthy indoor climate is to improve the thermal conductance of envelopes. Problem to solve is, how to get the optimal result in minimising energy use over the buildings life cycle. Main components we shall account are: total energy consumption during exploitation, the thermal conductance of the external wall, the embodied energy in the materials of external wall.

As many of people are interested in living in sustainable buildings and in many cases local natural insulation materials are simply agricultural waste, like straw, in our research we studied them (Miljan, M.-J. & Miljan, J., 2013). In calculating energy efficiency embodied energy of materials is not taken into account. In such tense energy saving situation and in designing of nearly zero-energy buildings this calculation gives a surprising result.

MATERIALS AND METHODS

In our study we took building's life cycle equal to 30 years. In calculating heating energy consumption we used Tartu region's degree days 4,933 and indoor temperature of 21 °C (Masso, 2012).

In this study we compared embodied energy of materials and consumed heating energy over 30 years of 5 external walls. Three walls were built using local renewable building materials: timber, clay, straw and lime (Fig. 3, Table 1). The fourth structure was theoretical wall built using straw and clay plaster with steel bars and thermal conductance of the wall was calculated on the data taken from literature sources (Minke & Mahlke, 2004; Wihan, 2007). The fifth theoretical wall (Table 2) was constructed from timber frame and insulated with glass wool. In calculations we used also data from the tests done during several years in the department of rural building in Estonian University of Life Sciences and the database of University of Bath (ICE, 2008). Building physics calculations were done according to EVS 908-1

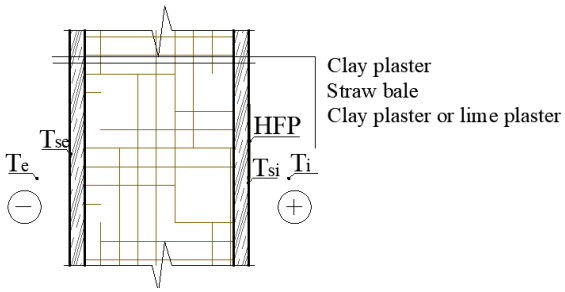

Figure 3. The scheme of external wall's structure (T – temperature sensor; HFP – heat flow plate).

(EVS 908-1, 2016). Placement of measuring devices and scheme of the walls no 1, no 2 and no 3 is presented on the Fig. 3.

Method to measure thermal conductance and temperatures was the same in all objects. The wall no 1 was a wall element built into the window opening of the laboratory (Miljan, M.-J. et al., 2013). The wall no 2 was office (case study building), built at Tammistu (Miljan, M. & Miljan, J., 2015) and the wall no 3 was sauna (case study building), built at Leigo (Miljan, M.-J. et al., 2017; Allikmae & Jurgenson, 2017). Data about structure and main results get from these objects are presented in the Table 1.

Table 1. Technical and physical indicators of external walls according to measured results on objects

Number of the external wall	Wall no 1	Wall no 2	Wall no 3
Measuring period	2009–2010	2012–2013	2016–2017
Used Materials and units	(mm)	(mm)	(mm)
Clay plaster (internal)	50	40	40
Straw	480	900	500
Clay plaster (external)	50	40	-
Lime plaster (external)	-	-	40
External wall - TOTAL THICKNESS	580	980	580
Thermal conductance of the external wall W m^{-2} K^{-1}	0.182	0.148	0.150

From the Table 1 we can see that measured thermal conductivity in case studies differs a lot. Results are influenced by climate, location of the building and the homogeneity of natural materials. Get results were actually not that good as we supposed basing on literature sources. From the literature data we found that thermal conductivity of straw (longitudinal fibre) is $\lambda = 0.085$ W m^{-1} K^{-1} (Wihan, 2007) and of clay plaster is $\lambda = 0.8$ W m^{-1} K^{-1} (Minke & Mahlke, 2004). Calculating the thermal conductance of external wall by these values we got that U = 0.092 W m^{-2} K^{-1}, if d_{wall} = 900 mm (later named as wall no 4).

To compare embodied energy consumption of different wall structures we constructed an theoretical timber frame external wall – the wall no 5, insulated with glass wool and with the same thermal conductance as the wall no 4. In Table 1 used materials and their building physics properties of external wall are presented.

Table 2. Building physics properties of timber frame wall no 5 insulated with glass wool

Properties of layer Used Materials	Thickness of the layer (m)	Thermal conductivity (W m^{-1} K^{-1})	Thermal resistance (m^2 K W^{-1})
Cladding (external)	0.025	-	-
Air cap	0.0025	-	-
Fixed external layer's thermal resistance	-		0.13
Wind resistance board	0.03	0.037	0.81
Glass wool	d_{wool}	0.04	R_{wool}
Vapour resistance barrier	0.0002	0.4	0.0005
Gypsum board	0.014	0.21	0.066
Fixed internal layer's thermal resistance	-	-	0.13
TOTAL			1.14

Needed thermal resistance of timber frame wall is:

$R = \frac{1}{U} = \frac{1}{0.092} = 10.87\ \mathrm{m^2\ K\ W^{-1}}$.

So the wool layer's needed thermal resistance R_{wool} = 9.73 m^2 K W^{-1}. The thickness of the wool layer should be $d_{wool} = 9.73 \times 0.04 = 0.389\ m$.

Embodied energy consumption of external walls materials' is presented in Tables 3 and 4.

Table 3. Embodied energy of the external walls (no 1, no 2 and no 3) insulated with straw

Wall	Material	Density (kg m^{-3})	Thick-ness of layer (m)	Consumed material (kg m^{-2})	Embodied energy (MJ kg^{-1})	Embodied energy of layer (MJ m^{-2})	Embodied energy of wall (MJ m^{-2})	(kWh m^{-2})
1	Clay plaster	1,700	2×0.05	170	0.09[2]	15.30		
	Straw bale	150	0.48	72	0.24[1]	17.28	50.22	13.90
	Timber*	450	-	4.50	3.93[3]	17.64		
2	Clay plaster	1,700	2×0.04	136	0.09[2]	12.24		
	Straw bale	200	0.9	180	0.24[1]	43.20	71.19	19.65
	Steel bars*	-	-	1.79	8.80[1]	15.75		
3	Clay plaster	1,700	0.04	68	0.09[2]	6.12		
	Straw bale	150	0.5	75	0.24[1]	18.00	119.60	33.39
	Lime plaster	1,400	0.04	56	1.39[3,4]	77.87		
	Timber*	450	-	4.50	3.93[3]	17.64		

*Amount of timber and steel bars is calculated to build one square meter of external wall. Indexes in the table [1] (ICE, 2008), [2] (Berge, 2009), [3] (Teor, 2016), [4] (Allikmae & Jurgenson, 2017).

In the Table 4 the embodied energy consumed in materials of the timber frame wall is described.

Table 4. Embodied energy of timber frame wall (the wall no 5) materials in the case if thermal conductance U = 0.092 W m^{-2} K^{-1}

	Material	Density (kg m^{-3})	Thickness of layer (m)	Material (kg m^{-2})	Embodied energy (MJ kg^{-1})	Material layer's embodied energy (MJ kg^{-1})	(kWh m^{-2})
1	Linseed oil (external)	-	-	-	-	13.54	3.76
2	Cladding	450	0.025	11.25	3.92	44.1	12.25
3	Distance lath	450	0.0019	0.84	3.92	3.35	0.93
4	Wind barrier	50	0.03	0.0015	7.40	11.10	3.08
5	Glass wool	40	0.389	0.015	43.00	669.08	185.86
6	Timber frame	450	0.027	12.15	3.92	47.63	13.23
7	Vapour resistance film	1,390	0.0002	0.278	83.10	23.10	6.42
8	Gypsum board	900	0.014	12.6	6.75	85.05	23.63
9	Colour (internal)	-	-	-	5.27	5.27	1.46
Embodied energy of external wall's square meter						902.22	250.62

From Table 3 we can see that embodied energy of ones square meter of external wall from alternative materials is in the range 13.90–33.39 kWh m^{-2}. Comparing this result to the result from Table 4, we see that embodied energy of timber frame wall will exceed the embodied energy of straw wall 8–18 times. Fig. 4 is compiled to illustrate this difference better.

From the Fig. 4 we can see that the wall no 4 has smallest energy consumption over 30 years and the wall no 5 (industrial materials and U = 0.092 W m^{-2} K^{-1}) consumed even more energy than walls no 2 and 3 with not so good thermal conductance as wall no 5.

In our article the calculation (formula 1) was done to find heating energy consumed during 30 exploitation years.

$$Q_k = H \cdot S \cdot 24 \cdot 10^{-3} \qquad (1)$$

where H – heat loss which is equalised with U-value; S – degree days in Tartu region, 4,933 days (Masso, T. 2012); 24 – hours in.

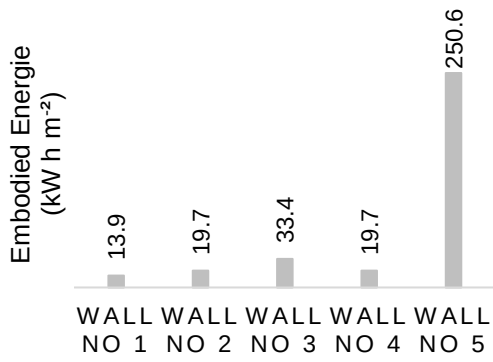

Figure 4. Embodied energy of investigated walls.

Graphs on the Fig. 5 presenting the combined impact of heat energy and embodied energy of all five investigated walls over 30 years. The consumed heat energy depends on U-value.

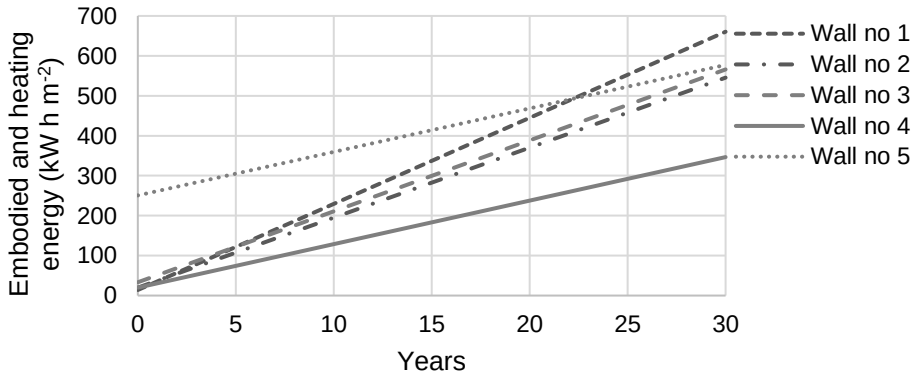

Figure 5. Combined impact of consumed heating and embodied energy of the wall's materials during 30 years.

From the Fig. 5 we can see that the wall no 5 has the best energy saving properties over 30 years and the wall no 4 (industrial materials and U = 0.092 W m^{-2} K^{-1}) consumed more energy than walls no 2 and no 3 with not so good thermal conductance as the wall no 5.

RESULTS AND DISCUSSION

Looking at the walls described in Tables 3 and 4, we see that embodied energy of the walls of local natural materials (the range is 13.90–33.39 kWh m^{-2}) is significantly smaller than that of the wall no 5 (250.62 kWh m^{-2}) constructed from industrial building materials. Comparing results the embodied energy of timber frame wall will exceed the embodied energy of straw wall 8–18 times. Even during 30 years the embodied energy

together with heating energy is smaller, comparing walls no 2 and no 3 to the wall no 4. Exceptionally big difference in energy consumption is between the walls no 5 and no 4. The wall no 4 was the theoretical wall where U-value was calculated using thermal conductivity values taken from literature sources: $\lambda = 0.085$ W m^{-1} K^{-1} (straw) and $\lambda = 0.8$ W m^{-1} K^{-1} (clay plaster) and the got U value was 0.092 W m^{-2} K^{-1}. The wall no 5 was with the equal U-value and thermal conductivities of used materials were taken also from different sources. The comparison of these two theoretical walls show that the materials used in wall no 4 (natural materials) is 1.67 times more sustainable and energy saving than used materials in the wall no 5. So local natural materials are worth researching.

CONCLUSIONS

Embodied energy of external wall's materials had been evaluated for five different walls design with target to estimate 30 years' life cycle energy consumption of the envelope. Looking at the results of the article the embodied energy of external wall's building materials should be taken into account in evaluating the energy efficiency of the envelope. On the whole the suggestion is to study this phenomenon in the future to figure out the more exact conditions which may influence total energy consumption. The future plan is to continue the research of local natural building materials, so called alternative materials, for instance lime and hempcrete. Data about embodied energy of lime based on literature sources may be smaller in Estonia. In the future researches it will be fascinating to find how the recycling energy amount will influence the total amount of used energy.

ACKNOWLEDGEMENTS. This research was supported by the Estonian Centre of Excellence in Zero Energy and Resource Efficient Smart Buildings and Districts, ZEBE, (grant No. 2014-2020.4.01.15-0016) funded by the European Regional Development Fund.

REFERENCES

Allikmae, R. & Jurgenson, A. 2017. *The exploitation and construction technology of straw-bale insulated timber-framed buildings*. Master Thesis, Estonian University of Life Sciences, Tartu, Estonia, 131 pp, (in Estonian).

Berge, B., 2009. *The Ecology of Building Materials*, 2nd Ed. Architectural Press, pp. 446.

Brencis, R., Pleiksnis, S., Skujans, J., Adamovics, A. & Gross, U. 2017. Lightweight Composite Building Materials with Hemp (Cannabis Sativa L.) Additives. *Chemical Engineering Transactions* **57**, 1375–1380. doi: 10.3303/CET1757230

Cornaro, C., Zanella, V., Robazza, P. Belloni, E. & Buratti, C. 2020. An innovative straw bale wall package for sustainable buildings: experimental characterization, energy and environmental performance assessment. *Energy & Buildings* **208**.

ECS (Energy Consumption by Sector) in the EU 2014. 2016. https://epthinktank.eu/2016/07/08/energy-efficiency-in-buildings/energy-consuption-by-sector/. Accessed 15.01.2020.

EPB-EU (Energy performance of buildings in EU) 2019. Energy performance of buildings directive, https://ec.europa.eu/energy/en/topics/energy-efficiency/energy-performance-of-buildings. Accessed 15.01.2020.

EC (European Commission) 2019. Communication from the Commission to the European Parliament, the European Council, the Council, the European Economic and Social Committee and the Committee of the regions, The European Green Deal, pp. 9.

EVS 908-1. 2016. 'Guidance for calculation of thermal transmittance of building envelope Part 1: Opaque building envelope in contact with outdoor-air'. Estonia centre for standardization, Tallinn, Estonia.

Fernandes, J., Peixoto, M., Mateus, R. & Gervasio, H. 2019. Life cycle analysis of environmental impacts of earthen materials in the Portuguese context: Rammed earth and compressed earth blocks. *Journal of Cleaner Production* **241**, 1–19.

GBS, (GLOBAL STATUS REPORT). Towards zero-emission efficient and resilient buildings 2016. 8–9, https://wedocs.unep.org/rest/bitstreams/45611/retrieve. Accessed 15.01.2020.

ICE (Inventory of Carbon and Energy, version 1.6a). 2008. University of Bath. Hammond, G., Jones, C.

Masso, T. 2012. *Building physic ABC*, 146 pp. (in Estonian).

May, B., England J.R., Raison, R. J. & Paul, K.I. 2012, Cradle-to-gate inventory of wood production from Australian softwood plantations and native hardwood forests: Embodied energy, water use and other inputs. *Forest Ecology and Management* **264**, 37–50.

Miljan, J. & Miljan, R. 2012. Embodied energy in building materials. *The use of local natural building materials*, 6–13 (in Estonian).

Miljan, M. & Miljan, J. 2013. Energy consumption of reed products. *Reed and the possibilities to use it*, 72–78 (in Estonian).

Miljan, M. & Miljan, J. 2015. Thermal Transmittance and the Embodied Energy of Timber Frame Lightweight Walls Insulated with Straw and Reed. *2nd International Conference on Innovative Materials, Structures and Technologies, Materials Science and Engineering* **96**. doi: 10.1088/1757-899X/96/1/012076

Miljan, M.-J., Miljan, M. & Miljan, J. 2013. Thermal conductivity of walls insulated with natural materials. *Proceedings of 4th International Scientific Conference CIVIL ENGINEERING'13* **4**, 175–179.

Miljan, M.-J. & Miljan, J. 2013. Thermal Transmittance of Wall Fragments Insulated with Reed. *Guidebook of reed business*, 29–31.

Miljan, M.-J., Allikmäe, R., Jürgenson, A., Miljan, M. & Miljan, J. 2017. Hygrothermal Behaviour of the TimberFramed Sauna with Straw-Bale Walls, *"Civil Engineering`17" Proceedings of International Scientific conference*, pp. 124–130. doi: 10.22616/CE.2018.017

Minke, G. & Mahlke, F. 2004. *Strawball building. Construction handbook*. ('Der Strohballenbau. Ein Konstruktionshandbuch'), 28 pp. (in German).

NECP 2030, 2014. Accessed 30.01.2020.

Probst, L., Erica, M., Laurent, F. & Safaâ, M. 2014. Smart Living Advanced building materials. Business Innovation Observatory. *Directorate-General for Enterprise and Industry, Directorate B* 'Sustainable Growth and EU 2020', Unit B3 'Innovation Policy for Growth'.

Schroeder, H. 2019. *Clay building. With clay ecologically planning and building* (Lehmbau. Mit Lehm ökologische plane und bauen). *Springer Fachmedien Wiesbaden (Verlag),* 593 pp. (in German) doi: 10.1007/978-3-658-23121-7

SGF (The State Gazette in Force) 2014. The Government of the Republic of Estonia, *Minimum energy performance requirement*, § 12 (3). https://www.riigiteataja.ee/en/eli/52010201400. Accessed 30.01.2020.

Teor, M. 2016. *Embodied energy of building materials and structures*. Master Thesis, Estonian University of Life Sciences, Tartu, Estonia, 77 pp. (in Estonian).

Wang, F., Yang, W.-J. & Sun, W.-F. 2020. Heat Transfer and Energy Consumption of Passive House in a Severely Cold Area: Simulation Analyses. *Energies* **13**(3), 626 pp. doi: 10.3390/en13030626

Wihan, J. 2007. Humidity in straw bale walls and its effect on the decomposition of straw, pp. 93. https://tallerconco.org/wp-content/uploads/2017/05/Thesis-Humidity-In-Straw-Bale-Walls-Jakub-Wihan.pdf. Accessed 30.01.2020.

Agronomy Research **18**(3), 2156–2165, 2020
https://doi.org/10.15159/AR.20.171

'GENETIC LOAD' and changes in the chronology of early mortality in mini-pigs of ICG SB RAS

S.V. Nikitin[1], K.S. Shatokhin[2,*], V.I. Zaporozhets[1], N.N. Kochnev[2], D.S. Bashur[1], A.V. Khodakova[2] and V.I. Ermolaev[1]

[1]Institute of Cytology and Genetics of Siberian Department of Russian Academy of Sciences, RU630090 Novosibirsk, Russia
[2]Novosibirsk State Agrarian University, RU630039 Novosibirsk, Russia
[*]Correspondence: true_genetic@mail.ru

Abstract. This paper describes the study of the common factors of mortality of suckling piglets. It is assumed that this parameter is influenced by recessive lethal factors of the genetic load in population. An immediate subject of study was the chronological analysis of mortality in piglets from the breeding group of mini-pigs of ICG SB RAS (Institute of Cytology and Genetics Siberian Branch of Russian Academy of Sciences) for the period from 2013 through 2019. The results revealed increased number of dead piglets in the early postnatal period (first five days after farrowing) over this time period. This observation was confirmed by a statistically significant correlation coefficient between the year of birth and the number of animals that died during the first five days of life. Mortality in the period from the 6th day to weaning, on the contrary, decreased to probable accidental death which was non-related to genetic causes. Observed redistribution of mortality may be associated with increased general homozygosity in population and, in part, with the optimization of the excessive for mini-pigs multiple fertility. It is possible that the consequence of the second cause is an increase in mortality and a decrease in multiple pregnancy. It is assumed that in the breeding group of mini-pigs of the ICG SB RAS, there is the process of eliminating excessive lethal 'genetic load' and optimizing homozygosity to a level ensuring maximum survival of piglets on the 6th day after birth. Results of regression analysis showed that the mortality of piglets in 2018 reached its maximum level and in future a decrease to the optimum level which is typical for domestic pigs is possible. In general, results of this study suggest that newborn piglets are represented by two types. The first type includes animals whose viability potential determined by recessive lethal 'genetic load' is zero – they cannot live outside mother's body. The second type is represented by animals with a genetic viability potential equal to one –they can die only from accidental death.

Key words: mini-pigs of ICG SB RAS, 'genetic load', homozygosity, inbreeding, mortality, optimization of piglets number, genetic viability potential, agriculture.

INTRODUCTION

Gene pool of a domestic pig, as well as of on any other species, has the so-called 'genetic load' which includes neutral and lethal components (Ingue-Vechtomov, 1989; Lyons et al., 2009). Domestic pigs exist somehowin isolated populations (herds) with limited number of members (Bekenev, 2012; Christensen et al., 2019) where genetic

processes typical forsuch populations take place; one of these is an increase in homozygosity. This is caused by both random stochastic processes, such as gene drift, and elimination of lethal and semi-lethal mutations through selection (Li, 1976; Ingue-Vechtomov, 1989; Nikitin & Knyazev, 2015). Depletion of gene pool due to gene drift is somewhat balanced by the selection vector for adaptive heterozygosity, as well as due to continuous mutagenesis of the satellite DNA (Ollivier, 2007; Jaeger et al., 2016). At the same time, protein-coding fragments of genome are subject to elimination which depletes not only gene pool, but also population phenofund (Markov & Naimark, 2015). The rate of these processes depends on the size of population and the presence of inbreeding (Li, 1976; Huisman et al., 2016). Moreover, if there is inbreeding in the population, then not only separate loci but the entire genomes (Severtsov, 1990) or, what is obviously more true, their rather large fragments, become homozygous.

The aim of this research is to study the process of elimination 'genetic load' from the breeding group of mini-pigs of the ICG SB RAS associated with early mortality. During the study period, this group was 'closed' (isolated), small in number, and there was a systematic planned inbreeding in it. Herd homozygosity increased from 0.25 in 2012 to 0.90 in 2018 (Nikitin et al., 2014 and 2018). 'Genetic load' of the breeding group of mini-pigs of the ICG SB RAS should be very high and various since four initial breeds were used for its forming – Svetlogorsk mini pigs, Large White, Landrace and Vietnamese breeds (Nikitin et al., 2014). Moreover, it should be taken into account that the allele pool of mini-pigs of the ICG SB RAS was formed not by the general gene pool of these breeds, but rather by total genomes of the founders (Shatokhin et al., 2014). Ultimately, a unique gene pool, different from other forms of domestic pig, has developed in this population what is confirmed by the unique sets of frequencies of erythrocyte antigens of blood groups, allotypes of serum proteins (Shatokhin et al., 2019), endogenous retroviruses (Aitnazarov et al., 2014) and microsatellites (Traspov et al., 2016). Each of the founders, accordingly, brought its share of genetic load into the herd. Studying of the variety of colors of mini-pigs of the ICG SB RAS showed the presence of 'hidden' variants in the initial forms (Nikitin et al., 2016 and 2017) which are obviously a manifestation of a neutral recessive 'genetic load', however, the question about the presence of early mortality lethal 'genetic load' remained unanswered.

MATERIALS AND METHODS

The studies were carried out according to the data of zootechnical registration of farrowing in the breeding group of mini-pigs of the ICG SB RAS for the period of 2013–2019. The number of animals in reproductive group during each coupling campaign in the study period ranged from 5 to 10 boars and from 20 to 30 sows (Nikitin et al., 2018). In the period from 01.01.2013 to 31.12.2019 were conducted 14 coupling campaigns. There was culling of small and weak at birth animals in the first five days of their life. All animals were separately weighed at birth and 1 month age. Upon the each fact of mortality of an animal, the date and reason for it was specified in the zootechnical document.

Mini-pigs of the ICG SB RAS is kept in 'Mini-pigs farm' of the Federal State Budget Scientific Institution 'Federal Research Center Institute of Cytology and Genetics of the Siberian Branch of the Russian Academy of Sciences' (ICG SB RAS) in the suburban area of Novosibirsk, in the village of Kainskaya Zaimka, Russia. Animals

are kept in unheated pig house, on concrete floors, using sawdust as bedding (Sada & Reppo, 2011). Feeding of animals carried out with concentrates consisting of bran, wheat stock feed and boiled meat waste. The content and ratio of nutrients in the feeding corresponded to the standards for feeding pigs with calculation on a live weight of 50–80 kg (Vladimirov et al., 2003). Currently, mini-pigs of the ICG SB RAS are used as a model for cardiac surgery experiments conducted at Meshalkin National Medical Research Center (Chepeleva et al., 2017).

In domestic pigs, early mortality of piglets is commonly divided into two main periods (Topchin, 2012):

1. Before registration in zootechnical journal, i.e. first five days after birth. This group includes stillborn, dead at birth, small, weak and ugly pigs.
2. After registration, on the sixth day after birth and before weaning to sows.

Mortality was estimated as the ratio of the number of deaths during the first of second period to the total number of birth expressed as a percentage. Thus, three parameters were used:

1. Total mortality –ratio of the number of deaths before weaning to sows, including stillborn and ugly ones, to the number of births (%);
2. Mortality before the 6th day – ratio of the number of deaths during first five days, including stillbirths and ugly ones, to the number of births (%);
3. Mortality of sucklings – ratio of the number of deaths starting from the 6thday until weaning to the number of births (%).

For plottingin accordance to studied parameters, we used Microsoft Excel. Regression and correlation analyses were carried out according to recommendation (Lakin, 1990). Significance of differences in statistical parameters was evaluated using Student's test (Lakin, 1990). The trend was calculated by using software Microsoft Exel 2007.

RESULTS

Six-year dynamics of changes in mortality of piglets of mini-pigs in the ICG SB RAS can be described by linear regression equations (Fig. 1); it allows estimating the significance of these changes through correlation coefficients between the year of birth and the proportion of dead piglets (Table 1).

These changes show a relevant increased death rate of piglets until the 6th day after birth with a relevant decreased mortality starting from the 6thday. In general, mortality growth from birth to weaning is statistically insignificant (Table 1). This combination of changesin three mortality parameters allows suggesting that there is a shift in the time of piglets' death to the earlier period, i.e. first five days after birth. If this assumption is true, changes in mortality before the 6thday after birth and starting from it should be:

1) symmetrical,
2) with a negative correlation between them.

Symmetry of the changesobserved means the symmetry of their linear trends, through the intersection of which and parallel to *x* axis, the line of symmetry will run. To determine the $_y$ coordinate of this line, we used linear regressionequationsfor mortality before the 6thday and starting from it (Fig. 1). The equations were reduced to $x = \frac{y+6472.2}{3.2225}$ and $x = \frac{-y+4491.7}{2.2238}$ and, and then combined into equation $\frac{y+6472.2}{3.2225} = \frac{-y+4491.7}{2.2238}$ from which $y \approx 14.99$ (Fig. 1).

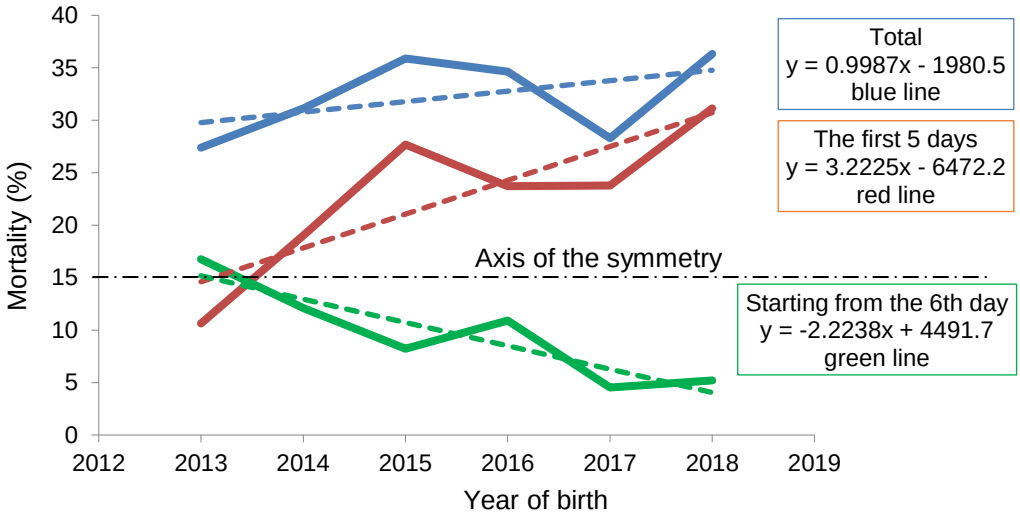

Figure 1. Changes in postnatal mortality of piglets of mini-pigs at the ICG SB RAS during the period from 2013 to 2018.

Table 1. Changes in mortality of piglets of mini-pigs in ICG SB RAS

Parameter			Year						Correlation coefficient
			2013	2014	2015	2016	2017	2018	
Born	total	heads	555	331	365	413	265	212	–
Died	total	heads	152	103	131	143	75	77	–
		%	27.38 ± 1.89	31.12 ± 2.54	35.89 ± 2.51	34.62 ± 2.34	28.30 ± 2.77	36.32 ± 3.30	0.48
	before the 6th day	heads	59	63	101	98	63	66	–
		%	10.63 ± 1.31	19.03 ± 2.16	27.67 ± 2.34	23.73 ± 2.09	23.77 ± 2.61	31.13 ± 3.18	0.84 $P < 0.05$
		trend	14.69	17.92	21.14	24.36	27.58	30.81	–
	After the 6th day	heads	93	40	30	45	12	11	–
		%	16.76 ± 1.59	12.08 ± 1.79	8.22 ± 1.44	10.90 ± 1.53	4.53 ± 1.28	5.19 ± 1.52	-0.90 $P < 0.01$
		trend	15.19	12.97	10.74	8.52	6.30	4.07	–
Trend deviation from the line of symmetry	before the 6th day	%	0.30	2.93	6.15	9.37	12.59	15.82	–
	Afterthe 6th day	%	0.20	2.02	4.25	6.47	8.69	10.92	–
	difference	%	0.10	0.91	1.90	2.90	3.90	4.90	–
Difference between actual proportions of died before and after the 6th day		%	-6.13	6.95	19.45	12.83	19.24	25.94	0.89 $P < 0.01$
Average weight at birth		g	701.29	709.28	669.05	682.31	706.75	651.39	-0.56

Paired values of deviations of trend lines from the line of symmetry should be equal in absolute values, and their difference should be equal to zero, both in each comparison pair and in general. However, the absolute values of deviations were actually not equal (Table 1), and their average value over six measurements, 2.435 ± 0.742, is definitely

($P < 0.01$) not equal to zero. Thus, the changesin mortality before and after the 6thday after birth are not symmetrical, however, relevant negative correlation is observed between them ($r = -0.98$, $P < 0.01$). This result showed that, along with a redistribution of the death time of piglets, there was a direct increase in their mortality up to the 6thday after birth, as it is indicated by a relevant positive correlation between the year of birth and the difference between observed mortality values before the 6thdays after birth and starting from it (Table 1).

To assess the nature of changes in the growth rate of piglet mortality during the first five days after birth, the dynamics of this process was developed (Fig. 2) showing that although this process can be described by linear regression equation in the time period under study, it can be more adequately expressed by parabolic equation (Fig. 2). According to parabolic equation, in 2018, the death rate of piglets in the first five days after birth reached its maximum and will continue to decline. It is known that low weight of newborn piglets (less than 600 g) is accompanied by their reduced life and competitiveness (Pond & Houpt, 1978; Nikitin & Knyazev, 2015). Correlation between mortality from birth to weaning and average birth weight during this year was statistically significant ($r = -0.87$, $P < 0.05$). At the same time, in this research, the correlation between the year of birth and the average weight of piglet born this year is statistically insignificant (Table 1). That is, the variation in average birth weight, unlike mortality, is not related to the year of birth. Therefore, the correlation between mortality and average birth weightis not indirect (mediated by year of birth), but a direct one.

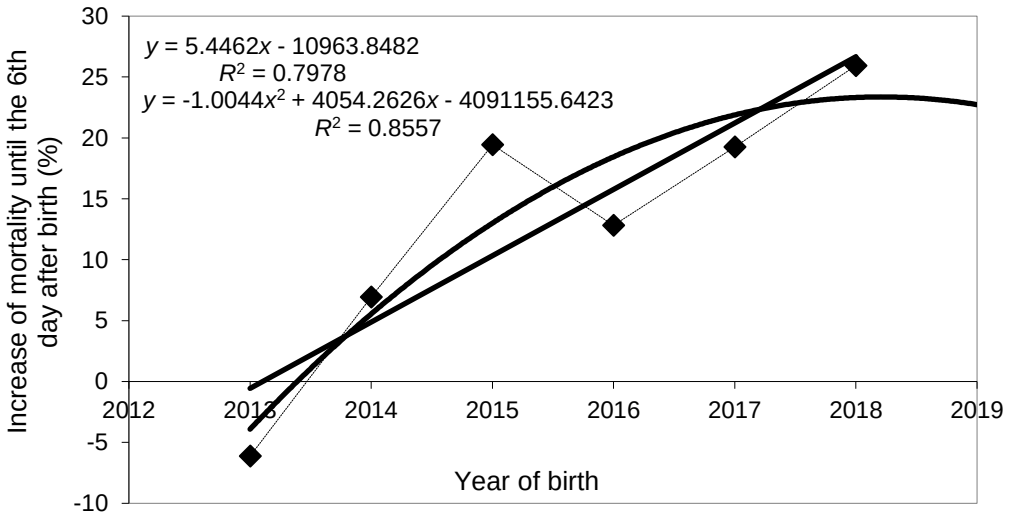

Figure 2. Increase in mortality of piglets of mini-pigs at the ICG SB RAS during the first five days after birth in the period from 2013 to 2018.

Piglets mortality from birth to weaning will result in a reduction in the number of piglet reared from sow (live on the 6thday after birth) and in the number of weaned piglets received on average from one sow. Since it cannot be excluded out that a shift in mortality can also affect prenatal period, a decrease in total number of piglets (including stillborn piglets) is possible.

To assess these parameters, the dynamics of their changes were plotted (Fig. 3). It turned out that although a decrease in multiple pregnancy was observed for six years, correlation coefficient between it and the year of birth of piglets is statistically insignificant and equals to -0.64. However, for parameters directly related to mortality, it is statistically significant ($P < 0.01$) and amounts to:

1) for the number of born piglets on the 6th day after birth $r = -0.98$;
2) for the number of piglets at weaning $r = -0.91$.

Statistical insignificance of correlation between multiple pregnancy and the year of birth suggests that there is no shift in mortality to prenatal period. However, there is a parallelism in the trends of multiple pregnancy and the number of piglets in a litter at weaning (Fig. 3), but at the same time, correlation coefficient between these parameters is irrelevant ($r = 0.70$). Since the inclination of line is determined by regression coefficient, the absence of significant differences between two regression coefficients indicates their possible parallelism. Regression coefficient for multiple pregnancy is -0.1591 ± 0.0954, for the number of live piglets before weaning -0.1771 ± 0.0395 (Fig. 3). Difference between them is irrelevant (Student's criterion is 0.17). Parallelism of trends, one of which is statistically significant and the other irrelevant, as well as irrelevant correlation between them indicate a greater exposure of the second parameter to the influence of random factors. Thus, there is reason to believe that a shift in mortality to prenatal period exists, and itmakes sense much more than the absence of such shift.

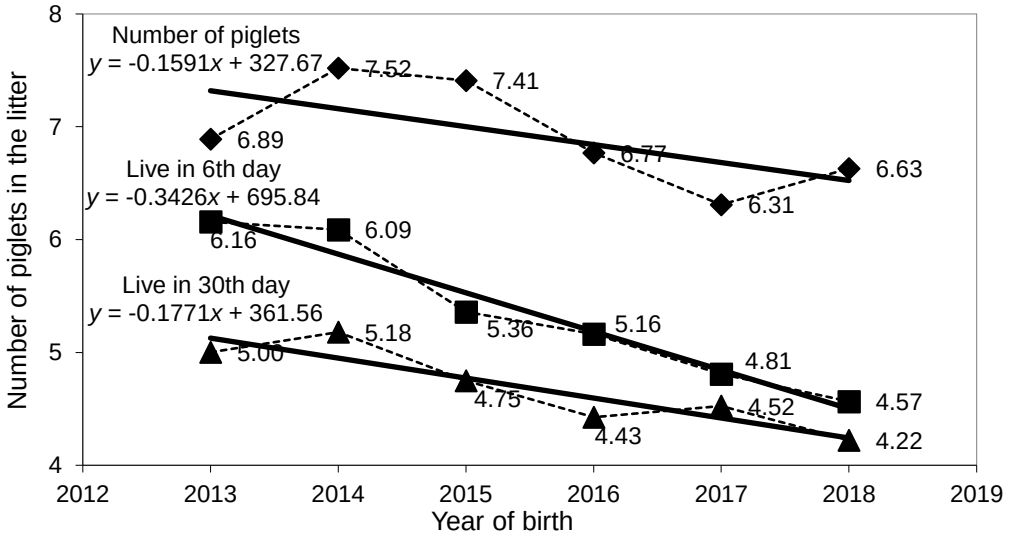

Figure 3. Dynamics of changes in total multiple pregnancy; piglets reared from mother and the number of piglets at weaning per sow.

DISCUSSION

This study showed the relevancy of common division of piglets' mortality into two periods:

1) before the 6thday after birth;
2) starting from the 6th day after birth.

Genetic background of this dividing is obvious. It is due to genetically determined viability potential of newborns which are naturally divided into two types (Rosendo et al., 2007; Andersen et al., 2011; Topchin, 2012; Nikitin & Knyazev, 2015):

1) Animals whose genetic viability potential (the probability of surviving until weaning) is equal to zero. Their genotype and, accordingly, phenotype are incompatible with life outside mother's body. The proportion of such animals shows the level of burdening the reproductive part of population with lethal 'genetic load' but is not related to the viability of young animals during suckling period.

2) Animals whose genetic viability potential in early postnatal period of ontogenesis can be considered as equal to one. In them, just accidental death can happen which is not related to their genetic characteristics.

The features of mortality changes are obviously associated with increased homozygosity in a limited population with systematic inbreeding hat was observed earlier (Dubinin & Glembotskiy, 1967). Was shown that the maximum frequency of lethal alleles can reach 10%, after which these alleles were eliminated by selection (Derks et al., 2019). Since each dying and naturally not leaving offspring animal reduces the frequency of allele responsible for its death (Li, 1976; Altukhov, 2003), this should form the dynamics of increased mortality described by parabolic equation (Fig. 2). Increased homozygosity of selection group is also associated with redistribution of mortality to an earlier period. This seems quite logical given the four-factor system of piglets ' safety, which consists of feeding sows, their maternal qualities, size of the litter and genetic components (Andersen et al., 2011). Moreover, the latter is also very difficult (Rothschild et al., 2007; Wang et al., 2016; Stafuzza et al., 2019) and it in turn can be decomposed into the presence of alleles that reduce viability, homozygosity and genes that determine the live weight, since it is also a factor of survival (Pond & Houpt, 1978; Smith et al., 2007). With constant litter size and feeding conditions, as well as with the elimination of sublethal alleles and a decrease in homozygosity, the shift in mortality terms to an earlier period can be explained by the fact that the proportion of mortality of small-weight piglets in the herd increases.

Culling of weak newborns could simulate shifting mortality to an earlier period but such cases are recorded as culling, and not as death, so this assumption is untenable. At the same time, cumulative effect of homozygosity in many loci that reduce viability should shift the time of death to an earlier period. It is known that one of the significant factors of animal mortality in a highly inbreed population is the homozygous state of lethal and sublethal alleles (Latter, 1998; Charlesworth & Willis, 2009). Therefore, the more such loci are homozygous, the earlier the animal will die. Shift in mortality to the first five days after birth has led to minimal mortality of piglets during later period; during last two years, it has stabilized and amounts to about 5%. This value is consistent with the probability of accidental death non-dependent of genetic factors (Muns et al., 2016). Therefore, there is reason to believe that, other things being equal, achieved level will remain such in the future.

The idea that a negative 'genetic load' can also perform positive functions seems to be very interesting. If multiple pregnancy is excessive, homozygosity for recessive lethal and sublethal alleles reduces its size and, thereby, reducing the 'damage' to mother's body and competition between littermates, increases the possibility of survival of the remaining animals. Breeding mini-pigs aimed at downsizing is, in fact, an artificially created situation when multiple fertility inherited from large pigs is clearly

excessive. A rapid decrease in actual multiple pregnancy (the number of ovulated eggs) is hardly possible, therefore, the optimization of the number of offspring in litter (bringing it in line with the size of mother) is achieved by increasing homozygosity for the alleles of early death. Moreover, the sooner this death occurs, the more beneficial it will be, both for mother and for remained piglets. Mortality changes observed in the breeding group of mini-pigs of the ICG SB RAS are consistent with this hypothesis. They show a rapid increase in early mortality (the whole process took just six years), with the same rapid decrease in mortality during later period. At the same time, the number of piglets survived to weaning is reduced what can be considered as an adaptively determined tendency for an optimal number for breeding group. It should be noted that a decrease in the number of piglets at weaning to the value obtained in 2018 (4.22 piglets per sow) is not critical for mini-pigs at the ICG SB RAS. Much more important is the positive effect of this reduction, i.e. lesser burden on sows, their better development, fatness, and health of piglets; the latter, therefore, in less age become ready for use in surgical experiments.

CONCLUSION

In general, results of this study show that in the breeding group of mini-pigs of the Institute of Cytology and Genetics of SB RAS, the process of removing 'genetic load' and optimization of multiple pregnancy has reached its completion stage. A herd of mini-pigs at the ICG SB RAS is highly inbred. According to 2018 data, similarity index forthe animals of reproductive core calculated on the basis of the 'blood share' of founder is close to the figure of one, that is, genetic similarity between them is close to that between siblings. It is clear that the level of homozygosity with this genetic background is rapidly growing including this in the alleles that form 'genetic' load which caused increased mortality. However, death of young animals from the 6thday until weaning in 2017–2018 stopped at a value close to 5%, that is, it obviously does not have genetic background and is due to random reasons. The shift of death to the first days after birth and achievement of maximal annual increase in mortality during this period indicate that in the future, a decrease in piglet mortality is expected to reach the level optimal for the breeding group of mini pigs of the Institute of Cytology and Genetics SB RAS.

ACKNOWLEDGEMENTS. This study was supported by budget financing on a state assignment (project No. AAAA-A17-117071240065-4).

REFERENSES

Aitnazarov, R.B., Yudin, N.S., Nikitin, S.V., Ermolayev, V.I. & Voevoda, M.I. 2014. Identification of whole genomes of endogenous retroviruses in Siberian miniature pigs. */Vavilovskii Zhurnal Genetiki i Selektsii/ Vavilov Journal of Genetics and Breeding* **18**(2), 294–297 (in Russian).

Altukhov, Yu.P. 2003. *Genetic processes in populations: Manual*. 3ed. Moscow, Academkniga, 431 pp. (in Russian).

Andersen, I.S., Naevdal, E. & Bøe, K.E. 2011. Maternal investment, sibling competition, and offspring survival with increasing litter size and parity in pigs (*Sus scrofa*). *Behav Ecol Sociobiol.* **65**(6), 1159–1167. doi: 10.1007/s00265-010-1128-4

Bekenev, V.A. 2012. *Technology of Pig Keeping and Breeding*. St. Petersburg: Lan Publ., 416 pp. (in Russian).

Charlesworth, D. & Willis, J.H. 2009. The genetics of inbreeding depression. *Nat Rev Genet*. **10**, 783–796. doi: 10.1038/nrg2664

Chepeleva, E.V., Balashov, V.A., Dokuchaeva, A.A., Korobejnikov, A.A., Strelnikov, A.G., Lependin, S.O., Pavlova, S.V., Agladze, K.I., Sergeevichev, D.S. & Pokushalov, E.A. 2017. Analyis of biological compatibility of polylactidenanofibrous matrix vitalized with cardiac fibroblasts in a porcine model. /*Geny I kletki* / *Genes & Cells* **XII**(4). doi: 10.23868/201707031 (in Russian).

Christensen, O.F., Nielsen, B., Su, G., Xiang, T., Madsen, P., Ostersen, T., Velander, I. & Strathe, A.B. 2019. A bivariate genomic model with additive, dominance and inbreeding depression effects for sire line and three-way crossbred pigs. *Genet SelEvol*. **51**, 45. doi: 10.1186/s12711-019-0486-2

Derks, M.F.L., Gjuvsland, A.B., Bosse, M., Lopes, M.S., van Son, M., Harlizius, B., Tan, B.F., Hamland, H., Grindflek, E., Groenen, M.A.M. & Megens, H.-J. 2019. Loss of function mutations in essential genes cause embryonic lethality in pigs. *PLoS Genet*. **15**(3), e1008055. doi: 10.1371/journal.pgen.1008055

Dubinin, N.P. & Glembotskiy, Ya.L. 1967. *Population genetics and selection*. Moscow, Nauka, 592 pp. (in Russian).

Huisman, J., Kruuk, L.E.B., Ellis, P.A., Clutton-Brock, T. & Pemberton, J.M. 2016. Inbreeding depression across the lifespan in a wild mammal population. *Proc Natl AcadSci*. **113**(13), 3585–3590. doi: 10.1073/pnas.1518046113

Ingue-Vechtomov, S.G. 1989. *Genetics with the basics of breeding*. Moscow, Vyshayashkola, 591 pp. (in Russian).

Jaeger, C.P., Duvall, M.R., Swanson, B.J., Phillips, C.A., Dreslik, M.J., Baker, S.J. & King, R.B. 2016. Microsatellite and major histocompatibility complex variation in an endangered rattlesnake, the Eastern Massasauga (*Sistruruscatenatus*). *EcolEvol*.**6**(12), 3991–4003. doi: 10.1002/ece3.2159

Lakin, G.F. 1990. *Biometrics. Fourth edition revised and expanded*. Moscow, Vysshayashkola, 352 pp. (in Russian).

Latter B.D. 1998. Mutant alleles of small effect are primarily responsible for the loss of fitness with slow inbreeding in Drosophila melanogaster. *Genetics*; **148**(3), 1143–1158.

Li, C.C. 1976. *First course in population genetics.* The Boxwood Press Pacific Grove, California, 556 pp.

Lyons, E.J., Amos, W., Berkley, J.A., Mwangi, I., Shafi, M., Williams, T.N., Newton, C.N., Peshu, N., Marsh, K., Scott, J.A.G. & Hill, A.V.S. 2009. Homozygosity and risk of childhood death due to invasive bacterial disease. *BMC Med Genet.* **10**, 55.doi: 10.1186/1471-2350-10-55

Markov, A. & Naimark, E. 2015. Evolution. Classical Ideas in the Light of New Discoveries. Moscow, ACT: CORPUS, 656 pp. (in Russian).

Muns, R., Nuntapaitoon, M. & Tummaruk, P. 2016. Non-infectious causes of pre-weaning mortality in piglets. *Livestock Science* **184**, 46–57. doi: 10.1016/j.livsci.2015.11.025

Nikitin, S.V. & Knyazev, S.P. 2015. *Selection and Adaptation in Domestic Pig Populations.* Saarbrucken, Lambert Academy, 228 pp. (in Russian).

Nikitin, S.V., Knyazev, S.P. & Shatokhin, K.S. 2014. Miniature pigs of ICG as a model object for morphogenetic research. *Russ. J. Genet.: Appl. Res*. **4**(6), 511–522. doi: 10.1134/S207905971406015X

Nikitin, S.V., Knyazev, S.P., Shatokhin, K.S., Goncharenko, G.M., Zaporozhets, V.I. & Ermolayev, V.I. 2017. Juvenile coat colours in mini-pigs at ICG. /*Vavilovskii Zhurnal Genetiki i Selektsii / Vavilov Journal of Genetics and Breeding* **21**(6), 638–645. doi: 10.18699/VJ17.280 (in Russian).

Nikitin, S.V., Knyazev, S.P., Shatokhin, K.S., Zaporozhets, V.I. & Ermolaev, V.I.2018.Breeding and selection of mini-pigs in the ICG SB RAS. /*Vavilovskii Zhurnal Genetiki i Selektsii / Vavilov Journal of Genetics and Breeding* **22**(8), 922–930. doi: 10.18699/ VJ18.434 (in Russian).

Nikitin, S.V., Shatokhin, K.S., Knyazev, S.P., Goncharenko, G.M., Zaporozhets, V.I. & Ermolayev, V.I. 2016. Polymorphic loci of coat color inmini-pigs. /*Vavilovskii Zhurnal Genetiki i Selektsii / Vavilov Journal of Genetics and Breeding* **20**(5), 584–595. doi: 10.18699/VJ16.180 (in Russian).

Ollivier, L. 2007. Analyses of the European pig diversity using genetic marcers. In: *Proceedings of 6th International Symposium on the Mediterranean Pig* (Ed. L. Nanni, Costa, P. Zambonelli, V. Russo). October 11–13, 2007. Messina - Capo d'Orlando (ME), Italy, pp. 10–22.

Pond, W.G. & Houpt, K.A. 1978. *The Biology of the Pig*. Cornell University Press, Ithaca, New York, 356 pp.

Rosendo, A., Druet, T., Gogué, J., Canario, L. & Bidanel, J.P. 2007. Correlated responses for litter traits to six generations of selection for ovulation rate or prenatal survival in French Large White pigs. *J Anim Sci*. **85**(7), 1615–1624. doi: 10.2527/jas.2006-690

Rothschild, M.F., Zhi-Liang, H. & Zhihua, J. 2007. Advances in QTL mapping pigs. *Internation J. Biological Sci.* **3**, 192–197. doi: 10.7150/ijbs.3.192

Severtsov, A.S. 1990. *The direction of the evolution*. Moscow State Univercity Publ., 272 pp. (in Russian).

Sada, O. & Reppo, B. 2011. Indoor climate in pigsty with deep litter system in winter. *Agronomy Research* **9**(Special Issue 1) 203–212.

Shatokhin, K.S., Knyazev, S.P., Goncharenko, G.M., Nikitin, S.V. 2014. The effect of allele introduction on the status of the allele pool of blood group system loci in the population of minipigs in the Institute of Cytology and Genetics, Novosibirsk. /*Vestnik NGAU / Bulletin of the Novosibirsk State Agrarian University* **33**(4), 119–124 (in Russian).

Shatokhin, K.S., Nikitin, S.V., Knyazev, S.P., Goncharenko, G.M., Ermolaev, V.I. & Zaporozhets, V.I. 2019. Livestock, physiology and genetic of the mini-pigs of ICG SB RAS. Novosibirsk, Siberian Federal Research Centre for AgroBiotechnology Publ.URL: https://elibrary.ru/ author_items.asp? authorid=805266 (in Russian).

Smith, A.L., Stalder, K.J., Serenius, T.V., Baas, T.J. & Mabry, J.W. 2007. Effect of piglet birth weight on weights at weaning and 42 days post weaning. *J Swine Health Prod*. **15**(4), 213–218.

Stafuzza, N.B., de Oliveira Silva, R.M., de Oliveira Fragomeni, B., Masuda, Y., Huang, Y., Gray, K., Lino Lourenco, D.A. 2019. A genome-wide single nucleotide polymorphism and copy number variation analysis for number of piglets born alive. *BMC Genomics* **20**, 321. doi: 10.1186/s12864-019-5687-0

Topchin, A.V. 2012. Safety of young animals– the most important factor in increasing profitability in pig farming. /*VestnikVNIMZh / Journal of VNIIMZH* **3**(7), 38–42 (in Russian).

Traspov, A., Deng, W., Kostyunina, O., Ji, J., Shatokhin, K., Lugovoy, S., Zinovieva, N., Yang, B. & Huang, L. 2016. Population structure and genome characterization of local pig breeds in Russia, Belorussia, Kazakhstan and Ukraine. *Genet SelEvol*. **48**(16) doi: 10.1186/s12711-016-0196-y

Vladimirov, N.I., Cheremnyakova, L.N., Lunicyn, V.G., Kocarev, A.P. & Popelyaev, A.S. 2008. *Feeding of farm animals*. Barnaul, Russia, Altai State Agricultural University Publ., 212 pp. (in Russian).

Wang, X., Liu, X., Deng, D., Yu, M. & Li, X. 2016. Genetic determinants of pig birth weight variability. *BMC Genet*. **17**(1), 15. doi:10.1186/s12863-015-0309-6

Agronomy Research **18**(3), 2166–2184, 2020
https://doi.org/10.15159/AR.20.164

Thermal performance of a solar hybrid dryer for Conilon coffee (*Coffea canephora*)

J.L. Paes[1,*], B.C. Vargas[1], J.P.B. Cunha[1], D.S.C. Silva[1], G.A.S. Ferraz[2], M.R.S. Braz[1], P.F.P. Ferraz[2], L. Conti[3] and G. Rossi[3]

[1]Rural Federal University of Rio de Janeiro, Engineering Department, Campus Seropédica, ZIP Code BR23890000, Seropédica, Rio de Janeiro, Brazil
[2]Federal University of Lavras, Agricultural Engineering Department, ZIP Code BR37200000, Lavras, Minas Gerais, Brazil
[3]University of Florence, Department of Agricultural, Food, Environment and Forestry (DAGRI), Via San Bonaventura, 13, IT50145, Florence, Italy
[*]Correspondence: juliana.lobop@gmail.com

Abstract. The study was aimed at design and development of an energy efficient hybrid solar dryer suitable for drying of organic Conilon coffee placed in the town of Seropédica, Rio de Janeiro, Brazil. The energy efficiency and the drying efficiency were the evaluation criteria for thermal performance of the hybrid solar dryer during the coffee drying. Temperature and relative humidity (RH) of the drying and ambient air, solar radiation intensity and coffee weight loss were monitored during the drying process. The process occurred over six consecutive days; the drying time was from 07:00 to 17:00 h, totalling 120 h of operation with an intermittent period (at night) of 14 h. During intermittence, the exhaust system kept off and solar collector and drying chamber sealed. The effective drying period took 60 h, with temperature and RH, respectively, of 38.3 °C and 60.6% outlet of the solar collector, 32.7 °C and 72.2% outlet drying chamber and 27.8 °C and 74.5% ambient air. The maximum temperature in the solar collector and drying chamber reached 54 and 47.7 °C, respectively, with an ambient air temperature of 32 °C at 12:00 h. These values showing temperature increase 22.2 °C in solar collector and 10 ºC drying chamber. The mean variation for the reduction in RH between the drying air inside the solar collector and the ambient air was 28%, while in the chamber obtained in a range of 10.5% at 13:00 h. The solar collector and dryer chamber efficiency were 29.1 and 40.8%, respectively, while the overall dryer efficiency 39.7%.

Key words: organic Conilon coffee, drying, sustainable processing, energy efficiency.

INTRODUCTION

In the processing of coffee fruits there are different methods to obtain sensory characteristics to be consumed as a beverage. Among the methods, those that make up the post-harvest processing can be highlighted. The first stage can be divided into dry pre-processing to obtain natural grain and washing pre-processing generating peeled, pulped and mucilage-free coffee (Lima Filho et al., 2015). These stages is followed by drying of the coffee fruit, in which there is a reduction in their moisture content, thus leading to reductions in chemical reactions and in the proliferation of microorganisms

that often deteriorate the final product (Borém et al., 2013, Nakayama et al., 2020). Coffee is one of the products with highest costs in the drying process, not only due to the high initial moisture content but also because the structural characteristics of fruits and grains are susceptible to damage that can depreciate the quality of the dry product, decreasing its commercial value (Palacin et al., 2009).

Specifically, conventional methods of drying coffee can be on the ground (earth and concrete) and in mechanical dryers. The sun drying and air natural stages at the ground is possible in environments with low relative humidity and little cloudiness, having as main advantage the saving of energy. However, this type of drying is a relatively slow process that can lead to considerable losses of product quality, besides requiring extensive areas and long drying time (Deeto et al., 2018). On the other hand, dryers that use energy sources through electricity, firewood or fossil fuels avoid the problems of ground terraces, but they are equipment that increase production costs, harmful to the environment and generate energy dependence for producers (Moreira et al., 2019).

Nowadays, sustainable food processing is becoming an increasingly important issue in developing countries. Within this concept, solar drying is able to meet the growing demand for healthy and low-cost natural foods (Azouma et al., 2019). In view of energy issues, an alternative to the drying process is the use of solar dryers because it is a process that uses renewable and non-polluting energy sources (Altobelli et al., 2014, Azouma et al., 2019). Solar dryers for agricultural products are the most useful device from the point of view of energy conservation that not only saves energy, but also drying time, occupying less area, improving product quality and the employee's lives (Kant et al., 2016; Camelo et al., 2019; Moreira et al., 2019). In Brazil, solar drying of agricultural products becomes a promising methodology due to the use of the abundance of solar radiation (Alves et al., 2019). With this it is possible to convert solar energy into thermal energy in the solar collector coupled to the dryer and to heat the ambient air (Camelo et al., 2019). Therefore, solar dryers are an alternative to current conventional drying methods for coffee (Moreira et al., 2019).

Solar drying is based on the use of direct and indirect dryers with natural or forced convection, making it possible to control the drying rate (Kumar et al., 2016; Lingayat et al., 2020a). In the first dryer, the solar collector and drying chamber perform the same function with the incidence of radiation directly on the agricultural product (Almeida et al., 2016). These dryers have advantages such as simple construction and low cost, but they present greater product deterioration, slower drying and loss of efficiency due to decreased transmittivity of the glass lid from condensation and moisture (Sandali et al., 2019; Lingayat et al., 2020b). In contrast, in the indirect dryer, the radiation does not act directly on the agricultural product, which results in quality improvements, besides reducing drying time and contaminants, ideal characteristics for coffee drying (Lingayat et al., 2017).

Furthermore, solar dryers can be classified as hybrids in terms of how they are activated by means of energy. In other words, hybrids can be mentioned, in which different forms of generation obtain the same type of energy, whether electrical or thermal (Montero et al., 2010; Oliveira et al., 2019). In addition, hybrid active mode enabled a considerable reduction in drying time, being an aspect to take into account for its use during low solar radiation or at night time (Montero et al., 2015). Hybrid dryers are a viable option as they can make use of solar thermal energy, in heating the drying

air, and electrical energy by conventional source or photovoltaic plates, to activate the exhaust system, making that this system is more flexible and economical than the conventional one (Oliveira et al., 2019). Different design and performance evaluation of hybrid dryer has been studies. Solar energy during peak sunshine hours and liquefied petroleum gas (LPG) water heater as auxiliary heat source during low sunshine hours was evaluated to drying of shrimps. In this hybrid dryer, solar system supplied 73.93% of the energy requirement of the solar-LPG hybrid dryer for shrimp drying (Murali et al., 2019).

In association with the construction, design and performance evaluation of different types of dryers, one must take into account the efficiency of these technologies when drying agricultural products. In a study for the development and technical-economic evaluation of an electric hybrid solar dryer for tomato cultivation, Boughali et al. (2009) verified the influence of the increase in air flow on the efficiency of the dryer, thus obtaining efficiency of up to 47.5% for a flow of 2 m s^{-1}. The authors also conclude that under the conditions evaluated, the return on investment was 1.27 years compared to the estimated dryer life of 15 years, indicating that it is a viable option for drying agricultural products.

Currently, several studies are being developed to improve and increase the efficiency of solar dryers through the search for materials that allow greater transfer and conduction of heat. However, complex material combinations make these dryer designs less sustainable and more economical. Khanlari et al. (2020a) mention that when drying agricultural products, temperature is a limiting factor. Thus, evaluating a tube-type air heater associated with the greenhouse dryer, showed a maximum efficiency of 56.77% for an air flow of 0.015 kg s^{-1} and reducing the drying time by 30%.

Evaluating the solar drying of cucumber fruits (*Solanum muricatum* L.), two dryers were developed, an indirect double-pass dryer (DIPSD) and another indirect double-pass dryer with modification of the mesh absorber (DPISDMA). The solar dryer showed an average efficiency of the collector between 70 and 80%, and the addition of the mesh with a thickness of 5 mm improved the thermal performance of the collector, allowing a better quality drying of the cucumber fruits (Güler et al. 2020). By studying the drying behavior of celery (*Apium Graveolens* L.) in a parallel pass solar dryer (PPSC), deflectors were added to the dryer in order to improve thermal performance. The dryer during the evaluation presented instantaneous efficiency of 84.3% for higher flow and higher thermal efficiency as more deflectors are added (Khanlari et al., 2020b).

The drying process and the dynamics of the internal mass transfer mechanisms are specific to each product (Dermirpolate, 2019). There are still few studies on the behavior of coffee drying in such dryers, so in general there is the need for technical and operational information, such as knowledge on the intermittence of the process and on the performance of these dryers (Amunugoda et al., 2013; Shalaby & Bek, 2014; Camelo et al., 2019, Montero et al., 2019). Thus, the objective was to developing a hybrid solar-electric dryer (HSED) for effective use on coffee drying applications. For that purpose, it was studied the thermal efficiency of the solar collector and of the drying chamber, and, subsequently, the overall thermal efficiency of the hybrid solar-electric dryer (HSED) during the drying of conilon coffee.

MATHERIAL AND METHODS

The experiment was conducted at the Laboratory of Rural Electrification and Alternative Energies and at the Laboratory of Storage of Agricultural Products of the Institute of Technology (IT)/Department of Engineering (DE) of the Federal Rural University of Rio de Janeiro (UFRRJ), Campus of Seropédica - Rio de Janeiro, Brazil. The climate of the region is classified as Aw according to Köppen's classification, with average annual temperature of 24.5 °C (Carvalho et al., 2006).

Emcapa 8121 clonal variety of Conilon coffee (*Coffea canephora* Pierre ex Froehner) harvested from organic production systems was used in the experiment. Fruits were harvested manually coming from the Agroecological Farm km 49, located in the municipality of Seropédica, state of Rio de Janeiro. Two types of coffee preparation were analyzed: washed cherry, where the skin and part of the mucilage were removed before they were dried at the HSED and natural coffee, where the fruits were harvested at the green, beginning maturation, and mature stages and taken to the drying at the HSED. The performance of the developed hybrid solar dryer was evaluated using natural (0.88 ± 1 wb, decimal wet base) and washed organic Conilon coffee (0.83 ± 1 wb), until the coffee reached 0.09 ± 1 wb.

The HSED consists of solar collector, drying chamber, exhaust system and photovoltaic panel with solar tracker. In order to make greater use of the incidence of solar radiation for a maximum period of 12 h, the face of the solar collector was installed pointing North with a tilting angle equal to the latitude of the municipality of Seropédica - RJ (23°), plus 15° (Fig. 1).

a)  b) 

Figure 1. Hybrid solar-electric dryer (HSED) a) Solar collector, drying chamber, photovoltaic panel and b) Conductive air channels of solar collector drying.

The solar collector consists of a rectangular aluminum plate, with dimensions of 0.68×3.00×0.14 m (width × length × height). The adopted solar collector was sized so that an area of 8 m^2 of solar collector is required for each cubic meter of the drying chamber, forming the ratio of 1 m^3:8 m^2, as adopted by Oliveira et al. (2019). The solar radiation-absorbing surface consists of a corrugated aluminum structure in a triangular profile with dimensions of 0.10×0.08 m (base × height) and thickness of the 0.01 m, painted matte black. The surface area exposed to solar radiation consists of a transparent, flat glass plate (0.004 m thick) with area of 2.04 m^2. The absorpsivity and transmissivity of the flat glass plate was 0.07 and 0.85, respectively. The ambient air travels in the thermal fluid circuit in the solar collector through the six lower channels of the absorbing

surface to receive thermal energy to the drying chamber. The upper channels of the absorbing surface are sealed so that the ambient air passes only through the lower triangular section. The cross-section area of the solar collector was determined as a function of the quantity and triangular area of the six drying air-conducting channels, being equal to 0.024 m².

The drying chamber was made of metal, lined with a glass wool (thermal conductivity - 0.04 W (m K)$^{-1}$), and had dimensions of 1.79×1.01×0.85 m (width × height × depth), which resulted in an area of 1.80 m² and a volume of 1.54 m³. Inside it there are three trays containing nine removable metal basket with oblong holes to hold agricultural products, equally distanced from each other. The baskets have a screened bottom to allow the passage of the drying air, through the sample.

There is a rectangular entrance at the bottom of the drying chamber with dimensions of 0.815×0.185 m to fit a connection duct between the solar collector. In the upper part of the chamber, an exhaust fan was installed, with a power of 144 W, in order to guarantee the forced convection of the drying air inside. The exhaust fan accompanies a Dimmer in the form of a potentiometer (Speed Control) that allows to control the rotation of the device.

In order to generate electrical energy to drive the exhaust fan, the photovoltaic system with a 500 W solar tracker was installed. In addition to these electrical energy generating components, the hybrid system consists of a charge controller, batteries and a sinusoidal inverter. The energy storage in batteries guarantees the reliability of the system, as they allow to consume this energy in seasons when no wind is verified. The charge controller manages and controls the charging and discharging process of the battery bank. This controller allows the batteries to be fully charged and prevents them from being discharged below a safe value.

Monitoring of drying air and ambient air parameters

Throughout the drying process, the solar collector and drying chamber of the HSED were monitored for temperature ($T_{air\ dry}$), relative humidity ($RH_{air\ dry}$) and drying air velocity ($V_{air\ dry}$). Ambient air was monitored for temperature ($T_{air\ amb}$), relative humidity ($RH_{air\ amb}$), light intensity and solar radiation. The parameters were obtained at regular periods every hour. Thermocouples connected to a millivoltmeter with accuracy of ± 0.1 °C were used to monitor $T_{air\ dry}$ and $T_{air\ amb}$. $RH_{air\ dry}$ and $RH_{air\ amb}$ were measured using an MTH-1380 thermo-hygrometer. $V_{air\ dry}$ was monitored with a Minipa MDA II digital thermo-anemometer every hour throughout the effective drying period, in order to keep it fixed at 0.98 m s^{-1}. In case of variation, the adjustment of the drying air speed was carried out with the Dimmer attached to the exhaust fan. This value of the present study has been used by Mirzaee et al. (2010), who satisfactorily described the apricot drying curve through a logarithmic model, and by Kant et al. (2016) for the indirect solar drying of potatoes.

Solar radiation data along the solar drying period were obtained from the National Institute of Meteorology (INMET), coming from the automatic weather station of Agricultural Ecology, located in the municipality of Seropédica, Rio de Janeiro, Brazil. This weather station is situated 2.73 km away from the IT of UFRRJ.

Adopted procedure for coffee drying

Initially, the removable basket of each tray were filled with coffee fruits, forming a thin layer of 0.03 m. Then, the trays were arranged in the drying chamber to start the process. The baskets were periodically removed every hour to be weighed during the drying process. The condition of hygroscopic equilibrium was considered so that the variation in the mass of the baskets with coffee did not exceed 0.01 g for three times consecutive weighing procedures, where a final water content of 0.09 ± 1% wb was reached.

The solar drying of the samples was carried out in six consecutive days, being from 07:00 to 17:00 h, totaling 120 h of operation. At night, when the exhaust system was turned off and the solar collector and drying chamber were sealed in order to avoid external interference in the internal microclimate, it was considered an intermittence of 14 h (between 17:00 and 7:00 h). The effective drying time of the coffee, without considering the intermittence period, was 60 h.

Thermal performance of the HSED

After collecting the drying parameters, the thermal efficiency of the solar collector, drying chamber and the overall thermal efficiency of the HSED were evaluated.

Thermal efficiency of the solar collector

The thermal efficiency of the solar collector was determined according to the ratio between the useful energy supplied and the incident solar energy along the drying period (Eq. 1).

$$\eta_c = \frac{E_u}{E_i} = \frac{\int P_{u\,col}\, dt}{A_d \int I_t\, dt} = \frac{P_{u\,col}}{P_i} = \frac{\dot{m} \times c_p \times (T_o - T_i)}{I_t \times A_d} \quad (1)$$

where η_c – Thermal efficiency of the collector; E_u – Useful energy supplied by the solar collector along the drying period t; E_i – Incident solar energy on the solar collector along the drying period t; $P_{u\,col}$ – Useful energy gain of the collector, W; A_d – Surface area of the solar collector exposed to solar radiation, m²; I_t – Solar radiation on the tilted surface, W m^{-2}; P_i – Potential related to solar energy, W; $\dot{m}$ – Mass flow rate of the air, kg s^{-1}; c_p – Specific heat of the air, J (kg °C)$^{-1}$; T_o – Outlet temperature of the collector, ºC and T_i – Inlet temperature of the collector, °C.

Eq. 2 was adopted to calculate ṁ (Montero et al., 2010).

$$\dot{m} = \rho \times A_c \times v_m \quad (2)$$

where ρ – Specific mass of the incoming air of the solar collector, kg m^{-3}; A_c – Transverse area of the solar collector, m² and v_m – Average air velocity at the inlet of the solar collector, m s^{-1}.

The ρ was determined as a function of the inlet temperature of the solar collector, according to Eq. 3 (Montero et al., 2010).

$$\rho = \frac{353.44}{T_i + 273.15} \quad (3)$$

According to the study conducted by Silveira (2016), the efficiency of the solar collector was evaluated considering the insulation of the system does not allow air leakage. The air inside the solar collector behaves as an ideal gas at constant pressure, and the transmittance-absorbance between the glass and the absorbing plate is negligible. The radiation measured on a flat surface (weather station) is the same for the tilted

surface. A value of 1,006 J (kg °C)$^{-1}$ was adopted for the specific heat of the air to calculate the efficiency of the collector (Silveira, 2016).

Thermal efficiency of the drying chamber

The thermal efficiency of the HSED drying chamber was determined considering the useful energy gain obtained, potential related to solar energy and to the power required by the exhaust (Eq. 4).

$$\eta_{chm} = \frac{P_{u\,chm}}{P_{u\,col} + P_e} = \frac{\dot{m}_w \times l_v}{P_{u\,col} + P_e} \quad (4)$$

where η_{chm} – Thermal efficiency of the drying chamber; $P_{u\,chm}$ – Useful energy gain of the drying chamber, W; P_e – Exhaust power, W; $\dot{m}_w$ – Water evaporation rate in the grains, kg s^{-1} and l_v – Latent heat of water evaporation at the air saturation temperature, J kg^{-1}.

To calculate the thermal efficiency of the drying chamber, a value of 2,256 J kg^{-1} was adopted for the latent heat of water evaporation at the air saturation temperature. Eq. 5 was used to determine $\dot{m}_w$.

$$\dot{m}_w = \dot{m}_{chm} \times (AM_o - AM_i) \quad (5)$$

where $\dot{m}_{chm}$ – Mass flow rate of the air in the drying chamber, kg s^{-1}; AM_o – Outlet absolute moisture of the drying chamber, decimal and AM_i – Inlet absolute moisture of the drying chamber, decimal.

Equal 6 was used to determine $\dot{m}_{chm}$.

$$\dot{m}_{chm} = \rho_{chm} \times v_{m\,chm} \times A_{chm} \quad (6)$$

where ρ_{chm} – Specific mass of moist air for the drying chamber, kg m^{-3}; $v_{m\,chm}$ – Average air velocity in the drying chamber, m s^{-1} and A_{chm} – Area of the drying chamber, m².

The ρ_{chm} was determined as a function of T_{ichm} according to Eq. 7 (Montero et al., 2010).

$$\rho_{chm} = \frac{353.44}{T_{e\,chm} + 273.15} \quad (7)$$

Overall thermal efficiency of the HSED

The overall thermal efficiency of the hybrid solar-electric dryer was determined considering the useful energy gain of the drying chamber, the potential related to solar energy and the power of the exhaust (Eq. 8).

$$\eta_g = \frac{P_{u\,chm}}{P_i + P_e} \quad (8)$$

RESULTS AND DISCUSSION

It was observed that during the solar drying of conilon coffee, the ambient temperature did not vary along the six days of process, averaging 27.8 °C. The average minimum temperature reached was 20.0 °C, at 7:00 h, and the average maximum was 31.6 °C, from 12:00 to 14:00 h. From 14:00 h the ambient temperature decreased until reaching 25.3 °C at 17:00 h (Fig. 2).

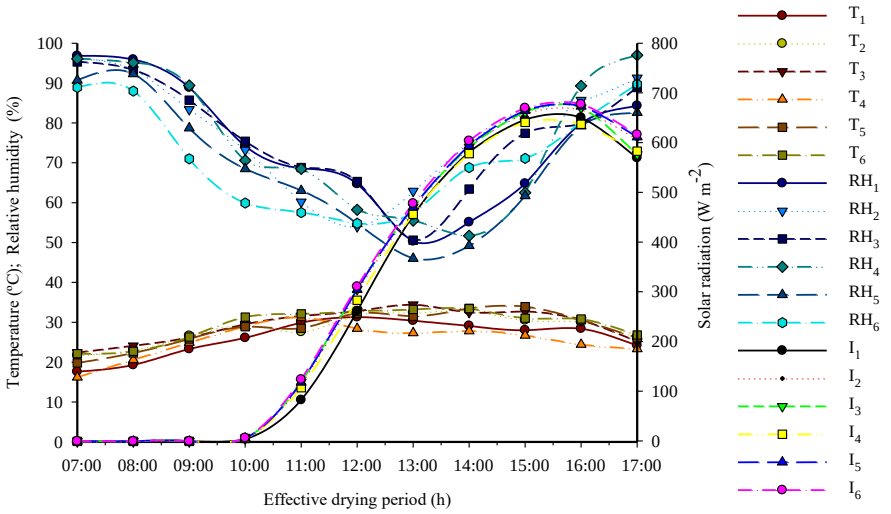

Figure 2. Temperature (ºC), relative humidity (%) and global solar radiation (W m^{-2}) over the drying period: T_n – Temperature; RH_n – Relative humidity; I_n – Solar radiation; n – drying day.

Regarding the relative humidity, it can be observed that this drying indicator showed the same behavior over the six days of the process, with an average of 74.5%. The highest values of relative humidity occurred was 94.0% at 07:00 h, and the minimum was 53.8% at 13:00 h.

The average global solar radiation obtained during the drying period of coffee in the HSED was approximately 306.9 W m^{-2}, with peaked was 662.3 W m^{-2} at 16:00 h. The period of maximum average value of global radiation does not coincide with that achieved by the temperature. Furthermore, it can be observed that in the daytime between 07:00 and 10:00 h there was low availability of radiant energy, with an average of 0.5 W m^{-2}. In the period of availability of solar energy (11:00 to 17:00 h), the average global solar radiation was 482.0 W m^{-2} (Fig. 2). Lingayat et al. (2017) when using indirect solar dryer (solar flat plate air collector with V-corrugated absorption plates, insulated drying chamber, and chimney for exhaust air) for banana drying in India obtained maximum and average incident solar radiation values of 1,219.1 and 897.4 W m^{-2}, respectively.

It was verified that environmental conditions are favorable to coffee drying, since the period of higher temperature coincides with lower value of relative humidity and higher availability of solar energy. Additionally, on the fourth day of drying, there was a low incidence of rain, leading to lower temperatures from 12:00 h. In the evaluation of the solar dryer thermal efficiency low incidence of rain, including collector and drying chamber, it is essential to take into account the environmental conditions, such as temperature, relative humidity and radiation, as well as the geographical location (Altobelli et al., 2014).

In specific case of coffee drying, in Brazil, its harvest occurs in the months between May and August (autumn/winter season), so there are excellent environmental conditions such as high level of solar radiation and low level of rainfall. In order to maintain its quality for processing and, subsequently, marketing at any period of the year, coffee is immediately dried. Thus, the drying period of the different lots of conilon

coffee are consistent with the Brazilian reality in any season for the metropolitan region of Rio de Janeiro, Brazil.

Thermal efficiency of the solar collector

The thermal efficiency of the solar collector can be influenced by its size, mode of operation, geographical location, mass flow rate, temperature, relative humidity and local radiation (Montero et al., 2010; Lingayat et al., 2017). Fig. 3 shows the curve of drying air temperature (inlet, middle and outlet of the solar collector) along the drying period.

The ambient air temperature and solar collector's inlet temperature did not show great variations among themselves during the coffee drying period, being the average of 27.9 ± 0.02 °C. In contrast, the average temperature in the middle and at the outlet of the solar collector were respectively 10 and 27% higher than that of the inlet.

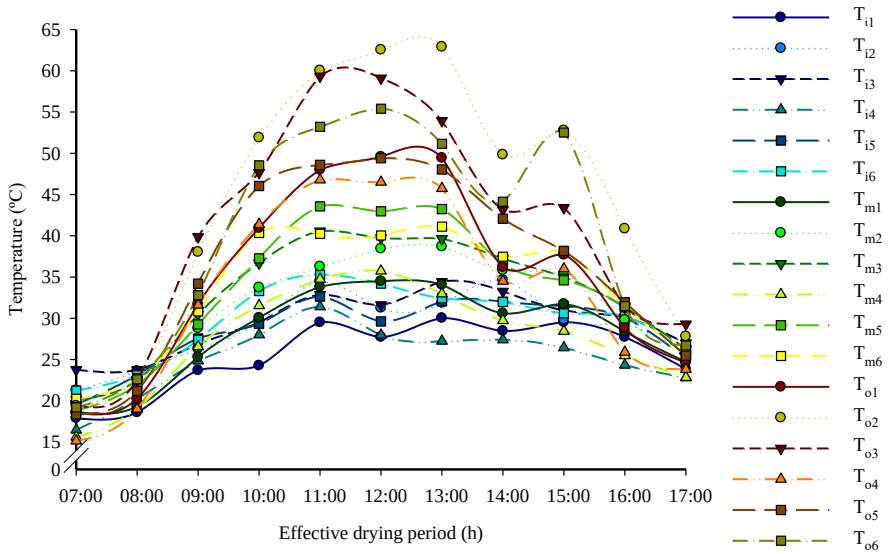

Figure 3. Temperature (ºC) as function of effective drying period in the solar collector: T_n – Temperature; i – inlet; m – middle; o – outlet; n – drying day.

The highest average temperatures were recorded at noon, being equal to 32 °C for ambient temperature and at the inlet, to 39 °C in the middle and to 54 °C at the outlet of the solar collector. At this moment, an increase of 21.1 °C was observed in the collector's outlet temperature compared to the inlet temperature. Then, there was a reduction in the temperatures, regardless of the data collection position, equal to 25 °C at 17:00 h (Fig. 3). Shuck et al. (2014) evaluated the efficiency of flat solar collector for tobacco drying and considered the inlet temperature of the solar collector as the ambient temperature itself, because there was no significant difference between the two.

In addition to the increase in drying air temperature and global solar radiation, the reduction of relative humidity is a factor that proves the efficiency of the solar collector. Combined with this, indicators such as temperature and relative humidity are tools to be considered when there are variables other than solar radiation taken as energy sources (Altobelli et al., 2014).

Therefore, in Fig. 4 presents the relative humidity recorded at the outlet of the solar collector, which decreased by 33% at 12:00 h, compared to air at the inlet (Fig. 2). In general, the relative humidity of the ambient air and at the inlet of the solar collector showed a difference of no more than 5% at 09:00 and 11:00 h.

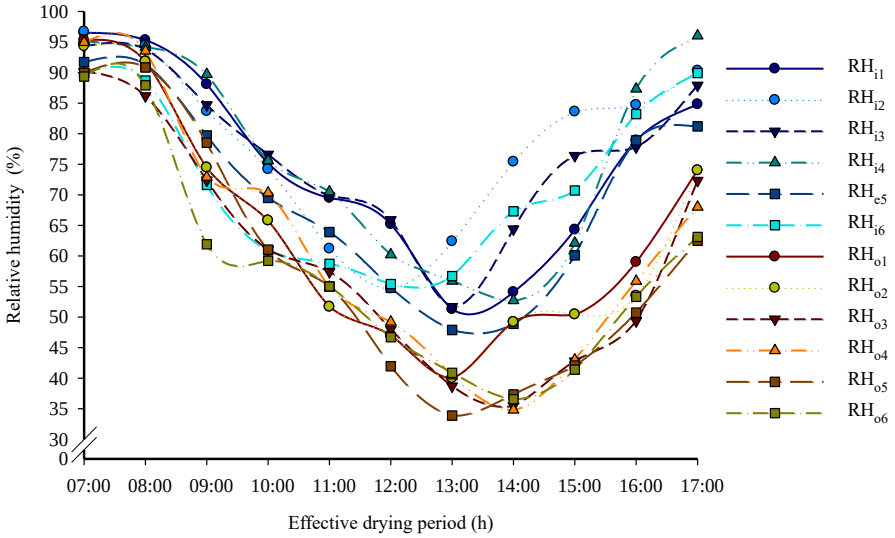

Figure 4. Relative humidity (%) as function of effective drying period in the solar collector: RH_n – Relative humidity; i – inlet; m – middle; o – outlet; n – drying day.

In terms of instantaneous thermal efficiency of the solar collector, at the beginning of the daytime there were average values higher than 100%, equal to 1,201% at 07:00 h, 490% at 08:00 h, -6,187% at 09:00 h and 2,421% at 10:00 h. The high values of instantaneous thermal efficiency of the solar collector in the coffee drying period from 07:00 to 10:00 h can be justified by the combination between low global solar radiation and temperature, as observed in Fig. 2. When determining the thermal efficiency of the solar collector of continuous solar dryer integrated with desiccant thermal storage for drying cocoa beans, Dina et al. (2015) did not adopt the day time due to the low availability of solar energy.

In particular at 11:00 h, there was an increase in global solar radiation, which, together with the variation of temperature (Fig. 2), reduced the efficiency of the solar collector (Fig. 5). However, when considering the six days of coffee drying, the average instantaneous thermal efficiency of the solar collector was 120%, that is, higher than 100%. Thus, for 11:00 h the average instantaneous thermal efficiency was calculated only with daily values below 100%.

Altobelli et al. (2014) evaluated the instantaneous thermal efficiency of the flat solar collector coupled to a dryer in Argentina, considering only values below 100%, since they obtained higher values in the afternoon, as the intensity of solar radiation decreases. These authors also observed a similar behavior with the performance of the system, solar collector and drying chamber, because at the beginning they observed values similar to the total performance, but reached values beyond possible when radiation was zero. Due to the dependence only on solar radiation, the authors considered

that the thermal efficiency of the solar collector alone does not adequately describe the behavior of the solar dryer, so the system needs to be considered as a whole to determine the thermal efficiency.

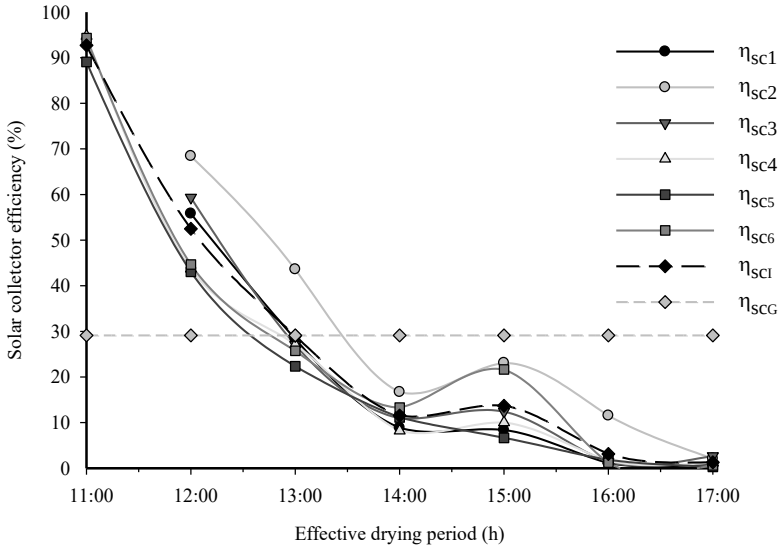

Figure 5. Thermal, instantaneous and global average efficiency of the solar collector throughout the drying period: η_{scn} – Solar collector efficiency; n – drying day; I – Instantaneous; G – Global.

In the drying period from 11:00 to 17:00 h, there was a reduction in the instantaneous thermal efficiency, regardless of the drying day. In calculating the average thermal efficiency of the solar collector at 11:00 am, only the fourth (95%), fifth (89%) and sixth (94%) day of coffee drying was taken into account (Fig. 5). From 12:00 h, the second day showed higher values of instantaneous thermal efficiency. The increase in instantaneous thermal efficiency at 15:00 h, followed by reduction, confirms the interference of the drying indicators, that is, temperature variation associated with higher values of global solar radiation (Fig. 2).

Similar behavior was reported by Kareem et al. (2017), according to whom the instantaneous thermal efficiency of the multi-pass solar air heating collector system for drying of screw-pine leaf (*Pandanus tectorius*) reduced as a function of the drying period, showing 50% efficiency at 09:00 h with solar irradiation close to zero Watts per square meter and temperature (ambient and outlet of the collector) of 20 °C. Demirpolat (2019) analyzed the behavior of apple drying in a convective indirect solar dryer and found that the maximum thermal efficiency of the collector occurred between 12:00 and 13:30 h, with 65% thermal efficiency in the collector.

Oliveira et al. (2019), performing the drying of mangoes in a convective indirect solar dryer, reported that the peak of maximum instantaneous thermal efficiency of solar collector was approximately 60% at 14:00 h at four days of drying, with global solar radiation and ambient temperature ranging from 400 to 600 W m^{-2} and from 35 to 60 °C, respectively. Gulcimen et al. (2016), during the drying of sweet basil in a convective indirect solar dryer, obtained maximum instantaneous efficiency of solar collector of

42% at 13:00 h, with global solar radiation between 720 and 750 W m^{-2} and mass flow rate of 0.012 kg s^{-1}.

The average thermal efficiency of the solar collector of 29% is higher than that found in the literature by Oliveira et al. (2019), who obtained 26% during solar drying, under conditions of average solar radiation of 361 W m^{-2}. This value is also higher than those found by Fudholi et al. (2015), equal to 28%, in the back-passV-groove solar collector coupled in solar drying of red pepper, and by Altobelli et al. (2014), equal to 27%, evaluating drying indicators in northwestern Argentina. On the other hand, Lingayat et al. (2017) evaluated the performance of indirect solar dryer for banana drying obtained average overall efficiency of 31%. The authors conducted the experiment under conditions of average incident radiation of 724 W m^{-2}, more than twice the one mentioned in the present study (306.9 W m^{-2}).

Thermal efficiency values higher than that found in the present study were reported by Hedge et al. (2015), 36% higher. However, these authors adopted thermal systems to maintain the temperature high inside the flat plate solar collector during the period of low solar energy availability and ambient temperature.

Thermal efficiency of the drying chamber

During the solar drying of coffee, it was observed that both the temperature and relative humidity of the drying air show differences when compared at the inlet and outlet of the drying chamber (Fig. 6). The average differences in temperature and relative humidity between drying air at the inlet and at the outlet were 5.7 °C and 1.7%, respectively.

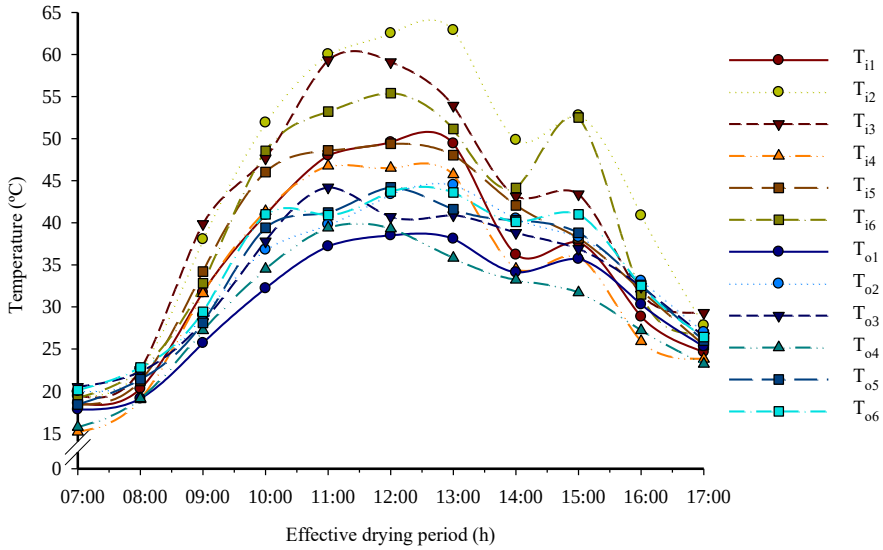

Figure 6. Temperature of the drying air in the SHSE chamber over the drying period: T_n – Temperature; i – inlet; o – outlet; n – drying day.

Furthermore, it can be observed that the highest temperatures and lowest values of relative humidity occurred inside the drying chamber when compared to the air ambient. The highest temperatures at the inlet and outlet of the drying chamber occurred from

11:00 to 13:00 h, while the lowest ones occurred during the early morning and late afternoon (Fig. 6). On the other hand, the minimum relative humidity at the inlet and outlet of the drying chamber occurred at 13:00 h and the maximum values occurred at 07:00 and 17:00 h (Fig. 7).

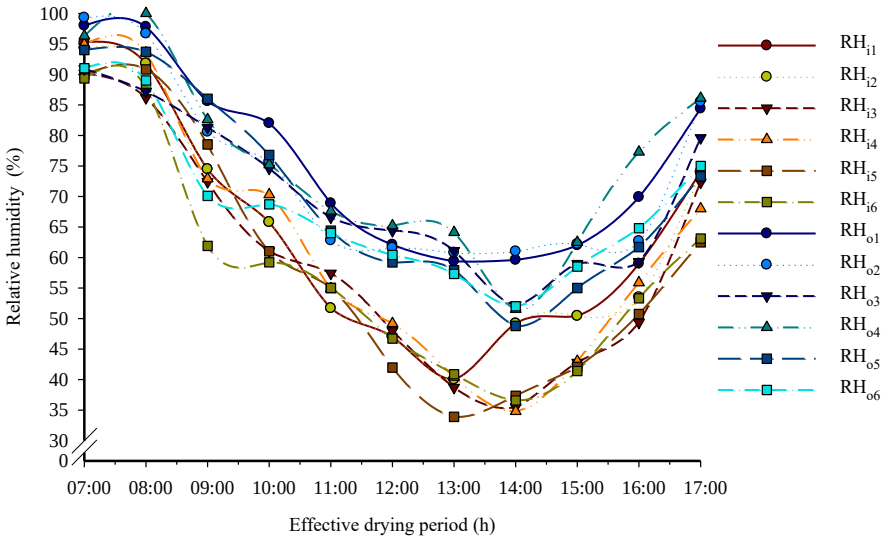

Figure 7. Relative humidity of the drying air in the SHSE chamber over the drying period: RH_n – Relative humidity; i – inlet; o – outlet; n – drying day.

The average value of drying air temperature and UR inside the SHSE chamber was 35.5 °C and 66.4%, respectively. The average maximum temperature reached inside the drying chamber was 47.7 °C at 12:00 h. At that same time, the ambient air had a temperature of 31.6 °C, that is, an increase of 16.1 °C. Regarding the average minimum relative humidity reached in the drying chamber was 39.7% at 13:00 h, with 53.2% in the ambient air, a reduction of 13.5%. The average variation in the temperature increment and the reduction of relative humidity between the drying air inside the chamber and the ambient air was 7.7 °C and 5.5%, respectively. The higher temperature and lower relative humidity inside the drying chamber when compared to the ambient meteorological conditions indicate the capacity of the drying chamber to not lose heat to the environment.

It was found that the relative humidity decreases with the increase of temperature, as evidenced by the air exiting the solar collector and entering the drying chamber. High relative humidity was observed at the outlet of the drying chamber, compared to the inlet, and this can be attributed to the variation in the drying rate of the material as the moisture content decreases.

Dina et al. (2015) evaluated the continuous solar drying of cocoa seeds using a flat-plate solar collector and obtained lower results of thermal variation than those of the present experiment. The authors obtained an increase of 12 °C in the air temperature inside the drying chamber comparison to the ambient. In addition, the increase obtained was also higher than that reported by Shalaby & Bek (2014), who evaluated the

performance of an indirect solar dryer and found an increase of 7.5 °C between drying air temperature and ambient temperature.

For the study of the thermal efficiency of the drying chamber for conilon coffee, the average values of temperature, relative humidity, drying air velocity were 38.9 °C, 53.6% and 0.98 m s^{-1}, respectively. As adopted for the solar collector, only the fourth, fifth and sixth day were considered for calculating the average values of the thermal efficiency of the drying chamber at 11:00 h. As expected, the highest average values of instantaneous thermal efficiency occurred at 11:00 and 12:00 h (66.3%), while the lowest at 17 h (17.6%). Considering the six days of coffee drying, the average instantaneous thermal efficiency of the drying chamber was 40.8%.

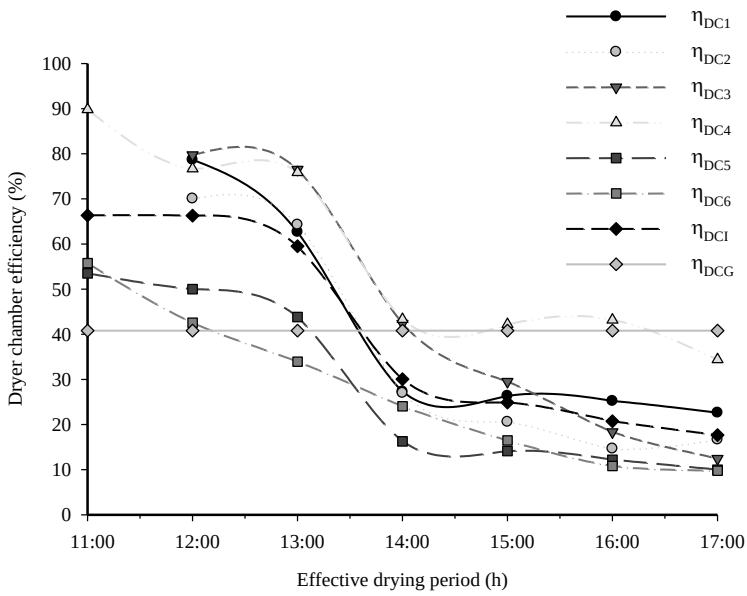

Figure 8. Thermal efficiency of the drying chamber of the hybrid solar-electric dryer over the drying period: η_{DCn} – Dryer chamber efficiency; n – drying day; I – Instantaneous; G – Global.

The maximum and minimum value of instantaneous thermal efficiency reached was 89.8% at 11:00 h on the fourth day and 9.7% at 17:00 h on the six day, respectively (Fig. 8). The high values of instantaneous thermal efficiency in the drying chamber along the coffee drying period from 11:00 to 13:00 h can be justified by the combination between high temperature (Fig. 6) and the reduction in relative humidity (Fig. 7).

In the drying period from 13:00 to 17:00 h, there was a reduction in the instantaneous thermal efficiency, regardless of the drying day. The relative humidity of the air entering the drying chamber was more stable until 10:00 h, while that of the air inside the drying chamber continuously decreases until about 13:00 h (Fig. 7). Such behavior may be an indication that most of the moisture in the product had already evaporated at that time, although solar radiation has increased at the same time, leading to a reduction in the thermal efficiency of the drying chamber (Fig. 8). Musembi et al. (2016), when analyzing an indirect solar dryer by natural convection for medium latitudes, obtained similar results. The authors observed stability in the inlet relative

humidity during the first 40 min of the drying days, noting that the value in the air of the drying chamber decreases until 15:00 h. The average overall thermal efficiency of the drying chamber was 48.8% for the six days of drying, value that is within the range obtained by Hao et al. (2020), evaluating a hybrid dryer for lemon drying.

Overall thermal efficiency of the HSED

Regarding the overall thermal efficiency, the same profile shown by the drying chamber can be observed (Fig. 8). The highest values of global thermal efficiency occurred at 11:00 am from the fourth day of solar drying. For this period of solar drying, the average global efficiency was 64.1%. Considering the six days of coffee drying, the average overall thermal efficiency of the drying chamber was 39.7% (Fig. 9).

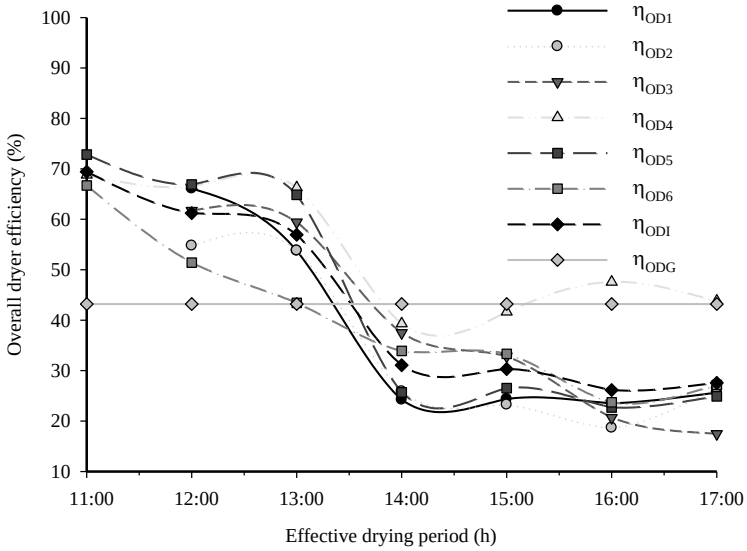

Figure 9. Overall thermal efficiency of the hybrid solar-electric dryer over the drying period: η_{ODn} – Overall dryer efficiency; n – drying day; I – Instantaneous; G – Global.

Lingayat et al. (2017) and Altobelli et al. (2014) obtained values of 22.38 and 17%, respectively, for the average overall thermal efficiency of their experiments. This confirms that the local climatic conditions of Brazil are excellent for the use of indirect solar drying, combining the drying indicators such as temperature, relative humidity and solar radiation.

Mass reduction in natural and pulped coffees

Fig. 10 shows the reduction in the mass of natural and pulped grains, respectively, over the drying period. It should be noted that the initial mass of the natural grain (Fig. 10, a) is lower than the pulped grain (Fig. 10, b), being 291.2 and 295.4 g, respectively, at 7:00 am on the first day. However, it did not affect the solar drying process. This difference in initial mass is justified due to the wet treatment used for pulping.

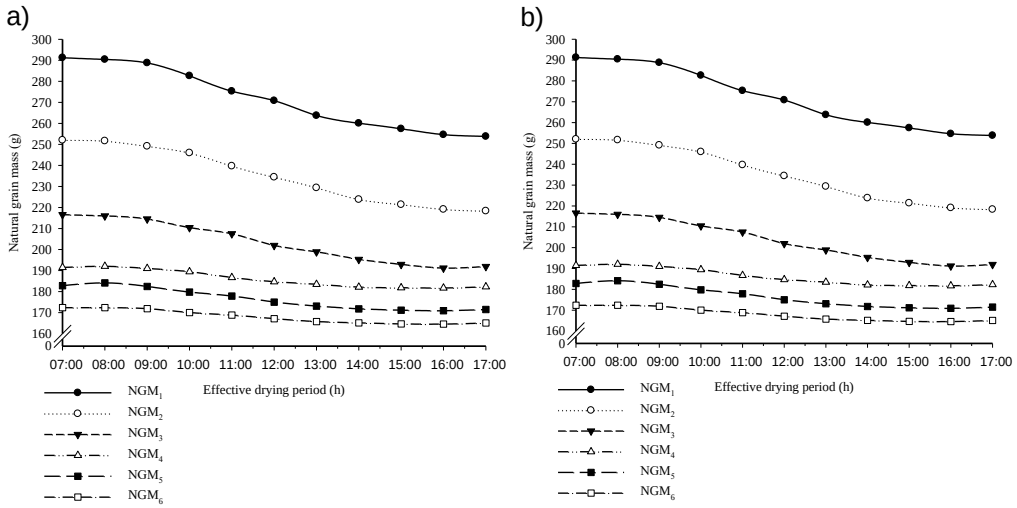

Figure 10. Reduction in the mass of a) natural and b) washed grains throughout the drying period: NGM_n – Natural grain mass; WGM_n – Washed grain mass; n – drying day.

It is also observed that, during the drying of the conilon coffee, the period of intermittence did not interfere with the mass loss of the product. However, greater mass loss can be observed on the first two days in both pulped and natural grains. The highest rate of water removal in the first two days is due to the initial elimination of free water from the grain surface.

It can be observed that there was a reduction in grain mass every day of solar drying, being more pronounced on the first day. Thus, it can be inferred that the rainy season did not interfere in the coffee drying as commonly occurs in conventional processes. On earth and suspended terraces in the rainy season, coffee drying is delayed, which leads to an increase in the period and a probable interference in the final quality of the product.

It can also be verified that, from the third day, the mass of both lots of grains remained constant along the drying period. Regarding the effect of the intermittence period, the product did not absorb moisture, as reported by Camelo et al. (2019) in solar drying of banana. The final masses of natural grains and pulped grains were 165.1 and 186.8 g, respectively. Thus, it can be considered that on the last day the product reached the hygroscopic equilibrium with the environment, and the results are similar to those obtained by Silvia et al. (2019) for the drying of conilon coffee fruits in a hybrid dryer.

CONCLUSIONS

The studied electric solar hybrid dryer proved efficient in the drying process of conillon coffee. Results show that the temperature increases 18.1 °C in the solar collector and in the drying chamber of 21.3 °C, allowing the coffee to dry at acceptable and ideal temperatures for the drying process. The average variation for the reduction of RH between the drying air inside the solar collector and the ambient air was 10.8%, while in the chamber obtained in the range of 13.5% at 13:00 h. During the drying of conilon coffee, the intermittence period did not interfere in the loss of mass of the product. Regarding the values obtained for efficiency, the solar collector and dryer chamber

efficiency were 27.1 and 45.3%, respectively, while the overall dryer efficiency 39.7%. The drying of coffee is one of the processes with the greatest attention due to the direct influence on the quality of the drink and marketing price. As most of the producers still use conventional drying methods, the data obtained in the present study allow us to say the hybrid solar-electric dryer proved to be an economically viable and economical tool for processing a differentiated and gourmet coffee in small rural. It is seen that HSED is promising in view of sustainability and this simple structure can be utilized as an alternative to drying applications.

ACKNOWLEDGEMENTS. The authors wish to thank the Conselho Nacional de Desenvolvimento Científico e Tecnológico (CNPq) that provided support for this research project.

REFERENCES

Almeida, I.B., Lima, M.A.A. & Souza, L.G.M. 2016. Solar dryer development built from recycled material. *Holos* **4**, 197–205 (in Portuguese).

Altobelli, F., Condorí, M., Duran, G. & Martinez, C. 2014. Solar dryer efficiency considering the total drying potential. Application of this potential as a resource indicator in north-western Argentina. *Solar Energy* **105**, 742–759.

Alves, R.A., Queiroz, A.J.M., Figueiredo, R.M.F., Silva, W.P. & Gomes, J. P. 2019. Solar drying of cowpea bean combined with drying in a heat accumulator dryer. *Revista Brasileira de Engenharia Agrícola e Ambiental* **9**, 709–715.

Amunugoda, P.N.R.J., Senanayake, N.S., Wilson Wijeratnam, R.S. & Kulatunga, K.D.G. 2013. Quality enhancement of dehydrated products through the modification of solar tunnel dryer for continuous operation in rural communities. *International Journal of Energy Engineering* **1**, 7–14.

Azouma, Y.O., Drigalski, L., Jegla, Z., Reppich, M., Turek, V. & Weiz, 2019. M. Indirect convective solar drying process of pineapples as part of circular economy strategy. *Energies* **12**, 2841.

Borém, F.M., Oliveira, P.D., Isquierdo, E.P., Giomo, G.S., Saath, R. & Cardoso, R.A. 2013. Scanning electron microscopy of coffee beans subjected to different forms of processing and drying. *Coffee Science* **2**, 227–237 (in Portuguese).

Boughali, S., Benmoussa, H., Bouchekima, B., Mennouche, D., Bouguettaia, H. & Bechki, D. 2009. Crop drying by indirect active hybrid solar - electrical dryer in the eastern Algerian Septentrional Sahara. *Solar Energy* **83**, 2223–2232.

Camelo, R.S.S., Paes, J.L., Brás, M.R.S., Bruggianesi, G. & Guimarães, C.L. 2019. Kinetics drying of silver banana (*Musa* spp.) in hybrid dryer. *Ciência Agronômica* **3**, 353–360.

Carvalho, D.F., Silva, L.D.B., Folegatti, M.V., Costa, J.R. & Cruz, F.A. 2009. Evaluation of reference evapotranspiration in the Seropédica-RJ region, using weighing lysimeter. *Revista Brasileira de Agrometeorologia* **14**, 108–116 (in Portuguese).

Deeto, S., Thepa, S., Monyakul, V. & Songprakorp, R. 2018. The experimental new hybrid solar dryer and hot water storage system of thin layer coffee bean dehumidification. *Renewable Energy* **115**, 954–968.

Demirpolat, A.B. 2019. Investigation of mass transfer with different models in a solar energy food-drying system. *Energies* **12**, 3447–3461.

Dina, S.F., Ambarita, H., Napitupulu, F.H. & Kawai, H. 2015. Study on effective ness of continuous solar dryer integrated with desiccant thermal storage for drying cocoa beans. *Case Studies in Thermal Engineering* **5**, 32–40.

Fudholi, A., Sopian, K., Bakhtyar, B., Gabbasa, M., Othman, M.Y. & Ruslan, M.H. Review of solar drying systems with air based solar collectors in Malasia. 2015. *Renewable and Sustainable Energy Reviews* **51**, 1191–1204.

Gulcimen, F., Karakaya, H. & Durmus, A. 2016. Drying of sweet basil with solar air collectors. *Renewable Energy* **93**, 77–86.

Güler, H.O., Sözen, A., Tuncer, A.D., Afshari, F. & Khanlari, A. 2020. Experimental and CFD survey of indirect solar dryer modified with low-cost iron mesh. *Solar Energy* **197**, 371–384.

Hao, W., Liu, S., Mi, B. & Lai, Y. 2020. Mathematical modeling and performance analysis of a new hybrid solar dryer of lemon slices for controlling drying temperature. *Energies* **13**, 350–373.

Hedge, V.N., Hosur, V.S., Rathod, S.K., Harsoor, P.A. & Narayana, K.B. 2015. Design, fabrication and performance evaluation of solar dryer for banana. *Energy* **1**, 5–23.

Kant, K., Shukla, A., Sharma, A., Kumarm A. & Jain, A. 2016. Thermal energy storage based solar drying systems: A review. *Innovative Food Science and Emerging Technologies* **34**, 86–99.

Kareem, M.W., Habib, K., Sopian, K. & Ruslan, M.H. 2017. Multi-pass solar air heating collector system for drying of screw-pine leaf (*Pandanus tectorius*). *Renewable Energy* **112**, 413–424.

Khanlari, A, Sözen, A, Şirin, C, Tuncer, A.D. & Gungor, A. 2020a. Performance enhancement of a greenhouse dryer: Analysis of a cost-effective alternative solar air heater. *Journal of Cleaner Production* **19**, 1–30.

Khanlari, A., Güler H.O., Tuncer, A.D., Sirin, C., Bilge Y.C., Yılmaz, Y. & Güngor A. 2020b. Experimental and numerical study of the effect of integrating plus-shaped perforated baffles to solar air collector in drying application. *Renewable Energy* **145**, 1677–1692.

Kumar, M., Sansaniwal, S.K. & Khatak, P. 2016. Progress in solar dryers for drying various commodities. *Renewable and Sustainable Energy Reviews* **55**, 346–60.

Lima Filho, T., Lucia, S.M.D., Saraiva, S.H. & Lima, R.M. 2015. Physico-chemical characterization of espresso coffee beverage prepared from blends of arabica and conilon coffees. *Revista Ceres* **4**, 333–339 (in Portuguese).

Lingayat, A., Chandramohan, V.P. & Raju, V.R.K. 2017. Design, Development and performance of indirect type solar dryer for banana drying. *Energy Procedia* **109**, 409–416.

Lingayat, A., Chandramohan, V.P., Raju, V.R.K. & Kumar, A. 2020a. Development of indirect type solar dryer and experiments for estimation of drying parameters of apple and watermelon. *Thermal Science and Engineering Progress* **16**, 1–65.

Lingayat, A., Chandramohan, V.P., Raju, V.R.K. & Meda, V. 2020b. A review on indirect type solar dryers for agricultural crops – Dryer setup, its performance, energy storage and important highlights. *Applied Energy* **258**, 1–22.

Mirzaee, E., Rafiee, S. & Keyhani, A. 2010. Evaluation and selection of thin-layer models for drying kinetics of apricot (cv. NASIRY). *Agric Eng Int: CIGR Journal* **12**, 111–116.

Montero, I, Miranda, M.T., Sepúlveda, F.J., Arranz, J.I., Rojas, C.V. & Nogales, S. 2015. Solar dryer application for olive oil mill wastes. Energies **8**, 14049–14063.

Montero, I., Blanco, J., Miranda, T, Rojasa, S. & Celma, A.R. 2010. Design, construction and performance testing of a solar dryer for agroindustrial by-products. *Energy Conversion and Management* **7**, 1510–1521.

Moreira, D.H.F., Freitas, F.F., Landy, C.C.R. & Charbel, A.L.T. 2019. Analysis of coffee drying in direct passive solar dryer. *Brazilian Journal of Development* **9**, 16556–16573.

Murali, S., Amulya, P.R., Alfiya, P.V., Delfiya, D.S.A. & Samuel, P.M. 2019. Design and Performance Evaluation of Solar - LPG Hybrid Dryer for Drying of Shrimps, *Renewable Energy* **147**, 2417–2428.

Musembi, M.N., Kiptoo, K.S. & Yuichi, N. 2016. Design and analysis of solar dryer for mid-latitude region. *Energy Procedia* **100**, p. 98–110.

Nakayama, C.C., Teixeira, A.A., Teixeira, R.R., Reis, M. Montero, A. & Bueno, J. 2020. Microorganism succession at different coffee drying stages and its influence on the beverage. *Brazilian Journal of Development* **6**, 2402–2418.

Oliveira, L.C.T.G., Paes, J.L., Guimarães, C.L., Camelo, R.S.S., Misquita, Í.S. & Lovisi, T.A.P. 2019. Evaluation of the efficiency of the flat solar collector coupled in hybrid dryer. *Energia Solar e Eólica*, vol. 01. Ponta Grossa (PR): Atena Editora, Cap.**13**, 194–211 (in Portuguese).

Palacin, J.J.F., Lacerda Filho, A.F., Melo, E.C. & Teixeira, E. C. 2009. Secagem combinada de café cereja descascado. *Engenharia na Agricultura* **3**, 244–258 (in Portuguese).

Sandali, M., Boubekri, A., Mennouche, D. & Gherraf, N. 2019. Improvement of a direct solar dryer performance using a geothermal water heat exchanger as supplementary energetic supply. An experimental investigation and simulation study. *Renewable Energy* **10**, 186–196.

Schuck, M.L.R., Santos, J.P., Soares, R.M.D., Zófoli, G.R., Garlet, L. & Gricoletti, G.C. 2014. Solar collector for air pre-heating on drying systems case study - curing tobacco. *Extensão Rural* **21**, 106–130 (in Portuguese).

Shalaby, S.M. & Bek, M.A. 2014. Experimental investigation of a novel indirect solar dryer implementing PCM as energy storage medium. *Energy Conversionand Management* **83**, 1–8.

Silveira, L.R. 2016. *Modeling of a solar dryer for agricultural products with thermal energy storage system.* PhD Thesis Thesis in Engenharia de Sistemas Agrícolas, Piracicaba: Escola Superior de Agricultura Luiz de Queiroz, University of São Paulo, 60 pp. (in Portuguese).

Silvia, E., Yuwana, Y. & Bosman, S. 2019. Performance of modified hybrid solar dryer on the drying process of robusta cherry coffee. *Journal Agroindustrial* **9**, 94–101 (in Indonesian).

Agronomy Research **18**(3), 2185–2196, 2020
https://doi.org/10.15159/AR.20.166

Determination of heavy metals in corn (*Zea Mays* L.) using silver nanoparticles/graphene/nafion modified glassy carbon electrode

S. Palisoc[1,2], A.J. Gallardo[1], C.B. Laurito[1] and M. Natividad[1,2,*]

[1]De La Salle University, Condensed Matter Research Laboratory, Physics Department, 2401 Taft Avenue, PH922 Manila, Philippines
[2]De La Salle University, Condensed Matter Research Unit, CENSER, 2401 Taft Avenue, PH922 Manila, Philippines
[*]Correspondence: michelle.natividad@dlsu.edu.ph

Abstract. Silver nanoparticles (AgNP)/graphene/Nafion modified glassy carbon electrodes were fabricated for the determination of trace amounts of cadmium (Cd^{2+}) and lead (Pb^{2+}) via anodic stripping voltammetry (ASV). The electrode modifiers and the ASV parameters were optimized. The fabricated electrode was characterized by field emission scanning electron microscopy and energy dispersive x-ray spectroscopy. A linear relationship between anodic peak current and heavy metal concentration was obtained in the range of 25 parts per billion (ppb) to 250 ppb. The limit of detection of the modified electrode is 25 ppb for both Cd^{2+} and Pb^{2+}, while the limits of quantitation are 155.7 ppb for Cd^{2+} and 159.5 ppb for Pb^{2+}. Real sample analysis using corn plant and soil samples was performed to show the utility of the fabricated electrode in sensing applications. Trace amounts of Cd^{2+} and Pb^{2+} were found in the said samples.

Key words: anodic stripping voltammetry, heavy metals, silver nanoparticles, graphene, Nafion.

INTRODUCTION

Heavy metal pollution is one of the main environmental problems of third world countries as well as industrialized countries. Due to anthropogenic activities such as smoking, mining, industrial processing, automobile exhausts, and application of organic manure and fertilizers, heavy metals accumulate in the air, soil, and water sources (Ganeshamurthy et al., 2008). Soil pollution is a serious problem since plants easily absorb heavy metals through their roots and accumulate them in their leaves, stems, and fruits. Consumption of food from plants such as crops, fruits, and vegetables with high levels of heavy metals has detrimental effects on human health (Baghaie & Fereydoni, 2019). Heavy metals can cause severe ailments such as kidney damage and cancer, lung and neurological damage, neurological effects, behavioral changes, loss of motor response, and disturbance in the cardiovascular and central nervous systems, bone marrow depression, hemolysis, hepatomegaly, melanosis, polyneuropathy, and encephalopathy (Jarup, 2003).

Corn (*Zea Mays* L.) is one of the most important crops in the Philippines. It is the best substitute staple food during rice shortages and is one of the primary sources of animal feeds. A study (Ibrahim, 2015) has shown that corn absorbs heavy metals like nickel (Ni), copper (Cu), iron (Fe), lead (Pb), and zinc (Zn) from soil and accumulates them in the grain, stem, silk, and stalk. Another study determined high levels of Pb on roots, leaves and seeds of corn grown on dumpsite soil (Cortez & Ching, 2014). Due to the adverse effects of heavy metals on human health, there is a need to detect heavy metals in corn.

There are different methods of detecting heavy metals viz., UV-Vis spectroscopy, atomic fluorescence spectroscopy, inductively coupled plasma mass spectroscopy (ICP-MS), surface enhanced Raman spectroscopy (SERS), ion chromatography, and atomic absorption spectroscopy (AAS). Although effective, these methods are considered to be complicated and expensive (March et al., 2015). A relatively low-cost and simpler alternate method (Bohrill et al., 2019) is anodic stripping voltammetry (ASV).

Anodic stripping voltammetry is an electrochemical method which offers a simple, low cost, and highly sensitive technique to determine various compounds, which gives it an upper hand (Zhai et al., 2015). It utilizes three electrodes; a working electrode, a counter electrode, and a reference electrode. The working electrode acts as the sensor and is usually modified to further increase its sensitivity. One of the common modifiers used is graphene which has a very unique set of physical and chemical properties such as large surface area and high conductivity (Er et al., 2017; Palisoc et al., 2017a). Other modifiers commonly used are gold nanoparticles (Palisoc et al., 2017b; Palisoc et al., 2017c; Palisoc et al., 2019b; Palisoc et al., 2019c), silver nanoparticles (AgNP) (He et al., 2017; Palisoc et al., 2018a), and bismuth nanoparticles (Palisoc et al., 2019a; Palisoc et al., 2020). Nanomaterials are usually used because of their remarkable properties, high adsorption and reactive capacity due to active sites and abundant functional groups on the nanomaterials' surface (Kurbanoglu et al., 2017), high surface-to-volume ratio, as well as enhanced sensitivity (Maduraiveeran & Jin W, 2017). The aforementioned nanomaterials are common in electrochemical detection for their unique physical and chemical properties like high-efficiency electrochemical sensing and quantum conductance (Hamidi-Asl et al., 2016). Silver nanoparticles, in particular, have excellent conductivity and biocompatibility, and electrocatalytic properties that can accelerate electron transfer and sensor stabilization (Zhai et al., 2015). Nafion has been widely used as an electrode modifier due to its anti-fouling capabilities, as well as its impressive optical quality, ability to load metal ions, and its simple handling (Zhai et al., 2015).

In this study, AgNP/graphene/Nafion modified glassy carbon electrodes (GCE) were fabricated for the detection and assessment of cadmium (Cd^{2+}) and lead (Pb^{2+}) accumulation in Philippine corn via ASV.

MATERIALS AND METHODS

AgNP/Graphene/Nafion modified glassy carbon electrode was fabricated by using the drop-coating method. The AgNP and graphene concentrations were each varied at 1 mg, 2 mg, and 3 mg. The modified GCEs were then used as the working electrode for detecting Pb^{2+} and Cd^{2+} in standard and real sample solutions via anodic stripping voltammetry.

Glassware and equipment

The following are the glassware and equipment that were used in this study: beaker, graduated cylinder, petri dish, Transferpette micropipette, teflon tape, glass slide, crucibles, Bosch SAE 200 electronic balance, Rocker Ultrasonic cleaner soner bath, AUTOLAB potentiostat, AA-6300 Shimadzu Atomic Absorption Spectrophotometer, glassy carbon electrode, and a voltammetric cell.

Chemicals and Reagents

Silver nanopowder (< 100 nm particle size), sodium chloride, lead chloride, cadmium chloride, copper chloride, mineral oil, nitric acid, concentrated hydrochloric acid, methanol, ethanol, 0.3 and 0.05-micron alumina slurry were purchased from Sigma Aldrich (Sigma-Aldrich Pte Ltd, Singapore). Graphene nanopowder (multilayer graphene; average flake thickness: 60 nm) was purchased from Graphene Supermarket (Calverton, NY, USA). Nafion (15-wt%) was purchased from Fuel Cell Earth (Woburn, MA, USA).

Preparation of AgNP/Graphene/Nafion casting solution

A Bosch SAE 200 electronic balance was used to measure the concentrations of AgNP and graphene. A 10 mL graduated cylinder was then used to measure ten weight-percentage (10-wt%) of Nafion. Since 15% Nafion was utilized, it was diluted with ethanol. Ethanol (4.667 mL) was added to 0.333 mL of 15% Nafion. The diluted Nafion was kept constant while the AgNP and graphene concentrations were each varied at 1 mg, 2 mg, and 3 mg.

Fabrication of the modified GCE

The bare GCE was polished with alumina slurry. This is to ensure an even surface for an even distribution of the casting solution. The alumina slurry was placed on a glass slide to serve as a surface to smoothen the GCE. The GCE was polished with 0.3-micron alumina slurry followed by 0.05-micron alumina slurry. Once the tip of the GCE was smoothened, the GCE was placed in a petri dish with nitric acid and was sonicated for 15 minutes. It was then rinsed with running water for 5 minutes and was sonicated in ethanol for 15 minutes. After the sonication, the electrode was rinsed with deionized water and was allowed to dry in air.

The AgNP/Graphene/Nafion solution was deposited onto the bare GCE via the using a Transferpette micropipette. The modified GCE was air dried at room temperature for at least two (2) hours.

Characterization of the modified GCE

The AgNP/Graphene/Nafion modified glassy carbon electrode was characterized using field emission scanning electron microscopy (FESEM) and energy dispersive X-ray (EDX) point analysis.

Anodic Stripping Voltammetry

An AUTOLAB potentiostat was used to perform anodic stripping voltammetry (ASV). A three-electrode voltammetry setup was utilized wherein Ag/AgCl served as the counter electrode, Pt wire as the reference electrode, and the AgNP/Graphene/Nafion modified GCE as the working electrode. Deionized water (100 mL) with 0.5844 g of

NaCl was used as the electrolyte solution. It was sparged with nitrogen to prevent oxygen from interfering with the scans.

Preparation of Stock Solution for Optimization of ASV Parameters

For the optimization of the parameters, 10 parts per million (ppm) stock solutions of Pb and Cd was prepared. The analyte solution is composed of 0.1 M NaCl, 1.6307 mg of $CdCl_2$, and 1.3389 mg of $PbCl_2$. The solutions were all diluted with 100 mL deionized water.

Preparation of stock solution for Calibration curve

For the calibration curve, 25, 50, 75, 100, 150, 200, and 250 ppb stock solutions of Pb and Cd were prepared. A 10-ppm solution was first prepared and was then diluted to obtain the desired concentration. All stock solutions were diluted with deionized water.

Real Sampling

Three corn plant (Zea mays) samples from a local farm were used for this study. Sample 1 was obtained nearest to a road used by cars and tractors. Sample 2 was obtained in between the nearest and farthest from the said road, and Sample 3 was obtained farthest from the road (sample 3). This was done to test if being closer to a source of pollution such as vehicle exhaust would affect heavy metal concentrations in plants, thus, the samples were not washed prior to testing. After one week of air drying, the samples were segregated and blenderized. There were a total of eighteen (18) samples that were tested. All the samples were subjected to acid digestion. All the samples, except the soil, were ashed beforehand. One gram (1 g) of soil and 2 g each of silk, leaf, stem, crop, and root were used in the real sampling. Using the AgNP/graphene/Nafion modified electrode, Cd^{2+} and Pb^{2+} were determined in the corn plant's silk, crop, leaf, stem, root, and the soil sample where it was planted on.

The fifteen (15) samples (silk, leaf, stem, crop, and root) were placed in crucibles and were ashed in a furnace with a temperature of 450 °C for 5 to 6 hours or until the samples have turned to white ash. Nitric acid (1.5 mL) was added to each sample and was allowed to evaporate to dryness over a hot plate. Once dried, the samples were placed in a 450 °C furnace for 15 mins. Hydrochloric acid (1 mL) was then added to each sample. The samples were then diluted with 100 mL of deionized water. The analyte was filtered with filter paper to remove larger particles and sodium chloride (0.5844 g) was added to the filtered analyte to form the analyte solution.

Determination of Pb^{2+} and Cd^{2+}

Anodic stripping voltammetry was performed to determine the concentraions of Pb^{2+} and Cd^{2+} in the samples of this study. The optimal electrode and optimized parameters were used todetermine the heavy metal concentrations in each of the samples. The calibration curves of Pb^{2+} and Cd^{2+} were used to compute for the concentrations present in the sample. Statistical analysis was performed via histograms for the optimization of the ASV parameters and linear regression for the calibration curves.

RESULTS AND DISCUSSION

Optimization of the electrode modifiers

The modifiers of the electrode were optimized by the amounts of AgNP and graphene at 1 mg, 2 mg, and 3 mg while the concentration of the Nafion solution (4.667 mL ethanol and 0.333 mL Nafion) was held constant. The resulting electrodes were then used for the simultaneous detection of 10 ppm of Cd^{2+} and Pb^{2+} in an electrolyte solution via anodic stripping voltammetry. The deposition potential, deposition time, and accumulation time were held constant at -1 V s^{-1}, 60 s, and 15 s, respectively.

Fig. 1 shows the comparison of the current peaks for varying amounts of AgNP and graphene for the simultaneous detection of Cd^{2+} and Pb^{2+}. It can be observed from the figure that for 1 mg AgNP, the anodic current peaks of Cd^{2+} and Pb^{2+} decrease with increasing amounts of graphene, while for 3 mg AgNP, the anodic current peaks of Cd^{2+} and Pb^{2+} are almost constant with varying amounts of graphene. Since the electrode fabricated with 2 mg AgNP and 1 mg graphene manifested the highest anodic current peaks of Cd^{2+} and Pb^{2+}, it was considered as the optimized electrode.

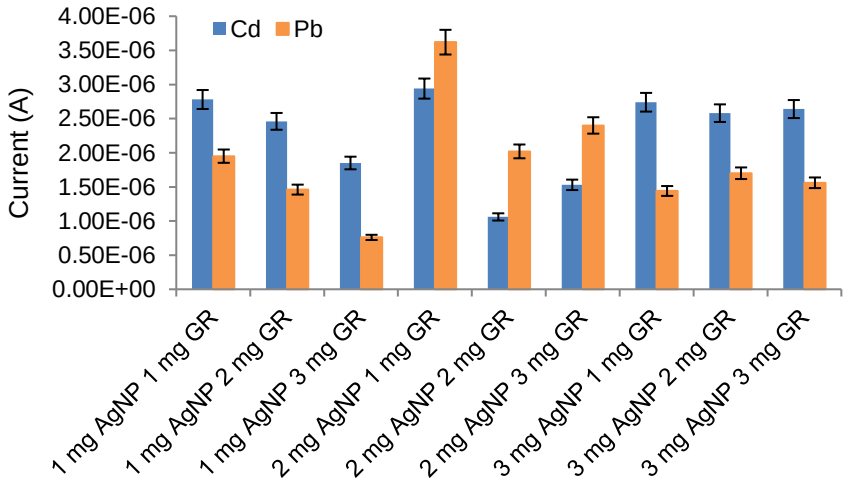

Figure 1. Anodic current peaks for varying amounts of AgNP and graphene for the simultaneous detection of Cd^{2+} and Pb^{2+}.

Optimization of ASV Parameters

The deposition potential was varied at -1.05 V, -1.0 V, -0.95 V, -0.9 V, -0.85 V and -0.8 V while the deposition time and accumulation time were held constant at 60s and 30s, respectively. Fig. 2 shows the comparison of the anodic current peaks for varying deposition potential. From the figure, it can be noted that as the deposition potential increased, the anodic peak current also increased. However, when it reached -0.95 V, the peaks started to plateau and decrease. Thus, the optimized deposition potential is -0.90 V since it showed the highest anodic current peak.

The deposition time was varied at 30, 40, 50, 55, and 60 s while deposition potential was held constant at -0.9 V, and accumulation time at 30 s. As seen in Fig. 3, as the accumulation time increased, the anodic peak current also increased. However, at 60 s,

the anodic peak current significantly decreased. Thus, the optimized deposition time is 55 s because it showed the highest anodic current peak.

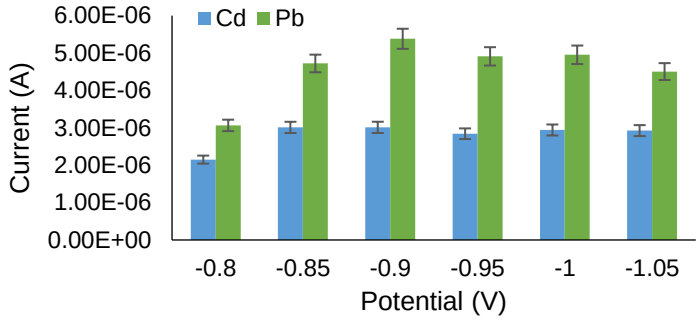

Figure 2. Anodic peak currents for varying deposition potential for the simultaneous detection of Cd^{2+} and Pb^{2+}.

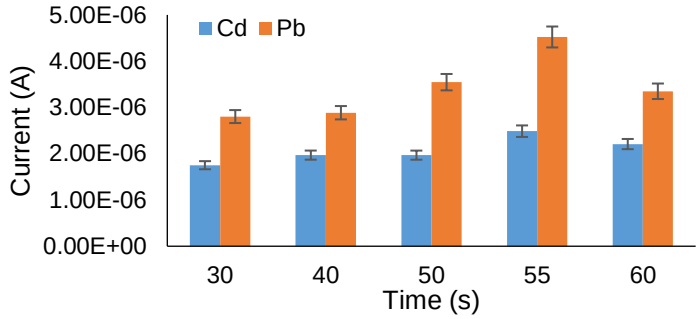

Figure 3. Anodic peak currents for varying deposition time for the simultaneous detection of Cd^{2+} and Pb^{2+}.

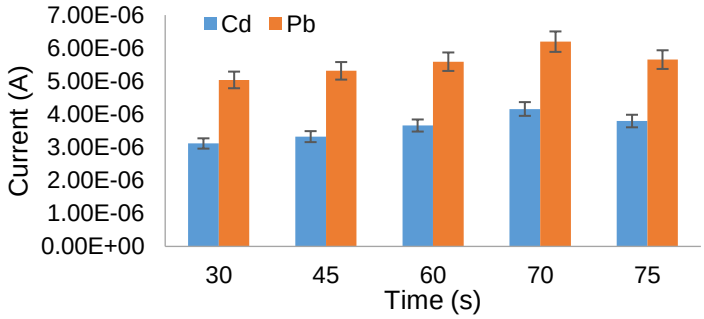

Figure 4. Anodic peak currents for varying resting time for the simultaneous detection of Cd^{2+} and Pb^{2+}.

The accumulation time was varied at 30, 45, 60, 65, 70, and 75 s while the deposition potential was held constant at -0.9 V, and deposition time at 55 s. As seen in Fig. 4, as the accumulation time increased, the anodic peak current increased as well. However, at 75 s, the anodic peak currents started to decrease. Thus, 70 s is the optimized resting time since it gave the highest anodic current peak.

Characterization of the modified electrode

Field emission scanning electron microscopy and energy dispersive X-ray spectroscopy were used to verify the presence of AgNP and graphene on the electrode surface, as well as to characterize the morphology of the modified electrode surface.

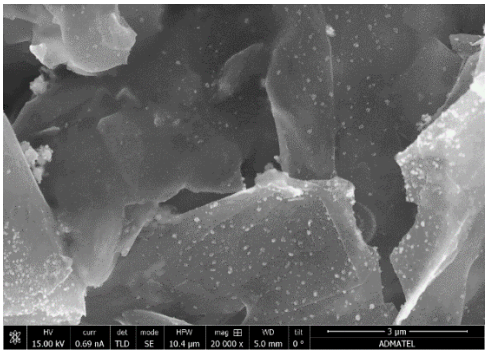

Figure 5. FESEM image of AgNP/ Graphene/ Nafion modified GCE.

Fig. 5 shows the scanning electron micrograph of the modified electrode surface. The image confirms the dendritic shape of the silver nanoparticles and the sheet like structure of graphene. It also shows that AgNP was dispersed uniformly on the modified GCE surface. The SEM image is in agreement with previous studies (Song et al., 2013; Molina et al., 2016).

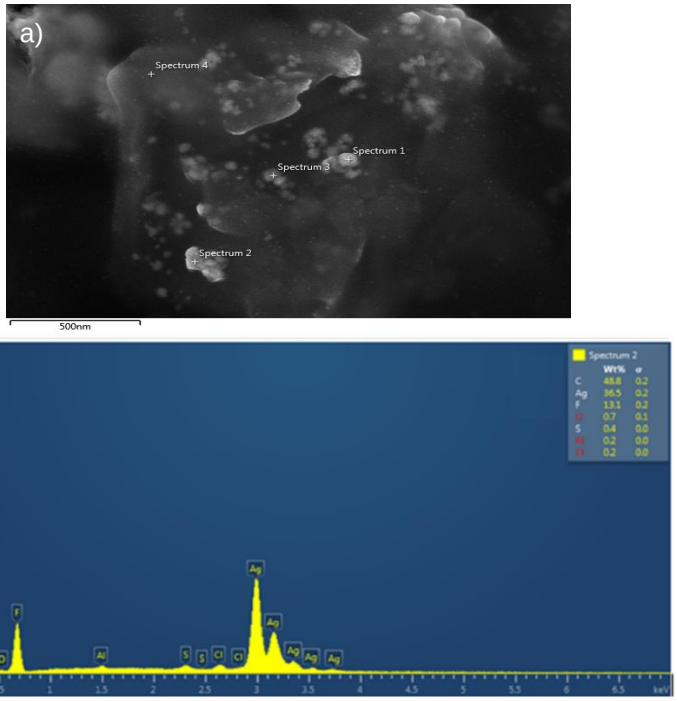

Figure 6. (a) FESEM point analysis micrograph and (b) the corresponding EDX spectrum of AgNP/Graphene/Nafion modified GCE.

Fig. 6 shows the FESEM point analysis micrograph and the corresponding EDX spectrum of the modified electrode. As seen in the figure, the EDX spectrum confirms the presence of AgNP and graphene on the GCE surface. Aluminum found in the spectrum is attributed to the alumina slurry used in polishing the bare GCEs. Alumina

slurry is the common polishing reagent for carbon electrodes. It has been found that even after sonication, the aluminum layer still remains (Kiema et al. 2013). Fluorine (F), Sulfur (S), and Oxygen (O) found in the spectrum are from Nafion's composition.

Calibration Curve

Using the prepared stock solutions, the calibration curves for Pb^{2+} and Cd^{2+} concentrations were obtained (Fig. 7). The calibration curve of each of the said heavy metals were obtained by plotting the heavy metal concentrations against their respective anodic current peaks. With an R^2 value close to 1 for both heavy metals, it can be stated that the current peaks and the heavy metal concentration have a strong linear relationship.

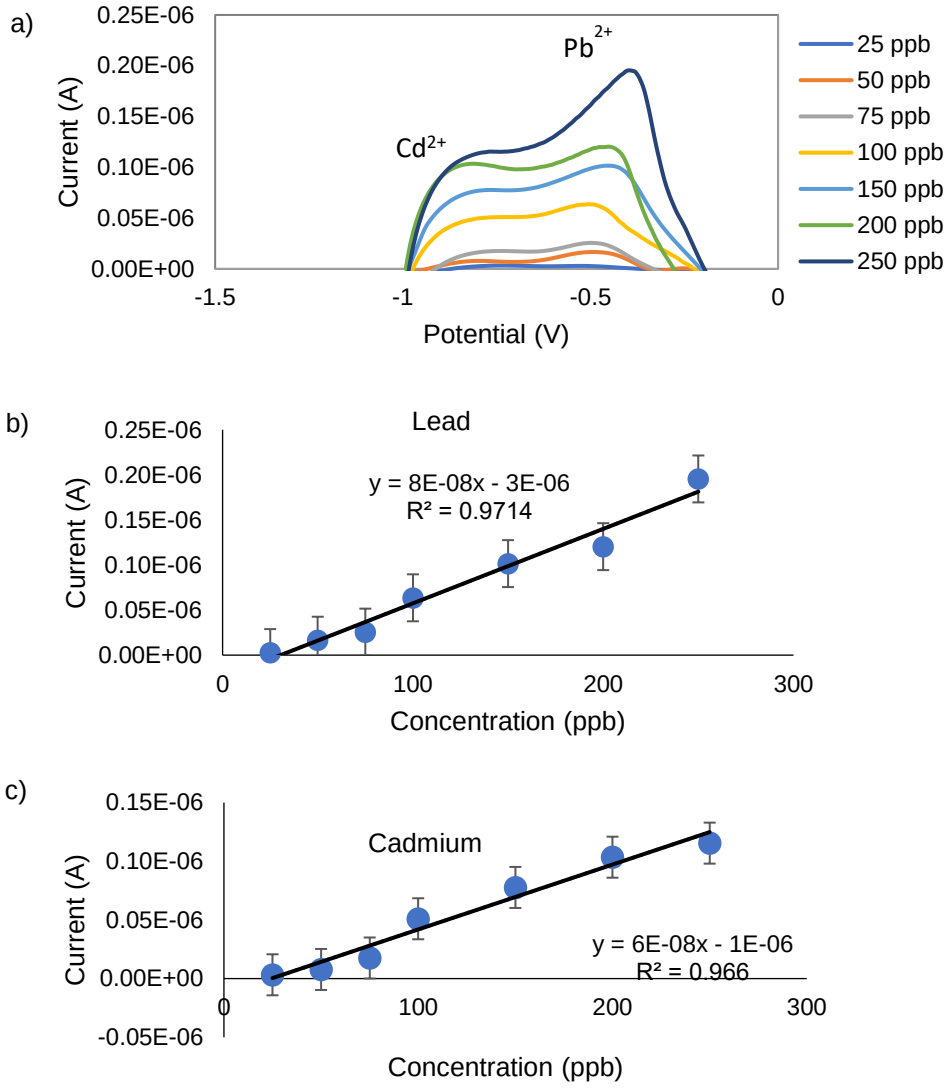

Figure 7. (a) Anodic stripping voltammograms for varying concentrations of Cd^{2+} and Pb^{2+}. Calibration curves for (b) Pb^{2+} and (c) Cd^{2+}.

Limit of Detection and Limit of Quantitation

The limit of detection (LOD) and limit of quantitation (LOQ) for both Cd^{2+} and Pb^{2+} were computed to determine the lowest concentration that the AgNP/graphene/Nafion modified GCE can detect. The limit of detection of the modified electrode was determined to be 25 ppb for both Cd^{2+} and Pb^{2+}. The limits of quantitation are 155.7 ppb for Cd^{2+} and 159.5 ppb for Pb^{2+}. These values were computed using the line equations obtained from the calibration curves.

Table 1 shows the performance comparison of the AgNP/Graphene/Nafion modified glassy carbon electrode with other works. From this, it can be concluded that the modified electrode in this study has a lower LOD than most of the electrodes presented in the table.

Table 1. Comparison of the AgNP/Graphene/Nafion modified GCE with other works

Electrode	Modifier	Method	Limit of Detection	Reference
Indium Tin Oxide	$[Ru(NH_3)_6]^{3+}$/Nafion	ASV	Pb – 500 ppb Cd – 500 ppb	(Palisoc et al., 2015)
Glassy Carbon	AuNP/$[Ru(NH_3)_6]^{3+}$/ Nafion	ASV	Pb – 45 ppb Cd – 200 ppb	(Palisoc et al., 2017b)
Glassy Carbon	Chitosan/carbon nanotubes	SWASV	Pb – 600 ppb Cd – 800 ppb	(Wu et al., 2017)
Glassy carbon	$[Ru(bpy)_3]^{2+}$/graphene/ Nafion	DPV	Pb – 48 ppb Cd – 49 ppb	(Palisoc et al., 2017a)
Carbon Paste	Coconut Shell powder	ASV	Cd – 105 ppb	(Rajawat et al., 2014)
Multilayer Graphene paste	Activated carbon from coconut husk	ASV	Pb – 44 ppb Cd – 56 ppb	(Palisoc et al., 2018b)
Graphene paste	Bismuth nanoparticles	ASV	Pb & Cd – 100 ppb	(Palisoc et al., 2019a)
Graphene paste	Gold nanoparticles	ASV	Pb–256 ppb Cd – 267 ppb	(Palisoc et al., 2019b)
Glassy Carbon	AgNP/Graphene/Nafion	DPV	Cd –25 ppb Pb – 25 ppb	This work

Real Sampling

Using the optimized modified electrode and optimized ASV parameters for obtaining the highest possible anodic peak currents for Pb^{2+} and Cd^{2+}, ASV was performed for the real sample analysis.

Table 2 shows the Cd^{2+} and Pb^{2+} concentrations present in the three different plant and soil locations. It can be observed that soil 3, root 1, stem 3, leaves 1, corn 2, and silk 3 have the highest concentration of the two heavy metals for their respective parts. The plant part that accumulated the most Pb^{2+} concentration was stem 3 with 142.375 ppb; while the part that absorbed the least amount of Pb^{2+} was leaves 3, with only 51.25 ppb. For Cd^{2+}, the highest concentration was also found to be in stem 3, with 261.67 ppb. The lowest Cd^{2+} concentration was found in root 2, with only 22.92 ppb.

It has been observed that the soil and the plant samples had an increase in heavy metal content as it got planted further away from the road, leading to location 3 having most of the highest concentrations for both metals. This may be due to the environment enclosing location 3, such as smaller roads accessible to the locals. According to Peralta-Videa (Peralta-Videa et al., 2009), the main source of Cd^{2+} intake is due to anthropogenic activities such as smoking. It can also be noted that Cd^{2+} utilizes the same biosorption pathway as calcium when absorbed by plants, which means it could easily be absorbed and stored in stems. For the concentration of Pb^{2+}, Peralta-Videa also mentioned that plants do not have channels for the uptake of Pb^{2+}. However, there have been observations that Pb^{2+} enters through the roots and builds up in the plant's phloem, which would most likely end up accumulating in the plant's leaves as it grows. This would explain the presence of Pb^{2+} in leaves 1 and 3. The minimal uptake of Pb^{2+} is also in agreement with previous studies (Mirecki et al., 2015; Wang et al., 2017).

Table 2. Concentrations of Cd^{2+} and Pb^{2+} and in the soil, corn grain, silk, leaves, stem and roots using ASV (ND-Not detected)

Samples	Cadmium (ppb)	Lead (ppb)
Soil 1	113.17	121.13
Soil 2	35.17	ND
Soil 3	221.6	162.5
Root 1	39.3	107.75
Root 2	22.92	ND
Root 3	ND	ND
Stem 1	ND	ND
Stem 2	ND	ND
Stem 3	261.67	142.38
Leaves 1	ND	109.88
Leaves 2	ND	ND
Leaves 3	ND	51.25
Corn 1	ND	ND
Corn 2	ND	88
Corn 3	ND	67.13
Silk 1	25.13	ND
Silk 2	50.3	ND
Silk 3	57.5	ND

According to the World Health Organization (WHO), the maximum amount of lead and cadmium that a person is allowed to consume is 50 ppb and 5 ppb, respectively (Palisoc et al., 2017). The corn 2 and corn 3 samples had lead contents of 88 and 67.125 ppb, respectively. This is way beyond the acceptable WHO limits and are therefore deemed toxic for human consumption.

CONCLUSIONS

A AgNP/Grahphene/Nafion modified glassy carbon electrode has been successfully fabricated via the drop-coating method. It was determined that 2mg AgNP and 1mg graphene were the optimum modifier amounts for detecting Cd^{2+} and Pb^{2+} since they obtained the highest anodic peak current for the detection of lead and cadmium. Characterization of the modified electrode by FESEM and EDX showed that the silver nanoparticles and graphene have successfully been deposited on to the electrode surface. The limit of detection for the modified electrode was found to be at 25 ppb for both Cd^{2+} and Pb^{2+}. The limit of quantitation was found to be at 155.7 ppb for Cd^{2+} and 159.5 ppb for Pb^{2+}. In future studies, it is suggested to use other nanomaterials as modifiers of the GCE to obtain a lower LOD. Moreover, using a standard method such as inductively coupled plasma mass spectroscopy is recommended to verify the ASV results.

REFERENCES

Baghaie, A.H. & Fereydoni, M. 2019. The potential risk of heavy metals on human health due to the daily consumption of vegetables. *Environmental Health Engineering and Management* **6**, 11–16.

Borrill, A., Reily, N. & Macpherson, J. 2019. Addressing the practicalities of anodic stripping voltammetry for heavy metal detection: a tutorial review. *Analyst* **144**, 6834–6849.

Cortez, L.A. & Ching, J. 2014. Heavy Metal Concentration of Dumpsite Soil and Accumulation in Zea mays (corn) Growing in a Closed Dumpsite in Manila, Philippines. *International Journal of Environmental Science and Techenology* **5**, 77–80.

Er, E., Çelikkan, H. & Erk, N. 2017. A novel electrochemical nano-platform based on graphene/platinum nanoparticles/nafion composites for the electrochemical sensing of metoprolol. *Sensors and Actuators B-Chemistry* **238**, 779–787.

Ganeshamurthy, A.N., Varalakshmi, L.R. & Sumangala, H.P. 2008. Environmental risks associated with heavy metal contamination in soil, water and plants in urban and periurban agriculture. *Journal of Horticultural Sciences* **3**, 1–29.

Hamidi-Asl, E., Dardenne, F., Pilehvar, S., Blust, R. & Wael, K.D. 2016. Unique Properties of Core Shell Ag@Au Nanoparticles for the Aptasensing of Bacterial Cells. *Chemosensors* **4**, 1–11.

He, D., Rauwel, E., Malpass-Evans, R., Carta, M., McKeown, N., Gorle, D.B., Kulandainathan, M.A. & Marken, F. 2017. Redox reactivity at silver microparticle–glassy carbon contacts under a coating of polymer of intrinsic microporosity (PIM). *Journal of Solid State Electrochemistry* **21**, 2141–2146.

Ibrahim, K.N. 2015. Heavy Metal Concentration (Pb, Cu, Fe, Zn, Ni) in Plant Parts of *Zea Mays* L. Cultivated in Agricultural Area Near Alor Gajah, Melaka, Malaysia. *American Journal of Environmental Engineering* **5**, 8–12.

Jarup, L. 2003. Hazards of heavy metal contamination. *British Medical Bulletin* **68**, 167–182.

Kiema, G.K., Aktay, M. & Mcdermott, M.T. 2003. Preparation of reproducible glassy carbon electrodes by removal of polishing impurities. *Journal of Electroanalytical Chemistry* **540**, 7–15.

Kurbanoglu, S., Ozkan, S.A. & Merkoçi, A. 2017. Nanomaterials-based enzyme electrochemical biosensors operating through inhibition for biosensing applications. *Biosensors and Bioelectronics* **89**, 886–898.

Maduraiveeran, G. & Jin, W. 2017. Nanomaterials based electrochemical sensor and biosensor platforms for environmental applications. *Trends in Environmental Analytical Chemistry* **13**, 10–23.

March, G., Nguyen, T.D. & Piro, B. 2015. Modified Electrodes Used for Electrochemical Detection of Metal Ions in Environmental Analysis. *Biosensors* **5**, 241–275.

Mirecki, N., Sunic, L., Agic, R. & Ilic, ZS. 2015. Transfer factor as indicator of heavy metals content in plants. *Fresenius Environmental Bulletin* **24,** 4212–4219.

Molina, J., Cases, F. & Moretto, L. 2016. Graphene-based materials for the electrochemical determination of hazardous ions. *Analytica Chimica Acta* **946**, 9–39.

Palisoc, S., Chua, R. & Natividad, M. 2020. Highly sensitive determination of heavy metals in Upland and Lowland Rice using AgNP/BiNP/MWCNT/Nafion modified glassy carbon electrode via anodic stripping voltammetry. *Materials Research Express* **7**, 1–14.

Palisoc, S., Natividad, M., Malabuyo, Y.A. & Pereja, R.C. 2019a. Determination of heavy metals in root crops using bismuth nanoparticles modified graphene paste electrode. *Agronomy Research* **17**, 245–260.

Palisoc, S., Leoncini, J. & Natividad, M. 2019b. Trace level determination of cadmium and lead in coffee (Coffea) using gold nanoparticles modified graphene paste electrode. *Agronomy Research* **17**, 229–239.

Palisoc, S., Bentulan, J.M. & Natividad, M. 2019c. Determination of trace heavy metals in canned food using Graphene/AuNPs/$[Ru(NH_3)_6]^{3+}$/Nafion modified glassy carbon electrodes. *Journal of Food Measurement and Characterization* **13**, 169–176.

Palisoc, S., Lee, E., Natividad, M. & Racines, L. 2018a. Silver Nanoparticle Modified Graphene Paste Electrode for the Electrochemical Detection of Lead, Cadmium and Copper. *International Journal of Electrochemical Science* **13**, 8854–8866.

Palisoc, S., Estioko, L.C. & Natividad, M. 2018b. Voltammetric Determination of Lead and Cadmium in Vegetables by Graphene Paste Electrode Modified with Activated Carbon from Coconut Husk. *Materials Research Express* **5**, 1–10.

Palisoc, S., Uy, D.J., Natividad, M. & Lopez, T.B. 2017a. Determination of heavy metals in mussel and oyster samples with tris (2,2′-bipyridyl) ruthenium (II)/graphene/Nafion® modified glassy carbon electrodes. *Materials Research Express* **4**, 1–13.

Palisoc, S., Causing, N. & Natividad, M. 2017b. Gold nanoparticle/hexaammineruthenium/Nafion® modified glassy carbon electrodes for trace heavy metal detection in commercial hair dyes. *Analytical Methods* **9**, 4240–4246.

Palisoc, S., Valeza, N.C. & Natividad,M. 2017c. Fabrication of an Effective Gold Nanoparticle/Graphene/Nafion® Modified Glassy Carbon Electrode for High Sensitive Detection of Trace Cd^{2+}, Pb^{2+} and Cu^{2+} in Tobacco and Tobacco Products. *International Journal of Electrochemical Science* **12**, 3859–3872.

Palisoc, S., Natividad, M., Martinez, N., Ramos, R. & Kaw, K. 2015. Fabrication and electrochemical study of $[Ru(NH_3)_6]^{3+}$/Nafion modified electrodes for the determination of trace amounts of Pb^{2+}, Cd^{2+}, and Zn^{2+} via anodic stripping voltammetry. *e-Polymers* **16**, 117–123.

Peralta-Videa, J.R., Lopez, M.L., Narayan, M., Saupe, G. & Gardea-Torresdey, J. 2009. The biochemistry of environmental heavy metal uptake by plants: Implications for the food chain. *The International Journal of Biochemistry and Cell Biology* **41**, 1665–1677.

Rajawat, D.S., Kumar, N. & Satsangee, S.P. 2014. Trace determination of cadmium in water using anodic stripping voltammetry at a carbon paste electrode modified with coconut shell powder. *Journal of Analytical Science and Technology* **5**, 1–8.

Song, Y.Z., Ma, K., Zhu, F.X. & Xu, J. 2013. Synthesis of Silver Nanoparticles Using Cefopernazone as a Stabilizing Reagent and Its Catalysis for Sodium Sulfide. *International Jouranl of Electrochemical Science* **8**, 3628–3635.

Wang, S., Wu, W., Liu, F, Liao, R. & Hu, Y. 2017. Accumulation of heavy metals in soil-crop systems: a review for wheat and corn. *Environmental Science and Pollution Research* **24**, 15209–15225.

Wu, K., Lo, H., Wang, J., Yu, S. & Yan, B. 2017. Electrochemical detection of heavy metal pollutant using crosslinked chitosan/carbon nanotubes thin film electrodes. *Materials Express* **7**, 15–24.

Zhai, H., Liang, Z., Chen, Z., Wang, H., Liu, Z., Su, Z. & Zhou, Q. 2015. Simultaneous detection of metronidazole and chloramphenicol by differential pulse stripping voltammetry using a silver nanoparticles/sulfonate functionalized graphene modified glassy carbon electrode. *Electrochimica Acta* **171**, 105–113.

Agronomy Research **18**(3), 2197–2210, 2020
https://doi.org/10.15159/AR.20.163

Conversion of cellulose to activated carbons for high-performance supercapacitors

E. Sermyagina[1,*], K. Murashko[2], D. Nevstrueva[1], A. Pihlajamäki[1] and E. Vakkilainen[1]

[1]LUT University, Energy Technology, Laboratory of Sustainable Energy Systems, Skinnarilankatu 34, FI53850 Lappeenranta, Finland
[2]University of Eastern Finland, Fine Particle and Aerosol Technology Laboratory, Yliopistonranta 1 C, FI70210 Kuopio, Finland
[*]Correspondence: ekaterina.sermyagina@lut.fi

Abstract. Biomass-derived activated carbons are promising materials that can be used in various applications. Current work investigates the possibilities of the cellulose-derived activated carbons in substituting the commercial alternatives for the supercapacitors' electrodes with high efficiency, stable performance and relatively low cost. Hydrothermal carbonization (HTC) followed by chemical activation with KOH is used to convert cellulose into highly porous activated carbons. The effect of HTC parameters on the material porosity development and electrochemical properties of the electrodes is evaluated with several variations of the residence time and the weight ratio between cellulose and water during the pretreatment. The analysis shows that intensification of the HTC process (longer residence time and higher water/cellulose ratio) results in increase of the surface area of both hydrochar samples and subsequent activated carbons: with the highest surface area for the sample produced after 2 h HTC treatment with water/cellulose ratio of 6/1 - 2,645 $m^2 g^{-1}$. As for the electrochemical analysis, the highest values of the specific capacitance are found for the samples produced from 2 h HTC treatment: 110.3 F g^{-1} (water/cellulose ratio of 3/1) and 102.5 F g^{-1} (water/cellulose ratio of 6/1). Additionally, it is noted that electrodes produced from the samples treated during 4 h have higher impedance at low operation frequency. The present study proves the possibility to substitute commercial activated carbons with cellulose-derived materials, the porosity of which can be tuned accordingly already during the pretreatment step.

Key words: cellulose, hydrothermal carbonization, activated carbon, electrodes, supercapacitors.

INTRODUCTION

Activated carbons (AC) present the carbonaceous materials with high specific surface areas and adjustable surface-containing functional groups (Kuzmenko et al., 2015). The beneficial features of AC make them highly widespread in various modern applications and technologies. Their versatile properties allow them to be efficiently applied as adsorbents: in applications including the removal of heavy metals, organic compounds and dyes, toxic substances and different impurities in water and in air (Rengaraj et al., 2002; Babeł & Kurniawan, 2003; Jiang et al., 2003; Crini, 2006; Mohan & Pittman Jr., 2007). Another important area for the AC is the electrical energy storage

applications: carbonaceous materials are widely used for lithium-ion batteries and for supercapacitors due to physical and chemical stability and high conductivity, significant surface area and porosity (Pandolfo & Hollenkamp, 2006; Zhu et al., 2011).

The activated carbons can be produced by several activation methods: physical (thermal), chemical or physicochemical activation (a combination of both) (Hernández-Montoya et al., 2012; Kuzmenko et al., 2015). During thermal activation, the precursor is carbonized under an inert atmosphere, and the resulting carbon is subjected to a partial gasification with an oxidizing gas (air, steam, CO_2, etc.) at high temperature (800–1,100 °C). Within the chemical activation, the feedstock is mixed with a chemical compound, generally a dehydrating agent (H_3PO_4, H_2SO_4, HNO_3, NaOH, KOH or $ZnCl_2$), and the mixture is subsequently heated to the temperature between 400 and 800 °C in an inert atmosphere. As for the physicochemical activation, the process is carried out with changing the activation atmosphere of the chemical activation to a gasification atmosphere (e.g. steam) at higher temperatures (Hernández-Montoya et al., 2012). As a rule, the chemical activation produces AC with the highest specific surface area. Additionally, the chemical activation provides more intensive development of micropores and requires lower temperatures than physical activation (Khezami et al., 2005). At the same time, the applied chemical agents make the process corrosive and require additional washing step for the products (Lozano-Castelló et al., 2001).

The majority of the commercial AC are the fossil fuel-based. Relatively high production cost and environmental concerns about the consequences of the coal and oil utilization drive the attention to alternative feedstock to produce the activated carbons from cheaper, renewable and widely available precursors (Mohamad Nor et al., 2013). Considering the increasing energy demand in the world and the promotion of sustainable materials and processes in different industrial spheres, biomass-derived activated carbons are highly promising materials for the supercapacitors' electrodes with high efficiency, stable performance and relatively low cost (Hernández-Montoya et al., 2012; Kuzmenko et al., 2015; Mesfun et al., 2019).

Alternative sources for activated carbons

The specific surface area and porosity of the activated carbons are determined by the feedstock material and activation procedure (Jiang et al., 2003). Hydrothermal carbonization (HTC) presents an attractive pathway to convert the organic materials into carbonaceous precursors for AC production (Li et al., 2020). Thermal treatment of the feedstock in a mixture with water in temperature range of 150–350 °C under autogenous pressures converts biomass into highly functionalized carbon materials (Titirici et al., 2007; Titirici & Antonietti, 2010). The resulted coal-like product (hydrochar) obtains a rudimental porosity due to the depolymerization and decomposition of the structural components and the consequent release of such elements as hydrogen, oxygen and nitrogen in form of condensable and non-condensable gases and tars (Hernández-Montoya et al., 2012). The liquid products of the HTC process contain volatile fatty acids and furfurals, which can be then effectively used in other applications (Sun et al., 2019).

In order to optimize the activation process towards the required resulting properties, the comprehensive knowledge of chemical components' behaviour during both carbonization and activation steps is needed. Several researchers have been investigating the possibilities of producing functional carbonaceous products from the main lignocellulosic structural components: glucose (Khezami et al., 2005; Lee et al., 2016;

Yuan et al., 2019), starch (Sevilla et al., 2011; Cao et al., 2018), cellulose (Deng et al., 2013; Wang et al., 2017) and lignin (Saha et al., 2014; Zhang et al., 2019). Cellulose has a significant impact on the microporosity development of the activated carbons from lignocellulosic feedstock: da Silva Lacerda et al. (2015) reported the increase of the adsorption properties of the activated carbons with artificially increased cellulose content. Sevilla et al. (2011) investigated the impact of activation parameters (temperature and hydrochar/KOH ratio) on the AC from hydrothermally carbonized cellulose and other lignocellulosic compounds for the gas storage applications. It was proven that the pore characteristics can be adjusted by changing the activation conditions: the highest porosity for cellulose derived AC was developed at the activation temperature of 700 °C and the hydrochar/KOH weight ratio of 1/4. The results presented by Wei et al. (2011) demonstrated a high potential to convert hydrothermally carbonized lignocellulosic materials (cellulose, starch and wood) into high surface area supercapacitors. Other researchers investigated the impact HTC temperature. In the work of Falco et al. (2013), three temperatures were tested (180, 240 and 280 °C) for cellulose, glucose and rye straw, and the highest surface area and total pore volume values were found for AC produced from samples carbonized at 240 °C. At the same time, more research is needed to evaluate in detail the effect of carbonization step on the resulted product, i.e. how the process severity (time, temperature, feedstock/water ratio) affects the porosity of activated carbons.

Tuning the microporosity of the ACs is important for some energy and environmental related applications (e.g., natural gas and hydrogen storage, supercapacitors, volatile organic compounds removal), where advanced porous materials with tailored porosity (extremely high development of microporosity together with a narrow micropore size distribution) are required (Hartmann et al., 2020). Using supercapacitors as an energy storage device is attracting an increasing attention worldwide (Kim et al., 2019). In the previous paper (Murashko et al., 2017), the material preparation methodology for a natural cellulose-activated carbon composite material was developed and described. The flexible self-standing electrodes for electrical double layer capacitors (EDLCs) were produced from the commercially available activated carbon with cellulose as a binding material. The aim of the current study is to investigate the possibility of substituting the commercial AC with the activated carbon from the cellulose derived hydrochar. Above all, the effect of HTC reaction parameters on porous structure evolution during activation and, as a result, on electrochemical characteristics of the produced electrodes was evaluated.

MATERIALS AND METHODS

Materials

High-purity cellulose (quality 2100 type, degree of polymerization 780, α-cellulose content ≥ 93%) produced by Domsjö Fabriker AB from softwood was used as a carbon precursor and an electrode binder. The material was cut to pieces with dimensions around 5–10 mm on average for the HTC experiments and grinded at the Retsch PM100 planetary ball mill to the powder state for the electrode preparation. Potassium hydroxide pellets (Sigma-Aldrich) were used as an activation agent and were grinded in the agate mortar before the experiments. Ionic liquid (IL), 1-ethyl-3-methylimidazolium acetate, was acquired from BASF (BasionicsTM BC01, CAS: 143314-17-4, assay > 98%) and

used as received in preparation of an electrode casting solution. Sulphuric acid from Merck (CAS: 7664-93-9, assay 95–97%) was used to prepare a 1 mol sulphuric acid aqueous electrolyte. Deionized water was used for electrolyte preparation, for all electrode samples (as a coagulant) and during storage of the samples.

Preparation of hydrochar materials

Hydrochars were prepared by hydrothermal carbonization in 1 l stainless steel tube batch reactor. For each run, the feedstock material was dispersed in water, stirred manually and then loaded into the reactor. Heating (at the rate of 2 °C min^{-1}) to the process was provided by the electrical heater and controlled with a PID controller. The reaction temperature was maintained at 250 °C for all HTC runs. In this work, the following reaction parameters were tested: the residence time of 2 and 4 h; water-to-cellulose weight ratios of 3:1 and 6:1. The resulting solid product was recovered by vacuum filtration using the Büchner funnel with a Whatman glass microfiber filter paper (grade GF/A). Hydrochar samples were subsequently dried overnight in the oven at a temperature of 105 ± 2 °C.

Hydrochar samples were named in accordance with the reaction parameters as HTC-*t*-r_{HTC}, where *t* denotes the reaction time, h, and r_{HTC} the unitless water/cellulose weight ratio.

Preparation of porous carbons

The hydrochar samples were chemically activated at 700 °C with KOH. Hydrochar was thoroughly mixed with the activating agent at impregnation ratio (KOH/ hydrochar) of 4:1 in an agate mortar. Powder mixture was then loaded into the reactor where it was heated to the activation temperature with the heating ramp rate of 3 °C min^{-1} under nitrogen gas flow and hold at the target temperature for 1 h. Finally, the activated carbon samples were washed with distilled water to neutral pH and dried in an oven at 50 ± 2 °C for 16 h. Dried AC was subsequently milled to the powder state (particle size ≤ 200 μm).

Burn-off values (*BO*, %) for ACs were determined as following

$$BO = \frac{wt_0 - wt}{wt_0} \cdot 100\% \quad (1)$$

where wt_0 and wt – respectively the initial weight of the dry hydrochar and the final weight of activated carbon, g.

Preparation of electrodes

The electrodes were prepared by the phase inversion method, immersion precipitation, using activated carbon as the active material and cellulose as the electrode binder (Mulder, 1996). The procedure of the electrode preparation was described in detail in the previous paper (Murashko et al., 2017). On the whole, the cellulose was ground in the planetary ball-mill and dissolved in the ionic liquid under vigorous stirring at 90 °C for 12 h to produce a 6 wt% casting solution. Respective amount of obtained activated carbon was mixed with the ionic liquid and the dispersion was placed under an ultrasound homogenizer Bandelin UW 2200 for 10 min to prevent possible formation of carbon particle agglomerates. The hot cellulose solution was added to the activated carbon dispersion and the obtained slurry with cellulose/activated carbon ratio of 1/6 was mixed by ultrasound for 5 min to ensure a homogeneous particle distribution. The casting solution was then distributed on a glass plate with an adjustable casting knife

(BYK Additives & Instruments) using an automatic film applicator BYK Additives & Instruments at room temperature. The casting thickness for all samples was 250 μm and the casting speed was 50 mm s^{-1}. All prepared materials were immersed in a deionized water coagulation bath at room temperature for 24 h. The electrodes were denoted according to the HTC conditions – AC-*t*-r_{HTC}.

Analytical methods

The moisture content of both hydrochar samples and activated carbons was measured with the moisture analyser balance Sartorius 7093. The morphology of the activated carbon samples was examined by Scanning Electron Microscopy (SEM) using a Hitachi SU3500 microscope. The characterization of porous carbons was carried out by nitrogen adsorption–desorption isotherms measured at 77 K using a Gemini VII Micromeritics instrument. Prior to gas adsorption measurement, the carbon samples were degassed at 300 °C under nitrogen for 3 h. BET surface area was calculated from N_2 adsorption isotherms by using the Brunauer–Emmett–Teller (BET) equation. The relative pressure range applied for the hydrochar samples was p/p_0 = 0.05–0.25 and for the activated carbons – p/p_0 = 0.01–0.15. More narrow and lower pressure region in case of activated carbons is required due to limitations of applying BET equation: only linear and continuously increasing portion of the BET plot can be used for the calculations, and in case of microporous materials this usually appear to be at the low relative pressures where the monolayer formation occurs (Rouquerol et al., 2007; De Lange et al., 2014). The total pore volume was determined from experimental isotherm by calculating the amount of nitrogen adsorbed at a relative pressure of 0.99.

The electrochemical tests were performed by using a Swagelok-type cell (Fig. 1). Two flexible self-standing electrodes were prepared from the derived cellulose composite material and dipped into 1 M H_2SO_4 (H_2SO_4/H_2O) electrolyte before placing into the Swagelok-type cell. The electrodes were clamped between two graphite current collectors and a cellulosic separator. The pressure between the current collectors was adjusted by screws with butterfly nuts. The Swagelok-type cell was connected to a potentiostat/galvanostat (Gamry Reference 3000), which was used for the measurement of cyclic voltammetry (CV) curves and electrochemical impedance spectroscopy (EIS) measurements.

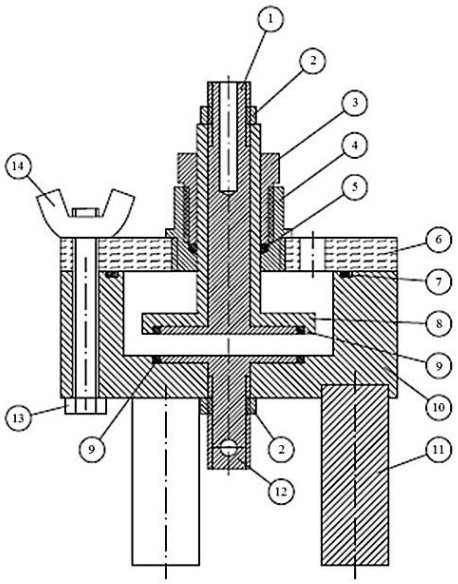

Figure 1. Swagelok-type cell used in measurements. Graphite current collectors are used due to their good chemical compatibility: 1) current collector; 2) nut; 3) seal tightening nut; 4) stud; 5) O-ring; 6) cover; 7) O-ring; 8) current collector insulation; 9) seal; 10) test chamber; 11) feet; 12) current collector; 13) screw; 14) butterfly nut.

RESULTS AND DISCUSSION

Mass yields of carbonization and activation processes

During HTC process, the solid feedstock undergoes several complex processes, which essentially modify its physical and chemical properties. Reactions of dehydration, decarboxylation with additional polymerization and aromatization are the major mechanisms of the material decomposition (Funke & Ziegler, 2010). Physical changes in the cellulose during hydrothermal carbonization lead to significant mass loss. The hydrochar mass yield (ratio between the hydrochar weight and the initial weight of feedstock on dry basis) depends on the reaction conditions (with temperature as a dominating factor) and feedstock structural properties. In the current paper, the mass yield values are in rather narrow range: 44% (HTC-2-3/1), 38% (HTC-2-6/1), 40% (HTC-4-3/1) and 36% (HTC-4-6/1). The results are consistent with data available in the literature for the hydrothermal treatment of cellulose. Sevilla & Fuertes (2009) reported the cellulose hydrochar mass yield values from 34% (at 250 °C, 2 h, 25/1 ratio) to 44% (250 °C, 2 h, 6/1 ratio) and 42.7% (250 °C, 2 h, 3/1 ratio). Reza et al. (2015) measured the product yields from 38% (250 °C, 20 min, 9/1) to 44.3% (250 °C, 8 h, 3/1). Slightly higher mass yields were reported by Diakite et al. (2013) 46.3–48.5% (230 °C, 2, 6 and 10 h, 10/1) and by Kang et al. (2012) from 48% (265 °C, 20 h, 3/1) to 53% (225 °C, 20 h, 3/1).

During chemical activation, the activation agent acts as a dehydration agent intensifying the pyrolytic decomposition of carbonaceous feedstock leading to further mass loss with simultaneous porosity development (Viswanathan et al., 2009). In current work, the burn-off of the activated carbon was on the average level of 62% for all testing runs. Sevilla et al. (2011) reported similar values of the product yield for cellulose activation with KOH at 700 °C: 34% (1/4 ratio of hydrochar/KOH) and 48% (1/2 ratio of hydrochar/KOH) which correspond to the burn-off values of 66% and 52%.

Structural properties of hydrochar samples and activated carbons

The morphology of the cellulose derived hydrochars and the obtained activated carbons is shown in Fig. 2. The figure illustrates the effect of cellulose concentration in the mixture with water during HTC process. It can be noted that hydrothermal carbonization with lower feedstock concentration (HTC-2-6/1) leads to the formation of smaller diameter spherical agglomerates (Fig. 2, b). While quite many microspheres of approx. Ø10 μm are formed on the surface of the cellulose hydrochar HTC-2-3/1 with higher cellulose concentration (Fig. 2, a). The microspherical particles on the hydrochar resulted from the cellulose depolymerization and hydrolysis (Kang et al., 2012). Falco et al. (2011) noticed the similar formation of the spherical agglomerates during glucose carbonization, however with the higher level of homogeneity. It was noted by Kang et al. (2012) that the amount of microspheres increases with process severity (higher reaction temperature and longer reaction time). In another work by Sevilla & Fuertes (2009), an abrupt morphological change in the cellulose structure during the hydrothermal treatment was noted at the temperature around 220 °C: cellulose treatment at this temperature increases the solubility of cellulose and significantly decreases its crystallinity. The following reactions are taking place during the hydrothermal carbonization of cellulose according to their study: (i) hydrolysis of the feedstock, (ii) dehydration and fragmentation into soluble products of the monomers from the hydrolysis, (iii) polymerization or condensation of the soluble products, (iv) aromatization of the

polymers, (v) appearance of a short burst of nucleation and (vi) growth of the nuclei. It was also mentioned that high functionalization of the hydrochar makes this material an excellent precursor for the activation carbon production (Sevilla et al., 2011).

The morphology of the activated carbons is characterized with particularly irregular shapes, smooth surfaces and large cavities (Figs 2, c and 2, d). The resulted structures differ significantly from the hydrochar precursors. Sevilla & Fuertes (2009) and Falco et al. (2013) reported on the similar morphology for the activated carbons produced from different lignocellulosic components regardless of the hydrochar precursor.

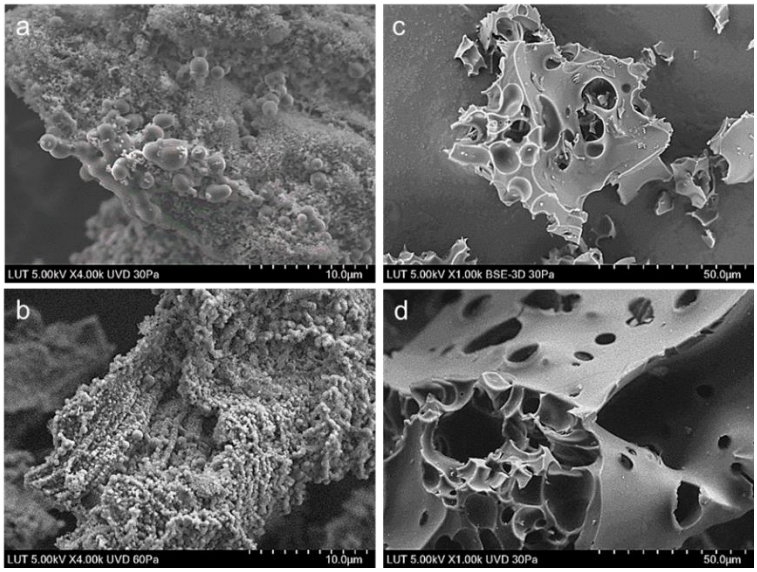

Figure 2. SEM images of the hydrochar samples before chemical activation: (a) HTC-2-3/1; (b) HTC-2-6/1. And activated carbons after chemical activation: (c) AC-2-3/1; (d) AC-2-6/1.

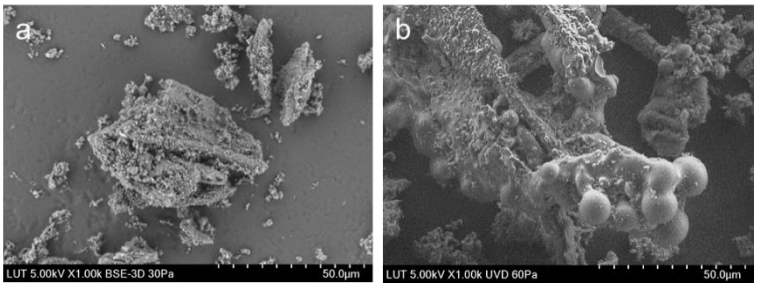

Figure 3. SEM images of the hydrochar samples HTC-2-3/1 (a) and HTC-4-3/1 (b).

Fig. 3 compares the morphology of the hydrochar samples after HTC treatment during 2 h (Fig. 3, a) and 4 h (Fig. 3, b). The carbonization structurally modifies the cellulose fibres, but they are still visible. Longer residence time results in the formation of bigger separate spheres of around Ø100 µm each. This can be the result of the secondary reactions that can occur with higher intensity of HTC treatment.

Porous textural characteristics of hydrochar samples activated carbons

During the carbonization step (e.g., HTC), the lignocellulosic components release oxygen, hydrogen and nitrogen in liquid or gaseous form and are converted into coal-like material enriched in carbon char with a rudimentary porosity (Hernández-Montoya et al., 2012; Diakite et al., 2013). Simple pyrolysis of the wood basic components in an inert atmosphere resulted in the somewhat moderate increase of the surface area: from 2.5 $m^2 g^{-1}$ for a virgin cellulose to 394 $m^2 g^{-1}$ for the cellulose after pyrolysis (700 °C, 1 h, 3 °C min^{-1} heating rate) (Khezami et al., 2005). The final elemental composition as well as the developed surface area of carbonized cellulose strongly depends on such parameters as heating rate, reaction temperature and residence time (Khezami et al., 2005). In general, the surface area of the hydrochars from cellulose reported in the literature is on the level of ca. 30 $m^2 g^{-1}$ which corresponds relatively well with the external surface area (Sevilla & Fuertes, 2009). Table 1 presents the values of the BET surface area for hydrothermally carbonized materials from cellulose found in the literature and compared with the results of the current work. Although the values from the current study are in rather narrow range, the effect of HTC intensification (longer residence time and higher amount of water in the mixture) on the product porosity can be still noticed. An effect of the higher water-to-cellulose ratio can be due to the greater effect of water in the hydrolysis reaction during HTC treatment (Román et al., 2012). At the same time, the results confirm that the hydrochar samples has only rudimentary porosity before the activation step.

Table 1. BET surface areas of the cellulose derived hydrochars

Feedstock	Conditions			BET	Source
	T [°C]	t [h]	r_{HTC} [-]	[$m^2 g^{-1}$]	
Microcrystalline cellulose	250	6	1/9	21	(Reza et al., 2015)
Microcrystalline cellulose	230	6	1/10	28	(Diakite et al., 2013)
Cellulose	230	6	n/r	28	(Mumme et al., 2011)
Cellulose	250	4	1/25	30	(Sevilla & Fuertes, 2009)
Cellulose	250	2	1/3	24	Current work
	250	2	1/6	26	
	250	4	1/3	25	
	250	4	1/6	27	

T – temperature; t – residence time; r_{HTC} – cellulose/water weight ratio; n/r – not reported.

During chemical activation with KOH, all hydrothermally carbonized cellulose samples are converted into porous carbons with high surface areas in the range of 2,300–2,645 $m^2 g^{-1}$. Results obtained in the present study are compared with data available in the literature (Table 2). The most advanced development of porous structure is found for the sample AC-2-6/1. As compared to the initial surface area after HTC, the surface area increases tenfold after the activation.

The total pore volume is also the highest among the studied samples – 1.6 $cm^3 g^{-1}$, while other AC samples have slightly lower values: 1.3 $cm^3 g^{-1}$ (AC-2-3/1), 1.4 $cm^3 g^{-1}$ (AC-4-3/1) and 1.5 $cm^3 g^{-1}$ (AC-4-6/1). In overall, the obtained values are consistent with the values from other investigators. In the majority of the chemical activation tests with KOH, the temperature was on the level 700–800 °C with residence time of 1 h, generally. The impregnation ratio of KOH/char varies in the range of 0.25–4 in the

considered literature. As a rule, the use of simple pyrolysis for char preparation results in lower values of porosity in comparison with HTC treatment (with the exception for the tests by Fujishige et al. (2017)).

Table 2. BET surface areas of the cellulose derived activated carbons

Carbonization Process conditions	Activation				BET [m^2 g^{-1}]	Source
	Activation agent	T [°C]	t [h]	r_{imp} [-]		
Pyrolysis (N_2, 300 °C)	KOH	700	1	0.25	678	(Khezami et al., 2005)
Pyrolysis (Ar, 600 °C)	steam	850	0.5	n/a	1,044	(Babeł, 2004)
Slow pyrolysis (N_2, 400 °C) + fast pyrolysis (N_2, 900 °C)	steam	800	n/r*	n/a	1,317	(Lorenc-Grabowska & Rutkowski, 2014)
HTC	KOH	700	1	2	1,283	(Sevilla, Fuertes & Mokaya, 2011)
(250 °C, 2 h, 1/3 ratio)	KOH	800	1	4	2,047	
	KOH	700	1	4	2,370	
HTC (240 °C, 2 h, 1/10 ratio)	KOH	750	2	3	2,250	(Falco et al., 2013)
HTC	KOH	700	1	4	2,457	(Wei et al., 2011)
(250 °C, 2 h, 1/3 ratio)	KOH	800	1	4	2,125	
Pyrolysis (Ar, 600 °C)	NaOH	720	n/r	2.5	2,366	(Fujishige et al., 2017)
HTC (250 °C, 2 h, 1/3 ratio)	KOH	700	1	4	2,296	Current work
HTC (250 °C, 2 h, 1/6 ratio)	KOH	700	1	4	2,645	
HTC (250 °C, 4 h, 1/3 ratio)	KOH	700	1	4	2,494	
HTC (250 °C, 4 h, 1/6 ratio)	KOH	700	1	4	2,580	

* to 50% burn-off; T – temperature; t – residence time; r_{imp} – KOH/cellulose weight ratio; n/r – not reported; n/a – not applicable.

Electrochemical tests

The results of the electrochemical analysis of the prepared samples are presented in Fig. 4. The specific capacitance of the samples (Fig. 4, a) was measured with 50 mV s^{-1} scan rate and the obtained values are given in Table 3. Additionally, the different values of the scan rates were applied to evaluate the capacity retention of the prepared electrodes (Fig. 4, b).

As it can be seen in Fig. 4, a, the effect of residence time during HTC on the electrodes performance is more pronounced than the effect of feedstock concentration within the studied reaction parameters. The electrodes produced from the samples carbonized during 2 h (AC-2-3/1 and AC-2-6/1) show comparable performance and have higher specific capacitances than other two samples carbonized during 4 h. The sample AC-2-3/1 reveals the highest value of the specific capacitance in spite of the fact that it has not the highest BET surface area among others. As one of the possible reasons for such results, the nanopores of the prepared AC are not fully used during the creation of the electrochemical double layer, where the charge is stored.

The variations of capacity retention within different scan rates show relatively similar results for all samples. However, the capacity retention is slightly higher for the samples AC-4-3/1 and AC-4-6/1 than for the samples AC-2-3/1 and AC-2-6/1. The obtained results may be explained by the influence of the secondary reaction products during the carbonization process that may have an influence on the final product characteristics. With higher severity of the carbonization process, the additional chemical reactions occur during the HTC process. If the products of those reactions were not fully removed from the material, the purity of the final product is decreased, which in it turn leads to the decreasing of the electrochemical properties of the prepared material (by increasing the material resistance). The trace metals and salts (e.g., Ca and Mg salts) that originally containing in the cellulose may have an impact on the properties of the final product.

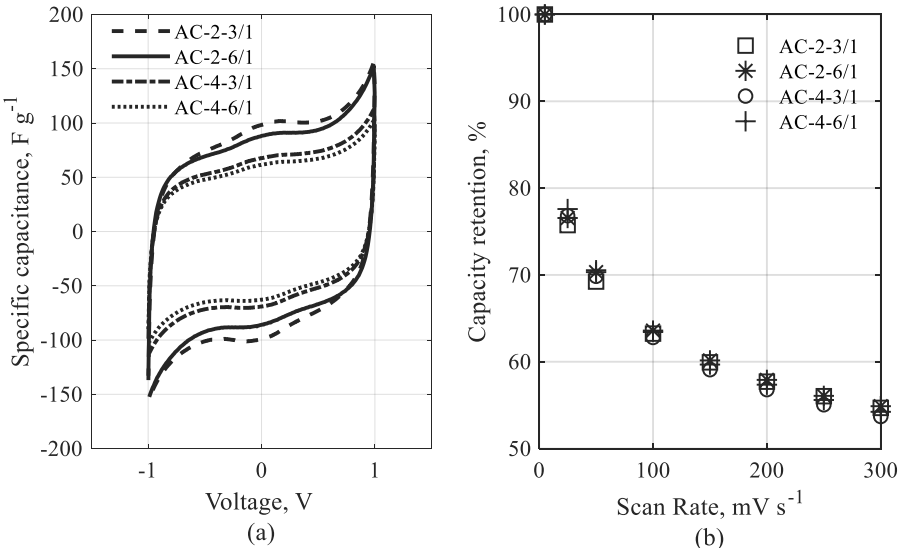

Figure 4. Specific capacitance (a) and capacity retention (b) of the created EDLCs from prepared composite materials.

Table 3. Specific capacitance of the studied samples at 50 mV s^{-1} scan rate

Samples	AC-2-3/1	AC-2-6/1	AC-4-3/1	AC-4-6/1
Specific capacitance, F g^{-1}	110.3	102.5	77.2	69.4

The similar result was obtained from the impedance analysis of the prepared samples, which is shown in Fig. 5. The samples AC-4-3/1 and AC-4-6/1 have higher value of the impedance at low operation frequency than samples AC-2-3/1 and AC-2-6/1. Similarly to the explanation above, the products of the side reactions may influence on the diffusion of electrolyte ions into the pores of electrode materials which may lead to the increase of the impedance values for the prepared electrodes. Therefore, with purpose to improve the quality of the produced AC an additional purification of the material, prepared by using a long residence time during hydrothermal carbonization, may be necessary.

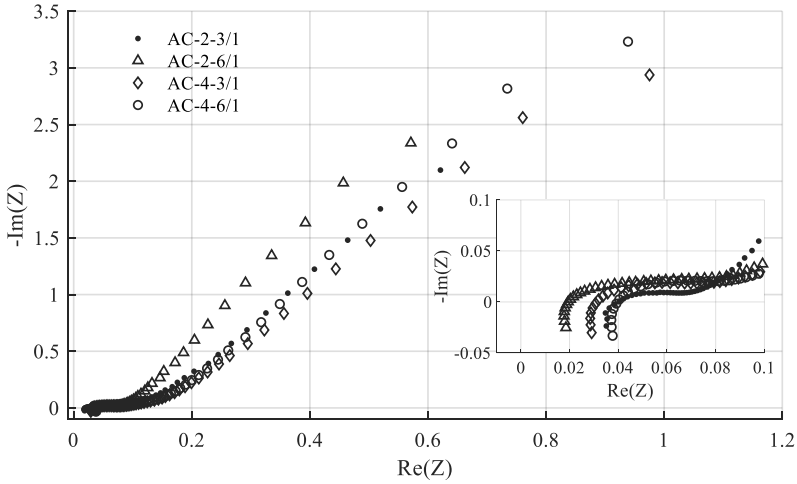

Figure 5. Impedance of the created EDLCs from prepared composite materials.

CONCLUSIONS

Porous activated carbons were produced from cellulose-derived hydrochars with KOH chemical activation. The presented results proved that cellulose can be successfully used as a feedstock for electrodes of electrical double layer capacitors. The possibility to tune the porosity of activated carbons is essential for various application. Several variations of reaction conditions during the hydrothermal carbonization were tested in order to evaluate the influence of hydrochar preparation on the characteristics of the final product. This work demonstrates that not only the HTC reaction temperature but also the ratio between the feedstock and water and the residence time have certain effect on the porosity development of the final product. The significance of these reaction parameters is generally underestimated and their effect is not well studied. The increase of the process severity (longer reaction time and higher amount of water in water-cellulose mixture) increases the surface area of the derived hydrochar samples. Within the frames of the studied reaction parameters, the sample HTC-4-6/1 after the HTC treatment during 4 h and with water/cellulose ratio of 6/1 have the highest BET surface area of 27 m^2 g^{-1}. Chemical activation allows to convert the hydrochar samples into porous activated carbons with high surface areas in the range of 2,300–2,645 m^2 g^{-1}. The highest surface areas of activated carbons were found for the samples produced from the cellulose hydrochars after 2 and 4 h with water/cellulose ratio of 6/1.

The flexible self-standing electrodes for an electrical double layer capacitors were successfully produced and their electrochemical characteristics were analysed. Even though all studied samples show rather comparable values for the capacity retention, the levels of specific capacity differ significantly for the samples after different reaction times. Despite the fact that the samples AC-4-3/1 and AC-4-6/1 have the higher BET surface areas than samples produced during 2 h of HTC, the highest specific capacitances are found for AC-2-3/1 and AC-2-6/1: 110.3 and 102.5 F g^{-1} correspondingly. That can be possibly explained by non-complete use of the developed nanopores of the activated carbon during the creation of the electrochemical double layer. Moreover, the samples

AC-4-3/1 and AC-4-6/1 have the higher value of the impedance at low operation frequency than samples AC-2-3/1 and AC-2-6/1. The products of the secondary reactions during HTC may influence on the diffusion of electrolyte ions into the pores of electrode materials that may lead to such results.

The obtained results prove that HTC in combination with chemical activation may be effectively used to convert the feedstock material into highly porous activated carbon. Higher intensity of the HTC process (longer residence time and higher water-to-feedstock ratio) leads to more severe decomposition of the initial material and, as a consequence, higher porosity. At the same time, more research is required to determine accurate correlations between the reaction parameters and final characteristics of the product. Possible side effects during longer time of reaction should be thoroughly studied with wider variation of the process parameters. Moreover, the possibility to use some organic by-products and wastes instead of pure cellulose would be extremely beneficial for future research.

ACKNOWLEDGEMENTS. The authors would like to thank Toni Väkiparta and Liisa Puro from Chemical Technology Unit of LUT University for valuable help and assistance during the analysis of the samples.

REFERENCES

Babeł, K. 2004. Porous structure evolution of cellulose carbon fibres during heating in the initial activation stage. *Fuel Processing Technology* **85**(1), 75–89.

Babeł, S. & Kurniawan, T.A. 2003. Low-cost adsorbents for heavy metals uptake from contaminated water: a review. *Journal of Hazardous Materials* **97**(3), 219–243.

Cao, J., Zhu, C., Aoki, Y. & Habazaki, H. 2018. Starch-Derived Hierarchical Porous Carbon with Controlled Porosity for High Performance Supercapacitors. *ACS Sustainable Chemistry & Engineering* **6**(6), 7292–7303.

Crini, G. 2006. Non-conventional low-cost adsorbents for dye removal: A review. *Bioresource Technology* **97**(9), 1061–1085.

da Silva Lacerda, V., Lopez-Sotelo, J.B., Correa-Guimaraes, A., Hernandez-Navarro, S., Sanchez-Bascones, M., Navas-Gracia, L. M. & Martin-Gil, J. 2015. Rhodamine B removal with activated carbons obtained from lignocellulosic waste. *Journal of Environmental Managemen* **155**, 67–76.

De Lange, M.F., Vlugt, T. J.H., Gascon, J. & Kapteijn, F. 2014. Adsorptive characterization of porous solids: Error analysis guides the way. *Microporous and Mesoporous Materials* **200**, 199–215.

Deng, L., Young, R.J., Kinloch, I.A., Abdelkader, A.M., Holmes, S.M., De Haro-Del Rio, D.A. & Eichhorn, S.J. 2013. Supercapacitance from cellulose and carbon nanotube nanocomposite fibers. *ACS Applied Materials and Interfaces* **5**(20), 9983–9990.

Diakite, M., Paul, A., Jäger, C., Pielert, J. & Mumme, J. 2013. Chemical and morphological changes in hydrochars derived from microcrystalline cellulose and investigated by chromatographic, spectroscopic and adsorption techniques. *Bioresource Technology* **150**, 98–105.

Falco, C., Baccile, N. & Titirici, M.-M. 2011. Morphological and structural differences between glucose, cellulose and lignocellulosic biomass derived hydrothermal carbons. *Green Chemistry* **13**(11), 3273.

Falco, C., Marco-Lozar, J.P., Salinas-Torres, D., Morallón, E., Cazorla-Amorós, D., Titirici, M.M. & Lozano-Castelló, D. 2013. Tailoring the porosity of chemically activated hydrothermal carbons: Influence of the precursor and hydrothermal carbonization temperature. *Carbon* **62**, 346–355.

Fujishige, M., Yoshida, I., Toya, Y., Banba, Y., Oshida, K., Tanaka, Y., Dulyaseree P., Wongwiriyapan, W. & Takeuchi, K. 2017. Preparation of activated carbon from bamboo-cellulose fiber and its use for EDLC electrode material. *Journal of Environmental Chemical Engineering* **5**(2), 1801–1808.

Funke, A. & Ziegler, F. 2010. Hydrothermal carbonization of biomass: A summary and discussion of chemical mechanisms for process engineering. *Biofuels, Bioproducts and Biorefining* **4**(2), 160–177.

Hartmann, S., Iurchenkova, A., Kallio, T. & Fedorovskaya, E. 2020. Electrochemical Properties of Nitrogen and Oxygen Doped Reduced Graphene Oxide. *Energies* **13**(2), 312.

Hernández-Montoya, V., García-Servin, J. & Bueno-López, J.I. 2012. Thermal Treatments and Activation Procedures Used in the Preparation of Activated Carbons. Lignocellulosic Precursors Used in the Synthesis of Activated Carbon - Characterization Techniques and Applications in the Wastewater Treatment, Chapter 2, pp. 19–36.

Jiang, Z., Liu, Y., Sun, X., Tian, F., Sun, F., Liang, C., You, W., Han, C. & Li, C. 2003. Activated carbons chemically modified by concentrated H2SO4 for the adsorption of the pollutants from wastewater and the dibenzothiophene from fuel oils. *Langmuir* **19**(3), 731–736.

Kang, S., Li, X., Fan, J. & Chang, J. 2012. Characterization of hydrochars produced by hydrothermal carbonization of lignin, cellulose, d-xylose, and wood meal. *Industrial and Engineering Chemistry Research* **51**(26), 9023–9031.

Kim, H., Shin, J., Jang, I. & Ju, Y. 2019. Hydrothermal Synthesis of Three-Dimensional Perovskite NiMnO3 Oxide and Application in Supercapacitor Electrode. *Energies* **13**(1), 36.

Khezami, L., Chetouani, A., Taouk, B. & Capart, R. 2005. Production and characterisation of activated carbon from wood components in powder: Cellulose, lignin, xylan. *Powder Technology* **157**(1), 48–56.

Kuzmenko, V., Naboka, O., Haque, M., Staaf, H., Göransson, G., Gatenholm, P. & Enoksson, P. 2015. Sustainable carbon nanofibers/nanotubes composites from cellulose as electrodes for supercapacitors. *Energy*, **90**, Part 2, 1490–1496.

Lee, K.K., Hao, W., Gustafsson, M., Tai, C.-W., Morin, D., Björkman, E., Lilliestråle, M., Björefors, F., Andersson, A.M. & Hedin, N. 2016. Tailored activated carbons for supercapacitors derived from hydrothermally carbonized sugars by chemical activation. *RSC Advances* **6**(112), 110629–110641.

Li, Z., Yi, W., Li, Z., Tian, C., Fu, P., Zhang, Y. & Teng, J. 2020. Preparation of Solid Fuel Hydrochar over Hydrothermal Carbonization of Red Jujube Branch. *Energies* **13**(2), 480.

Lorenc-Grabowska, E. & Rutkowski, P. 2014. High basicity adsorbents from solid residue of cellulose and synthetic polymer co-pyrolysis for phenol removal: Kinetics and mechanism. *Applied Surface Science* **316**(1), 435–442.

Lozano-Castelló, D., Lillo-Ródenas, M.A., Cazorla-Amorós, D. & Linares-Solano, A. 2001. Preparation of activated carbons from Spanish anthracite - I. Activation by KOH. *Carbon* **39**(5), 741–749.

Mesfun, S., Matsakas, L., Rova, U. & Christakopoulos, P. 2019. Technoeconomic Assessment of Hybrid Organosolv–Steam Explosion Pretreatment of Woody Biomass. *Energies* **12**(21), 4206.

Mohamad, N., Lau, L.C., Lee, K. T. & Mohamed, A.R. 2013. Synthesis of activated carbon from lignocellulosic biomass and its applications in air pollution control–a review. *Journal of Environmental Chemical Engineering* **1**(4), 658–666.

Mohan, D. & Pittman Jr., C.U. 2007. Arsenic removal from water/wastewater using adsorbents–A critical review. *Journal of Hazardous Materials* **142**(1), 1–53.

Mulder, M. 1996. Preparation of Synthetic Membranes. *In Basic Principles of Membrane Technology*. Springer, Netherlands, pp. 71–156.

Mumme, J., Eckervogt, L., Pielert, J., Diakité, M., Rupp, F. & Kern, J. 2011. Hydrothermal carbonization of anaerobically digested maize silage. *Bioresource Technology* **102**(19), 9255–9260.

Murashko, K., Nevstrueva, D., Pihlajamaki, A., Koiranen, T. & Pyrhonen, J. 2017. Cellulose and activated carbon based flexible electrical double-layer capacitor electrode: Preparation and characterization. *Energy* **119**, 435–441.

Pandolfo, A.G. & Hollenkamp, A.F. 2006. Carbon properties and their role in supercapacitors. *Journal of Power Sources* **157**(1), 11–27.

Rengaraj, S., Moon, S.-H., Sivabalan, R., Arabindoo, B. & Murugesan, V. 2002. Agricultural solid waste for the removal of organics: adsorption of phenol from water and wastewater by palm seed coat activated carbon. *Waste Management* **22**(5), 543–548.

Reza, M.T., Rottler, E., Tölle, R., Werner, M., Ramm, P. & Mumme, J. 2015. Production, characterization, and biogas application of magnetic hydrochar from cellulose. *Bioresource Technology* **186**, 34–43.

Román, S., Nabais, J.M.V, Laginhas, C., Ledesma, B. & González, J.F. 2012. Hydrothermal carbonization as an effective way of densifying the energy content of biomass. *Fuel Processing Technology* **103**, 78–83.

Rouquerol, J., Llewellyn, P. & Rouquerol, F. 2007. Is the BET equation applicable to microporous adsorbents? *Studies in Surface Science and Catalysis* **160**, 49–56.

Saha, D., Li, Y., Bi, Z., Chen, J., Keum, J., Hensley, D. & Naskar, A. 2014. Studies on Supercapacitor Electrode Material from Activated Lignin-Derived Mesoporous Carbon. *Langmuir* **30**(3), 900–910.

Sevilla, M. & Fuertes, A.B. 2009. The production of carbon materials by hydrothermal carbonization of cellulose. *Carbon* **47**(9), 2281–2289.

Sevilla, M., Fuertes, A.B. & Mokaya, R. 2011. High density hydrogen storage in superactivated carbons from hydrothermally carbonized renewable organic materials. *Energy & Environmental Science* **4**(4), 1400–1410.

Sun, Y., Wang, Z., Liu, Y., Meng, X., Qu, J., Liu, C. & Qu, B. 2019. A Review on the Transformation of Furfural Residue for Value-Added Products. *Energies* **13**(1), 21.

Titirici, M.M., Thomas, A., Yu, S.-H., Müller, J.-O. & Antonietti, M. 2007. A direct synthesis of mesoporous carbons with bicontinuous pore morphology from crude plant material by hydrothermal carbonization. *Chemistry of Materials* **19**(17), 4205–4212.

Titirici, M.-M. & Antonietti, M. 2010. Chemistry and materials options of sustainable carbon materials made by hydrothermal carbonization. *Chemical Society Reviews* **39**(1), 103–116.

Viswanathan, B., Neel, P. & Varadarajan, T. 2009. Methods of activation and specific applications of carbon materials. *Methods of Activation and Specific Applications of Carbon Materials*, pp. 16–17.

Wang, Z., Tammela, P., Strømme, M. & Nyholm, L. 2017. Cellulose-based Supercapacitors: Material and Performance Considerations. *Advanced Energy Materials* **7**(18).

Wei, L., Sevilla, M., Fuertes, A.B., Mokaya, R. & Yushin, G. 2011. Hydrothermal carbonization of abundant renewable natural organic chemicals for high-performance supercapacitor electrodes. *Advanced Energy Materials* **1**(3), 356–361.

Yuan, M., Que, H., Yang, X. & Li, M. 2019. Nitrogen and oxygen co-doped glucose-based carbon materials with enhanced electrochemical performances as supercapacitors. *Ionic* **25**(9), 4305–4314.

Zhang, K., Liu, M., Zhang, T., Min, X., Wang, Z., Chaiab, L. & Shi, Y. 2019. High-performance supercapacitor energy storage using a carbon material derived from lignin by bacterial activation before carbonization. *Journal of Materials Chemistry A* **7**(47), 26838–26848.

Zhu, Y., Murali, S., Stoller, M.D., Ganesh, K.J., Cai, W., Ferreira, P.J. & Ruoff, R.S. 2011. Carbon-based supercapacitors produced by activation of graphene. *Science* **332**(6037), 1537–1541.

Agronomy Research **18**(3), 2211–2216, 2020
https://doi.org/10.15159/AR.20.167

Manufacturing technologies for slide bushings from powder materials for lever brake systems of vehicles

P. Stankevics[1,*], V. Mironovs[2] and N. Muracova[3]

[1]Riga Technical University, Transport Institute, 12 Azenes street, LV–1048 Riga, Latvia
pavels.stankevics@rtu.lv
[2]Riga Technical University, Laboratory of Powder Materials, 12 Azenes street, LV–1048 Riga, Latvia
[3]ICFSD, Riga Technical University, 1 Kalku street, LV–1050 Riga, Latvia
[*]Correspondence: pavels.stankevics@rtu.lv

Abstract. Slide bushings made of metal powder materials are used in many parts of vehicles. The current trend is to reduce the unit cost of products, increase the durability of components and assemblies, and reduce the harmful effects on the environment. One of these solutions is the use of powder materials. In this article, we consider some manufacturing techniques for sliding bushings of a lever brake system of a rolling stock using one-sided and two-sided pressing, pulse and combined sealing. The areas of their rational use are demonstrated as well.

Key words: metal powder materials, pulsed compaction, slide bushings.

INTRODUCTION

To ensure maximum efficiency and safety when transporting goods by rail, it is necessary to constantly seek and implement innovative solutions. To a large extent, this applies to the technical part, primarily to the mechanisms of rolling stock. Many railway transport nodes operate at high specific loads and significant temperature fluctuations (Kruse et al., 2015), (Ivaskovska & Mihailovs, 2019). Bearing sleeves in articulated joints are subject to particularly intense wear, which requires frequent adjustment and repair.

In nodes of increased dimensions under heavy loads, as well as when working in a humid environment, the plain bearings are the most suitable. The main element of the bearings is an insert (sleeve) made of antifriction material, which is installed between the shaft and the bearing housing (Karpichev, 2000). The disadvantages of such bearings are of higher friction than rolling bearings and the need for relatively expensive antifriction materials.

In railway transport, anti-friction bushings are widely used in lever brake systems, auxiliary and low-speed mechanisms. Characteristic defects in antifriction bushings are caused by friction (abrasive wear) and fatigue failure under the influence of load pulsation. Increased wear or destruction of the slide bushings can lead to both premature destruction of the elements themselves and jamming of the entire structure as a whole. Intensive oscillatory movements are also characteristic features of bearing assemblies of hinge systems of brake mechanisms. This is another serious condition that can lead to

accelerated wear on the sleeve. The position at zero speed between each oscillation cycle is the point at which the lubricant will be broken, which leads to increased wear of the material. Self-lubricating bushings are the best choice for oscillatory motion due to the rigid sliding surface, which generates a small amount of wear particles, as well as the presence of internal lubrication.

Modern technology allows the manufacture of bearing bushings of metal powders that meet the most stringent requirements. The criterion for the strength and, consequently, the performance of the sleeve are contact stresses in the friction zone or contact pressure. The estimated contact pressure p can be estimated (Dunajev & Lelikov, 2001).

$$p = N/(ld)\ [p] \tag{1}$$

where N – is the force of the normal shaft pressure on the sleeve (support reaction); l – is the working length of the bearing sleeve; d – is the diameter of the shaft journal; $[p]$ – permissible specific pressure.

One of the main advantages of bushings made of metal powder materials is the presence of pores in them, which contribute to the formation of a stable oil film in the bearing. As a result of the preliminary impregnation of the sleeve in heated oil, a large number of its capillaries are filled with oil. Due to this, a lubricating film is formed on the rubbing surface of the sleeve, which remains for a sufficiently long time. The use of so-called pockets in plain bearings is known. They accumulate oil during parking and low speeds. Then the oil is used when the mechanism is triggered.

Different operating modes require the use of cermet bearings with varying degrees of porosity. In studies (Leitans et al., 2015), it was shown that one of the reasons for increased wear of parts of hinge assemblies is damage to the surface layer of the antifriction sleeve and vertical dynamic forces of an impact nature. In this regard, greater importance should be given to the strength properties of the elements of the system (Ivanovs & Gavrilovs, 2017; Evsejev et al., 2019).

It is possible to increase the strength of sliding bushings made of powder materials by increasing the density of the product and selecting material from the class of high alloy, containing an increased value of chromium, manganese and nickel Oberacker, 2011). However, this increases the cost of parts and makes the use of powder metallurgy unprofitable. The use of low-alloy powder mixtures makes it possible to reduce the cost of production of parts of brake assemblies (Mironovs et al., 2019). But this requires increased attention to the choice of material, porosity and manufacturing technology. For medium loads, a porosity of 20–25% is recommended. In the production of metal-powder products, there are four main stages: the selection and preparation of the powder composition, pressing, sintering to the desired density and additional (finishing) operations after sintering to the final product. Each of these steps is very important to obtain a product with desired properties.

In this paper, a number of technologies for the manufacture of sliding bushings for a lever brake system of a rolling stock from low-alloy powder raw materials using one-sided and two-sided pressing is considered. The use of pulsed and combined seals allows the manufacture of bushings with a wider range of sizes and configurations. The areas of their rational application of technologies are shown.

MATERIALS AND METHODS

Experimental studies have been conducted at the Powder Materials Laboratory of Riga Technical University. The samples of slide bushings with an outer diameter of 25–50, a length of 25 to 120 mm and a wall thickness of 5–15 mm were made.

For the preparation of samples, iron-based powder mixtures were used (Fe – 94%, Ni – 2.5%, Cu–2.0%, Mn – 0.5%, < C – 0.7%) (Mironovs et al., 2019).

The simplest compaction method is single-sided pressing. It is recommended to be used if $0.5d < l < 1.5d$, where d is the diameter of the sleeve and l is its length. Sealing was carried out on a hydraulic press at a pressure of 400 to 600 MPa.

The pressing device (Fig. 1, a) consisted of a die, upper and lower punches, the space between which was filled with pressed powder. The mold matrix was made of carbon steel with a hardness of HRB 58-64. A steel bar was used to form the inner hole. To ensure the specified accuracy of the dimensions of the workpiece, limiters were used. The force was applied to the upper punch. The experiments showed that uniform porosity in height can be obtained provided: $0.5\ d < l < 1.5\ d$.

Double-ended pressing was carried out in the same matrix; however, a compression force was applied to both punches (Fig. 1, b).

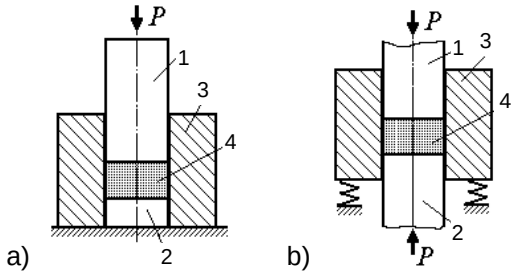

Figure 1. Scheme for powder compaction: 1 – upper punch; 2 – lower punch; 3 – die; 4 – powder.

The following recommendation (German, 2005) was considered here, which indicated that the ratio of the diameter and wall thickness is an important factor in choosing a two-sided pressing method. It is recommended within (2).

$$3 < s/d < 17 \qquad (2)$$

where s – wall thickness; d – diameter.

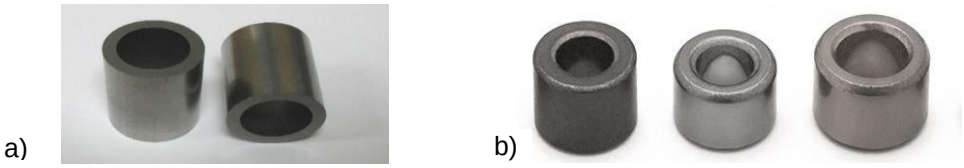

Figure 2. Sliding bushings after compaction (a) and after sintering (b).

When the sleeve length was increased to more than $1 \geq 1.5$ d, the method of magnetic pulse pressing was applied by crimping the powder material in an electrically conductive shell. This method also turns out to be suitable for calibrating the bushings, as well as in the manufacture of bushings of a more complex configuration, for example, in the manufacture of bushings with a shoulder (Fig. 3).

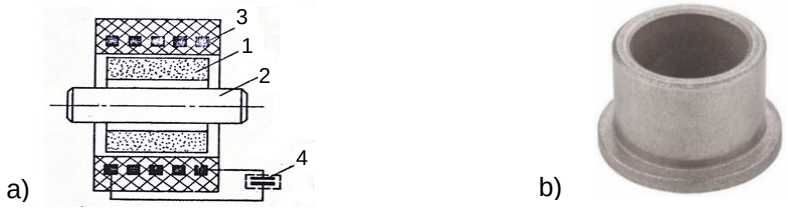

Figure 3. The scheme of magnetic pulse pressing of the bushings (a) and the sample sleeve with a shoulder: 1 – powder; 2 rod; 3 – inductor; 4 – pulse current generator.

To increase the density of products, the combined static-dynamic sealing scheme developed in (Mironovs et al., 2016) is used. In this case, the powder was pre-compacted on a hydraulic press at a pressure of up to 400 MPa, and then subjected to repeated pulsed exposure by applying

To obtain bushings with the ratio 3 d < l < 10 d, combined pressing was used: pulse compaction followed by drawing (Glushenkov et al., 2017).

In the manufacture of powder parts, attention was paid to the basic characteristics of metal powders. The stability of the bulk mass (mass per unit volume of the freely sprinkled powder) provides a more constant shrinkage during sintering. It depends mainly on the shape and size of the powder particles. The presence of protrusions and irregularities on the surface of the particles increase interparticle friction, which complicates their movement relative to each other and leads to a decrease in the bulk density of the powder. The granulometric composition of the powder is of significant importance – with an increase in the content of finer particles, the bulk density of the powder decreased, apparently due to an increase in the friction surface. The fluidity of the powder worsened with decreasing particle size of the powder.

All samples were sintered in a protective atmosphere of endogas at a temperature of 1,120 °C. For 30 minutes.

RESULTS AND DISCUSSION

Changes in the volume of the powder body during compression are the result of ongoing processes during compaction. The density of the workpiece depends on the pressing pressure and the form of its application. In all processes, with an increase in compaction pressure, the specific gravity increased and the porosity decreased. Porosity is evenly distributed throughout the volume (Fig. 4).

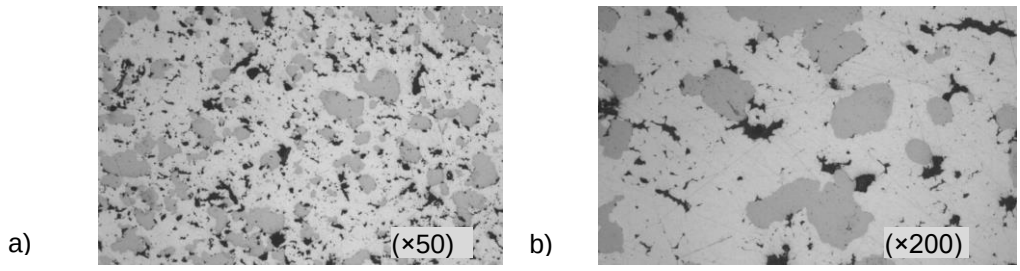

Figure 4. Microstructure of powder sleeves made of low-alloyed iron powder with porosity of 18%.

Particle shape affects bulk density and bulkability. Associated with it is their surface energy, which increases with increasing particle surface (Freeman et al., 2009). Along with the adhesion forces, mechanical factors also act, in particular, jamming of particles and interweaving of the protrusions. The particle size of the powder is one of the factors determining the specific pressure during pressing, necessary to achieve a given porosity, as well as shrinkage during sintering and the mechanical properties of sintered products (Fig. 5). This was especially evident with pulse compaction. Smaller powders were pressed much worse, and some billets cracked during sintering.

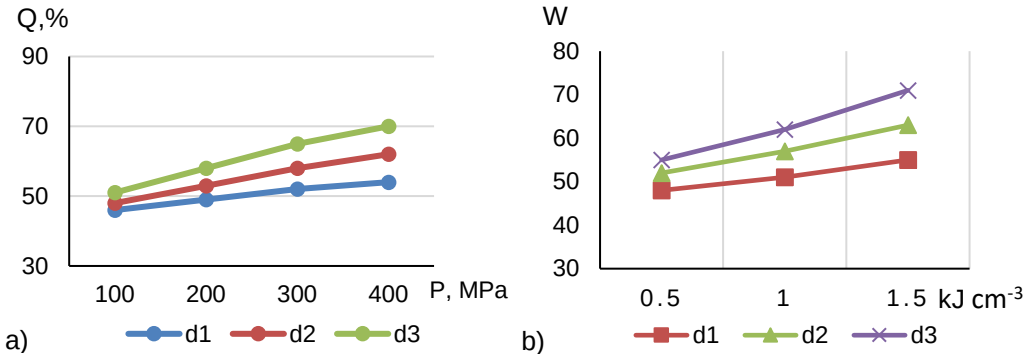

Figure 5. Change in the relative density of iron powder depending on the particle size during static (a) and by impulse pressing (b), d_1 = 100, d_2 = 50, d_3 = 20, – particle size μm; p – pressure; w – specific pulse energy.

Particular attention was paid to the method of manufacturing bushings with side holes (pockets) for subsequent grease retention (Fig. 6, a). A special device has been developed for this purpose (Fig. 6, b).

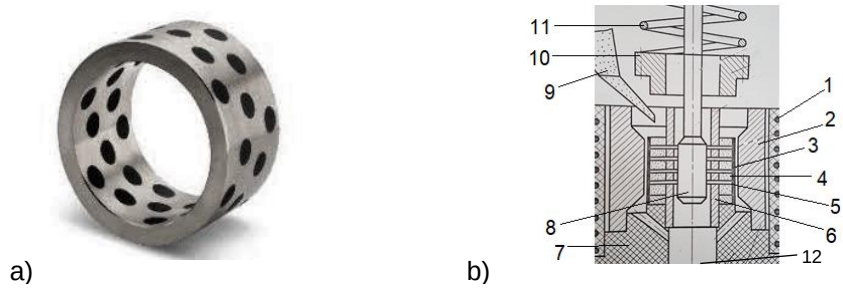

Figure 6. A sleeve with an outer diameter of 50 mm and side holes with a diameter of 3 mm (a) and a device for its manufacture (b), where: 1 – inductor; 2 – hub magnetic field; 3 – metal shell; 4 – powder; 5 – fingers; 6 – sleeve; 7 – base; 8 – stem; 9 – gutter for powder; 10 – cap; 11 – spring; 12 – device for pressing.

The device (Fig. 6, b) is intended for magnetic pulse pressing. It contains a multi-turn inductor 1, a magnetic field concentrator 2, a metal shell 3, a sleeve for forming an internal hole 6, a mandrel with sliding fingers 5 for forming side holes, and also a powder filling mechanism in mold 9 and a device for extruding products 12.

As experiments showed, the device is advisable to use in the manufacture of bushings of large diameter (more than 50 mm).

CONCLUSIONS

1. The technology of manufacturing powder sleeves for railway nodes is constantly being improved. Technologies based on the use of combined static-dynamic compaction methods deserve more and more attention.

2. New technological possibilities for the manufacture of slide bushings with side openings, used as pockets to hold grease, are presented.

REFERENCES

Dunajev, P. & Lelikov, O. 2001. *Construction of units and machine parts.* High scool. Moscow. 444 pp. (in Russian).

Evsejev, D., Medvedev, B., Medvedev, P., Strautmanis, G. & Samoshkin, S. 2019. Acoustic emission approach to determining survivability in fatigue tests. *ICTE 2018 in Transportation and Logistics. Procedia Computer Science* **149**, pp. 340–344.

Freeman, R., Cooke, J. & Schneider, L. 2009. Measuring shear properties and normal stresses generated within a rotational shear cell for consolidated and non-consolidated powders. *Powder Technology* **190**(2), 65–69.

German, R. 2005. *Powder Metallurgy & Particulate Materials Processing*. Metal Powder Industries Federation, Princeton, NJ, 528 pp.

Glushenkov, V., Beljaeva, I., Mironovs, V. & Burmistrov, A. 2017. Obtaining long products from waste powder compositions Al-B. *Modern methods and technologies for the creation and processing of materials.* Minsk, Belarus, pp. 22–28 (in Russian).

Ivanovs, V. & Gavrilovs, P. 2017. Research of the Defective Frog Wing of 1/11 Mark. *Journal Transport Problems* **11**, 1–11.

Ivaskovska, N. & Mihailovs, F. 2019. Reliability and profitability of rail fastenings. *ICTE 2018 in Transportation and Logistics. Procedia Computer Science* **149**. doi: 10.1016/j.procs.2019.01.147, ISSN: 18770509

Karpichev, V. 2000. *Development of method for system analysis of an automatic brake of a freight rolling stock.* MIIT, Moscow, 316. pp. (in Russian).

Kruse, S., Tiedemann, M., Zeumer, B., Reuss, P., Hetzler, H. & Hoffmann, N. 2015. The influence of joints of friction induced vibration in brake squeal. *Journal of Sound and Vibration* **340**, 239–252.

Leitans, A., Boiko, I., Lungevics, J. & Mironovs, V. 2015. The Influence of the Technological Process on the Surface Quality and Tribological Properties of Powder Detail. *Environment. Technology. Resources*: In: *10th International Scientific and Practical Conference. Vol.**1**, Latvia, Rezekne*, pp. 116–120.

Mironovs, V., Stankevich, P., Tatarinov, A., Zemchenkov, V. & Boyko, I. 2015. Mechanical and Acoustical Properties of Bushings Made of Low-Alloyed Materials and Used in Brake Systems of Transport Vehicles. *Materials Science and Engineering* **96**(1), 1–9.

Mironovs, V., Stankevics, P., Beljaeva, I. & Glushenkov, V. 2016. Static-Dynamic Powder Material Compaction Methods. In: *15th International Scientific Conference "Engineering for Rural Development"*. **15**, Latvia, Jelgava, University of Agriculture, pp. 1128–1132.

Mironovs, V., Stankevics, P. & Eiduks, J. 2019. Tendencies in the field of application of metal-powder materials for repair and maintenance of railway equipment. *ICTE 2018 in Transportation and Logistics.* Procedia Computer Science, **149**, pp. 344–348.

Oberacker, R. 2011. Powder compaction by dry pressing. In: Riedel, R., Chen, I.-W. (eds.) *Ceramics Science and Technology***3**, pp. 1–37. Wiley-VCH, Weinheim.

Agronomy Research **18**(3), 2217–2244, 2020
https://doi.org/10.15159/AR.20.219

Formation and determination of the individual area of oilseed radish leaves in agrophytocenosises of different technological construction

Y. Tsytsiura

Vinnytsia National Agrarian University, Faculty of Agronomy and Forestry, Sonyachna street 3, UA21008 Vinnytsia, Ukraine
Correspondence: yaroslavtsytsyura@ukr.net

Abstract. For the successful control of the production process, determining the leaf area is a basic requirement. In this context, it is important to determine the regularities of leaf formation within the plant, considering technological parameters of agrophytocenosis construction. These are the important issues covered in this paper based on the years of research conducted between 2013 and 2018 on three cultivars of oilseed radish: one of the poorly explored members of the cruciferous family of multipurpose use. The conducted researches allowed to distinguish features of longline leaf formation of oilseed radish cultivars and mathematically describe features of formation of their area, length and width at the early flowering phase according to the Richards growth curve. The peculiarities of formation of individual leaf area depending on the combination of the variations of the stand density and fertilization in the context of the recommended process regulation of oilseed radish cultivation are also determined. It has been proved possible to use a non–destructive method of determining the individual leaf area of oilseed radish, basing on the evaluation of 29 models, using the following formula $S = 7.9316 – 2.3613L + 0.6897 (LW)+0.0458L^2–0.0005 (LW)^2$ (under the following test parameters of the model: R^2 0.9106; *RMSE* 9.75; *d* 0.956; *BIAS* –0.1523).

Key words: oilseed radish, leaf formation, leaf area estimation, non-destructive methods, mathematical model.

INTRODUCTION

Assimilating surface of agrophytocenosis of any crop is a complex longline structure, which reacts sensitively enough to the hydrothermal vegetation regime, technological nature of cenosis creation, phenotypic features of the main crop forming cenosis, level of soil and additional mineral nutrition, and nature of weediness (Long et al., 2006; Lamptey et al., 2017; Seetseng et al., 2020). On the other hand, the area of the assimilating surface of a plant is a combination of the number of leaves per plant and their individual area (Kotula, 1951; Lewis, 1972; Smith et al., 1997; Tsukaya, 2003; Doust, 2007). A common scientific challenge is the fact that a simple product of the number of leaves per leaf area is only appropriate in case of equal leaf sizes by their placement on the plant's stem (Stewart & Dwyer, 1999; Gielis, 2003; Watanabe et al., 2005; Dornbusch et al., 2011). In the majority of cases there are significant deviations for the plant body both in the size of leaves and in their shape in the direction from the

first leaves to the upper leaves (Terashima & Hikosaka, 1995; Terashima et al., 2001; Bylesjö et al., 2008; Pérez-Pérez et al., 2010). Such nature of the formation of differences may take the form of a change in the leaf type (due to a combination of different separation moduses) and is called pinnation, and is expressed in a change in the character of the complexity of the leaf blade, starting with juvenile leaves to leaves which are formed at late stages of growth and development of plants (Corona & Vasilyev, 2007). Another type of differences is related to the parameters of fluctuating asymmetry of leaves, which in fact reflects the format of lateral leaf blade variability (Parsons, 1992; Semiarti et al., 2001; Shi et al., 2018). It should be remembered that there is one more component of the differences between the leaves of plants of different tiers, in particular the thickness of the leaf blade, venetion nature, anatomical differences in the tissue texture, space angular orientation towards the stem (Wofford & Allen, 1982; Ivanov et al., 1994; Rosa & Forseth, 1995; Deckmyn et al., 2000; Terashima et al., 2001; Runions et al., 2005; Milla & Reich, 2007; Ford et al., 2008; Nam et al., 2008; Nicotra et al., 2011; Dornbusch et al., 2011). In summary, there is an appropriate level of morphological variability for plants, which can be characterized as a morphological gradient, which in some research works is expressed as a ratio of leaf area of certain upper tiers to lower tiers, or their individual linear sizes, in particular leaf length, leaf width or other morphological parameter (Ivanov et al., 1994; Gielis, 2003; Breda, 2003; Efroni et al., 2010). It is also believed that the nature and value of the mentioned variability is determined by the main technological aspects of agrophytocenosis formation (Loomis et al., 1967; Nanda et al., 1995; Long et al., 2006; Ro´zyło & Pałys, 2014). Most researches show that the intensive variability of leaf morphological parameters in the vertical gradient is determined by a number of factors from the most to the least determinant: the density of agrophytocenosis considering the feeding area of one plant, the level of fertilization in interaction with the density, the edaphic conditions of growth and development of plants (Morrison & Stewart, 1995; Nanda et al., 1995; Schurr et al., 2000; Jullien et al., 2009; Biskup et al., 2009; Ma et al., 2014; Boudaoud, 2016). The above mentioned number of factors has a determining basis from the perspective of hydrothermal conditions of vegetation with the maximum reduction in morphometry of individual leaves of the plant in combination with the maximum formats of stand density, fertilization and favorable ground conditions, as well as the most favorable, and vice versa the most unfavorable hydrothermal regimes of the vegetation period of the respective crop (Stefanowska et al., 1999; Nicotra et al., 2008; Hosoi & Omasa, 2012; Li et al., 2013; Wright et al., 2017).

On the other hand, it is noted that the nature of individual leaf parameters, considering the linear growth of plants and the multiple–age staging of functioning of leaves from different tiers, is in some degree determining in providing the appropriate levels of photosynthesis productivity in cruciferous crops, and as a result provides both the formation of the appropriate leaf–stem complex structure and the formation of appropriate seed yield levels (Freyman et al., 1973; Thurling, 1974; Clarke, 1977 and 1978; Pecham & Morgan, 1985; Kasa & Kondra, 1986; Gabrielle et al., 1998; Khan, 2003 and 2005; Mullen et al., 2006; Jansen et al., 2009; Kirkegaard et al., 2012; Cargnelutti Filho et al., 2015; Fochesatto, et al., 2016).

It should be also noted that there is an important aspect of leaf variability expressed in heterophylly. Almost all plants are heterophyllous, as it is difficult to find morphologically identical leaf blades on the stem. The approaches to this issue distinguish the typification of heterophylly: dimensional, geometric, venational, etc.

(Korona and Vasilyev, 2007; Chitwood & Sinha, 2016; Nakayama et al., 2017). Due to heterophylly on the plant stem, different morphotypes (categories or formations) of leaves can be found sequentially: basal, middle and apical (Baker–Brosh & Peet, 1997; Kuwabara et al., 2001; Corona and Vasilyev, 2007; Merks et al., 2011; Nakayama et al., 2012; Yamaguchi et al., 2012; Maugarny-Cales & Laufs, 2018). Basal leaves perform a protective function and therefore have a simplified structure. Middle leaves are typical for this species and constitute the basic mass of the shoot. Their primary function is photosynthesis. Within this formation, they differ. In the beginning, they have a simplified structure. In complex leaves of the basal formation a smaller number of leaves are formed, then the number of leaves increases towards the middle part of the stem, and then decreases up to the top. The apical leaves are formed in the upper part of the stem. They cover flowers (bracts) or inflorescences, have a poorly developed leaf blade, as well as basal leaves, sometimes change their color and function.

Given the above aspects of the importance of exploring the formation of individual leaf morphological parameters, the researches show evidence of scientific novelty and topicality. The developments in modern approaches to determining the area of both individual leaves and the entire assimilation surface of plants should also be considered. In this context, the defining methodological approach is the determination of regression models of leaf area dependencies on its linear parameters, such as leaf length and width or a combination of these parameters in product or power expressions. Nowadays, this method of estimation of leaf area formation regularities is applied for many crops from different botanical families and leaf morphological complexity (Robbins & Pharr, 1987; Elsner & Jubb, 1988; Firman & Allen, 1989; Schultz, 1992; Uzun & Celik, 1999; Montero et al., 2000; Kandiannan et al., 2002; Blanco & Folegatti, 2003; Stoppani et al., 2003; Lizaso et al., 2003; de Swart et al., 2004; Demirsoy et al., 2004; Demirsoy et al., 2005; Tsialtas & Maslaris, 2005; Gamper, 2005; Rouphael et al., 2006; Serdar & Demirsoy, 2006; Cristofori et al., 2007; Rouphael et al., 2007; Mendoza–de Gyves et al., 2007; Cristofori et al., 2007; Rivera et al., 2007; Peksen, 2007; Ramesh et al., 2007; Carmassi et al., 2007; Tsialtas & Maslaris, 2008; Mendoza–de Gyves et al., 2008; Antunes et al., 2008; Cristofori et al., 2008; Fallovo et al., 2008; Kumar, 2009; Mazzini et al., 2010; Rouphael et al., 2010a and 2010b; Bakhshandeh et al., 2011; Giuffrida et al., 2011; Cemek et al., 2011; Chavarria et al., 2011; Pompelli et al., 2012; Richter et al., 2014; Buttaro et al., 2015; Corcoles et al., 2015; Zanetti et al., 2017) including members of cruciferous family (Stoppani et al., 2003; Salerno et al., 2005; Olfati, 2010; Tartaglia et al., 2016; Aminifard et al., 2019). This issue, however, remains unexplored and conceptually important for oilseed radish plants in order to clarify the features and regularities of leaf apparatus formation among members of the cruciferous family.

MATERIALS AND METHODS

The research was conducted on the experimental field of the VNAU (N 49°11′31″, E 28°22′16″) on dark gray forest soils Luvic Greyic Phaeozem soils (IUSS Working Group WRB, 2015). Agrochemical field potential: humus content: 2.02–3.2%, lightly hydrolyzed nitrogen 67–92, mobile phosphorus 149–220, exchangeable potassium 92–126 mg kg^{-1} of soil at pH_{kcl} 5.5–6.0. The research on peculiarities of leaf apparatus formation of the oilseed radish Zhuravka variety plants was carried out on the basis of two cardinally distant technological options of its construction at the rate of sowing of

4.0 million pcs. ha^{-1} of germinable seeds of row sowing (15 cm) and 0.5 million pcs. ha^{-1} of germinable seeds of wide-row (30 cm) sowing. The research of both options was conducted on a nonfertilized ground. The sowing period for both options corresponded to the end of the first and beginning of the second ten-day period of April. The climate of the region is moderately continental (Dfb according to the Köppen-Geiger climate classification (Pivoshenko, 1997)), average January temperature: -5 °C, average July temperature: 20 °C; annual precipitation: 420–590 mm, 80% of which occurs during a warm period. The increase in the overall favorability of hydrothermal vegetation regimes of oilseed radish towards reduction of weather risks should be placed in the following order: 2018–2015–2017–2016–2013–2014 (Table 1). The research covered three varieties of oilseed radish (*Raphanus sativus L.* var. *oleiformis Pers.*), namely 'Zhuravka', 'Raiduha' and 'Lybid'. The study of the variability of the fodder radish fruits was carried out with a scheme including extreme gradations of the technological spectrum of agrophytocenosis formation in the study area, taking into consideration the borderline formats of the recommended mineral nutrition of the specimen (Table 2).

Table 1. Monthly average hydrothermal coefficient* over the growing season of oilseed radish, 2013–2018

Year of research	Months					Average for the years of vegetation
	V	VI	VII	VIII	IX	
2013	1.305	2.202	0.377	1.047	3.441	1.527
2014	2.783	1.078	1.137	0.750	0.736	1.269
2015	0.719	0.613	0.230	0.061	0.684	0.430
2016	1.227	0.893	0.682	0.486	0.063	0.663
2017	0.645	0.349	0.806	0.563	1.983	0.824
2018	0.258	3.124	1.349	0.349	0.680	1.179

* – $GTC = \frac{\sum R}{0.1 \cdot \sum t_{>10}}$, where the amount of precipitation (ΣR) in mm over a period with temperatures above 10 °C, the sum of effective temperatures (Σt > 10) over the same period, decreased by a factor of 10.

Table 2. The range of acceptable common options for the formation of oilseed radish agrophytocenosis in the study area (Tsytsiura, 2019)

Planting method and seeding rates (million germinable seeds·ha^{-1})		Fertilization (of the active substance), kg·ha^{-1}
row method (15 cm)	wide-row method (30 cm)	
1.0	0.5	without fertilizers
2.0	1.0	$N_{30}P_{30}K_{30}$
3.0	1.5	$N_{60}P_{60}K_{60}$
4.0	2.0	$N_{90}P_{90}K_{90}$

** – underlined are variants for studying.

The experiments were set in randomized blocks, in a split–plot scheme, with four replicates. Three manual weedings were performed for weed control, while pests (*Phyllotreta crusiferae* Kutsch.), *Ph. atra var. cruciferae* Goeze., *Ph. armoraciae* Koch., *Meligethes aeneus* F.) were controlled through the application of insecticide in the vegetative stage.

Samples were collected in different phenological stages and in leaves of different sizes and shapes, because radish plants produce leaves of different shapes along the

cycle. After plant collection, the leaves were separated from the stem and only those photosynthetically active, with no damage or deformation caused by diseases, insects or other external factors, were selected. The annual number of the analyzed leaves was determined by the foliage level of plants in different years of observations, and according to the principle of single elimination, it provided for the analysis of leaves from 10 typical plants in non–contiguous repetitions for each technological variation of agrophytocenosis construction. The typicality of plants was determined for the middle dominating tier of oilseed radish plants of each studied variety according to a number of recommendations (Rabotnov, 1978; Ramensky, 1971).

Leaf parameters were determined using the Digimizer image analysis software (v 4.2) (Schoonjans, 2019). This software allows determining such leaf parameters as length (L), width (W), perimeter (P), area (LA). The specified morphometric parameters were determined in cm and cm^2, according to the image processing calibration system. The image of the leaves to be processed in the specified program is obtained by scanning with a CanoScan LIDE 700F scanner with the appropriate software for processing the obtained scanned images. Scanning of leaves within individual phenological periods of growth and development of oilseed radish plants was performed according to the order of their placement on the plant from the bottom to the top.

Typification of morphotypes of the leaf blade was performed in accordance with Fedorov et al. (1956), considering Cuptar (2019). Comparison of the significance of average values in comparison with the studied technological variations of the agrophytocenosis construction was carried out using a four-factor system of dispersion analysis. The general research methodology, associated observations and surveys were conducted in accordance with the baseline recommendations for studies on cruciferous crops (Saiko et al., 2011) with the methodological and descriptive recommendations of the classification ranking tables of variety examination (Test Guidelines for the conduct of tests for distinctness, uniformity and stability of Fodder Radish (*Raphanus sativus* L. var. *oleiformis* Pers., 2017) using correlation and regression methods of analysis (Sharma, 2005) and using a software package of statistical application programs Statistica 10, Exel 2013, Past 324.

RESULTS AND DISCUSSION

According to the results of morphometric analysis of oilseed radish leaves in their successive placement from the lower to the upper tiers, the presence of longline heterophylly with complex transient types of leaf blade between the tiers along the stem height was determined. For the oilseed radish, two types of changes were observed. In the early stages of vegetation up to the rosette phase – the beginning of the stem formation (BBCH 10–21), there is a gradual complication of the leaf blade from a simple morphotype in the cotyledons (obcordate) to a more complex morphotype (pinnatisect lyrate) for the leaves, which are formed during the period of the rosette formation and the beginning of the stem prolongation. In the subsequent process of plant growth from the stage of stooling to the stage of budding (BBCH 22–52), there is a domination of morphotypes of the middle tier leaves mainly of various transitional shapes of pinnatisect divided lyrate shape with signs of symmetry, asymmetry and disproportions with a marked deformation of the central vein. Already at the stage of the budding beginning (BBCH 48–50) in the zone of formed buds, the leaves of morphotypes of the upper tier

are distinguished (pinnately divided and pinnatisect lyrate leaves, pedate, subulate, linear, wedge–shaped, sagittate, palmate, ovoid leaves, etc.). The morphotypes of oilseed radish leaves are shown in Fig. 1. According to the presented character of the longline morphology of leaves, oilseed radish plants can be attributed to the highly differentiated heterophyllous type according to Corona & Vasilyev (2007) with a clear division into the morphological types of leaf according to its height placement on the stem. In addition, by the nature of the dominance of a certain leaf fraction, i.e. the prevalence of the corresponding tier of leaf morphotypes, by the tier of their placement it is possible to evaluate the optimality of applied technological parameters in the construction of agrophytocenosis, which corresponds to the general conclusions in a number of researches on other cruciferous crops (Clarke, 1977; Mullen et al., 2006; Maugarny-Cales & Laufs, 2018; Aminifard et al., 2019).

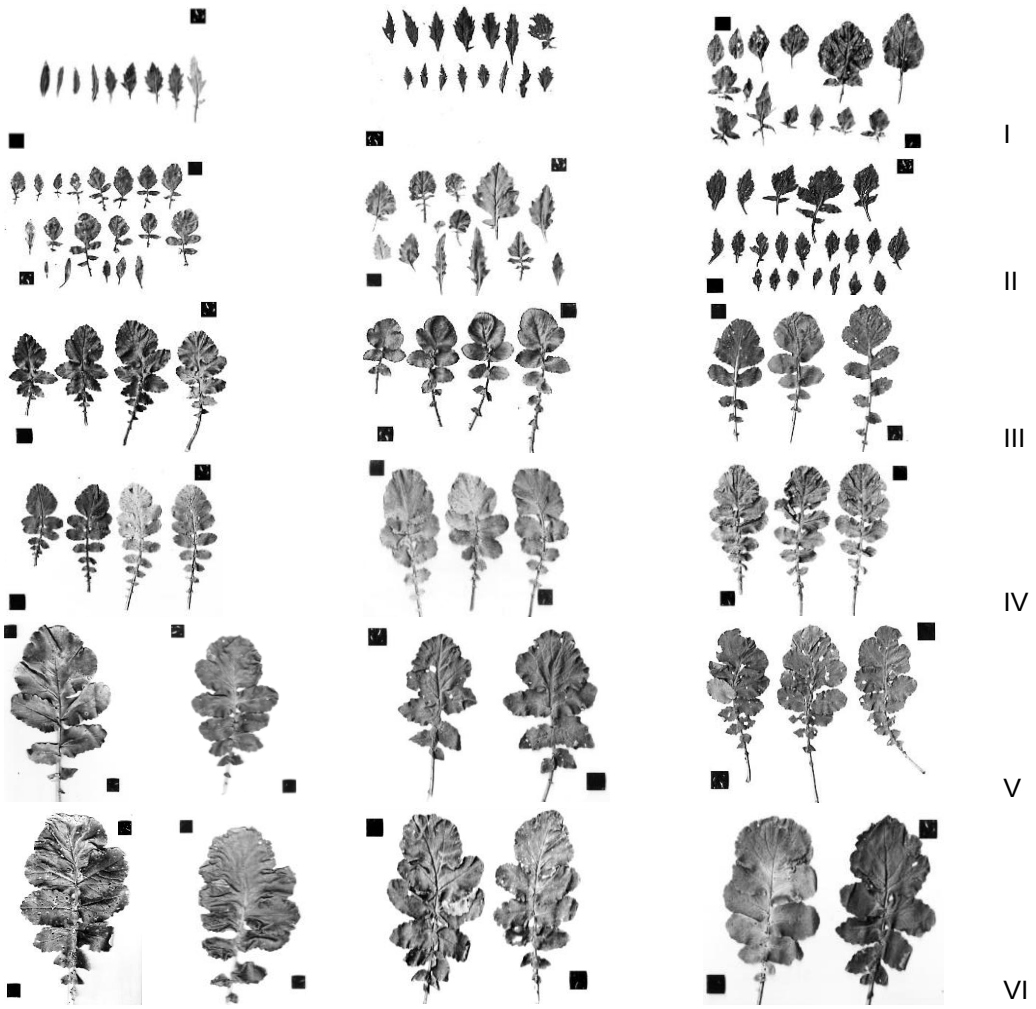

Figure 1. Morphotypes of oilseed radish leaves by tiers at the phenological flowering phase (BBCH 59–61) (I–II – upper tier leaves (zone of inflorescence branches and inflorescence itself)); III–IV – middle tier leaves; V–VI – lower tier leaves). Positioning of specimens sequentially from the lowest to the highest in a vertical sequence along the stem (composed for three varieties, marker black square with an area of 2 cm^2).

Considering the determined tier features in the morphology of oilseed radish leaves, different character of the structural complexity of leaves by the nature of their dwelling structure was also determined, including the character of the right–hand and left–hand placement of the serratures of the leaf blade edge, the presence of signs of fluctuating asymmetry and other signs, which are expressed in the total points of the number of differences (dwells) (Corona & Vasilyev, 2007). Given the above features, several basic types (metamers) of the leaf and a number of intermediate types, which are transitional between the main metamers within the selected axial stem tiers by leaf arrangement, can be considered in the oilseed radish, which is clearly demonstrated in Figs 1–3. Thus, leaves of the lower tier are characterized by the formation of an ovoid-lyrate type with dissected or divided almost symmetrical type of leaf blade lobes, which often overlap each other, or form a complex morphological growth type which artificially masks the dissection of the general morphology of the leaf. Leaves of the lower tier are typical for cruciferous crops of lyrate-sected type with 3–8 one-sided lobes of the leaf blade with the maximum width of the leaf on the last or penultimate leaf lobe.

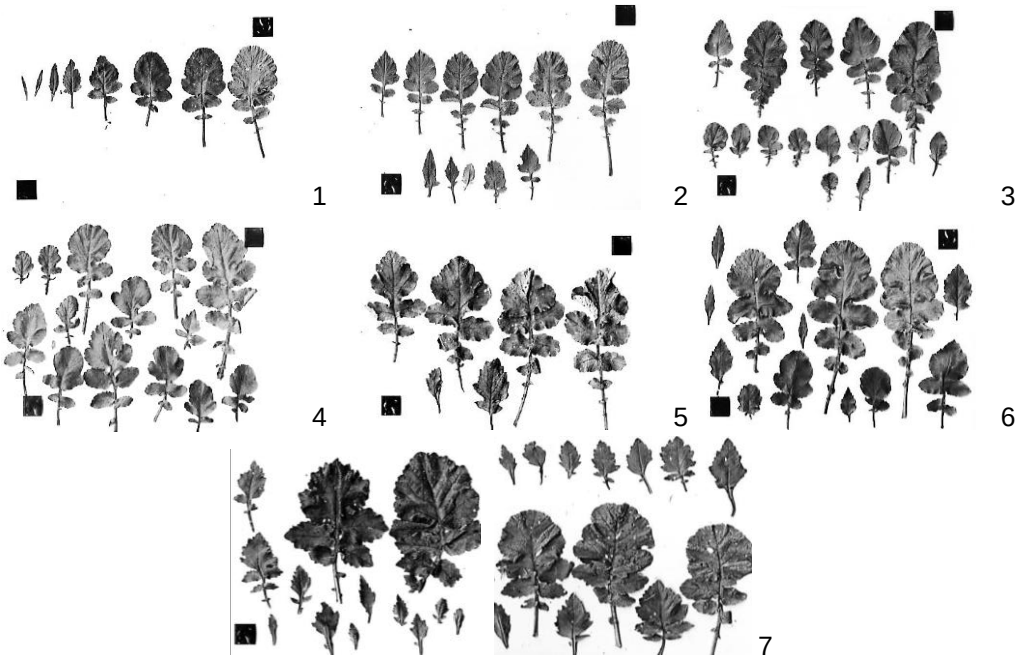

Figure 2. General morphotypology of oilseed radish leaves with different stand density during the flowering phase (BBCH 59–61) on a nonfertilized ground for 'Raiduha' variety (for inter-row spacing of 15 cm: 1 – 4.0 million pcs. ha^{-1} of germinable seeds; 2 – 3.0 million pcs. ha^{-1} of germinable seeds; 3 – 2.0 million pcs. ha^{-1} of germinable seeds; 4 –1.0 million pcs. ha^{-1} of germinable seeds; for inter-row spacing of 30 cm: 5 – 2.0 million pcs. ha^{-1} of germinable seeds; 6 – 1.5 million pcs. ha^{-1} of germinable seeds; 7–0.5 million pcs. ha^{-1} of germinable seeds), 2017. (marker black square with an area of 2 cm^2).

Progressively to the upper zone, transitional leaf morphotypes with different asymmetrical number of leaf parts of the distinct dissected leaf blade appear. These leaves show signs of fluctuating asymmetry with less development of the left side of the

leaf by the field of view. Leaves of the upper tier, which are mainly adjacent to the generative part of plants, both behind the main flower stalk and lateral reproductive branches, have the most diverse morphological structure, which consistently passes from the dissected 1–4 lobular leaf blades to the already specified morphotypes: subulate, linear, wedge–shaped, sagittate, palmate, ovoid, etc. Similar, but less distinct, nature of formation of morphological parameters of the leaf is noted in other cruciferous crops of spring rape (Pecham, P.A. & Morgan et al., 1985; Chavarria et al., 2011; Cargnelutti Filho et al., 2015), winter rape (Jullien et al., 2009), white mustard (Khader & Bhargava, 1984; Kumar et al., 1997) and other cruciferous crops (Paul, 1980; Gupta, 2009; Weraduwage et al., 2015). As a result, morphological rows with certain regular changes of both morphological types and morphological parameters in length, width and perimeter of the leaf can be identified for oilseed radish plants (Fig. 2). Moreover, the character of dynamic increase of linear parameters of a leaf (Fig. 3) during the flowering phase differs in different technological variations of oilseed radish agrophytocenosis construction, distinguishing two types: stably descending, providing for a constant decrease in the linear size of a leaf and its area from leaves of the lower tier to leaves of the upper tier, and oscillating – with a gradual increase in the morphological parameters of a leaf to 3–5 leaves in a row and a subsequent constant decrease in the specified parameters for subsequent leaves in a row up to the uppermost ones. We marked the first type for technological variations of 2.0–4.0 million pcs. ha^{-1} of germinable seeds, and the second type for all other variations under study. For the variation of 0.5–1.0 million pcs. ha^{-1} of germinable seeds in the dynamic row for the first 2–6 leaves a relative constancy in morphological development with subsequent decrease towards the upper tier was noted. It should also be noted that the total number of leaves on the plant during the flowering phase differs significantly from 5–10 leaves in variations of 4.0 million pcs. ha^{-1} of germinable seeds to 15–22 leaves in variations of 0.5 million pcs. ha^{-1} of germinable seeds. However, for the indication of the number of leaves for the various technological variants under study, a significant scale of the indicator values was also noted. So, if for a variation of 4.0 million pcs. ha^{-1} of germinable seeds it was within the range of 5–11 leaves during the period of estimations, then for a variation of 0.5 million pcs. ha^{-1} of germinable seeds it was within the range of 11–19 and even up to 40–75 leaves. It should be noted that with a decrease in sowing rate and fertilizer growth, the number of leaves of the upper tier of the plant, which belong to its generative zone, increases intensively, and the majority of leaves, which determine the main course of the assimilation process, remains relatively stable and is within the limits from 5–8 to 10–17 leaves with a range of values up to 12–24 depending on the variation. This is clearly illustrated by Figs 1–4.

The specified features of the dynamic changes of the leaf blade area within the plant by their height gradation of placement are most noticeable in the period of the end of budding (BBCH 53–57) – the beginning of flowering (BBCH 61–62), since during this period it is possible to distinguish the entire typology of leaf morphological forms within the plant's upper tiers.

We researched the nature of these changes in the form of graphical interpretation with the description of the corresponding dependence on the basis of selection of the corresponding classical function. For our technological variations with averaging of values on the variety factor, year of research and technological variation, these dependencies are shown in Fig. 4.

Figure 3. Dynamic rows of leaves in the order of their placement on the plant from the base to the top during the flowering phase (BBCH 59–61) for different technological variations of agrophytocenosis construction for 'Zhuravka' variety (1 – 3.0 million pcs. ha^{-} of germinable seeds (inter–row spacing of 15 cm); 2 – 2.0 million pcs. ha^{-1} of germinable seeds (inter-row spacing of 15 cm); 3 – 1.0 million pcs. ha^{-1} of germinable seeds (inter–row spacing of 15 cm); 4 – 1.0 million pcs. ha^{-1} of germinable seeds (inter–row spacing of 30 cm); 5 – 0.5 million pcs. ha^{-1} of germinable seeds (inter–row spacing of 30 cm), 2016.

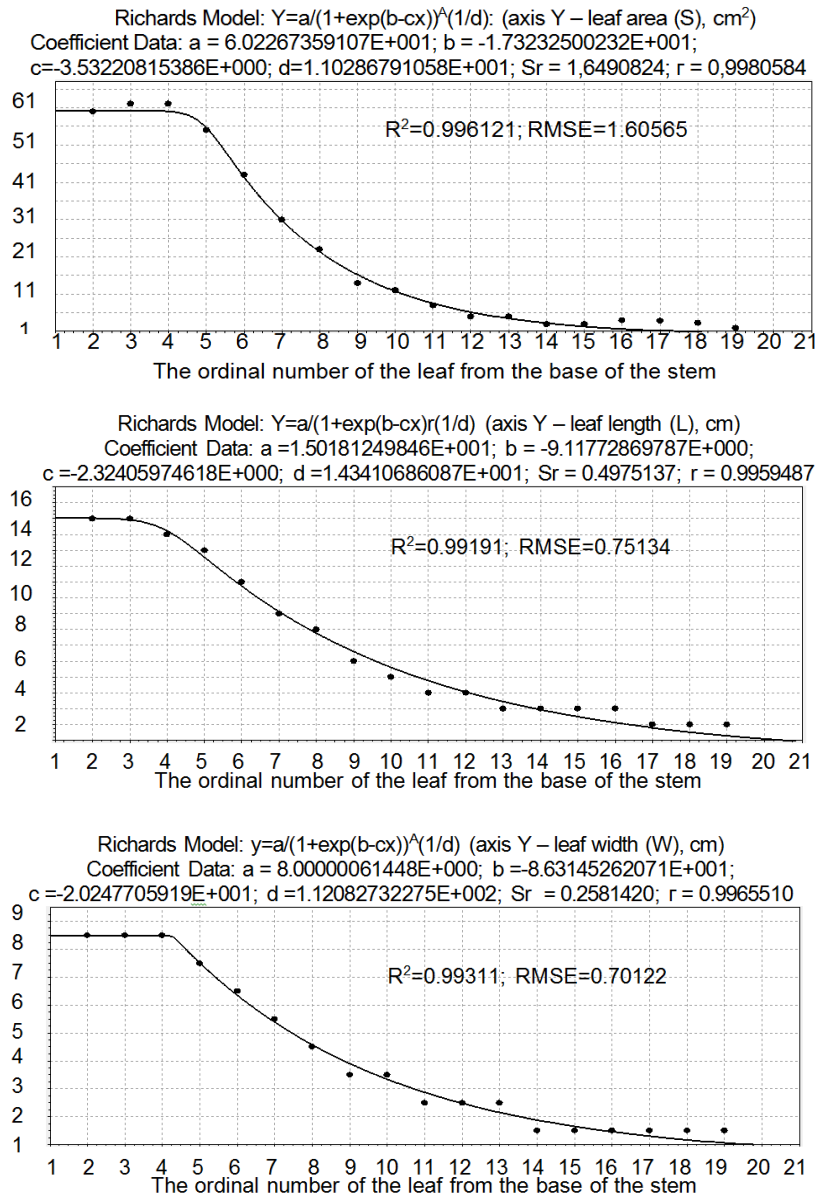

Figure 4. The change model of leaf area and its morphological parameters for the average row of three oilseed radish varieties and 32 technological variations of their agrophytocenosis construction for the consolidated period between 2013–2018 during the phase of the end of budding – the beginning of flowering (BBCH 57–61).

The results of selection of the corresponding dependence of changes in both the area of the average model leaf of oilseed radish varieties and its morphological parameters with the use of CurveExpert Pro: 2.6.5 software package allowed describing its character with maximum approximation according to the Richards model (at R^2 99.01–99.31). The Richards curve or generalized logistic is a widely used growth model that will fit a wide range of S-shaped growth curves. Among the closest in terms

of approximation R^2 to describe the regularities of the specified changes in leaf morphology we have considered the Weibull model (leaf area parameters (S) $R^2 = 0.98974$; *RMSE* = 1.92674, for the leaf length parameter (L) $R^2 = 0.990527$; *RMSE* = 0.87914, for the leaf width parameter (W) $R^2 = 0.98756$; *RMSE* = 0.91257) and the Rational Function model (corresponding parameters (S) $R^2 = 0.97956$; *RMSE* = 2.2584; L: $R^2 = 0.980421$; *RMSE* = 1.17894; W: $R^2 = 0.97456$; *RMSE* = 1.21475). Given that the Richards model belongs to the category of complex asymmetric models, formation of linear parameters of an oilseed radish leaf has certain regularities determined by us, but it also has certain cautions and features. Particularly, the general regularities in the budding–flowering period include the evident persistence of the reduction of leaf length and width in the height gradient. Moreover, 1–5 leaves should be attributed to morphological forms with the largest linear sizes and area located in the lower and main middle tier of the stem, 6–11 leaves to transitional forms of the middle and upper tier, and the rest to morphological forms of the upper (generative) tier.

The plateau presence in 3–4 initial points indicates a certain oscillatory nature of leaf size formation from the rosette phase to the flowering phase noted by us, in particular the formation of intermediate leaves by the order of their appearance from the seedling phase to the rosette phase with a gradual increase of linear parameters of the following leaves by the order of their formation on the stem up to the phase of the beginning of budding and, accordingly, a constant decrease in leaf size by the order of their formation from the phase of the end of budding to the phase of the end of flowering.

Similar observations on the search for regularities in the formation of shape and size of the leaf within the plant by the height gradient of the stem have been made in application to higher plants during the 80s–90s of the last century (Meinhardt & Gierer, 1974; Green & Poething, 1982; Cote et al., 1992; Gould et al., 1992; LAWG 1999) and in modern times (Pugnaire et al., 2007; Shi et al., 2018). Nevertheless, the real actions, except for the general approaches to plant modeling on the basis of botanical specification of plant parts (Lintermann & Deussen, 1999; Prusinkiewicz, 2004) have not been made. In this context, our researches in some aspects allow us to re-evaluate the peculiarities of formation of individual parameters of the assimilation surface of plants from the cruciferous family.

Also important is the assessment of both the variability in leaf morphology and the influence of major technological approaches on its value, the results of which are presented in Table 3. On the one hand, the data provided indicate both the high degree of variability in the morphological parameters of the leaves and the corresponding changes in the application of different combinations of sowing rate, row-width spacing and fertilization. In terms of the spread of values, the overall variability of the forms and area of the leaf has a strong tendency to increase both within the range of row and wide-row sowing method with a decrease in sowing rate. The application of the growing fertilization rates enhances both the overall size of the leaves and their area, and provides for an intensive increase in the variability of leaf morphotypes, widening the differentiation of the leaf row to the extreme morphological gradations between large and small leaves and an overall widening of the spread of values. In addition, we noted that this dynamics is more typical for the leaf length than its width. Thus, from this perspective the elongation of the oilseed radish leaf blade is more sensitive to the coenotic tension in agrophytocenosis than width changes.

Table 3. Summary morphological individual parameters of oilseed radish leaf at the flowering phase (BBCH 59–61) depending on the technological variation of agrophytocenosis construction, 2013–2018

Sowing rate (million pcs.ha of germinable seeds) (C), sowing method (B)	Fertilizer (D)	Average for 3 varieties (Zhuravka, Raiduha and Lybid)								
		Range of			S, cm^2	W, cm	L, cm	V_R*		
		S, cm^2	W, cm	L, cm				S	W	L
4.0, row	1**	0.38–31.54	0.29–7.15	1.41–15.14	16.27	3.46	8.6	1.92	1.98	1.60
	2	0.31–40.82	0.37–7.63	1.58–16.29	18.82	3.87	8.95	2.15	1.88	1.64
	3	0.27–46.24	0.31–7.89	1.45–17.91	19.64	4.06	9.44	2.34	1.87	1.74
	4	0.22–42.29	0.28–6.71	1.24–16.18	19.44	4.04	9.32	2.16	1.59	1.60
3.0, row	1	0.53–44.94	0.43–8.25	1.75–16.50	18.88	4.45	9.59	2.35	1.76	1.54
	2	0.48–60.37	0.43–8.48	1.52–19.19	23.40	4.8	10.49	2.56	1.68	1.68
	3	0.46–70.61	0.43–9.25	1.49–21.21	24.88	5.08	10.88	2.82	1.74	1.81
	4	0.35–68.92	0.35–8.69	1.18–20.69	23.11	4.94	9.86	2.97	1.69	1.98
2.0, row	1	0.59–48.11	0.51–6.85	1.49–14.66	19.39	3.95	8.51	2.45	1.61	1.55
	2	0.63–98.04	0.49–18.54	1.71–25.53	23.95	5.16	11.3	4.07	3.50	2.11
	3	0.36–105.91	0.34–19.44	1.63–26.85	29.41	5.25	10.55	3.59	3.64	2.39
	4	0.28–99.69	0.27–18.72	1.36–25.69	31.12	5.89	11.25	3.19	3.13	2.16
1.0, row	1	0.72–82.89	0.70–12.77	1.69–20.57	24.87	4.19	9.05	3.30	2.88	2.09
	2	0.92–92.14	0.67–16.83	1.74–21.17	34.69	5.63	12.01	2.63	2.87	1.62
	3	1.34–166.22	0.67–18.86	1.99–29.12	37.37	5.95	12.44	4.41	3.06	2.18
	4	1.28–174.82	0.55–19.48	1.51–32.87	40.53	6.74	12.97	4.28	2.81	2.42
2.0, wide-row	1	0.63–88.71	0.42–11.52	1.47–16.56	21.59	4.3	9.02	4.08	2.58	1.67
	2	1.19–109.74	0.96–14.82	1.84–17.68	28.74	5.4	9.89	3.78	2.57	1.60
	3	1.68–141.87	1.28–16.29	1.67–19.12	33.54	5.86	10.4	4.18	2.56	1.68
	4	1.44–126.81	1.19–15.12	1.48–18.20	33.75	5.93	10.52	3.71	2.35	1.59
1.5, wide-row	1	0.72–106.84	0.50–10.70	2.53–29.43	27.58	4.87	10.38	3.85	2.09	2.59
	2	3.14–193.85	1.65–16.45	3.72–29.68	33.45	5.94	12.09	5.70	2.49	2.15
	3	2.02–191.1	1.03–30.34	2.39–33.13	42.39	6.34	13.29	4.46	4.62	2.31
	4	1.54–172.63	1.02–27.28	1.89–27.44	45.84	6.98	13.72	3.73	3.76	1.86
1.0, wide-row	1	1.13–101.33	0.63–9.97	2.13–23.56	40.19	5.35	11.2	2.49	1.75	1.91
	2	0.96–294.84	0.65–26.39	2.26–31.92	49.27	5.99	12.08	5.96	4.30	2.46
	3	4.52–310.48	1.46–27.05	3.94–31.80	57.36	6.71	12.2	5.33	3.81	2.28
	4	4.18–339.47	1.28–28.57	2.73–32.82	64.44	7.6	13.43	5.20	3.59	2.24
0.5, wide-row	1	3.87–277.64	1.63–24.02	3.74–29.96	51.12	6.19	12.59	5.36	3.62	2.08
	2	2.67–286.91	1.47–26.97	2.68–31.51	64.6	8.24	16.08	4.40	3.09	1.79
	3	3.02–359.57	1.64–30.62	2.96–34.33	70.68	8.31	16.48	5.04	3.49	1.90
	4	2.84–396.80	1.55–33.61	2.75–36.27	79.22	9.16	17.87	4.97	3.50	1.88

For average values	S	W	L	Impact share	S	W	L
LSD_{05} factor A	0.21	0.05	0.09	A	19.77	15.91	21.64
LSD_{05} factor B	0.12	0.03	0.05	B	30.80	24.42	15.36
LSD_{05} factor C	0.17	0.04	0.08	C	28.60	28.18	32.78
LSD_{05} factor D	0.17	0.04	0.08	D	9.82	22.46	17.38
LSD_{05} interaction AB	0.30	0.07	0.13	AB	1.45	0.26	0.23
LSD_{05} interaction AC	0.42	0.10	0.19	AC	1.33	0.36	0.46
LSD_{05} interaction AD	0.42	0.10	0.19	AD	0.48	0.20	0.15
LSD_{05} interaction BC	0.24	0.06	0.11	BC	4.99	4.00	7.32
LSD_{05} interaction BD	0.24	0.06	0.11	BD	1.32	0.87	0.60
LSD_{05} interaction CD	0.34	0.08	0.15	CD	1.01	2.76	3.19
LSD_{05} interaction ABC	0.60	0.14	0.27	ABC	0.22	0.11	0.15
LSD_{05} interaction ABD	0.60	0.14	0.27	ABD	0.06	0.01	0.01
LSD_{05} interaction ACD	0.85	0.20	0.38	ACD	0.06	0.07	0.08
LSD_{05} interaction BCD	0.49	0.12	0.22	BCD	0.08	0.35	0.64
LSD_{05} interaction ABCD	1.20	0.29	0.54	ABCD	0.01	0.02	0.02

* – oscillation coefficient by Gumbel (1947);

** – 1 – without Fertilizer, 2 – $N_{30}P_{30}K_{30?}$, 3 – $N_{60}P_{60}K_{60}$, 4 – $N_{90}P_{90}K_{90}$.

This effect is more noticeable in the variations of row sowing than in wide-row sowing, and corresponds to the general typology of reaction of plants with relatively tolerant type to clotting (Rabotnov, 1978). The high variability of the leaf morphological parameters also confirms the value of the oscillation coefficient (V_R). The proximity of the values of this indicator for all the studied parameters S, L, and W indicates the possibility of a non-destructive method of determining the leaf area by the corresponding ratio of its length and width. On the other hand, its constant growth in comparison with non–fertilized and fertilized variations indicates that the application of additional fertilizer contributes to the expansion of the spread of variation and the corresponding range of leaf parameters within the plant. At the same time, the maximum variation of the leaf morphological features is maximum in the variants of 0.5 million pcs. ha^{-1} of germinable seeds. For this variation, the average V_R for certain leaf parameters was 3.43 with the same indicator in the variation 4.0 million pcs. ha^{-1} of germinable seeds 1.87.

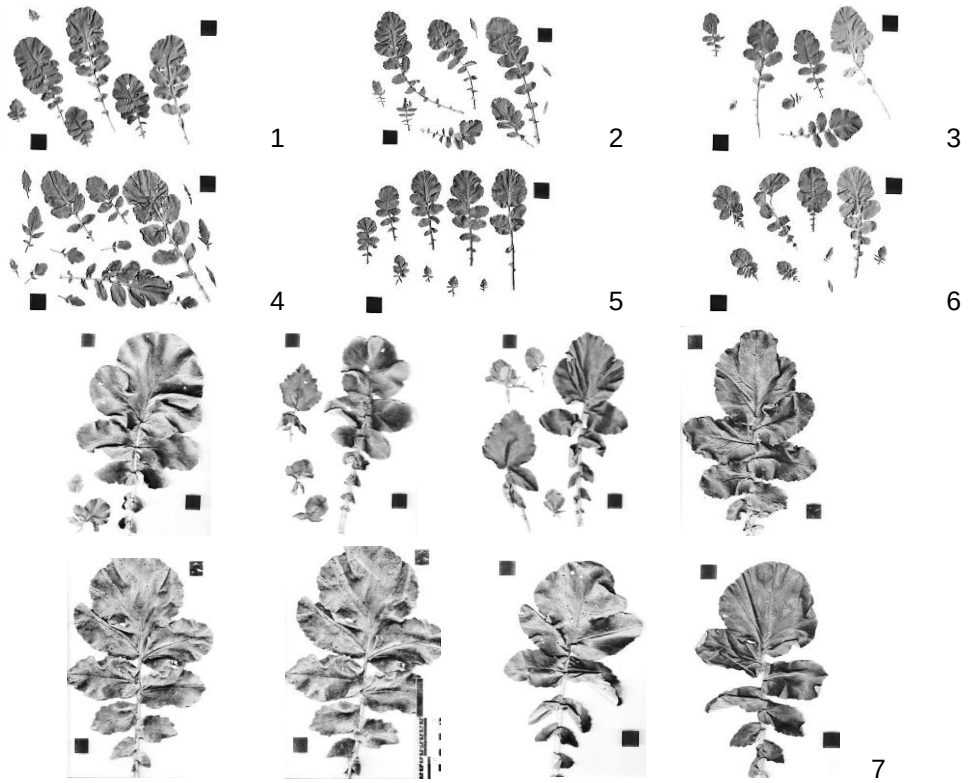

Figure 5. Scanned assimilation surface of 6 typical oilseed radish plants of 'Lybid' variety in the flowering phase with a sowing rate of 3.0 million pcs. ha^{-1} a of germinable seeds in the ground with the application of $N_{60}P_{60}K_{60}$ (position 1–6) and one typical plant with a sowing rate of 0.5 million pcs. ha^{-1} of germinable seeds in the same fertilization ground (position 7) (marker black square with an area of 2 cm^2), 2014.

This is clearly confirmed by the data presented in Fig. 5, which shows a comparable comparison of the morphological row of leaves of the plant, namely for variations 4.0 and 0.5 pcs. ha^{-1} of germinable seeds of the 'Lybid' variety in 2014, which was favorable

for intensive growth processes. It should also be noted that wide-row sowing variations ensured much higher variability of leaf morphological features than ordinary row sowing: the average V_R for row sowing was 2.40, meanwhile for wide-row sowing variations this value was 3.22. For different fertilizer options in comparison of non–fertilized ground and ground at application of 90 kg ha^{-1} of the primary material – 2.46 and 2.85, respectively. The conducted 4-factor dispersion analysis of morphological features of oilseed radish leaf confirms the previously made summaries concerning the influence of technological parameters of oilseed radish agrophytocenosis construction on the size of its leaf (the share of corresponding B and C factors is from 15 to almost 33% with the maximum combined effect on the leaf area indicator).

The results of the dispersion analysis also showed the determinant role of hydrothermal conditions during the year (factor A) in the range from 15 to 22% with the highest level of impact on the formation of leaf length indicator (L). Graphically, this dependence (Fig. 6, position 4) has a complex power nature.

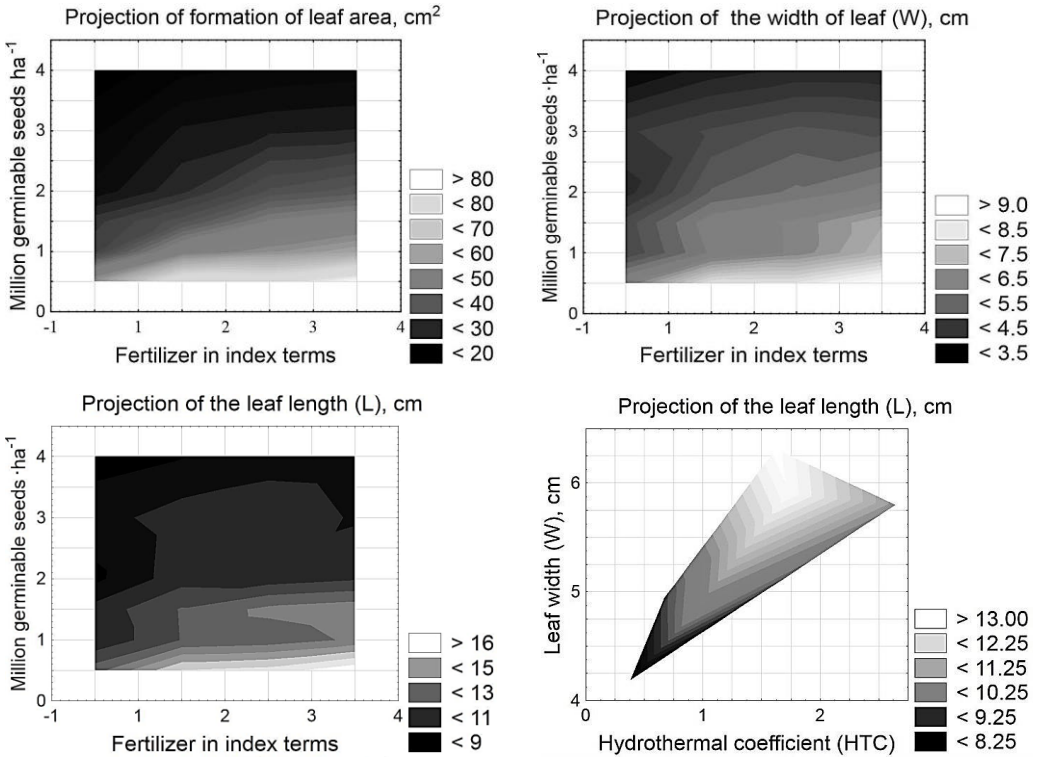

Figure 6. The reaction surface (projection (axis z)) of the formation of area depending on the sowing rate (stand density) of plants and fertilization in the index expression linear parameters of the leaf (width (W) and length (L)). The graphical dependence between the hydrothermal coefficient of the seedling–flowering period and the linear sizes of the leaf during the flowering period (position 4 (the relationship between the parameters: $z = -3.1375-0.7967x+3.5622y-1.5772x^2+1.0431xy-0.2929y^2$)) for the average value of varieties and years of study over the period 2013–2018.

Although, the growth of leaf length is associated with the growth of leaf width, but hydrothermal conditions during the period of leaf formation up to the flowering phase at their growth according to the hydrothermal coefficient (HTC) contribute to the overall growth of morphological parameters of the leaf with peak growth up to the HTC level of 1.6–1.8 with subsequent reduction of the overall length of the leaf blade at the HTC growth to the level of 1.8–2.6. The angular inclination of the reaction curve indicates the already determined advance effect of elongation of the leaf in comparison with the increase in its width. The determined features point to the fact that the increase in the intensity of growth processes due to excessive hydrothermal resources leads to intensive disproportional growth in above-ground biomass, including intensive leaf-making. The general shading and the increase of the coenotic tension contribute to the reduction of the average values for the plant of leaf morphological indicators and provide, as an option, the formation of a larger number of leaves with their significantly smaller average area. This distinguishes the average HTC level of 1.7 as the threshold for oilseed radish varieties from the perspective of combination of optimal growth rates and formation rates of individual leaf parameters. The results obtained correspond to the biological components of cruciferous crops growth processes and their reaction to stress factors (Paul, 1980; Nanda et al., 1995; Kumar et al., 1997; Kirkegaard et al., 2012), particularly positive reaction to the improvement of hydrothermal conditions in combination with sufficient humidity and moderate temperatures, guarantees the growth of HTC to 1.2–1.5 1.2–1.5.

The conclusions about the formation of average linear sizes of the leaf and its area depending on the range of applied technological solutions for growing oilseed radish varieties are also confirmed by the results of cluster analysis (Vard method) (Fig. 7), the index of Euclidean distances the system

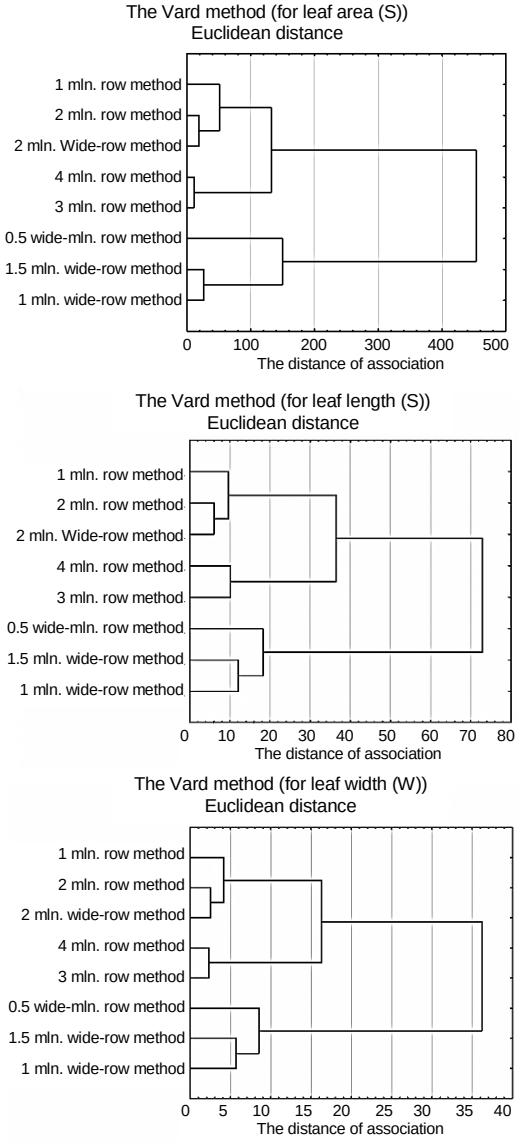

Figure 7. Cluster dendrograms of formation of the leaf average individual area and leaf linear sizes at various technological variations of the oil radish agrophytocenosis construction at the flowering phase (BBCH 59-61) on the average by the fertilizer options, 2013–2018.

of row sowing according to which by and wide-row sowing have significant differences in the size of morphological features of the leaf on the plant, starting with the sowing rate of 1.5 million pcs. ha^{-1} of germinable seeds due to the classification of the variation of 2.0 million pcs. ha^{-1} of germinable seeds at wide-row sowing to one cluster group with row sowing variations. The morphological parameters of the leaf are significantly higher in the variation of 0.5 million pcs. ha^{-1} of germinable seeds. Close in terms of formation of both length and width of the leaf were variations of 4.0 and 3.0 million pcs. ha^{-1} of germinable seeds with row sowing and 1.0 and 1.5 million pcs. ha^{-1} of germinable seeds with wide row sowing. Generally speaking, in terms of the association distances indicator, as it has been noted, the variability range of the leaf width within the oilseed radish plant is significantly less variable than its length in terms of the ratio of the specified distances as 1:2 in favor of the leaf width indicator (W).

Thus, the analysis and the intermediate generalizations that have been done confirm that it is possible to determine the leaf area using a non–destructive method of calculating it by selecting the appropriate functional connection between the initial parameters S, L and W. Possibility of such methodical approach is caused by the established features of uniformity of value formation of both width, and length of a leaf at various technological variations and certain proximity of determining factors in system of conditions year–variety–sowing method–sowing rate–fertilizer.

This is also confirmed by the conducted correlation analysis for the totality of the examined leaves between the formation of its main morphological features, their combinations and the leaf area (Table 4, Fig 8).

Table 4. Correlation coefficients between the area (S), length (L) and width (W) of individual leaves of oilseed radish and some its combination (in the cumulative total of accounted plant leaves for all varieties, technological variations and years of research)

Parameters	S, cm^2	L, cm	W, cm	L+W, cm	W^2, cm^2	L^2, cm^2	L^2+W^2, m^2	L W, cm^2
S, cm^2	1.000	0.880	0.885	0.903	0.914	0.809	0.926	0.928
L, cm	0.880	1.000	0.896	0.989	0.952	0.729	0.937	0.894
W, cm	0.885	0.896	1.000	0.953	0.847	0.885	0.892	0.927
L+W, cm	0.903	0.989	0.953	1.000	0.939	0.799	0.944	0.927
W^2, cm^2	0.914	0.952	0.847	0.939	1.000	0.782	0.988	0.943
L^2, cm^2	0.809	0.729	0.885	0.799	0.782	1.000	0.868	0.939
L^2+W^2, cm^2	0.926	0.937	0.892	0.944	0.988	0.868	1.000	0.981
L W, cm^2	0.926	0.937	0.892	0.944	0.988	0.868	1.000	0.981

* – all correlations are significant at the level $p < 0.001$.

The provided data show that there is a direct close relation between the leaf area and its linear parameters. At the same time, the closeness of relation with the parameter of its width is higher by 4.4%.

This confirms our conclusions on different rates of linear and latitudinal increase of the oilseed radish leaf blade and the significantly higher reaction of the leaf length parameter on changing the agrophytocenosis density against the background of increasing fertilizer rates. Due to this difference, the reaction plane between the length, width of the leaf and the hydrothermal coefficient has an angular inclination with respect

to the Z axis (see Fig. 6, position 4). Thus, the established closeness of the relation enabled us to search for an appropriate regression equation of the relation between the leaf area and the variants of attracting to the equation its length (L) and width (W), or their respective combinations (Table 5). The results obtained on 29 models of different combinations of leaf parameters in the consolidated totality proved the complexity of dependencies between the leaf area and its basic dimensions.

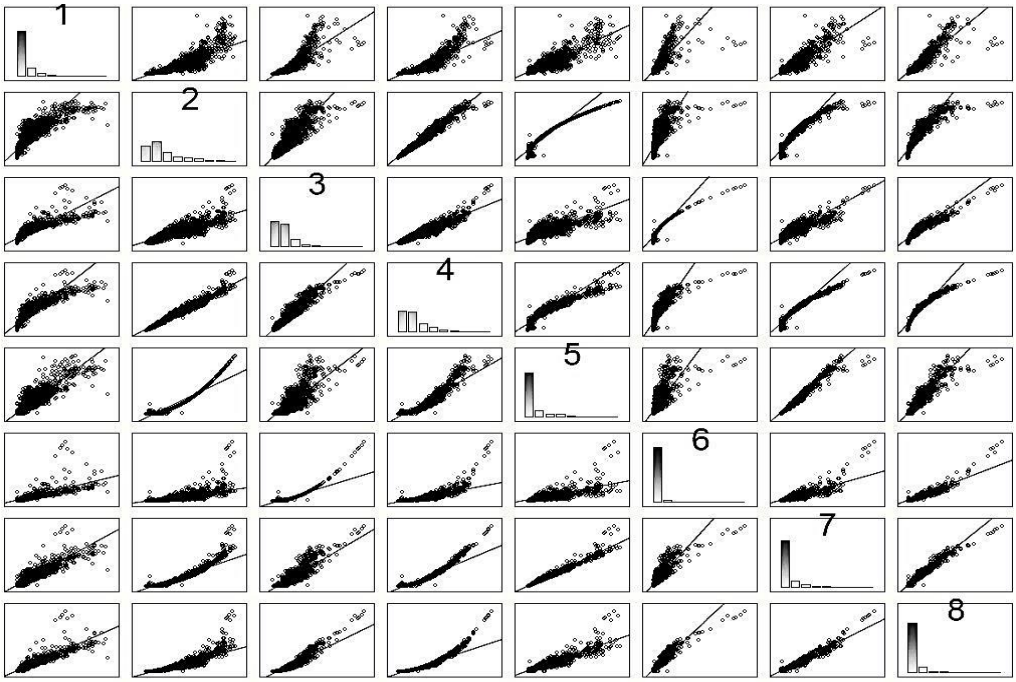

Figure 8. Correlation matrix of dependencies between leaf area (S, cm^2) its length (L, cm) and width (W, cm) for oil radish varieties in the totality of data for the period between 2013 and 2018 (matrix diagonal from left to right; 1 – S (cm^2); 2 – L (cm); 3 – W (cm); 4 – L+W (cm); 5 – W^2 (cm^2); 6 – L^2 (cm^2); 7 – $(L+W)^2$ (cm^2); 8 – LW (cm^2)).

In comparison with similar researches on rapeseed (Chavarria et al., 2011; Cargnelutti Filho et al., 2015; Tartaglia et al., 2016) and radish (Salerno et al., 2005; Aminifard et al., 2019), where models of correlation of leaf area with its morphological parameters were determined, which provide the level of approximation (R^2) 0.972–0.984 with the *RMSE* value 6.19–11.28, in our case, the approximation level of the examined models in the maximum value was 0.9106 (model 26) with a spread of *RMSE* values 9.75–21.19.

Table 5. Regression models for the estimation of canola leaf area (S, cm^2) with the respective coefficients of determination (R^2) of their generation and the Akaike information criterion (*AIC*), root–mean–square error (*RMSE*), Willmott's index (Willmott et al., 1985 and 2012) of agreement (*d*) and *BIAS* index of their test, as a function of length (L), width (W) and the product of length versus width (L.W) (in the cumulative total of accounted plant leaves for all varieties, technological variations for the period between 2013 and 2018)

Model no.	Form of model tested	Fitted coefficients and constant					R^2	Test of the models			
		a	b	c	d	e		AIC_C	*RMSE*	*d*	*BIAS*
1	$S = a + bL$	–17.9815	5.0238				0.7751	41268.9	15.45	0.885	–0.0005
2	$S = a + bW$	–20.0172	10.1400				0.7835	41335.7	15.16	0.888	0.0001
3	$S = a + b\ LW$	3.1566	0.4090				0.8605	41913.2	12.17	0.927	–0.0099
4	$S = a + b(L + W)$	–20.7099	3.5219				0.8156	41583.5	13.99	0.908	0.0014
5	$S = a + b(L^2 + W^2)$	2.9473	0.1623				0.8579	41892.6	12.28	0.928	–0.0061
6	$S = a + bL^2$	3.3383	0.2012				0.8353	41728.6	13.22	0.915	0.0202
7	$S = a + bW^2$	8.3645	0.5772				0.6539	40222.9	19.17	0.773	0.0013
8	$S = a + bL + cL^2$	0.9069	0.5280	0.1819			0.8374	41744.2	13.18	0.916	–0.0189
9	$S = a + bW + cW^2$	–17.1133	8.9509	0.0835			0.7865	41358.6	15.05	0.889	–0.0042
10	$S = a + bLW + c\ (LW)^2$	–0.9993	0.5428	–0.0003			0.9018	42201.5	10.25	0.953	0.8305
11	$S = a + b\ (L + W) + c\ (L + W)^2$	–3.6447	0.9003	0.0700			0.8737	42006.8	11.58	0.937	–0.0337
12	$S = aL^b$	0.3712	1.8147				0.8349	41726.0	13.24	0.917	–2.6743
13	$S = aW^b$	2.7911	1.4442				0.7760	41276.1	15.42	0.867	9.2928
14	$S = a(LW)^b$	0.9075	0.8623				0.8773	42032.2	11.41	0.937	3.5065
15	$S = a(L + W)^b$	0.2078	1.7745				0.8751	42017.1	11.51	0.937	1.3669
16	$S = a(W^2)^b$	2.7897	0.7220				0.7729	41255.5	15.52	0.865	9.1994
17	$S = a(L^2)^b$	0.3687	0.9084				0.8334	41718.6	13.29	0.917	–2.7293
18	$S = a(L^2 + W^2)^b$	0.3211	0.8990				0.8609	41916.2	12.15	0.930	–0.3281
19	$S = a + bL + cW$	–21.3902	2.5252	5.5975			0.8222	41633.2	13.74	0.912	0.0001
20	$S = a + bL^2 + cW^2$	2.9555	0.1724	0.1596			0.8580	41895.1	12.41	0.930	4.0421
21	$S = a + bL + c(LW)$	–3.8599	1.4526	0.3087			0.8735	42005.4	11.59	0.937	0.0034
22	$S = a + bW + c(LW)$	–2.0309	2.0582	0.3356			0.8650	41945.5	11.97	0.931	0.0008
23	$S = a + bL + c(L + W)$	–21.3902	–3.0722	5.5975			0.8222	41633.2	13.74	0.912	0.0036
24	$S = a + bW + c(L + W)$	–21.3902	–3.0722	5.5975			0.8222	41633.2	21.19	0.852	51.5648
25	$S = a + bL + cW + dL^2 + eW^2$	–2.1694	–4.2264	9.4815	0.2470	-0.1859	0.8959	42165.5	10.52	0.948	0.0214
26	$S = a + bL + c\ (LW) + dL^2 + e\ (LW)^2$	7.9316	–2.3613	0.6897	0.0458	-0.0005	0.9106	42265.1	9.75	0.956	–0.1523
27	$S = a + bW + c\ (LW) + dW^2 + e\ (LW)^2$	–1.2284	0.5111	0.5902	-0.2003	-0.0002	0.9048	42226.1	10.07	0.954	0.0443
28	$S = a + bL + c\ (L + W) + dL^2 + e\ (L + W)^2$	–2.1808	–11.4602	8.0457	0.2831	-0.0400	0.8911	42132.3	10.85	0.945	0.0501
29	$S = a + bW + c\ (L + W) + dW^2 + e\ (L + W)^2$	–0.6683	13.1036	-4.2612	-0.6174	0.1666	0.9073	42242.8	10.04	0.953	0.0285

According to the criteria of correlation of the model evaluation parameters, four models have been distinguished, which ensure the combination of the above criteria with the possibility of meeting the requirements of the regression model between the defined and calculated value of the individual leaf area (Fig. 9).

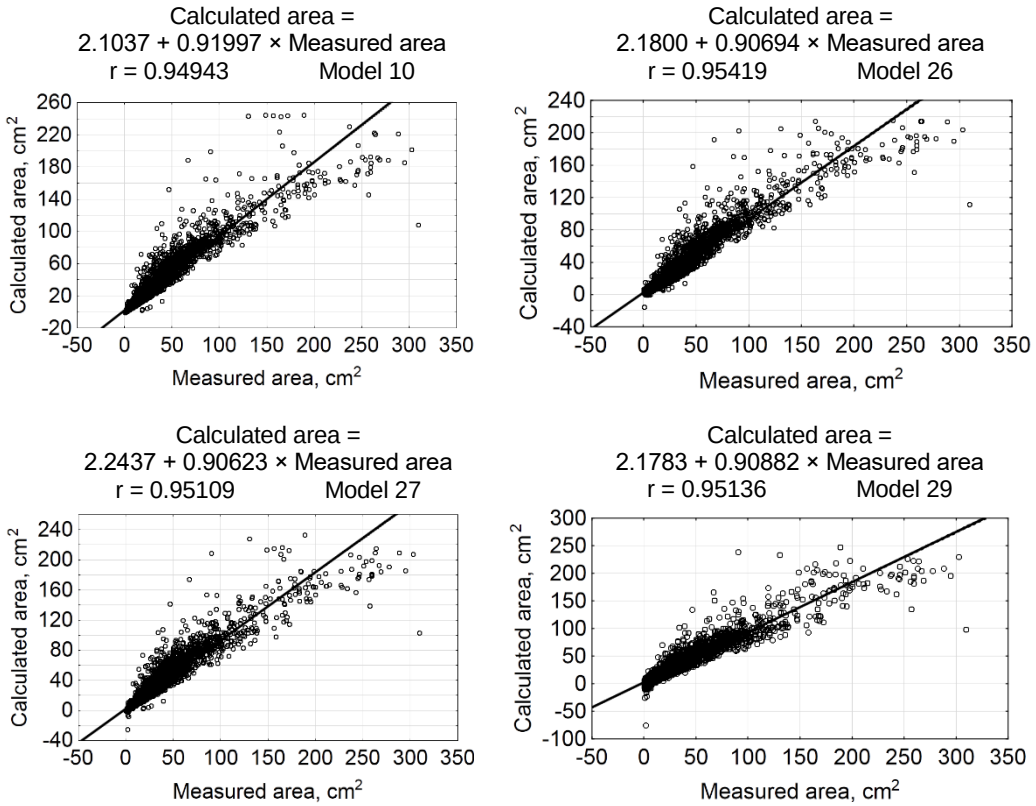

Figure 9. The dependence between the individual area of the oilseed radish leaf defined using appropriate mathematical models that include the appropriate morphological parameters of the leaf and the same area defined by scanning the entire leaf. The solid line represents the linear regression line; the line represents the 1:1 relationship.

Assessing the accuracy of the prediction in the system of non-destructive determination of individual leaf area, we can distinguish the model 26 with the highest level of approximation (R^2), the d criterion and the lowest *RMSE* value. Although there are general cautions concerning the application of this model and similar to it among 29 analyzed oilseed radish plants. Particularly, the high variability of the leaf area within the plant and the complexity of its morphotypes, defined by us in the first part of the paper, caused certain difficulty in observing the regular correlations between the length (L) and width (W) of an oilseed radish leaf. As a result, direct dependencies of both non–power and direct power linear nature do not provide sufficient level of regression ratio significance. The effectiveness of predictive models based on a combination of power and linear dependencies is higher, especially when using the leaf length criterion (L) in equations. Thus, the L criterion is parametrically more informative for determining the

area of an oilseed radish leaf (R^2 level was 0.823 on average for models using the L criterion and 0.755 for using the leaf width criterion (W)), than the width criterion (W), which is consistent with the results of researches Chavarria et al. (2011) on the use of leaf length in the variations of determining the leaf area by indirect methods of its measurement. Relatively high values of the *BIAS* criterion for models with the highest level of approximation R^2 indicate, according to the properties of this indicator (Leite et al., 2002), an increase in the regression dependence bias for leaves with an intensively developed leaf blade of large sizes, which, as we have already noted, may have the nature of a mutual overlap of the divided lobes, and often a complex corrugated surface (see Fig. 5, position 7). As a result, the overall variability predetermines the expansion of the deviation from the desired regression dependence for leaves with an area of more than 150 cm^2. Thus, regression dependence nature for prognostic and actual leaf area value has a sectoral nature with an extension from the minimum point of regression values to the maximum point, which attributes the dependence model to a multi–component in which linear and power variations can be combined (Sheskin, 2007). This nature is confirmed by the value of the *AICS* indicator, which according to the obtained parameters of values attributes morphological parameters of oilseed radish leaves within the plant to the highly variable ones (Motulsky & Christopoulos, 2003; Floriano et al., 2006). The nature of morphological misbalance between L and W parameters also confirms the nature of approximation of a certain model of oilseed radish leaf formation according to a height gradient (see Fig. 4), where approximation expression of the leaf area is lower than its linear parameters, that, according to the determination of the area of geometrical parts of plants (Klingenberg, 2015), attributes oilseed radish leaf to the body of complex morphologic configuration (Efroni et al., 2010).

CONCLUSIONS

1. The leaves of oilseed radish differ both in morphological features, and in the regularities of formation within the plant from other representatives of the cruciferous family, with the possibility of distinguishing a number of its morphotypes typical for three tiers of plants, of which the most variable is the upper tier, which forms their pre–generative and generative part.

2. The analysis of a variation range of leaf morphotypes allowed us to distinguish a longline type in the nature of leaf formation by a height gradient of oilseed radish plants, respectively, of the lower, middle and upper tier with maximum expressions of such nature of leaf formation at the phase of the beginning of flowering.

3. The peculiarities of leaf placement along the high gradient from the lower tier to the upper one are described by the Richards model with the approximation value (R^2) 99.01 (at *RMSE* 1,605) for leaf area, 99.19 (at *RMSE* 1.605) for leaf length (L) and 99.31 (at *RMSE* 0.70122) for leaf width (W).

4. It has been determined that the reduction of the feeding area of one plant with fertilization increase under favorable hydrothermal conditions in the period of seedling and beginning of flowering with the threshold optimal HTC for this period of 1,7 ensures the growth of both the variation of morphological parameters of the leaf and its average sizes in all linear parameters with the impact on the formation of the annual conditions 15.91–21.64%, sowing rate 28.18–32.78%, fertilization rate 9.82–17.38%.

5. The cluster analysis, including leaf morphology indicators for the examined technological groups of options for oilseed radish agrophytocenosis construction, determined a smaller scale interval of leaf width variability in comparison with its length in relation to the Euclidean distances as 1:2 in favor of leaf width indicator (W).

6. The individual area of the oilseed radish leaves can be determined without their selection, by measuring their length and width using the S model = 7.9316-2.3613L+0.6897 (LW)+0.0458L^2-0.0005 $(LW)^2$ (under the following test parameters of the model: R^2 0.9106; *RMSE* 9.75; *d* 0.956; *BIAS* 0.1523).

7. Further researches on the non–destructive way of determining the individual area of oilseed radish leaf should focus on approaches to exploring models for area determination for its different morphotypes, considering the tier of their placement along a height gradient on the stem.

REFERENCES

Antunes, W.C., Pompelli, M.F., Carretero, D.M. & DaMatta, F.M. 2008. Allometric models for non–destructive leaf area estimation in coffea (*Coffea arabica* and *Coffea canephora*). *Annals of Applied Biology* **153**, 33–40.

Aminifard, M.H., Bayat, H. & Khayyat, M. 2019. Individual modelling of leaf area in cress and radish using leaf dimensions and weight. *Journal Hortic. Postharvest Research* **2**, 83–94.

Baker–Brosh, K.F. & Peet, R.K. 1997. The ecological significance of lobed and toothed leaves in temperate forest trees. *Ecology* **78**, 1250–1255.

Bakhshandeh, E., Kamkar, B. & Tsialtas, J.T. 2011. Application of linear models for estimation of leaf area in soybean [*Glycine max* (L.) Merr]. *Photosynthetica*. **49**, 405–416.

Biology and Breeding of Crucifers. 2009. Edited by Surinder Kumar Gupta. CRC Press. Boca Raton (Florida): *Taylor & Francis*, 385 pp.

Biskup, B, Kuesters, R, Scharr, H, Walter, A & Rascher, U. 2009. Quantification of plant surface structures from small baseline stereo images to measure the three–dimensional surface from the leaf to the canopy scale. *Nova Acta Leopoldina* **96**(357), 31–47.

Blanco, F.F. & Folegatti, M.V. 2003. A new method for estimating the leaf area index of cucumber and tomato plants. *Horticultura Brasileira*, v.**21**, 666–669.

Boudaoud, A. 2016. Mechanical stress induces remodeling of vascular networks in growing leaves. *PLoS Computational Biology* **12**, 1–21.

Breda, N.J.J. 2003. Ground–based measurements of leaf area index: a review of methods, instruments and current controversies. *Journal of Experimental Botany* **54**, 2403–2417.

Buttaro, D., Rouphael, Y., Rivera, C.M., Colla, G. & Gonella, M. 2015. Simple and accurate allometric model for leaf area estimation in Vitis vinifera L. genotypes. *Photosynthetica* **53**, 342–348.

Bylesjö, M., Segura, V., Soolanayakanahally, R.Y., Rae, A.M., Trygg, J., Gustafsson, P., Jansson, S, & Street, N.R. 2008. LAMINA: a tool for rapid quantification of leaf size and shape parameters. *BMC Plant Biology*. **8**(1), 82.

Cargnelutti Filho, A. Toebe, M., Mendonça, A. B., Burin, C. & Kleinpaul, J.A. 2015. Estimation of rapeseed leaf area by linear leaf size. *Bragantia*, **74**(2), 139–148 (in Portuguese).

Carmassi, G., Incrocci, L., Incrocci, G. & Pardossi, A. 2007. Non-destructive estimation of leaf area in *Solanum lycopersicum* L. and gerbera (*Gerbera jamesonii* H. Bolus). *Agronomy. Med*. **137**, 172–176.

Cemek, B., Unlukara, A. & Kurunc, A. 2011. Non-destructive leaf area estimation and validation for green pepper (*Capsicum annuum* L.) grown under different stress conditions. *Photosynthetica***49**(1), 98–106.

Chavarria, G., Tomm, G.O., Muller, A., Mendonɜa, H.F., Mello, N. & Betto, M.S. 2011. Índice de área foliar em canola cultivada sob variações de espaçamento e de densidade de semeadura. *Ciencia Rural*. **41**(12), 2084–2089.

Chitwood, D.H. & Sinha, N.R. 2016. Evolutionary and environmental forces sculpting leaf development. *Current Biology* **26**, 297–306.

Clarke, J.M. 1977. *Growth relationships and yield of Brasslca napus*. Ph.D. Thesis. University of Saskatchewan, Saskatoon, Sask. 158 pp.

Clarke, J.M. 1978. The effects of leaf removal on yield and yield components of Brassica napus. *Canadian Journal Plant Science* **58**, 1103–1105.

Corcoles, J.I., A. Domínguez, M.A., Moreno, J.F. & Ortega, J.A. de Juan. 2015. A non-destructive method for estimating onion leaf area. *Irish Journal Agricultural Food Research* **54** (1), 17–30.

Corona, V.V. & Vasilyev, A.G. 2007. *Structure and variability of plant leaves: Fundamentals of modular theory*. Ekaterinburg: Ekaterinburg Publishing House. 279 pp. (in Russian).

Cote, R., Gerrath, J.M., Posluszny, U. & Grodzinski, B. 1992. Comparative leaf development of conventional and semileafless peas (Pisum sativum). *Canadian Journal of Botany* **70**, 571–580.

Cristofori, V., Rouphael, Y., Mendoza–de Gyves, E. & Bignami, C. 2007. A simple model for estimating leaf area of hazelnut from linear measurements. *Scientia Horticulturae*. Amsterdam **113**, 221–225.

Cristofori, V., Gyves, E.M., Bignami, C. & Rouphael, Y. 2008. Nondestructive, analogue model for leaf area estimation in persimmon (*Diospyros kaki* L.f.) based on leaf length and width measurement. *European Journal of Horticultural Science* **73**, 216–221.

Cuptar, H. 2019. Leaf: Definition, Parts and Types (With Diagram) http://www.biologydiscussion.com/leaf/leaf–definition–parts–and–types–with–diagram–botany/20137.

De Swart, E.A.M., Groenwold, R., Kanne, H.J., Stam, P., Marcelis, L.F.M. & Voorrips, R.E. 2004. Nondestructive estimation of leaf area for different plant ages and accessions of *Capsicum annuum* L. *Journal of Horticultural Science and Biotechnology* **79**, 764–770.

Deckmyn, G., Nijs, I. & Ceulemans, R. 2000. A simple method to determine leaf angles of grass species. *Journal of Experimental Botany* **51**(349), 1467–70.

Demirsoy, H., Demirsoy, L., Uzun, S. & Ersoy, B. 2004. Nondestructive leaf area estimation in peach. *European Journal of Horticultural Science* **69**, 144–146.

Demirsoy, H., Demirsoy, L. & Ozturk, A. 2005. Improved model for the non–destructive estimation of strawberry leaf area. *Fruits* **60**(1), 69–73.

Dornbusch, T., Watt, J., Baccar, R., Fournier, C. & Andrieu, B. 2011. A comparative analysis of leaf shape of wheat, barley and maize using an empirical shape model. *Annals of Botany* **107**, 865–873.

Doust, A. 2007. Architectural evolution and its implications for domestication in grasses. *Annals of Botany* **100**, 941–950.

Efroni, I., Eshed, Y & Lifschitz, E. 2010. Morphogenesis of simple and compound leaves: a critical review. *Plant Cell.* **22**(4), 1019–32.

Elsner, E.A. & Jubb, Jr. G.L. 1988. Leaf area estimation of Concord grape leaves from simple linear measurements. *American Journal of Enology and Viticulture* **39**, 95–97.

Fallovo, C., Cristofori, V., Mendoza-de Gyves, E., Rivera, C.M. & Rea, R., Fanasca, S. 2008. Leaf area estimation model for small fruits from linear measurements. – *HortScience* **43**, 2263–2267.

Fedorov, A.A. 1956. *Atlas of descriptive morphology of higher plants*. Letter. Moscow–Leningrad. Published by the USSR Academy of Sciences. 312 pp. (in Russian).

Firman, D.M. & Allen, E.J. 1989. Estimating individual leaf area of potato from leaf length. J. *Agricultural Science* **112**, 425–426.

Floriano, E.P., Müller, I., Finger, C.A.G. & Schneider, P.R. 2006. Adjustment and selection of traditional models to estimate the periodic increase in tree height. *Ciência Florestal*, v. **16**, pp. 177–199 (in Spanish).

Fochesatto, E., Henrique, A., Homero, N., Genei, B., Dalmago, A., Pinto, D.G., Kovaleski, S., Roca da Cunha, G. & Gouvea, J.A. 2016. Interception of solar radiation by the reproductive structures of canola hybrids. *Ciência Rural* **46**(10), 1790–1796.

Ford, E.D., Cocke, A., Horton, L., Fellner, E. & Van Volkenburgh, M. 2008. Estimation, variation and importance of leaf curvature in zea mays hybrids. *Agric Forest Meteorology* **148**(10), 1598–610.

Freyman, S., Charnetski, W.A. & Crookston, R.K. 1973. Role of leaves in the formation of seed in rape. *Canadian Journal Plant Science* **53**, 693–694.

Gabrielle, B., Denoroy, P., Gosse, G., Justes, E. & Andersen, M.N. 1998. A model of leaf area development and senescence for winter oilseed rape. *Field Crops Research* **57**(2), 209–222.

Gamper, H. 2005. Nondestructive estimates of leaf area in white clover using predictive formulae: the contribution of genotype identity to trifoliate leaf area. *Crop Science* **45**(6), 2552–2556.

Gould, K.S., Young, J.P.W. & Cutter, E.G. 1992. L–system analysis of compound leaf development in Pisum sativum. *Annals of Botany* **70**, 189–196.

Gielis, J. 2003. A generic geometric transformation that unifies a wide range of natural and abstract shapes. *American Journal of Botany* **90**, 333–338.

Giuffrida, F., Rouphael, Y., Toscano, S., Scuderi, D., Romano, D., Rivera, C.M., Colla G. & Leonardi, C.2011. Simple model for nondestructive leaf area estimation in bedding plants. *Photosynthetica* **49**, 380–388.

Green, P.B. & Poething, R.S. 1982. *Biophysics of the Extension and Initiation of Plant Organs*. In Developmental Order, its Origin and Regulation, S.Subtelny and P.B. Green (eds), New York, pp. 485–509.

Gumbel, E.J. 1947. The Distribution of the Range. *The Annals of Mathematical Statistics* **18**(3), 5142, 384–412.

Hosoi, F. & Omasa, K. 2012. Estimation of vertical plant area density profiles in a rice canopy at different growth stages by high–resolution portable scanning LIDAR with a lightweight mirror. *ISPRS Journal Photogram Remote Sensors* **74**, 11–19.

IUSS Working Group WRB: *World Reference Base for Soil Resources 2014. Update 2015*. *World Soil Resources Reports* **106**, FAO, Rome. 203 pp.

Ivanov, N., Boissard, P., Chapron, M. & Valery, P. 1994. Estimation of the height and angles of orientation of the upper leaves in the maize canopy using stereovision. *Agronomie* **2**, 183–94.

Jansen, M., Gilmer, F., Biskup, B., Nagel, K.A., Rascher, U., Fischbach, A., Briem, S., Dreissen, G., Tittmann, S., Braun, S., De Jaeger, I., Metzlaff, M., Schurr, U., Scharr, H. & Walter, A. 2009. Simultaneous phenotyping of leaf growth and chlorophyll fluorescence via growscreen fluoro allows detection of stress tolerance in Arabidopsis thaliana and other rosette plants. *Function Plant Biology* **36**(11), 902–914.

Jullien, A., Allirand, J.–M., Mathieu, A., Andrieu, B. & Ney, B. 2009. Variations in leaf mass per area according to N nutrition, plant age, and leaf position reflect ontogenetic plasticity in winter oilseed rape (Brassica napus L.). *Field Crop Research* **114**, 188–197.

Kandiannan, K., Kailasam, C., Chandaragiri, K.K., Sankaran, N. 2002. Allometric Model for Leaf Area Estimation in Black Pepper *(Piper nigrum* L.). *Journal Agronomy & Crop Science* **188**, 138–140.

Kasa, G.R. & Kondra, Z.P. 1986. Growth analysis of spring type oilseed rape. *Field Crop Research* **14**, 361–370.

Khader, S.S.E. & Bhargava, S.C. 1984. Physiological aspects of yield improvement of Brassica species with references to plant density 1. Dry matter accumulation arid growth attributes. *Journal Oilseeds Research* **1**, 37–48.

Khan, N.A. 2003. Changes in photosynthetic biomass accumulation, auxin and ethylene level following defoliation in *Brassica juncea*. *Food Agronomy Environmental* **1**, 125–128.

Khan, N.A. 2005. The influence of exogenous ethylene on growth and photosynthesis of mustard (*Brassica juncea*) followin defoliation. *Scientia Horticulturae* **105**, 499–505.

Kirkegaard, J.A., Sprague, S.J., Lilley, J.M., McCormick, J.I., Virgona, J.M. & Morrison, M.J. 2012. Physiological response of spring canola (Brassica napus) to defoliation in diverse environments. *Field Crops Research* **125**(18), 61–68.

Klingenberg, C.P. 2015. Analyzing fluctuating asymmetry with geometric morphometrics: Concepts, methods, and applications. *Symmetry* **7**, 843–934.

Kotula. Determinations on the basis of a single leaf 1951. *Bulletin International de l'Academie Polonaise des Sciences* et *des Lettres Série B.* pp. 1–40.

Kumar, S., Singh, J. & Dhingra, K.K. 1997. Leaf area index relationship with solar radiation interception and yield of Indian mustard (Brassica juncea L.) as influenced by plant population and nitrogen. *Indian Journal of Agronomy* **42**(2), 348–351.

Kumar, R. 2009. Calibration and validation of regression model for non–destructive leaf área estimation of saffron (*Crocus sativus* L.). *Scientia Horticulturae* **122**.142–145.

Kuwabara, A, Tsukaya, H & Nagata, T. 2001. Identification of factors that cause heterophylly in Ludwigia arcuata Walt.(Onagraceae). *Plant Biology* **3**(1), 98–105.

LAWG 1999. *Manual of Leaf Architecture: Morphological Description and Categorization of Dicotyledonous and Net-Veined Monocotyledonous Angiosperms*. Smithsonian Institution, Washington DC. 65 pp.

Leite, H.G. & Lima, V.C.A. de. 2002. A Method for Conducting Forest Inventories without Using Volumetric Equations. *Revista Árvore* **26**(3), 321–328 (in Spanish).

Lamptey, S., Yeboah, S., Li, L. & Zhang, R. 2017. *Agronomy Research* **15**(4), 1646–1658.

Lewis, M.C. 1972. The physiological significance of variation in leaf structure. *Science Progress*, pp. 25–51.

Li, H., Tang, C. & Xu, Z. 2013. The effects of different light qualities on rapeseed (Brassica napus L.) plantlet growth and morphogenesis in vitro. *Scientia Horticulturae. Amsterdam* **150**, 117–124.

Lintermann, B. & Deussen, O. 1999. Interactive modeling of plants, *IEEE Computer Graphics and Application*. vol. **19**, 56–65.

Lizaso, J.I., Batchelo,r, W.D. & Westgate, M.E. 2003. A leaf area model to simulate cultivar–specific expansion and senescence of maize leaves. *Field Crops Research* **80**, 1–17.

Loomis, R.S., Williams, W.A. & Duncan, W.G. 1967. Community architecture and the productivity of terrestrial plant communities. New York, USA: *New York Academic*. pp. 291–308.

Long, S.P., Zhu, X.G., Naidu, S.L. & Ort, D.R. 2006. Can improvement in photosynthesis increase crop yields? *Plant Cell and Environment* **29**, 315–30.

Ma, N., Yuan, J., Li, M., Li, J., Zhang, L., Liu, L., Naeem, M.S. & Zhang, C. 2014. Ideotype population exploration: growth, photosynthesis, and yield components at different planting densities in winter oilseed rape (Brassica napus L.) *PLoS ONE* **9**(12), Article ID e114232.

Mazzini, R.B., Ribeiro, R.V. & Pio, R.M. 2010 A simple and nondestructive model for individual leaf area estimation in citrus. *Fruits.* **65**, 269–275.

Maugarny-Cales, A. & Laufs, P. 2018. Getting leaves into shape: a molecular, cellular, environmental and evolutionary view. *Development* **145**(13), dev161646.

Meinhardt, H. & Gierer, A. 1974. Applications of a Theory of Biological Pattern Formation Based on Lateral Inhibition. *Journal Cell Science* **15**. 321–346.

Mendoza–de Gyves, E., Rouphael, Y., Cristofori, V. & Rosana Mira, F. 2007. A non–destructive, simple and accurate model for estimating the individual leaf area of kiwi (Actinidia deliciosa). *Fruits* **62**, 171–176.

Mendoza–de Gyves E., Cristofori V., Fallovo, C., Rouphael, Y. & Bignami, C. 2008. Accurate and rapid technique for leaf area measurement in medlar (Mespilus germanica L.). *Advances in Horticultural Science* **22**, 223–226.

Merks, R.M., Guravage, M., Inze, D. & Beemster, G.T. 2011. VirtualLeaf: an open– ´ source framework for cell–based modeling of plant tissue growth and development. *Plant physiology* **155**(2), 656–666.

Milla, R. & Reich, P.B. 2007. The scaling of leaf area and mass: The cost of light interception increases with leaf size. *Proceedings of the Royal Society B: Biological Sciences* **274**, 2109–2114.

Montero, F.J., de Juan, J.A., Cuesta, A. & Brasa, A. 2000. Nondestructive methods to estimate leaf area in Vitis vinifera L. *Horticultural Science* **35**, 696–698.

Morrison, M.J. & Stewart, D.W. 1995. Radiation-use efficiency in summer rape. *Agronomy Journal* **87**(6), 1139.

Motulsky, H. & Christopoulos, A. 2003. *Fitting models to biological data using linear e nonlinear regression: a pratical guide to curve fitting*. San Diego: *GraphPad Software*, 351 pp.

Mullen, J.L., Weinig, C. & Hangarter, R.P. 2006. Shade avoidance and the regulation of leaf inclination in Arabidopsis. *Plant Cell and Environment* **29**, 1099–106.

Nakayama, H., Nakayama, N., Nakamasu, A., Sinha, N. & Kimura, S. 2012. Toward elucidating the mechanisms that regulate heterophylly. *Plant Morphology* **24**, 57–63.

Nakayama, H., Sinha, N.R. & Kimura, S. 2017. How do plants and phytohormones accomplish heterophylly, leaf phenotypic plasticity, in response to environmental cues. *Frontiers in Plant Science* **8**, 1717.

Nam, Y., Hwang, E. & Kim, D. 2008. A similarity–based leaf image retrieval scheme: joining shape and venation features. *Computer Vision and Image Understanding* **110**(2), 245–59.

Nanda, R., Bhargava, S.C. & Rawson, H.M. 1995. Effect of sowing date on rates of leaf appearance, final leaf numbers and areas in Brassica campestris, B. juncea, B. napus and B. carinata. *Field Crops Research* **2**(2–3), 125–134.

Nicotra, A.B., Cosgrove, M.J., Cowling, A., Schlichting, C.D. & Jones, C.S. 2008. Leaf shape linked to photosynthetic rates and temperature optima in South African Pelargonium species. *Oecologia* **154**, 625–635.

Nicotra, A.B., Leigh, A., Boyce, C.K., Jones, C.S., Niklas, K.J., Royer, D.L. & Tsukaya, H. 2011. The evolution and functional significance of leaf shape in the angiosperms. *Functional Plant Biology* **38**, 535–552.

Olfati, J.A., Peyvast, G.H., Shabani, H. & Nosratie–Rad, Z. 2010. An estimation of individual leaf area in cabbage and broccoli using non–destructive methods. *Journal of Agricultural Science and Technology* **12**, 627–632.

Parsons, P.A. 1992. Fluctuating asymmetry: a biological monitor of environmental and genomic stress. *Heredity* **68**(4), 361–364.

Paul, N.K. 1980. *Environmental effects on growth and development of Brassicae*. Ph.D. Thesis. University of Wales. U. K. pp. 62–72.

Pecham, P.A. & Morgan, D.G. 1985. Defoliation and its effects on pod and seed development in oil seed rape (*Brassica napus* L.). *Journal of Experimental Botany* **36**, 458–468.

Peksen, E. 2007. Non-destructive leaf area estimation model for faba bean (Vicia faba L.). *Scientia Horticulturae* **113**(4), 322–328.

Pérez-Pérez, J.M., Esteve–Bruna, D. & Micol, J.L. 2010. QTL analysis of leaf architecture. *Journal Plant Research* **123**(1), 15–23.

Pivoshenko, I.M. 1997. *Climate of Vinnytsia region*. Vinnytsia: OJSC Vinoblprint, 240 pp. (in Russian).

Pompelli, M.F., Antunes, W.C., Ferreira, D.T.R.G., Cavalcante, P.G.S., Wanderley-Filho, H.C.L. & Endres, L.2012. Allometric models for non–destructive leaf area estimation of Jatropha curcas. *Biomass and Bioenergy* **36**, 77–85.

Prusinkiewicz, P. 2004. Modeling plant growth development. *Current Opinion in Plant Biology* **7**, 79–83.

Pugnaire, F.I. & Valladares, F. eds. 2007. *Functional plant ecology*. 2nd edn. Boca Raton: CRC Press/Taylor & Francis Group. 724 pp.

Rabotnov, T.A. 1978. *Phytocenology*. Moscow Publishing House Univ., Moscow, 384 pp. (in Russian).

Ramensky, L.G. 1971. *Problems and methods of studying the vegetation cover*. Selected works. Nauka, Leningrad, 426 pp. (in Russian).

Ramesh, K., Ramawat, N. & Singh, V. 2007. Leaf area distribution pattern and non–destructive estimation methods of leaf area for Stevia rebaudiana (Bert) Bertoni. *Asian Journal of Plant Sciences* **6**(7), 1037–1043.

Richter, G.L., Zanon, J.A., Streck, N.A., Guedes, J.V.C., Kräulich, B., Rocha, T.S.M. da, Winck, J.E.M. & Cera, J.C. 2014. Estimating leaf area of modern soybean cultivars by a non-destructive method. *Bragantia*, v.**73**, 416–425 (in Spanish).

Rivera, C.M., Rouphael, Y., Cardarelli, M. & Colla, G. 2007. A simple and accurate equation for estimating individual leaf area of eggplant from linear measurements. *European Journal of Horticultural Science* **72** (5), 228–230.

Robbins, S.N. & Pharr, D.M. 1987. Leaf area prediction models for cucumber from linear measurements. *HortScience* **22**, 1264–1266.

Rosa, L.M. & Forseth, I.N. 1995. Diurnal patterns of soybean leaf inclination angles and azimuthal orientation under different levels of UVb radiation. *Agricultural and Forest Meteorology* **78**, 107–19.

Rouphael, Y., Rivera, C.M., Cardarelli, M., Fanasca, S. & Colla G. 2006. Leaf area estimation from linear measurements in zucchini plants of different ages. *Journal of Horticultural Science and Biotechnology* **81**, 238–241.

Rouphael, Y., Colla, G., Fanasca, S. & Karam, F. 2007. Leaf area estimation of sunflower leaves from simple linear measurements. *Photosynthetica* **45**, 306–308.

Rouphael, Y., Mouneimne, A.H., Ismail, A., Mendoza-de Gyves, E., Rivera, C.M. & Colla, G. 2010a. Modeling individual leaf area of rose (Rosa hybrida L.) based on leaf length and width measurement. *Photosynthetica* **48**, 9–15.

Rouphael, Y., Mouneimne, A.H., Rivera, C.M., Cardarelli, M., Marucci, A. & Colla, G. 2010b. Allometric models for non–destructive leaf area estimation in grafted and ungrafted watermelon (Citrillus lanatus Thunb.). *Journal of Food, Agriculture and Environment* **8**, 161–165.

Ro´zyło, K. & Pałys, E. 2014. New oilseed rape (Brassica napus L.) varieties–canopy development, yield components and plant density," Acta Agriculture a Scandinavica Section B–Soil. *Plant Science* **64**(3), 260–266.

Runions, A., Fuhrer, M., Lane, B., Federl, P., Rolland–Lagan, A.–G. & Prusinkiewicz, P. 2005. Modeling and visualization of leaf venation patterns. Generate ACM *Transactions on Graphics journal* **24**, 702–711.

Saiko, V.F., Kaminsky, V.F., Vishnevsky, P.S. [and others]. 2011. *Features of research with oilseeds cruciferous*, 76 pp. (in Ukrainian).

Salerno, A., Rivera, C.M., Rouphael, Y., Colla, G., Cardarelli, M., Pierandrei, F., Rea, E. & Saccardo, F. 2005. Leaf area estimation of radish from simple linear measurements. *Advances in Horticultural Science* **19**, 213–215.

Schoonjans, F. 2019. *Digimizer manual: Easy–to–use image analysis software*. Independently Published, 108 pp.

Schultz, H.R. 1992. An empirical model for the simulation of leaf appearance and leaf area development of primary shoots of several grapevine (Vitis vinifera L.) canopy-systems. *Scientia Horticulturae. Amsterdam* **52**, 179–200.

Schurr, U., Heckenberger, U., Herdel, K., Walter, A. & Feil, R. 2000. Leaf development in Ricinus communis during drought stress: dynamics of growth processes, of cellular structure and of sink–source transition. *Journal of Experimental Botany* **51**(350), 1515–1529.

Semiarti, E., Ueno, Y., Tsukaya, H., Iwakawa, H., Machida, C. & Machida, Y. 2001. The asymmetric leaves gene of Arabidopsis thaliana regulates formation of a symmetric lamina, establishment of venation and repression of meristem–related homeobox genes in leaves. *Development* **128**, 1771–1783.

Serdar, Ü. & Demirsoy, H. 2006. Non–destructive leaf area estimation in chestnut. *Scientia Horticulturae* **108**, 227–230.

Seetseng, K.A., Gerrano, A.S., Mavengahama, S., Araya, H.T. & Du Plooy, C.P. 2020. Influence of fertilizer application on biomass yield and nutritional quality of Mustard Spinach (Florida) Broadleaf in South Africa. *Agronomy Research* **18**(1), 256–266.

Sharma, A.K. 2005. *Text Book of Correlations and Regression*. Discovery Publishing House, 212 pp.

Sheskin, D.J. 2007. *The Handbook of Parametric and Nonparametric Statistical Procedures*. Chapman & Hall/CRC. 1707 pp.

Shi, P., Zheng, X., Ratkowsky, D.A., Li, Y., Wang, P. & Cheng, L. 2018. A simple method for measuring the bilateral symmetry of leaves. *Symmetry* **10**. 118.

Smith, W.K., Vogelmann, T.C., DeLucia, E.H., Bell, D.T. & Shepherd, K.A. 1997. Leaf form and photosynthesis: Do leaf structure and orientation interact to regulate internal light and carbon dioxide? *BioScience* **47**, 785–793.

Stefanowska, M., Kuraś, M., Kubacka-Zębalska, M. & Kacperska, A. 1999. Low temperature affects pattern of leaf growth and structure of cell walls in winter oilseed rape (Brassica napus L., var. oleifera L.). *Annals of Botany* **84**(3), 313–319.

Stewart, D.W. & Dwyer, L.M. 1999. Mathematical characterization of leaf shape and area of maize hybrids. *Crop Science* **39**(2), 422–427.

Stoppani, M.I., Wolf, R., Francescangeli, N., Martí, H.R., 2003 A nondestructive and rapid method for estimating leaf area of broccoli. *Advances in Horticultural Science* **17**(3), 173–175.

Tartaglia, F.L., Righi, E.Z., Rocha, L., Loose, L.H., Maldaner, I.C. & Heldwein, A.B. 2016. Non–destructive models for leaf area determination in canola. *Revista Brasileira de Engenharia Agrícola e Ambiental* **20**(6), 551–556.

Terashima, I. & Hikosaka, K. 1995. Comparative ecophysiology of leaf and canopy photosynthesis. *Plant Cell and Environment* **18**, 1111–1128.

Terashima, I., Miyazawa, S.–I. & Hanba, Y.T. 2001. Why are sun leaves thicker than shade leaves? Consideration based on analyses of CO2 diffusion in the leaf. *Journal Plant Research* **114**, 93–105.

Test Guidelines for the conduct of tests for distinctness. uniformity and stability of Fodder Radish (Raphanus sativus L. var. oleiformis Pers.). Geneva. 2017. 19 p.

Thurling, N.W. 1974. Morphophysiological determinants of yield in rapeseed (Brassica campestris and B. napus) I. Growth and morphological characters. *Australian Journal of Agricultural Research* **25**(6), 700–710.

Tsialtas, J.T. & Maslaris, N. 2005. Leaf area estimation in a sugar beet cultivar by linear models. *Photosynthetica* **43**, 477–479.

Tsialtas, J.T. & Maslaris, N. 2008. Leaf area prediction model for sugar beet (Beta vulgaris L.) cultivars. *Photosynthetica* **46**(2), 291–293.

Tsukaya, H. 2003. Organ shape and size: a lesson from studies of leaf morphogenesis. *Current Opinion in Plant Biology* **6**(1), 57–62.

Tsytsiura, Y.H. 2019. Evaluation of the efficiency of oil radish agrofitocenosis construction by the factor of reproductive effort. *Bulgarian Journal of Agricultural Science* **25**(6), 1161–1174.

Uzun, S. & Celik, H. 1999. Leaf area prediction models (Uzcelik–I) for different horticultural plants. *Turkish Journal of Agriculture and Forestry* **23**, 645–650.

Watanabe, T., Hanan, J.S., Room, P.M., Hasegawa, T., Nakagawa, H. & Takahashi, W. 2005. Rice morphogenesis and plant architecture: Measurement, specification and the reconstruction of structural development by 3d architectural modelling. *Annals Botany* **95**, 1131–43.

Weraduwage, S.M., Chen, J., Anozie, F.C., Morales, A., Weise, S.E. & Sharkey, T.D. 2015. The relationship between leaf area growth and biomass accumulation in Arabidopsis thaliana. *Frontiers in Plant Science* **6**, 167.

Willmott, C.J., Ackleson, S.G., Davis, J.J., Feddema, K.M. & Klink, D.R. 1985. Statistics for the evaluation and comparison of models. *Journal of Geophysical Research* **90**, 8995–9005.

Willmott, C.J., Robeson, S.M. & Matsuura, K. 2012. A refined index of model performance. *International Journal of Climatology* **32**, 2088–2094.

Wofford, T.J. & Allen, F.L. 1982. Variation in leaflet orientation among soybean cultivars. *Crop Science* **22**, 999–1004.

Wright, I.J., Dong, N., Maire, V., Prentice, C., Westoby, M., Díaz, S., Gallagher, R.V., Jacobs, B.F., Kooyman, R., Law, E.A., Leishman, M.R., Niinemets, Ü., Reich, P.B., Sack, L., Villar, R., Wang, H. & Wilf, P. 2017. Global climatic derivers of leaf size. *Science* **357**, 917–921.

Yamaguchi, T, Nukazuka, A & Tsukaya, H. 2012. Leaf adaxial-abaxial polarity specification and lamina outgrowth: evolution and development. *Plant* & *Cell Physiology* **53**(7), 1180–94.

Zanetti, S., Pereira, L.F.M., Sartori, M.M.P. & Silva, M.A. 2017. Leaf area estimation of cassava from linear dimensions. *Annals of the Brazilian Academy of Sciences* **89**(3), 1729–1736.

Agronomy Research **18**(3), 2245–2258, 2020
https://doi.org/10.15159/AR.20.172

The influence of amino acids on the activity of antioxidant enzimes, malonic dialdehyde content and productivity of garlic (*Allium Sativum* L.)

O. Ulianych[1], V. Yatsenko[1,*], P. Kondratenko[2], O. Lazariev[1], L. Voievoda[1], O. Lukianets[1] and D. Adamenko[1]

[1]Uman National University of Horticulture, Faculty of Horticulture, Ecology and Plants Protection, Department of Vegetable Growing, Department of Plant Protection and Quarantine, Faculty of Management, Department of Ukrainian and Foreign Languages, Instytutska street, 1, UA20300 Uman, Ukraine
[2]The National Academy of Agrarian Sciences, Mykhayla Omelyanovycha-Pavlenka street, 9, UA01010 Kyiv, Ukraine
[*]Correspondence: slavikskavin16@gmail.com

Abstract. The research was carried out in 2017–2019 in the conditions of the Right-Bank Forest Steppe of Ukraine. The results of study, the effect of spraying by certain amino acids; salicylic(300 ppm), gibberellin (150 ppm) and ascorbic acids (200 ppm) on garlic (*Allium sativum* L.) plants are presented in the article. It was found that amino acid solutions improves the antioxidant state: the activities of SOD, CAT, POD, GR, GST in treated leaves tended to increase, the activity of SOD was higher than the control of 7.5–15.0%; CAT (27.4–45.9%); POD (7.0–83.0%); GR (5.4–49.9%); and GST (14.8–41.3%). It was noted that the content of chlorophyll *a+b* in the leaves significantly increased (2.6–10.8%), The use of amino acids increased the accumulation of dry matter by 1.4–4.0%. The yield increase was 1.14–2.27 t ha^{-1} (7.7–15.3% compared to control). The content of B vitamins in the garlic cloves was greatly influenced by gibberellic acid, where increasing the amount of B vitamins reached to 21.9% relative to control The use of salicylic and ascorbic acids increased the amount of B vitamins by 7.6 and 8.2%, respectively. The most significant increasing of C vitamin content was observed by spraying of plants with ascorbic acid (+12.5%), whereas by spraying with salicylic and gibberellic acids its content increased by 6.0 and 7.5%, respectively. In the future, the data obtained can be used to reduce the impact of abiotic factors on the physiological state and productivity of garlic plants. Also, the obtained data will serve as a theoretical basis for producers in view of the purposes for which the products are grown (for sale in fresh form, processing or storage).

Key words: *Allium sativum* L., antioxidant enzyme activity, bulb, chlorophyll, vitamins, yield.

INTRODUCTION

One of the important goals of modern agriculture is to get foods that are high in vitamins. The productivity of plants depends on the environmental conditions. Water scarcity is a major limiting factor in crop production under the continental climate and

therefore, there is a constant problem of increasing the drought resistance of vegetables. One possibility to improve the drought resistance of cultivated crops is amino acids, which have a direct or indirect effect on physiological processes. In addition, amino acids are well known as biostimulants that have a positive effect on plant growth, yield and they significantly reduce plant stress caused by abiotic factors (El-Shabasi et al., 2005; Kowalczyk & Zielony, 2008; Abd El-Aal et al., 2010).

Drought is one type of oxidative stress that, at the cellular level, enhances the generation of active oxygen species (AOS), such as superoxide radicals (O_2^-), hydrogen peroxide (H_2O_2) and hydroxyl radicals (OH). Plants have developed different enzymatic and non-enzymatic scavenging mechanisms to control the level of AOS. Superoxide radicals can be converted to hydrogen peroxide enzymatically by superoxide dismutases (SOD). Cellular hydrogen peroxide is removed by catalase (CAT) enzymes and other enzymatic defence systems e.g. ascorbate peroxidase (APX) and other peroxidases. The level of antioxidants and the activities of antioxidant enzymes such as H_2O_2 related SOD, CAT, APX, guaiacol peroxidase (POD), and glutathione related enzymes (glutathione reductase, GR and glutathione S-transferase, GST) are generally increased in plants under stress conditions and in several cases their activities correlate well with enhanced tolerance (Prasad et al., 1994; Foyer et al., 1997).

Salicylic acid is a natural plant hormone and participates in plant responses to various biotic and abiotic factors (Shama et al., 2016). It plays a vital role in plant growth, ion uptake transport, and photosynthesis (Kazemi, 2013) as well as Salicylic acid has a diverse regulatory role in plant metabolism.

Salicylic acid an organic signal molecule has been reported to play a key part in regulating many physiological processes in plants. Its external application has encouraged plant productivity under biotic and abiotic stress conditions (Senaratna et al., 2000). Foliar spray of salicylic acid has been shown to increase vegetative growth, yield and bulb quality of garlic (Bardisi, 2004a and 2004b), Amin et al. (2007) on onion, El-Zohiri (2009) on globe artichoke and Bideshki et al. (2013), Khadr (2015) on garlic, Pradhan et al. (2016) and Prajapati et al. (2016) on onion, Shama et al. (2016) and Meena et al. (2017) on garlic.

The foliar application of salicylic acid promoted growth and development of plants. In this regard (Li et al., 2000), salicylic acid has been found to play an important role in bulb formation. Khadr (2015) specified that spraying of garlic plants by salicylic acid gave the highest indices of plant height, total crude and dry weights, and leaf area. In addition, the highest yields were achieved, and the total content of chlorophyll ($a+b$) increased.

Gibberellic acid (GA_3) plays an important role in the formation of garlic bulbs (Rahim, 1988 and Rahim & Forhad, 1988). Foliar spraying by gibberellic acid stimulates the formation of more cloves in the bulb. Gibberellic acid improves the growth and development of chloroplasts and enhances the efficiency of photosynthesis, which in turn increases yields (Yuan & Xu, 2001). On the basis of experiment Kumar et al. (2014), it is concluded that, gibberellic acid had significant influence on growth, quality and yield of tomato, application of GA_3 showed an increased plant height, number of leaves, number of fruits, fruit weight, ascorbic acid and total soluble solids.

Ascorbic acid exerts a stimulating effect on plants, for example, its use has led to a significant increase in the growth parameters and overall yield of tomatoes in the cold season (Abdel-Halim, 1995). Similar results were found in other plants (Helal et al., 2005; El-Banna et al., 2006).

Ascorbic acid (AA) is an antioxidant molecule and a key substrate for the detoxification of reactive oxygen entities (Foyer & Noctor, 2011; Qian et al., 2014). Physiologically active form of AA is the resonance stabilized anionic form (formed due to deprotonation of the hydroxy group at C_3) which is termed as ascorbate.

Foliar application of ascorbic acid previously increased plant height, leaves number, dry weight of plant and total yield (El-Morsy et al., 2010) on garlic and (Gouda et al., 2015) on potato, and increased bulbing ratio as well as average bulb weight and diameter and clove weight (El-Morsy et al., 2010) on garlic.

Garlic is the second most common species of the Onion Family after onion. It has long been recognized around the world as a valuable condiment for food and a popular remedy for various ailments and physiological disorders. Garlic is also considered to be one of the most important medicinal plants that have broad nutritional properties. (Petropoulos et al., 2018).

In review of all the above, it follows that these amino acids have been studied separately or in certain combinations in different natural conditions, but their effect on the physiological state of plants, productivity and storage of garlic has not been studied and did not compare with each other. Therefore, the comparison of the effect of salicylic, gibberellin and ascorbic acids on plant growth and yield, oxidative state, total content of chlorophylls $a+b$ in the leaves, B vitamins and C vitamin content in the bulb became the purpose of the study.

MATERIAL AND METHODS

The research of the influence of amino acids was carried out in 2017–2019 in the conditions of the Right-Bank Forest Steppe of Ukraine on the experimental field of the Department of Vegetable Growing of Uman National University of Horticulture in accordance with generally accepted methods (Bondarenko & Yakovenko, 2001; Ulianych et al., 2019; 2020). The soil of the experimental field is black, puddle, heavy loam with a well developed humus horizon (about 2.9% of humus) in the deep of 40–45 cm. Planting was carried out by the scheme of 45×6 cm at the end of the 5–10 of October.

The total area: for the experiment 400 m², for plot 100 m²; for sampling 10 m². The plots were arranged in a systematic order with a four replication. The location of the plots was systemic.

Plant spraying was carried out after 40 and 50th DAP. In the conditions of the Right-Bank Forest Steppe of Ukraine after 40 and 50th DAP there is an intensive growth of the vegetative mass of garlic plants and it is during this period that the last spring frosts - abiotic stress.

Single factor experiment consisted of foliar spraying salicylic acid (SA) - $C_6H_4(OH)COOH$ (300 ppm) (Shama et al., 2016) gibberellic acid (GA_3) - $C_{19}H_{22}O_6$ (150 ppm) (Abd-Elkader, 2016), and ascorbic acids (AA) - $C_6H_8O_6$ (200 ppm) (Naz et al., 2016) as well as control treatment (foliar spraying with water).

This experiment included the following treatments:

1. Control (foliar spraying with water).
2. Salicylic acid (SA) at 300 ppm.
3. Gibberellic acid (GA_3) at 150 ppm
4. Ascorbic acid (AA) at 200 ppm.

During the investigation, parameters including length and width of leaf, leaf blade area and total leaf area per plant on the 60th day after planting (DAP) were determined, plant height and the number of leaves (per plant, pcs) were calculated by, and the leaf blade area was determined by a calculated (linear) method, using the parameters of length and width of the leaf by the formula:

$$Sn = 0.67 \times ab \quad (1)$$

where Sn – one leaf area, cm²; a – the largest leaf width, cm; b – leaf length, cm; 0.67 is the coefficient that reflects the configuration of the leaf.

We studied the effect of spraying plants by amino acids on enzymes activity, productivity of plants, pigments contents in leaf, vitamins B complex and vitamin C of garlic cloves, and storability.

Plant material

Garlic (*Allium sativum* L.) cv. Lyubasha.

Assimilating pigments content were determined by spectrophotometric method (Ermakova et al., 1987).

Activity measurements of antioxidant enzymes

Enzyme activities were determined, 10 days after spraying plants by organic acids solutions. A one g of plant tissue from control and treated plants was homogenized on ice in 4 mL extraction buffer (50mM phosphate buffer pH 7.0, containing 1mM EDTA, 1mM phenylmethylsulfonyl fluoride and 1% polyvinylpolypirrolidone). The homogenate was centrifuged for 25 min at 15,000×g and 4 °C. The supernatant was used for enzyme activity assays. The means ± SD were calculated from the data of at least 3 independent measurements. SOD activity was determined spectrophotometrically by measuring the ability of the enzyme to inhibit the photochemical reduction of nitro blue tetrazolium (NBT) in the presence of riboflavin in light (Dhindsa et al., 1981). One unit (U) of SOD was the amount that causes 50% inhibition of NBT reduction in light. The enzyme activity was expressed in terms of specific activity (U mg protein^{-1}). CAT activity was determined by the decomposition of H_2O_2 which, in turn, was measured by the decrease in absorbance at 240 nm (Upadhyaya et al., 1985). One U equals the amount of H_2O_2 (in μmol) decomposed in 1 min. POD activity was determined by monitoring the increase in absorbance at 470 nm during the oxidation of guaiacol (Upadhyaya et al., 1985). The amount of enzyme producing 1 μmol min^{-1} of oxidized guaiacol was defined as 1 U. GR activity was determined by measuring the absorbance increment at 412 nm when 5.5 dithiobis(2–nitrobenzoic acid) (DTNB) was reduced by GSH, generated from glutathione disulfide (GSSG) (Smith et al., 1988). The specific activity was calculated as the amount of reduced DTNB, in μmol min^{-1} protein mg, ε_{420} = 13.6mM cm^{-1}. GST activity was determined spectrophotometrically by using an artificial substrate, 1-chloro-2.4-dinitrobenzene (CDNB), according to Habig et al. (1974). One U is the amount of enzyme producing 1 μmol conjugated product in 1 min, ε_{340} = 9.6 mM^{-1} cm^{-1}. The protein contents of the extracts were determined by the method of Bradford (1976).

Malondialdehyde (MDA) content

MDA content was calculated, taking into account optical density of the sample and its corresponding dilutions under the coefficient of micro molar absorption TBA $\varepsilon = 155\ \mu M\ cm^{-1}$ at the wave length 532 nm and was expressed in $\mu mol\ g^{-1}$ of raw substance. Intensity of oxidative stress was evaluated by the reaction of POL by the accumulation of a final product of peroxide oxidation of lipids malondialdehyde (MDA), by the reaction with thiobarbituric acid (TBA) at 532 nm on spectrophotometer LEKI SS1104 according to the technique (Rogozhin, 2006; Karpenko et al., 2019). The method is based on determining the amount of a coloured product at the wave length 532 nm, obtained as the result of interaction of 2 molecules of TBA with one molecule of MDA as one of the by–products of POL. For this purpose, a 1 g of leaves tissue was homogenized with 3 mL of 50% ethanol and centrifuged 10 min at 7,000 rpm. A 0.5 mL of 1% triton X-100 solution, 0.2 mL of 0.6 M HCl and 0.8 mL 0.06 M of TBA were added to the obtained 0.5 mL of supernatant and heated in the boiling water bath (100 °C) for 10 min and then cooled to 15 °C for 30 min and added 0.2 mL 5 mM solution of Trilon B and 5–10 mL of 96% ethanol. As a control served testtube in which all chemical reagents except TBA were added. MDA content was calculated, taking into account optical density of the sample and its corresponding dilutions under the coefficient of micro molar absorption TBA $\varepsilon = 155\ \mu M^{-1}\ cm^{-1}$ at the wave length 532 nm and was expressed in $\mu mol\ g^{-1}$ of raw substance.

Bulb dry matter (%)

The average dry matter weight (g) of bulbs after curing were measured by drying 10 randomly sampled bulbs in an oven with a forced hot air circulation at 70 °C until a constant weight was obtained. The percentage of bulb dry matter was calculated by taking the ratio of the dry weight to the fresh weight of the sampled bulbs and multiplying it by 100.

Determination of content of vitamins B complex

A weight 50 g was cut into small pieces and extracted with 0.1 NHCL (sodium chloride) on the water bath at suitable temperature and time period. All extracts were filtered through 0.40 micron filter and taken into 100 mL volumetric flask which was added up for mobile phase.

The standard preparation: stock of standard (Sigma Aldrich Analytical grade Reagent) prepared by dissolving 0.01 g of each standard in 100 mL of mobile phase followed by successive dilutions.

High-performance liquid chromatography (HPLC)

Analysis of HPLC (Shimadzu, Model Prominence 20A) equipped with UV detector and Supelco Discovery Cis18 column (25-cm in length and 0.45-cm internal diameter) was used. Mobile phase was 50 m MK_2HPO_4 and MeOH (70:30) at 1 mL min^{-1} flow rate and 10 µL of each sample/standard was injected and monitored at UV 254 nm.

Analysis of vitamin C

Lyophilized samples (each 0.2 g) were ground and added to 30 mL of 3% metaphosphoric acid solution and homogenized at 11,000 rpm for 2 min using a T25 basic ULTRA–TURRAX homogenizer (IKAWerke GmbH & Co. KG, Staufen,

Germany). The volume was made up to 50 mL with 3% metaphosphoric acid solution. The extract (2 mL) was centrifuged at 12,000 rpm for 3 min, and the supernatant filtered through a 0.45 lm polyvinylidene difluoride (PVDF) membrane filter (Whatman I nternational Ltd., Maidstone, UK). All samples were immediately analyzed using an HPLC system, equipped with a PU (2089 pump), an AS (2057 auto injector), and a MD (2010 UV) vis variable wavelength detector (JASCO Corp., Tokyo, Japan). Separation was carried out in a Crest Pak C18S column (15094.6 mm, i. d., 5 lm, JASCO Corp.), and the isocratic elution was carried out with 0.1% trifluoroacetic acid in distilled water as a mobile phase for 15 min (flow rate 0.8 mL min^{-1}). The peak was read at 254 nm using an UV detector and quantification was determined via external calibration against ascorbic acid.

Statistical analysis

For the food and chemical composition, three samples analyzed were performed in three replicates. The results were expressed as averages. The antioxidant activity, and chemical composition were analyzed using a one-way dispersion analysis, followed by the Tvyxi's Honesty Difference (TQ) Test at $P \leq 0.05$ (for yield and bulb weight), 0.01 (for enzyme activities, pigments content in leaf, vitamins B complex and vitamin C in cloves, dry matter) using statistical analysis program (SAS) v. 9.1.3.

RESULTS

The results of the studies showed that the highest increase in plant height was the best by gibberellic acid, and was higher than the control by 10.8%, whereas the use of salicylic and ascorbic acids increased the height of plants by 7.8 and 3.9%, respectively (Table 1).

The main indicator of growth and the index on which the productivity of garlic plants depends is the leaf apparatus, so we studied it thoroughly. The number of leaves per plant increased by 0.46–0.55 pcs $plant^{-1}$ with the use of gibberellic and ascorbic acids (5.3–6.3% of control), while salicylic acid significantly decreased this indicator by 0.15 pcs plant-1 (1.7% of control), while the leaf area increased by 8.3; 27.7 and 4.8% by the use of salicylic, gibberellic and ascorbic acids, respectively. The leaf area/plant and the leaf index had slightly different dynamics, but gibberellic acid showed the best results.

Table 1. Plant height and leaf area of garlic plant (average 2017–2019)

Variant	Plant height (cm)	Number of leaves (pcs)	Leaf area (cm^2)	Leaf area index (LAI)
Control	63.37	8.73	95.70	1.82
Salicylic acid	68.33*	8.58	103.63*	1.94
Gibberellic acid	70.21*	9.28*	122.20*	2.47*
Ascorbic acid	65.86	9.19*	100.25	2.00*
LSD (0.05)	3.45	0.40	6.06	0.14

Means bearing same * in each column are statistically similar at $p \leq 0.05$.

Plants were treated by amino acids, increased the amount of chlorophylls (a + b), but with the use of gibberellic acid, the increase was the most significant (0.17% /dry matter which equal to 10.8% increase compared to control) (Fig 1).

It is known that the impact of unfavourable factors affects the status of oxidative stress (OS). Amino acids activate protective mechanisms and reduce the oxidative stress in plant chloroplasts under stress. According to obtained data in this study, spraying of garlic plants (*Allium sativum* L.) with the amino acids reduced the impact of the oxidative stress caused by adverse weather conditions (Fig 2).

In plants which have been treated with GA and SA, Malondialdehyde (MAD) contents decreased by 16.7 and 16.5%, respectively. Under the influence of AA, MAD content decreased by 11.7% (Fig. 2).

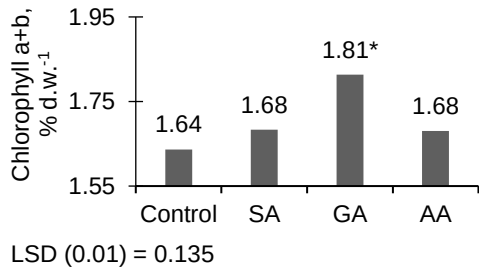

Figure 1. Leaf's total chlorophyll (*a*+*b*) content of the garlic plant (average 2017–2019).
(Means bearing same * in each column are statistically similar at $p \leq 0.01$).

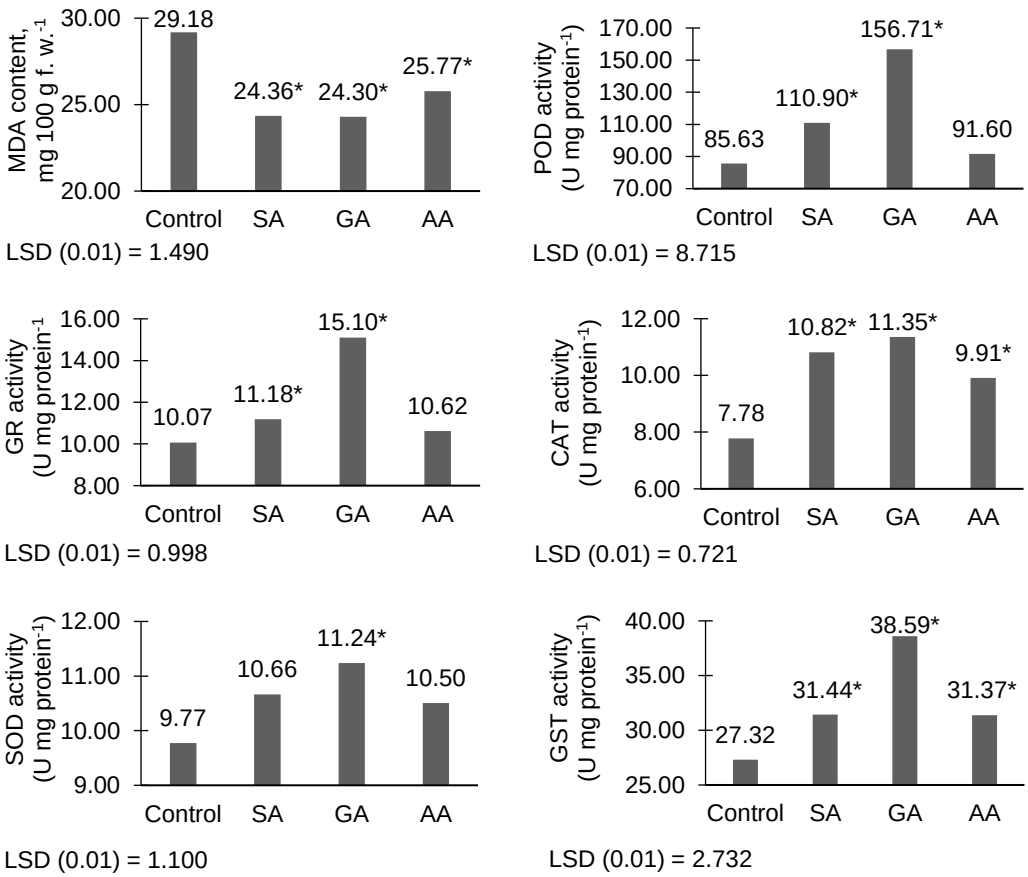

Figure 2. Malondialdehyde content and antioxidant enzyme activity in leaves of the garlic plant (average 2017–2019).
(Means bearing same * in each column are statistically similar at $p \leq 0.01$).

In plants treated by salicylic, gibberellin and ascorbic acids, increases in SOD activity were recorded, 9.1; 15.0 and 7.5% compared to the enzyme activity in the control variant. The use of amino acids ensured the activation of a complex of antioxidant enzymes (Fig. 2).

The activities of SOD, CAT, POD, GR, and GST in leaves treated by amino acids of garlic plants tended to increase (Fig. 2). Thus, SOD activity increses were 7.5–15.0%, CAT (27.4–45.9%); POD (7.0–83.0%); GR (5.4–49.9%) and GST (14.8–41.3%) higher than the control.

The results of the study indicated a significant effect of amino acids on the yield and its structure (Tables 2, 3; Fig. 3). So, the weight of the bulb and the dry matter content, vitamins B and vitamin C, had the best performance in all variants compared to control. The bulb weight increased by 4.73; 9.26 and 4.55 g (LSD (0.05) = 4.05) by the use of salicylic, gibberellic and ascorbic acids, respectively (Table 2).

Table 2. Weight of garlic bulbs (g) (average 2017–2019)

Variant	Weight of bulbs, g			
	2017	2018	2019	Average
Control	59.85	55.27	71.57	62.23
Salicylic acid	64.56*	61.01*	75.30	66.96*
Gibberellic acid	68.93*	65.14*	80.40*	71.49*
Ascorbic acid	64.39	60.85*	75.10	66.78*
LSD (0.05)	3.26	2.95	5.76	4.05

Means bearing same * in each column are statistically similar at $p \leq 0.05$.

The yield growth had the same dynamics. By using salicylic, gibberellic and ascorbic acids, the yield of garlic increased by 1.18; 2.27 and 1.14((LSD (0.05) = 0.89) (Table 3).

Table 3. Yield (t ha^{-1}) of garlic (average 2017–2019)

Variant	Yield, t ha^{-1}			Average	Yield, dry matter, t ha^{-1} (average 2017–2019)
	2017	2018	2019		
Control	14.36	13.26	17.0	14.87	4.65
Salicylicacid	15.48*	14.63*	18.06	16.06*	5.15
Gibberellic acid	16.53*	15.62*	19.28*	17.14	5.29
Ascorbic acid	15.44*	14.60*	18.01	16.02*	5.13
LSD (0.05)	0.73	0.86	1.14	0.89	0.91

Means bearing same * in each column are statistically similar at $p \leq 0.05$.

However, the solids contents of garlic bulbs (dry matter), at the highest amino acid utilization occurred by SA (+2.6%) followed by ascorbic acid (+ 2.5%) of the control. Gibberellic acid did not cause increase in dry matter (Fig. 3).

The study of the content of vitamins B_6 (Fig. 4) in garlic cloves showed that the best effect on their accumulation was by gibberellic acid, where the increase in the amount of vitamins B reached to 21.9% of control.

The use of salicylic and ascorbic acids increased their amounts to 7.6 and 8.2%, respectively.

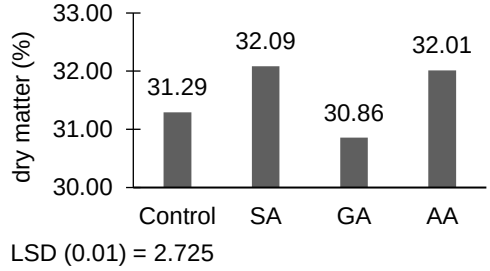

Figure 3. Bulb's dry matter content (average 2017–2019).

(Means bearing same * in each column are statistically similar at $p \leq 0.05$).

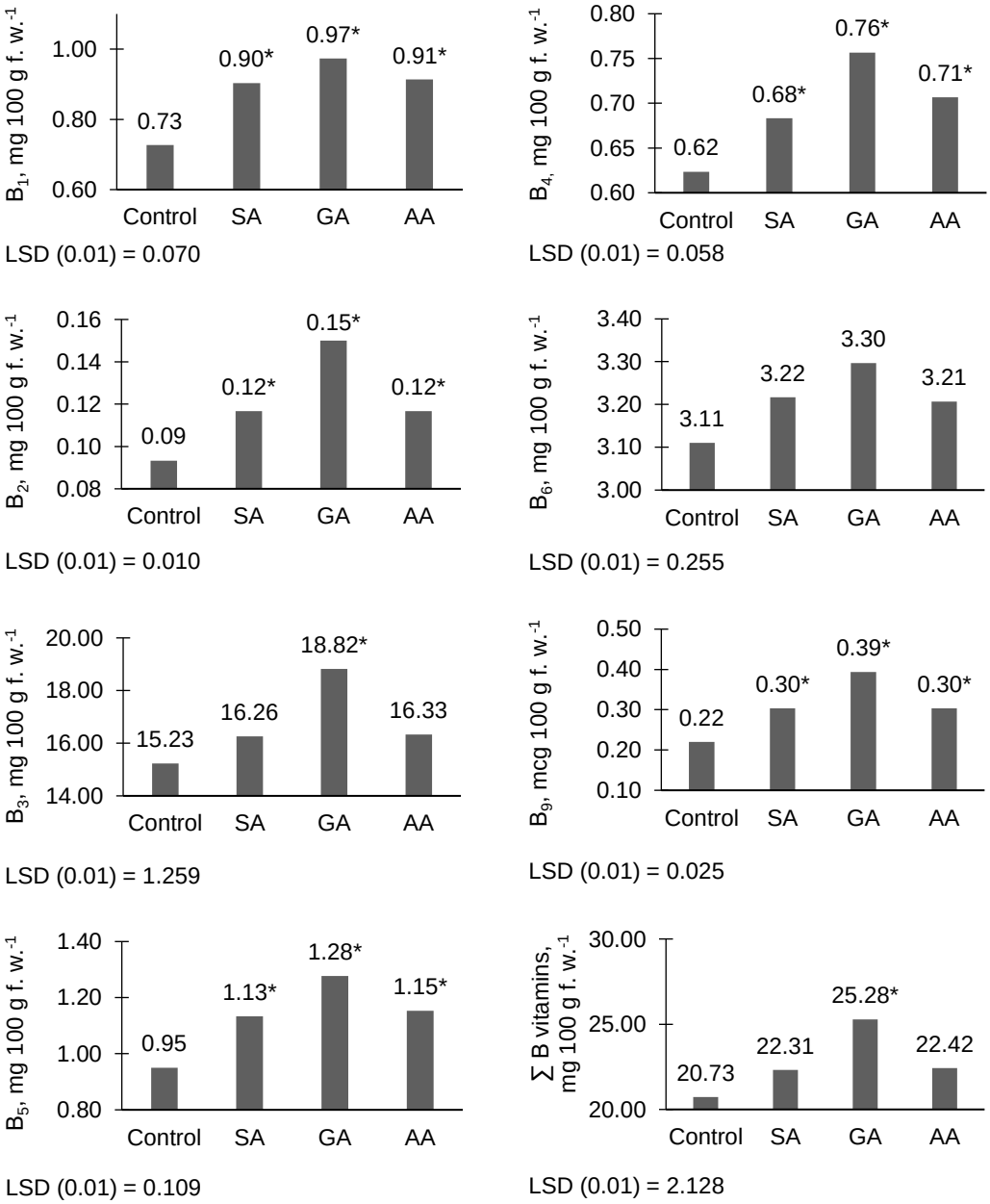

Figure 4. Vitamins B complex content (average 2017–2019).
(Means bearing same * in each column are statistically similar at $p \leq 0.01$).

The most significant increase in vitamin C content was observed for spraying of plants by ascorbic acid (+12.5%of control), whereas for spraying by salicylic and gibberellic acids, its content increased by 6.0 and 7.5%, respectively (Fig. 5).

The maximum weight loss of the bulbs (14.8–18.2%) was observed in the first month of storage, regardless of the variants (Fig. 6).

The percentage of weight loss was steadily increased until 6 months of storage, then, it gradually decreased until the end of storage. Salicylic acid treatment had the most pronounced effect on bulb weight loss during storage, compared to the control and other variants. All other treatments showed smaller percentages of weight loss compared to the control during all storage times(Table 4 and Fig. 6).

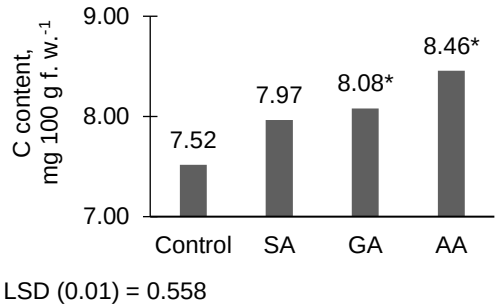

Figure 5. Vitamins C content (average 2017–2019).

(Means bearing same * in each column are statistically similar at $p \leq 0.01$).

Table 4. Bulb weight loss (%) during storage, days after harvest (average 2017–2019)

Variant	days after harvest									∑ weight loss, %
	30	60	90	120	150	180	210	240	270	
	bulb weight loss, %									
Control	18.2	2.2	2.5	2.7	3.0	3.5	3.1	2.6	2.0	39.8
Salicylic acid	14.8*	1.4*	1.6*	1.9*	2.3*	2.6*	2.5*	2.0*	1.3*	30.4*
Gibberellic acid	17.8	1.8*	1.9*	2.2*	2.7*	3.3*	2.8*	2.5	2.5	37.5*
Ascorbic acid	17.3*	1.8*	1.8*	2.1*	2.7*	3.1*	2.6*	2.4*	2.1	35.9*
LSD (0.05)	0.912	0.106	0.108	0.118	0.116	0.169	0.199	0.136	0.076	2.241

Means bearing same * in each column are statistically similar at $p \leq 0.01$.

During the germination of garlic cloves, their marketability is lost. During the storage period, the marketability of garlic bulbs was maintained with the use of GA_3 for up to 140–150 days on average over the years of research.

The use of SA and AA contributed to the extension of the marketability period to 210 days. After 210 days there was a mass germination of cloves. Control bulbs and GK3 germinated after 120 and 140–150 days, respectively. The results of the study indicate that the use of GC3 on garlic crops is impractical if the grown products will be stored for a long time.

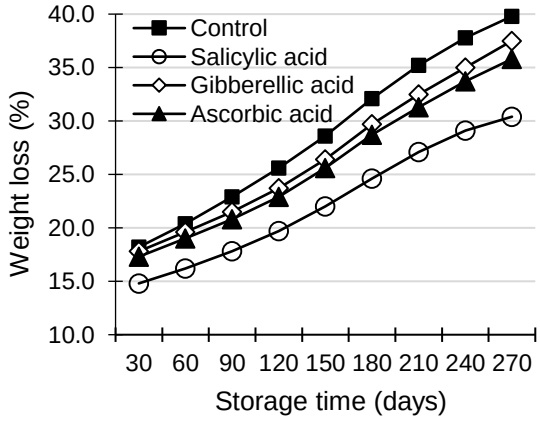

Figure 6. Effect of foliar spray with amino acids on weight loss (%) of garlic during 9 months (270 days) of storage under room temperature (average 2017–2019).

Subsequent storage shows only theoretical data on the weight loss of the bulbs.

DISCUSSION

According to research results, it is followed that the formation of ROS caused significant oxidative destruction in control plant's leaves and bulbs as compared to plants sprayed amino acids. The control plants are characterized by lower antioxidant protection capacity than plants spraying with amino acid.

In multiple studies carried out previously, it has been shown that dehydration of organs induced by drought is the direct sequence of stomatal closure, disorganization of photosynthesis, and inhibition of mechanisms of antioxidant protection(Neill et al., 2002).

Saturated fatty acids are very sensitive to reactive oxygen species (ROS) attack as a single $OH^{\bullet}$ can peroxidize more polyunsaturated acids, being the reason of chain disruptions in the structure and metabolic processes. Taking into account the level of MDA (Fig. 2), it can be concluded that ROS production in garlic plant organs treated with amino acids, and, especially, with gibberellinic acid, is actually much lower as compared to control plants.

In plant cells, there is a certain level of lipid for oxidation, which remains constant due to antioxidant protection systems. The enzyme system, in particular, superoxide dismutase (SOD), which catalyzes the reaction of superoxide radicals ($O^{\bullet-}$), plays an essential role in protecting cells from oxidative degradation. The rate of interaction between SOD and O depends on the degree of cell hydration (Asada, 2006). Depending on the intensity of the stressful fact, the activity of SOD varies differently.

The obtained results indicate that the highest physiological activity is exhibited by gibberellic acid, where the activity of the antioxidant complex is significantly higher against both control and other experimental variants.

The results of this study revealed that foliar spray by amino acids increased vegetative growth parameters. This might be due to the fact that amino acids enhance the metabolism processes in plant tissues.In this respect,foliar application of ascorbic and gibberellic acid resulted in higher growth and yield of eggplant (El-Tohamy et al., 2008; Islam et al., 2008). Our results are similarwith that of Paul et al. (2001); Pourtan, et al. (2004); Abd El-Aal et al. (2010). Similar results on the stimulatory effects of ascorbic acid on other plants were also noticed (Abdel-Halim (1995); Helal et al., 2005; El-Banna et al., 2006).) found that the application of ascorbic acid on tomato plants significantly improved certain plant growth criteria.

CONCLUSION

The antioxidant impact of amino acids manifested itself by a tendency to optimize these parameters; DAM values significantly decreased as compared to those of untreated plants.Amino acids increased the adaptive potential of plants and optimized the processes of growth and productivity. The study found that the use of amino acids improves the garlic productivity as a whole compared to the control. Increase in height of garlic plant, number of leaves, structural elements of yield, and crude and dry weights of the bulb. The highest yield and weight of the bulb were obtained in spraying plants by gibberellic acid, but the accumulation of dry weight was noted by using of salicylic and ascorbic acids.

REFERENCES

Abd El-Aal, F.S., Shaheen, A.M., Ahmed, A.A. & Mahmoud, R. 2010. Effect of foliar application of urea and amino acids mixtures as antioxidants on the growth and yield and characteristics of squash. *Res J Agric Biol Sci*. **6**(5), 583–588.

Abdel-Halim, S.M. 1995. Effect of some vitamins as growth regulators on growth, yield and endogenous hormones of tomato plants during winter. *Egypt J Appl Sci*.**10**(12), 322–334.

Abd-Elkader, D.Y. 2016. Effect of Foliar Spraying with Micronutrients and Salicylic Acid on Growth, Yield and Quality of Garlic Plants. *Alexandria Journal of Agricultural Sciences*. **61**(6), pp. 649–658.

Amin, A.A., Rashad, S.M. & El-Abagy, H.M.H. 2007. Physiological effect of indol-3-butyric acid and salicylic acid on growth, yield and chemical constituents of onion plants. *Journal of Applied Sciences Research* **3**(11), 1554–1563.

Asada, K. 2006. Production and scavenging of reactive oxygen species in chloroplasts and their functions. *Plant Physiol*. **41**(2), 391–396.

Bardisi, A. 2004a. Influence of vitamin C and Salicylic acid foliar application on garlic plants under sandy soil condition. 1. Growth and plant chemical composition. *Zagazig Journal of Agricultural Research* **31**(4A), 1337–1348.

Bardisi, A. 2004b. Influence of vitamin C and Salicylic acid foliar application on garlic plants under sandy soil condition. 2. Yield and its Storability. *Zagazig Journal of Agricultural Research* **31**(4A), 1349–1360.

Bideshki, A., Arvin, M.J. & Darini, M. 2013. Interactive effects of Indole-3-butyric acid (IBA) and salicylic acid (SA) on growth parameters, bulb yield and allicin contents of garlic (*Allium sativum*) under drought stress in field. *International Journal of Agronomy and Plant Production* **4**(2), 271–279.

Bondarenko, H.L.& Yakovenko, K.I. 2001. *Methodology of experimental work in vegetable and melon.* Kharkiv. Osnova, 369 pp. (in Ukrainian).

Bradford, M.M. 1976. A rapid and sensitive method for the quantitation of microgram quantities of protein utilizing the principle of protein-dye binding. *Anal. Biochem*. **72**, 248–254.

Dhindsa, R.S., Plumb-Dhindsa, P. & Thorpe, T.A. 1981. Leaf senescence: correlated with increased levels of membrane permeability and lipid peroxidation, and decreased levels of superoxide dismutase and catalase. *J. Exp. Bot*. **32**, 93–101.

El-Banna, E.N., Ashour, S.A. & Abd-El-Salam, H.Z. 2006. Effect of foliar application with organic compounds on growth, yield and tubers quality of potato (*Solanum tuberosum* L.). *J Agric Sci Mansoura Univ*. **31**(2), 1165–1173.

El-Morsy, A.H.A., Ezzat, A.S. & Saif El-Deen, U.M. 2010. Effect of some phosphorus and potassium rates and foliar spray with antioxidants on growth, yield and yield quality of garlic (*Allium sativum* L.). *Annals of Agricultural Science Moshtohor Journal* **48**(3), 27–40.

El-Shabasi, M.S.S., Mohamed, S.M.A., Mahfouz, S.A. 2005. Effect of foliar spray with some amino acids on growth, yield and chemical composition of garlic plants. *Proc. the 6th Arabian Conference for Horticulture, March 20–22, Faculty of Agric., Suez Canal University, Ismailia, Egypt*, pp. 365–369.

El-Tohamy, W.A., El-Abagy, H.M., El-Greadly, H.M. 2008. Studies on the effect of putrescine, yeast and vitamin C on growth, yield and physiological responses of eggplant (*Solanummelongena* L.) under sandy soil conditions. *Aust J Basic Appl Sci.* **2**(2), 296–300.

El-Zohiri, S.S.M. 2009. Role of the salicylic and ascorbic acid on the control of growth, flowering and yield of globe artichoke. *Annals of Agricultural Science Moshtohor Journal* **47**(3), 393–402.

Ermakova, A.I., Arasimovich, V.V. & Yarosh, N.P. 1987. *Methods of biochemical research of plants.* Ed. Ermakova A.I., 3 rd ed., Rev. and ext. L Agropromizdat. Leningrad branch, 430 pp.

Foyer, C.H., Lopez-Delgado, H., Dat, J.F. & Scott, I.M. 1997. Hydrogen peroxide- and glutathione-associated mechanisms of acclimatory stress tolerance and signalling. *Physiol. Plant*. **100**, 241–254.

Foyer, C.H., and Noctor, G. 2011. Ascorbate and glutathione: the heart of the redox hub. *Plant Physiol*. **155**, 2–18. doi: 10.1104/pp.110.167569

Habig, W.H., Pabst, M.J. & Jakoby, W.B. 1974. Glutathione S-transferases. The first enzymatic step in mercapturic acid formation. *J. Biol. Chem*. **246**, 7130–7139.

Helal, FA, Farag, S.T. & El-Sayed, SA 2005. Studies on growth, yield and its components and chemical composition under effect of vitamin C, vitamin B_1, boric acid and sulphur on pea (*Pisum sativum* L.) plants. *J AgricSci*, Mansoura Univ. **30**(6), 3343–3353.

Islam, M.A,Reza, M.H., Kamal, S.M.A.H.M., Wazed, M.A. & Islam, K.M. 2008. Effect of Planting Date and Gibberellic Acid on the Growth and Yield of Garlic. *The Agriculturists* **6**(1&2), 132–139.

Karpenko, V., Pavlyshyn, S., Prytuliak, R. & Naherniuk, D. 2019. Content of malondialdehyde and activity of enzyme glutathioneS-transferase in the leaves of emmer wheat under the action of herbicide and plant growth regulator. *Agronomy Research* **17**(1), 144–154, https://doi.org/10.15159/AR.19.014

Kazemi, M. 2013. Foliar Application of Salicylic Acid and Calcium on Yield, Yield Component and Chemical properties of Strawberry. *Bull. Env. Phar. Life Sci*. **2**(11), 19–23.

Khadr, A.A.I. 2015. *Effect of salicylic acid and calcium on growth, yield and quality of garlic (Allium sativum L.) plants*. M.Sc. thesis, Fac. Damanhour univ., Egypt, 110 pp.

Kowalczyk, K. & Zielony, T. 2008. Effect of aminoplant and asahi on yield and quality of lettuce grown on rockwool. *Proc. Conf. of Biostimulators in Modern Agriculture, 7–8 Febuary, Warsaw, Poland*, pp. 124.

Kumar, A., Biswas, T. K., Singh N. & Lal, E.P. 2014. Effect of Gibberellic Acid on Growth, Quality and Yield of Tomato (*Lycopersicon esculentum* Mill.) *Journal of Agriculture and Veterinary Science* **7(**7) Ver. IV, 28–30.

Li, C. X.; Yang, J., Wang, S. C., Xia, K., Li S. & Zhou, X. 2000. The role of salicylic acid in the swelling of garlic (*Allium statium* L.) bulb. *Acta. Hort. Sin*. **27**, 220–222.

Meena, B., Aravindakshan, K., Maurya, I. B., Yadav, I. & Singh, D. 2017. Effect of Foliar Application of Salicylic Acid and Ethrel on Growth, Yield and Quality of Garlic (*Allium Sativum* L.) var. G282. *Chemical Science Review and Letters* **6**(21), 600–605.

Naz, H., Akram, N.A. & Ashraf, M. 2016. Impact of ascorbic acid on growth and some physiological attributes of cucumber (cucumis sativus) plants under water-deficit conditions. *Pakistan Journal of Botany* **48**(3), 877–883.

Neill, S., Desikan, R. & Hancock, J. 2002. Hydrogen peroxide signalling. *Curr Opin Plant Biol.* **5**(5), 388–395.

Paul M.K., Pelling T.& Godding O. 2001. Enhancing photosynthesis with sugar signals. *Trends Plant Sci*. **6**, 197–200.

Petropoulos, S.A., Fernandes, A., Ntatsi, G., Petrotos, K., Barros, L. & Ferreira, I.C.F.R. 2018. Nutritional Value, Chemical Characterization and Bulb Morphology of Greek Garlic Landraces. *Molecules* **23**(2), 319. doi:10.3390/molecules23020319

Pourtan, N., Mares, M., Purdy, S., Quentinum, N., Rue, I.A. & Wingler, A. 2004. Interactions of bscisic acid and sugar signaling in the regulation of leaf senescence. *Planta* **219**, 765–772.

Pradhan, M., Tripathy, P., Mandal, P., Sahoo, B.B., Pradhan, R., Mishra, S.P. & Mishra, H.N. 2016. Effect of Salicylic Acid on Growth and Bulb Yield of Onion (*Allium Cepa* L.). *International Journal of Bio-resource and Stress Management* **7**(4), 960–963.

Prajapati, S., Jain, P. K. & Tiwari, A. 2016. Effects of Salicylic acid (SA) and Azospirillum on growth and bulb yield of Onion (*Allium cepa* L.) cv. *Agrifound Light Red. International Journal of Agriculture, Environment and Biotechnology* **9**(3), 393–402.

Prasad, T.K., Anderson, M.D., Martin, B.A. & Stewart, C.R. 1994. Evidence for chilling-induced oxidative stress in maize seedlings and a regulatory role for hydrogen peroxide. *Plant Cell*. **6**, 65–74.

Qian, H. F., Pen, X. F., Han, X., Ren, J., Zhan, K. Y. & Zhu, M. 2014. The stress factor, exogenous ascorbic acid, affects plant growth and the antioxidant system in Arabidopsis thaliana. Russ. *J. Plant Physiol*. **61**, 467–475. doi: 10.1134/S1021443714040141

Rahim, M.A. 1988. Control of growth and bulbing of garlic (*Allium sativum* L.) Ph.D. Thesis, University of London, 174 pp.

Rahim, M.A. & Forhad, R. 1988. *Effect of storage temperature on the initiation and development of garlic cloves (Allium sativum L.). Horticultural Science* **37**, 25–38.

Rogozhin, V.V. 2006. *Practical guide on biological chemistry*. Lan. St. Petersburg, 256 pp. (in Russian).

Senaratna, T., Touchell, D., Bunn, E. & Dixon, K. 2000. Acetyl salicylic acid (Aspirin) and salicylic acid induce multiple stress tolerance in bean and tomato plants. *Plant Growth Regulation* **30**, 157–161.

Shama, M.A., Moussa, S.A.M. & Abo El Fade, N.I. 2016. Salicylic acid efficacy on resistance of garlic plants (*Allium sativum*, L.) to water salinity stress on growth, yield and its quality.*Alex. Sci. Exc. J*. **37**(2), 165–174.

Smith, I.K., Vierheller, T.L., Thorne, C.A. 1988. Assay of glutathione reductase in crude tissue homogenates using 5,5'-dithiobis(2-nitrobenzoic acid). *Anal. Biochem*. **175**, 408–413.

Ulianych, O., Kostetska, K., Vorobiova, N., Shchetyna, S., Slobodyanyk, G. & Shevchuk, K. 2020. Growth and yield of spinach depending on absorbents' action. *Agronomy Research* **18**(2), 619–627. https://doi.org/10.15159/ar.20.012

Ulianych, O., Yatsenko, V., Didenko, I., Vorobiova, N., Kuhnyuk, O., Lazariev, O. & Tretiakova, S. 2019. Agrobiological evaluation of *Allium ampeloprasum* L. variety samples in comparison with Allium sativumL. Cultivars. *Agronomy Research* **17**(4), 1788–1799, https://doi.org/10.15159/AR.19.192

Upadhyaya, A., Sankhla, D., Davis, T.D., Sankhla, N. & Smith, B.N. 1985. Effect of paclobutrazol on the activities of some enzymes of activated oxygen metabolism and lipid peroxidation in senescing soybean leaves. *J. Plant Physiol*. **121**, 453–461.

Yuan, L. & Xu, D.Q. 2001. Stimulation effect of gibberellic acid short-term treatment on the photosynthesis related to the increase in Rubisco content in broad bean and soybean. *Photosynthesis Research* **68**, 39–47. doi: 10.1023/A:1011894912421

Agronomy Research **18**(3), 2259–2270, 2020
https://doi.org/10.15159/AR.20.209

Genetic Variation of Traits Affecting Meal Quality in Black × Yellow Seeded Doubled Haploid Population of Winter Oilseed Rape

J. Wolko[1], A. Dobrzycka[1], J. Bocianowski[2], L. Szala[1], T. Cegielska-Taras[1], I. Bartkowiak-Broda[1] and K. Gacek[1,*]

[1]Plant Breeding and Acclimatization Institute - National Research Institute (PBAI-NRI), Oilseed Crops Research Center, Strzeszynska 36, PL60-479 Poznan, Poland
[2]Poznan University of Life Sciences, Wojska Polskiego 28, PL60-637 Poznan, Poland
[*]Correspondence: k.gacek@ihar.edu.pl

Abstract. The by-product of oil production from oilseed rape (*Brassica napus* L.) is protein rich rapeseed meal. It is of great interest to improve the quality of rapeseed meal for poultry feed by reducing the level of anti-nutritional factors, mainly fibre and glucosinolates. The aim of the study was to assess genetic variation of traits affecting rapeseed meal quality in seeds from the M305 (black-seeded) × Z114 (yellow seeded) population of winter oilseed rape doubled haploid (DH) plants. The influence of weather conditions on these traits was tested under two-year field growing conditions in Poland. Significant effect of genotypes and the year of experiment was found for all of the studied traits, apart from neutral detergent fibre (NDF). The significant phenotypic variation in all of these traits makes future selection to improve quality of rapeseed meal possible. It was also found that all of the traits, apart from neutral detergent fibre, are regulated in a complex genetic manner involving additive and epistatic gene action. NDF is regulated by the additive gene action indicating that this trait might be easier for selection. Low heritability found for seed colour, fibre and glucobrassicin indicates great environmental effect on these traits. Large phenotypic variation for protein, oil, acid detergent fibre, neutral detergent fibre and glucosinolates found in this study will allow future genetic mapping analysis to identify key genes regulating these traits. The application of such genetic markers could enhance breeding programs aiming to improve oilseed rape which could be successfully introduced as poultry feed.

Key words: rapeseed meal quality, yellow-seeded oilseed rape, protein, oil, fibre.

INTRODUCTION

Oilseed rape (OSR) also known as rapeseed, canola (*Brassica napus*), is the second largest oil producing crop in the world (FAO). The by-product of oil production from this crop is protein rich rapeseed meal (RSM) or cake. When compared to protein meals from soybean or other legumes, RSM contains an excellent balance of essential amino acids, including high levels of desirable sulphur containing amino acids (cystine, methionine) and a slightly limited amount of lysine (Gacek et al., 2018). However, improvement of RSM is desired in order to make it a useful source of protein, especially for poultry feed, by reducing level of anti-nutritional components such as glucosinolates

(GLS), fibre, non-starch polysaccharides (NSP), and phytic acid present in rapeseed meal (Nesi et al., 2008; Swiech et al., 2016). Phytic acid is a primary storage form of *P* in the seed, while also being a low bioavailability source of *P* and also reduces the bioavailability of other essential nutrients especially cations like Fe or Zn. Glucosinolates induce enlargement of thyroid, therefore have negative effect on growth and health of animals (Quinsac et al., 1994; Swiech et al., 2016). The content of GLS has been significantly reduced in modern double-zero cultivars of OSR (< 25 μmol g^{-1} of seeds) but it is still desired to reduce its content especially for poultry feed purposes. Fibre, mainly present in the seed coat, reduces metabolizable energy content, protein digestibility, and bioavailability of minerals, therefore lowering its level in RSM meal is of great interest (Simbaya et al., 1995; Rahman et al., 2001; Mailer et al., 2008). The Van Soest system (Vansoest et al., 1991) classifies fibre as neutral detergent fibre, NDF (hemicellulose, cellulose, and lignin) and acid detergent fibre, ADF (cellulose and lignin).

Yellow-seeded oilseed rape genotypes of *B. napus* have a thinner and translucent seed coat resulting in lower fibre proportion and consequently higher protein and oil content in seeds (Rahman & McVetty, 2011). The level of proanthocyanidins and tannins, the major compounds involved in seed pigmentation known to reduce digestibility of seed meal, is also lowered in yellow-seeded OSR (Rahman & McVetty, 2011). The study on nutritive value of seed meal derived from yellow-seeded *B. napus* indicated that it could be successfully used in poultry industry for broilers (Slominski et al., 1994; Slominski et al., 1999). In contrast, the nutritional value and digestibility of yellow-seeded cakes was not improved when fed to young pigs, most likely due to presence of non-starch polysaccharides (NSP) and pectins in RSM (Simbaya et al., 1995; Rahman et al., 2001; Swiech et al., 2016). Although yellow-seeded OSR genotypes seem to be valuable for feeding industry, these varieties also have a number of negative qualities, many associated with yield, that limit their current utility for the wider market. Thus efforts have been dedicated to create new 'triple low' varieties with ultra low fibre meal (less than 2% of acid detergent lignin) and enhanced yield qualities from yellow by black seeded crosses. The yellow-seeded genotypes and intermediate genotypes derived from a cross between yellow-seeded and black-seeded OSR are valuable material in genetic and genomic studies aiming to understand genetic regulation of traits affecting RSM quality (Liu et al., 2013; Stein et al., 2013; Wang et al., 2015). Seed coat colour is a complex quantitative trait, known to be controlled by the interaction of many genes which are greatly affected by maternal and environmental effects (Penfield & MacGregor, 2017). The genetic analysis of yellow-seeded lines indicated that three to four genes, all in homozygous recessive state, were involved in regulation of seed coat colour (Rahman et al., 2001). Numerous genetic mapping studies have been performed in *Brassica* to understand the genetic basis of seed colour (Snowdon et al., 2010; Liu et al., 2013; Qu et al., 2015; Stein et al., 2017; Wang et al., 2017; Behnke et al., 2018) but the improvement of RSM as poultry feed is still a challenge. Further investigations of genetic regulation of traits affecting RSM quality in oilseed rape using different genetic backgrounds and environments, as well as development of targeted mapping populations would be advantageous for future marker assisted breeding programmes in this crop species.

Here a winter oilseed rape black-seeded × yellow-seeded mapping population of DH plants has been analysed under field conditions to assess genetic variability of traits affecting RSM quality including oil, protein, fibre and GLS content in seeds. The results

illustrate large genetic variation for these traits and interrelationship among them. The analysis of heritability and gene effect on the studied traits allowed estimation of genetic basis controlling these traits. Moreover, the data obtained could be used in our subsequent mapping studies to identify molecular markers associated with RSM quality in *B. napus*.

MATERIALS AND METHODS

Plant material

The experimental population consisted of 78 doubled haploid (DH) lines, developed from F_1 plants of a cross between M305, a black-seeded *B. napus* DH line and Z114, a yellow-seeded *B. napus* DH line. The two parental lines were selected for contrasting seed coat colour and seed fibre content. The population was developed in the Laboratory of Plant Tissue Culture, Plant Breeding and Acclimatization Institute-National Research Institute (PBAI-NRI), Oilseed Crops Division in Poznan, Poland through microspore culture according to the procedure described by Cegielska-Taras (Cegielska-Taras et al., 2002).

Field experiments

The M305×Z114 mapping population lines and parental lines were cultivated in PBAI-NRI experimental field in Poznan, Poland during two growing seasons: 2015/2016 and 2017/2018. The field trials were carried out in randomized block design with three replicates of double 2 m-long rows with 30 cm spacing seeded at a rate of 100 seeds per each row. The field was managed with standard methods. Seeds were harvested at maturity from five self-pollinated plants per genotype and threshed for further analysis.

Phenotypic evaluation

The contents of oil, protein, fibre (ADF and NDF), glucosinolates (GLS): 4-OH glucobrassicin, glucobrassicin, glucobrassicanapin, gluconapin, napoleiferin, progoitrin, and total GLS were determined in the Laboratory of Biochemistry PBAI-NRI in Poznan from each seed sample using near-infrared reflectance spectroscopy (NIRS) - Infratec 1255 analyser (Michalski & Czernik-Kolodziej, 2000). The quantification of seed coat colour was determined with The Hunter Labs spectrocolorimeter (Colorflex) and classified using 0 (black) to 5 (yellow) scale (Michalski, 2009).

Statistical analysis

The normality of the distributions of the traits value were tested using Shapiro-Wilk's normality test (Shapiro & Wilk, 1965). The two-way analysis of variance (ANOVA) were performed in order to verify the zero hypothesis of a lack of effects of years, DH lines and year × DH line interaction in terms of the values of the observed traits. The minimal and maximal values of the traits, as well as the arithmetic means and coefficients of variation (CV in %), were calculated. Fisher's least significant differences (LSDs) were estimated at a significance level of $\alpha = 0.001$. The relationships between the observed traits were assessed based on Pearson's correlation coefficients.

Estimation of the additive gene effect and additive-by-additive interaction of homozygous loci (epistasis) effect on the basis of phenotypic observations of DH lines and on the basis of parental observations as well as the test statistics to verify hypotheses about genetic parameters different than zero were described by following Bocianowski et al. (2017).

The heritability values were estimated using the standard units method of Frey and Horner (1957) in each year of study. Quantitative estimates of the number of genes segregating for observed traits were made using the Wright's formula (Frey and Horner 1957; Bjarko and Line 1988).

The statistical analysis was performed using GenStat 18 software package (https://genstat.kb.vsni.co.uk/).

RESULTS

Phenotypic variation of seed coat colour, oil, protein, fibre, and glucosinolates in seeds

Traits affecting RSM quality, including content of oil, protein, fibre (ADF and NDF), two indole glucosinolates: 4OH-glucobrassicin (4OH-GBS), glucobrassicin (GBS), four alkene glucosinolates: glucobrassicanapin (GBN), gluconapin (GNA), napoleiferin (NAP), progoitrin (PRO), and seed coat colour (SCC) were measured in the parental lines and each of the 78 DH lines of the *B. napus* population. The parental lines contrasted in SCC: line M305 displayed black seeds and Z114 yellow seeds. The SCC in the DH lines showed great variation in seed coat colour representing black, dark brown, dark brown with single light colour seeds, light brown, red, yellow with single brown seeds, yellow seeds (Fig. 1, M).

The results of ANOVA revealed that the main effects of years were significant for all tested traits, except NDF. The main effects of DH lines and year × DH lines interactions were statistically significant for all traits (data not shown). Higher or lower values for all of the tested traits in DH lines when compared to the parental lines indicate transgressive segregation in this population (Fig. 1, A–J and Table 1).

The mean oil content in Z114 seeds was 42%, 44% in 2016 and 2018, respectively whereas in M305 was 40%, 43% in 2016 and 2018, respectively. DH lines showed greater variation in oil content ranging from 30% -49% in both years of the study. The mean content of seed protein in the parental lines was 24% (Z114) and 25% (M305) in 2016, with similar values in 2018. The protein content in the DH lines showed bigger variation, ranging from 19% to 29% in 2016 and 20% to 28% in 2018. The mean content of NDF contrasted in seeds of the parental lines, with 18% (2016) and 16% (2018) for Z114 and 23% in 2016, 2018 for M305 line. The NDF content in the DH lines ranged from 17% to 25% in 2016, and 16% to 27% in 2018. The mean content of ADF in the parental lines was 11% (2016) and 10% (2018) for Z114 and about 17% (2016, 2018) for M305. The content of ADF fibre ranged in DH lines from 7% to 20% in 2016, and 9% to 22% in 2018. The mean content of 4OH-GBS glucosinolate was slightly higher for Z114 (5.2 and 4.7 μmol g^{-1} in 2016 and 2018, respectively) than for M305 (4.6 and 4.4 μmol g^{-1} in 2016 and 2018, respectively). In DH lines the variation for this glucosinolate ranged between 2.1–6.8 μmol g^{-1} in 2016 and 2.86–6.24 μmol g^{-1} in 2018.

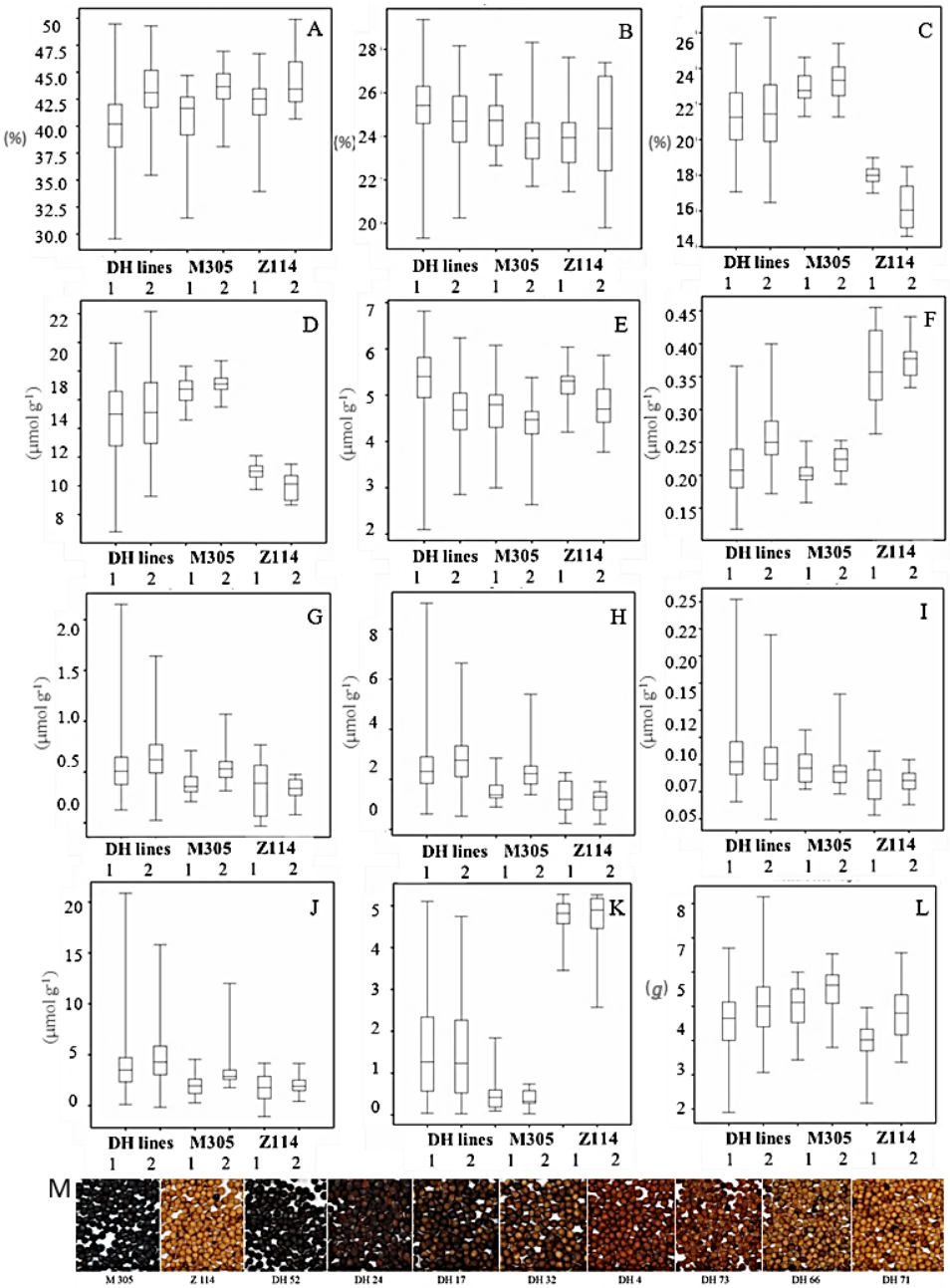

Figure 1. Boxplots showing content of (A) oil, (B) protein, (C) NDF fibre, (D) ADF fibre, (E) 4OH glucobrassicin, (F) glucobrassicin, (G) glucobrassicanapin, (H) gluconapin, (I) napoleiferin, (J) progroitrin, (K) seed coat colour, and (L) thousand seed weight in seeds of the M305×Z114 mapping population (DH lines) and the parental lines M305 and Z114 in two growing seasons (1) 2015/2016 (2) 2017/2018. (M) The images panel shows variation in seed coat colour in the parental lines: M305, Z114 and selection of DH lines representing colours black (DH52), dark brown (DH24), dark brown with single light colour seeds (DH17), light brown (DH32), red (DH4, DH73), yellow with single brown seeds (DH66), and yellow seeds (DH71).

The variation of GBS content ranged from 0.1 to 0.4 μmol g^{-1} in seeds collected in both years. Mean GBN content was lower in Z114 (0.33 μmol g^{-1} in both years) than in M305 (0.38 and 0.56 μmol g^{-1} in 2016 and 2018), whereas in the DH lines it ranged from 0.03 to 2.2 μmol g^{-1}. Mean GNA seed content was slightly lower in Z114 (1.3 μmol g^{-1} in 2016 and 1.1 μmol g^{-1} in 2018) when compared to M305 parent (1.5 in 2016 and 2.3 μmol g^{-1} in 2018). The mean NAP content was similar in both years of the study and was 0.08 μmol g^{-1} for Z114 and 0.09 μmol g^{-1} for M305, whereas in the DH lines NAP content ranged between 0.05–0.2 μmol g^{-1}. The mean PRO content was slightly higher in the black-seeded parent M305 (1.9 and 3.5 μmol g^{-1} in 2016 and 2018, respectively) when compared to yellow seeded parent Z114 with 1.8 and 2.01 μmol g^{-1} in 2016 and 2018, respectively. The content of PRO showed great variation in the DH lines which ranged between 0.1–21 μmol g^{-1} in both years of the study. Together this data shows that the largest variation among the traits affecting RSM quality was found in the DH lines from the M305×Z114 mapping population, whereas parental lines contrasted the most for SCC, ADF, and NDF. All of the traits were affected by the weather conditions (temperature and rainfall) which differed extremely in both years of the study (data not shown).

Table 1. Performance of traits affecting RSM quality for 2016 and 2018 in M305×Z114 mapping population

Trait	Year	Z114 mean	M305 mean	DH mean	DH range
Oil	2016	41.56 ± 3.1	40.35 ± 3.4	39.8 ± 3.5	29.55–49.46
	2018	44.04 ± 2.6	43.4 ± 2.06	43.29 ± 2.5	35.45–49.29
Protein	2016	24.02 ± 1.5	24.58 ± 1.1	25.42 ± 1.3	19.33–29.36
	2018	24.4 ± 2.4	24.02 ± 1.5	24.68 ± 1.5	20.25–28.17
NDF	2016	18.01 ± 0.5	22.92 ± 0.9	21.32 ± 1.7	17.06–25.4
	2018	16.25 ± 1.2	23.25 ± 0.9	21.41 ± 2.1	16.47–26.86
ADF	2016	11.01 ± 0.5	16.64 ± 0.9	14.62 ± 2.3	6.79–19.95
	2018	10.01 ± 0.9	17.17 ± 0.7	15.14 ± 2.6	9.27–22.15
40H–GBS	2016	5.21 ± 0.4	4.61 ± 0.7	5.3 ± 0.7	2.1–6.82
	2018	4.72±0.5	4.44 ± 0.5	4.67 ± 0.7	2.86–6.24
GBS	2016	0.37±0.05	0.2 ± 0.01	0.21 ± 0.04	0.12–0.37
	2018	0.38 ± 0.02	0.22 ± 0.01	0.26 ± 0.04	0.17–0.4
GBN	2016	0.33 ± 0.2	0.38 ± 0.1	0.52 ± 0.2	0.13–2.15
	2018	0.34 ± 0.1	0.56 ± 0.1	0.63 ± 0.2	0.03–1.64
GNA	2016	1.32 ± 0.6	1.54 ± 0.4	2.44 ± 0.9	0.62–9.04
	2018	1.14 ± 0.4	2.34 ± 0.8	2.75 ± 0.9	0.54–6.65
NAP	2016	0.083 ± 0.01	0.099 ± 0.01	0.108±0.02	0.066–0.252
	2018	0.085 ± 0.01	0.095 ± 0.01	0.102 ± 0.02	0.051–0.22
PRO	2016	1.82 ± 1.3	1.96 ± 1.02	3.77 ± 2.3	0.1–20.9
	2018	2.01 ± 1.09	3.5 ± 2.09	4.59 ± 2.2	0.17–15.8
SCC	2016	4.72 ± 0.4	0.55 ± 0.5	1.58 ± 0.4	0.04–5.1
	2018	4.69 ± 0.8	0.4 ± 1.2	1.51 ± 1.1	0.03–4.74
TSW	2016	3.97 ± 0.6	4.97 ± 0.6	4.53 ± 0.8	1.9–6.7
	2018	4.81 ± 0.9	5.52 ± 0.6	5.01 ± 0.8	3.07–8.2

NDF: neutral detergent fibre; ADF: acid detergent fibre; 4OH-GBS: 4OH-glucobrassicin; GBS: glucobrassicin; GBN: glucobrassicanapin; GNA: gluconapin; NAP: napoleiferin; PRO: progoitrin; SCC: seed coat colour; TSW: thousand seed weight.

Table 2. Correlations between traits affecting RSM quality for 2016 (above diagonal) and 2018 (below diagonal) in M305×Z114 mapping population

2016 2018	Oil	Protein	NDF	ADF	4OH-GBS	GBS	GBN	GNA	NAP	PRO	SCC	TSW
Oil	1	-0.65***	0.42***	0.31**	0.47***	0.04	-0.48***	-0.2	-0.50***	-0.36**	-0.23*	0.48***
Protein	-0.41***	1	-0.39***	-0.27*	-0.04	0.2	0.1	0.14	0	0.21	0.09	-0.18
NDF	0.08	-0.44***	1	0.92***	-0.14	-0.61***	-0.3**	-0.35**	0.07	0.19	-0.87***	0.26*
ADF	0.12	-0.33**	0.96***	1	-0.25*	-0.86***	0.28*	0.08	0.48***	0.23*	-0.89***	0.2
4OH-GBS	0.43***	0.13	-0.44***	-0.41***	1	0.43***	0.07	0.25*	-0.06	0.08	0.18	0.3**
GBS	0.08	-0.16	-0.91***	-0.71***	0.21	1	-0.08	-0.02	-0.38***	-0.22	0.83***	-0.21
GBN	-0.13	0.34**	0.21	-0.19	-0.1	-0.2	1	0.90***	0.88***	0.8***	0.2	-0.3**
GNA	0.04	0.22	0.04	-0.28*	0.12	0	0.85***	1	0.72***	0.79***	0.29**	-0.15
NAP	-0.16	0.22	0.41***	0.13	-0.41***	-0.26*	0.62***	0.43**	1	0.81***	-0.17	-0.25*
PRO	-0.14	0.31**	-0.32**	-0.25*	-0.11	-0.07	0.82***	0.82***	0.59***	1	0.22	-0.04
SCC	-0.11	0.12	-0.90***	-0.91***	0.35**	0.9***	-0.26*	-0.14	-0.41***	-0.21	1	-0.14
TSW	0.16	0.04	0.03	0.03	0.01	0	-0.17	-0.02	-0.1	0	-0.32**	1

NDF: neutral detergent fibre; ADF: acid detergent fibre; 4OH-GBS: 4OH-glucobrassicin; GBS: glucobrassicin; GBN: glucobrassicanapin; GNA: gluconapin, NAP: napoleiferin; PRO: progoitrin; SCC: seed coat colour; TSW: thousand seed weight.

Correlations between traits affecting RSM quality

The correlations between Oil-Protein, Oil-4OH-GBS, Protein-NDF, Protein-ADF, NDF-ADF, NDF-GBS, NDF-SCC, ADF-4OH-GBS, ADF-GBS, ADF-SCC, GBS-NAP, GBS-SCC, GBN-GNA, GBN-NAP, GBN-PRO, GNA-NAP, GNA-PRO, NAP-PRO were statistically significant across both years (Table 2). Correlation coefficients statistically significant in 2016 and not-significant in 2018 were observed for: Oil-NDF, OIL-ADF, OIL-GBN, OIL-NAP, OIL-PRO, OIL-SCC, OIL-TSW, NDF-GBN, NDF-GNA, NDF-TSW, ADF-GBN, ADF-NAP, 4OH-GBS-GBS, 4OH-GBS-GNA, 4OH-GBS-TSW, GBN-TSW, GNA-SCC, NAP-TSW (Table 2). Correlation coefficients statistically significant in 2018 and not-significant in 2016 were observed for: Protein-GBN, Protein-PRO, NDF-4OH-GBS, NDF-NAP, NDF-PRO, ADF-GNA, 4OH-GBS-NAP, 4OH-GBS-SCC, GBN-SCC, NAP-SCC, and SCC-TSW (Table 2). For ADF-PRO the observed correlation coefficients was significant in both years but negative in one year and positive in the other (Table 2). The correlations between the above traits are important factors to be considered in breeding programmes of improved RSM quality in oilseed rape.

Genetic regulation of traits affecting seed meal quality

To elucidate the mechanism of inheritance and genetic regulation of the traits affecting RSM quality, the estimation of heritability and the effect of additive and epistatic gene action were performed in the M305×Z114 mapping population (Table 3). The analysis of inheritance in the mapping population showed low heritability estimates for SCC (0.1), ADF (0.2), NDF (0.1), and GBS (0.1) in both years. High heritability estimates were observed for oil (0.9), protein (0.9), GBN (0.9 in 2016), GNA (0.9 in 2016), PRO (0.9), and NAP (0.8). The number of genes segregating for the analysed traits ranged from 0.0 (for protein content in 2018 and progoitrin in 2016) to 18.9 (for glucobrassicin in 2016) (Table 3). The number of genes segregating were significant negative correlated with heritability in 2018 (r = -0.889, $p < 0.001$) and not statistically significant in 2016 (r = -0.527, p = 0.078) (Table 3). Both additive and epistatic gene effects were found to be significant for SCC and GBN, GBS, GNA, NAP, PRO content in seeds whereas significant additive effect and non-significant epistasis was found for TSW, 4OH-GBS, ADF, and NDF fibre. The seed oil and protein content showed additive gene effect only in the first year of study.

Table 3. Estimation heritability of additive and epistatic effects as well as the number of genes segregating for RSM quality traits M305×Z114 mapping population

Trait	Year	Additive effect based on parental lines	Additive effect based on DH lines	Epistatic effect based on DH lines	Mean value	Heritability	Number of genes segregating
Oil	2016	-0.605	6.442*	-0.484	39.749	0.916	0.2
	2018	-0.320	3.980	-0.479	43.285	0.946	0.1
Protein	2016	0.280	2.648*	-0.364	25.459	0.898	3.7
content	2018	-0.190	2.235	-0.215	24.680	0.947	0.0
PRO	2016	0.070	3.957***	1.290***	3.737	0.997	0.0
	2018	0.746*	4.176***	1.121**	4.592	0.769	0.2
NDF	2016	2.455*	2.813*	-0.160	21.276	0.157	2.3
	2018	3.500*	3.955*	-0.179	21.410	0.134	3.4

Table 3(continued)

ADF	2016	2.815*	3.827*	-0.182	14.598	0.210	1.6
	2018	3.580*	4.787*	0.110	15.136	0.193	1.9
40H-GBS	2016	-0.300	1.266*	-0.171	5.294	0.624	0.4
	2018	-0.138	0.907*	0.048	4.673	0.848	0.5
GBS	2016	-0.081**	0.097**	0.019*	0.216	0.124	18.9
	2018	-0.077*	0.084*	0.020*	0.259	0.108	4.8
GNA	2016	0.109	1.665***	0.445**	2.408	0.958	0.0
	2018	0.599*	1.641***	0.197*	2.752	0.435	0.9
NAP	2016	0.008	0.042**	0.011**	0.107	0.751	0.1
	2018	0.005	0.045**	0.007*	0.102	0.851	0.1
GBN	2016	0.025	0.354***	0.089**	0.518	0.960	0.1
	2018	0.109*	0.412***	0.035*	0.629	0.582	0.3
SCC	2016	-2.085***	2.086***	0.638***	1.618	0.123	3.3
	2018	-2.145***	2.055***	0.711***	1.508	0.115	4.4
TSW	2016	0.503*	1.607**	-0.379*	4.511	0.489	0.9
	2018	0.356	1.245*	0.165	5.009	0.551	2.0

* $P < 0.05$; ** $P < 0.01$; *** $P < 0.001$; NDF: neutral detergent fibre; ADF: acid detergent fibre; 4OH-GBS: 4OH-glucobrassicin; GBS: glucobrassicin; GBN: glucobrassicanapin; GNA: gluconapin; NAP: napoleiferin; PRO: progoitrin; SCC: seed coat colour; TSW: thousand seed weight.

DISCUSSION

The significant effects of years on all tested traits, apart from NDF, were most likely caused by the differences in weather conditions in both experimental seasons. The rainfall and temperature recorded in meteorological station at PBAI-NRI for the growing seasons 2016 and 2018 (between April and September) showed extreme differences, with very high temperatures and very low rainfall level in 2018 (data not shown). The significant effect of weather on the content of fatty acid, glucosinolates and oil in seeds of winter oilseed rape have already been observed in previous studies (Liersch et al., 2013; Lääniste et al., 2016; Nowosad et al., 2017).

The ideal range of seed fibre content in OSR cultivars which could be used as poultry feed should be on a similar level to that found in the yellow-seeded genotypes. Unfortunately, the yellow-seeded OSR displays many unfavourable traits of agronomic importance (pre-harvest sprouting, seed deterioration during storage and problems with oil extraction) which makes them difficult to incorporate into the market. One of the strategies of RSM improvement would be introducing intermediate SCC genotypes of OSR with enhanced nutritional value. It is expected that reduction of seed coat thickness in yellow seeded genotypes results in increased contribution of the embryo to the seed weight and for this reason the content of oil and protein should rise too (Slominski et al., 1999). In contrast to this view the protein and oil content in the yellow-seeded line Z114 was not much higher than in the black-seeded parent M305. The selection of the parental lines for the development of our mapping population was based on great contrast in seed coat colour and seed fibre content, not protein and oil. In other studies no significant effect on oil content was observed in the yellow seeded genotypes too, which indicates a variation in protein and oil content in yellow-seeded genotypes (Wittkop et al., 2009). The observed variation for seed protein content (19–29%) in M305×Z114 mapping population was slightly smaller when compared to values in other studied population

KNDH (19–34%) (Chao et al., 2017). The protein content showed negative correlation with oil and fibre content which was also observed in other studies (Hannoufa et al., 2014). Seeds containing less fibre have thinner seed coat with decreased amount of cell wall polysaccharides which can cause increased carbon availability for protein deposition (Stombaugh et al., 2000). The analysis of the 78 DH lines in the mapping population allowed identification of line DH53 which contained lower amount of fibre and slightly higher protein content. This finding indicates that selection for lighter colour seeds could lead to higher protein content in seeds. The NDF content in the mapping population varied in both seasons between 16% and 27%, whereas in other studies the content of NDF ranged between 11–21% (Snowdon et al., 2010; Wittkop et al., 2012). The ADF fibre ranged in DH lines from 7% to 20% in 2016, and 9% to 22% in 2018, which shows wider variation in comparison to previously published studies (Mailer et al., 2008; Dimov et al., 2012). Strong negative correlation found between SCC and fibre is expected since yellow-seeded genotypes contain lower levels of fibre (Rahman & McVetty, 2011). Interestingly, negative correlation in both years was also observed between fibre and GBS content. In Suprainto study (PhD thesis https://d-nb.info/1052337953/34) the QTL for GLS colocalises with QTL for cellulose content which indicates that such correlation could be due to common QTLs for these two traits. Although no correlation was found between progoitrin and seed coat colour, the yellow-seeded parental line (Z114) contained lower level of progoitrin when compared to M305 line. It would also be very desired to eliminate progoitrin from the intermediate genotypes of OSR, which could be challenging since this glucosinolate showed negative correlation with fibre content in 2018. In some of the DH lines, the mean value of this major compound responsible for anti-nutritional effect in RSM was greatly reduced (e.g. 0.9 $\mu mol\ g^{-1}$ in line DH78) which makes these lines valuable genetic material for future breeding improvement work.

Both additive and epistasis gene effects were found to be significant for SCC, GBN, GBS, GNA, NAP and PRO content in seeds. It means that these traits are regulated in a complex manner involving many genes with small effect and also by gene-by-gene interactions. Significant additive effect and non-significant epistasis for TSW, 4OH-GBS, ADF, and NDF fibre means that these traits are regulated by many genes with small individual effect. Selection for genotypes with low fibre content in the future should be less challenging since this anti-nutritional component was found to be regulated by the additive action of genes.

CONCLUSION

In conclusion, this data shows that seed quality traits affecting RSM quality are complex and are regulated by interaction of genes which are influenced by the environment. Although some interesting DH lines were found in this study which are already being introduced to breeding programmes, future work includes application of the latest bioinformatic tools in genetic mapping studies using this population to identify key genomic regions affecting RSM quality traits. Recent advances in sequencing technologies and bioinformatics facilitate high density marker discovery with sufficient resolution to give closely linked markers with traits of interest using the DH mapping population developed in this study (Gacek et al., 2017). Identification of such regions

would enhance selection process of valuable genetic material for improvement of RSM quality regardless of environmental impact.

REFERENCES

Behnke, N., Suprianto, E. & Mollers, C. 2018. A major QTL on chromosome C05 significantly reduces acid detergent lignin (ADL) content and increases seed oil and protein content in oilseed rape (*Brassica napus* L.). *Theoretical and Applied Genetics* **131**(11), 2477–2492.

Bjarko, M.E. & Line, R.F. 1988. Quantitative determination of the gene action of leaf rust resistance in four cultivars of wheat. *Phytopathology* **78**, 457–461.

Bocianowski, J., Nowosad, K., Dobrzycka, A. & Wolko, J. 2017. Estimation of additive and epistatic gene effects of doubled haploid lines of winter oilseed rape (*Brassica napus* L.). *Euphytica* **213**(5), 122. doi: 10.1007/s10681-017-1905-5

Cegielska-Taras, T., Tykarska, T., Szala, L., Kuras, M. & Krzymanski, J. 2002. Direct plant development from microspore-derived embryos of winter oilseed rape *Brassica napus* L. ssp *oleifera* (DC.) Metzger." *Euphytica* **124**(3), 341–347.

Chao, H.B., Wang, H., Wang, X.D., Guo, L.X., Gu, J.W., Zhao, W.G., Li, B.J., Chen, D.Y., Raboanatahiry, N. & Li, M.T. 2017. Genetic dissection of seed oil and protein content and identification of networks associated with oil content in *Brassica napus*. *Scientific Reports* **7**.

Dimov, Z., Suprianto, E., Hermann, F. & Mollers, C. 2012. Genetic variation for seed hull and fibre content in a collection of European winter oilseed rape material (*Brassica napus* L.) and development of NIRS calibrations. *Plant Breeding* **131**(3), 361–368.

Frey, K.J. & Horner, T. 1957. Heritability in standard units. *Agronomy Journal* **49**, 59–62.

Gacek, K., Bartkowiak-Broda, I. & Batley, J. 2018. Genetic and Molecular Regulation of Seed Storage Proteins (SSPs) to Improve Protein Nutritional Value of Oilseed Rape (*Brassica napus* L.) Seeds. *Frontiers in Plant Science* **9**.

Gacek, K., Bayer, P.E., Bartkowiak-Broda, I., Szala, L., Bocianowski, J., Edwards, D. & Batley, J. 2017. Genome-Wide Association Study of Genetic Control of Seed Fatty Acid Biosynthesis in *Brassica napus*. *Frontiers in Plant Science* **7**.

Hannoufa, A., Pillai, B.V.S. & Chellamma, S. 2014. Genetic enhancement of *Brassica napus* seed quality. *Transgenic Research* **23**(1), 39–52.

Lääniste, P., Eremeev, V., Mäeorg, E. & Jõudu, J. 2016. Effect of sowing date on oil, protein and glucosinolate concentration of winter oilseed rape (*Brassica napus* L.). *Agronomy Research* **14**(S2), 1384–1395.

Liersch, A., Bocianowski, J. & Bartkowiak-Broda, I. 2013. Fatty acid and glucosinolate level in seeds of different types of winter oilseed rape cultivars (*Brassica napus* L.). *Communications in Biometry and Crop Science* **8**(2), 39–47.

Liu, L.Z., Qu, C.M., Wittkop, B., Yi, B., Xiao, Y., He, Y.J., Snowdon, R.J. & Li, J.N. 2013. A High-Density SNP Map for Accurate Mapping of Seed Fibre QTL in *Brassica napus* L. *Plos One* **8**(12).

Mailer, R.J., McFadden, A., Ayton, J. & Redden, B. 2008. Anti-nutritional components, fibre, sinapine and glucosinolate content, in Australian canola (*Brassica napus* L.) meal. *Journal of the American Oil Chemists Society* **85**(10), 937–944.

Michalski, K. & Czernik-Kolodziej, K. 2000. Application of NIR spectrometry for analysis of basic chemical constituent of rapeseed. *Rosliny Oleiste - Oilseed Crops* **21**(3), 801–806.

Michalski, K. 2009. Seed color assessment in rapeseed seeds using Color and Near Infrared Reflectance Spectrometers. *Rosliny Oleiste - Oilseed Crops* **30**(1), 119–132.

Nesi, N., Delourme, R., Bregeon, M., Falentin, C. & Renard, M. 2008. Genetic and molecular approaches to improve nutritional value of *Brassica napus* L. seed. *Comptes Rendus Biologies* **331**(10), 763–771.

Nowosad, K., Liersch, A., Popławska, W. & Bocianowski, J. 2017. Genotype by environment interaction for oil content in winter oilseed rape (*Brassica napus* L.) using additive main effects and multiplicative interaction model. *Indian J. Genet. Plant Breed.* **77**, 293–297.

Penfield, S. & MacGregor, D.R. 2017. Effects of environmental variation during seed production on seed dormancy and germination. *Journal of Experimental Botany* **68**(4), 819–825.

Qu, C.M., Hasan, M., Lu, K., Liu, L.Z., Zhang, K., Fu, F.Y., Wang, M., Liu, S.Y., Bu, H.D., Wang, R., Xu, X.F., Chen, L. & Li, J.N. 2015. Identification of QTL for seed coat colour and oil content in *Brassica napus* by association mapping using SSR markers. *Canadian Journal of Plant Science* **95**(2), 387–395.

Quinsac, A., Lessire, M., Krouti, M., Ribaillier, D. Coic, J.P., Fauduet, H. & Rollin, P. 1994. Improvement in the nutritive-value of high and low glucosinolate rapeseed meal by aqueous extraction. *Animal Feed Science and Technology* **48**(3–4), 265–272.

Rahman, M. & McVetty, P.B.E. 2011. A review of *Brassica* seed color. *Canadian Journal of Plant Science* **91**(3), 437–446.

Rahman, M.H., Joersbo, M. & Poulsen, M.H. 2001. Development of yellow-seeded *Brassica napus* of double low quality. *Plant Breeding* **120**(6), 473–478.

Shapiro, S.S. & Wilk, M.B. 1965. An analysis of variance test for normality (complete samples). *Biometrika* **52**, 591–611.

Simbaya, J., Slominski, B.A., Rakow, G., Campbell, L.D., Downey, R.K. & Bell, J.M. 1995. Quality Characteristics of Yellow-Seeded Brassica Seed Meals - Protein, Carbohydrates, and Dietary Fiber Components. *Journal of Agricultural and Food Chemistry* **43**(8), 2062–2066.

Slominski, B.A., Campbellm, L.D. & Guenter, W. 1994. Carbohydrates and Dietary Fiber Components of Yellow-Seeded and Brown-Seeded Canola. *Journal of Agricultural and Food Chemistry* **42**(3), 704–707.

Slominski, B.A., Simbaya, J., Campbell, L.D., Rakow, G. & Guenter, W. 1999. Nutritive value for broilers of meals derived from newly developed varieties of yellow-seeded canola. *Animal Feed Science and Technology* **78**(3–4), 249–262.

Snowdon, R.J., Wittkop, B., Rezaidad, A., Hasan, M., Lipsa, F., Stein, A. & Friedt, W. 2010. Regional association analysis delineates a sequenced chromosome region influencing antinutritive seed meal compounds in oilseed rape. *Genome* **53**(11), 917–928.

Stein, A., Coriton, O., Rousseau-Gueutin, M., Samans, B., Schiessl, S.V., Obermeier, C., Parkin, I.A.P., Chevre, A.M. & Snowdon, R.J. 2017. Mapping of homoeologous chromosome exchanges influencing quantitative trait variation in *Brassica napus*. *Plant Biotechnology Journal* **15**(11), 1478–1489.

Stein, A., Wittkop, B., Liu, L.Z., Obermeier, C., Friedt, W. & Snowdon, R.J. 2013. Dissection of a major QTL for seed colour and fibre content in *Brassica napus* reveals colocalization with candidate genes for phenylpropanoid biosynthesis and flavonoid deposition. *Plant Breeding* **132**(4), 382–389.

Stombaugh, S.K., Jung, H.G., Orf, J.H. & Somers, D.A. 2000. Genotypic and environmental variation in soybean seed cell wall polysaccharides. *Crop Science* **40**(2), 408–412.

Swiech, E., Raj, S., Pastuszewska, B., Taciak, M., Bartkowiak-Broda, I. & Smulikowska, S. 2016. Nutritional value of yellow-seeded winter rapeseed cakes for growing pigs. *Agricultural and Food Science* **25**(2), 99–110.

Vansoest, P.J., Robertson, J.B. & Lewis, B.A. 1991. Methods for Dietary Fiber, Neutral Detergent Fiber, and Nonstarch Polysaccharides in Relation to Animal Nutrition. *Journal of Dairy Science* **74**(10), 3583–3597.

Wang, J., Jian, H.J., Wei, L.J., Qu, C.M., Xu, X.F., Lu, K., Qian, W., Li, J.N., Li, M.T. & Liu, L.Z. 2015. Genome-Wide Analysis of Seed Acid Detergent Lignin (ADL) and Hull Content in Rapeseed (*Brassica napus* L.). *Plos One* **10**(12).

Wang, J., Xian, X.H., Xu, X.F., Qu, C.M., Lu, K., Li, J.N. & Liu, L.Z. 2017. Genome-Wide Association Mapping of Seed Coat Color in *Brassica napus*. *Journal of Agricultural and Food Chemistry* **65**(26), 5229–5237.

Wittkop, B., Snowdon, R.J. & Friedt, W. 2012. New NIRS Calibrations for Fiber Fractions Reveal Broad Genetic Variation in *Brassica napus* Seed Quality. *Journal of Agricultural and Food Chemistry* **60**(9), 2248–2256.

http://www.fao.org/fileadmin/templates/est/COMM_MARKETS_MONITORING/Oilcrops/Documents/Food_outlook_oilseeds/FO_May_2015.pdf

Agronomy Research **18**(3), 2271–2284, 2020
https://doi.org/10.15159/AR.20.199

Studying the storage and processing quality of the carrot taproots *(Daucus carota)* of various hybrids

O. Zavadska[1], I. Bobos[1], I. Fedosiy[1], G. Podpryatov[1] and J. Olt[2,*]

[1]National University of Life and Environmental Sciences of Ukraine, 15 Heroyiv Oborony Str., UA 03041 Kyiv, Ukraine
[2]Estonian University of Life Sciences, Institute of Technology, 56 F.R. Kreutzwaldi Str., 51006 Tartu, Estonia
[*]Correspondence: jyri.olt@emu.ee

Abstract. This paper presents the results acquired from the study of eight carrot hybrids which are suitable for growing in the climatic zone of woodland steppes, while considering a set of economical and/or biological, biochemical, and organoleptic properties. The carrot hybrids that were studied have a wide range of variation in their economic value indicators, which makes it possible to grow them for storage and processing in various soils and climate conditions without irrigation. The most productive carrot hybrids are White Sabine F_1 and Yellowstone F_1 with a commercial yield of 55.8–58.7 t ha^{-1} and an average taproot weight of 118.7–136.2 g. The levels of preservation of the taproot of the hybrids White Sabine F_1 and Purple Haze F_1 after seven months of storage in conditions that involved the use of a stationary pit storage facility was at 81.4% and 80.2% respectively. The use of the taproots of the hybrids Yellowstone F_1 and Viking F_1 for drying ensures a yield of a high-quality, biologically-valuable finished product with a yield of 11.4–11.7%. Dry hybrid Evolyutsiya F_1 and Mars F_1 carrots contain more than 40 mg (100 g)$^{-1}$ of β-carotene.

Key words: carrot, drying, quality, processing, storage, yield.

INTRODUCTION

The carrot is one of the world's most widespread vegetable crops, and is certainly not limited merely to Ukraine's borders (Arscott & Tanumihardjo, 2010). According to statistics, carrots are grown annually on more than 43,000 hectares of land (Sych, 2010; Bobos & Zavadska, 2015). The carrot is also one of the most high-yielding and biologically-valuable vegetable crops. If all of the agricultural rules of growing carrots are observed, the taproot crop can reach between 60–70 t ha^{-1} (Skaletska et al., 2013a; Bobos & Zavadska, 2015).

On average over the vegetation period, the total nutritional content of carrot taproots can be broken down firstly into 12–15% dry matter, and secondly into 8–12% carbohydrates, of which 6–9% are sugars, plus 1.0–1.2% cellular tissue, 0.37–2.93% pectins, 1.0–2.2% proteins, and 0.2–0.3% fats. This crop's taproots are also a source of minerals, water-soluble vitamins B_1, B_2, and B_6, and fat-soluble vitamins E and D (Skaletska et al., 2014a, 2014c; Zavadska & Kravchenko, 2016b). They are especially

valuable due to their high content of pro-vitamin A – carotene, which they contain at levels that are higher than for any other vegetable (8–12 mg $(100\ g)^{-1}$, for some variations and with hybrids this figure can exceed 20 mg $(100\ g)^{-1}$. It is known that β-carotene has antioxidant properties; its daily consumption in food improves vision, facilitates the slowing of the growth of cancer cells and prevents their multiplication (Piyarach et al., 2020). In order to satisfy the body's daily need for that vitamin, an intake of between 12–30 g of fresh carrot taproots is required. It is also better to consume them with vegetable oil because β-carotene is considered to be a fat-soluble vitamin (Skaletska et al., 2014a). The carrot's pectin ingredients, which contain calcium salts, are able to absorb heavy and radioactive metals and other toxins, which is why they have an anti-radiation and anti-toxin effect (Borisov et al., 2016).

Carrot production in Ukraine, Estonia, and other countries has a pronouncedly seasonal nature. Most crops (approximately 75% of the total) enter the market in the summer and autumn. The crops are not used up immediately and are instead sent to storage or processing. According to statistics, about 25–30% of stored vegetables are lost each year due to the lack of specialised storage facilities and processing at the necessary volumes (Skaletska et al., 2014a). This is why research into alternative methods of storage and processing for harvested carrot crops is relevant and necessary, in order to provide consumers with high-quality produce throughout the year (Wismer, 2003; Seljasen et al., 2013; Skaletska et al., 2014a).

It must be noted that, nowadays, the most relevant processing type for many vegetables is drying (Zielinska & Markowski, 2012; Hryshchenko et al., 2019). Dried vegetables form a concentrate of beneficial ingredients because drying removes free water and also some of the bound water. The advantages of dried vegetables are their prolonged shelf life, the absence of preservatives and other chemicals, the biological value, and the convenience and simplicity of preparing them as a dish. Moreover, dried vegetables take up considerably less space in storage and transport when compared to fresh vegetables (between 6–8 times less), which has the positive effect of significantly reducing the cost and complexity of logistics (Skaletska et al., 2014a; Skaletska & Zavadska, 2015). Drinks that are made using as a basis lyophilised fruit and vegetable powders have a high antioxidant content, nutritional value, and bioavailability (Bochnak-Niedźwiecka &Świeca, 2020).

Carrots are one of the most widespread agricultural crops to be used for drying. Dried carrots are a necessary ingredient in almost all vegetable mixtures and seasonings, and in its powder form it is also used as a natural pigment. It gives finished dishes their pleasant colour, smell, and taste, but what's most important is the fact that it enriches dishes with nutritional and biologically-valuable substances and minerals, which it contains in high quantities (Lewicki & Duszczyk, 1998; Zavadska et al., 2013; Skaletska & Zavadska, 2014c). The quality of dried vegetable produce depends significantly upon the drying methods being used and on subsequent storage conditions хранения (Macura et al., 2019). Currently the most widespread and economically feasible method of drying taproot vegetables is convective drying (Piyarach et al., 2020).

Regardless of their relatively good levels of preservation, losses in storage for carrot taproots are often huge (above 15%). This is related primarily to growing conditions for the carrots, plus the non-observance of optimum storage conditions, the lack of storage space, and the stacking of unfit produce (Skaletska et al., 2014a; Bobos

& Zavadska, 2015). Changes in the structure of taproot vegetables during their storage are the most pronounced in their central parts (Haq & Prasad, 2017).

The fitness of taproots for storage or various types of processing depends upon a large number of factors, important amongst them being their biological properties and cultivars. It is known that not every cultivar or hybrid is suitable for processing even if they have valuable agricultural indicators and appropriate taste properties. Moreover, cultivars of vegetables are rarely universal and cannot be used similarly well for fresh consumption, storage, and processing.

Every year in Ukraine, new carrot cultivars and hybrids are developed. These differ in terms of the shape of their taproot, the length of their vegetation period, their nutritional content, and their fitness for storage and processing. For fresh produce markets, early and medium-early maturing carrot cultivars are grown with conical and cylindrical taproot shapes, a rounded end, and uniform colouring. For storage purposes, later maturing carrot cultivars are more suitable with a uniform taproot shape, a high commercial value, and high biochemical indicators (Skaletska & Zavadska, 2013b; Skaletska et al., 2016; Zavadska & Kravchenko, 2016a and 2016b). For industrial processing purposes, suitable carrot cultivars are those that possess high dry matter content (6–16%) and carotene content, as well as appropriate properties for mechanical processing (Zavadska et al., 2013; Skaletska et al., 2014a and 2014c).

More recently botanical carrot cultivars with bright yellow, violet, or even white colourings have become increasingly popular (Burenin et al., 2017; Kornev et al., 2017). This is an eastern assortment, one which is mainly grown in China, Japan, and Uzbekistan. Dutch scientists have studied the beneficial properties of violet carrots. They found that the taproots of violet-coloured carrot cultivars provide the body with long term protection against tumours and cardiovascular diseases because they contain not only high amounts of carotene but also a significant level of anthocyanins (Alasalvar et al., 2005; Arscott & Tanumihardjo, 2010; Bobos & Zavadska, 2015). The antioxidant properties of purple carrots are much higher than are those in orange carrots (Algarra et al., 2014). Questions regarding the quality of the new cultivars and hybrids that are grown in certain soils and climate conditions have not involved sufficient levels of study to be able to answer them.

The goal of the research was to study the economic value, plus the biometric, biochemical, and technological parameters, of the quality of fresh and dried produce in terms of eight carrot hybrids with various taproot colours, in order to determine the most suitable variants for long-term storage when utilising stationary underground storage facilities and convective drying.

MATERIALS AND METHODS

The studies were conducted within the period between 2013–2015 at the National University of Biological Resources and Nature Utilisation of Ukraine, using single-factor tests (Bondarenko & Yakovenko, 2001). The carrot cultivar taproots that were being studied were grown on a collection plot without irrigation. The total area of crop being used for field tests was 0.2 ha. Each hybrid's plot covered an area of at least 6 m^2. The studies took place in triplicate. The seeds were sown according to a 20 + 50 cm scheme, forming a plant density of 600,000 plants per hectare. All of the hybrids were sown simultaneously and had a follow-up check in the second week of April, at the

following dates: 14 April 2013, 11 April 2014, and 15 April 2015. All of the hybrids were sown simultaneously and had a follow-up check in the second week of April, on the following dates: 14 April 2013, 11 April 2014, and 15 April 2015.

The plot being used for the field tests is located in Ukraine's climatic zone which largely consists of woodland steppe. The plot's soil is dark grey, medium ashy (podsolised), and slightly loamy. The thickness of the humus layer is 24–28 cm. The test plot is characterised by the low humus content, at between 1.5–2.2%, plus its medium content hydrolysed nitrogen, between 26–38 mg kg^{-1}, its mobile phosphor, between 43–61 mg kg^{-1}, and its potassium, between 28–34 mg kg^{-1} (Bobos et al., 2019).

In terms of crop rotation, the carrots were grown following a cucumber harvest. The main treatment for the soil being used for the crop was the autumn elimination of the previous crop's plant residue and weeds, as well as deep autumn ploughing. In the first week of April and prior to sowing, the test plot was cultivated to a depth of between 12–15 cm and 6–8 cm respectively, using a КПСП-4 cultivator in combination with a DT-75 tractor, levelled with a harrow, following which the carrot seeds were sown.

After the initial research phase, the studies included eight hybrids that were suitable for cultivation in the woodland steppe climatic zone. In addition to traditional carrot cultivars with their typical orange taproot colouring, use was also made of hybrids that had been produced by the company Bejo, each variety being distinctive thanks to its white colouring (White Sabine F_1), bright yellow colouring (Yellowstone F_1), or violet colouring and orange core (Purple Haze F_1) (Fig. 1). As a control crop, the highly-studied Dutch hybrid Vita Longa F_1, was used which had been introduced on a regional basis into Ukraine in 1997. The testing scheme is presented in Table 1.

a)  b) 

Figure 1. The taproots of carrot hybrids: a) Purple Haze F_1; b) Yellowstone F_1.

The crop harvesting took place simultaneously for all hybrids in the test, at the onset of the technical maturity of the carrot taproots, namely between 16–20 October in 2013, between 20–21 October in 2014, and between 25–27 September in 2015. The arid weather conditions in August and September 2015 led to an earlier harvesting of the crops, as any delay in harvesting could have led to premature aging of the taproots, a shortening of their shelf life, and a reduction in the quality of fresh taproots and processed produce.

The analyses of fresh taproots and dried produce were conducted using generally accepted methods (Skaletska et al., 2014b). The dry matter content was determined using the ДСТУ ISO 751:2004 method and thermal gravimetry, with drying taking place in a dryer at a temperature of 100–105 °C until a stable weight was achieved; the dry soluble matter content was determined using a refractometer pursuant to the requirements of ДСТУ ISO 2173: 2007. From the laboratory sample, after its careful mixing, 20 g of minced taproots were taken; this mass was filtered to yield between 1–2 cm^3 of juice, two or three drops of which were applied to the prism of a refractometer. After that, the top prism was lowered, taking between three to five counts with a clear boundary between the dark and light parts of the field of view, and calculating the average refraction rate. Sugars (sum) were determined using Bertran's method (ДСТУ 4954:2008); β-carotene content was determined pursuant to the requirements of ДСТУ 4305:2004. The volume of carotenes is determined from the intensity of the yellow colour in the solution by way of comparing it in a colorimeter with a solution of dichromate acid potassium that has been standardised on pure carotene. Degustation of fresh taproots and dried produce was carried out by a committee of at least seven people, using a nine-point scale. To determine the organoleptic properties of dry carrots, the laboratory sample was mixed on white paper and all available parameters were determined in daylight. Firstly, the outer appearance was determined, and then the colour was taken into account (taking note of its intensity, uniformity, and how it corresponded to the initial colour of the raw materials), followed by its consistency, aroma, and taste. When determining consistency, the material's elasticity, hardness, and fragility were all taken into account.

Standard taproots were stored in nylon mesh sacks, at up to 5 kg of weight, quadrupled, in stationary pit storage areas within the main storage period (between October and February), at a temperature of between zero degrees to +2 °C, and keeping relative air humidity at a level of 85–90%. Storage does not make use of artificial refrigeration units; therefore the temperature increased to between +4–5 °C at the end of March. Inspections were carried out after two months and five months of storage time, and again at the end of the storage period (after seven months had elapsed).

For the purpose of drying, 4 kg of carrot taproots were taken, as quadruples. The taproots were weighed, sorted, washed by hand, and cleaned, and the offshoots were counted. After cleaning the carrot taproots, they were washed again and cut with a SIRMAN mechanic shredder into pieces of the following dimensions: length 5–6 mm, width 2–3 mm, and thickness 2–3 mm. The cut produce was uniformly spread onto the dryer's trays as 3 kg m^{-2} and loaded into the dryer (Fig. 2).

A standard dryer C-2M (ТУУ 23061103.001-98) was used for drying the taproots, with it belonging to the category of convective air dryers with a chamber and periodic operation. The minced produce was dried at a temperature of 60 °C until a moisture content of 10–12% has been achieved.

The study's results were processed using mathematical methods on a PC, determining the least significant difference (LSD) and the correlation relationships between the studied indicators by means of generally accepted methods (Bondarenko & Yakovenko, 2001; Skaletska et al., 2014b). The statistical processing of the yielded data took place using two computer programs: Agrostat and Microsoft Excel.

a)  b) 

Figure 2. A general view of the convective dryer: a) carrot quantities prepared and loaded into the dryer's chamber; b) dried carrot quantities.

The stability of the carrot taproot crop yield was assessed using the Levis stability coefficient as SF = HE/LE, where HE and LE are the highest and lowest crop yield indicators respectively, depending upon the weather conditions seen in the vegetation period.

RESULTS AND DISCUSSION

From the results of the three years of field tests and laboratory research, the relevant measurements that were taken, and the processing of the gathered data on a PC, the indicators were determined to characterise the properties of carrot taproots of various hybrids for storage and processing purposes.

Economic value indicators for the carrot hybrids that were received in the period between 2013–2015 are set out in Table 1.

Table 1. The yield and commercial value of carrot hybrids, averaged for 2013–2015

Hybrid name	Commercial yield by years, t ha^{-1}			Average commercial yield, t ha^{-1}	Yield increase		Weight of standard taproot, g.	Commercial weight, %	Coefficient of stability (SF)
	2013	2014	2015		t ha^{-1}	%			
Vita Longa F_1 (*)	47.4	51.3	50.1	49.6	–	100	106.8	77	1.1
Viking F_1	37.2	46.6	40.1	41.3	–8.3	–17	82.2	83	1.3
Evolyutsiya F_1	48.6	51.7	51.2	50.5	+0.9	+2	98.6	85	1.1
Mars F_1	41.7	46.7	48.4	45.6	–4.0	–8	87.4	87	1.2
Napoli F_1	48.6	54.1	52.1	51.6	+2.0	+4	92.0	93	1.1
Purple Haze F_1	46.5	48.0	46.5	47.0	–2.6	–5	81.4	96	1.0
White Sabine F_1	61.0	55.9	59.2	58.7	+9.1	+18	136.2	78	1.1
Yellowstone F_1	53.7	59.5	54.2	55.8	+6.2	+12	118.7	80	1.1
$LSD_{0.5}$	4.7	3.8	4.1				12.4		

* Control group.

The carrot hybrids have a commercial taproot weight of between 81.4–136.2 g and have a characteristic commercial yield of 41.3–58.7 t ha^{-1}. The hybrid White Sabine F_1 is characterised by white taproots and a weight of 136.2 g. The hybrid's commercial yield (58.7 t ha^{-1}) stems from the large size of its taproot, making it possible to achieve a yield increase of 9.1 t ha^{-1}. On the other hand, the hybrid has a low commercial yield of 78%, which speaks of its weak adaptability to growing conditions, including its reactions to a lack of moisture due to the absence of irrigation. The unfavourable weather conditions of 2013, especially in the arid months of May to July, caused the taproots to be formed with a low average weight, which affected their commercial yield.

The hybrids Evolyutsiya F_1 and Napoli F_1 were determined as being high-yield cultivars with an average commercial yield of between 50.5–51.6 t ha^{-1} and an average taproot weight of 92.0–98.6 g. Their yield increase is 2–4%, which is not significantly different from that of the control crop. Additionally, the hybrid Napoli F_1 is characterised by the relatively small size of its taproots (92.0 g) but with a high commercial yield (93%), which has affected its high average commercial yield of 51.6 t ha^{-1} (Fig. 4).

Figure 4. The taproots of carrot hybrids Napoli F_1.

Among the carrot hybrids to be studied, the hybrid Viking F_1 has quite a low commercial yield (41.3 t ha^{-1}). This is related to its low taproot weight of 82.2 g, being 24.6 g lower than that of the control group. In that light, Viking F_1 is determined as being less adaptive to growth conditions, with a stability coefficient of 1.3.

On average over the three years, the most stable hybrid in terms of yield turned out to be Purple Haze F_1 with its violet taproots and a stability coefficient of one. On the other hand, this hybrid has a low commercial yield of 47.0 t ha^{-1}, which is 2.6 t ha^{-1} less than that of the control crop. The significant difference between the hybrid Purple Haze F_1 and the control crop was established throughout the entire three-year study period. Crop losses during harvesting were minimal (up to 0.5%), as the taproots were harvested manually (Fig. 5).

Figure 5. Harvesting the carrot taproots in 2015.

Therefore the carrot hybrids that have been studied have a wide range of variation in terms of their economic value indicators, which makes it possible to grow them for storage and processing in various soils and climate conditions without irrigation. The most productive carrot hybrids are White Sabine F_1 and Yellowstone F_1 with a commercial yield of 55.8–58.7 t ha^{-1} and an average taproot weight of between 118.7–136.2 g.

As indicated by the data in the available literature and the studies that are at hand, taproots with stable biometric properties are the most suitable when it comes to processing and storage, as these properties determine their suitability for mechanical cleaning, low waste levels, and low losses during storage. The most stable weights and diameters for their taproots were displayed by the hybrids Vita Longa F_1 (the control crop) and White Sabine F_1, and the most stable lengths by the hybrids Napoli F_1 and Purple Haze F_1.

In the complex assessment of the suitability of any carrot variation for storage and processing, the biochemical content of the produce is important. It is known that the higher the content of dry matter and sugars in taproots, the better its suitability for long-term storage (Skaletska et al., 2016; Zadadska & Kravchenko, 2016a, 2016b). These indicators also have a significant effect on the yield and quality of the processed produce (Skaletska et al., 2013; Skaletska & Zavadska, 2014c). The results of the biochemical assessment of the studied taproots are provided in Table 2.

Table 2. The content of the main biochemical indicators and the degustation assessment of the taproots of various carrot hybrids, averaged for 2013–2015

Hybrid name	Content in taproots						Degustation assessment, points*
	Dry matter, %	Dry soluble matter, %	Sugars, %			β-carotene, mg ($100g^{-1}$)	
			Mono-sugars	Sucroses	Total		
Vita Longa F_1 (control crop)	11.83	9.0	1.38	3.25	4.63	8.2	9.0
Viking F_1	12.69	10.0	1.77	3.47	5.24	9.2	8.6
Evolyutsiya F_1	12.86	9.0	1.90	3.88	5.78	10.4	9.0
Mars F_1	10.02	8.0	2.01	2.31	4.32	10.2	8.8
Napoli F_1	10.52	8.0	2.15	2.46	4.61	7.7	9.0
Purple Haze F_1	13.51	10.8	2.31	3.92	6.23	6.4	8.8
White Sabine F_1	11.24	9.5	2.91	1.97	4.88	2.3	8.0
Yellowstone F_1	12.40	9.3	2.11	3.09	5.20	5.2	8.4

* On a nine-point scale.

The studies indicated that the highest content of dry matter is in the taproots of carrot cultivar Purple Haze F_1, which has violet skin and orange core, with the content being at 13.51% (higher by 1.67% than the control crop), and the lowest content is in the hybrid Mars F_1 (9.1%). The taproots of the hybrids Evolyutsiya (12.86%), Viking (12.69%), and Yellowstone F_1 (12.40%) contained a sufficiently large amount of dry matter.

As shown by the results of the studies that had been conducted by the authors, the content of sugars is important for produce that is intended for drying, because it affects the taste and the commercial value of the finished produce (Skaletska & Zavadska, 2014c, 2015). It was determined that the taproots of the carrot hybrids, Purple Haze F_1 and Evolyutsiya F_1, had the highest content of such sugars and dry matter, at 6.23% and 5.78% respectively. Of the sugars in the taproots of the carrot hybrids that were studied (except the hybrid White Sabine F_1), sucrose was predominant.

The taproots of orange coloured hybrids contained more β-carotene, between 7.7–10.4 mg $(100\ g)^{-1}$ of raw material. Of the assortment that was studied, the taproots

of the hybrids Evolyutsiya F_1 and Mars F_1 had the highest content of β-carotene, which was in excess of 10 mg $(100\ g)^{-1}$.

The taproots of all of those carrot hybrids that have been included in the study received high grades in the degustation assessment: between 8–9 points on a nine-point scale. Maximum points were given to samples of the hybrids Vita Longa F_1 (control crop), Evolyutsiya F_1, and Napoli F_1. The taproots of these carrot hybrids had a small core, no discernible line between the core and the cortex, and a cortex that was juicy with a characteristic pleasant, saturated taste.

Therefore, over the entire vegetation period, the taproots of the hybrids Purple Haze F_1, Evolyutsiya F_1, Viking F_1, and Yellowstone F_1 collected 12% dry matter and 5% sugars. The highest concentration of those substances were contained in the taproots of the carrot hybrid Purple Haze F_1: 13.51% dry matter and 6.23% sugars (total). More than 10 mg $(100\ g)^{-1}$ of β-carotene was collected from the taproots of the carrot hybrids Evolyutsiya and Mars. The maximum number of points (nine points) from the degustation assessment were given to samples of the hybrids Vita Longa F_1 (the control crop), Evolyutsiya F_1, and Napoli F_1.

In order to be able to research the suitability for drying of taproots of the carrot hybrids that were studied, their technological properties were determined (Table 3).

Table 3. The volume of waste and the yield of dried produce from various carrot hybrids, averaged for 2013–2015

Hybrid name	Volume of waste		Yield of dried produce		Amount of fresh raw material for 1 kg of dried produce, kg	
	%	± comp. w/ control crop	%	± comp. w/ control crop	unprepared	prepared
Vita Longa F_1 (control crop)	19.6	–	9.8	–	12.1	10.2
Viking F_1	10.8	–8.8	11.4	+1.6	9.8	8.8
Evolyutsiya F_1	7.7	–11.9	10.6	+0.8	10.1	9.4
Mars F_1	13.5	–6.1	10.1	+0.3	11.2	9.9
Napoli F_1	14.7	–4.9	8.8	–1.0	13.0	11.4
Purple Haze F_1	18.8	–0.8	11.9	+2.1	11.6	8.4
White Sabine F_1	19.2	–0.4	8.4	–1.4	14.2	11.9
Yellowstone F_1	11.8	–7.8	11.7	+1.9	9.6	8.5
$LSD_{0.5}$	3.1		1.1		0.8	1.2

The volume of waste in the process of preparing the carrot taproots for drying varied within the range of 7.7% to 19.6%. The largest volume of waste was generated from samples of the control crop - the hybrid Vita Longa F_1 (19.6%) - due to its significant branching of taproots and their low commercial yield. The lowest level of waste when preparing taproots for drying was generated from the carrot hybrid Evolyutsiya: 7.7% (11.95% less when compared to the results for the control crop). There was no significant difference in terms of waste being generated from the taproots of the control crop and that for the hybrids Purple Haze F_1 and White Sabine F_1 (the difference was within the LSD).

The yield of dried produce is determined to be within the range of 8.4–11.9% of the total mass of the average sample, depending upon the cultivar. This indicator was at its lowest in the taproots of the hybrid Napoli: 8.4% (1.0% less than in the taproots of the control crop), and at its highest in the taproots of the hybrids Purple Haze F_1 (11.9%),

Yellowstone F_1 (11.7%), and Viking F_1 (11.4%).

The calculations that have been carried out indicated that between 9.6 kg and 14.2 kg of unprepared (not cleaned) raw material or between 8.4 kg and 11.9 kg of prepared raw material is required for 1 kg of dried produce. This indicator was most greatly affected by the dry matter content and the amount of waste. The quantity of fresh carrot taproots that is needed for 1 kg of dried produce was at its lowest when using the hybrid Yellowstone F_1: 8.5 kg of uncleaned raw material and 9.6 kg of cleaned raw material; as well as Viking F_1: with figures at 8.8 kg and 9.8 kg respectively.

Those properties that are important for consumers of processed produce include its nutritional value, its biological value, and also its organoleptic properties. The studies that have been carried out have provided the following indicators, as shown in Table 4.

It was determined that the amount of moisture in the dried carrots varied, depending upon the specific nature of the cultivars. The tissue structure in the taproots affected the speed and level of drying. The lowest content levels could be found in samples of the hybrids Vita Longa and White Sabine F_1: at 7.7 ±1.1 and 7.5 ±1.2% respectively. Fresh raw material from these hybrids was dried under identical conditions. This affected the organoleptic properties of the finished produce, the existence of darkened chips, their hard structure, and the significant volume of fine particulates. Those hybrids which had a moisture content that was closest to the standard moisture content level (10%) were Evolyutsiya F_1, Yellowstone F_1, and Napoli F_1. Their structure was sufficiently firm and elastic.

Table 4. The content of the main biochemical components and a degustation assessment of dried carrots from various carrot hybrids, averaged for 2013–2015

Hybrid name	Moisture content, %	Content in dried produce		Degustation assessment, points*
		Total sugars (total)	β-carotene, mg (100 g)$^{-1}$	
Vita Longa F_1 (control crop)	7.7 ± 1.1	36.10 ± 2.1	36.8 ± 1.4	7.7
Viking F_1	9.4 ± 0.7	39.0 ± 1.8	39.8 ± 2.5	8.5
Evolyutsiya F_1	10.2 ± 0.6	41.87 ± 1.4	42.5 ± 1.8	8.7
Mars F_1	8.7 ± 0.9	33.46 ± 2.3	41.6 ± 2.3	7.9
Napoli F_1	10.4 ± 0.4	36.71 ± 2.0	36.0 ± 0.8	7.8
Purple Haze F_1	10.8 ± 0.5	41.78 ± 1.7	32.4 ± 2.6	7.2
White Sabine F_1	7.5 ± 1.2	37.27 ± 2.3	14.8 ± 1.0	7.0
Yellowstone F_1	9.7 ± 0.5	40.92 ± 1.1	20.8 ± 1.4	8.8

* On a nine-point scale.

In the process of drying, the sugars content became significantly concentrated and changed, depending upon the cultivar. Similar to fresh raw materials, the highest sugars content was found in samples of the hybrids Evolyutsiya, Purple Haze F_1, and Yellowstone F_1: at more than 40%. It was determined that their amount significantly affected the taste of the finished produce ($r = 0.72 \pm 0.1$). As a result of the calculations that had been carried out in connection with changes in the sugars content during the course of drying carrots, it was determined that their content in dried produce increased by only negligible amounts when compared to the results from fresh raw material (by between 2–5%, depending upon the cultivar).

Research has already shown that β-carotene is quite stable whilst it is being heated. Therefore a significant amount of it was preserved in the dried produce: from 14.8 ± 1.0 mg $(100\ g)^{-1}$ in white-coloured carrots to 42.5 ± 1.8 in orange-coloured carrots. More than 40 mg $(100\ g)^{-1}$ of carotene was contained in the dried produce of the carrot hybrids Evolyutsiya and Mars: 42.5 ± 1.8 and 41.6 ± 2.3 mg $(100\ g)^{-1}$ respectively. Dried versions of those carrot hybrids can be recommended to consumers as a biologically valuable, natural dietary supplement.

Based on the complex of organoleptic indicators (involving outer appearance, structure, smell, taste, and colour), more than eight points on a nine-point scale were given to dried samples of the carrot hybrids Yellowstone F_1 (8.8), Evolyutsiya F_1 (8.7), and Viking F_1 (8.5). Produce involving the hybrid Yellowstone F_1 was uniform in shape and dimensions, as well as being coloured bright yellow and having a pleasant saturated taste (Fig. 3).

Dried samples of the hybrid White Sabine F_1 contained a significant amount of darkened particulates; dried samples of the hybrid Purple Haze F_1 had a mixed, uneven colour. Based on the results of the degustation assessment, these were assigned to the second commercial cultivar.

As indicated by the results of the study, the suitability of the taproots for long-term storage was significantly dependent upon the cultivar's specifics (Fig. 4).

During the first two months of storage in conditions that involved the use of a stationary pit storage area with no artificial cooling, the preservation rate for taproots of the hybrids Viking F_1, Purple Haze F_1, and White Sabine F_1 were at 100%. The taproots of the hybrid Napoli F_1 had even started sprouting (10% of them had sprouted) and then wilting during that first period. After five months of storage the taproots of the hybrid Mars F_1 started

Figure 3. Dried and restored versions of carrot hybrids: a) Vita Longa (the control crop); b) Yellowstone F_1.

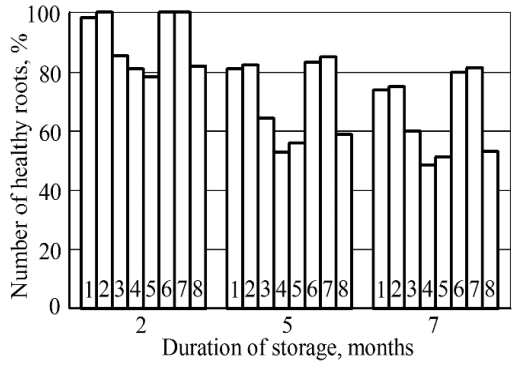

Figure 4. The number of healthy carrot taproots from various hybrids that are in the process of long-term storage (averaged for 2013–2015): 1) Vita Longa (the control crop); 2) Viking F_1; 3) Evolyutsiya F_1; 4) Mars F_1; 5) Napoli F_1; 6) Purple Haze F_1; 7) White Sabine F_1; 8) Yellowstone F_1.

sprouting *en masse* - more than half of them had sprouted within that storage period. The highest ratio of healthy taproots after five months of storage was observed for the hybrids Purple Haze F_1 and White Sabine F_1: 85.2 and 83.4% respectively.

It was determined that, after seven months of storage, the preservation rate for the taproots of the hybrids that were being studied tended to vary within the range of 8.5% to 81.4%. The most suitable hybrids for long-term storage were White Sabine F_1 and Purple Haze F_1: preservation rates for these taproots were at 81.4% and 80.2% respectively, which exceeded those of the control cultivar by 7.4% and 6.2%. By the end of the storage period the samples of all of the hybrids being studied included a significant amount of sprouted, wilted, and pathogen-damaged carrot taproots. If storage facilities with artificial cooling are not available during the storage period, carrot taproots should be utilised within the first two months after having been harvested as this ensures their high commercial yield and minimum losses.

CONCLUSIONS

In agricultural field tests and laboratory tests that were carried out over the course of three years, the carrot hybrids White Sabine F_1 and Yellowstone F_1, were determined to be the most productive of all the hybrids studied, with a commercial yield of between 55.8–58.7 t ha^{-1} and an average taproot weight of 118.7–136.2 g.

The highest nutritional value was found in fresh taproots of the carrot hybrid Purple Haze F_1, as they contain 13.51% dry matter and 6.23% sugars (total); the highest biological value was found in taproots of the hybrids Evolyutsiya F_1 and Mars F_1, as they collect more than 10 mg $(100\ g)^{-1}$ of β-carotene in them.

Of the carrot cultivars that are grown in the woodland steppes of Ukraine, taproots of the hybrids Yellowstone F_1 and Viking F_1 are the most suitable for drying. They are characterised by a negligible amount of waste being generated from the process of preparing the raw material for drying (10.8–11.8%), by quite a high yield of finished produce (11.4–11.7%), and by good organoleptic indicators (with a degustation assessment of between 8.5–8.8 points on a nine-point scale). The dried produce of carrot hybrids such as Evolyutsiya F_1 and Mars F_1 contains more than 40 mg $(100\ g)^{-1}$ of β-carotene and can be used as a biologically valuable natural dietary supplement.

The most suitable taproots for long-term storage in stationary pit storage facilities without any artificial cooling are those of the hybrids White Sabine F_1 and Purple Haze F_1. After a period of seven months the preservation rate of taproots for those hybrids exceeds 80%.

REFERENCES

Alasalvar, C., Al-Farsi, M., Quantick, P.C., Shahidi, F. & Wiktorowicz, R. 2005. Effect of chill storage and modified atmosphere packaging (MAP) on antioxidant activity, anthocyanins, carotenoids, phenolics and sensory quality of ready-to-eat shredded orange and purple carrots. *Food Chemistry* **89**(1), 69–76. doi: 10.1016/j.foodchem.2004.02.013

Algarra, M., Fernandes, A., Mateus, N., de Freitas, V., Esteves da Silva, J.C.G. & Casado, J. 2014. Anthocyanin profile and antioxidant capacity of black carrots (Daucus carota L. ssp. sativus var. atrorubens Alef.) from Cuevas Bajas, Spain (2014) *Journal of Food Composition and Analysis* **33**(1), 71–76. doi: 10.1016/j.jfca.2013.11.005

Arscott, S.A. & Tanumihardjo, S.A. 2010. Carrots of many colors provide basic nutrition and bioavailable phytochemicals acting as a functional food. *Comprehensive Reviews in Food Science and Food Safety* **9**(2), 223–239. doi: 10.1111/j.1541-4337.2009.00103.x

Bobos, I.M. & Zavadska, O.B. 2015. *Improved technology for growing taproots for storage and processing*. A Monograph, Kiev: CP Komprint, 304 pp. (in Ukrainian).

Bobos, I., Fedosy, I., Zavadska, O., Tonha, O. & Olt, J. 2019. Optimization of plant densities of dolichos (Dolichos lablab l. var. lignosus) bean in the right-bank of forest-steppe of Ukraine. *Agronomy Research* **17**(6), 2195–2202. doi: 10.15159/AR.19.223

Bochnak-Niedźwiecka, J. & Świeca, M. 2020. Quality of new functional powdered beverages enriched with lyophilized fruits-potentially bioaccessible antioxidant properties, nutritional value, and consumer analysis. *Applied Sciences (Switzerland)* **10**(11), art. no. 3668. doi: 10.3390/app10113668

Bondarenko, G.L. & Yakovenko, K.I., 2001. *Methodology of Experimental Research in Vegetable and Pumpkins*, Kharkiv: Osnova, 369 pp. (in Ukrainian).

Borisov, V.A., Romanova, A.V., Yanchenko, E.V., Gasparian, S.V., Piskounova, N.A., Maslovsky, S.A. & Zamyatina, M.E. 2016. Evaluation of varieties and hybrids of carrots on the suitability of fast-frozen products. *Vestnik MAX* **2**, 10–14. doi: 10.21047/1606-4313-2016-15-2-10-14

Burenin, V.I., Piskunova, T.M. & Khmelinskaya, T.V. 2017. The gene pool for breeding of carrot and table beet. Breeding and seed production of agricultural crops. *Vegetable crops of Russia*, ISSN 2618-7132, **37**(4), 28–31.

Haq, R.-U. & Prasad, K. 2017. Antioxidant activity, phenolic, carotenoid and color changes in packaged fresh carrots stored under refrigeration temperature. *Journal of Food Measurement and Characterization* **11**(4), 1542–1549. doi:10.1007/s11694-017-9533-2

Hryshchenko, A., Bilyk, O., Bondarenko, Y., Kovbasa, V. & Drobot, V. 2019. Use of dried carrot pomace in the technology of wheat bread for elderly people. *Food Science and Technology* **13**(1). 98–105. doi. 10.15673/fst.v13i1.1338

Kornev, A.V., Leunov, V.I. & Khovrin, A.N. 2017. Variation of some traits in carrot with different root colors. *Vegetable crops of Russia*, ISSN 2618-7132, **37**(4), 41–44.

Lewicki, P.P. & Duszczyk, E. 1998. Color change of selected vegetables during convective air drying. *International Journal of Food Properties* **1**(3), 263–273. doi: 10.1080/10942919809524582

Macura, R., Michalczyk, M., Fiutak, G. & Maciejaszek, I. 2019. Effect of freeze-drying and air-drying on the content of carotenoids and anthocyanins in stored purple carrot. *Acta Scientiarum Polonorum, Technologia Alimentaria* **18**(2), 135–142. doi: 10.17306/J.AFS.2019.0637

Piyarach, K., Nipawan, K., Chadapon, C., Daluwan, S. & Kunjana, R. 2020. Effect of Drying on β-Carotene, α Carotene, Lutein and Zeaxanthin Content in Vegetables and Its Application for Vegetable Seasoning, *E3S Web of Conferences* **141**, *art. no. 0200*, doi: 10.1051/e3sconf/202014102007.

Seljasen, R., Kristensen, H.L., Lauridsen, C., Wyss, G.S., Kretzschmar, U., Birlouez-Aragone, I. & Kah, J. 2013. Quality of carrots as affected by pre- and postharvest factors and processing. *Journal of the Science of Food and Agriculture* **93**(11), 2611–2626. doi: 10.1002/jsfa.6189

Skaletskaya, L.F., Bobos, I.M. & Djadenko, T.V. 2013a. The suitability of carrot cultivar taproot (Daucus carota) for processing. *Cultivar studies and protecting cultivar planting rights* **18**(1), 51–55 (in Ukrainian).

Skaletskaya, L.F., Zavadska, O.B. & Djadenko, T.V. 2013b. The effectiveness of producing various cultivars of dried carrots. *A research publication issued by the Ukrainian National University of Biological Resources and Nature Utilisation, Series: Agronomia*, Kiev, **183**(2), 269–274 (in Ukrainian).

Skaletska L.F. & Zavadska, O.B. 2013. Selection of carrots varieties for storage. *Journal of Scientific World of the Modern scientific research and their practical application*, J11307, 61–63.

Skaletska, L.F., Podpriatov, G.I. & Zavadska, O.B. 2014a. *Storage and processing technology: methods for the effective use of farm and garden crops*: A Monograph. Kiev: Centre of Information Technologies, 202 pp. (in Ukrainian).

Skaletska, L.F., Podpriatov, G.I. & Zavadska, O.B. 2014b. *Scientific research methods for storing and processing plant crops*. Kiev: CP KOMPRINT, 416 pp. (in Ukrainian).

Skaletska, L.F. & Zavadska, O.V. 2014c. The quality of dried carrots, depending upon cultivar and drying method. *Journal of Scientific World of the Modern scientific research and their practical application* **36**(3), 28, 56–60.

Skaletska L.F. & Zavadska O.V. 2015. *Selection* of carrots varieties for storage and processing. *Journal of Scientific World of the Modern scientific research and their practical application*, Ivanovo, J11510, 76–80.

Skaletska, L.F., Zavadska, O.V. & Ostrova, T.V. 2016. The suitability for storage of carrot taproots (Daucus carota) from various cultivars and hybrids grown in Ukrainian woodland steppes. *Research journal of the National Agricultural University of Moldova, Agricultural Science* **1**, 66–70. ISSN 1857-0003

Sych, Z.D. 2010. Recommendations for the growing of leguminous vegetable crops in the forest-steppe Ukraine, NULES of Ukraine, Kyiv, 41 pp.

Zavadska, O.V., Bobos, I.M. & Djadenko, T.V. 2013. The suitability of carrot cultivar taproot (Daucus carota) for processing. *Cultivar studies and protecting cultivar planting rights* **18**(1), 51–55 (in Ukrainian).

Zavadska, O.V. & Kravchenko, O. 2016a. Selecting taproots from various carrot hybrids for long-term storage. *The World of Science and Innovation* **12**(3), Ivanovo: ResearchWorld, 26–30 (in Russian).

Zavadska, O.V. & Kravchenko, O. 2016b. The quality and suitability for storage carrots hybrids cultivation in the conditions of Ukraine's forest-steppe. *Journal of Scientific World of the Modern scientific research and their practical application*, Ivanovo, **J116**(10), 40–46.

Zielinska, M. & Markowski, M. 2012. Color Characteristics of Carrots: Effect of Drying and Rehydration. *International Journal of Food Properties* **15**(2), 450–466. doi: 10.1080/10942912.2010.489209

Wismer, W.V. 2003. Low temperature as a causative agent of oxidative stress in postharvest crop. Postharvest oxidative stress in horticultural crops, Ed. D.M. Hodges, New York: Food Products Press, pp. 55–68.

INSTRUCTIONS TO AUTHORS

Papers must be in English (British spelling). English will be revised by a proofreader, but authors are strongly urged to have their manuscripts reviewed linguistically prior to submission. Contributions should be sent electronically. Papers are considered by referees before acceptance. The manuscript should follow the instructions below.

Structure: Title, Authors (initials & surname; an asterisk indicates the corresponding author), Authors' affiliation with postal address (each on a separate line) and e-mail of the corresponding author, Abstract (up to 250 words), Key words (not repeating words in the title), Introduction, Materials and methods, Results and discussion, Conclusions, Acknowledgements (optional), References.

Layout, page size and font

- Use preferably the latest version of **Microsoft Word**, doc., docx. format.
- Set page size to **ISO B5 (17.6×25 cm)**, all **margins at 2 cm**. All text, tables, and figures must fit within the text margins.
- Use single line spacing and **justify the text**. Do not use page numbering. Use **indent 0.8 cm** (do not use tab or spaces instead).
- Use font Times New Roman, point size for the title of article **14 (Bold)**, author's names 12, core text 11; Abstract, Key words, Acknowledgements, References, tables, and figure captions 10.
- Use *italics* for Latin biological names, mathematical variables and statistical terms.
- Use single ('…') instead of double quotation marks ("…").

Tables

- All tables must be referred to in the text (Table 1; Tables 1, 3; Tables 2–3).
- Use font Times New Roman, regular, 10 pt. Insert tables by Word's 'Insert' menu.
- Do not use vertical lines as dividers; only horizontal lines (1/2 pt) are allowed. Primary column and row headings should start with an initial capital.

Figures

- All figures must be referred to in the text (Fig. 1; Fig. 1 A; Figs 1, 3; Figs 1–3). Use only black and white or greyscale for figures. Avoid 3D charts, background shading, gridlines and excessive symbols. Use font **Arial, 10 pt** within the figures. Make sure that thickness of the lines is greater than 0.3 pt.
- Do not put caption in the frame of the figure.
- The preferred graphic format is Excel object; for diagrams and charts EPS; for half-tones please use TIFF. MS Office files are also acceptable. Please include these files in your submission.
- Check and double-check spelling in figures and graphs. Proof-readers may not be able to change mistakes in a different program.

References

- **Within the text**

In case of two authors, use '&', if more than two authors, provide first author 'et al.':

Smith & Jones (1996); (Smith & Jones, 1996);

Brown et al. (1997); (Brown et al., 1997)

When referring to more than one publication, arrange them by following keys: 1. year of publication (ascending), 2. alphabetical order for the same year of publication:

(Smith & Jones, 1996; Brown et al., 1997; Adams, 1998; Smith, 1998)

- **For whole books**

Name(s) and initials of the author(s). Year of publication. *Title of the book* (*in italics*). Publisher, place of publication, number of pages.

Shiyatov, S.G. 1986. *Dendrochronology of the upper timberline in the Urals*. Nauka, Moscow, 350 pp. (in Russian).

- **For articles in a journal**

Name(s) and initials of the author(s). Year of publication. Title of the article. *Abbreviated journal title* (*in italic*) volume (in bold), page numbers.

Titles of papers published in languages other than English, should be replaced by an English translation, with an explanatory note at the end, e.g., (in Russian, English abstr.).

Karube, I. & Tamiyra, M.Y. 1987. Biosensors for environmental control. *Pure Appl. Chem.* **59**, 545–554.

Frey, R. 1958. Zur Kenntnis der Diptera brachycera p.p. der Kapverdischen Inseln. *Commentat.Biol*. **18**(4), 1–61.

Danielyan, S.G. & Nabaldiyan, K.M. 1971. The causal agents of meloids in bees. *Veterinariya* **8**, 64–65 (in Russian).

- **For articles in collections:**

Name(s) and initials of the author(s). Year of publication. Title of the article. Name(s) and initials of the editor(s) (preceded by In:) *Title of the collection (in italics)*, publisher, place of publication, page numbers.

Yurtsev, B.A., Tolmachev, A.I. & Rebristaya, O.V. 1978. The floristic delimitation and subdivisions of the Arctic. In: Yurtsev, B. A. (ed.) *The Arctic Floristic Region*. Nauka, Leningrad, pp. 9–104 (in Russian).

- **For conference proceedings:**

Name(s) and initials of the author(s). Year of publication. Name(s) and initials of the editor(s) (preceded by In:) *Proceedings name (in italics)*, publisher, place of publishing, page numbers.

Ritchie, M.E. & Olff, H. 1999. Herbivore diversity and plant dynamics: compensatory and additive effects. In: Olff, H., Brown, V.K. & Drent R.H. (eds) *Herbivores between plants and predators. Proc. Int. Conf. The 38th Symposium of the British Ecological Society*, Blackwell Science, Oxford, UK, pp. 175–204.

Please note

- Use '.' (not ',') for decimal point: 0.6 ± 0.2; Use ',' for thousands – 1,230.4;
- Use '–' (not '-') and without space: pp. 27–36, 1998–2000, 4–6 min, 3–5 kg
- With spaces: 5 h, 5 kg, 5 m, 5 °C, C : D = 0.6 ± 0.2; $p < 0.001$
- Without space: 55°, 5% (not 55 °, 5 %)
- Use 'kg ha^{-1}' (not 'kg/ha');
- Use degree sign ' ° ' : 5 °C (not 5 ^{O}C).